Synthesis of Reactive Polyether Copolymers

Dissertation zur Erlangung des Grades
„Doktor der Naturwissenschaften"
im Promotionsfach Chemie

am Fachbereich Chemie, Pharmazie und Geowissenschaften
der Johannes Gutenberg-Universität Mainz

Kamil Norbert Maciol

geboren in Malapane, Polen

Mainz, 2018

JOHANNES GUTENBERG UNIVERSITÄT MAINZ

JG|U

Dekan: ▮▮▮▮▮▮▮▮▮▮▮▮

Prodekanin: ▮▮▮▮▮▮▮▮▮▮▮

1. Berichterstatter: ▮▮▮▮▮▮▮▮▮

2. Berichterstatter: ▮▮▮▮▮▮▮▮▮

Tag der mündlichen Prüfung: ▮▮▮▮▮▮▮

Die als Dissertation vorgelegte Arbeit wurde in der Zeit von Oktober 2015 bis Dezember 2018 am Institut für Organische Chemie der Johannes Gutenberg-Universität Mainz im Arbeitskreis von Herrn Prof. Dr. Holger Frey angefertigt.

Hiermit versichere ich gemäß § 10 Abs. 3d der Promotionsordnung vom 24.07.2007

a) Ich habe die jetzt als Dissertation vorgelegte Arbeit selbst angefertigt und alle benutzten Hilfsmittel (Literatur, Apparaturen, Material) in der Arbeit angegeben.

b) Ich habe oder hatte die jetzt als Dissertation vorgelegte Arbeit nicht als Prüfungsarbeit für eine staatliche oder andere wissenschaftliche Prüfung eingereicht.

c) Ich hatte weder die jetzt als Dissertation vorgelegte Arbeit noch Teile davon bei einer anderen Fakultät bzw. einem anderen Fachbereich als Dissertation eingereicht.

_____

Kamil Maciol

„Mit dem Wissen wächst der Zweifel."

Johann Wolfgang von Goethe

Danksagung

██
██

██
██
██
██
██
██ ████████ ████████ ██████ █████ ██ ██████ ██████ ██
██████████████

██
██
██
██
██████████████████████████ ██████████████████████████
██
████████████████████████████

██
██████████████████████████████

██
██

██
████████████████████████████

██
██████████████████████████████████████

██
██
██████████

Danksagung

██
███████████████████████████████

██
██
██
██
██
████████████████████████████

██
████████████ ██ ██ ████ ██ ████████████ ████████
██
██
██
██
██
██
███████████████████████

██

██
████████████████████████████████

██
██
██
██████████████████████

██
██
██
██

██
██
██

███

███

██

███

██

███

███

███

███

████████████████████████████

███

███

███

███

██

██ ████████ ██████ ██ ██████ ████ █████ ██ ██ ████████

███

████

███

███

███

███████████████████████████████████

Table of Contents

Motivation and Objectives

Poly(ethylene glycol) (PEG) is considered to be one of the most important aliphatic polyethers and is predominantly synthesized by the anionic ring-opening polymerization (AROP) of ethylene oxide (EO). For molecular weights below 30,000 g mol^{-1} these non-ionic homopolymers of EO are referred to as poly(ethylene glycol), in the case of higher molecular weights as poly(ethylene oxide) (PEO).[1] Under standard conditions, the appearance of PEG is strongly dependent on its molecular weight and ranges from viscous liquids (400−600 g mol^{-1}) to waxy structures and to colorless, crystalline solids ($\geq$ 2,000 g mol^{-1}). The same applies to the melting point (T_m) and glass transition temperature (T_g), which level off at around 68.6 °C[2] for T_m and -60.5 °C[3] for T_g at high molecular weights. Unlike other prominent polyethers such as poly(oxymethylene) (POM) or poly(propylene oxide) (PPO), PEG exhibits exceptionally high solubility in water.[4] Moreover, PEG shows extremely low toxicity, immunogenicity and antigenicity,[5] leading to significant interest for medical, pharmaceutic and cosmetic applications.[6] Using bioconjugation with PEG ("PEGylation"), protein and peptide biopharmaceuticals can be protected against immune response by shielding with PEG chains. This concept, introduced by Abuchowski *et al.* in the 1970s, is used commercially, and a number of PEGylated pharmaceuticals, such as Adagen® and Oncaspar®, are approved by the U.S. Food and Drug Administration (FDA).[7–9] Besides these protein conjugates, PEG is also applied in liposomes (Doxil®/Caelyx®) or in imaging techniques in echocardiography (Definity®).[10] Another well-known application is the use as non-ionic surfactants. Here, established representatives are poloxamers, which are commercialized under the names Synperonic®, Pluronic® or Kolliphor® among others.[11] These non-toxic poloxamers are triblock copolymers consisting of a hydrophobic PPO block, flanked by two hydrophilic PEG blocks. As the covalently connected blocks have different polarity, they tend to self-assemble in water. Here, the hydrophilic PEG is at the polymer aggregate surface in aqueous solutions, while the hydrophobic PPO block is the core of the commonly micellar aggregates.[12] These surfactants are used for multiple applications, such as drug delivery systems, as dispersants for inks/ pigments or in coatings.[13,14] Apart from these mostly pharmaceutical applications, PEG tensides are also used as a component of emulsifying agent, for plasticizers or for textile lubricants.[15]

Linear PEG possesses only two functional groups (hydroxyl groups) at the chain ends. However, many applications require specific terminal functionalities. Two strategies are feasible for the synthesis of α,ω-modified PEGs.[16] In the direct synthesis functional initiators and terminating agents are used for the introduction of reactive groups. In the second method,

the functionalization of the end groups is achieved by post-polymerization modification reactions. When aiming at pharmaceutical applications, the limited loading capacity for active ingredients is disadvantageous, which is a consequence of the low number of functional groups. In this context, multi-functional PEGs provide a solution. The copolymerization of EO with functional epoxides permits the incorporation of reactive groups along the polymer backbone (**Scheme 1a**). In this fashion, the properties of poly(ethylene glycol) can be tailored and therefore the range of applications expanded, making multi-functional PEGs a very attractive platform. By copolymerization of EO with propylene oxide (PO)[17] or glycidyl methyl ether (GME)[18], PEG's thermoresponsive behavior in water can be selectively adjusted in dependence of the comonomer amount, as this has an impact on its lower critical solution temperature (LCST) behavior in aqueous solutions. Complementary, pendant ferrocene[19,20] moieties are used to introduce redox properties to the polymer, while acid cleavable[21] and amine[22] groups trigger a pH-sensing response.

By further expanding the range of established multi-functional PEGs via the copolymerization of a variety of innovative epoxide monomers, this doctoral thesis ties in with the previous research. In this context, a wide variety of architectures are realized here: statistical and gradient-like copolymers, as well as novel block copolymers (**Scheme 1b**).
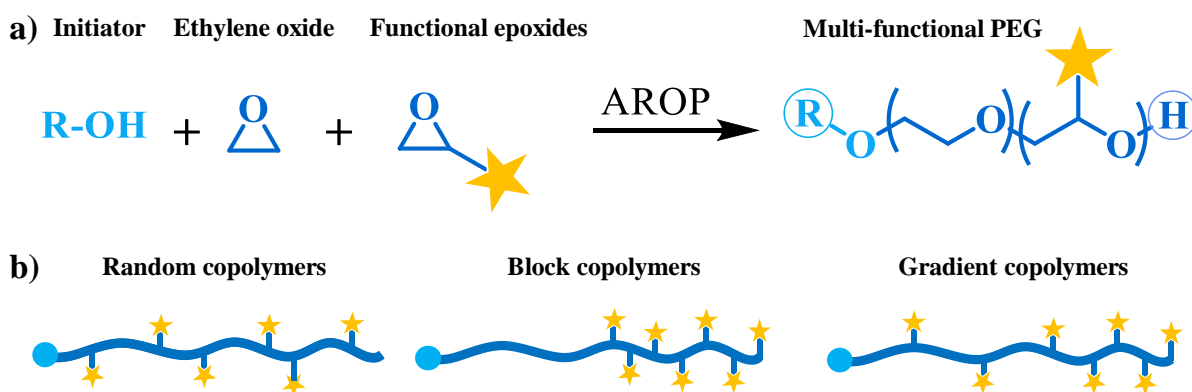
Scheme 1. a) Synthesis of multi-functional PEGs by the anionic ring-opening copolymerization of EO with functional epoxides. b) Synthesis of various polyether architectures: random-, block- and gradient copolymers.

In this context, the following key questions are addressed in this thesis:

1)   Can tailored epoxide derivatives be developed for the synthesis of novel, multi-functional PEGs via AROP, targeting potential biomedical applications?

Stimuli-responsive materials are capable of changing their chemical and/ or physical properties when exposed to external stimuli. In this context, two acid-labile monomer building blocks have been established: ethoxy allyl glycidyl ether (EAGE) (**Chapter 2.1**) and ethoxy butoxy vinyl glycidyl ether (EBVGE) (**Chapter 3.1**). Different concepts are used for the application of PEG-based copolymers of these two monomers. In basic studies for potential biomedical applications, the scope of EAGE for the preparation of acid-labile hydrogels is investigated. In contrast, water-soluble EBVGE block copolymers are studied in detail with respect to their aggregation to micelles and subsequent crosslinking. Interestingly, to date there is no direct access to aliphatic ketones in a polyether backbone. Instead, polymer modification reactions have to be carried out. The synthesis of the ketone-based monomer ketone dioxolane glycidyl ether (KDGE) (**Chapter 2.2**) and its copolymers with ethylene oxide is investigated. In addition, the potential of KDGE for the synthesis of reversible hydrogels is examined in more detail.

2)   Can the limits of AROP be overcome and novel multi-functional polyether structures be established through the use of monomer-activated AROP?

As a consequence of the harsh, basic conditions of oxyanionic ROP, the polymerization of reactive or protic monomers is not feasible. A remedy may be the monomer-activated AROP, as it operates under considerably milder conditions. This polymerization strategy is applied to prepare polyethers based on glycidyl cinnamate (GC) (**Chapter 2.3**), epoxy undecane methacrylate (EUMA) (**Chapter 3.2**) and tridecafluorooctyl glycidyl ether (TDFOGE) (**Chapter 4.1**). As has been shown, cinnamoyl groups are a promising candidate for the synthesis of photoresponsive hydrogels and methacrylates are very well-suited for crosslinking of micellar cores. Perfluorinated polyethers are an obvious choice for oil- and water repellent surface coatings.

3)   What does the reaction kinetics for the copolymerization of EO/ EEGE with the novel epoxide derivatives look like and how does this affect the final copolymer microstructure?

The copolymer microstructure does not only influence the properties, but also determines possible applications. Accordingly, the examination of reaction kinetics of the copolymerizations in **Chapters 2−3** is a central point of this thesis and also plays a role in the **Appendix** chapters. Here, the quantification of reactivity ratios and the determination of the resulting microstructure is conducted using real-time ^{1}H NMR spectroscopy.

REFERENCES

(1) Herzberger, J.; Niederer, K.; Pohlit, H.; Seiwert, J.; Worm, M.; Wurm, F. R.; Frey, H. Polymerization of Ethylene Oxide, Propylene Oxide, and Other Alkylene Oxides: Synthesis, Novel Polymer Architectures, and Bioconjugation. *Chem. Rev.* **2016**, *116*, 2170–2243, DOI: 10.1021/acs.chemrev.5b00441.

(2) Hay, J.N.; Sabir, M.; Steven, R.L.T. Crystallization kinetics of high polymers. Polyethylene oxide—Part I. *Polymer* **1969**, *10*, 187–202, DOI: 10.1016/0032-3861(69)90030-5.

(3) Wetton, R. E.; Allen, G. The dynamic mechanical properties of some polyethers. *Polymer* **1966**, *7*, 331–365, DOI: 10.1016/0032-3861(66)90028-0.

(4) Bailey, F. E.; Koleske, J. V. *Poly(ethylene oxide)*; Academic Press: New York, 1976.

(5) Fruijtier-Pölloth, C. Safety assessment on polyethylene glycols (PEGs) and their derivatives as used in cosmetic products. *Toxicology* **2005**, *214*, 1–38, DOI: 10.1016/j.tox.2005.06.001.

(6) Dingels, C.; Schömer, M.; Frey, H. Die vielen Gesichter des Poly(ethylenglykol)s. *Chem. unserer Zeit* **2011**, *45*, 338–349, DOI: 10.1002/ciuz.201100551.

(7) Abuchowski, A.; van Es, T.; Palczuk, N. C.; Davis, F. F. Alteration of immunological properties of bovine serum albumin by covalent attachment of polyethylene glycol. *J. Biol. Chem.* **1977**, *252*, 3578–3581.

(8) Abuchowski, A.; McCoy, J. R.; Palczuk, N. C.; van Es, T.; Davis, F. F. Effect of covalent attachment of polyethylene glycol on immunogenicity and circulating life of bovine liver catalase. *J. Biol. Chem.* **1977**, *252*, 3582–3586.

(9) Pfister, D.; Morbidelli, M. Process for protein PEGylation. *J. Control. Release* **2014**, *180*, 134–149, DOI: 10.1016/j.jconrel.2014.02.002.

(10) *Die Pharmaindustrie: Einblick - Durchblick - Perspektiven;* Fischer, D.; Breitenbach, J., Eds., 4. Auflage; Springer Spektrum: Berlin, 2017.

(11) Almeida, M.; Magalhães, M.; Veiga, F.; Figueiras, A. Poloxamers, poloxamines and polymeric micelles: Definition, structure and therapeutic applications in cancer. *J. Polym. Res.* **2018**, *25*, 248, DOI: 10.1007/s10965-017-1426-x.

(12) Pitto-Barry, A.; Barry, N. P. E. Pluronic® block-copolymers in medicine: from chemical and biological versatility to rationalisation and clinical advances. *Polym. Chem.* **2014**, *5*, 3291–3297, DOI: 10.1039/C4PY00039K.

(13) Bodratti, A. M.; Alexandridis, P. Formulation of Poloxamers for Drug Delivery. *J. Funct. Biomater.* **2018**, *9,* DOI: 10.3390/jfb9010011.

(14) Dumortier, G.; Grossiord, J. L.; Agnely, F.; Chaumeil, J. C. A review of poloxamer 407 pharmaceutical and pharmacological characteristics. *Pharm. Res.* **2006**, *23*, 2709–2728, DOI: 10.1007/s11095-006-9104-4.

(15) Lee, S. M. *Dictionary of composite materials technology*; Technomic Publ: Lancaster, 1989.

(16) Thompson, M. S.; Vadala, T. P.; Vadala, M. L.; Lin, Y.; Riffle, J. S. Synthesis and applications of heterobifunctional poly(ethylene oxide) oligomers. *Polymer* **2008**, *49*, 345–373, DOI: 10.1016/j.polymer.2007.10.029.

(17) Louai, A.; Sarazin, D.; Pollet, G.; François, J.; Moreaux, F. Properties of ethylene oxide-propylene oxide statistical copolymers in aqueous solution. *Polymer* **1991**, *32*, 703–712, DOI: 10.1016/0032-3861(91)90484-Z.

(18) Müller, S. S.; Moers, C.; Frey, H. A Challenging Comonomer Pair: Copolymerization of Ethylene Oxide and Glycidyl Methyl Ether to Thermoresponsive Polyethers. *Macromolecules* **2014**, *47*, 5492–5500, DOI: 10.1021/ma501280k.

(19) Tonhauser, C.; Alkan, A.; Schömer, M.; Dingels, C.; Ritz, S.; Mailänder, V.; Frey, H.; Wurm, F. R. Ferrocenyl Glycidyl Ether: A Versatile Ferrocene Monomer for Copolymerization with Ethylene Oxide to Water-Soluble, Thermoresponsive Copolymers. *Macromolecules* **2013**, *46*, 647–655, DOI: 10.1021/ma302241w.

(20) Alkan, A.; Thomi, L.; Gleede, T.; Wurm, F. R. Vinyl ferrocenyl glycidyl ether: An unprotected orthogonal ferrocene monomer for anionic and radical polymerization. *Polym. Chem.* **2015**, *6*, 3617–3624, DOI: 10.1039/C5PY00404G.

(21) Song, J.; Palanikumar, L.; Choi, Y.; Kim, I.; Heo, T.-y.; Ahn, E.; Choi, S.-H.; Lee, E.; Shibasaki, Y.; Ryu, J.-H. *et al.* The power of the ring: a pH-responsive hydrophobic epoxide monomer for superior micelle stability. *Polym. Chem.* **2017**, *8*, 7119–7132, DOI: 10.1039/C7PY01613A.

(22) Herzberger, J.; Kurzbach, D.; Werre, M.; Fischer, K.; Hinderberger, D.; Frey, H. Stimuli-Responsive Tertiary Amine Functional PEGs Based on N,N -Dialkylglycidylamines. *Macromolecules* **2014**, *47*, 7679–7690, DOI: 10.1021/ma501367b.

Abstract

The main focus of this thesis is the development of concepts for novel reactive and multi-functional poly(ethylene glycol)s (PEGs). A variety of synthetic strategies based on the ring-opening polymerization (AROP) of epoxides were explored, and the obtained polyether materials were characterized in great detail. Prospective areas of application of these polymers include functional hydrogels, surfactants as well as surface coatings. In particular, this work was motivated by the aim to establish new functional monomers and polyether structures. An overview of the key epoxide building blocks employed is shown in **Scheme 1**.
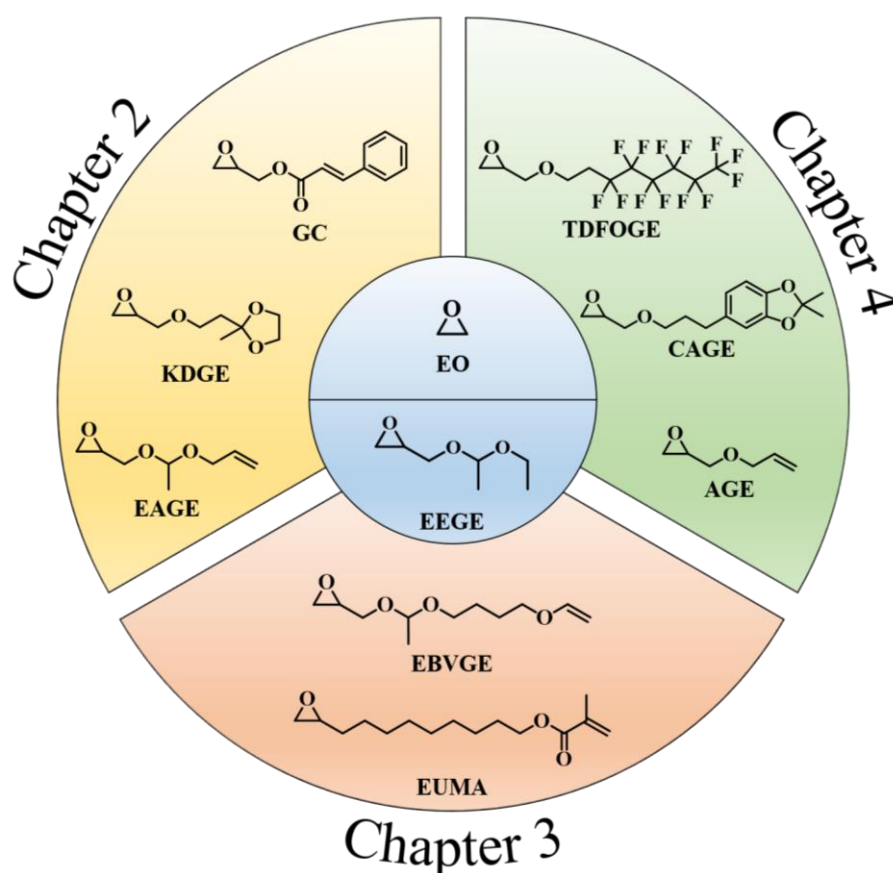
Scheme 1. Synopsis of the epoxide derivatives used for copolymerization with EO/ EEGE (shown in the center) in this thesis, arranged according to the respective chapters.

Chapter 1 provides a brief introduction into the topic. In this section, the properties of PEG and strategies for the synthesis of multi-functional PEGs are shortly outlined. This section focuses on mechanistic aspects as well as on the reaction kinetics of the copolymerization of substituted epoxides and the resulting microstructure of the corresponding copolymers. An emphasis is placed on ^{1}H NMR spectroscopy as a key evaluation method for copolymerizations.

An in-depth literature review is followed by an overview of the respective monomer pairs and their copolymerization reactivity ratios. This chapter also gives a perspective for works beyond the scope of this thesis.

Hydrogels are valuable due to their capacity to absorb water and are important materials for application in wound care, tissue engineering and numerous other biomedical areas. Their synthesis is the main focus of **Chapter 2**. In **Chapter 2.1**, a novel acid-cleavable, acetal-containing epoxide monomer, ethoxy allyl glycidyl ether (EAGE), is introduced. Copolymerization with ethylene oxide (EO) led to random incorporation of the comonomers, as was evidenced by real-time ^{1}H NMR kinetics studies. To demonstrate the potential for drug carrier systems, a cysteine derivative was successfully attached via thiol-ene click reaction. Moreover, triblock copolymers were prepared using PEG macroinitiators of different molecular weight. Photo-crosslinking was applied to synthesize acid-labile hydrogels. In this context, the material properties of the hydrogels were investigated, using rheology. Degradability at different pH values was explored as well. Studies of the swelling behavior revealed maximum swelling of up to 5,400%. In **Chapter 2.2** the novel monomer ketone dioxolane glycidyl ether (KDGE) is presented. Two approaches were pursued: on the one hand, random copolymers with varied KDGE content (5−100 mol%) were synthesized by copolymerization with EO. The polymers were modified with a hydrazine derivative after *in-situ* cleavage of the dioxolane protecting groups. On the other hand, triblock copolymers based on PEG were used for the preparation of hydrogels containing reversible oxime crosslinks by reaction with a difunctional alkoxyamines after deprotection of the ketone units. The addition of monofunctional alkoxyamines led to the decomposition of the gels. **Chapter 2.3** deals with the copolymerization of the glycidyl ester glycidyl cinnamate (GC) and ethoxyethyl glycidyl ether (EEGE), which was conducted using the activated monomer polymerization technique, since the conventional AROP could not be applied due to the harsh, basic conditions. For the first time, an adjustable content of cinnamoyl units (3−100 mol%) could be directly incorporated into a polyglycerol backbone without the need for post-polymerization modification. Kinetic studies of the copolymerization reaction demonstrated preferential incorporation of GC. The primary glycerol hydroxyl groups were first selectively released by removing the EEGE acetal protecting groups to prepare polyglycerol hydrogels. Subsequently, the photoreactive cinnamoyl groups were photo-crosslinked by dimerization through exposing to UV light.

It is crucial to increase the stability of micelles by crosslinking in order to utilize them as potential drug nanocarriers, as will be discussed in more detail in **Chapter 3**. The novel

monomer building block ethoxy butoxy vinyl glycidyl ether (EBVGE) is a vinyl-containing structural analogue to the acid-labile EAGE monomer. EBVGE has been converted with orthogonal polymerization strategies based on its bifunctionality and is discussed in **Chapter 3.1**. Epoxy-substituted polyethylene structures were accessible by the non-trivial, free radical copolymerization of the electron-rich EBVGE vinyl functionalities with electron-poor monomers such as maleic anhydride. Vinyl ether-functional polyethers, however, were obtained by AROP of EBVGE with EO or PEG macroinitiators. While the random copolymers exhibited thermoresponsive behavior in aqueous solution, block copolymers assembled to acid-labile, well-defined micelles. These stimuli-responsive aggregates were monitored and investigated by fluorescence correlation spectroscopy (FCS) as well as light scattering and examined regarding their biocompatibility. Crosslinking of the hydrophobic micellar core by thiol-ene click chemistry resulted in a significantly increased stability compared to non-crosslinked micelles. The synthesis of the novel monomer epoxy undecane methacrylate (EUMA) is presented in **Chapter 3.2**. EUMA allowed the direct access to methacrylate functionalities in a polyether backbone by copolymerization with EO, using the monomer-activated AROP. The copolymers exhibited a pronounced gradient microstructure, as demonstrated by *in-situ* ^{1}H NMR studies. As a result, the copolymers showed surface activity in aqueous solution, which was used for the preparation of crosslinkable micelles. Due to their enhanced stability, the defined micelle distribution was maintained compared to the non-crosslinked particles even in organic solvents as proved by light scattering studies. Furthermore, swelling behavior in organic solution was demonstrated. On account of its bifunctionality, the methacrylate units of the EUMA monomer could be selectively addressed by reversible addition-fragmentation chain transfer (RAFT) polymerization. This enabled access to organogels by crosslinking the pendant epoxy groups with a primary diamine.

Chapter 4 primarily addresses surface coatings, which are widely used nowadays, for instance for corrosion protection or to prevent fouling. In order to specifically control hydrophobicity, the perfluorinated glycidyl ether tridecafluoroctyl glycidyl ether (TDFOGE) was copolymerized with allyl glycidyl ether (AGE) or EEGE and catechol acetonide glycidyl ether (CAGE). After removal of the acetonide protecting groups, the reactive catechol units were used for the coating of glass surfaces. Contact angle measurements revealed a systematic variation of the water-repellent surface properties up to 120° depending on the perfluorinated glycidyl ether content.

The appendix of this thesis contains several chapters with contributions from the authors of this thesis. Aldehyde multi-functional PEGs are presented in **Appendix A1**. In this context, two epoxide monomers were developed and copolymerized with EO. The copolymerization parameters and the microstructure of the copolymers were derived from ^{1}H NMR kinetics. Polyethers with ester, nitrile and hydrazone groups were obtained by post-polymerization modification.

Appendix A2 describes the one-step, solvent-free synthesis of ketone-containing polycarbonates by terpolymerization of KDGE, propylene oxide (PO) and carbon dioxide (CO_2). These polymers had a tailor-made KDGE content between 2−100 mol% and as a result of their high reactivity, released ketone units were successfully functionalized with carboxylic acid hydrazides.

In **Appendix A3** the synthesis of linear polyglycerols with an adjustable degree of methylation up to 91% by copolymerization of glycidyl methyl ether (GME) and EEGE using monomer-activated AROP is depicted. In addition to thermoresponsive properties, reaction kinetics and thermorheological behavior were investigated.

Appendix A4 introduces an efficient and stoichiometric coupling strategy for the preparation of gradient star polymers in a one-pot synthesis. Despite the high steric demands of the polystyryllithium (PS-Li) chain ends, this coupling succeeded within minutes using tetra[3-(chloro-dimethylsilyl)propyl]silane (TCDMSPS) as the linking agent. As the reactive mono-chloro dimethyl silane groups are separated from each other by alkyl spacers, a remarkably high coupling efficiency (98%) was reached, demonstrated via size exclusion chromatography (SEC) viscometry with universal calibration. The materials, which were synthesized in only two steps, were finally spun into nanofibers using electrospinning.

Zusammenfassung

Im Zentrum dieser Arbeit standen die Synthese und Anwendung von reaktiven, linearen, multifunktionellen Polyethylenglykolen (PEGs). Hierzu wurden verschiedenste Synthesestrategien wie die anionische ringöffnende Polymerisation (AROP) angewendet und die Polymere im Detail untersucht. Die Anwendungsgebiete der Polymere erstreckten sich dabei von Hydrogelen über Mizellen bis hin zu Oberflächenbeschichtungen. Die besondere Motivation der Arbeit bestand in der Etablierung neuer funktioneller Monomere und Polyetherstrukturen. **Abbildung 1** stellt eine Übersicht der eingesetzten Epoxidbausteine dar.
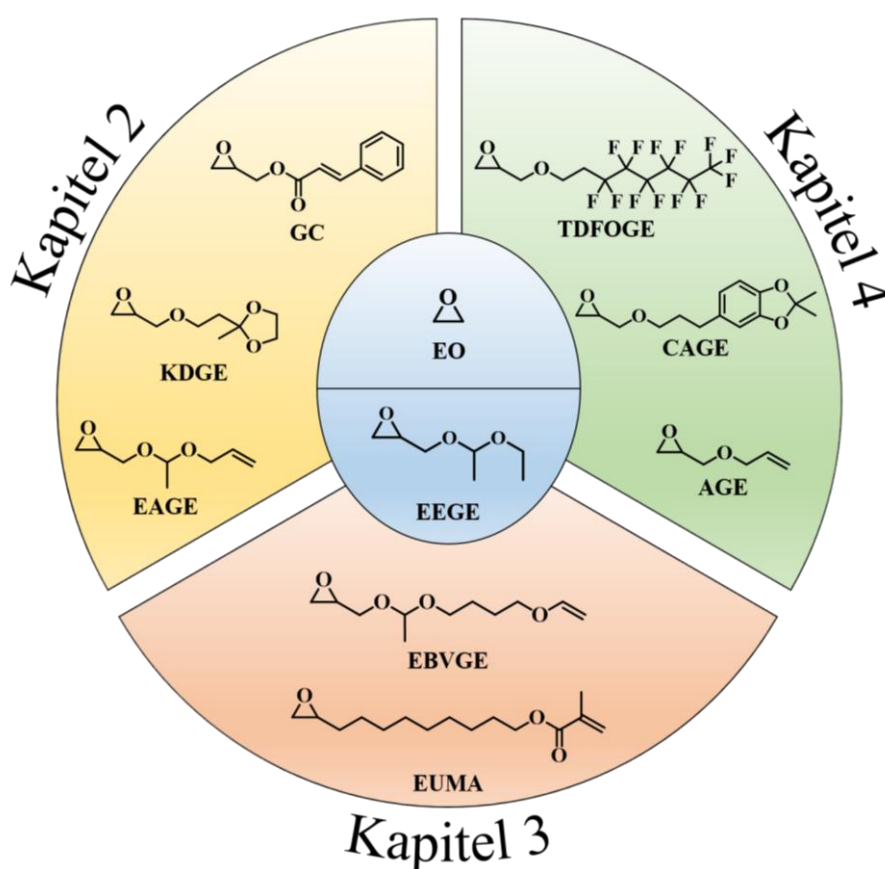
Abbildung 1. Übersicht der verwendeten Epoxyderivate, die nach den jeweiligen Kapiteln geordnet sind und mit den im Zentrum abgebildeten Monomeren EO/ EEGE umgesetzt wurden.

Kapitel 1 dient als eine kurze Einführung in das Themenfeld. In diesem Abschnitt werden Strategien zur Synthese von multifunktionellen PEGs skizziert. Neben den mechanistischen Aspekten ist die Reaktionskinetik der Copolymerisation von substituierten Epoxiden und die daraus resultierende Mikrostruktur der entsprechenden Copolymere ein Schwerpunkt. Der Fokus liegt dabei auf der NMR Spektroskopie als Auswertungsmethode. Nach einem

detaillierten Literaturüberblick folgt eine Auflistung der Monomerpaare und deren Copolymerisationsparametern.

Hydrogele zeichnen sich durch ihre hohe Wasseraufnahmefähigkeit aus und sind unter anderem für Anwendungen in der Wundversorgung sehr interessant. Ihre Synthese steht im Zentrum von **Kapitel 2**. In **Unterkapitel 2.1** wird das neue, säurespaltbare Epoxidmonomer Ethoxyallylglycidylether (EAGE) vorgestellt. Die Copolymerisation mittels Ethylenoxid (EO) führte zu einem statistischen Einbau der Comonomere, was mittels Echtzeit ^{1}H NMR Kinetikstudien nachgewiesen werden konnte. Die potentielle Anwendung als Wirkstoffträger wurde durch das erfolgreiche Anbringen eines Cysteinderivat per Klick-Reaktion demonstriert. Zusätzlich wurden ausgehend von unterschiedlich großen PEG Makroinitiatoren Triblockcopolymere hergestellt, die zur Synthese von säurelabilen Hydrogelen mittels Photovernetzung verwendet wurden. Hierbei wurden die Hydrogele hinsichtlich ihrer Materialeigenschaften mittels Rheologie charakterisiert und ihre Abbaubarkeit bei verschiedenen pH-Werten beleuchtet. Untersuchungen des Quellverhaltens zeigten Wasseraufnahmen von bis zu 5400%. In **Abschnitt 2.2** wird das neue Monomer Ketondioxolanglycidylether (KDGE) vorgestellt, wobei zwei Ansätze verfolgt wurden. Zum einen wurden statistische Copolymere mit einem variablen KDGE-Gehalt (5−100 mol%) durch Copolymerisation mit EO synthetisiert, welche mit einem Hydrazinderivat nach *in-situ* Abspaltung der Dioxolan-Schutzgruppen adressiert werden konnten. Zum anderen wurden Triblockcopolymere auf Basis von PEG Makroinitiatoren nach Freisetzung der Ketoneinheiten durch Reaktion mit einem bifunktionelle Alkoxyamin zu reversiblen Hydrogelen umgesetzt, die durch Zugabe von monofunktionellem Alkoxyamin wieder zersetzt werden konnten. In **Unterkapitel 2.3** wird die Copolymerisation von Glycidylcinnamat (GC) und Ethoxyethylglycidylether (EEGE) diskutiert, die aufgrund der harschen und basischen Bedingungen der konventionellen AROP unter Verwendung der monomer-aktivierten AROP durchgeführt wurde. Erstmalig konnten so Cinnamoyl-Einheiten direkt und mit einem einstellbaren GC-Gehalt (3−100 mol%) in ein Polyglycerinrückgrat eingebaut werden, ohne auf polymeranaloge Reaktionen zurückgreifen zu müssen. Durch die kinetische Untersuchung der Copolymerisationsreaktion konnte ein präferierter Einbau von GC nachgewiesen werden. Für die Herstellung der Polyglycerinhydrogele wurden zunächst die primären Hydroxylgruppen durch Abspaltung der EEGE-Acetalschutzgruppen selektiv freigesetzt. Anschließend erfolgte die Vernetzung der photoreaktiven Cinnamoyl-Gruppen durch Dimerisierung unter Bestrahlung mit UV-Licht.

Für den Einsatz als potentielle Wirkstoffträger ist es nahezu unabdingbar, die Stabilität von Mizellen durch deren Vernetzung zu erhöhen, was in **Kapitel 3** genauer erörtert wird. Der neue Monomerbaustein Ethoxybutoxyvinylglycidylether (EBVGE) ist das vinylhaltige, strukturelle Analogon zum säurelabilen EAGE Monomer, welches aufgrund seiner Bifunktionalität mit orthogonalen Polymerisationsstrategien umgesetzt wurde und in **Unterkapitel 3.1** thematisiert wird. Epoxysubstituierte Polyethylenstrukturen wurden durch die nicht triviale, freie radikalische Copolymerisationen der elektronenreichen EBVGE Vinylfunktionalitäten mit elektronenarmen Monomeren wie Maleinsäureanhydrid zugänglich gemacht. Vinylfunktionelle Polyether hingegen wurden durch die AROP von EBVGE mit EO oder PEG Makroinitiatoren erhalten. Während die statistischen Copolymere in wässriger Lösung ein thermoresponsives Verhalten zeigten, bildeten hier die Blockcopolymere durch Selbstassemblierung säurelabile, definierte Mizellen aus. Diese stimuli-responsiven Aggregate wurden mithilfe von Fluoreszenzkorrelationsspektroskopie (FCS) und Lichtstreuung nachgewiesen, untersucht und hinsichtlich ihrer Biokompatibilität überprüft. Eine Vernetzung des hydrophoben mizellaren Kerns mittels Klick-Chemie resultierte in einer wesentlich erhöhten Stabilität im Vergleich zu unvernetzten Mizellen. Die Synthese des neuen Monomers Epoxyundecanmethacrylat (EUMA), welches in **Abschnitt 3.2** behandelt wird, ermöglichte den direkten Zugang zu Methacrylatfunktionalitäten in einem Polyetherbackbone durch Copolymerisation mit Ethylenoxid unter Verwendung der monomer-aktivierten AROP. Der tensidische Charakter der Copolymere, der auf die ausgeprägte gradientartige Morphologie zurückzuführen ist, was mit *in-situ* ^{1}H NMR Untersuchungen nachgewiesen werden konnte, wurde zur Synthese von vernetzbaren Mizellen verwendet. Hierdurch blieb ihre definierte Verteilung verglichen mit den unvernetzten Partikeln auch in organischen Lösungsmitteln erhalten; ferner konnte hier auch ein Quellungsverhalten nachgewiesen werden. Aufgrund der Bifunktionalität des EUMA-Monomers konnten neben den polymerisierbaren Epoxyfunktionalitäten auch die Methacrylateinheiten selektiv mittels reversibler Additions-Fragmentierungs-Kettenübertragung (RAFT) adressiert werden. Dies ermöglichte den Zugang zu Organogelen durch Vernetzung der Epoxygruppen mit einem primären Diamin.

Im Mittelpunkt von **Kapitel 4** stehen Oberflächenbeschichtungen, die bereits heutzutage unter anderem als Korrosionsschutz oder zum Verhindern von Anwuchs vielfach Anwendung finden. Um die Hydrophobizität gezielt zu steuern, wurde der perfluorierte Glycidylether Tridecafluoroctylglycidylether (TDFOGE) mit Allylgylcidylether (AGE) bzw. EEGE und Catecholacetonidglyciylether umgesetzt. Nach der Abspaltung der Acetonid-Schutzgruppen wurden die reaktiven Catecholeinheiten zur Beschichtung von Glasoberflächen genutzt. Durch

Kontaktwinkelmessungen konnte gezeigt werden, dass die wasserabstoßenden Eigenschaften der Oberfläche in Abhängigkeit an perfluorierte Glycidylethergehalt systematisch bis zu 120° variiert werden konnten.

Die Synthese von aldehydfunktionalisiertem PEG wird in **Anhang A1** vorgestellt. Hierzu wurden zwei Epoxymonomere entwickelt, welche mit EO polymerisiert wurden. Die Copolymerisationsparameter und die Mikrostruktur der Copolymere wurden aus ^{1}H NMR Kinetiken abgeleitet. Um Polyether mit Ester-, Nitril-, und Hydrazon-Gruppen zu erhalten, wurden polymeranaloge Reaktionen durchgeführt.

Anhang A2 beschreibt die einstufige und lösungsmittelfreie Synthese von ketonhaltigen Polycarbonaten, welche durch die Terpolymerisation von KDGE, Propylenoxid (PO) und Kohlenstoffdioxid (CO_2) realisiert wurde. Die Polymere wiesen einen maßgeschneiderten KDGE-Gehalt zwischen 2−100 mol% auf. Bedingt durch ihre hohe Reaktivität konnten die freigesetzten Keton-Einheiten erfolgreich mit Carboxylsäurehydraziden funktionalisiert werden.

In **Anhang A3** wird die Synthese von linearen Polyglycerinen mit maßgeschneidertem Methylierungsgrad bis zu 91% durch Copolymerisation von Glycidylmethylether (GME) und EEGE mittels monomer-aktivierter AROP beschrieben. Neben den thermoresponsiven Eigenschaften wurde auch die Reaktionskinetik und das thermorheologische Verhalten untersucht.

In **Anhang A4** wird eine effiziente und stöchiometrische Kupplungsstrategie zur Herstellung von Gradienten-Sternpolymeren in einem Eintopfverfahren vorgestellt. Trotz des hohen sterischen Anspruchs der Polystyryllithium-Kettenenden gelang diese Kupplung innerhalb weniger Minuten mit Tetra[3-(Chlor-dimethylsilyl)propyl]silan (TCDMSPS) als Kupplungsreagenz. Durch die räumliche Separation der reaktiven Dimethylchlorsilan-Funktionalitäten mittels Alkylketten wurde eine bemerkenswert hohe Kopplungseffizienz (98%) erreicht, was durch GPC-Viskosimetrie Messungen (universelle Kalibrierung) belegt werden konnte. Die in nur zwei Schritten synthetisierten Materialien wurden schließlich durch Elektroverspinnen zu Nanofasern verarbeitet.

Graphical Abstract

Chapter 2. Preparation of Hydrogels

2.1.   Design of a Novel Epoxide Monomer for pH-Sensitive Poly(ethylene glycol) Hydrogels via Acid-Labile and Crosslinkable Allyl Side Groups
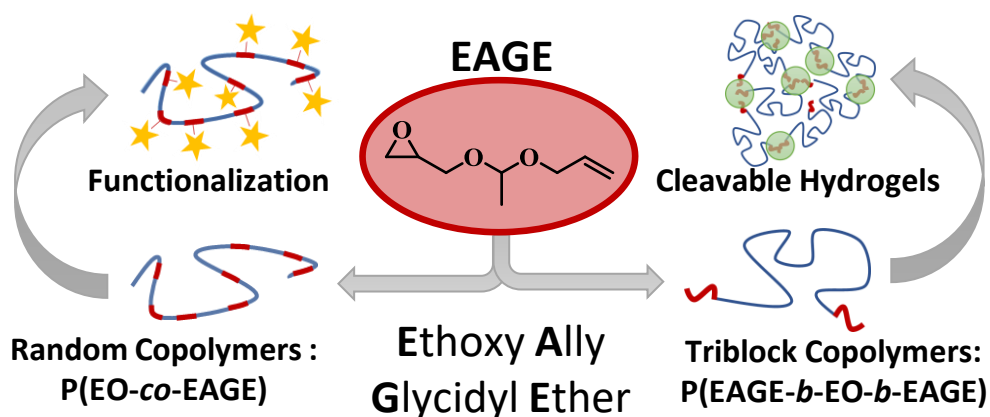
2.2.   Ketone Dioxolane Glycidyl Ether: Synthesis of Multi-Ketone-Functional Poly(ethylene glycol) as a Promising Candidate for Bioconjugation and Reversible Hydrogels
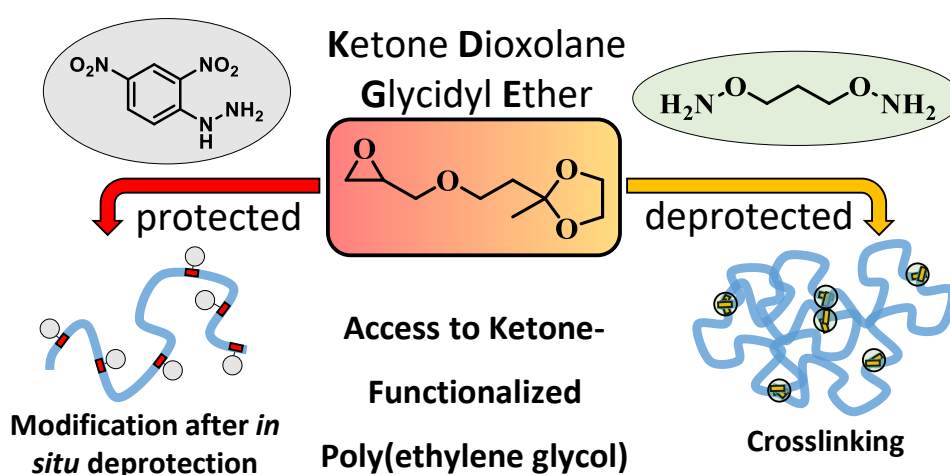
2.3. Glycidyl Cinnamate: Copolymerization with Glycidyl Ethers, *in-situ* NMR Kinetics and Photocrosslinking
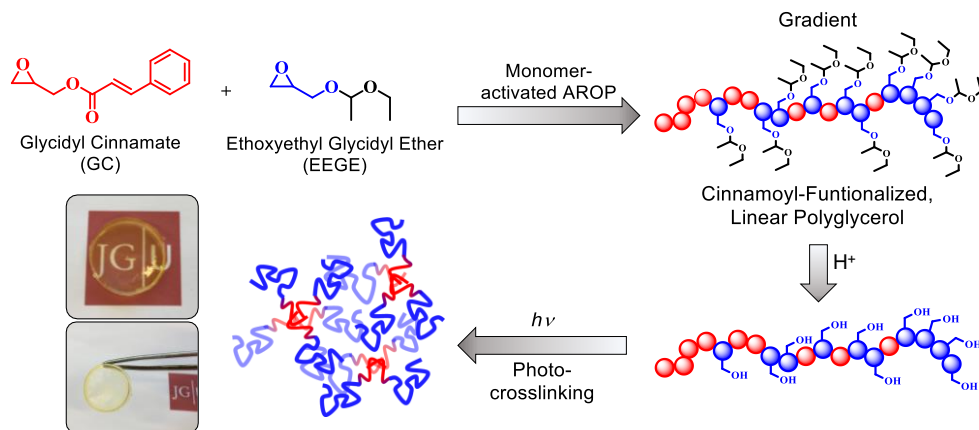
Chapter 3. Preparation of Crosslinkable Micelles

3.1. Ethoxy Butoxy Vinyl Glycidyl Ether: Reactive and Cleavable Multi-Vinyl Ether Functional Poly(ethylene glycol)s for Drug Delivery Applications
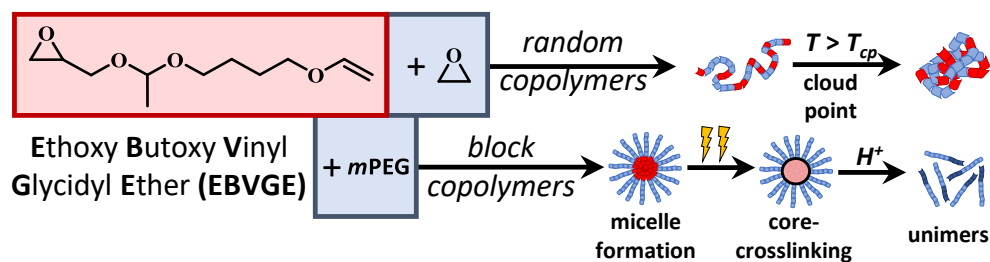
3.2.   Epoxy Undecane Methacrylate: A Symbiosis of Methacrylates and Poly(ethylene glycol)
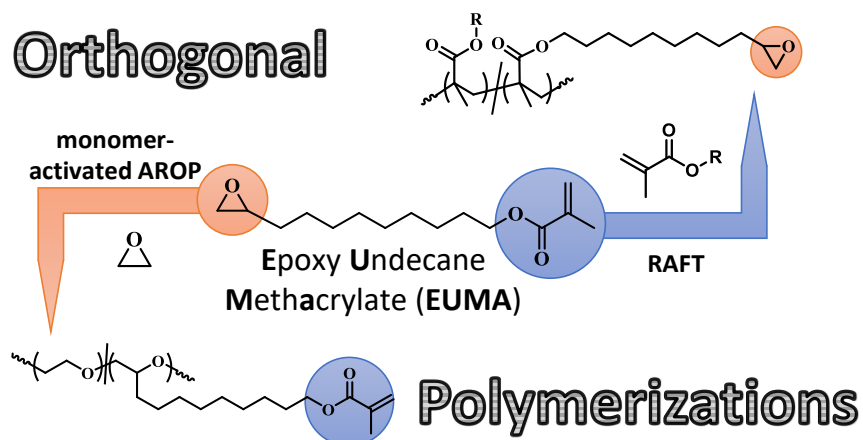
Chapter 4: Preparation of Surface Coatings

4.1.   Synthesis of Perfluoroalkyl-Bearing Polyether, Their Characterization and Application as Coating for Glass Slides
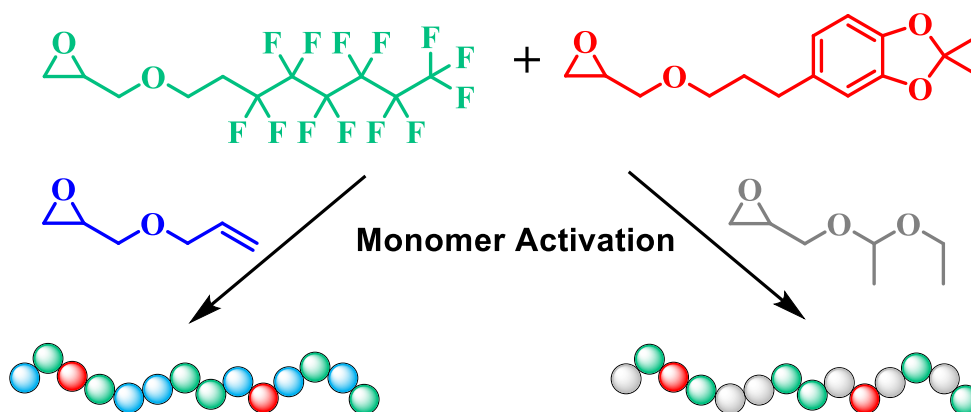
1. Introduction

This chapter is divided into three main sections. First, a brief overview regarding the class of aliphatic polyethers and their most important representatives is given. Second, the focus is on poly(ethylene glycol) (PEG). In this context, its properties, important polymerization techniques and the synthesis of multi-functional PEGs are discussed. The last part addresses reactivity ratios of various functional epoxide comonomers and the microstructure of polyether copolymers analyzed by NMR spectroscopic methods.

Aliphatic Polyethers

This section deals with industrially relevant aliphatic polyethers in a general overview, excluding PEG.

Aliphatic polyethers are characterized by the general formula $HO(R-O)_nH$, where R is an alkyl group and n is the degree of polymerization. Typical for this class of polymers are their ether groups as repeating unit, which share similar chemical bonding properties as alcohols and water.[1] The bond angle between the oxygen atom and alkyl groups is 112°, while the bond distance of the C-O bond is 143 pm, corresponding to that of alcohols.[2] Aliphatic polyethers are accessible via various polymerization techniques such as step-growth, cationic or anionic polymerization of carbonyl compounds or cyclic ethers and have a wide range of applications.[3] Well-known and commercial representatives of this polymer class are poly(oxymethylene) (POM, in fact a polyacetal), poly(propylene glycol) (PPO), poly(epichlorohydrin) (PECH), PEG, poly[3,3-bis(chloromethyl)oxetane] (PBCMO) and poly(tetrahydrofuran) (PTHF) (**Scheme 1**). In the following, PEG is not further discussed, as it is the focus of the next section.
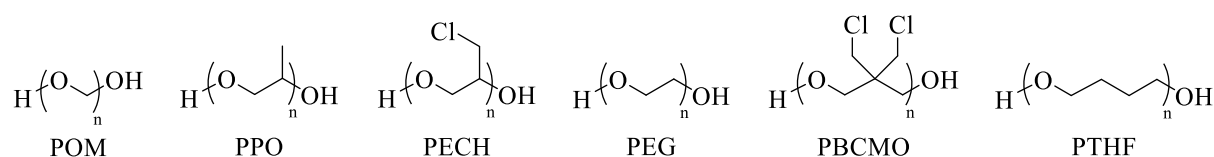
Scheme 1. Overview of industrially relevant aliphatic polyethers: POM, PPO, PECH, PEG, PBCMO and PTHF.

Initial work on the simplest aliphatic polyether POM, goes back to Auerbach and Barschall[4] and was further extended by Staudinger and co-workers[5–7] in the 1920s. Commercialization did not take place until the 1950s due to stability- and solubility problems in the solvents commonly used at that time.[3] The main reason for this is the zipper-like degradation of the thermolabile semi-acetal end groups, which can be prevented by end-capping via acetalization or by co-polymerization of trioxane with ethylene oxide or other cyclic ethers. After years of research

DuPont commercialized POM under the product name Delrin® in 1959.[8] POM is distinguished by a high melting point (T_m = 180 °C) and a low glass transition temperature (T_g = -75 °C) and is used as durable engineering plastics in many different applications for instance for gear wheels, Playmobil® toys or ski binding parts.[9,10]

Propylene oxide (PO) was discovered by Wurtz in 1859.[11] Early attempts regarding its polymerization can be attributed to studies by Levene and Walti in 1927.[12] In this context, further investigations by Staudinger, Meerwein and patents by the I.G. Farbenindustrie AG followed.[13–15] In the first applications, PPO was used for lubricants and hydraulic fluids. A basis for this were patents of H.R. Fife and F.H. Roberts describing the polymerization of PO in the presence of alcohols, resulting in methoxy- and butoxy-initiated PPO chains.[16] As a result of these findings, studies of the copolymerization of PO and ethylene oxide (EO) soon followed, and the copolymers were used as anti-foaming agents, emulsifiers, ceramic glazes or binders.[13] Nowadays, PPOs with lower molecular weights ($M_n \leq$ 3,500 g mol^{-1}) are used in the production of flexible and rigid polyurethane (PU) foams. For flexible foams, linear PPOs with a molecular weight of approximately of 2,000 g mol^{-1} or three-arm star-shaped PPOs with an M_n in the range of 3,000−3,500 g mol^{-1} based on glycerol- or 1,1,1-trimethylolpropane initiators are used. For rigid PU foams PPO polytriols with an M_n around 500 g mol^{-1} are utilized.[3] PPO is also used for the synthesis of surfactants, namely poloxamers (PEO-*b*-PPO-*b*-PEO triblock copolymers) or polyether amines (linear PPO with amino termini).[2] The typical atactic and industrially relevant PPO is amorphous and has a low T_g of -70 °C. In contrast, isotactic PPO crystallizes and the melting point is around 75 °C.[17] The increased hydrophobicity compared to PEG is attributable to the additional methyl groups along the polymer backbone.[17]

Epichlorohydrin (ECH) was first synthesized in 1848 by Marcellin Berthelot, who investigated the derivatives of glycerol.[18] The polymerization of ECH was based on the work of E.J. Vandenberg in 1957, who developed the organometallic catalyst system AlEt$_3$/H$_2$O/acetylacetone.[19,20] 8 years later B.F. Goodrich commercialized PECH under the trade name Hydrin®. This was a license agreement from Hercules Inc., the company that also distributed ECH-based polymers under the name Herclor®. In 1986, the epichlorohydrin division of Hercules Inc. was taken over by B.F. Goodrich and continued under the trade name Hydrin®. Then in 1989, the entire elastomer division was purchased by Zeon Chemicals, retaining the trade name Hydrin®. Its parent company Nippon Zeon has its own ECH production line, which is marketed under the trade name Gechron®. The competitor Daiso Chemical Co., Ltd. also sells PECHs (Epichlomer®).[21,22] PECH and its copolymers combine various

outstanding properties. In addition to fuel, heat, ozone and permeation resistance, the polymers also exhibit fire resistance. Furthermore, chloromethyl groups are suitable for vulcanization for instance via ethylene thiourea.[23] A characteristic feature of the amorphous PECH is the T_g of -24 °C, whereas EO containing copolymers improve the low temperature flexibility by decreasing the T_g to -41 °C ($x_{EO} = 50$ mol%). The exceptional elastic properties of ECH based polymers are used in the automotive industry (fuel hoses, engine seals, etc.).[21]

The first oxetane polymers were established in 1954 by the polymerization of 3,3-bis(chloromethyl)oxetanes (BCMO),[24] followed by further unsubstituted[25] and substituted[26] oxetanes. Polymers based on the unsubstituted oxetane exhibit poor physical properties ($T_m = 35$ °C) and were never relevant for industrial applications.[3] However, PBCMO was commercialized in the 1950s by Hercules Inc and marketed under the trade name Penton® for 15 years.[27] In addition to very good thermal properties ($T_m = 180$ °C), PBCMO also exhibits excellent chemical resistance. As a consequence, PBMCO was mainly applied as resistant material in corrosive conditions. In this context, it was used as adhesive, coating and in lining pipes or tanks.[22]

The development of poly(tetrahydrofuran) (PTHF) goes back to Meerwein and co-workers in the late 1930s. However, worldwide interest started after World War II.[22,28] The use as a polyether component in flexible polyurethane foams was intended.[3] However, the comparatively high manufacturing costs prevented the commercial breakthrough and led to the use of cheaper materials such as PPO-based polyethers instead. For instance, in 1996 the cost of a general-purpose rubber was about $1 per kilogram, whereas PTHF cost between $3.5−4.2 per kilogram.[29] The state of matter and the thermal properties correlate with the molecular weight. While low molecular weights ($M_n = 250$ g mol^{-1}) show a T_m of -15 °C and a T_g of -98 °C, higher molecular weights ($M_n = 2{,}000$ g mol^{-1}) exhibit a T_m of 33 °C and a T_g of -84 °C.[30] With increasing molecular weight, the state of matter at room temperature changes from a viscous oil, through a wax-like structure, to a solid.

Poly(ethylene glycol) and its properties

Following this short outline of various aliphatic polyethers and their eminent representatives, the focal point of the following section is now on PEG and its properties.

PEG is one of the best-known representatives of the aliphatic polyethers with the repeat unit -(CH$_2$-CH$_2$-O)$_n$- and is obtained by polymerization of ethylene oxide (EO). The term "poly(ethylene glycol)" is used for molecular weight range from 200−35,000 g mol^{-1}, polymers with molecular weights above these limits are called "poly(ethylene oxide)s" (PEOs). Furthermore, the term PEG is used wherever biocompatibility is involved.[31] Common trade names are ALKOX® (Meisei Chemical Works, Ltd.), CARBOWAX™ (Dow Chemical), Genapol® (Clariant AG), POGOL® (Huntsman Corporation) and Pluracol®/ Pluracare® (BASF SE).

The appearance at room temperature and the specific properties are strongly related to the degree of polymerization (X_n) of PEG. PEGs with molecular weights between 200−400 g mol^{-1} are clear, colorless, hygroscopic liquids at room temperature. Around 600 g mol^{-1}, PEG has a paste-like consistency owing to its melting range of 15 to 25 °C. Above molecular weights of 1,000 g mol^{-1} it is a solid with a wax-like behavior. The hygroscopicity of the polymers decreases with increasing molecular weight. Thus, PEGs with an M_n above 1,500 g mol^{-1} are not hygroscopic.[32]

The thermal properties correlate strongly with the X_n of PEG. Thus PEG-750 has a melting point of 30 °C, PEG-4,000 shows a T_m of 59.6 °C and PEG-20,000 displays a T_m of 63.1 °C.[33] Godovsky *et al.* proved an asymptotic convergence to a T_m of 70 °C for infinitely high molecular weights of PEG based on the Flory equation for melting points:[34]

$$\frac{1}{T_m} - \frac{1}{T_m^\circ} = \frac{2 \cdot R}{H_f \cdot X_n} \tag{1}$$

where T_m is the measured melting point, T_m° is the equilibrium melting point for the polymer of infinite T_m, R is the gas constant, H_f is the molar heat of fusion per chain unit and X_n is the degree of polymerization.[35] These theoretical results are consistent with the measured values for ultrahigh molecular weight PEO-6,000,000, for which a T_m of 68.6 °C was determined.[36] The situation is more complex regarding the glass transition temperatures (T_gs). According to Flory and Fox, T_g correlates with the molecular weight and decreases with decreasing molecular weight. For high molecular weights the glass transition temperature asymptotically approaches a limiting value:[37]

$$T_g = T_{g,\infty} - \frac{K}{M_n} \tag{2}$$

Here, $T_{g,\infty}$ is the glass transition temperature of an infinite molecular weight polymer and K is constant. Studies by Faucher *et al.*[38] and Read[39] showed no correlation in this respect. The experimental values were higher in a very broad M_n range compared to the theoretically calculated T_gs and passed through a maximum of -20 °C at approximately 6,000 g mol^{-1}. The reason for this is the crystallinity of PEG. In contrast, completely amorphous PEG obtained by quenching displayed the expected monotonic increase of T_g with increasing M_n.[33] Thus, PEG-194 has a T_g of -72 °C, PEG-400 a T_g of -70 °C, PEG-1,540 a T_g of -65 °C and PEG-12,000 a T_g of -60 °C. For very high molecular weights ($M_n \geq 1,000,000$), the T_g fluctuates from -53 °C[38] over -59 °C[39] up to -60.5 °C[40] depending on the measuring method and parameters.

One of the special properties of poly(ethylene glycol)s is their exceptional water solubility, especially in comparison to other aliphatic polyethers (POM, PPO, etc.). While low molecular weight PEGs are miscible with water in any ratio, this ability decreases with increasing molar mass. However, even at a molecular weight of 35,000 g mol^{-1}, aqueous solutions with concentrations of up to 50 wt% can still be prepared at room temperature.[41] This is attributable to the distance of the repeating oxygen atoms in the polymer backbone, which roughly corresponds to the distance of the oxygen atoms in liquid water. As a consequence, a hydrogen bonding network can form between the water molecules and the PEG chains.[42] The solubility of polymers is temperature-dependent and is generally described by the critical solution temperatures, such as the lower and upper critical solution temperatures (LCST and UCST). In this context, it should be noted, that the LCST and the UCST in a binary mixture represent the minimum and maximum of the binodal (**Scheme 2**) in a phase diagram. All other points of the binodal curve are called "cloud points". If the temperature exceeds the LCST or falls below the UCST, a miscibility gap occurs.[9] Dielectric relaxation measurements demonstrated the hydration of a single PEG repeating unit of about 4 water molecules below 30 °C, which decreases with increasing temperature (approximately 2 water molecules at 70 °C).[43] The LCST of PEG is around 100 °C.
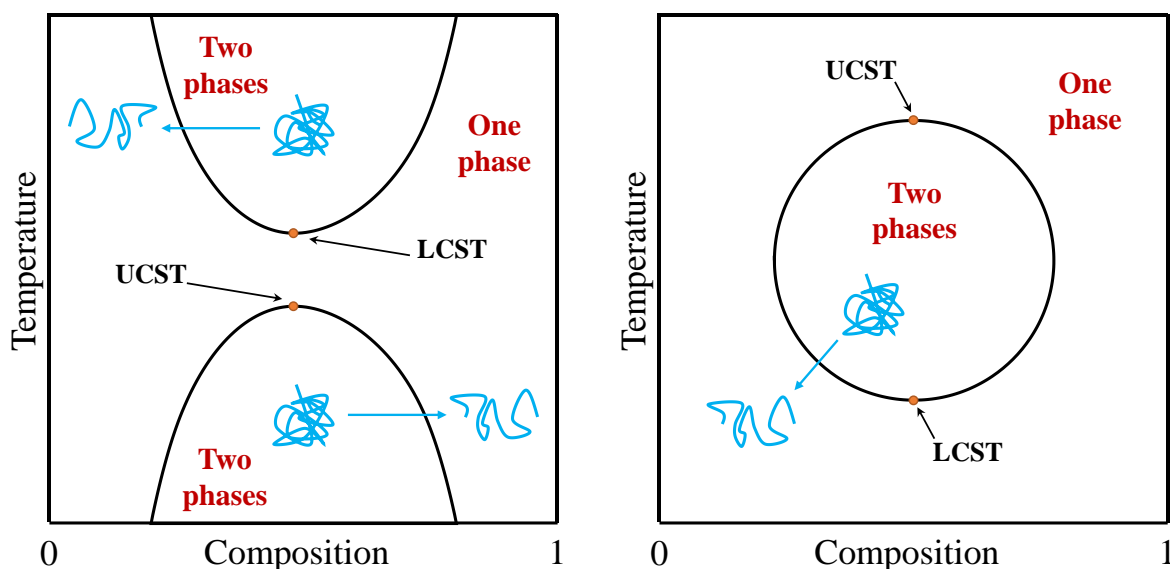
Scheme 2. Phase diagrams of a binary polymer mixture containing UCST, LCST and miscibility gaps. Left: LCST > UCST. Right: LCST < UCST.

Via the incorporation of substituted epoxides with lower polarity into the PEG backbone, the LCST can be reduced and tailored.[44–47] The fundamental Gibbs-Helmholtz equation (**3**) explains many phenomena of polymer solutions and provides important insights for understanding their thermodynamics:[9]

$$\Delta G = \Delta H - T \cdot \Delta S \tag{3}$$

where ΔG is the Gibbs free energy of the system, ΔH is the enthalpy, T is the absolute temperature and ΔS is the entropy. Polymers dissolve in a solvent when the change in ΔG is negative. Consequently, depending on the sign, the following scenarios can occur: complete miscibility ($\Delta H < 0$ and $\Delta S > 0$), UCST ($\Delta H > 0$ and $\Delta S > 0$), LCST ($\Delta H < 0$ and $\Delta S < 0$) or complete immiscibility ($\Delta H > 0$ and $\Delta S < 0$). An unfavorable entropy of the mixture results in phase separation when heating these solutions. When hydrated, extended polymer coils are present in aqueous solutions. As the temperature increases, the hydrogen bonds between solvent molecules and polymer chains are disrupted, enabling intra- and intermolecular hydrogen bonds and hydrophobic interactions between polymer chains to increase. Consequently, the polymer chains collapse and aggregate in a globular conformation. Accordingly, an LCST is caused by entropic reasons. In contrast, segregation below the UCST is an enthalpy-induced process. At low temperatures, the enthalpy of the mixture dominates over the entropic contribution, leading to an increase of the free enthalpy. Transferring the Gibbs-Helmholtz equation to a polymeric system is a simplification, since factors such as mobility and the different size of the polymer chains in relation to the solvent are not considered. A model to describe a binary solution of a

polymer in a low molecular weight solvent was developed by Flory[48] and Huggins[49]. A rigid lattice model serves as a basis, wherein the polymer chains are subdivided into single segments. Each of these segments and the solvent particles, which have the same size, occupies a lattice space:

$$\Delta G = R \cdot T \cdot \left(\varphi_1 \cdot ln\,\varphi_1 + \frac{\varphi_2}{X_N} \cdot ln\,\varphi_2 + \varphi_1 \cdot \varphi_2 \cdot \chi \right) \tag{4}$$

Here, R is the universal gas constant, φ is the volume fraction of the polymer/solvent, X_N is the degree of polymerization and χ is the interaction parameter. The first two terms can be combined as entropy terms and the last as enthalpy term.[9] Since the volume fraction φ always includes values between zero and one, the entropy term is negative. Is the attraction between molecules of the same species stronger than that between molecules of a different species, χ is positive. If the polymer-solvent interactions are energetically favored, χ has a negative value. According to the Flory-Huggins theory, the solubility of polymers decreases with increasing chain length. The entropy contribution to the free enthalpy of mixing decreases with increasing molecular weight.

Apart from its extraordinary solubility in water, PEG also shows extremely low toxicity, immunogenicity and antigenicity.[50] For pharmaceutical applications of polymers, certain requirements must be met. Besides biocompatibility, polymers should have a narrow molecular weight distribution. The latter should avoid unforeseen, molecular weight-dependent effects. For instance, polymers with a broad distribution can have different biological properties, especially in terms of residence time in the body and immunogenicity.[51] Further, a certain molecular weight must not be exceeded. As the glomerular filtration rate in the kidneys correlates inversely with the molecular weight of a polymer, higher molecular weight polymers are more efficient in increasing the circulation rate, which is of relevance in drug transport.[52,53] However, PEG is not biodegradable due to its inert ether units. Hence, PEG cannot be metabolized and must be excreted through the kidney. The kidney's filtration limit is 45 Å, corresponding to a hydrodynamic radius of PEGs with molecular weights of approximately 40,000 g mol^{-1}.[54] While below 20,000 g mol^{-1} the body is able to excrete the polymer via urine, higher molecular weight PEGs are eliminated more slowly and clearance through the liver takes place.[55] High molecular weights exceeding the filtration threshold, lead to a longer circulation time and accumulation in the liver.[56] Hence, PEG with low molecular weights is important for medical purposes.

Unsurprisingly, PEG's exceptional properties make it suitable for a wide range of applications in the fields of medicine, pharmacy, cosmetics and the food industry.[31] In the following, the focus will be on commercial applications of PEG homopolymers. The applications differ depending on the molecular weight. Smaller molecular weights ($M_n \leq 8{,}000$ g mol^{-1}) are used in the formulation of ointments due to their water solubility and compatibility with active ingredients.[57] PEGs with molecular weights between 1,000-4,000 g mol^{-1} are used as suppository bases, since PEG does not melt at body temperature. Instead, it slowly dissolves in the body and releases the active ingredient. Depending on the molecular weight or by mixing different PEGs, the consistence of the suppositories can be specifically adjusted.[58] In cosmetics, PEG is used in formulations of creams, lotions or powders. Industrially, PEGs are used as pigment dispersants or as anti-static agents or mold release agents.[33] Besides its uses in biomedical applications, its properties are beneficial for other areas. Thus, PEG can be used for restoration purposes. The royal warship Vasa, which is located in the Vasa Museum in Stockholm, was preserved by PEG for 17 years to prevent drying damage in the wood.[59]

PEOs with molecular weights above 1,000,000 g mol^{-1} have a unique property: small amounts dissolved in water (40−50 ppm) increase the flow rate in a pipeline by lowering the friction without the need to increase the pump pressure. This effect, known as Toms effect, is used, for example, to pump crude oil in pipelines or to fight fires, by pumping more water through the hoses.[60] PEO is used as seed tapes to ensure uniform planting of the seed. PEO can also be used as a flocculant for finely dispersed solids in water. For sedimentation, very small amounts in the ppm range are sufficient for the filtration of coal washery suspensions and uranium- or bentonite slime, for instance.[33]

Amphiphilic triblock copolymers of type A-B-A, where B is PPO and A is PEG, are used as drug delivery platforms, biological response modifiers, non-ionic surfactants and coating agents for pharmaceutical formulation.[61] The properties of these ABA triblock copolymers can be specifically tailored by variation of the block length. Such structures are referred to as poloxamers and are commercially marketed under the name Pluronic® (BASF SE) or Synperonic® (Croda International PLC).[62]

Modifying therapeutics with hydrophilic, non-ionic polymers can prevent a recognition by the immune system. In the context of PEG, the term "PEGylation" is used.[51,63] The first protein conjugate Adagen® (PEGylated bovine adenosine deaminase) was approved by the U.S. Food

and Drug Administration (FDA) in 1990 and is applied for the treatment of severe combined immunodeficiency disease.[64]

Polymerization techniques

Anionic ring-opening polymerization

In this section, the conventional anionic ring-opening polymerization (AROP) of ethylene oxide (EO) will be examined in more detail, starting with a historical review.

Historically, the first synthesis of low molecular poly(ethylene glycol) (PEG) dates back to Lourenço and Wurtz in the 19th century.[65–68] In the late 1920s the synthesis of higher molecular weight PEGs by using sodium hydroxide as a base was described in detail by Staudinger and Schweitzer.[69] With correspondingly long polymerization times of up to two years, Staudinger and Lohmann were even able to achieve molecular weights of 120,000 g mol^{-1}.[70] In 1940, Flory was able to demonstrate the living character of the AROP and he also proved that the molecular weight distribution of PEG obtained via the AROP of EO corresponds to a Poisson distribution.[71] In this respect, the relationship between the dispersity ($Đ$) and the degree of polymerization (X_N) is as follows:

$$Đ = \frac{M_w}{M_n} = 1 + \left[\frac{X_N}{(1+X_N)^2} \right] \approx 1 + \frac{1}{X_N} \tag{1}$$

where M_w is the weight- and M_n the number average molar mass.

Hydroxides, alkoxides, amides, metal alkyls and -aryls are suitable initiators for the AROP.[72] The polymerization mechanism depicted in **Scheme 3** can be described by a bimolecular nucleophilic substitution.

Partial deprotonation: $2\,ROH \;+\; X^{\oplus}OH^{\ominus} \longrightarrow RO^{\ominus}X^{\oplus} \;+\; ROH \;+\; H_2O$

X = Na, K, Cs

Initiation:

Propargation:

active

Fast proton exchange || ROH

dormant

Termination:

Y = OH, RO, Cl
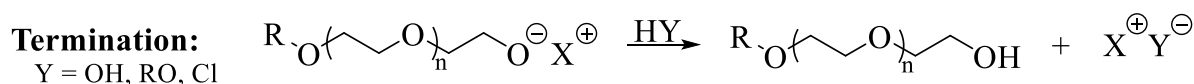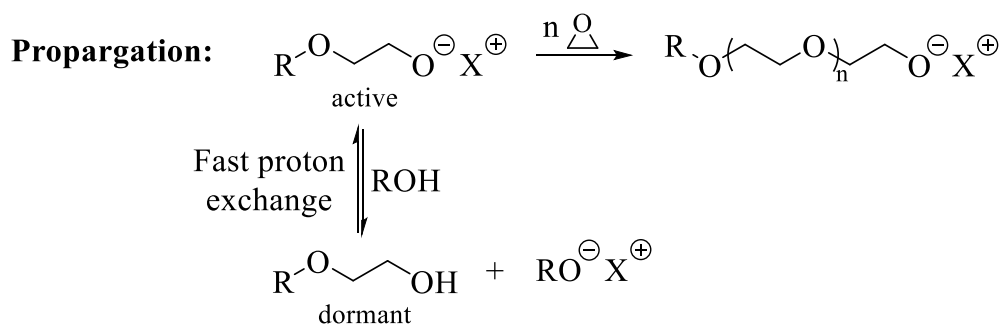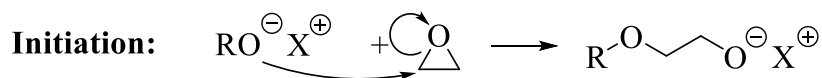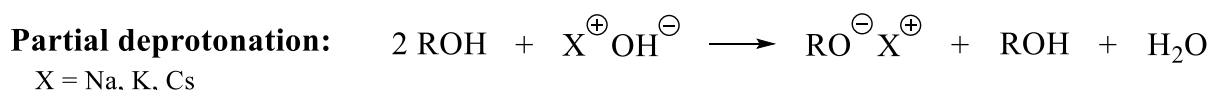
Scheme 3. Anionic ring-opening polymerization (AROP) of ethylene oxide (EO) via alkali metal alkoxides.

The driving force of the ring-opening polymerization is the reduction of ring strain. Whereas the ring strain for oxiranes is $114\,kJ\,mol^{-1}$, it decreases to $107\,kJ\,mol^{-1}$ for oxetanes and to $23\,kJ\,mol^{-1}$ for oxolanes.[73] For this reason, EO (oxirane) can be successfully polymerized via AROP, but tetrahydrofuran (oxolane) cannot. In the AROP, initiating hydroxide compounds are usually partially deprotonated to ensure better solubility and to prevent alkoxide aggregation. Moreover, a quantitative deprotonation is not necessary, since the proton exchange between the active and the dormant species is faster than initiation and propagation. As transfer reactions and temporary deactivation occur during the polymerization of EO, the criteria for "living" anionic polymerization are not met.[74] In this regard, the term "degenerative chain transfer" is used. In both initiation and propagation, a nucleophilic attack of the alkoxide oxygen anion occurs at the carbon atom of the epoxide derivative. The polymerization mechanisms of EO can be transferred to other epoxide derivatives. On account of the steric effects of substitutes, the attack occurs at the primary carbon atom and thus guarantees high regional specificity.[75] Protic solvents such as methanol can be used for termination to obtain a hydroxyl group as the end group. Alternatively, block copolymers can be obtained by addition of another oxirane monomer to the active chain end.

A crucial parameter for AROP is the choice of solvent and counter ion (**Scheme 4**). These two parameters have an influence on the propagation rate of the polymerization. The more the active chain end is separated from the counter ion, which correlates with the increasing polarity of the solvent, the higher is the propagation rate of the polymerization. Besides the bulk (solvent free) polymerization, there is a wide range of suitable, aprotic solvents available, namely dimethylformamide (DMF), *N*-methyl-2-pyrrolidone (NMP), dimethyl sulfoxide (DMSO), tetrahydrofuran (THF), 1,4-dioxane and many more.[76–78] Cryptands such as 18-crown-6 can further significantly increase the propagation rate.[79–81] Since a negatively charged oxygen atom is present as the active chain end in the case of EO, the interaction between the active center and the counterion must be taken into account. Based on the hard and soft acids and bases (HSAB) principle,[82] an oxygen anion is a hard base. According to this concept, lithium counterions are attached to the alkoxide oxygen atom, thus preventing polymerization through pronounced aggregation. Consequently, soft and bulky counterions such as potassium or cesium are required in order to avoid aggregation. Examinations have demonstrated that in the case of lithium cations no polymerizations took place and hence confirmed the trend that the softer the counterion, the higher the rate constant: $Na^+ < K^+ < Cs^+$.[77,83,84]
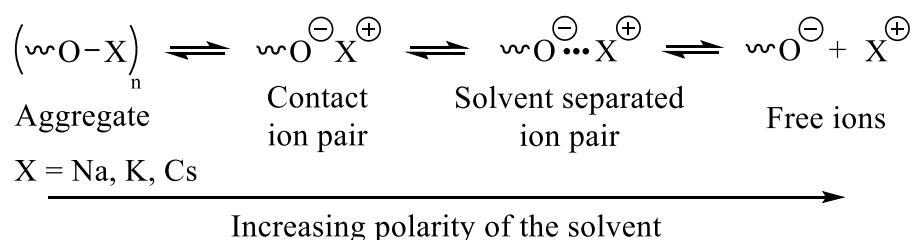
Scheme 4. Ion solvation in dependence of the solvent polarity.

Conventional PEG possesses two functional hydroxyl groups at the chain ends. These functionalities can be modified in different ways: either by the choice of initiator and termination reagent (**Scheme 5A**) or via post-polymerization modification (**Scheme 5B**). In the first method, functional initiators are used for AROP, followed by termination with a functional reagent. The second method involves derivatization of the terminal PEG hydroxyl groups after polymerization and without chain degradation. In this context, Thompson *et al.* wrote an exceptional review article on heterobifunctional PEGs.[85] In the following, the emphasis is placed on the first method. The scope of initiators for α-functionalization is very wide.[78,86] It extends for instance from amine,[87–89] azide,[90] carboxylic acid[91] and acetal[92,93] to aldehyde groups[94–96]. A precondition is the stability of the initiators with regard to the harsh AROP conditions, which is why protecting group chemistry must be used in case of catechol

functionalities.[97] Similar applies to the termination reagent. In addition to azide and alkyne groups,[98] methacrylate[99] and carboxylic acid[100] functionalities can also be introduced.

A) $\boxed{X}$-OH + (epoxide) $\xrightarrow{\text{AROP, terminating reagent Y}}$ X-(O)$_n$-Y

B) HO-(O)$_n$-H $\xrightarrow{\text{Functionalization reagent X}}$ X-(O)$_n$-X
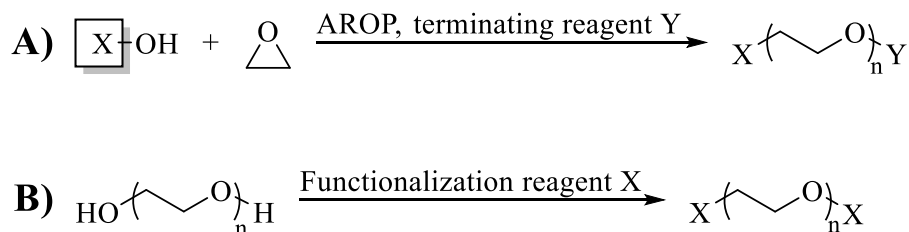
Scheme 5. Introduction of end groups and end group modification.

Monomer-activated anionic ring-opening polymerization

This section deals with the Lewis acid activated, controlled anionic polymerization according to Deffieux and Carlotti.

Aluminum-based catalysts for the activation and polymerization of epoxides are not new. Vandenberg pioneered this approach in the 1960s. On the other hand, diethyl aluminum chloride-based 5,10,15,20-tetraphenylporphine system were introduced by Aida and Inoue.[20,101] The key issue addressed was the non-uniform polymerization rate of epoxides fluctuating from minutes (in the case of EO) to days (e.g. styrene oxides),[102] which could be drastically improved by the addition of sterically demanding Lewis acids.[103] Tsvetanov *et al.* on the other hand, introduced a porphyrin-free catalyst. For this purpose, EO was reacted with $NaAlBu_4$ in various solvents such as THF, toluene and *n*-heptane and studied with regard to polymerization kinetics.[104] The group was also able to effectively polymerize EO with sodium tetrabutyl aluminate. Another porphyrin-free system was developed by Braune and Okuda, who combined neutral Lewis acid precursors and "ate" complexes for the polymerization of PO.[105]

A seminal work published in 2004 by Deffieux and Carlotti on the polymerization of PO marked the birth of a polymerization technique that is now commonly referred to as "activated monomer technique".[106] The activated monomer strategy has become an important alternative to conventional AROP.[78] The key element of this method is the use of an initiator-catalyst system. An organic salt, such as tetraoctylammonium bromide ($NOct_4Br$) or methyltriphenylphosphonium bromide ($MePPh_3Br$) serves as the initiator, which is combined with a Lewis acid such as triisobutylaluminum (iBu_3Al).[107] The following scheme (**Scheme 7**) shows the proposed mechanism:

Formation of "ate" complex: $i\text{Bu}_3\text{Al} + X^{\ominus}Y^{\oplus} \longrightarrow X\text{-}\overset{\ominus}{\underset{i\text{-Bu}}{\overset{i\text{-Bu}}{Al}}}\text{-}i\text{-Bu}\ \ Y^{\oplus}$

X = iPrO, Cl, Br, N$_3$
Y = Na, NBu$_4$, NOct$_4$, PBu$_3$, MePPh$_3$

Complexation: [epoxide with R] $\xrightarrow{\ i\text{Bu}_3\text{Al}\ }$ [epoxide–O $\cdots$ Al(i-Bu)$_3$ complex with R]

Initiation: [epoxide–O $\cdots$ Al(i-Bu)(i-Bu)(i-Bu) with R] $+\ X\text{-}\overset{\ominus}{Al(i\text{-Bu})_3}\ Y^{\oplus} \xrightarrow[-\ i\text{Bu}_3\text{Al}]{} X\underset{R}{\frown}O\text{-}\overset{\ominus}{Al(i\text{Bu})_3}\ Y^{\oplus}$

Propargation: $X\underset{R}{\frown}O\text{-}\overset{\ominus}{Al(i\text{Bu})_3}\ Y^{\oplus} \xrightarrow[-\ i\text{Bu}_3\text{Al}]{\text{[epoxide–O}\cdots\text{Al}(i\text{-Bu})_3\text{, R]}} X\left(\underset{R}{\frown}O\right)_2\overset{\ominus}{Al(i\text{Bu})_3}\ Y^{\oplus}$

Termination: $X\left(\underset{R}{\frown}O\right)\overset{\ominus}{Al(i\text{Bu})_3}\ Y^{\oplus} \xrightarrow{\ \text{MeOH}\ } X\left(\underset{R}{\frown}O\right)H$
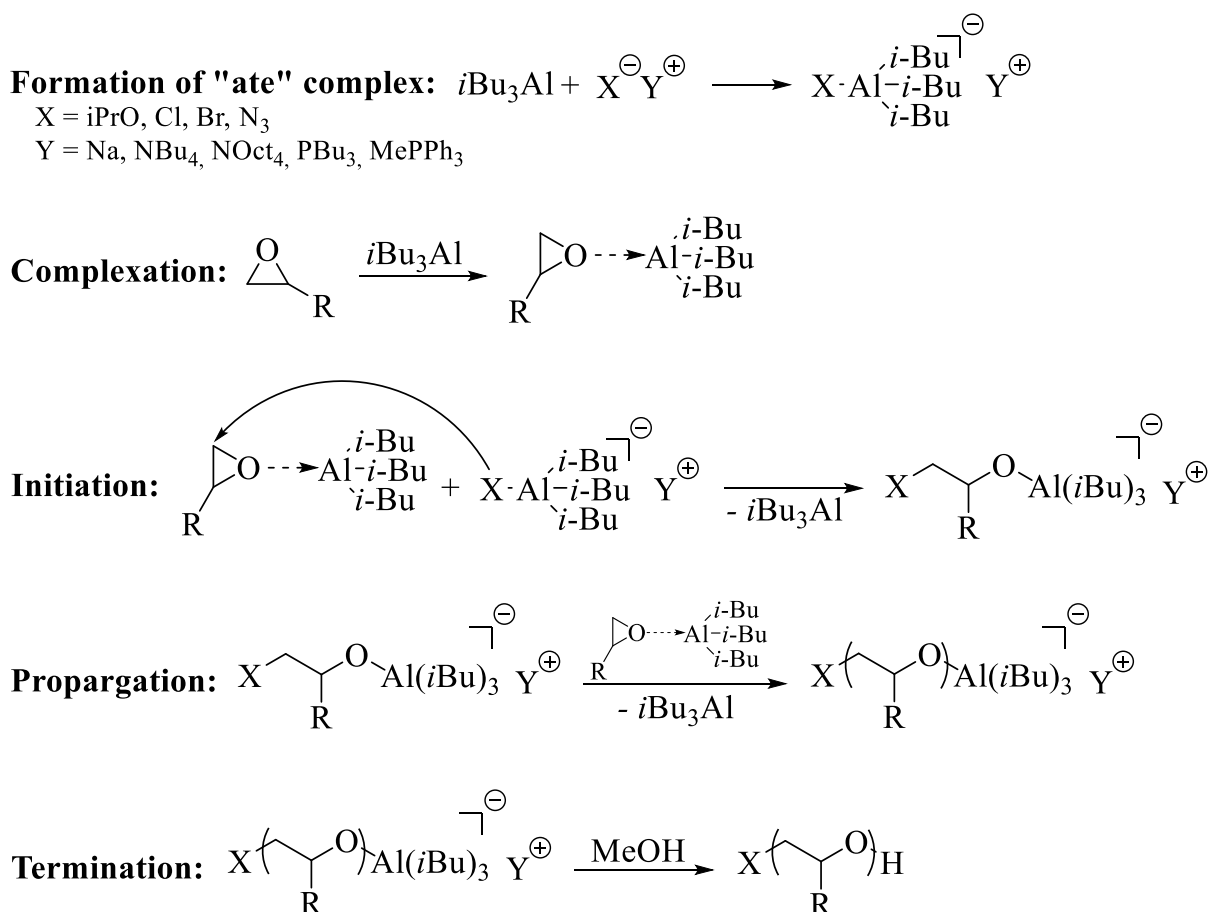
Scheme 7. Polymerization mechanism according to the activated monomer technique.

In the activated monomer strategy, the catalyst is used in excess of the initiator. First, an "ate" complex of low nucleophilicity is formed between the initiator as a weak nucleophile and the catalyst iBu$_3$Al. Furthermore, monomer activation occurs through interaction between the excess Lewis acid catalyst and the epoxide ring. The electron density in the epoxide ring is reduced, and its electrophilicity and reactivity towards nucleophiles is increased, facilitating the subsequent ring-opening. In the initiation step, a nucleophilic attack of the "ate" complex on the activated monomer occurs. The halide ion initiates polymerization, the monomer is inserted and further monomer activation takes place for subsequent chain growth. Similar to conventional AROP, termination takes place using protic solvents. Moreover, ^{13}C NMR spectroscopic analyses revealed no stereoselectivity, but regioselectivity for almost exclusively head-to-tail-linkages.[106] By synthesizing different block copolymers, the "living character" of this polymerization strategy was demonstrated by the successive addition of comonomers. In this fashion, amphiphilic diblock copolymers were prepared based on PEG and poly(butylene oxide) (PBO) respectively poly(hexylene oxide) (PHO)[108], poly(glycerol) and poly(glycidyl amine)[109] or PPO and PECH[110].

As already mentioned at the beginning, an excess of iBu$_3$Al is indispensable for the polymerization technique according to Carlotti and Deffieux. If the ratio of catalyst to initiator is too high, broad molecular weight distributions result.[111] Another point worth mentioning is the aluminum-complexing capability of oxygen atoms. As a result, rather high catalyst amounts have to be utilized in the polymerization of acetal-protected ethoxyethyl glycidyl ether (EEGE), owing to its three oxygen atoms in comparison, e.g. to EO. Because of the nucleophilic oxygen atoms of the acetal protecting group, EEGE shows strong complexation and thus reduces the activity of iBu$_3$Al.

An interesting parameter is the choice of the initiator, allowing the end groups to be controlled specifically. However, the spectrum of available initiators is very limited compared to the conventional AROP. For example, when NOct$_4$Br is used, a bromide anion initiates polymerization, whereas tetrabutylammonium azide (NBu$_4$N$_3$)[112] is used to obtain azido-functionalized polyethers. However, Sakakibara et $al.$ were able to demonstrate by MALDI-ToF investigations that undesired initiations occur through transfer of hydride or isobutyl groups, as depicted in **Scheme 8**.[113]
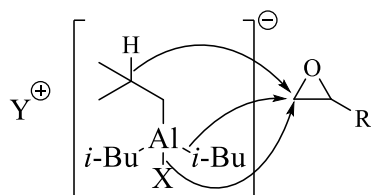
Scheme 8. Possible initiation modes by abstraction of a proton, the isobutyl group or (halide) anions.

With regard to solvent selection, the only restriction is the use of aprotic solvents. In this respect, the use of 2-methyltetrahydrofuran (2-MTHF)[114], cyclohexane[106], dichloromethane[111], chlorobenzene[115] and toluene[45] as well as fluorinated solvents[113] are described. The complexation of the catalyst by solvent oxygen atoms mentioned above should be considered. For this reason, the use of 2-MTHF is preferable to tetrahydrofuran (THF) due to its shielding methyl group.

By employing this polymerization technique, molecular weights of PPO in the range of 170,000 g mol^{-1} were achieved for the first time.[116] In addition, the strong activation of epoxide rings allows both the (co)polymerization of less reactive and sterically hindered epoxides, such as glycidyl methyl ether (GME)[45]. Strong tolerance to functional groups is evident in the polymerization of benzophenone-based glycidyl ether (EEBP)[117], glycidyl propargyl ether

(GPgE)[118], epicyanohydrin (EPICH)[115], glycidyl methacrylate (GMA)[119], ECH[120], as well as fluorinated epoxide monomers[113,121]. An overview of these sensitive epoxide derivatives that are only suitable for the activated monomer technique is displayed in **Scheme 9**:
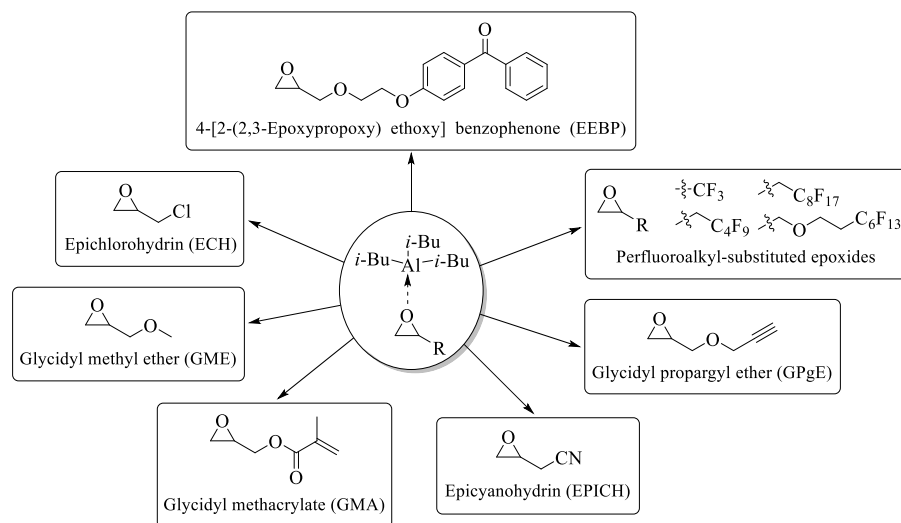
Scheme 9. Overview of established, functional epoxide monomers that cannot be polymerized by "classical" oxyanionic polymerization, but are suitable for the activated monomer technique.

Multi-functional poly(ethylene glycol)s and their application

The following section is intended to provide information on multi-functional PEGs.[122]

The above described functionalization possibilities of the terminal PEG hydroxyl groups have a decisive disadvantage: the total number of functionalities is strongly limited. Especially for drug delivery, a high loading capacity is crucial. This is precisely where multi-functional PEGs come in. Although poly(ethylene glycol) is highly established, multi-functional PEGs were only introduced in recent decades.[123,124] The copolymerization of EO with epoxide derivatives distributes functional groups along the polymer backbone resulting in multi-functional PEGs. In this fashion, also new properties are obtained and the application spectrum of the polyethers is expanded.[122,125]

For instance, the incorporation of glycidyl amines such as *N,N*-diethyl glycidyl amine (DEGA) introduces pH-responsive behavior, while the copolymerization of EO with ferrocenyl glycidyl ether (fcGE) leads to electroactive and thermoresponsive behavior.[126–128] Catechol units are highly suitable for complexing ions or coating surfaces. By incorporation and acidic deprotection of the acetonide-protected catechol glycidyl ether CAGE, these properties can be

transferred to PEG.[129] In addition, these properties can be tailored by the variation of the comonomer amount.

Alternatively, apart from the direct incorporation of functional monomer building blocks, functionalities can also be introduced by post-polymerization modification, e.g. via thiol-ene click- [130,131] or Diels-Alder chemistry[132,133]. The former can be realized by copolymerization of EO with allyl glycidyl ether (AGE)[134] or ethoxy vinyl glycidyl ether (EVGE)[135]. In these structures the pendant allyl (or respectively vinyl) moieties serve as a platform for subsequent reactions at the polymer. For the latter, furfuryl glycidyl ether (FGE) units can also be incorporated.[136,137] Another possibility is the incorporation of hydroxyl groups along the polyether backbone. Linear polyether polyols (polyglycerols, *lin*PG) are obtained by the incorporation and subsequent cleavage of EEGE[124], an acetal-protected glycidol derivative. Li and Chau reported in detail on the post-polymerization modification possibilities of these PGs, including for instance carboxyl-, tosylate-, primary amine- or azido functionalities.[138]

The AROP of EO with functional epoxide building blocks not only allows to tailor the properties of PEG, but also to tailor the polymer architecture. In this manner, the successive addition of monomers leads to block copolymers, while the AROP of a monomer mixture results in statistical copolymers.[139] It should be noted that the microstructure is strongly dependent on the reactivity of the epoxide comonomers, and thus ideal random copolymers or gradient copolymers can be obtained.[140] A more detailed discussion on this topic is given in the next section.

Functional epoxide derivatives can be roughly divided into four classes: glycidyl ethers, glycidyl amines, alkylene oxides and others (**Scheme 6a**).[86] In general, the former are accessible by etherification of alcohols with ECH. Glycidyl amines can be synthesized by the reaction of secondary amines with epichlorohydrin. In contrast, alkylene oxides are obtained by oxidation of the corresponding alkenes. In the class of other functional monomers, a case-specific subdivision must be made. While glycidyl esters can be synthesized e.g. by the reaction of ECH with activated carboxylic acids, epihalohydrins such as ECH can be prepared analogous to alkylene oxides from the epoxidation of allylic halides. The asymmetry of functional epoxides raises the additional question of regioselectivity. Due to steric reasons, they are mainly incorporated regioselectively by head-to-tail connections.[86,141]

One critical issue in the polymerization of substituted oxiranes is that undesirable chain transfer reactions are frequently observed under conventional oxyanionic polymerization

conditions.[142-144] The abstraction of a proton from the methyl- or methylene group at the epoxide moiety leads to the formation of an allyl alkoxide, which may act as an initiator itself, resulting in a limitation of the molecular weights. For this reason, the molecular weight of PEEGE obtained by the conventional AROP is limited to 27,400 g mol^{-1}.[144] The process is illustrated in **Scheme 6b**. A further limitation are the harsh reaction conditions of the conventional AROP, such as the increased reaction temperatures and the use of strong bases. As a result, the variety of functionalities is limited, making the direct polymerization of glycidyl esters[119] or the incorporation of hydroxyl (EEGE)[124], catechol (CAGE)[129], nitrile[115] or alkylene units (GPgE)[118] impossible. Instead, protecting group chemistry or the much milder monomer-activation technique must be applied.

a)

Glycidyl ethers

Classes of functional epoxide derivatives

Alkylene oxides

Glycidyl amines

Glycidyl methacrylate (GMA)　　Epicyanohydrin (EPICH)

Trifluoropropene oxide (TFPO)　　Epihalohydrins

b)
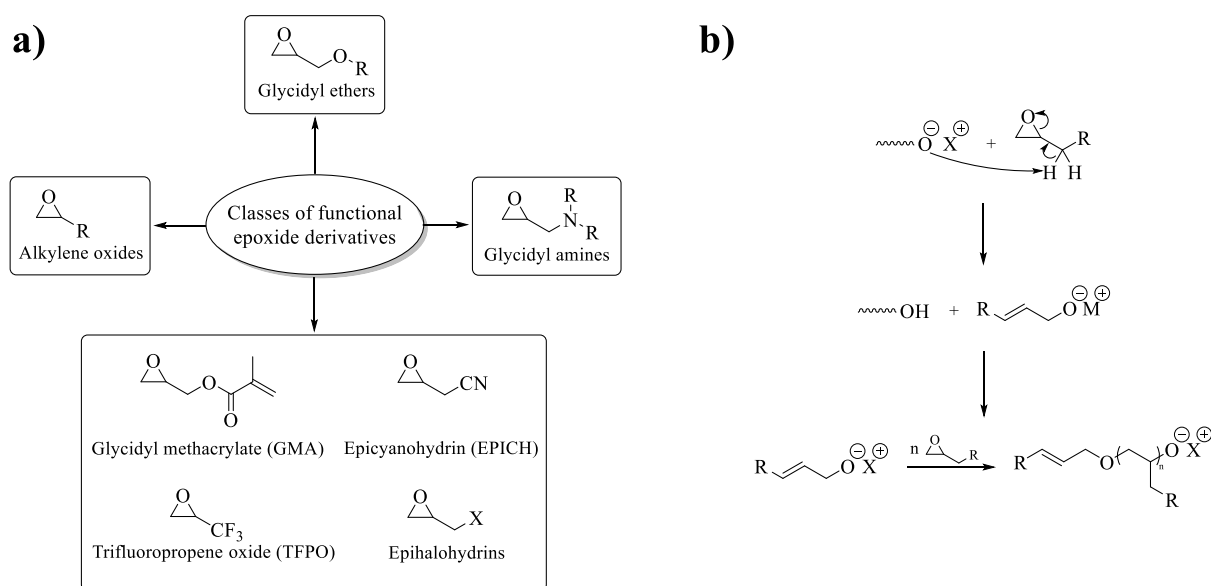
Scheme 6. a) Classification of the functional epoxide building blocks in glycidyl ethers, glycidyl amines, alkylene oxides and others (here, a selection is shown); b) chain transfer reaction in the polymerization of an epoxide derivatives including undesired initiation of the allyl alkoxide species.

Monomer sequence matters: NMR investigation of copolymerization kinetics

In the following section, epoxide copolymerization kinetics will be examined in detail, using (*in-situ*) NMR spectroscopy. Following a short introduction to the topic, the copolymerization of EO and PO with various epoxide derivatives is discussed. Moreover, monomer pairs that do not include EO or PO are also listed. Copolymerization kinetics from both conventional and monomer-activated AROP are illuminated.

The reactivity of comonomers is decisive for the microstructure of copolymers. In the early 1930s Staudinger already investigated the copolymerization of vinyl acetate (VA) and vinyl chloride (VC). For an equimolar mixture, he observed a shift in the copolymer composition from 9:3 to 7 : 3 to 5 : 3 to 5 : 7 (VC to VA).[145] This effect is known as composition drift and is attributable to differences the reactivity of the comonomers. Similar reactivity of both comonomers leads to a kinetically indistinguishable incorporation of the comonomers and an ideal, random copolymer is obtained. In addition, there is a variety of further possibilities for arranging comonomer units within a polymer chain, leading to alternating or gradient-like copolymer structures among others. A schematic overview is shown in **Scheme 10**.

Ideal (random) copolymer

Strictly alternating copolymer

Gradient copolymer

Tapered block copolymer

Statistical block copolymer
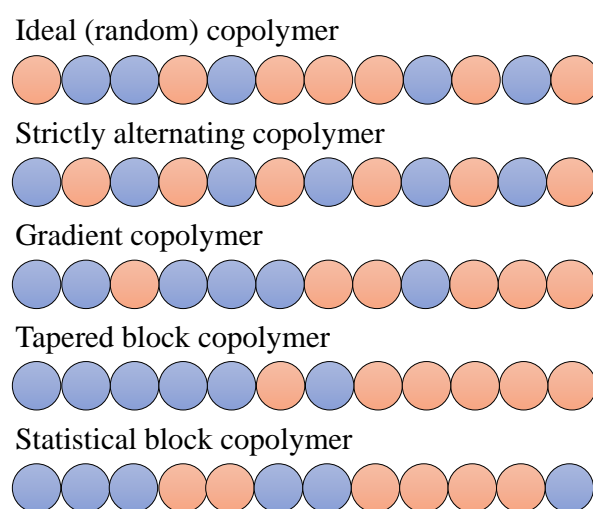
Scheme 10. Schematic representation of different types of copolymers.

In particular, gradient copolymers show special properties.[146,147] Establishing living ionic- or living free-radical polymerization methods have made it possible to access this rather new class of copolymers, since termination reactions lead to heterogeneity in the copolymer composition.[148] A characteristic feature of gradient copolymers is their wide glass transition temperature range, located between the T_gs of the respective homopolymers. In addition, the T_g for gradient copolymers is strongly dependent on the thermal history.[148] Further, Karaky *et al.* demonstrated for poly(octadecyl acrylate)-*grad*-poly(methyl acrylate) (PODA-*grad*-PMA) copolymers a decrease of the T_m by 10 °C compared to the corresponding block copolymers and respectively the PODA homopolymer, which showed constant T_m values in the range of 45 °C due to the strong phase separation of ODA and MMA sequences.[149] The reason for this is a disturbance of the octadecyl acrylate crystal lattice by the MA moieties. Similar to block copolymers, gradient copolymers may show amphiphilic behavior. For aqueous solutions of ethoxyethyl vinyl ether/ methoxyethyl vinyl ether gradient copolymers, Okabe *et al.* observed

an interesting effect.[150,151] While the diameter of micelles made of block copolymers did not change with increasing temperatures, a "reel-in" effect was observed for the gradient copolymers: the simultaneous shrinkage of the micellar shell with simultaneous expansion of the micellar nucleus. In view of the differences in the microstructure, the fields of application of the copolymers also differ. Thus, random P(EO-*co*-PO) are used as water-soluble lubricants, preventing foaming due their higher surface tension compared to PEO-*b*-PPO block copolymers.[152,153] In contrast, the poloxamers (PEO-*b*-PPO-*b*-PEO triblock copolymers) mentioned above are non-ionic surfactants and are used for instance as pharmaceutical ingredients and agricultural products or food additives.[154] Potential applications for gradient copolymers are polymer blend compatibilizers[155] or damping materials[156,157]. In this context, recently, Harrisson *et al.* reviewed the synthesis, properties and applications of gradient and other partially segregated copolymers.[158] In the light of this discussion, it is evident why it is essential to understand the microstructure of copolymers.

A quantitative description of the copolymerization is given by the copolymerization model introduced by Mayo and Lewis.[159] This model is a so-called terminal model, this means the reactivity of monomers can be influenced by the last monomer unit in the growing chain:

$$\sim M_1^* + M_1 \xrightarrow{k_{11}} \sim M_1 M_1^* \tag{5}$$

$$\sim M_1^* + M_2 \xrightarrow{k_{12}} \sim M_1 M_2^* \tag{6}$$

$$\sim M_2^* + M_2 \xrightarrow{k_{22}} \sim M_2 M_2^* \tag{7}$$

$$\sim M_2^* + M_1 \xrightarrow{k_{21}} \sim M_2 M_1^* \tag{8}$$

Here, k_x is the rate constant, M_x^* is the active chain end and M_x is the monomer. The temporal decrease of the respective monomer concentration can be determined as follows:

$$-\frac{dM_1}{dt} = k_{11} \cdot \left[M_1^*\right] \cdot [M_1] + k_{21} \cdot \left[M_2^*\right] \cdot [M_1] \tag{9}$$

$$-\frac{dM_2}{dt} = k_{12} \cdot \left[M_1^*\right] \cdot [M_2] + k_{22} \cdot \left[M_2^*\right] \cdot [M_2] \tag{10}$$

By dividing **Equations 9** by **10** and subsequently rearrangement, expression **12** is obtained, describing the incorporation rate of the comonomers:

$$\frac{dM_1}{dM_2} = \frac{k_{11} \cdot \left[M_1^*\right] \cdot [M_1] + k_{21} \cdot \left[M_2^*\right] \cdot [M_1]}{k_{12} \cdot \left[M_1^*\right] \cdot [M_2] + k_{22} \cdot \left[M_2^*\right] \cdot [M_2]} \tag{11}$$

$$\frac{dM_1}{dM_2} = \frac{[M_1]}{[M_2]} \cdot \left[\frac{k_{11}\cdot[M_1^*] + k_{21}[M_2^*]}{k_{12}\cdot[M_1^*] + k_{22}[M_2^*]}\right] \tag{12}$$

The assumption of the steady state approximation leads to **Equation 14** after rearrangement:

$$k_{21} \cdot [M_2^*] \cdot [M_1] = k_{12} \cdot [M_1^*] \cdot [M_2] \tag{13}$$

$$\frac{[M_2]}{[M_1]} = \frac{k_{21}\cdot[M_2^*]}{k_{12}\cdot[M_1^*]} \tag{14}$$

Using this approximation, **Equation 12** results in:

$$\frac{dM_1}{dM_2} = \frac{[M_1]}{[M_2]} \cdot \left[\frac{\frac{k_{11}\cdot[M_1]}{k_{12}} + [M_2]}{[M_1] + \frac{k_{22}[M_2]}{k_{21}}}\right] \tag{15}$$

The reactivity ratios r_1 and r_2 can be defined as the ratio of the addition of the respective comonomer to the active polymer chain:

$$r_1 = \frac{k_{11}}{k_{12}} \quad \& \quad r_2 = \frac{k_{22}}{k_{21}} \tag{16}$$

The copolymer equation is obtained by simplifying **Equation 15** with the expressions just derived for the reactivity ratios:

$$\frac{dM_1}{dM_2} = \frac{m_1}{m_2} = \frac{[M_1]}{[M_2]} \cdot \left[\frac{r_1\cdot[M_1] + [M_2]}{r_2\cdot[M_2] + [M_1]}\right] \tag{17}$$

This equation, also known as the Mayo-Lewis equation[159], describes the copolymer composition as a function of the respective (instantaneous) monomer ratio during the copolymerization. It can be noted that the monomer rate as well as the resulting copolymer ratio changes throughout the course of the copolymerization. A linear relationship between r_1 and r_2 is obtained by rearrangement of the copolymerization equation:

$$r_1 = r_1 \cdot \frac{m_1}{m_2} \cdot \frac{[M_2]^2}{[M_1]^2} + \frac{[M_2]}{[M_1]} \cdot \left(\frac{m_1}{m_2} - 1\right) \tag{18}$$

M_1/ M_2 are known from the initial monomer concentrations, while m_1/ m_2 can be determined from the copolymer composition using suitable analytical methods (NMR, UV/VIS, etc.). **Equation 18** gives a linear equation for any pair of copolymerization experiments. Thus, the reactivity ratios r_1 and r_2 can be obtained from the intersection of these straight lines. The challenge with this method is that intersections often do not meet at a single point. Hence, in

the next method only one single linear equation is defined for the calculation of the reactivity ratios.

An alternative method for determining r_1 and r_2 is the Fineman and Ross method.[160] Here, the copolymerization equation is converted to the following form:

$$\frac{m_2}{m_1} \cdot \frac{[M_1]}{[M_2]} \cdot \left(\frac{m_1}{m_2} - 1\right) = r_1 \cdot \frac{m_2}{m_1} \cdot \frac{[M_1]^2}{[M_2]^2} - r_2 \tag{19}$$

$$\frac{[M_2]}{[M_1]} \cdot \left(\frac{m_1}{m_2} - 1\right) = -r_2 \cdot \frac{m_1}{m_2} \cdot \frac{[M_2]^2}{[M_1]^2} + r_1 \tag{20}$$

Equations 19/ 20 provide linear equations of the shape $y = r_1 \cdot x - r_2$, respectively $y = -r_2 \cdot x + r_1$. Plotting y against x leads to a straight line with a slope r_1 $(-r_2)$ and an intercept $-r_2$ (r_1). Using both equations, it is possible to determine the reactivity ratios from the slope, which is more accurate. A disadvantage of the method is the uneven distribution of the measured values, which gives a distorted error structure. Therefore, other methods were developed.

The third well-known graphical method for determination of the reactivity ratios is based on work of Kelen and Tüdős.[161] Division of **Equation 19** with $\alpha + \frac{m_2}{m_1} \cdot \frac{[M_1]^2}{[M_2]^2}$ yields the following expression, where α is an auxiliary variable:

$$\frac{\frac{m_2}{m_1} \cdot \frac{[M_1]}{[M_2]} \cdot \left(\frac{m_1}{m_2} - 1\right)}{\alpha + \frac{m_2}{m_1} \cdot \frac{[M_1]^2}{[M_2]^2}} = \frac{r_1 \cdot \frac{m_2}{m_1} \cdot \frac{[M_1]^2}{[M_2]^2}}{\alpha + \frac{m_2}{m_1} \cdot \frac{[M_1]^2}{[M_2]^2}} - \frac{r_2}{\alpha + \frac{m_2}{m_1} \cdot \frac{[M_1]^2}{[M_2]^2}} \tag{21}$$

The following more practical equation can then be derived:

$$\eta = r_1 \cdot \xi - r_2 \cdot \frac{1 - \xi}{\alpha} \tag{22}$$

ξ can only take values between 0 and 1. The even distribution of the ξ values over this interval is achieved by defining α as the geometric mean of the smallest and the largest value for $\frac{m_2}{m_1} \cdot \frac{[M_1]^2}{[M_2]^2}$. A graph of η against ξ is thus a straight line. Here, r_1 is obtained for $\xi = 1$, whereas the intercept of $-\frac{r_2}{\alpha}$ is obtained for $\xi = 0$.

The reactivity ratios from **Equation 16** are essential for estimating the copolymer composition expected for a given monomer pair. In this context, a distinction can be made between four cases listed in **Table 1**:

Table 1. Various combinations of the reactivity ratios.

Types of copolymerization	Reactivity ratios	
Random (ideal)	$r_1 = 1$	$r_2 = 1$
Statistical Ideal, if $r_1 \cdot r_2 = 1$ Tapered block copolymerization, if $r_1 \gg 1$ and $r_2 \ll 1$ or vice versa	$r_1 > 1$ $r_1 < 1$	$r_2 < 1$ $r_2 > 1$
Statistical-alternating Strictly alternating, if $r_1 = r_2 = 0$	$r_1 < 1$	$r_2 < 1$
Statistical block copolymerization Homopolymerization, if $r_1 = r_2 \gg 1$	$r_1 > 1$	$r_2 > 1$

Apart from classical sampling out at different conversions and analysis of the copolymer composition at low conversion or triad analysis via NMR spectroscopy, the *in-situ* monitoring of copolymerization is an elegant approach for the exploration of copolymerization kinetics and to determine reactivity ratios in a single experiment. Besides methods like IR[162,163] and UV[164,165] spectroscopy, both ^{1}H NMR and ^{13}C NMR spectroscopy are suitable for this purpose. In this area, our group pioneered *in-situ* kinetics of both conventional AROP[166,167] as well as the monomer-activated AROP[140]. In the meantime, the technology is well established.[168–171]

In the following, the copolymerization kinetics based on conventional AROP of EO and afterwards PO with epoxide derivatives according to the classification in **Scheme 6** will be summarized and discussed. An emphasis is placed on NMR spectroscopy (^{1}H NMR analysis of aliquots obtained by sampling, ^{13}C NMR triad analysis, real-time ^{1}H NMR kinetics) as an evaluation method. Afterwards, copolymerizations under conditions of the monomer-activated AROP are illuminated before focusing on copolymerizations, in which neither EO nor PO are involved. **Table 2** presents a summary of numerous studies and indicates clearly that the common oxyanionic copolymerization of EO with a glycidyl ether is in general almost ideal and fully random. The minimum deviations for ideal conditions $r_1 \approx r_2 \approx 1$ can be traced back to steric reasons of the respective bulky glycidyl ethers.[129] By application of a new method for the determination of reactivity ratios, Lynd and co-workers obtained ratios which strongly deviated from the overall trend in case of EO-AGE/EVGE.[172] In this work, the authors determined the values for r_1 and r_2 based on the methylene signal of the benzyl alcohol initiator and supported the results with density functional theory (DFT) calculations. In contrast, DEGE,

also evaluated according to this method, behaves almost like other glycidyl ethers and displays nearly random behavior in the copolymerization with EO.

Table 2. Reactivity ratios obtained for the copolymerization of EO with various glycidyl ethers according by conventional AROP.
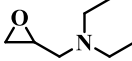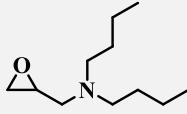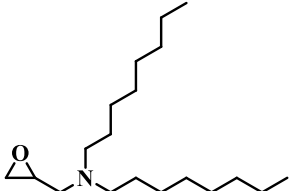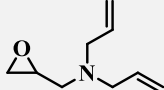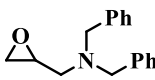
Comonomer structure	Comonomer name	$r_{comonomer}$	r_{EO}	Ref.
	ethoxyethyl glycidyl ether (EEGE)	0.94 random[a]	1.05	140 173
	N,N-diisopropyl ethanolamine glycidyl ether (DEGE)	1.28	0.82	174
	allyl glycidyl ether (AGE)	1.31 random[a]	0.54	172 134
	ethoxy vinyl glycidyl ether (EVGE)	3.5 random[a]	0.90	172 135
	catechol acetonide glycidyl ether (CAGE)	0.88	1.14	129
	2-(methylthio)ethyl glycidyl ether (MTEGE)	1.06	0.92	139
	ferrocenyl glycidyl ether (FcGE)	random		128
	Ruthenocenyl glycidyl ether (rcGE)	random		175
	Ethoxy ally glycidyl ether (EAGE)	0.95	1.05	Chapter 2.1
	Ketone dioxolane glycidyl ether (KDGE)	0.74	1.35	Chapter 2.2
	Ethoxy Butoxy Vinyl Glycidyl Ether (EBVGE)	0.99	1.01	Chapter 3.1

[a]Triad sequence analysis via ^{13}C NMR spectroscopy.

Table 3 lists the reactivity ratios for the copolymerization of EO with glycidyl amines and alkylene oxides. Obviously, glycidyl amines are less reactive compared to EO. It can be observed that the length of the glycidyl amine alkyl chains has no influence on the reactivity of the monomers. Reuss *et al.* attributed these observations to the lower electronegativity of the

nitrogen atom compared to oxygen atoms in case of glycidyl ethers and the less efficient coordination of the counterion with the glycidyl amines, which can be traced back to the shielding of nitrogen by the alkyl chains.[127] In comparison, the reactivity of alkylene oxides decreases with increasing length of the alkyl chains, with EO being more reactive in any case. Remarkably, the steric substituent constants E_s of PO ($E_s = 0.00$) and BO ($E_s = -0.07$) are quite similar.[176] Hence, this indicates an origin of the reactivity differences in electronic effects. The additional electron pressure of the ethyl substituent in BO increases the electron density in the epoxide ring, making it less attractive for a nucleophilic attack.
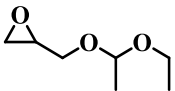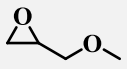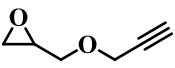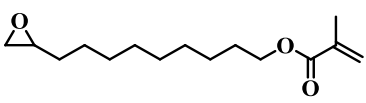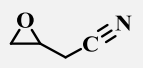
Table 3. Reactivity ratios determined for the copolymerization of EO with various glycidyl amines and alkylene oxides polymerized by conventional AROP.

Comonomer structure	Comonomer name	$r_{comonomer}$	r_{EO}	Ref.
	N,N-diethyl glycidyl amine (DEGA)	faster incorporation of EO		127
	N,N-di(*n*-butyl) glycidyl amine (DButGA)	0.49	1.84	177
	N,N-di(*n*-octyl) glycidyl amine (DoctGA).	0.42	1.78	177
	N,N-diallylglycidylamine *(DAGA)*	faster incorporation of EO		178
	N,N-dibenzyl glycidyl amine (DBAG)	faster incorporation of EO		166
	propylene oxide (PO)	0.25 0.30 1.49	2.8 3.1 2.35	179 179 180
	butylene oxide (BO)	0.148	6.46	171

Application of the activated monomer strategy leads to the formation of gradient copolymer microstructures. It is interesting to note that to date there is no comonomer capable of forming random copolymers with EO, when the activated monomer approach is used. Since this polymerization method represents still a rather recent technique, not many examples are found in literature (**Table 4**). Nevertheless, the general conclusion can be drawn that EO is always incorporated faster than glycidyl ethers. The complexation capability of the *i*Bu₃Al catalyst by

the additional oxygen atoms can be attributed to this.[45,140] Consequently, the activation of the monomers and thus their electrophilicity towards the nucleophilic, active chain end is reduced, resulting in slower incorporation.

Table 4. Reactivity ratios obtained for the copolymerization of EO with various glycidyl ethers, alkylene oxides and epoxide derivatives by monomer activated AROP.

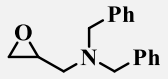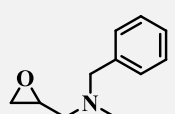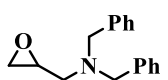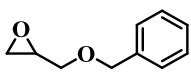| Comonomer structure	Comonomer name	$r_{comonomer}$	r_{EO}	Ref.
	ethoxyethyl glycidyl ether (EEGE)	0.125	8.00	140
	glycidyl methyl ether (GME)	gradient (EO faster)[a]		45
	glycidyl propargyl ether (GPgE)	0.076	14.8	118
	propylene oxide (PO)	0.013	2.05	111
	epoxy undecane methacrylate (EUMA)	0.10	9.43	Chapter 3.2
	epicyanohydrin (EPICH)	"rather random or gradient microstructure"[a]		115
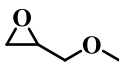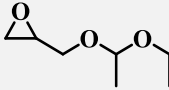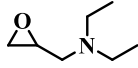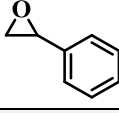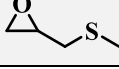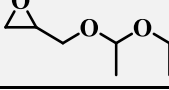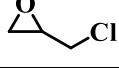
[a]Triad sequence analysis via ^{13}C NMR spectroscopy.

Table 5 outlines the results for the copolymerization of PO according to conventional and monomer-activated AROP. EPB, also an alkylene oxide, is the only known monomer providing random copolymers with PO, which can be explained by the structural similarity.[180] As mentioned above, glycidyl ethers exhibit similar behavior as EO. However, since the latter is also preferred in the copolymerization with PO, this also applies to the glycidyl ethers. Ponomarenko *et al.* attribute the higher reactivity of GME and GMT to the complexation of the alkali metal counterions, facilitating nucleophilic attack at the epoxide ring.[180] The above depicted steric shielding of the nitrogen atom in glycidyl amines caused by the alkyl residues interferes the coordination of ions, hence explaining the lower reactivity of DEGA in the copolymerization with PO. Owing to the fluorine atoms in TFEP, the reactivity of the structural analogue PO is significantly increased due to the strong electron pull on the epoxide ring, as evidenced by the reaction parameters of $r_{TFEP} = 18.0$ and $r_{PO} = 0.16$.

It is an intriguing fact that the reactivity ratios in the copolymerization of EEGE and PO are reversed under monomer-activated conditions ($r_{EEGE} = 0.18$, $r_{PO} = 3.58$) and are similar to those

of the monomer pair EEGE-EO ($r_{EEGE} = 0.125$, $r_{EO} = 8.00$). Again, the reason for this is the oxophilicity of the aluminum catalyst and the resulting complexation by the three EEGE oxygen atoms, weakening the activation of the monomer. Interactions between the lone pairs of the chloride in ECH and iBu$_3$Al catalyst could also be the reason for the reduced activity of this monomer.
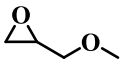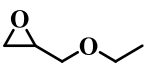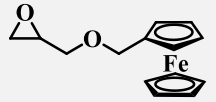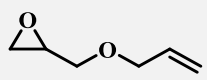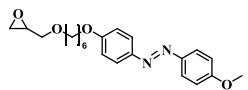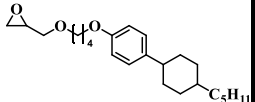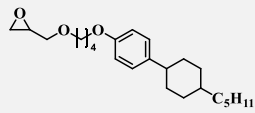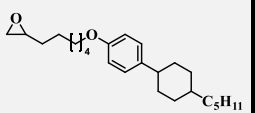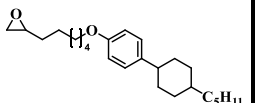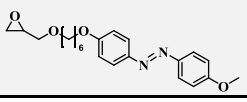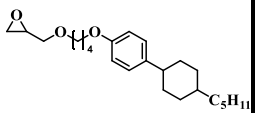
Table 5. Reactivity ratios determined for the copolymerization of PO with various glycidyl ethers, glycidyl amines, alkylene oxides and epoxide derivatives.

Comonomer structure	Comonomer name	Polymerization technique	$r_{comonomer}$	r_{PO}	Ref.
	glycidyl methy ether (GME)	con. AROP	3.15	0.305	180
	ethoxyethyl glycidyl ether (EEGE)	con. AROP	faster incorporated of EEGE		46
	N,N-diethyl glycidyl amine (DEGA)	con. AROP	0.3 0.9	1.9 1.7	180 181
	3,4-epoxy-1-butene (EPB)	con. AROP	1.0	1.0	180
	styrene oxide (SO)	con. AROP	2.07	0.62	180
	glycidyl methyl thioether (GMT)	con. AROP	4.45	0.54	180
	3,3,3-trifluoro-1,2-epoxypropane (TFEP)	con. AROP	18.0	0.16	180
	ethoxyethyl glycidyl ether (EEGE)	m. a. AROP	0.18	3.58	182
	epichlorohydrin (ECH)	m. a. AROP	0.16	1.21	110

Table 6 summarizes the copolymerization kinetics of monomers based on the to conventional AROP, in which neither PO nor EO were involved. Generally, it can be concluded that the copolymerization of two glycidyl ethers (FcGE-AGE, A-B) leads to rather random copolymers. In the copolymerization of GME and EGE, the small difference in monomer reactivity is due to the inductive effect of the alkyl groups. As a consequence of the methyl substituent in GME, this effect is less pronounced. Thus, the electron density at the oxygen atom and in the epoxide ring is lower, facilitating the attack of the nucleophilic, active chain end. In the case of the copolymerization of two alkylene oxide derivates (BO-C), the copolymerization is also ideal

and random. This is consistent with the above-mentioned copolymerization of PO with EPB. In analogy to the observations that glycidyl ethers react faster than PO, similar conclusions can also be drawn here (BO-A), whereas the difference is even more significant due to the lower reactivity of BO. With regard to glycidyl amines, it can be observed that the length of alkyl substituents has no influence on the reactivity of the monomers (cf. EO-glycidyl amine copolymers). Furthermore, the incorporation of glycidyl amines is slower in comparison to glycidyl ethers as a result of the lower electronegativity of nitrogen compared to oxygen and most likely also due to coordination effects.

Table 6. Reactivity ratios determined for the copolymerization of various glycidyl ethers, glycidyl amines and alkylene oxides polymerized by conventional AROP.

Monomer structure 1	Monomer name 1	Monomer structure 2	Monomer name 2	r_1	r_2	Ref.
	glycidyl methyl ether (GME)		ethyl glycidyl ether (EGE)	1.42	0.55	183
	ferrocenyl glycidyl ether (FcGE)		allyl glycidyl ether (AGE)	random		167
	A		B	0.96	1.02	170
	B		C	8.8	0.12	170
	butylene oxide (BO)		C	1.1	0.91	170
	butylene oxide (BO)		A	0.17	6.0	170
	butylene oxide (BO)		B	0.14	7.3	170
	N,N-dibenzyl glycidyl amine (DBAG)		*N*-benzyl-*N*-methyl glycidyl amine (BMGA)	0.91	0.98	184
	N,N-dibenzyl glycidyl amine (DBAG)		benzyl glycidyl ether (BGE)	0.80	3.24	184

An analogous survey for copolymerization kinetics according to the monomer active method can be found in **Table 7**. Structurally related monomers such as glycidyl ethers (EEGE-GME/EGE) copolymerize randomly. On the contrary, glycidyl esters as a scarcely investigated class of monomers are more reactive than glycidyl ethers (GME-GMA, EEGE-GC). This is attributable to the stronger complexation of the *i*Bu$_3$Al catalyst and the resulting lower activation of the glycidyl ethers. Concerning the copolymerization of ECH and glycidyl ethers (EEGE/AGE-ECH), resulting in gradient copolymers, the same rationale is valid.

Table 7. Reactivity ratios obtained for the copolymerization of various glycidyl ethers and various epoxide derivatives polymerized by monomer activated AROP.

Monomer structure 1	Monomer name 1	Monomer structure 2	Monomer name 2	r_1	r_2	Ref.
	ethoxyethyl glycidyl ether (EEGE)		glycidyl methyl ether (GME)	0.90	1.11	185
	ethoxyethyl glycidyl ether (EEGE)		ethyl glycidyl ether (EME)	0.98	0.95	186
	glycidyl methyl ether (GME)		glycidyl methacrylate (GMA)	0.37	1.24	119
	ethoxyethyl glycidyl ether (EEGE)		glycidyl cinnamate (GC)	0.2	2.9	Chapter 2.3
	ethoxyethyl glycidyl ether (EEGE)		epichlorohydrin (ECH)	smooth gradient (ECH faster)		109
	allyl glycidyl ether (AGE)		epichlorohydrin (ECH)	1.4	6.6	120

After this introduction, the following chapters deal with multi-functional PEGs and PGs. In addition to the synthesis and characterization, the focus was on the possible applications for these novel materials.

REFERENCES

(1) Allen, F. H.; Kennard, O.; Watson, D. G.; Brammer, L.; Orpen, A. G.; Taylor, R. Tables of bond lengths determined by X-ray and neutron diffraction. Part 1. Bond lengths in organic compounds. *J. Chem. Soc., Perkin Trans. 2* **1987**, S1, DOI: 10.1039/p298700000s1.

(2) Klein, R.; Wurm, F. R. Aliphatic Polyethers: Classical Polymers for the 21st Century. *Macromol. Rapid Commun.* **2015**, *36*, 1147–1165, DOI: 10.1002/marc.201500013.

(3) Saunders, K. J. *Organic Polymer Chemistry: An Introduction to the Organic Chemistry of Adhesives, Fibres, Paints, Plastics and Rubbers*, Second edition; Springer Netherlands: Dordrecht, 1988.

(4) Auerbach, F.; Barschall, H. Über die festen Polymeren des Formaldehyds. *Fresenius Z. Anal. Chem.* **1908**, *47*, 515–518, DOI: 10.1007/BF01362685.

(5) Staudinger, H. Hochpolymere Verbindungen. 5. Mitteilung. Über die Konstitution der Poly-oxymethylene und anderer hochpolymerer Verbindungen. *HCA* **1925**, *8*, 67–70, DOI: 10.1002/hlca.19250080113.

(6) Staudinger, H.; Lüthy, M. Hochpolymere Verbindungen. 3. Mitteilung. Über die Konstitution der Poly-oxymethylene. *HCA* **1925**, *8*, 41–64, DOI: 10.1002/hlca.19250080111.

(7) Staudinger, H.; Johner, H.; Signer, R.; Mie, G.; Hengstenberg, J. Der polymere Formaldehyd, ein Modell der Zellulose. *Z. Phys. Chem.* **1927**, *126U,* DOI: 10.1515/zpch-1927-12628.

(8) Carraher, C. E. *Introduction to polymer chemistry*, Fourth edition; Taylor & Francis: Boca Raton, London, New York, 2017.

(9) Koltzenburg, S.; Maskos, M.; Nuyken, O. *Polymer Chemistry*; Springer Berlin Heidelberg: Berlin, Heidelberg, 2017.

(10) Carraher Jr., C. E. *Introduction to Polymer Chemistry, Fourth Edition*, 4th ed.; CRC Press: Independence, 2017.

(11) Wurtz, A. Ueber das Aethylenoxyd. *Justus Liebigs Ann. Chem.* **1859**, *110*, 125–128, DOI: 10.1002/jlac.18591100116.

(12) Levene, P. A.; Walti, A. On condensation products of propylene oxide and of glycidol. *J. Biol. Chem.* **1927**, *75*, 325–336.

(13) Bailey, F. E. *Alkylene Oxides and Their Polymers*; Taylor & Francis, 1990.

(14) Franz, W. Production of polymerization products from alkylene oxides. U.S. Patent No. 1976678A.

(15) Max, W. Production of polymerization products. U.S. Patent No. 1976678A.

(16) Fife, H. R.; Roberts, F. H. Polyoxypropylene compounds. U.S. Patent No. 2448664A.

(17) Elias, H. G. *Makromoleküle: Anwendungen von Polymeren*; Wiley, 2009.

(18) Graebe, O. Marcelin Berthelot. *Ber. Dtsch. Chem. Ges.* **1908**, *41*, 4805–4872, DOI: 10.1002/cber.190804103193.

(19) Vandenberg, E. J. Discovery and Development of Epichlorohydrin Elastomers. *J. Elastomers Plast.* **1982**, *14*, 243–256, DOI: 10.1177/009524438201400405.

(20) Vandenberg, E. J. Organometallic catalysts for polymerizing monosubstituted epoxides. *J. Polym. Sci.* **1960**, *47*, 486–489, DOI: 10.1002/pol.1960.1204714947.

(21) Klingender, R. C. *Handbook of Specialty Elastomers*; CRC Press, 2008.

(22) Matyjaszewski, K. *Cationic Polymerizations: Mechanisms, Synthesis & Applications*; Taylor & Francis, 1996.

(23) Paulo, C.; Puskas, J. E.; Michel, A.; Barghi, S. *Ionic Polymerizations and Related Processes*; Springer Netherlands, 2012.

(24) Farthing, A. C.; Reynolds, R. J. W. Synthesis and properties of a new polyether: Poly-3,3-bis(chloromethyl)-1-oxabutene. *J. Polym. Sci.* **1954**, *12*, 503–507, DOI: 10.1002/pol.1954.120120142.

(25) Rose, J. B. 111. Cationic polymerisation of oxacyclobutanes. Part I. *J. Chem. Soc.* **1956**, 542, DOI: 10.1039/jr9560000542.

(26) Farthing, A. C. Preparation and polymerisation of some 3: 3-disubstituted oxacyclobutanes. *J. Chem. Soc.* **1955**, 3648, DOI: 10.1039/jr9550003648.

(27) *Handbook of Thermoplastics;* Olabisi, O., Ed.; Plastics Engineering 41; Dekker: New York, 1997.

(28) Dreyfuss, P. *Poly(tetrahydrofuran)*; Polymer monographs 8; Gordon and Breach: New York, 1982.

(29) Bhowmick, A. K.; Stephens, H. *Handbook of Elastomers, Second Edition*; Taylor & Francis, 2000.

(30) Olabisi, O.; Adewale, K. *Handbook of Thermoplastics, Second Edition*, 2nd ed.; Plastics Engineering v.41; CRC Press: Baton Rouge, 1997.

(31) Dingels, C.; Schömer, M.; Frey, H. Die vielen Gesichter des Poly(ethylenglykol)s. *Chem. unserer Zeit* **2011**, *45*, 338–349, DOI: 10.1002/ciuz.201100551.

(32) European Pharmacopoeia 7.0. Macrogels **2008**, *1444*, 2402–2404.

(33) Bailey, F. E.; Koleske, J. V. *Poly(ethylene oxide)*; Academic Press: New York, 1976.

(34) Flory, P. J. *Principles of Polymer Chemistry*; Cornell University Press: Ithaca, NY, 1953.

(35) Godovsky, Y. K.; Slonimsky, G. L.; Garbar, N. M. Effect of molecular weight on the crystallization and morphology of poly (ethylene oxide) fractions. *J. polym. sci., C Polym. symp.* **1972**, *38*, 1–21, DOI: 10.1002/polc.5070380103.

(36) Hay, J.N.; Sabir, M.; Steven, R.L.T. Crystallization kinetics of high polymers. Polyethylene oxide—Part I. *Polymer* **1969**, *10*, 187–202, DOI: 10.1016/0032-3861(69)90030-5.

(37) Fox, T. G.; Flory, P. J. Second-Order Transition Temperatures and Related Properties of Polystyrene. I. Influence of Molecular Weight. *J. Appl. Phys.* **1950**, *21*, 581–591, DOI: 10.1063/1.1699711.

(38) Faucher, J. A.; Koleske, J. V.; Santee, E. R.; Stratta, J. J.; Wilson, C. W. Glass Transitions of Ethylene Oxide Polymers. *J. Appl. Phys.* **1966**, *37*, 3962–3964, DOI: 10.1063/1.1707961.

(39) READ, B. Mechanical relaxation in some oxide polymers. *Polymer* **1962**, *3*, 529–542, DOI: 10.1016/0032-3861(62)90100-3.

(40) Wetton, R. E.; Allen, G. The dynamic mechanical properties of some polyethers. *Polymer* **1966**, *7*, 331–365, DOI: 10.1016/0032-3861(66)90028-0.

(41) Polyethylene glycol [MAK Value Documentation, 1998]. *The MAK-Collection for Occupational Health and Safety*; pp 248–270.

(42) Kjellander, R.; Florin, E. Water structure and changes in thermal stability of the system poly(ethylene oxide)–water. *J. Chem. Soc., Faraday Trans. 1* **1981**, *77*, 2053, DOI: 10.1039/f19817702053.

(43) Shikata, T.; Okuzono, M.; Sugimoto, N. Temperature-Dependent Hydration/Dehydration Behavior of Poly(ethylene oxide)s in Aqueous Solution. *Macromolecules* **2013**, *46*, 1956–1961, DOI: 10.1021/ma3026282.

(44) Lee, J.; McGrath, A. J.; Hawker, C. J.; Kim, B.-S. pH-Tunable Thermoresponsive PEO-Based Functional Polymers with Pendant Amine Groups. *ACS Macro Lett.* **2016**, *5*, 1391–1396, DOI: 10.1021/acsmacrolett.6b00830.

(45) Müller, S. S.; Moers, C.; Frey, H. A Challenging Comonomer Pair: Copolymerization of Ethylene Oxide and Glycidyl Methyl Ether to Thermoresponsive Polyethers. *Macromolecules* **2014**, *47*, 5492–5500, DOI: 10.1021/ma501280k.

(46) Schömer, M.; Frey, H. Water-Soluble "Poly(propylene oxide)" by Random Copolymerization of Propylene Oxide with a Protected Glycidol Monomer. *Macromolecules* **2012**, *45*, 3039–3046, DOI: 10.1021/ma300249c.

(47) Mangold, C.; Obermeier, B.; Wurm, F.; Frey, H. From an epoxide monomer toolkit to functional PEG copolymers with adjustable LCST behavior. *Macromol. Rapid Commun.* **2011**, *32*, 1930–1934, DOI: 10.1002/marc.201100489.

(48) Flory, P. J. Thermodynamics of High Polymer Solutions. *J. Chem. Phys.* **1942**, *10*, 51–61, DOI: 10.1063/1.1723621.

(49) Huggins, M. L. Solutions of Long Chain Compounds. *J. Chem. Phys.* **1941**, *9*, 440, DOI: 10.1063/1.1750930.

(50) Fruijtier-Pölloth, C. Safety assessment on polyethylene glycols (PEGs) and their derivatives as used in cosmetic products. *Toxicology* **2005**, *214*, 1–38, DOI: 10.1016/j.tox.2005.06.001.

(51) Veronese, F. M.; Pasut, G. PEGylation, successful approach to drug delivery. *Drug Discov. Today* **2005**, *10*, 1451–1458, DOI: 10.1016/S1359-6446(05)03575-0.

(52) Yamaoka, T.; Tabata, Y.; Ikada, Y. Fate of Water-Soluble Polymers Administered via Different Routes. *J. Pharm. Sci.* **1995**, *84*, 349–354, DOI: 10.1002/jps.2600840316.

(53) Yamaoka, T.; Tabata, Y.; Ikada, Y. Distribution and Tissue Uptake of Poly(ethylene glycol) with Different Molecular Weights after Intravenous Administration to Mice. *J. Pharm. Sci.* **1994**, *83*, 601–606, DOI: 10.1002/jps.2600830432.

(54) Jørgensen, K. E.; Møller, J. V. Use of flexible polymers as probes of glomerular pore size. *Am. J. Physiol.* **1979**, *236*, F103-11, DOI: 10.1152/ajprenal.1979.236.2.F103.

(55) Pasut, G.; Veronese, F. M. Polymer–drug conjugation, recent achievements and general strategies. *Prog. Polym. Sci.* **2007**, *32*, 933–961, DOI: 10.1016/j.progpolymsci.2007.05.008.

(56) Markovsky, E.; Baabur-Cohen, H.; Eldar-Boock, A.; Omer, L.; Tiram, G.; Ferber, S.; Ofek, P.; Polyak, D.; Scomparin, A.; Satchi-Fainaro, R. Administration, distribution, metabolism and elimination of polymer therapeutics. *J. Control. Release* **2012**, *161*, 446–460, DOI: 10.1016/j.jconrel.2011.12.021.

(57) Jang, H.-J.; Shin, C. Y.; Kim, K.-B. Safety Evaluation of Polyethylene Glycol (PEG) Compounds for Cosmetic Use. *Toxicol. Res.* **2015**, *31*, 105–136, DOI: 10.5487/TR.2015.31.2.105.

(58) *Gibaldi's drug delivery systems in pharmaceutical care;* Desai, A.; Lee, M., Eds.; American Society of Health-System Pharmacists: Bethesda, MD, 2007.

(59) Glastrup, J.; Shashoua, Y.; Egsgaard, H.; Mortensen, M. N. Degradation of PEG in the Warship Vasa. *Macromol. Symp.* **2006**, *238*, 22–29, DOI: 10.1002/masy.200650604.

(60) Graebel, W. P. *Engineering fluid mechanics*, Internat. student ed.; Taylor & Francis: New York, 2001.

(61) Pitto-Barry, A.; Barry, N. P. E. Pluronic® block-copolymers in medicine: from chemical and biological versatility to rationalisation and clinical advances. *Polym. Chem.* **2014**, *5*, 3291–3297, DOI: 10.1039/C4PY00039K.

(62) Almeida, M.; Magalhães, M.; Veiga, F.; Figueiras, A. Poloxamers, poloxamines and polymeric micelles: Definition, structure and therapeutic applications in cancer. *J. Polym. Res.* **2018**, *25*, 248, DOI: 10.1007/s10965-017-1426-x.

(63) Pelegri-O'Day, E. M.; Lin, E.-W.; Maynard, H. D. Therapeutic Protein–Polymer Conjugates: Advancing Beyond PEGylation. *J. Am. Chem. Soc.* **2014**, *136*, 14323–14332, DOI: 10.1021/ja504390x.

(64) Knop, K.; Hoogenboom, R.; Fischer, D.; Schubert, U. S. Poly(ethylene glycol) in Drug Delivery: Pros and Cons as Well as Potential Alternatives. *Angew. Chem. Int. Ed.* **2010**, *49*, 6288–6308, DOI: 10.1002/anie.200902672.

(65) Lourenço, A. V. Intermediäre Aether des Glykols. *J. Prakt. Chem.* **1860**, *79*, 212–213, DOI: 10.1002/prac.18600790130.

(66) Lourenço, A. V. Ueber die Polyäthylenalkohole. *J. Prakt. Chem.* **1862**, *85*, 389–392, DOI: 10.1002/prac.18620850149.

(67) Wurtz, A. Neue Untersuchungen über das Aethylenoxyd. *Justus Liebigs Ann. Chem.* **1860**, *116*, 249–252, DOI: 10.1002/jlac.18601160212.

(68) Wurtz, A. Synthese des Glycols aus Aethylenoxyd und Wasser. *Justus Liebigs Ann. Chem.* **1860**, *113*, 255–256, DOI: 10.1002/jlac.18601130218.

(69) Staudinger, H.; Schweitzer, O. Über hochpolymere Verbindungen, 20. Mitteil.: Über die Poly-äthylenoxyde. *Ber. dtsch. Chem. Ges. A/B* **1929**, *62*, 2395–2405, DOI: 10.1002/cber.19290620879.

(70) Staudinger, H.; Lohmann, H. Über hochpolymere Verbindungen. 81. Mitteilung. Über eukolloides Polyäthylenoxyd. *Justus Liebigs Ann. Chem.* **1933**, *505*, 41–51, DOI: 10.1002/jlac.19335050104.

(71) Flory, P. J. Molecular Size Distribution in Ethylene Oxide Polymers. *J. Am. Chem. Soc.* **1940**, *62*, 1561–1565, DOI: 10.1021/ja01863a066.

(72) PENCZEK, S.; CYPRYK, M.; DUDA, A.; KUBISA, P.; Slomkowski, S. Living ring-opening polymerizations of heterocyclic monomers. *Prog. Polym. Sci.* **2007**, *32*, 247–282, DOI: 10.1016/j.progpolymsci.2007.01.002.

(73) Sasaki, H. Oxetanes: Curing Properties in Photo-Cationic Polymerization. *J. Photopol. Sci. Technol.* **2000**, *13*, 119–124, DOI: 10.2494/photopolymer.13.119.

(74) Quirk, R. P.; Lee, B. Experimental Criteria for Living Polymerizations. *Polym. Int.* **1992**, *27*, 359–367, DOI: 10.1002/pi.4990270412.

(75) Adolphs, P.; Alberts, H.; Bachem, H.; Bartl, H.; Bieringer, H. *Houben-Weyl Methods of Organic Chemistry Vol. E 20, 4th Edition Supplement: Macromolecular Compounds*; Thieme Georg Verlag, 2014.

(76) *Anionic Polymerization: Principles, Practice, Strength, Consequences and Applications;* Hadjichristidis, N.; Hirao, A., Eds., 1st ed. 2015; Springer: Tokyo, 2015.

(77) Solov'yanov, A. A.; Kazanskii, K. S. The kinetics and mechanism of anionic polymerization of ethylene oxide in ether solvents. *Polym. Sci. USSR* **1972**, *14*, 1186–1195, DOI: 10.1016/0032-3950(72)90162-1.

(78) Brocas, A.-L.; Mantzaridis, C.; Tunc, D.; Carlotti, S. Polyether synthesis: From activated or metal-free anionic ring-opening polymerization of epoxides to functionalization. *Prog. Polym. Sci.* **2013**, *38*, 845–873, DOI: 10.1016/j.progpolymsci.2012.09.007.

(79) Deffieux, A.; Boileau, S. Anionic polymerization of ethylene oxide with cryptates as counterions: 1. *Polymer* **1977**, *18*, 1047–1050, DOI: 10.1016/0032-3861(77)90011-8.

(80) Deffieux, A.; Graf, E.; Boileau, S. Anionic polymerization of ethylene oxide with cryptates as counterions: 2. *Polymer* **1981**, *22*, 549–552, DOI: 10.1016/0032-3861(81)90178-6.

(81) Ding, J.; Price, C.; Booth, C. Use of crown ether in the anionic polymerization of propylene oxide—1. Rate of polymerization. *Eur. Polym. J.* **1991**, *27*, 891–894, DOI: 10.1016/0014-3057(91)90028-M.

(82) Pearson, R. G. Hard and Soft Acids and Bases. *J. Am. Chem. Soc.* **1963**, *85*, 3533–3539, DOI: 10.1021/ja00905a001.

(83) Kazanskii, K. S.; Solovyanov, A. A.; Entelis, S. G. Polymerization of ethylene oxide by alkali metal-naphthalene complexes in tetrahydrofuran. *Eur. Polym. J.* **1971**, *7*, 1421–1433, DOI: 10.1016/0014-3057(71)90036-X.

(84) Boileau, S. Anionic Ring-opening Polymerization: Epoxides and Episulfides. In *Comprehensive polymer science and supplements*; Allen, G., Ed.; [Elsevier]: [New York.], 1996; pp 467–487.

(85) Thompson, M. S.; Vadala, T. P.; Vadala, M. L.; Lin, Y.; Riffle, J. S. Synthesis and applications of heterobifunctional poly(ethylene oxide) oligomers. *Polymer* **2008**, *49*, 345–373, DOI: 10.1016/j.polymer.2007.10.029.

(86) Herzberger, J.; Niederer, K.; Pohlit, H.; Seiwert, J.; Worm, M.; Wurm, F. R.; Frey, H. Polymerization of Ethylene Oxide, Propylene Oxide, and Other Alkylene Oxides: Synthesis, Novel Polymer Architectures, and Bioconjugation. *Chem. Rev.* **2016**, *116*, 2170–2243, DOI: 10.1021/acs.chemrev.5b00441.

(87) Mosquet, M.; Chevalier, Y.; Le Perchec, P.; Guicquero, J.-P. Synthesis of poly(ethylene oxide) with a terminal amino group by anionic polymerization of ethylene oxide initiated by aminoalcoholates. *Macromol. Chem. Phys.* **1997**, *198*, 2457–2474, DOI: 10.1002/macp.1997.021980808.

(88) Yamamoto, Y.; Nakao, W.; Atago, Y.; Ito, K.; Yagci, Y. A novel macroinimer of polyethylene oxide: synthesis of hyper branched networks by photoinduced H-abstraction process. *Eur. Polym. J.* **2003**, *39*, 545–550, DOI: 10.1016/S0014-3057(02)00273-2.

(89) Yokoyama, M.; Okano, T.; Sakurai, Y.; Kikuchi, A.; Ohsako, N.; Nagasaki, Y.; Kataoka, K. Synthesis of poly(ethylene oxide) with heterobifunctional reactive groups at its terminals by an anionic initiator. *Bioconjugate Chem.* **1992**, *3*, 275–276, DOI: 10.1021/bc00016a003.

(90) Yang, S.; Kim, Y.; Kim, H. C.; Siddique, A. B.; Youn, G.; Kim, H. J.; Park, H. J.; Lee, J. Y.; Kim, S.; Kim, J. Azide-based heterobifunctional poly(ethylene oxide)s: NaN 3 -initiated "living" polymerization of ethylene oxide and chain end functionalizations. *Polym. Chem.* **2016**, *7*, 394–401, DOI: 10.1039/C5PY01444A.

(91) Zeng, F.; Allen, C. Synthesis of Carboxy-Functionalized Heterobifunctional Poly(ethylene glycol) by a Thiol-Anionic Polymerization Method. *Macromolecules* **2006**, *39*, 6391–6398, DOI: 10.1021/ma0607665.

(92) Li, Z.; Chau, Y. Synthesis of heterobifunctional poly(ethylene glycol)s by an acetal protection method. *Polym. Chem.* **2010**, *1*, 1599, DOI: 10.1039/c0py00310g.

(93) Dingels, C.; Müller, S. S.; Steinbach, T.; Tonhauser, C.; Frey, H. Universal concept for the implementation of a single cleavable unit at tunable position in functional poly(ethylene glycol)s. *Biomacromolecules* **2013**, *14*, 448–459, DOI: 10.1021/bm3016797.

(94) Akiyama, Y.; Nagasaki, Y.; Kataoka, K. Synthesis of heterotelechelic poly(ethylene glycol) derivatives having alpha-benzaldehyde and omega-pyridyl disulfide groups by ring opening polymerization of ethylene oxide using 4-(diethoxymethyl)benzyl alkoxide as a novel initiator. *Bioconjugate Chem.* **2004**, *15*, 424–427, DOI: 10.1021/bc0341775.

(95) Studer, P.; Limal, D.; Breton, P.; Riess, G. Synthesis and characterization of poly(ethylene oxide)-block-poly(methylidene malonate 2.1.2) block copolymers bearing a mannose group at the PEO chain end. *Bioconjugate Chem.* **2005**, *16*, 223–229, DOI: 10.1021/bc0498065.

(96) Otsuka, H.; Nagasaki, Y.; Kataoka, K. Characterization of aldehyde-PEG tethered surfaces: influence of PEG chain length on the specific biorecognition. *Langmuir* **2004**, *20*, 11285–11287, DOI: 10.1021/la0483414.

(97) Thomas, A.; Bauer, H.; Schilmann, A.-M.; Fischer, K.; Tremel, W.; Frey, H. The "Needle in the Haystack" Makes the Difference: Linear and Hyperbranched Polyglycerols with a Single Catechol Moiety for Metal Oxide Nanoparticle Coating. *Macromolecules* **2014**, *47*, 4557–4566, DOI: 10.1021/ma5003672.

(98) Hiki, S.; Kataoka, K. Versatile and selective synthesis of "click chemistry" compatible heterobifunctional poly(ethylene glycol)s possessing azide and alkyne functionalities. *Bioconjugate Chem.* **2010**, *21*, 248–254, DOI: 10.1021/bc900253p.

(99) Yagci, Y.; Ito, K. Macromolecular Architecture Based on Anionically Prepared Poly(ethylene oxide) Macromonomers. *Macromol. Symp.* **2005**, *226*, 87–96, DOI: 10.1002/masy.200550809.

(100) Ishii, T.; Yamada, M.; Hirase, T.; Nagasaki, Y. New Synthesis of Heterobifunctional Poly(ethylene glycol) Possessing a Pyridyl Disulfide at One End and a Carboxylic Acid at the Other End. *Polym. J.* **2005**, *37*, 221–228, DOI: 10.1295/polymj.37.221.

(101) Aida, T.; Inoue, S. Living polymerization of epoxides with metalloporphyrin and synthesis of block copolymers with controlled chain lengths. *Macromolecules* **1981**, *14*, 1162–1166, DOI: 10.1021/ma50006a004.

(102) Aida, T.; Mizuta, R.; Yoshida, Y.; Inoue, S. Polymerization of Epoxides Catalysed by Metalloporphine. *Makromol. Chem.* **1981**, *182*, 1073–1079, DOI: 10.1002/macp.1981.021820408.

(103) Sugimoto, H.; Kawamura, C.; Kuroki, M.; Aida, T.; Inoue, S. Lewis Acid-Assisted Anionic Ring-Opening Polymerization of Epoxide by the Aluminum Complexes of Porphyrin, Phthalocyanine, Tetraazaannulene, and Schiff Base as Initiators. *Macromolecules* **1994**, *27*, 2013–2018, DOI: 10.1021/ma00086a006.

(104) Tsvetanov, C. B.; Petrova, E. B.; Panayotov, I. M. Polymerization of 1,2-Epoxides Initiated by Tetraalkyl Aluminates. 1. Polymerization of Ethylene Oxide in the Presence of Sodium Tetrabutyl Aluminate. *J. Macromol. Sci., Chem.* **1985**, *22*, 1309–1324, DOI: 10.1080/00222338508063335.

(105) Braune, W.; Okuda, J. An Efficient Method for Controlled Propylene Oxide Polymerization: The Significance of Bimetallic Activation in Aluminum Lewis Acids. *Angew. Chem. Int. Ed.* **2003**, *42*, 64–68, DOI: 10.1002/anie.200390054.

(106) Billouard, C.; Carlotti, S.; Desbois, P.; Deffieux, A. "Controlled" High-Speed Anionic Polymerization of Propylene Oxide Initiated by Alkali Metal Alkoxide/Trialkylaluminum Systems. *Macromolecules* **2004**, *37*, 4038–4043, DOI: 10.1021/ma035768t.

(107) Carlotti, S.; Desbois, P.; Billouard, C.; Deffieux, A. Reactivity control in anionic polymerization of ethylenic and heterocyclic monomers through formation of 'ate' complexes. *Polym. Int.* **2006**, *55*, 1126–1131, DOI: 10.1002/pi.1981.

(108) Brocas, A.-L.; Gervais, M.; Carlotti, S.; Pispas, S. Amphiphilic diblock copolymers based on ethylene oxide and epoxides bearing aliphatic side chains. *Polym. Chem.* **2012**, *3*, 2148, DOI: 10.1039/c2py20189e.

(109) Meyer, J.; Keul, H.; Möller, M. Poly(glycidyl amine) and Copolymers with Glycidol and Glycidyl Amine Repeating Units: Synthesis and Characterization. *Macromolecules* **2011**, *44*, 4082–4091, DOI: 10.1021/ma200757v.

(110) Carlotti, S.; Labbé, A.; Rejsek, V.; Doutaz, S.; Gervais, M.; Deffieux, A. Living/Controlled Anionic Polymerization and Copolymerization of Epichlorohydrin with Tetraoctylammonium Bromide−Triisobutylaluminum Initiating Systems. *Macromolecules* **2008**, *41*, 7058–7062, DOI: 10.1021/ma801422c.

(111) Rejsek, V.; Sauvanier, D.; Billouard, C.; Desbois, P.; Deffieux, A.; Carlotti, S. Controlled Anionic Homo- and Copolymerization of Ethylene Oxide and Propylene Oxide by Monomer Activation. *Macromolecules* **2007**, *40*, 6510–6514, DOI: 10.1021/ma070450c.

(112) Gervais, M.; Labbé, A.; Carlotti, S.; Deffieux, A. Direct Synthesis of α-Azido,ω-hydroxypolyethers by Monomer-Activated Anionic Polymerization. *Macromolecules* **2009**, *42*, 2395–2400, DOI: 10.1021/ma802063s.

(113) Sakakibara, K.; Nakano, K.; Nozaki, K. Regio-controlled ring-opening polymerization of perfluoroalkyl-substituted epoxides. *Chem. Commun.* **2006**, *0*, 3334–3336, DOI: 10.1039/b606693c.

(114) Roos, K.; Carlotti, S. Grignard-based anionic ring-opening polymerization of propylene oxide activated by triisobutylaluminum. *Eur. Polym. J.* **2015**, *70*, 240–246, DOI: 10.1016/j.eurpolymj.2015.07.016.

(115) Herzberger, J.; Frey, H. Epicyanohydrin: Polymerization by Monomer Activation Gives Access to Nitrile-, Amino-, and Carboxyl-Functional Poly(ethylene glycol). *Macromolecules* **2015**, *48*, 8144–8153, DOI: 10.1021/acs.macromol.5b02178.

(116) Labbé, A.; Carlotti, S.; Billouard, C.; Desbois, P.; Deffieux, A. Controlled High-Speed Anionic Polymerization of Propylene Oxide Initiated by Onium Salts in the Presence of Triisobutylaluminum. *Macromolecules* **2007**, *40*, 7842–7847, DOI: 10.1021/ma070288d.

(117) Stöbener, D. D.; Uckert, M.; Cuellar-Camacho, J. L.; Hoppensack, A.; Weinhart, M. Ultrathin Poly(glycidyl ether) Coatings on Polystyrene for Temperature-Triggered Human Dermal Fibroblast Sheet Fabrication. *ACS Biomater. Sci. Eng.* **2017**, *3*, 2155–2165, DOI: 10.1021/acsbiomaterials.7b00270.

(118) Herzberger, J.; Leibig, D.; Langhanki, J.; Moers, C.; Opatz, T.; Frey, H. "Clickable PEG" via anionic copolymerization of ethylene oxide and glycidyl propargyl ether. *Polym. Chem.* **2017**, *8*, 1882–1887, DOI: 10.1039/C7PY00173H.

(119) Labbé, A.; Brocas, A.-L.; Ibarboure, E.; Ishizone, T.; Hirao, A.; Deffieux, A.; Carlotti, S. Selective Ring-Opening Polymerization of Glycidyl Methacrylate: Toward the Synthesis of

Cross-Linked (Co)polyethers with Thermoresponsive Properties. *Macromolecules* **2011**, *44*, 6356–6364, DOI: 10.1021/ma201075n.

(120) Brocas, A.-L.; Cendejas, G.; Caillol, S.; Deffieux, A.; Carlotti, S. Controlled synthesis of polyepichlorohydrin with pendant cyclic carbonate functions for isocyanate-free polyurethane networks. *J. Polym. Sci. A Polym. Chem.* **2011**, *49*, 2677–2684, DOI: 10.1002/pola.24699.

(121) Sakakibara, K.; Nakano, K.; Nozaki, K. Regioregular Polymerization of Fluorine-Containing Epoxides. *Macromolecules* **2007**, *40*, 6136–6142, DOI: 10.1021/ma070428j.

(122) Obermeier, B.; Wurm, F.; Mangold, C.; Frey, H. Multifunctional Poly(ethylene glycol)s. *Angew. Chem. Int. Ed. (English)* **2011**, *50*, 7988–7997, DOI: 10.1002/anie.201100027.

(123) Koyama, Y.; Umehara, M.; Mizuno, A.; Itaba, M.; Yasukouchi, T.; Natsume, K.; Suginaka, A. Synthesis of novel poly(ethylene glycol) derivatives having pendant amino groups and aggregating behavior of its mixture with fatty acid in water. *Bioconjugate Chem.* **1996**, *7*, 298–301, DOI: 10.1021/bc9600123.

(124) Taton, D.; Le Borgne, A.; Sepulchre, M.; Spassky, N. Synthesis of chiral and racemic functional polymers from glycidol and thioglycidol. *Macromol. Chem. Phys.* **1994**, *195*, 139–148, DOI: 10.1002/macp.1994.021950111.

(125) Mangold, C.; Wurm, F.; Frey, H. Functional PEG-based polymers with reactive groups via anionic ROP of tailor-made epoxides. *Polym. Chem.* **2012**, *3*, 1714, DOI: 10.1039/c2py00489e.

(126) Kurzbach, D.; Wilms, V. S.; Frey, H.; Hinderberger, D. Impact of Amino-Functionalization on the Response of Poly(ethylene glycol) (PEG) to External Stimuli. *ACS Macro Lett.* **2013**, *2*, 128–131, DOI: 10.1021/mz300596r.

(127) Reuss, V. S.; Werre, M.; Frey, H. Thermoresponsive copolymers of ethylene oxide and N,N-diethyl glycidyl amine: polyether polyelectrolytes and PEGylated gold nanoparticle formation. *Macromol. Rapid Commun.* **2012**, *33*, 1556–1561, DOI: 10.1002/marc.201200307.

(128) Tonhauser, C.; Alkan, A.; Schömer, M.; Dingels, C.; Ritz, S.; Mailänder, V.; Frey, H.; Wurm, F. R. Ferrocenyl Glycidyl Ether: A Versatile Ferrocene Monomer for Copolymerization with Ethylene Oxide to Water-Soluble, Thermoresponsive Copolymers. *Macromolecules* **2013**, *46*, 647–655, DOI: 10.1021/ma302241w.

(129) Niederer, K.; Schüll, C.; Leibig, D.; Johann, T.; Frey, H. Catechol Acetonide Glycidyl Ether (CAGE): A Functional Epoxide Monomer for Linear and Hyperbranched Multi-Catechol Functional Polyether Architectures. *Macromolecules* **2016**, *49*, 1655–1665, DOI: 10.1021/acs.macromol.5b02441.

(130) Lowe, A. B. Thiol–ene "click" reactions and recent applications in polymer and materials synthesis: A first update. *Polym. Chem.* **2014**, *5*, 4820, DOI: 10.1039/C4PY00339J.

(131) Hoyle, C. E.; Bowman, C. N. Thiol-ene click chemistry. *Angew. Chem. Int. Ed.* **2010**, *49*, 1540–1573, DOI: 10.1002/anie.200903924.

(132) Hall, D. J.; van den Berghe, H. M.; Dove, A. P. Synthesis and post-polymerization modification of maleimide-containing polymers by 'thiol-ene' click and Diels-Alder chemistries. *Polym. Int.* **2011**, *60*, 1149–1157, DOI: 10.1002/pi.3121.

(133) Sanyal, A. Diels-Alder Cycloaddition-Cycloreversion: A Powerful Combo in Materials Design. *Macromol. Chem. Phys.* **2010**, *211*, 1417–1425, DOI: 10.1002/macp.201000108.

(134) Obermeier, B.; Frey, H. Poly(ethylene glycol-co-allyl glycidyl ether)s: a PEG-based modular synthetic platform for multiple bioconjugation. *Bioconjugate Chem.* **2011**, *22*, 436–444, DOI: 10.1021/bc1004747.

(135) Mangold, C.; Dingels, C.; Obermeier, B.; Frey, H.; Wurm, F. PEG-based Multifunctional Polyethers with Highly Reactive Vinyl-Ether Side Chains for Click-Type Functionalization. *Macromolecules* **2011**, *44*, 6326–6334, DOI: 10.1021/ma200898n.

(136) Barthel, M. J.; Rudolph, T.; Crotty, S.; Schacher, F. H.; Schubert, U. S. Homo- and diblock copolymers of poly(furfuryl glycidyl ether) by living anionic polymerization: Toward reversibly core-crosslinked micelles. *J. Polym. Sci. A Polym. Chem.* **2012**, *50*, 4958–4965, DOI: 10.1002/pola.26327.

(137) Barthel, M. J.; Rudolph, T.; Teichler, A.; Paulus, R. M.; Vitz, J.; Hoeppener, S.; Hager, M. D.; Schacher, F. H.; Schubert, U. S. Self-Healing Materials via Reversible Crosslinking of Poly(ethylene oxide)- Block -Poly(furfuryl glycidyl ether) (PEO- b -PFGE) Block Copolymer Films. *Adv. Funct. Mater.* **2013**, *23*, 4921–4932, DOI: 10.1002/adfm.201300469.

(138) Li, Z.; Chau, Y. Synthesis of linear polyether polyol derivatives as new materials for bioconjugation. *Bioconjugate Chem.* **2009**, *20*, 780–789, DOI: 10.1021/bc900036f.

(139) Herzberger, J.; Fischer, K.; Leibig, D.; Bros, M.; Thiermann, R.; Frey, H. Oxidation-Responsive and "Clickable" Poly(ethylene glycol) via Copolymerization of 2-(Methylthio)ethyl Glycidyl Ether. *J. Am. Chem. Soc.* **2016**, *138*, 9212–9223, DOI: 10.1021/jacs.6b04548.

(140) Herzberger, J.; Leibig, D.; Liermann, J. C.; Frey, H. Conventional Oxyanionic versus Monomer-Activated Anionic Copolymerization of Ethylene Oxide with Glycidyl Ethers: Striking Differences in Reactivity Ratios. *ACS Macro Lett.* **2016**, *5*, 1206–1211, DOI: 10.1021/acsmacrolett.6b00701.

(141) Chisholm, M. H.; Navarro-Llobet, D. NMR Assignments of Regioregular Poly(propylene oxide) at the Triad and Tetrad Level. *Macromolecules* **2002**, *35*, 2389–2392, DOI: 10.1021/ma0119934.

(142) Stolarzewicz, A. A new chain transfer reaction in the anionic polymerization of 2,3-epoxypropyl phenyl ether and other oxiranes. *Makromol. Chem.* **1986**, *187*, 745–752, DOI: 10.1002/macp.1986.021870405.

(143) Price, C. C.; Atarashi, Y.; Yamamoto, R. Polymerization and copolymerization of some epoxides by potassium tert-butoxide in DMSO. *J. Polym. Sci. A-1 Polym. Chem.* **1969**, *7*, 569–574, DOI: 10.1002/pol.1969.150070211.

(144) Hans, M.; Keul, H.; Moeller, M. Chain transfer reactions limit the molecular weight of polyglycidol prepared via alkali metal based initiating systems. *Polymer* **2009**, *50*, 1103–1108, DOI: 10.1016/j.polymer.2009.01.012.

(145) Cowie, J.M.G.; Arrighi, V. *Polymers: Chemistry and Physics of Modern Materials, Third Edition*, 3rd ed.; CRC Press: Hoboken, 2007.

(146) Beginn, U. Gradient copolymers. *Kolloid-Z.* **2008**, *286*, 1465–1474, DOI: 10.1007/s00396-008-1922-y.

(147) Zaremski, M. Y.; Di Kalugin; Golubev, V. B. Gradient copolymers: Synthesis, structure, and properties. *Polym. Sci. Ser. A* **2009**, *51*, 103–122.

(148) Matyjaszewski, K.; Ziegler, M. J.; Arehart, S. V.; Greszta, D.; Pakula, T. Gradient copolymers by atom transfer radical copolymerization. *J. Phys. Org. Chem.* **2000**, *13*, 775–786, DOI: 10.1002/1099-1395(200012)13:12<775:AID-POC314>3.0.CO;2-D.

(149) Karaky, K.; Clisson, G.; Reiter, G.; Billon, L. Semicrystalline Macromolecular Design by Nitroxide-Mediated Polymerization. *Macromol. Chem. Phys.* **2008**, *209*, 715–722, DOI: 10.1002/macp.200700578.

(150) Okabe, S.; Fuse, C.; Sugihara, S.; Aoshima, S.; Shibayama, M. Structural transition in block and gradient copolymer aqueous solutions. *Physica B* **2006**, *385-386*, 756–758, DOI: 10.1016/j.physb.2006.06.055.

(151) Okabe, S.; Seno, K.-i.; Kanaoka, S.; Aoshima, S.; Shibayama, M. Micellization Study on Block and Gradient Copolymer Aqueous Solutions by DLS and SANS. *Macromolecules* **2006**, *39*, 1592–1597, DOI: 10.1021/ma052334k.

(152) Louai, A.; Sarazin, D.; Pollet, G.; François, J.; Moreaux, F. Properties of ethylene oxide-propylene oxide statistical copolymers in aqueous solution. *Polymer* **1991**, *32*, 703–712, DOI: 10.1016/0032-3861(91)90484-Z.

(153) Rudnick, L. R.; Shubkin, R. L. *Synthetic lubricants and high-performance functional fluids*, 2nd ed., rev. and expanded.; Chemical industries 77; Marcel Dekker: New York, 1999.

(154) Chiappetta, D. A.; Sosnik, A. Poly(ethylene oxide)-poly(propylene oxide) block copolymer micelles as drug delivery agents: improved hydrosolubility, stability and bioavailability of drugs. *Eur. J. Pharm. Biopharm.* **2007**, *66*, 303–317, DOI: 10.1016/j.ejpb.2007.03.022.

(155) Kim, J.; Gray, M. K.; Zhou, H.; Nguyen, S. T.; Torkelson, J. M. Polymer Blend Compatibilization by Gradient Copolymer Addition during Melt Processing: Stabilization of Dispersed Phase to Static Coarsening. *Macromolecules* **2005**, *38*, 1037–1040, DOI: 10.1021/ma047549t.

(156) Kim, J.; Mok, M. M.; Sandoval, R. W.; Woo, D. J.; Torkelson, J. M. Uniquely Broad Glass Transition Temperatures of Gradient Copolymers Relative to Random and Block Copolymers Containing Repulsive Comonomers. *Macromolecules* **2006**, *39*, 6152–6160, DOI: 10.1021/ma061241f.

(157) Mok, M. M.; Kim, J.; Torkelson, J. M. Gradient copolymers with broad glass transition temperature regions: Design of purely interphase compositions for damping applications. *J. Polym. Sci. B Polym. Phys.* **2008**, *46*, 48–58, DOI: 10.1002/polb.21341.

(158) Zhang, J.; Farias-Mancilla, B.; Destarac, M.; Schubert, U. S.; Keddie, D. J.; Guerrero-Sanchez, C.; Harrisson, S. Asymmetric Copolymers: Synthesis, Properties, and Applications of Gradient and Other Partially Segregated Copolymers. *Macromol. Rapid Commun.* **2018**, *39*, e1800357, DOI: 10.1002/marc.201800357.

(159) Mayo, F. R.; Lewis, F. M. Copolymerization. I. A Basis for Comparing the Behavior of Monomers in Copolymerization; The Copolymerization of Styrene and Methyl Methacrylate. *J. Am. Chem. Soc.* **1944**, *66*, 1594–1601, DOI: 10.1021/ja01237a052.

(160) Fineman, M.; Ross, S. D. Linear method for determining monomer reactivity ratios in copolymerization. *J. Polym. Sci.* **1950**, *5*, 259–262, DOI: 10.1002/pol.1950.120050210.

(161) Kelen, T.; Tüdos, F. Analysis of the Linear Methods for Determining Copolymerization Reactivity Ratios. I. A New Improved Linear Graphic Method. *J. Macromol. Sci., Chem.* **1975**, *9*, 1–27, DOI: 10.1080/00222337508068644.

(162) Pasquale, A. J.; Long, T. E. Real-Time Monitoring of the Stable Free Radical Polymerization of Styrene via in-Situ Mid-Infrared Spectroscopy. *Macromolecules* **1999**, *32*, 7954–7957, DOI: 10.1021/ma9912498.

(163) Long, T. E.; Liu, H. Y.; Schell, B. A.; Teegarden, D. M.; Uerz, D. S. Determination of solution polymerization kinetics by near-infrared spectroscopy. 1. Living anionic polymerization processes. *Macromolecules* **1993**, *26*, 6237–6242, DOI: 10.1021/ma00075a018.

(164) Quinebèche, S.; Navarro, C.; Gnanou, Y.; Fontanille, M. In situ mid-IR and UV–visible spectroscopies applied to the determination of kinetic parameters in the anionic copolymerization of styrene and isoprene. *Polymer* **2009**, *50*, 1351–1357, DOI: 10.1016/j.polymer.2009.01.041.

(165) Alb, A. M.; Enohnyaket, P.; Drenski, M. F.; Head, A.; Reed, A. W.; Reed, W. F. Online Monitoring of Copolymerization Involving Comonomers of Similar Spectral Characteristics. *Macromolecules* **2006**, *39*, 5705–5713, DOI: 10.1021/ma060800f.

(166) Obermeier, B.; Wurm, F.; Frey, H. Amino Functional Poly(ethylene glycol) Copolymers via Protected Amino Glycidol. *Macromolecules* **2010**, *43*, 2244–2251, DOI: 10.1021/ma902245d.

(167) Alkan, A.; Natalello, A.; Wagner, M.; Frey, H.; Wurm, F. R. Ferrocene-Containing Multifunctional Polyethers: Monomer Sequence Monitoring via Quantitative 13 C NMR Spectroscopy in Bulk. *Macromolecules* **2014**, *47*, 2242–2249, DOI: 10.1021/ma500323m.

(168) Son, S.; Shin, E.; Kim, B.-S. Redox-Degradable Biocompatible Hyperbranched Polyglycerols: Synthesis, Copolymerization Kinetics, Degradation, and Biocompatibility. *Macromolecules* **2015**, *48*, 600–609, DOI: 10.1021/ma502242v.

(169) Beckingham, B. S.; Sanoja, G. E.; Lynd, N. A. Simple and Accurate Determination of Reactivity Ratios Using a Nonterminal Model of Chain Copolymerization. *Macromolecules* **2015**, *48*, 6922–6930, DOI: 10.1021/acs.macromol.5b01631.

(170) Wu, Z.; Liu, P.; Liu, Y.; Wei, W.; Zhang, X.; Wang, P.; Xu, Z.; Xiong, H. Regulating sequence distribution of polyethers via ab initio kinetics control in anionic copolymerization. *Polym. Chem.* **2017**, *8*, 5673–5678, DOI: 10.1039/C7PY01073G.

(171) Zhang, W.; Allgaier, J.; Zorn, R.; Willbold, S. Determination of the Compositional Profile for Tapered Copolymers of Ethylene Oxide and 1,2-Butylene Oxide by In-situ-NMR. *Macromolecules* **2013**, *46*, 3931–3938, DOI: 10.1021/ma400166n.

(172) Lee, B. F.; Wolffs, M.; Delaney, K. T.; Sprafke, J. K.; Leibfarth, F. A.; Hawker, C. J.; Lynd, N. A. Reactivity ratios, and mechanistic insight for anionic ring-opening copolymerization of epoxides. *Macromolecules* **2012**, *45*, 3722–3731, DOI: 10.1021/ma300634d.

(173) Mangold, C.; Wurm, F.; Obermeier, B.; Frey, H. Hetero-Multifunctional Poly(ethylene glycol) Copolymers with Multiple Hydroxyl Groups and a Single Terminal Functionality. *Macromol. Rapid Commun.* **2010**, *31*, 258–264, DOI: 10.1002/marc.200900472.

(174) Lee, A.; Lundberg, P.; Klinger, D.; Lee, B. F.; Hawker, C. J.; Lynd, N. A. Physiologically relevant, pH-responsive PEG-based block and statistical copolymers with N,N-diisopropylamine units. *Polym. Chem.* **2013**, *4*, 5735–5742, DOI: 10.1039/C3PY00747B.

(175) Alkan, A.; Gleede, T.; Wurm, F. R. Ruthenocenyl Glycidyl Ether: A Ruthenium-Containing Epoxide for Anionic Polymerization. *Organometallics* **2017**, *36*, 3023–3028, DOI: 10.1021/acs.organomet.7b00278.

(176) Stolarzewicz, A.; Neugebauer, D. Influence of substituent on the polymerization of oxiranes by potassium hydride. *Macromol. Chem. Phys.* **1999**, *200*, 2467–2470, DOI: 10.1002/(SICI)1521-3935(19991101)200:11<2467:AID-MACP2467>3.0.CO;2-3.

(177) Herzberger, J.; Kurzbach, D.; Werre, M.; Fischer, K.; Hinderberger, D.; Frey, H. Stimuli-Responsive Tertiary Amine Functional PEGs Based on N,N -Dialkylglycidylamines. *Macromolecules* **2014**, *47*, 7679–7690, DOI: 10.1021/ma501367b.

(178) Reuss, V. S.; Obermeier, B.; Dingels, C.; Frey, H. N,N -Diallylglycidylamine: A Key Monomer for Amino-Functional Poly(ethylene glycol) Architectures. *Macromolecules* **2012**, *45*, 4581–4589, DOI: 10.1021/ma300292m.

(179) Heatley, F.; Yu, G.-E.; Booth, C.; Blease, T. G. Determination of reactivity ratios for the anionic copolymerization of ethylene oxide and propylene oxide in bulk. *Eur. Polym. J.* **1991**, *27*, 573–579, DOI: 10.1016/0014-3057(91)90138-E.

(180) Ponomarenko, V. A.; Khomutov, A. M.; Il'chenko, S. I.; Ignatenko, A. V. The effect of substituents of the anionic polymerization of α-oxides. *Polym. Sci. USSR* **1971**, *13*, 1735–1740, DOI: 10.1016/0032-3950(71)90364-9.

(181) Blankenburg, J.; Wagner, M.; Frey, H. Well-Defined Multi-Amino-Functional and Stimuli-Responsive Poly(propylene oxide) by Crown Ether Assisted Anionic Ring-Opening Polymerization. *Macromolecules* **2017**, *50*, 8885–8893, DOI: 10.1021/acs.macromol.7b01324.

(182) Gervais, M.; Brocas, A.-L.; Cendejas, G.; Deffieux, A.; Carlotti, S. Synthesis of Linear High Molar Mass Glycidol-Based Polymers by Monomer-Activated Anionic Polymerization. *Macromolecules* **2010**, *43*, 1778–1784, DOI: 10.1021/ma902286a.

(183) Reinicke, S.; Schmelz, J.; Lapp, A.; Karg, M.; Hellweg, T.; Schmalz, H. Smart hydrogels based on double responsive triblock terpolymers. *Soft Matter* **2009,** DOI: 10.1039/b900539k.

(184) Isono, T.; Asai, S.; Satoh, Y.; Takaoka, T.; Tajima, K.; Kakuchi, T.; Satoh, T. Controlled/Living Ring-Opening Polymerization of Glycidylamine Derivatives Using t-Bu-P4 /Alcohol Initiating System Leading to Polyethers with Pendant Primary, Secondary, and Tertiary Amino Groups. *Macromolecules* **2015**, *48*, 3217–3229, DOI: 10.1021/acs.macromol.5b00556.

(185) Schubert, C.; Dreier, P.; Nguyen, T.; Maciol, K.; Blankenburg, J.; Friedrich, C.; Frey, H. Synthesis of linear polyglycerols with tailored degree of methylation by copolymerization and

the effect on thermorheological behavior. *Polymer* **2017**, *121*, 328–339, DOI: 10.1016/j.polymer.2017.05.030.

(186) Heinen, S.; Rackow, S.; Schäfer, A.; Weinhart, M. A Perfect Match: Fast and Truly Random Copolymerization of Glycidyl Ether Monomers to Thermoresponsive Copolymers. *Macromolecules* **2017**, *50*, 44–53, DOI: 10.1021/acs.macromol.6b01904.

2. Preparation of Hydrogels

2.1. Design of a Novel Epoxide Monomer for pH-Sensitive Poly(ethylene glycol) Hydrogels via Acid-Labile and Crosslinkable Allyl Side Groups

Kamil Maciol[a], *Gregor Linden*[a], *Jan Blankenburg*[a,b], *Willi Schmolke*[a], *Sebastian Seiffert*[a,*] *and Holger Frey*[a,*]

[a] Institute of Organic Chemistry, Johannes Gutenberg University Mainz, Duesbergweg 10-14, 55128 Mainz, Germany

[b] Graduate School Materials Science in Mainz, Staudinger Weg 9, 55128 Mainz, Germany

* E-Mail: sebastian.seiffert@uni-mainz.de, hfrey@uni-mainz.de

To be submitted

ABSTRACT

We introduce the novel bifunctional and acid-cleavable ethoxy ally glycidyl ether (EAGE) monomer. Using the anionic ring-opening polymerization (AROP) PEAGE-*b*-PEG-*b*-PEAGE triblock copolymers were prepared from poly(ethylene glycol) (PEG) macroinitiators with different molecular weights (M_{PEG} = 2,000–20,000 g mol^{-1}). In addition to a detailed characterization (SEC, NMR spectroscopy, MALDI-TOF MS, DSC), hydrogels were formed via thiol-ene photo-click chemistry. To gain a deeper understanding of the materials properties, the triblock copolymers were crosslinked, while being analyzed on a rheometer. The materials were optimized regarding their water absorption capacity by varying the PEG block lengths, leading to swelling ratios up to 5,400%. Additionally, the stability of the hydrogels was investigated at various pH values in acidic, aqueous solutions. Random PEG-*ran*-PEAGE copolymers were synthesized by AROP of EAGE and ethylene oxide (EO). A well-defined and narrow-distributed copolymer series was synthesized (M_n = 3,800–5,800 g mol^{-1}, Đ ≤ 1.16) in which the incorporation ratio of EAGE was varied (5–100 mol%). Real-time ^{1}H NMR kinetic measurements revealed a random incorporation of both monomers. Thermal properties were investigated by DSC. Targeted addressing of the EAGE allylic double bonds was performed with a cysteine derivative by thiol-ene click chemistry.

Regarding biomedical applications, cleavable and reactive moieties are highly interesting. Conceivable is the use as a drug delivery system in which therapeutically effective drugs can be specifically bound to the polymer backbone and released at the appropriate pH range.

TABLE OF CONTENTS
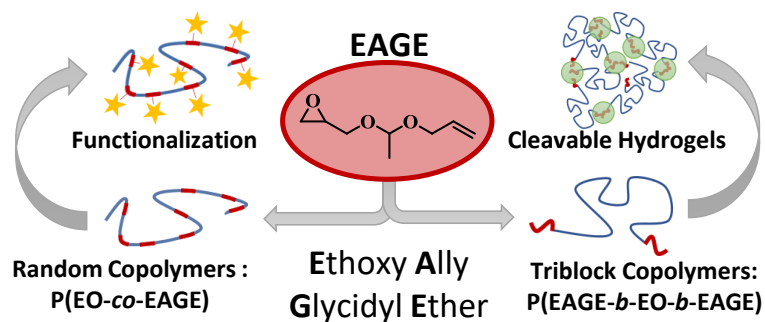
INTRODUCTION

Poly(ethylene glycol) (PEG), also known as poly(ethylene oxide) (PEO), is often referred to as the "gold standard" of biocompatible polymers and displays a unique water solubility.[1,2] This can be attributed to the distance of the oxygen atoms in the polymer backbone, which is ideal to form hydrogen bonds with the water molecules.[3] Due to its remarkable characteristics such as its low toxicity and immunogenicity,[4] PEG has a broad field of possible applications[5,6] especially in the biomedical field. One example is the so-called "PEGylation", which is a technique that allows an increase of the circulation time of therapeutically useful peptides or proteins in the blood.[7–9] Another application is the improvement of the solubility of hydrophobic drugs. Pegasys®, which is used to treat hepatitis C, is an example of such a drug.[10]

Because of its outstanding properties and biocompatibility, PEG is an ideal material for hydrogels.[11,12] Hydrogels are insoluble polymeric networks, which can absorb high amounts of water.[13] These polymeric networks can be formed by crosslinking. Different approaches for crosslinking have been established so far.[14] There is a tremendous range of potential applications for hydrogels, such as carriers for cell transplantation, scaffolds for tissue engineering or drug depots.[15] Particularly noteworthy are stimuli-responsive hydrogels which react to external stimuli such as changes in temperature, pH or chemical environment, for example by degradation.[16,17] In the field of degradable PEG hydrogels, there is a wealth of different cleavage mechanisms, such as photolytic,[18–20] reductive[21–23] or enzymatic[24,25]. Acid-degradable PEG hydrogels are particularly interesting in the area of tissue engineering and as nanogels, in cancer treatment.[26–30] The introduction of acid-labile units in PEG hydrogels has already been realized by various approaches. Messersmith *et al.* described the crosslinking of catechol functionalized 4-arm PEG by complexation with 1,3-benzenediboronic acid. Stable gels were formed at pH 9, which dissolved through acidification.[31] Covalently crosslinked, acid-cleavable PEGs were reported by Kim and co-workers. Here, phosphoesters and phosphoamides were used as cleavage sites to make the PEG hydrogels degradable and the use of these gels as drug delivery systems for doxorubicin was successfully demonstrated.[32] Hydrogels with acetal cleavage sites were already used as nanocarriers for allergen encapsulation[33] or as a promising candidate for the synthesis of bone biomaterials[34].

In this work, we introduce the novel acid-cleavable allyl glycidyl ether analogue: ethoxy ally glycidyl ether (EAGE). EAGE combines the acid-degradable character of 1-(glycidyloxy)ethyl ethylene glycol ether (GEGE)[35] or ethoxyethyl glycidyl ether (EEGE)[36] with an allyl group, offering a variety of post-polymerization modification possibilities.[37–41] Using anionic ring-

opening polymerization (AROP), random PEG-*ran*-PEAGE copolymers (**Scheme 1A**) were synthesized and functionalized with the cysteine derivative *N*-(*tert*-butoxycarbonyl)-L-cysteine methyl ester by thiol-ene click reactions. PEAGE-*b*-PEG-*b*-PEAGE triblock copolymers (**Scheme 1B**) were prepared from PEG macroinitiators with varying molecular weights. Crosslinking was successfully performed by thiol-ene click chemistry to obtain hydrogels which were optimized in order to achieve a high water uptake.

A) random copolymers
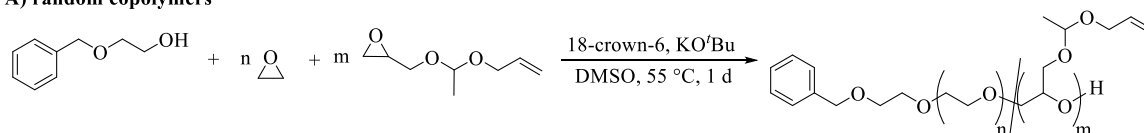
B) triblock copolymers
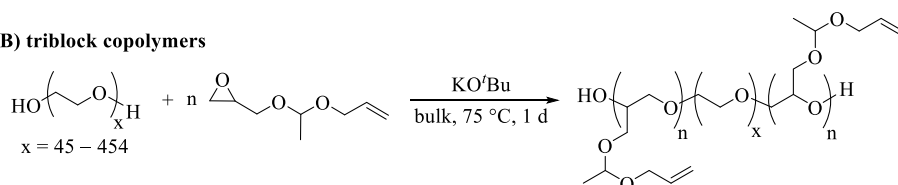
Scheme 1. Synthesis strategies for different polyether architectures using EAGE. A) Random PEG-*ran*-PEAGE copolymers. B) PEAGE-*b*-PEG-*b*-PEAGE triblock copolymers.

EXPERIMENTAL PART

Instrumentation. All ^{1}H NMR spectra were recorded on a Bruker Avance II 400 (5 mm BBFO Z-gradient probe and ATM, SampleXPress 60 auto sampler) at 400 MHz. Real-time ^{1}H NMR (400 MHz) kinetic studies, inverse gated ^{13}C NMR (100 MHz) and 2D NMR spectra were measured on a Bruker Avance III HD 400 spectrometer equipped with a 5 mm BBFO SmartProbe (Z-gradient probe) and an ATM as well as a SampleXPress 60 auto sampler. The chemical shifts were internally referred to residual proton signals of the deuterated solvent.

An Agilent 1,100 Series with Polymer Standards Service (PSS) HEMA columns (300/ 100/ 40 Å porosity) was used for size exclusion chromatography (SEC) measurements with DMF (containing 1 g L^{-1} lithium bromide) as eluent at 50 °C in combination with a RI and UV (275 nm) detector. Calibration was achieved using PEG standards by PSS.

Differential scanning calorimetry (DSC) was measured on a Perkin Elmer 8,500 in a temperature range from -95 °C to 95 °C using heating and cooling rates of 20 K min^{-1} (first cycle) and 10 K min^{-1} (second cycle) under a nitrogen atmosphere. The data points of the second heating cycle were used for evaluation.

Matrix-assisted laser desorption/ionization time-of-flight mass spectrometry (MALDI-TOF MS) measurements were conducted on a Shimadzu Axima CFR MALDI-TOF mass spectrometer with a pulsed nitrogen laser ($\lambda = 337$ nm, $t = 3$ ns), employing dithranol as matrix and potassium trifluoroacetate as cationization reagent.

Hydrodynamic radii were measured by dynamic light scattering (DLS) using a Malvern Zetasizer Nano ZS. For this purpose, aqueous solutions of the PEAGE-*b*-PEG-*b*-PEAGE copolymers were prepared in PBS buffer solution. The measuring cell holder was equipped with a Peltier-controlled thermostat. All measurements were carried out in polystyrene disposable cuvettes made by Brand GmbH at a constant temperature of 25 °C. The solutions were measured at a laser wavelength of 633 nm and a scattering angle of 173°. Malvern Zetasizer series software v7.11 was used for the evaluation.

Rheological studies were performed on a stress-controlled modular compact Anton Paar Physica MCR 302 rheometer with a cone-plate geometry (cone diameter: 25 mm, cone angle: 1°), equipped with the Peltier-temperature-controlled hood H-PTD 200. For irradiation, an OmniCure S1500 UV light curing system was used, operated with a high pressure 200 W mercury vapor short-arc lamp. Using the integrated shutter, which was 10% open, the intensity

of UV radiation was mitigated. The implemented bandpass filter transmitted UV-light between 320–500 nm (irradiance: 23 W cm^{-2}). UV-light was transferred to the Rheometer by an optical fiber cable, which was positioned central under the lower, UV-permeable glass plate to ensure homogenous illumination.

For the post-polymerization modification and crosslinking by thiol-ene click reaction, the UV lamp XX-15B (Ultra-Violet Products Ltd) was used, which consisted of two UV tubes (model T-15.M: 312 nm; T-15.L: 365 nm) provided by Vilber Lourmat Deutschland GmbH.

Materials. All reagents and solvents were obtained from common manufacturers, such as Sigma Aldrich, Alfa Aesar, Tokyo Chemical Industry (TCI) and abcr GmbH. DMSO-d_6 was purchased from Deutero GmbH. Dialysis membranes (regenerated cellulose, $MWCO = 1,000$ g mol^{-1}) were purchased from Orange Scientific. All chemicals were used without prior purification unless explicitly mentioned. In the case that purchased allyl vinyl ether (AVE) showed a brownish color, purification was conducted via flash column chromatography (SiO$_2$, pentane).[42] Initiator reagents were dried by azeotropic distillation of benzene and traces of THF. EAGE was purified by stirring over CaH$_2$ and distillation.

Monomer synthesis (ethoxy allyl glycidyl ether). The synthesis of EAGE was performed corresponding to the preparation of ethoxyethyl glycidyl ether (EEGE) according to Fitton *et al.*.[43] 0.9 mL Glycidol (13.5 mmol, 1 equiv) and 4.5 mL allyl vinyl ether (AVE, 42.6 mmol, 4 equiv) were mixed in a round bottom flask and cooled to 0 °C in an ice/water bath. Subsequently, 25.9 mg *p*-toluenesulfonic acid monohydrate (*p*-TsOH, 0.1 mmol, 1 mol% with respect to glycidol, dissolved in 0.5 mL THF) was added and the mixture was stirred under further cooling. After four hours, the colorless mixture was extracted twice with an aqueous solution of sodium bicarbonate (NaHCO$_3$). The organic phase was separated, dried over sodium sulfate (Na$_2$SO$_4$) and the excess of AVE was removed by distillation under atmospheric pressure at 80 °C. Afterwards, traces of AVE were removed under reduced pressure at room temperature. Then, the temperature was raised to 70 °C and EAGE was obtained as a colorless liquid with a yield of 50%. ^{1}H NMR (400 MHz, DMSO-d_6): δ (ppm) = 1.24 (m, 3H, H$_5$), 2.53–2.77 (m, 2H, H$_1$), 3.10 (m, 1H, H$_2$), 3.23–3.82 (m, 2H, H$_3$), 3.90–4.14(m, 2H, H$_6$), 4.75 (m, 1H, H$_4$), 5.13 (dd, 1H, H$_8$), 5.25 (dd, 1H, H$_9$), 5.90 (m, 1H, H$_7$). ^{13}C NMR (100 MHz, DMSO-d_6): δ (ppm) = 19.70 (C$_5$), 43.60 (C$_1$), 50.30 (C$_2$), 65.70 (C$_6$), 66.22 (C$_3$), 98.90 (C$_4$), 115.90 (C$_8$), 135.20 (C$_7$).

Poly(ethylene glycol)-ran-poly(ethoxy ally glycidyl ether) (PEG-ran-PEAGE). The described procedure corresponds to the preparation of PEG$_{86}$-*ran*-PEAGE$_{13}$ (entry 4, **Table 1**). Syntheses of other copolymers were performed analogously, whereby the ratios of EO and EAGE were varied. 32.7 mL 2-(Benzyloxy)ethanol (0.03 mL, 0.23 mmol, 1 equiv), 18-crown-6 (0.12 g, 0.46 mmol, 3 equiv) and KO^{t}Bu (0.02 g, 0.21 mmol, 0.9 equiv) were transferred into a 100 mL Schlenk flask. After addition of 3 mL benzene and 2 mL THF, the solution was stirred under reduced pressure at 60 °C for 30 min. The content of the flask was frozen using liquid nitrogen and evacuated overnight. In the next step, the flask was flushed with argon and 6 mL dimethyl sulfoxide (DMSO) was injected via syringe. After freezing with a dry ice/ethanol cool bath, 0.45 mL dried EAGE (2.87 mmol, 13 equiv) was added. After evacuation, 0.72 mL EO (15.87 mmol, 69 equiv) was condensed into the flask. The mixture was heated to 55 °C for 24 h. Thereafter, the reaction was terminated with addition of 1 mL MeOH. To remove DMSO, the solution was diluted with 40 mL dichloromethane (DCM) and extracted five times with 10 mL aqueous NaHCO$_3$ solution. For further purification, the concentrated organic phase was dialyzed against a mixture of MeOH/DCM (2 : 3) for 24 h. To prevent cleavage of the acetal groups by traces of acids, NaHCO$_3$ was added to the dialysis solution. The polymer was dried under reduced pressure, leading to a yield of 83%.

Sample preparation for real-time ^{1}H NMR kinetic studies. 2-(Benzyloxy)ethanol (30 mg, 0.2 mmol, 1 equiv), KO^{t}Bu (20 mg, 0.18 mmol, 0.9 equiv) and 18-crown-6 (156 mg, 0.59 mmol, 3 equiv) were dissolved in 2 mL of benzene and 1 mL of THF in a 10 mL Schlenk tube and stirred under reduced pressure for 30 min at 60 °C. The solvents were removed under reduced pressure over a period of 24 h. Subsequently, 1 mL DMSO-d_6 was added. A Norell S-5-400-VT-7 NMR tube was evacuated overnight and then flushed with argon. 0.1 mL was taken from the initiator solution under a stream of argon and transferred to the NMR tube. The solution was frozen in liquid nitrogen and 0.5 mL DMSO-d_6 was added. EAGE was dried over CaH$_2$ and distilled under reduced pressure prior to use. After addition of 78 μL EAGE (4.93 mmol, 25 equiv) to the NMR tube, vacuum was applied and a targeted amount of 22 μL EO (4.93 mmol, 25 equiv) was condensed inside the tube. The frozen NMR tube was sealed with a Teflon plug and after thawing vigorously shaken several times to homogenize the solution. Next, the NMR tube was placed in a pre-heated NMR spectrometer at 55 °C. After reaching a stable temperature (~10 min, $\Delta T = 0.1$ K), the measurement was started. The total measurement time was six hours, whereby two spectra were recorded every minute with one scan. Sample spinning was turned off. **SI-Figure 1** shows the SEC traces of the isolated PEG$_{132}$-*ran*-PEAGE$_{30}$ copolymer ($M_n = 2,500$ g mol^{-1}; Đ = 1.12).

Post-polymerization modification: thiol-ene functionalization of random PEG-ran-PEAGE copolymers. The procedure is based on a procedure of Feldmann and Martin.[44] 2,2-Dimethoxy-2-phenylacetophenone (DMPA) (1 wt%) was used as photoinitiator and added to a mixture of PEG$_{86}$-*ran*-PEAGE$_{13}$ (entry 4, **Table 1**) and *N*-(*tert*-butoxycarbonyl)-L-cysteine methyl ester (BCCME) (ratio ally double bond to thiol = 1 : 10) in MeOH/DCM (1 : 1). After three times degassing via the freeze pump thaw method, the solution was stirred for two hours under UV light irradiation. In the next step, the modified copolymer was purified using dialysis against MeOH/DCM (2 : 3) and subsequent dried under reduced pressure, leading to a yield of 90 %

Poly(ethoxy ally glycidyl ether)-block-poly(ethylene glycol)-block-poly(ethoxy ally glycidyl ether) (PEAGE-b-PEG-b-PEAGE). The approach shown here relates to the synthesis of PEAGE$_3$-*b*-PEG$_{45}$-*b*-PEAGE$_3$ (entry 1, **Table 4**). Preparations of the other triblock copolymers were performed analogously, wherein the size of the PEG macroinitiators was varied. PEG$_{45}$ (0.9 g, 0.45 mmol, 1 equiv) and KO^{t}Bu (91 mg, 0.81 mmol, 1.8 equiv) were transferred into a Schlenk flask and 3 mL benzene and 2 mL freshly distilled THF were added. Subsequently, the mixture was stirred for 30 min under reduced pressure at 60 °C. The mixture was frozen with liquid nitrogen and the solvents were removed overnight under vacuum. Then, the macroinitiator PEG$_{45}$ was melted at 75 °C and dried EAGE (0.57 mL, 3.60 mmol, 8 equiv) was added. After 24 h, 1 mL MeOH was added and the mixture was dialyzed against MeOH/DCM (2 : 3). To prevent acetal cleavage by traces of acids, NaHCO$_3$ was added. The polymer was dried under reduced pressure. The yield was 71%, with the loss being due to dialysis.

Hydrogel preparation and crosslinking. The respective PEAGE-*b*-PEG-*b*-PEAGE (1 equiv) and pentaerythritol tetrakis(3-mercaptopropionate) (PETMP) (2 equiv) were dissolved in PBS buffer solution (**SI-Table 1**). A solution of 2-hydroxy-2-methylpropiophenone (HMP) in ethanol (10 wt%) was added to the mixture (1.5 wt% with respect to the polymer and PETMP). After mixing, the solution was poured into a mold of aluminum foil, which was covered with a quartz glass lid and exposed for 30 minutes to UV light. Then, the resulting hydrogel disk was frozen in the refrigerator at -18 °C and subsequent transferred from the aluminum foil mold in a screw-top glass filled with PBS buffer solution. The hydrogel was allowed to swell for two days. After weighing, the gel was again placed in PBS and the weight was re-determined after one hour until three measured values were obtained. To determine the dry weight, the hydrogels were dried by lyophilization.

Network characterization. The overlap concentration was determined as[45]:

$$c^* = \frac{3 \cdot M_n}{4 \cdot \pi \cdot R_g^3 \cdot N_A} \tag{1}$$

where M_n is the number average molecular weight, R_g^3 is the radius of gyration and N_A is the Avogadro number. Here, R_g was calculated using the relation according to Burchard for a monodisperse random coil in a good solvent: $R_g = 1.78 \cdot r_H$.[46]

Hydrogel characteristics were calculated according to the following equations[47–49]:

$$\text{Swelling ratio } (SR) = \frac{W_s - W_d}{W_d} \tag{2}$$

$$\text{Mass degree } (Q_m) = \frac{W_s}{W_d} \tag{3}$$

$$\text{Volume degree } (Q_v) = 1 + \frac{\rho_p}{\rho_s} \cdot (Q_m - 1) \tag{4}$$

where W_s is the weight of the swollen gel, W_d is the weight of the dry gel, ρ_p is the density of PEG ($\rho_p = 1.12$ g mL^{-1})[50] and ρ_s the density of water ($\rho_s = 1$ g mL^{-1}).

To determine the hydrogel mesh size ξ, first the molecular weight between the crosslinks M_c was calculated based on a modified Flory-Rehner theory[51] according to Merrill and Peppas.[52,53] This modification applies to hydrogels prepared in solution.[54]

$$\frac{1}{M_c} = \frac{2}{M_n} - \frac{\left(\frac{\bar{v}}{V_1}\right) \cdot \left[\ln(1 - v_{2,s}) + v_{2,s} + \chi_1 \cdot v_{2,s}^2\right]}{v_{2,r} \cdot \left[(v_{2,s})^{\frac{1}{3}} - \left(\frac{1}{2} \cdot v_{2,s}\right)\right]} \tag{5}$$

To simplify the calculation, it was assumed that the triblock copolymers consist of EO units only. Thus, the resulting error is minimized with increasing size of the PEG macroinitiators. For M_n, the average molecular weights of the triblock copolymers determined from the ^{1}H NMR spectra were used. $\bar{v}$ is the specific volume of the polymers and obtained by $\frac{\rho_s}{\rho_p}$, $v_{2,s}$ is the polymer volume fraction in the swollen hydrogel and corresponds to the reciprocal value of Q_v, V_1 is the molar volume of water (18 mL mol^{-1}) and χ_1 is the polymer-solvent interaction parameter (for PEG-water interaction: $\chi_1 = 0.426$)[55].

The mesh size ξ was calculated according to Canal and Peppas[56]:

$$\xi = v_{2,s}^{-\frac{1}{3}} \cdot \left(2 \cdot C_n \cdot \frac{M_c}{M_r}\right)^{\frac{1}{2}} \cdot l \tag{6}$$

where C_n is the characteristic ratio of PEG ($C_n = 4.0$), M_r is the molecular weight of the repeating unit (44.05 g mol^{-1} for PEG) and l is the average bond length (0.154 nm).[55]

For the unperturbed root-mean-square end-to-end distance $\langle \overline{R}^2 \rangle$ of a freely-jointed polymer chain, the following expression was used[57]:

$$\langle \overline{R}^2 \rangle = n^{\frac{1}{2}} \cdot C_n^{\frac{1}{2}} \cdot l \tag{7}$$

where n is the number of repeating units.

Rheology measurements. The starting mixtures contained the respective PEAGE-*b*-PEG-*b*-PEAGE triblock copolymer (**Table 4**), the thiol PETMP, the photoinitiator HMP and PBS buffer solution in the same concentration as for the hydrogel preparations, which were used for the water uptake studies. In the first step, strain sweeps were measured before the photogelation. For this purpose, the sample was equilibrated at an angular frequency of $\omega = 1$ rad s^{-1} for 5 minutes at 25 °C. Subsequently, the shear deformation γ was varied (1–100%) at a constant angular frequency ($\omega = 1$ rad s^{-1}). Then, a value for γ was selected at which the moduli G' and G'' formed a plateau. For the following frequency sweeps, the chosen value for γ was kept constant and the frequency was varied in a range of 1–50 rad s^{-1}. From each measurement, a value for ω was selected, where the non-crosslinked mixture responded as a viscoelastic liquid. During the photogelation tests, the temporal changes in the moduli were observed at the respective constant values for γ and ω. The samples were given a few minutes lead time before the UV lamp was turned on. When G' leveled off in a constant plateau, the measurements were terminated. The following strain and frequency sweep measurements were performed analogous to the first measurements before photogelation.

Network stability tests. To study the hydrogel stability, the two triblock copolymers PEAGE$_3$-*b*-PEG$_{45}$-*b*-PEAGE$_3$ (entry 1, **Table 4**) and PEAGE$_3$-*b*-PEG$_{454}$-*b*-PEAGE$_3$ (entry 5, **Table 4**) were used, which consisted of the smallest ($M_n = 2,000$ g mol^{-1}) and the largest ($M_n = 20,000$ g mol^{-1}) PEG macroinitiator. After the preparation of the hydrogels, they were divided into three equal parts in the frozen state. These parts were transferred to a buffered solution of pH 3, pH 4 and pH 5. The time was measured until the gel dissolved in an optically clear solution.

RESULTS AND DISCUSSION

A. Synthesis of EAGE monomer.

The electrophilic addition of glycidol to ally vinyl ether (AVE) was performed with *p*-toluenesulfonic acid (*p*-TsOH) as an acid catalyst (**Scheme 2**).
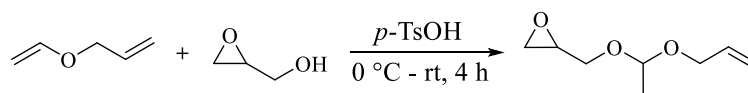
Scheme 2. Synthesis of EAGE monomer.

The reason for the preferred conversion of the vinyl ether group is the mesomeric effect. In the first step of the reaction, the addition of a proton to the vinyl double bond takes place. The resulting carbenium ion is stabilized by the mesomeric effect of the oxygen atom. In the next step, the nucleophilic attack of the glycidol takes place. To generate the highest possible yield with respect to glycidol, AVE was used in excess. The cooling of the reaction is essential, as it is exothermic. The reaction was optimized regarding the following parameter: reaction time, amount of catalyst and the ratio of the reactants glycidol/AVE. Crucial is the quantitative removal of *p*-TsOH via extraction with saturated $NaHCO_3$ solution before distillation, otherwise the combination of heat and acid traces can lead to acetal interchange.[58] The yield was on average 50% after optimization of these parameters. At temperatures below 4 °C, EAGE is storage stable for months. The ^{1}H NMR spectrum (**Figure 1**) shows all characteristic signals. ^{13}C NMR and 2D NMR spectra can be found in the Supporting Information (**SI-Figures 2−6**).
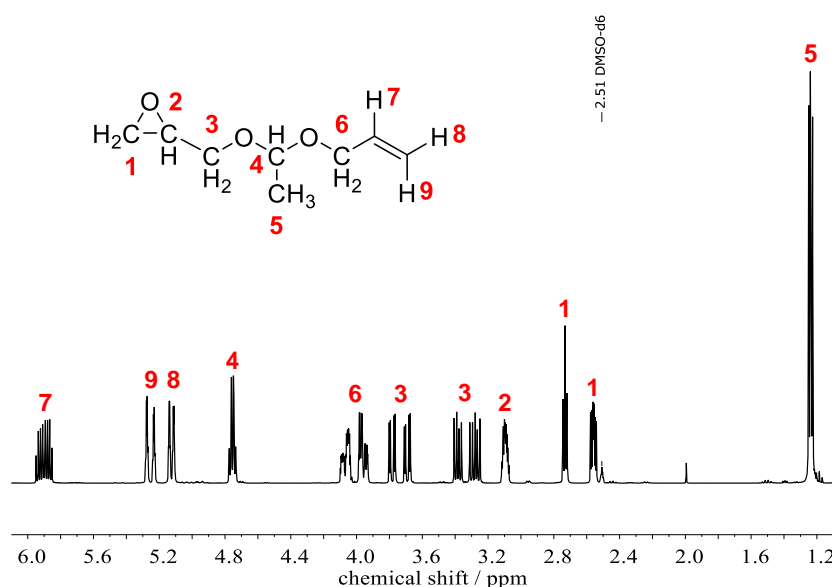
Figure 1. ^{1}H NMR spectrum (400 MHz, DMSO-d_6) of EAGE monomer.

B.   Synthesis & characterization of random PEG-*ran*-PEAGE copolymers, real-time ¹H NMR kinetics, thermal properties and post-polymerization modification.

Synthesis & characterization. The anionic ring-opening polymerization (AROP) of EO and EAGE was carried out under vacuum at 55 °C in DMSO. Higher reaction temperatures can lead to chain transfer reactions of DMSO. 2-(Benzyloxy)ethanol was used as the initiator, which comprises both an UV-active phenyl and a methylene group. Both signals do not overlap with other signals in ¹H NMR and can be used for integration and determination of the absolute molecular weight. The hydroxyl groups of the initiator were deprotonated with KO*t*Bu to 90%. Azeotropic distillation with benzene under vacuum removed traces of water in the reaction flask. The removal of the DMSO after the polymerization was quantitative by using a combination of liquid-liquid extraction and subsequent dialysis.

To investigate the random copolymers systematically, the EAGE content was varied from 5 mol% to 100 mol%. The anionic ring-opening polymerization of EAGE and EO resulted in monomodal molecular weight distributions (**Figure 2**).
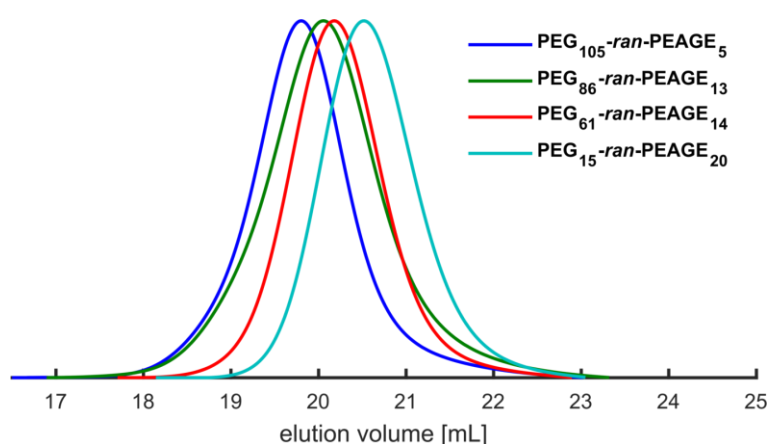
Figure 2. SEC traces (DMF, PEG-standard, RI detector) of selected copolymer samples: PEG$_{105}$-*ran*-PEAGE$_5$ (entry 2, **Table 1**); PEG$_{86}$-*ran*-PEAGE$_{13}$ (entry 4, **Table 1**); PEG$_{61}$-*ran*-PEAGE$_{14}$ (entry 5, **Table 1**); PEG$_{15}$-*ran*-PEAGE$_{20}$ (entry 7, **Table 1**).

Table 1 summarizes the SEC data for the copolymerization of EAGE and EO. The molecular weights range from 3,800 g mol^{-1} to 5,800 g mol^{-1} and show dispersities ($Đ = M_w M_n^{-1}$) below 1.17. The comparison of the theoretical molecular weights M_n^{th} with the measured values of M_n indicates a deviation with increasing EAGE content up to approximately 60%. This is attributable to the increasing hydrophobicity of the copolymers, which correlates with the amount of incorporated EAGE. Consequently, the hydrodynamic radii of the copolymers differ from those of the PEG-standards used in the SEC measurements in DMF. In addition, **Table 1**

clarifies that the difference between theoretical and calculated molecular weights from the NMR spectra increases with increasing amount of EAGE. This is due to the combination of reduced pressure and elevated temperature in the polymerization, which exceeded the boiling point both of EAGE and EO. Since EAGE exhibit a comparatively lower polarity than EO, the molecule has a higher gas permeability for the permeation through the rubber septum. Thus, EAGE probably diffused through the septum due to the reaction conditions during the polymerization. Such a behavior was already observed for the polymerization of 1,2-butylene oxide and glycidol.[59] This issue will be discussed again later in the kinetic section.

Table 1. Overview of synthesized PEG-*ran*-PEAGE copolymers.

No.	Composition[a]	EAGE / mol%[a]	M_n^{th} / g mol^{-1}	M_n^{b} / g mol^{-1}	M_n^{a} / g mol^{-1}	Đ
1	PEAGE$_{28}$	100	5,100	1,500	4,400	1.16
2	PEG$_{105}$-*ran*-PEAGE$_5$	5	5,100	2,800	5,400	1.10
3	PEG$_{72}$-*ran*-PEAGE$_9$	11	5,100	2,500	4,600	1.08
4	PEG$_{86}$-*ran*-PEAGE$_{13}$	13	5,100	2,500	5,800	1.12
5	PEG$_{61}$-*ran*-PEAGE$_{14}$	19	5,200	2,400	4,900	1.07
6	PEG$_{27}$-*ran*-PEAGE$_{18}$	40	5,100	2,400	4,000	1.07
7	PEG$_{15}$-*ran*-PEAGE$_{20}$	56	5,000	2,000	3,800	1.06

[a] Values calculated by ^{1}H NMR spectroscopy. [b] Determined by SEC in DMF (PEG-standard).

Characteristic signals of the EAGE could be assigned in the ^{1}H NMR spectra of the copolymers. Based on the initiator signals, the amount of EAGE and EO was also calculated. **Figure 3** exemplarily shows the ^{1}H NMR spectrum of PEG$_{86}$-*ran*-PEAGE$_{13}$ (entry 4, **Table 1**). Results of the ^{13}C NMR and 2D NMR investigations are given in the Supporting Information (**SI-Figures 7−11**).
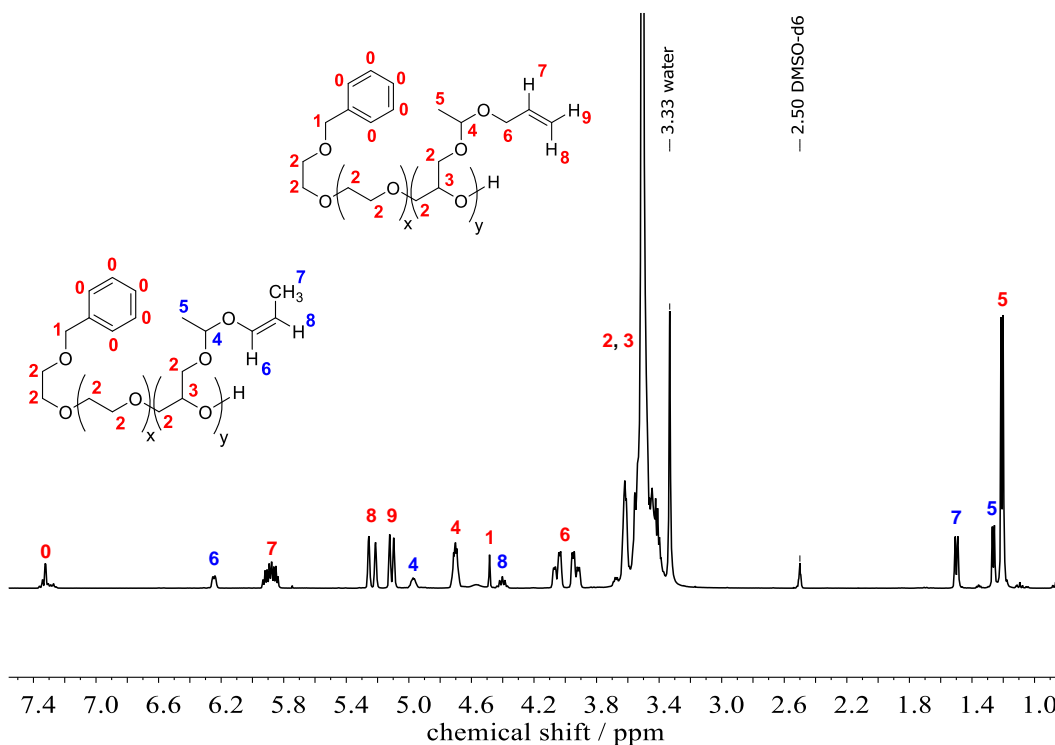
Figure 3. ^{1}H NMR spectrum of PEG$_{86}$-*ran*-PEAGE$_{13}$ (entry 4, **Table 1**) (400 MHz, DMSO-d_6); upper structure: ally structure (main product), lower structure: *cis*-prop-1-enyl isomer (side product).

It is known from the literature that the base-catalyzed C=C isomerization of allyl ethers to vinyl ethers works very well with the system KO^{t}Bu/DMSO.[60,61] Under comparable reaction conditions, the formation of the *cis*-isomer is nearly quantitative, presumably due to the formation of a cyclic transition complex.[62–64] To prevent this transition state and thus the isomerization, an excess of 18-crown-6 was used during the reaction. By addition of crown ether, an allyl content of about 80% was obtained. A quantitative suppression of *cis*-isomerization was not possible. In addition, the isomerization was only observed in combination with the solvent DMSO, which was essential for the copolymerization of EAGE with EO. In experiments in DMSO without 18-crown-6, almost only the *cis*-isomer was obtained, which is shown in the later section on the triblock copolymers. Nevertheless, the isomerization did not affect the modification via thiol-ene click chemistry (see section *post-polymerization modification*).

Real-time ^{1}H NMR kinetics. The chemical structure of the comonomers and the polymerization technique has a strong influence on the microstructure of the resulting copolymers. Previous studies revealed a random incorporation of glycidyl ethers with ethylene oxide.[65,66] For this purpose, real-time ^{1}H NMR kinetic measurements were performed in an evacuated NMR tube

at 55 °C using DMSO-d_6 as solvent to investigate the copolymerization of EAGE and EO. To evaluate the monomer incorporation, the decrease of the epoxide integrals of the respective monomers was monitored. For EAGE, the signal at 2.7 ppm (**Figure 4A**) was used and for EO the signal at 2.6 ppm (**Figure 4B**). In **SI-Figure 12**, it can be clearly seen that the intensity of the epoxide signals decreases with the same rate, indicating an ideally random incorporation of the monomers.
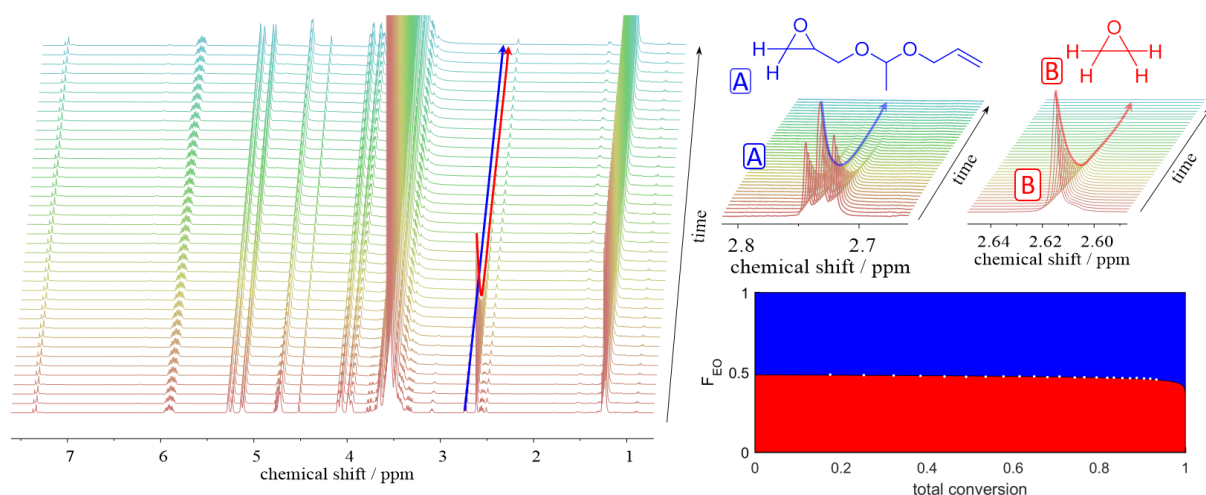
Figure 4. Left: ^{1}H NMR spectra of the copolymerization of EAGE and EO (400 MHz, 55 °C, DMSO-d_6). Upper right corner: zoom of relevant areas for evaluation. Lower right corner: Simulated composition plotted versus total conversion of both monomers. The white dots represent real measurement data, while the color gradient was simulated using reactivity ratios according to Meyer-Lowry.

The findings were underpinned by the determination of the reactivity ratios for EAGE and EO according to the methods of Jaacks[67] and Meyer-Lowry[68] (**Table 2**). The corresponding fits can be found in the Supporting Information (**SI-Figures 13−14**).

Table 2. Overview of the reactivity ratios determined by fits of the Jaacks and Meyer-Lowry equations.

	Ideal (Jaacks)	**Meyer-Lowry**
r_{EAGE}	0.95	0.98
r_{EO}	1.05	1.09

Another important finding is the calculated amount of EAGE (30 units), which almost corresponds to the theoretical value of 25 units with the inclusion of measuring and weighing errors. In this case, the highest EAGE incorporation rate was achieved (cf. **Table 1**). This

supports the assumption that the EAGE monomer diffused through the rubber septum, while the NMR tube was tightly sealed with a Teflon plug.

Thermal properties. The thermal properties of the copolymers were investigated by DSC measurements. **Table 3** shows the glass transition temperatures (T_gs) and melting temperatures (T_ms) of the PEG-*ran*-PEAGE copolymers and PEAGE homopolymer. The T_ms increase with increasing EO content. At lower EO incorporation rates, T_m completely disappears, as the atactic EAGE units hinders an ordered packing and crystallization of the PEG chains. As expected, the T_gs decrease with decreasing EO content. The incorporation of flexible EAGE side chains promotes binding rotation and thus lowers the T_g compared to pure PEG.

Table 3. Thermal properties of the PEAGE homopolymer and PEG-*ran*-PEAGE copolymers.

No.	Composition[a]	mol% EAGE	T_m / °C	ΔH / J g^{-1}	T_g / °C
1	PEAGE$_{28}$	100	-	-	-68
2	PEG$_{105}$-*ran*-PEAGE$_5$	5	35	81	-59
3	PEG$_{72}$-*ran*-PEAGE$_9$	11	9	45	-64
4	PEG$_{86}$-*ran*-PEAGE$_{13}$	13	-11	39	-66
5	PEG$_{61}$-*ran*-PEAGE$_{14}$	19	-	-	-66
6	PEG$_{27}$-*ran*-PEAGE$_{18}$	40	-	-	-64
7	PEG$_{15}$-*ran*-PEAGE$_{20}$	56	-	-	-64

[a] Values calculated by ^{1}H NMR spectroscopy

Post-polymerization modification. The linkage of the PEG-*ran*-PEAGE copolymers with the cysteine derivative *N*-(*tert*-butoxycarbonyl)-L-cysteine methyl ester (BCCME) was chosen as a model reaction to investigate the copolymers as pH-responsive nanocarriers for potential drug delivery applications (**Scheme 3**).[69]
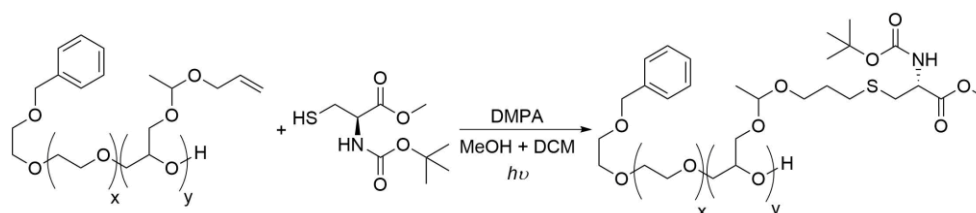
Scheme 3. Thiol-ene coupling of a random PEG-*ran*-PEAGE copolymer with the functional thiol BCCME.

Thiol-ene click chemistry is a powerful tool to modify polymers.[70,71] To this date, there is a wealth of works, demonstrating the linkage of various functionalities in the polymer backbone via thiol-ene click chemistry.[39,64,72–75] Here, the reaction progress was monitored by ^{1}H NMR spectroscopy. The quantitative disappearance of the signals for the EAGE double bonds of the main and side product confirmed the successful functionalization of the copolymer with BCCME (**Figure 5**). In addition to the signals for the main product, the signals of the functionalized *cis*-isomers could also be assigned in the ^{1}H NMR spectrum (**SI-Figure 15**). The Supporting Information includes additional ^{13}C NMR and 2D NMR spectra (**SI-Figures 16−19**).
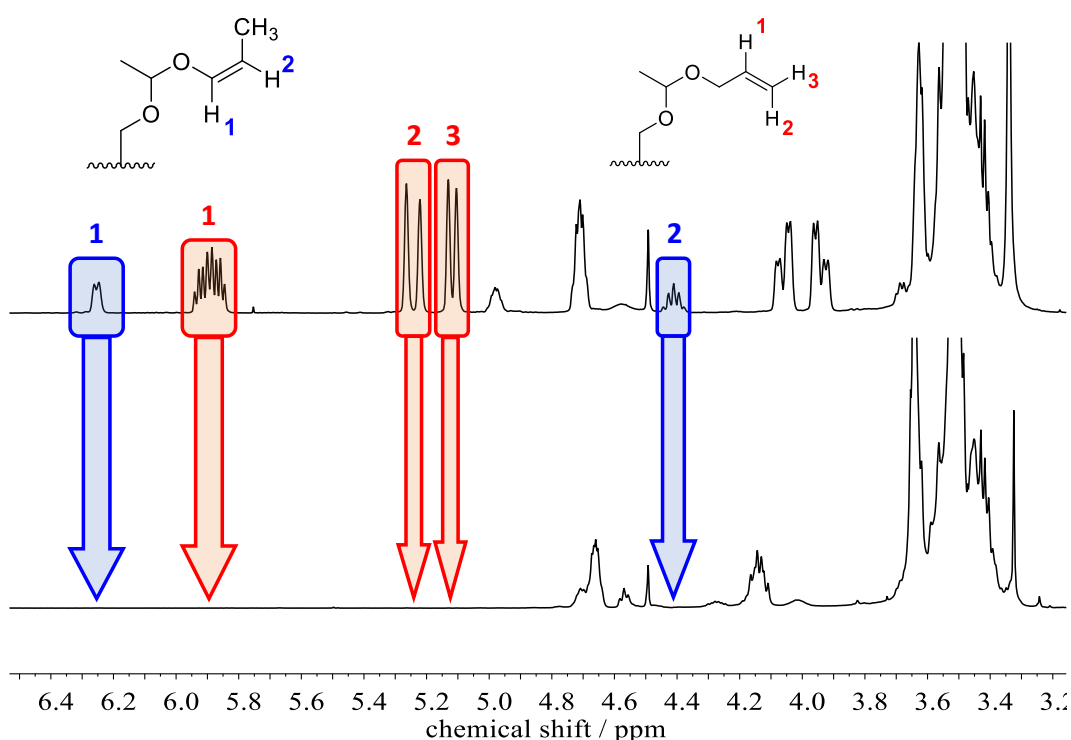
Figure 5. ^{1}H NMR spectrum (400 MHz, DMSO-*d_6*) of precursor PEG$_{86}$-*ran*-PEAGE$_{13}$ (entry 4, **Table 1**) and BCCME-modified copolymer before and after thiol-ene click reaction.

The comparison of the SEC traces of the precursor PEG$_{86}$-*ran*-PEAGE$_{13}$ (entry 4, **Table 1**) and BCCME-functionalized PEG$_{86}$-*ran*-PEAGE$_{13}$ demonstrates a clear und uniform shift of about 1,100 g mol^{-1}, proving a successful and quantitative modification (**SI-Figure 20**).

C. Synthesis of PEAGE-*b*-PEG-*b*-PEAGE triblock copolymers, characterization and crosslinking to acid-labile hydrogels.

Synthesis & characterization. For the synthesis of ABA type PEAGE-*b*-PEG-*b*-PEAGE triblock copolymers, PEG macroinitiators with different molecular weights (2,000, 3,000, 8,000, 10,000 and 20,000 g mol^{-1}) were used and deprotonated with KO^{t}Bu (**Scheme 1B**). The use of crown ether could be avoided since the reactions were conducted in bulk in contrast to the copolymerization with EO. **Table 4** summarizes the synthesized triblock copolymers in terms of theoretical and measured molecular weight as well as their dispersities determined by SEC. It also contains the calculated molar masses from the ^{1}H NMR spectra, which are consistent with the theoretical values except for slight deviations.

Table 4. Overview of synthesized PEAGE-*b*-PEG-*b*-PEAGE triblock copolymers.

No.	Composition[a]	M_n^{th} / g mol^{-1}	M_n^b / g mol^{-1}	M_n^a / g mol^{-1}	Đ
1	PEAGE$_3$-*b*-PEG$_{45}$-*b*-PEAGE$_3$	3,300	3,000	2,900	1.03
2	PEAGE$_3$-*b*-PEG$_{68}$-*b*-PEAGE$_3$	4,300	4,100	3,900	1.03
3	PEAGE$_4$-*b*-PEG$_{182}$-*b*-PEAGE$_4$	9,300	10,600	9,300	1.05
4	PEAGE$_4$-*b*-PEG$_{227}$-*b*-PEAGE$_4$	11,300	12,100	11,300	1.08
5	PEAGE$_3$-*b*-PEG$_{454}$-*b*-PEAGE$_3$	21,300	23,900	20,900	1.10

[a] Values calculated by ^{1}H NMR spectroscopy; theoretical composition was as follows: PEAGE$_4$-*b*-PEG$_x$-*b*-PEAGE$_4$. [b] Determined by SEC in DMF (PEG-standards).

SEC analysis shows narrow, monomodal distributions (**Figure 6**). The direct comparison between unfunctionalized homo-PEG macroinitiators and the EAGE-functionalized PEGs clearly verifies a shift of the SEC traces, which can be seen in **SI-Figure 21**. This shift is very pronounced for the smaller PEGs, since the first sample in **Table 4** contains 12 mol% EAGE, whereas the last sample (entry 5, **Table 4**) contains approximately 1 mol% EAGE.
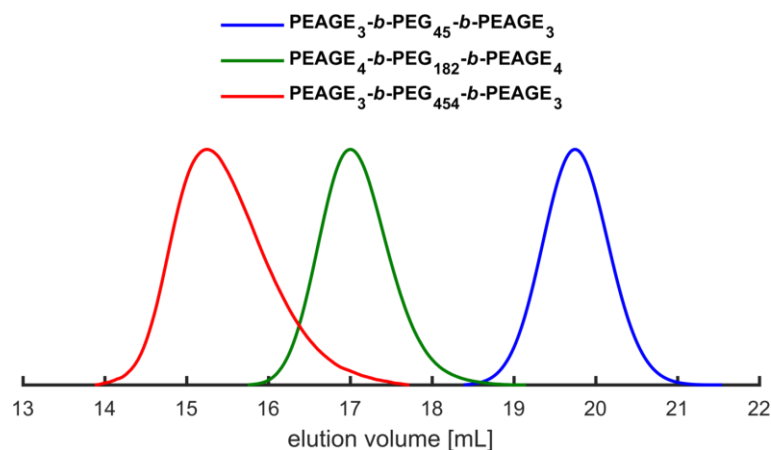
Figure 6. SEC traces (DMF, PEG-standard, RI detector) of selected copolymer samples: PEAGE₃-*b*-PEG₄₅-*b*-PEAGE₃ (entry 1, **Table 4**); PEAGE₄-*b*-PEG₁₈₂-*b*-PEAGE₄ (entry 3, **Table 4**); PEAGE₃-*b*-PEG₄₅₄-*b*-PEAGE₃ (entry 5, **Table 4**).

All characteristic signals of the PEAGE-*b*-PEG-*b*-PEAGE triblock copolymers could be assigned in the ^{1}H NMR spectrum (**Figure 7**). Since defined PEG macroinitiators were used, the number of EO repeating units was known. Thus, the number of EAGE units and the absolute molecular weights could be calculated. **SI-Figures 22−26** show the corresponding ^{13}C NMR and 2D NMR spectra.
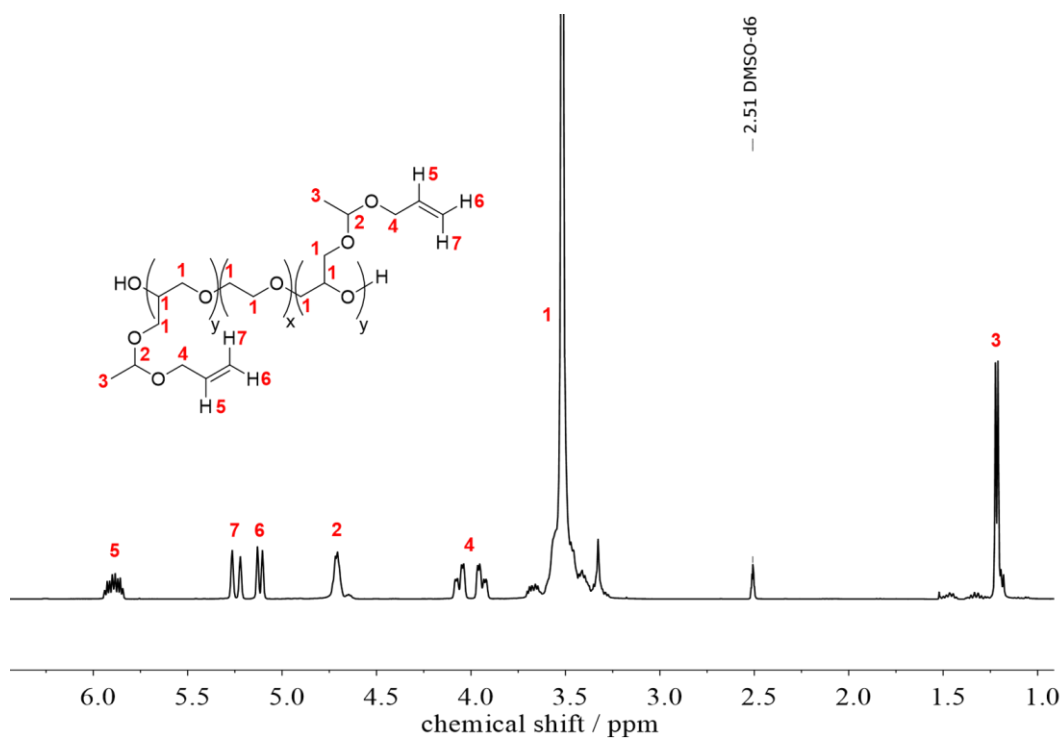
Figure 7. ^{1}H NMR spectrum of PEAGE₃-*b*-PEG₄₅-*b*-PEAGE₃ (entry 1, **Table 4**) in DMSO-*d₆* (400 MHz).

The ^{1}H NMR spectrum also shows that the formation of the *cis*-isomer did not occur. As mentioned above, this formation takes place only in combination with solvent. A test reaction in DMSO without using 18-crown-6 resulted in an almost quantitative formation of the cis isomer (**SI-Figure 27**).

Matrix-assisted laser desorption/ionization time-of-flight mass spectrometry (MALDI-TOF MS) investigations proved the successful formation of triblock copolymers. In **Figure 8** each peak could be assigned to the corresponding copolymer species, demonstrating the absence of unfunctionalized PEG chains. For the larger triblock copolymers, the measurement did not meet the resolution criteria, due to the high molecular weights ($M_n > 8,000$ g mol^{-1}).
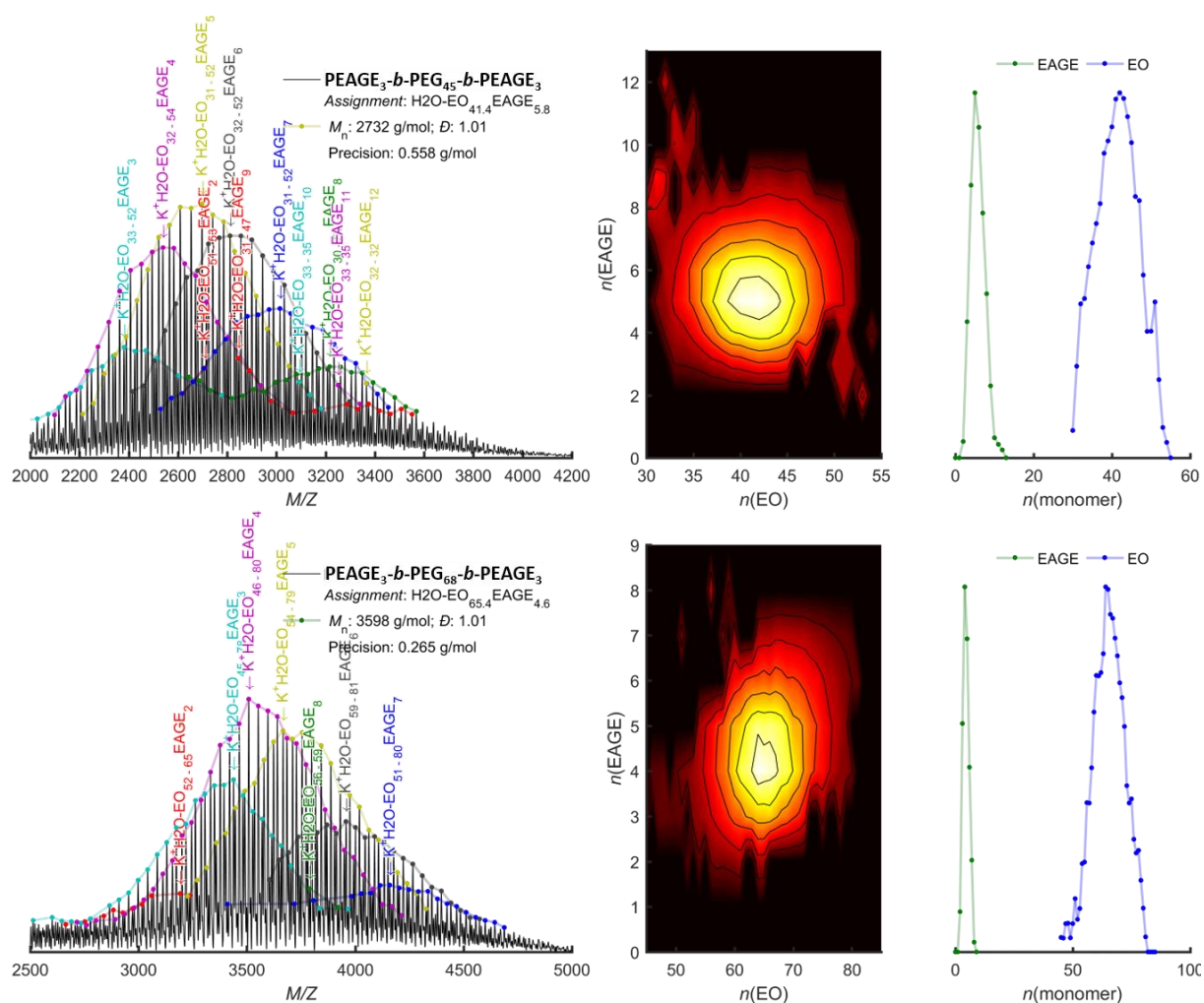
Figure 8. Left: MADLI-TOF mass spectra with assigned peaks for PEAGE$_3$-*b*-PEG$_{45}$-*b*-PEAGE$_3$ (top, entry 1, **Table 4**) and PEAGE$_3$-*b*-PEG$_{68}$-*b*-PEAGE$_3$ (bottom, entry 2, **Table 4**), Center: extracted 2D-composition from the mass spectra. Right: 2D distribution of the monomer distributions.[76–78]

Thermal properties. **Table 5** displays the T_gs, T_ms and enthalpies of fusion ΔH of the synthesized triblock copolymers.

Table 5. Thermal properties of PEAGE-*b*-PEG-*b*-PEAGE triblock copolymers.

No.	Composition[a]	T_m / °C	ΔH / J g^{-1}	T_g / °C
1	PEAGE$_3$-*b*-PEG$_{45}$-*b*-PEAGE$_3$	23	59	-69
2	PEAGE$_3$-*b*-PEG$_{68}$-*b*-PEAGE$_3$	40	79	-63
3	PEAGE$_4$-*b*-PEG$_{182}$-*b*-PEAGE$_4$	54	115	-62
4	PEAGE$_4$-*b*-PEG$_{227}$-*b*-PEAGE$_4$	56	121	-56
5	PEAGE$_3$-*b*-PEG$_{454}$-*b*-PEAGE$_3$	61	136	-53

[a] Values calculated by ^{1}H NMR spectroscopy

The T_ms increase with larger PEG chain length. The packing of longer PEG chains is less disturbed at higher EO to EAGE ratios, explaining the increase in melting temperature. The T_gs exhibit a similar trend as the random PEG-*ran*-PEAGE copolymers: with decreasing PEG chain length, the T_gs decrease. Phase separation did not occur due to the small size of the PEAGE blocks, which is why only a medium T_g of both, the PEG and the PEAGE block was observed.

Network formation. Thiol-ene click chemistry was used for the formation of pH-sensitive hydrogels based on the PEAGE-*b*-PEG-*b*-PEAGE triblock copolymers in combination with pentaerythritol tetrakis(3-mercaptopropionate) (PETMP) as thiol and 2-hydroxy-2-methylpropiophenone (HMP) as photoinitiator. Parameters such as the irradiation duration, initiator concentration, water content and thiol concentration were varied such to obtain gels with maximum water absorbency. In the first step, hydrogel disks were prepared by photocrosslinking, which were then allowed to swell further to reach their swelling equilibrium. The drastic swelling of the hydrogels is exemplarily demonstrated in **Figure 9**:

Hydrogels in state as prepared without further swelling   **Hydrogels in the fully swollen state**
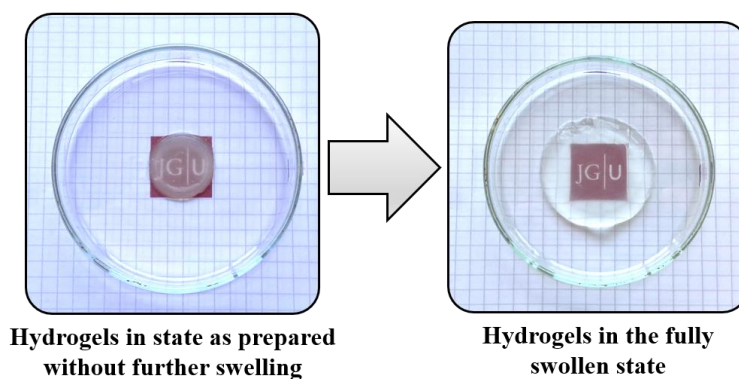
Figure 9. Comparison of crosslinked PEAGE$_3$-b-PEG$_{454}$-b-PEAGE$_3$ (entry 5, **Table 4**) before and after swelling in water. The grid in the background has a scale of 0.5 cm · 0.5 cm (1/5 inch · 1/5 inch).

Generally, the approaches were designed to employ a 1 : 1 ratio of PETMP thiol groups to the allyl double bonds of the triblock copolymers. HMP was added for each experiment with a mass fraction of 1.5 wt%. All samples were irradiated for 30 min with an UV lamp. The mass concentration of the triblock copolymers was varied depending on the size of the triblock copolymers. Exact compositions for the particular hydrogels can be found in the Supporting Information (**SI-Table 1**).

To verify whether the selected polymer concentration is sufficient for hydrogel synthesis, the overlap concentration c^* was determined (**Equation 1**), as compiled in **Table 6**. Hydrodynamic radii of the PEAGE-b-PEG-b-PEAGE triblock copolymers were calculated from dynamic light scattering (DLS)-estimates of their translational diffusivities with the Stokes-Einstein equation under assumption of spherical shapes and a Newtonian medium (particle distribution can be found in **SI-Figures 28−32**).

Table 6. Overlap concentrations of PEAGE-*b*-PEG-*b*-PEAGE triblock copolymers.

No.	Composition[a]	$R_{g,PEG}$[b] / nm	c^*_{PEG}[c] / g L^{-1}	$R_{g,Aggr.}$[b] / nm	$c^*_{Aggr.}$[c] / µg mL^{-1}	c^*_{Gel}[d] / g L^{-1}
1	PEAGE$_3$-*b*-PEG$_{45}$-*b*-PEAGE$_3$	2	56	94	1.5	200
2	PEAGE$_3$-*b*-PEG$_{68}$-*b*-PEAGE$_3$	3	41	152	0.4	200
3	PEAGE$_4$-*b*-PEG$_{182}$-*b*-PEAGE$_4$	5	24	155	1.0	150
4	PEAGE$_4$-*b*-PEG$_{227}$-*b*-PEAGE$_4$	6	20	161	1.1	150
5	PEAGE$_3$-*b*-PEG$_{454}$-*b*-PEAGE$_3$	9	14	171	1.6	150

[a] Values calculated by ^{1}H NMR spectroscopy. [b] Radii of gyration of pure PEG samples[79] and EAGE-containing triblock copolymers. [c] Overlap concentrations of pure PEG samples and EAGE-containing triblock copolymers. [d] Polymer mass concentration in PBS for crosslinking experiments.

The first two columns for R_g and c^* show the characteristics of pure aqueous PEG solutions of comparable molecular weight analogous to the PEAGE-*b*-PEG-*b*-PEAGE triblock copolymers, which were calculated according to **Equation 1**.[79] In strong contrast are the data of the triblock copolymers in the next two columns, which differ by several orders of magnitude for c^*. The reason for this difference is the formation of aggregates, which entail very large hydrodynamic particle radii r_H and therefore radii of gyration R_g, resulting in very small overlap concentrations. Independent of what value is more appropriate, the selected concentrations for the hydrogel preparation (last row) in this work exceed both of them, such that the overlap concentration was certainly exceeded in each case, ensuring sufficient overlap of the polymer chains for hydrogel formation.

To gain a deeper understanding of the crosslinking of PEAGE-*b*-PEG-*b*-PEAGE triblock copolymers, the process was investigated rheologically. For this purpose, strain and frequency sweeps were recorded before the photogelation. Subsequently, the samples were irradiated directly on the rheometer, and the changes in the moduli were observed. In the last step, the strain and frequency sweep measurements were repeated for the crosslinked hydrogels. Values for the shear deformation γ and angular frequency ω, which were set constant for the respective tests, are summarized in **SI-Table 2**. The results of the rheology experiments are exemplified for PEAGE$_3$-*b*-PEG$_{454}$-*b*-PEAGE$_3$ (entry 5, **Table 4**) in **Figure 10** (the remaining data are shown in **SI Figures 33−36**).
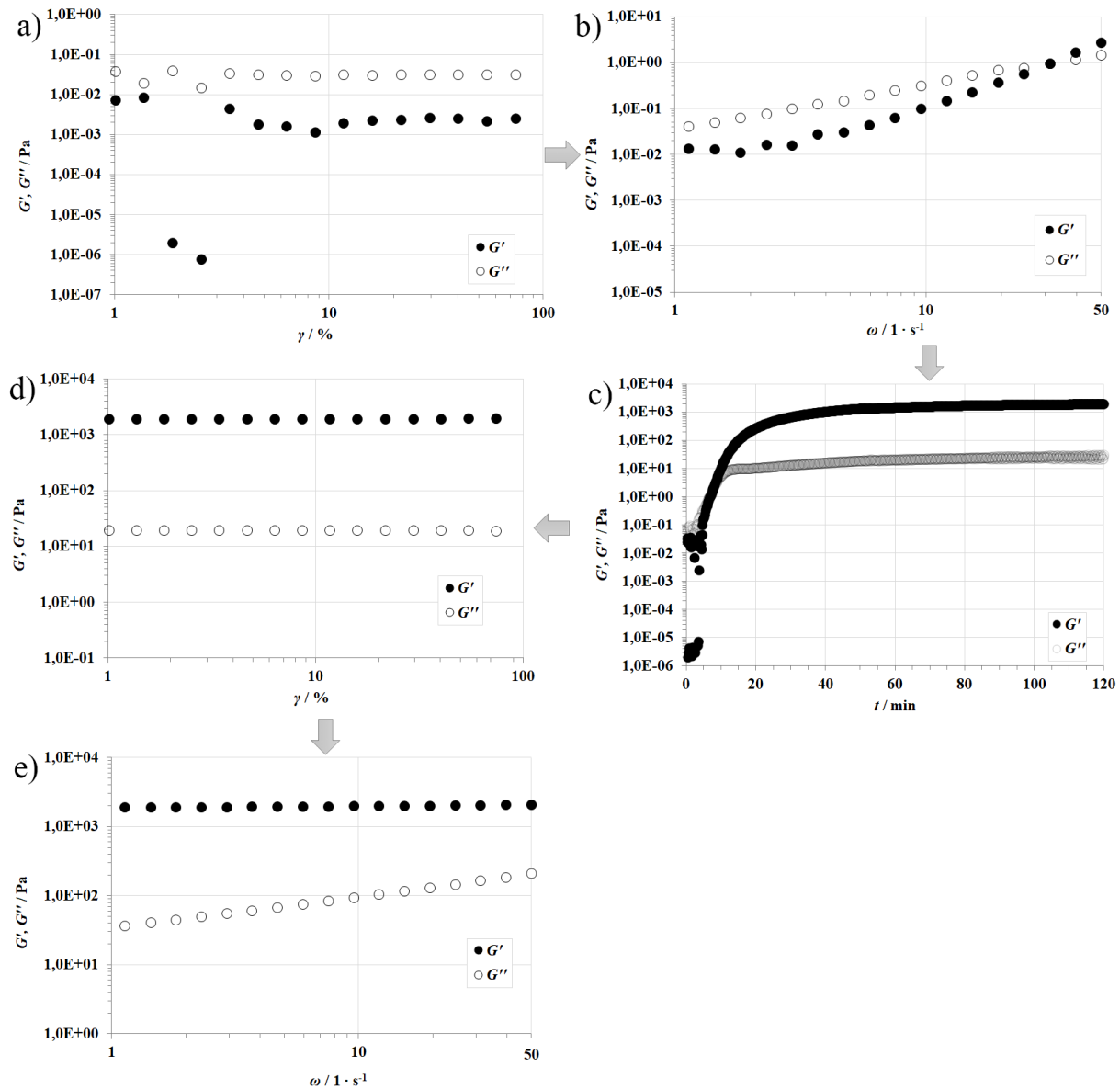
Figure 10. Rheological investigation of PEAGE$_3$-b-PEG$_{454}$-b-PEAGE$_3$ (entry 5, **Table 4**): a) strain sweep before photogelation, b) frequency sweep before photogelation, c) photogelation, d) strain sweep after photogelation, e) frequency sweep after photogelation.

The change in material properties due to photocrosslinking is clearly visible. Before gelation, the mixtures of the PEAGE-b-PEG-b-PEAGE triblock copolymers, thiol, photoinitiator and water behaved close to a Maxwell fluid, with a frequency-dependent scaling of the storage and loss moduli close to $G' \sim \omega^{1.6}$ and $G'' \sim \omega^{0.8}$. By irradiation with UV light, the gelation point was reached within a few seconds for all samples. Beyond that point, upon further irradiation, G' increased several orders of magnitude above G'' in each hydrogel sample, and the moduli formed a constant plateau within 40 minutes. Strain and frequency sweep measurements after the photogelation demonstrated that the moduli were several decades above the values of the

initial measurements and that their frequency-dependence was no longer that one of a Maxwell fluid, but instead, that one of a gel, with $G' \sim \omega^0$ and $G'' \sim \omega^{0.5}$.

For the study of water absorption, the non-equilibrated photocrosslinked hydrogel discs were placed in water and allowed to swell for two days. Subsequently, the water absorption capacity was determined (**Figure 11**). Here, the increase in water uptake correlates with the length of the PEG chains and varies between about 900% for sample 1 (entry 1, **Table 4**) and 5,400% for sample 5 (entry 5, **Table 4**). This is due to the larger hydrogel mesh sizes because of the larger PEG macroinitiators, corresponding to a softer gel that can swell more.
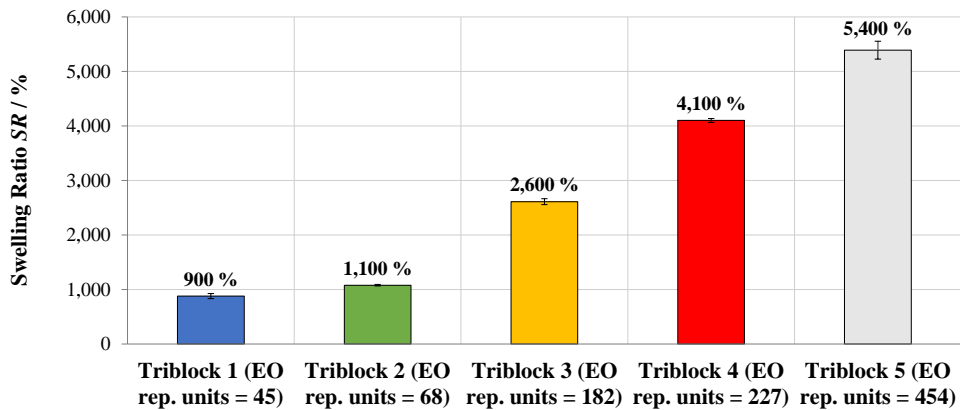
Figure 11. Overview of the water uptake of the equilibrated hydrogels based on the PEAGE-*b*-PEG-*b*-PEAGE triblock copolymers.

This fact was further clarified by calculating the mesh sizes ξ of the equilibrated hydrogels using the Flory-Rehner theory (**Table 7**).[51]

Table 7. Characteristics of the equilibrated hydrogels, including the volume swelling Q_v, the molecular weight between crosslinks M_c, the mesh size ξ and the root-mean-square end-to-end distance $\langle \overline{R}^2 \rangle$ of the PEG precursor polymers used to build the network meshes.

No.	Composition[a]	Q_V	M_c / g mol^{-1}	ξ / nm	$\langle \overline{R}^2 \rangle$ / nm
1	PEAGE$_3$-*b*-PEG$_{45}$-*b*-PEAGE$_3$	11	1,300	4.9	2.4
2	PEAGE$_3$-*b*-PEG$_{68}$-*b*-PEAGE$_3$	13	1,700	6.0	2.8
3	PEAGE$_4$-*b*-PEG$_{182}$-*b*-PEAGE$_4$	30	4,300	12.7	4.2
4	PEAGE$_4$-*b*-PEG$_{227}$-*b*-PEAGE$_4$	46	5,400	16.5	4.7
5	PEAGE$_3$-*b*-PEG$_{454}$-*b*-PEAGE$_3$	61	10,000	24.5	6.4

[a] Values calculated by ^{1}H NMR spectroscopy

ξ increases from 5 nm (entry 1, **Table 7**) to 24 nm (entry 5, **Table 7**). The same applies to the molecular weights between the individual crosslinking nodes. By comparing the mesh sizes ξ with the root-mean-square end-to-end distances $\langle \overline{R}^2 \rangle$ of the PEG precursors used to build the network meshes, it can be seen that the values for ξ of the first two samples (entries 1/2, **Table 7**) are about twice as large as end-to-end distances of the polymer coils. The value for next sample (entry 3, **Table 7**) is about three times larger than the theoretical values, whereas ξ is approximately four times larger as $\langle \overline{R}^2 \rangle$ for the last samples (entries 4/5, **Table 7**). These findings go hand in hand with the experimental results for water uptake (**Figure 11**). The hydrogels from the first two samples (entries 1/2, **Table 4**) are quite well crosslinked, indicated by the small deviations between ξ and $\langle \overline{R}^2 \rangle$ and the limited water uptake (*SR*). By doubling the molar masses of the PEG macroinitiators (entry 3, **Table 4**), network defects and inhomogeneity get more significant. This is reflected in the sudden increase in the *SR*s and deviations between ξ and $\langle \overline{R}^2 \rangle$. When re-enlarging the PEG backbone (entries 4/5, **Table 4**) analog observations can be made. The mesh size ξ and thus the water absorption increases by a multiple. Due to increasing extent of network defects and inhomogeneities, the deviation between experimental and theoretical distance is exacerbated.

To investigate the stability of the hydrogels in the acidic environment, the hydrogels based on the PEG$_{45}$ and PEG$_{454}$ macroinitiator were placed in different buffered solutions (**Figure 12**). It is particularly striking that the PEAGE$_3$-*b*-PEG$_{45}$-*b*-PEAGE$_3$ (entry 1, **Table 4**) hydrogels have a significantly higher stability in acidic solutions, regardless of the pH value, compared to the gels of PEAGE$_3$-*b*-PEG$_{454}$-*b*-PEAGE$_3$ (entry 5, **Table 4**). Thus, the former gel dissolved at pH 3 after approximately one week, while the latter one required one day. For pH 5, the stability studies were discontinued after 56 days for the smaller crosslinked triblock because the hydrogel still had not optically dissolved by that time. These observations can be attributed to the higher water absorption capacity of the crosslinked PEAGE$_3$-*b*-PEG$_{454}$-*b*-PEAGE$_3$ (entry 5, **Table 4**) triblock copolymer, facilitating the transport of protons to the cleavable acetal groups. Additionally, the more hydrophobic properties of the PEAGE$_3$-*b*-PEG$_{45}$-*b*-PEAGE$_3$ (entry 1, **Table 4**) hydrogels also play a role here, due to the significantly higher EAGE to EO ratio.
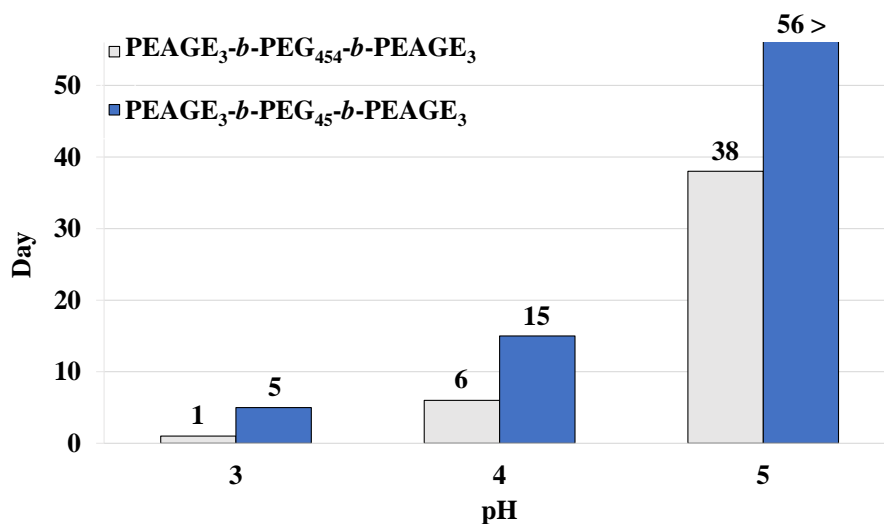
Figure 12. Duration until complete dissolution of PEAGE-*b*-PEG-*b*-PEAGE hydrogels in acidic, buffered solutions (pH 3, pH 4 and pH 5), prepared of the triblock copolymers PEAGE$_3$-*b*-PEG$_{45}$-*b*-PEAGE$_3$ (entry 1, **Table 4**) and PEAGE$_3$-*b*-PEG$_{454}$-*b*-PEAGE$_3$ (entry 5, **Table 4**).

CONCLUSION

In this work, we introduced and optimized the synthesis of the novel bifunctional and pH-sensitive monomer EAGE. Copolymerization of EAGE with EO via AROP led to PEG-*ran*-PEAGE copolymers. Random copolymers were obtained in the range from 3,800 g mol^{-1} to 5,800 g mol^{-1} with dispersities up to 1.16 and with EAGE incorporation rates between 5 mol% and 100 mol%. Despite the complexation of the potassium counterions of KO^{t}Bu by 18-crown-6 in the copolymerizations, the *cis*-isomerization of the EAGE allyl double bonds was observed. Nevertheless, the functionalization of PEG-*ran*-PEAGE copolymer double bonds with a cysteine derivative by thiol-ene click reaction was successful and quantitative for the main and side product. The investigation of the microstructure by real-time ^{1}H NMR spectroscopy revealed a random incorporation of both monomers ($r_{EO} = 1.1$, $r_{EAGE} = 1.0$). Due to the targeted incorporation of EAGE, the T_ms of the copolymers could be varied between 35 °C to -11 °C, while T_gs moved in a range from -59 to -68 °C.

The successful synthesis of the PEAGE-*b*-PEG-*b*-PEAGE triblock copolymers was confirmed by NMR, SEC and MALDI-TOF MS analysis. Triblock copolymers with molecular weights up to 20,900 g mol^{-1} and dispersities less than 1.11 were obtained. The investigation of the thermal properties revealed T_gs between -69 °C to -53 °C, while T_ms varied between 23 °C and 61 °C. Using thiol-ene click chemistry, the triblock copolymers were successfully photocrosslinked to hydrogels. The rheological analysis of the crosslinking process clearly demonstrated the change in material properties through gelation. Swelling ratios up to 5,400% were achieved, with mesh sizes in the range of 5 nm to 24 nm. Additionally, the stability of the hydrogels at different pH values in aqueous solutions was studied, demonstrating a cleavage between days and months.

The specific design of the novel reactive and acid-labile monomer EAGE provides access to a variety of cleavable polyether architectures. EAGE is polymerizable via the epoxy functionality and allows the functionalization via the allyl group. Contemporaneously, EAGE also provides acid cleavability of the allyl ether structure. These properties make EAGE-polymers highly interesting as pH-sensitive materials in biomedical applications.

REFERENCES

(1) Herzberger, J.; Niederer, K.; Pohlit, H.; Seiwert, J.; Worm, M.; Wurm, F. R.; Frey, H. Polymerization of Ethylene Oxide, Propylene Oxide, and Other Alkylene Oxides: Synthesis, Novel Polymer Architectures, and Bioconjugation. *Chem. Rev.* **2016**, *116*, 2170–2243, DOI: 10.1021/acs.chemrev.5b00441.

(2) Bailey, F. E.; Koleske, J. V. *Poly(ethylene oxide)*; Academic Press: New York, 1976.

(3) Kjellander, R.; Florin, E. Water structure and changes in thermal stability of the system poly(ethylene oxide)–water. *J. Chem. Soc., Faraday Trans. 1* **1981**, *77*, 2053, DOI: 10.1039/f19817702053.

(4) Fruijtier-Pölloth, C. Safety assessment on polyethylene glycols (PEGs) and their derivatives as used in cosmetic products. *Toxicology* **2005**, *214*, 1–38, DOI: 10.1016/j.tox.2005.06.001.

(5) *Poly(ethylene glycol): Chemistry and Biological Applications;* Harris, J. M.; Zalipsky, S., Eds.; ACS symposium series 680; American Chemical Society: Washington, 1997.

(6) Obermeier, B.; Wurm, F.; Mangold, C.; Frey, H. Multifunctional Poly(ethylene glycol)s. *Angew. Chem. Int. Ed. (English)* **2011**, *50*, 7988–7997, DOI: 10.1002/anie.201100027.

(7) Zalipsky, S. Chemistry of polyethylene glycol conjugates with biologically active molecules. *Adv. Drug Deliv. Rev.* **1995**, *16*, 157–182, DOI: 10.1016/0169-409X(95)00023-Z.

(8) Veronese, F. M. Peptide and protein PEGylation. *Biomaterials* **2001**, *22*, 405–417, DOI: 10.1016/S0142-9612(00)00193-9.

(9) Roberts, M. J.; Bentley, M. D.; Harris, J. M. Chemistry for peptide and protein PEGylation. *Adv. Drug Deliv. Rev.* **2012**, *64*, 116–127, DOI: 10.1016/j.addr.2012.09.025.

(10) Bailon, P.; Palleroni, A.; Schaffer, C. A.; Spence, C. L.; Fung, W.-J.; Porter, J. E.; Ehrlich, G. K.; Pan, W.; Xu, Z.-X.; Modi, M. W. *et al.* Rational Design of a Potent, Long-Lasting Form of Interferon: A 40 kDa Branched Polyethylene Glycol-Conjugated Interferon α-2a for the Treatment of Hepatitis C. *Bioconjugate Chem.* **2001**, *12*, 195–202, DOI: 10.1021/bc000082g.

(11) Zhu, J. Bioactive modification of poly(ethylene glycol) hydrogels for tissue engineering. *Biomaterials* **2010**, *31*, 4639–4656, DOI: 10.1016/j.biomaterials.2010.02.044.

(12) Lin, C.-C.; Anseth, K. S. PEG hydrogels for the controlled release of biomolecules in regenerative medicine. *Pharm. Res.* **2009**, *26*, 631–643, DOI: 10.1007/s11095-008-9801-2.

(13) Hoffman, A. S. Hydrogels for biomedical applications. *Adv. Drug Deliv. Rev.* **2002**, *54*, 3–12, DOI: 10.1016/S0169-409X(01)00239-3.

(14) Hennink, W.E.; van Nostrum, C.F. Novel crosslinking methods to design hydrogels. *Adv. Drug Deliv. Rev.* **2002**, *54*, 13–36, DOI: 10.1016/S0169-409X(01)00240-X.

(15) El-Sherbiny, I. M.; Yacoub, M. H. Hydrogel scaffolds for tissue engineering: Progress and challenges. *Glob. Cardiol. Sci. Pract.* **2013**, *2013*, 316–342, DOI: 10.5339/gcsp.2013.38.

(16) Koetting, M. C.; Peters, J. T.; Steichen, S. D.; Peppas, N. A. Stimulus-responsive hydrogels: Theory, modern advances, and applications. *Mater. Sci. Eng. R Rep.* **2015**, *93*, 1–49, DOI: 10.1016/j.mser.2015.04.001.

(17) Gil, E. S.; Hudson, S. M. Stimuli-reponsive polymers and their bioconjugates. *Prog. Polym. Sci.* **2004**, *29*, 1173–1222, DOI: 10.1016/j.progpolymsci.2004.08.003.

(18) Li, H.; Zheng, H.; Zhang, Y.; Zhang, W.; Tong, W.; Gao, C. Preparation of photo-responsive poly(ethylene glycol) microparticles and their influence on cell viability. *J. Colloid Interface Sci.* **2018**, *514*, 182–189, DOI: 10.1016/j.jcis.2017.12.031.

(19) Kloxin, A. M.; Kasko, A. M.; Salinas, C. N.; Anseth, K. S. Photodegradable hydrogels for dynamic tuning of physical and chemical properties. *Science* **2009**, *324*, 59–63, DOI: 10.1126/science.1169494.

(20) McKinnon, D. D.; Brown, T. E.; Kyburz, K. A.; Kiyotake, E.; Anseth, K. S. Design and characterization of a synthetically accessible, photodegradable hydrogel for user-directed formation of neural networks. *Biomacromolecules* **2014**, *15*, 2808–2816, DOI: 10.1021/bm500731b.

(21) Kar, M.; Vernon Shih, Y.-R.; Velez, D. O.; Cabrales, P.; Varghese, S. Poly(ethylene glycol) hydrogels with cell cleavable groups for autonomous cell delivery. *Biomaterials* **2016**, *77*, 186–197, DOI: 10.1016/j.biomaterials.2015.11.018.

(22) Choh, S.-Y.; Cross, D.; Wang, C. Facile synthesis and characterization of disulfide-cross-linked hyaluronic acid hydrogels for protein delivery and cell encapsulation. *Biomacromolecules* **2011**, *12*, 1126–1136, DOI: 10.1021/bm101451k.

(23) Jia, H.; Huang, Z.; Li, Z.; Zheng, Z.; Wang, X. One-pot synthesis of highly mechanical and redox-degradable polyurethane hydrogels based on tetra-PEG and disulfide/thiol chemistry. *RSC Adv.* **2016**, *6*, 48863–48869, DOI: 10.1039/C6RA04320H.

(24) Shubin, A. D.; Felong, T. J.; Schutrum, B. E.; Joe, D. S. L.; Ovitt, C. E.; Benoit, D. S. W. Encapsulation of primary salivary gland cells in enzymatically degradable poly(ethylene glycol) hydrogels promotes acinar cell characteristics. *Acta Biomater.* **2017**, *50*, 437–449, DOI: 10.1016/j.actbio.2016.12.049.

(25) Mann, B. K.; Gobin, A. S.; Tsai, A. T.; Schmedlen, R. H.; West, J. L. Smooth muscle cell growth in photopolymerized hydrogels with cell adhesive and proteolytically degradable domains: synthetic ECM analogs for tissue engineering. *Biomaterials* **2001**, *22*, 3045–3051, DOI: 10.1016/S0142-9612(01)00051-5.

(26) Soni, G.; Yadav, K. S. Nanogels as potential nanomedicine carrier for treatment of cancer: A mini review of the state of the art. *Saudi Pharm. J.* **2016**, *24*, 133–139, DOI: 10.1016/j.jsps.2014.04.001.

(27) Chacko, R. T.; Ventura, J.; Zhuang, J.; Thayumanavan, S. Polymer nanogels: a versatile nanoscopic drug delivery platform. *Adv. Drug Deliv. Rev.* **2012**, *64*, 836–851, DOI: 10.1016/j.addr.2012.02.002.

(28) Kaihara, S.; Matsumura, S.; Fisher, J. P. Synthesis and Properties of Poly[poly(ethylene glycol)- co -cyclic acetal] Based Hydrogels. *Macromolecules* **2007**, *40*, 7625–7632, DOI: 10.1021/ma071297p.

(29) Betz, M. W.; Caccamese, J. F.; Coletti, D. P.; Sauk, J. J.; Fisher, J. P. Tissue response and orbital floor regeneration using cyclic acetal hydrogels. *J. Biomed. Mater. Res. A* **2009**, *90*, 819–829, DOI: 10.1002/jbm.a.32131.

(30) Salimath, A. S.; García, A. J. Biofunctional hydrogels for skeletal muscle constructs. *J. Tissue Eng. Regen. Med.* **2016**, *10*, 967–976, DOI: 10.1002/term.1881.

(31) He, L.; Fullenkamp, D. E.; Rivera, J. G.; Messersmith, P. B. pH responsive self-healing hydrogels formed by boronate-catechol complexation. *Chem. Commun.* **2011**, *47*, 7497–7499, DOI: 10.1039/c1cc11928a.

(32) Zhang, L.; Jeong, Y.-I.; Zheng, S.; Jang, S. I.; Suh, H.; Kang, D. H.; Kim, I. Biocompatible and pH-sensitive PEG hydrogels with degradable phosphoester and phosphoamide linkers end-capped with amine for controlled drug delivery. *Polym. Chem.* **2013**, *4*, 1084–1094, DOI: 10.1039/C2PY20755A.

(33) Pohlit, H.; Bellinghausen, I.; Schömer, M.; Heydenreich, B.; Saloga, J.; Frey, H. Biodegradable pH-Sensitive Poly(ethylene glycol) Nanocarriers for Allergen Encapsulation and Controlled Release. *Biomacromolecules* **2015**, *16*, 3103–3111, DOI: 10.1021/acs.biomac.5b00458.

(34) Schröder, R.; Pohlit, H.; Schüler, T.; Panthöfer, M.; Unger, R. E.; Frey, H.; Tremel, W. Transformation of vaterite nanoparticles to hydroxycarbonate apatite in a hydrogel scaffold: relevance to bone formation. *J. Mater. Chem. B* **2015**, *3*, 7079–7089, DOI: 10.1039/C5TB01032B.

(35) Tonhauser, C.; Schüll, C.; Dingels, C.; Frey, H. Branched Acid-Degradable, Biocompatible Polyether Copolymers via Anionic Ring-Opening Polymerization Using an Epoxide Inimer. *ACS Macro Lett.* **2012**, *1*, 1094–1097, DOI: 10.1021/mz300265z.

(36) Taton, D.; Le Borgne, A.; Sepulchre, M.; Spassky, N. Synthesis of chiral and racemic functional polymers from glycidol and thioglycidol. *Macromol. Chem. Phys.* **1994**, *195*, 139–148, DOI: 10.1002/macp.1994.021950111.

(37) Tao, Y.; Wang, X.; Zhao, X.; Li, J.; Wang, F. Crosslinkable poly(propylene carbonate): High-yield synthesis and performance improvement. *J. Polym. Sci. A Polym. Chem.* **2006**, *44*, 5329–5336, DOI: 10.1002/pola.21595.

(38) Koyama, Y.; Ito, T.; Matsumoto, H.; Tanioka, A.; Okuda, T.; Yamaura, N.; Aoyagi, H.; Niidome, T. Novel poly(ethylene glycol) derivatives with carboxylic acid pendant groups: synthesis and their protection and enhancing effect on non-viral gene transfection systems. *J. Biomater. Sci., Polym. Ed.* **2003**, *14*, 515–531, DOI: 10.1163/15685620360674227.

(39) Barteau, K. P.; Wolffs, M.; Lynd, N. A.; Fredrickson, G. H.; Kramer, E. J.; Hawker, C. J. Allyl Glycidyl Ether-Based Polymer Electrolytes for Room Temperature Lithium Batteries. *Macromolecules* **2013**, *46*, 8988–8994, DOI: 10.1021/ma401267w.

(40) Zhou, L.; Cheng, R.; Tao, H.; Ma, S.; Guo, W.; Meng, F.; Liu, H.; Liu, Z.; Zhong, Z. Endosomal pH-activatable poly(ethylene oxide)-graft-doxorubicin prodrugs: synthesis, drug release, and biodistribution in tumor-bearing mice. *Biomacromolecules* **2011**, *12*, 1460–1467, DOI: 10.1021/bm101340u.

(41) Hrubý, M.; Konák, C.; Ulbrich, K. Polymeric micellar pH-sensitive drug delivery system for doxorubicin. *J. Control. Release* **2005**, *103*, 137–148, DOI: 10.1016/j.jconrel.2004.11.017.

(42) Wang, K. Development and Synthesis Applications of Olefin Isomerization-Claisen Rearrangement Reactions. Doctoral Dissertation, University of Pittsburgh, 2007.

(43) Fitton, A. O.; Hill, J.; Jane, D. E.; Millar, R. Synthesis of Simple Oxetanes Carrying Reactive 2-Substituents. *Synthesis* **1987**, *1987*, 1140–1142, DOI: 10.1055/s-1987-28203.

(44) Feldman, K. E.; Martin, D. C. Functional Conducting Polymers via Thiol-ene Chemistry. *Biosensors* **2012**, *2*, 305–317, DOI: 10.3390/bios2030305.

(45) Ying, Q.; Chu, B. Overlap concentration of macromolecules in solution. *Macromolecules* **1987**, *20*, 362–366, DOI: 10.1021/ma00168a023.

(46) Burchard, W. Solution Properties of Branched Macromolecules. In *Branched Polymers II*; Roovers, J., Ed.; Advances in Polymer Science 143; Springer: Berlin, Heidelberg, 1999; pp 113–194.

(47) Peter, M.; Tayalia, P. An alternative technique for patterning cells on poly(ethylene glycol) diacrylate hydrogels. *RSC Adv.* **2016**, *6*, 40878–40885, DOI: 10.1039/C6RA08852J.

(48) Karadağ, E.; Üzüm, Ö. B.; Saraydin, D. Swelling equilibria and dye adsorption studies of chemically crosslinked superabsorbent acrylamide/maleic acid hydrogels. *Eur. Polym. J.* **2002**, *38*, 2133–2141, DOI: 10.1016/S0014-3057(02)00117-9.

(49) Zustiak, S. P.; Leach, J. B. Hydrolytically degradable poly(ethylene glycol) hydrogel scaffolds with tunable degradation and mechanical properties. *Biomacromolecules* **2010**, *11*, 1348–1357, DOI: 10.1021/bm100137q.

(50) Elbert, D. L.; Pratt, A. B.; Lutolf, M. P.; Halstenberg, S.; Hubbell, J. A. Protein delivery from materials formed by self-selective conjugate addition reactions. *J. Control. Release* **2001**, *76*, 11–25, DOI: 10.1016/S0168-3659(01)00398-4.

(51) Flory, P. J.; Rehner, J. Statistical Mechanics of Cross-Linked Polymer Networks II. Swelling. *J. Chem. Phys.* **1943**, *11*, 521–526, DOI: 10.1063/1.1723792.

(52) Bray, J. C.; Merrill, E. W. Poly(vinyl alcohol) hydrogels. Formation by electron beam irradiation of aqueous solutions and subsequent crystallization. *J. Appl. Polym. Sci.* **1973**, *17*, 3779–3794, DOI: 10.1002/app.1973.070171219.

(53) Peppas, N. A.; Merrill, E. W. Crosslinked poly(vinyl alcohol) hydrogels as swollen elastic networks. *J. Appl. Polym. Sci.* **1977**, *21*, 1763–1770, DOI: 10.1002/app.1977.070210704.

(54) Slaughter, B. V.; Khurshid, S. S.; Fisher, O. Z.; Khademhosseini, A.; Peppas, N. A. Hydrogels in regenerative medicine. *Adv. Mater. (Weinheim, Ger.)* **2009**, *21*, 3307–3329, DOI: 10.1002/adma.200802106.

(55) Merrill, E. W.; Dennison, K. A.; Sung, C. Partitioning and diffusion of solutes in hydrogels of poly(ethylene oxide). *Biomaterials* **1993**, *14*, 1117–1126, DOI: 10.1016/0142-9612(93)90154-T.

(56) Canal, T.; Peppas, N. A. Correlation between mesh size and equilibrium degree of swelling of polymeric networks. *J. Biomed. Mater. Res.* **1989**, *23*, 1183–1193, DOI: 10.1002/jbm.820231007.

(57) Flory, P. J. *Statistical mechanics of chain molecules*; Interscience Publ: New York, 1969.

(58) Barot, B. C.; Pinnick, H. W. Preparation of formaldehyde and acetaldehyde acetals. *J. Org. Chem.* **1981**, *46*, 2981–2983, DOI: 10.1021/jo00327a032.

(59) Seiwert, J.; Leibig, D.; Kemmer-Jonas, U.; Bauer, M.; Perevyazko, I.; Preis, J.; Frey, H. Hyperbranched Polyols via Copolymerization of 1,2-Butylene Oxide and Glycidol: Comparison of Batch Synthesis and Slow Monomer Addition. *Macromolecules* **2016**, *49*, 38–47, DOI: 10.1021/acs.macromol.5b02402.

(60) Price, C. C.; Snyder, W. H. Solvent effects in the base-catalyzed isomerization of allyl to propenyl ethers. *J. Am. Chem. Soc.* **1961**, *83*, 1773, DOI: 10.1021/ja01468a062.

(61) Prosser, T. J. The Rearrangement of Allyl Ethers to Propenyl Ethers. *J. Am. Chem. Soc.* **1961**, *83*, 1701–1704, DOI: 10.1021/ja01468a035.

(62) Kropf, H.; Schaumann, E. *Methoden der organischen Chemie: En,X- und In,X-Verbindungen*; Georg Thieme Verlag: Stuttgart, 1993.

(63) Lee, B. F.; Kade, M. J.; Chute, J. A.; Gupta, N.; Campos, L. M.; Fredrickson, G. H.; Kramer, E. J.; Lynd, N. A.; Hawker, C. J. Poly(allyl glycidyl ether)-A versatile and functional polyether platform. *J. Polym. Sci. A Polym. Chem.* **2011**, *49*, 4498–4504, DOI: 10.1002/pola.24891.

(64) Murakami, T.; Kawamori, T.; Gopez, J. D.; McGrath, A. J.; Klinger, D.; Saito, K. Synthesis of PEO-based physical gels with tunable viscoelastic properties. *J. Polym. Sci. A Polym. Chem.* **2018**, *18*, 1345, DOI: 10.1002/pola.28992.

(65) Herzberger, J.; Fischer, K.; Leibig, D.; Bros, M.; Thiermann, R.; Frey, H. Oxidation-Responsive and "Clickable" Poly(ethylene glycol) via Copolymerization of 2-(Methylthio)ethyl Glycidyl Ether. *J. Am. Chem. Soc.* **2016**, *138*, 9212–9223, DOI: 10.1021/jacs.6b04548.

(66) Niederer, K.; Schüll, C.; Leibig, D.; Johann, T.; Frey, H. Catechol Acetonide Glycidyl Ether (CAGE): A Functional Epoxide Monomer for Linear and Hyperbranched Multi-Catechol Functional Polyether Architectures. *Macromolecules* **2016**, *49*, 1655–1665, DOI: 10.1021/acs.macromol.5b02441.

(67) Jaacks, V. A novel method of determination of reactivity ratios in binary and ternary copolymerizations. *Makromol. Chem.* **1972**, *161*, 161–172, DOI: 10.1002/macp.1972.021610110.

(68) Meyer, V. E.; Lowry, G. G. Integral and differential binary copolymerization equations. *J. Polym. Sci. A Gen. Pap.* **1965**, *3*, 2843–2851, DOI: 10.1002/pol.1965.100030811.

(69) Ganta, S.; Devalapally, H.; Shahiwala, A.; Amiji, M. A review of stimuli-responsive nanocarriers for drug and gene delivery. *J. Control. Release* **2008**, *126*, 187–204, DOI: 10.1016/j.jconrel.2007.12.017.

(70) Hoyle, C. E.; Bowman, C. N. Thiol-ene click chemistry. *Angew. Chem. Int. Ed.* **2010**, *49*, 1540–1573, DOI: 10.1002/anie.200903924.

(71) Lowe, A. B. Thiol–ene "click" reactions and recent applications in polymer and materials synthesis: A first update. *Polym. Chem.* **2014**, *5*, 4820, DOI: 10.1039/C4PY00339J.

(72) Obermeier, B.; Frey, H. Poly(ethylene glycol-co-allyl glycidyl ether)s: a PEG-based modular synthetic platform for multiple bioconjugation. *Bioconjugate Chem.* **2011**, *22*, 436–444, DOI: 10.1021/bc1004747.

(73) Stichler, S.; Jungst, T.; Schamel, M.; Zilkowski, I.; Kuhlmann, M.; Böck, T.; Blunk, T.; Teßmar, J.; Groll, J. Thiol-ene Clickable Poly(glycidol) Hydrogels for Biofabrication. *Ann. Biomed. Eng.* **2017**, *45*, 273–285, DOI: 10.1007/s10439-016-1633-3.

(74) Xia, Y.; Ding, S.; Liu, Y.; Qi, Z. Facile Synthesis and Self-Assembly of Amphiphilic Polyether-Octafunctionalized Polyhedral Oligomeric Silsesquioxane via Thiol-Ene Click Reaction. *Polymers* **2017**, *9*, 251, DOI: 10.3390/polym9070251.

(75) Fleischmann, C.; Gopez, J.; Lundberg, P.; Ritter, H.; Killops, K. L.; Hawker, C. J.; Klinger, D. A robust platform for functional microgels via thiol–ene chemistry with reactive polyether-based nanoparticles. *Polym. Chem.* **2015**, *6*, 2029–2037, DOI: 10.1039/C4PY01766H.

(76) Wilczek-Vera, G.; Danis, P. O.; Eisenberg, A. Individual Block Length Distributions of Block Copolymers of Polystyrene- block -Poly(α-methylstyrene) by MALDI/TOF Mass Spectrometry. *Macromolecules* **1996**, *29*, 4036–4044, DOI: 10.1021/ma9516394.

(77) van Rooij, G. J.; Duursma, M. C.; Koster, C. G. de; Heeren, R. M.; Boon, J. J.; Schuyl, P. J.; van der Hage, E. R. Determination of Block Length Distributions of Poly(oxypropylene) and Poly(oxyethylene) Block Copolymers by MALDI-FTICR Mass Spectrometry. *Anal. Chem.* **1998**, *70*, 843–850, DOI: 10.1021/ac970609r.

(78) Engler, M. S.; Crotty, S.; Barthel, M. J.; Pietsch, C.; Knop, K.; Schubert, U. S.; Böcker, S. COCONUT—An Efficient Tool for Estimating Copolymer Compositions from Mass Spectra. *Anal. Chem.* **2015**, *87*, 5223–5231, DOI: 10.1021/acs.analchem.5b00146.

(79) Armstrong, J. K.; Wenby, R. B.; Meiselman, H. J.; Fisher, T. C. The Hydrodynamic Radii of Macromolecules and Their Effect on Red Blood Cell Aggregation. *Biophys. J.* **2004**, *87*, 4259–4270, DOI: 10.1529/biophysj.104.047746.

Supporting Information

Design of a Novel Epoxide Monomer for pH-Sensitive Poly(ethylene glycol) Hydrogels via Acid-Labile and Crosslinkable Allyl Side Groups

Kamil Maciol[a], Gregor Linden[a], Jan Blankenburg[a,b], Willi Schmolke[a], Sebastian Seiffert[a,] and Holger Frey[a,*]*

[a] Institute of Organic Chemistry, Johannes Gutenberg University Mainz, Duesbergweg 10-14, 55128 Mainz, Germany

[b] Graduate School Materials Science in Mainz, Staudinger Weg 9, 55128 Mainz, Germany

*E-Mail: sebastian.seiffert@uni-mainz.de, hfrey@uni-mainz.de

To be submitted

SI-Figure 1. SEC trace of real-time ^{1}H NMR EO/EAGE copolymerization in DMSO-d_6 at 55 °C (M_n = 2,500 g mol^{-1}, $Đ$ = 1.12).
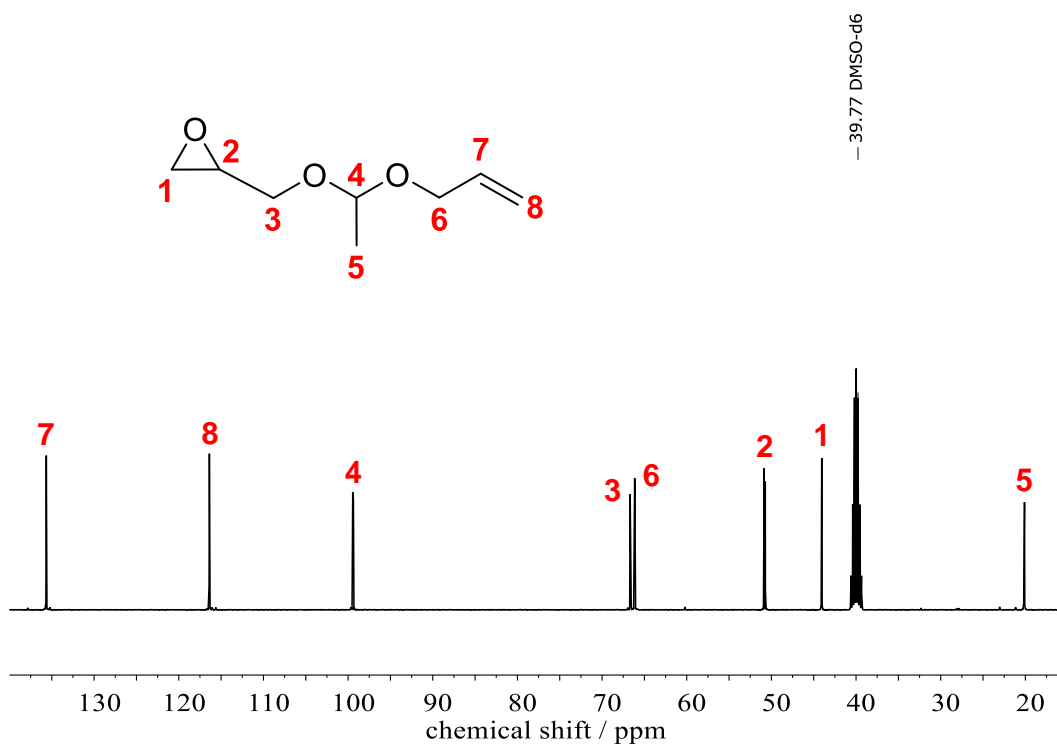
SI-Figure 2. Inverse gated 13C NMR spectrum (100 MHz, DMSO-d_6) of EAGE monomer.
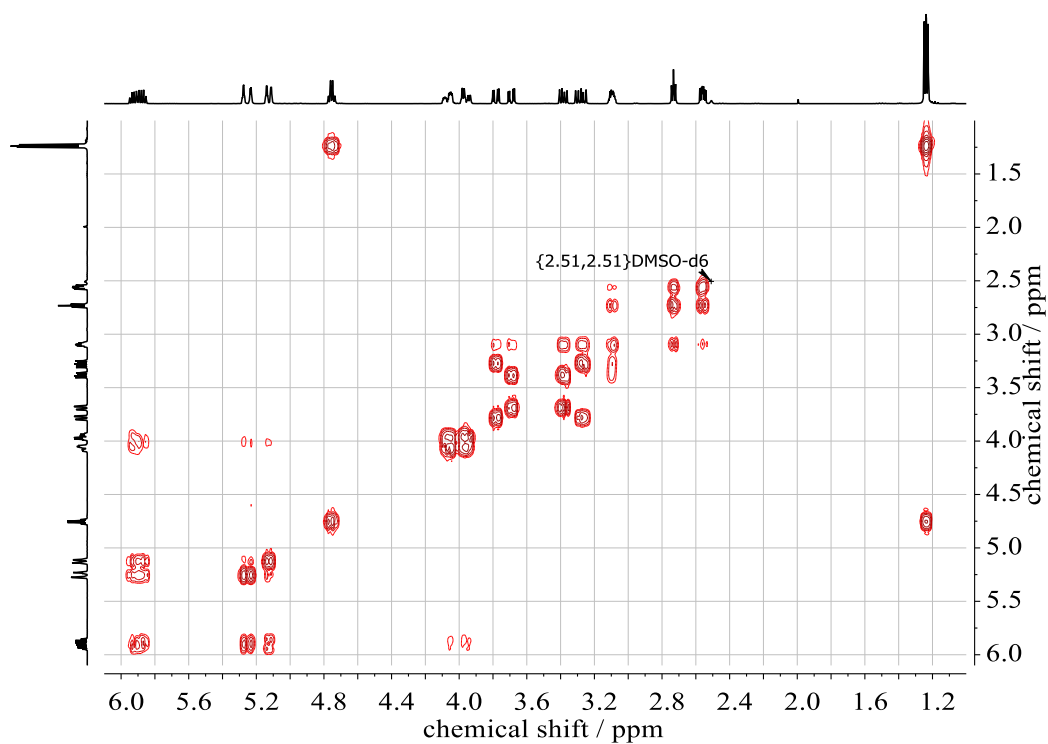
SI-Figure 3. ^{1}H, ^{1}H COSY NMR (400 MHz, DMSO-d_6) of EAGE monomer.
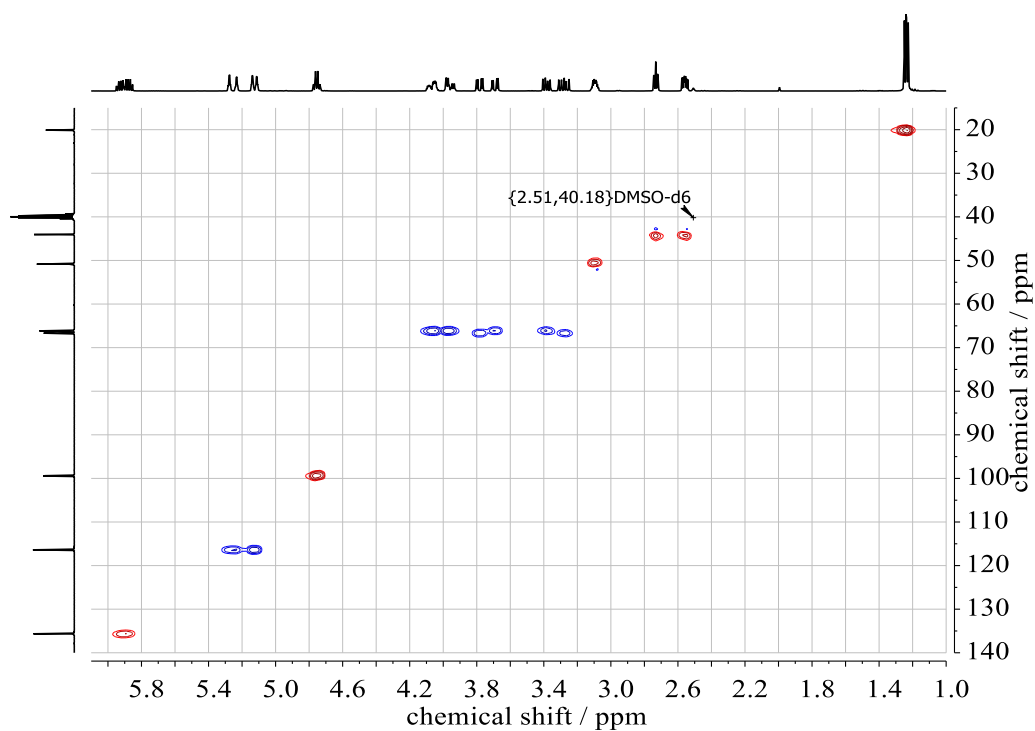
SI-Figure 4. ^{1}H, ^{13}C HSQC NMR of EAGE monomer in DMSO-d_6. Color of the signals indicates the phase information (red: methine proton, blue: methylene protons).
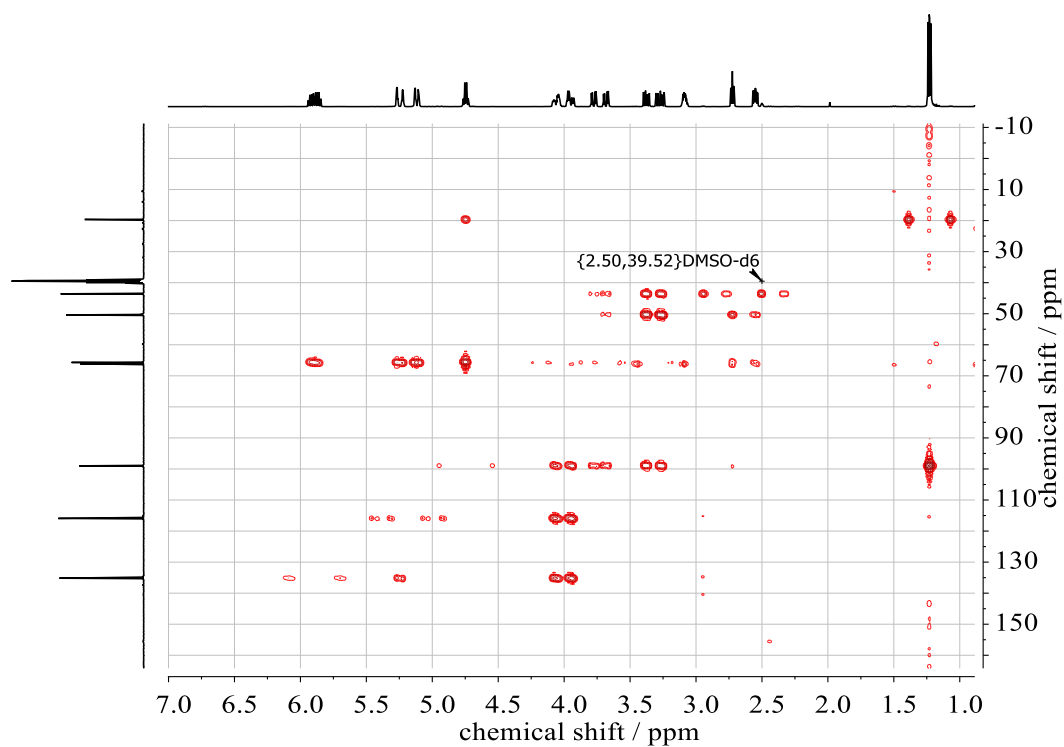
SI-Figure 5. ^{1}H, ^{13}C HMBC NMR of EAGE monomer in DMSO-d_6.
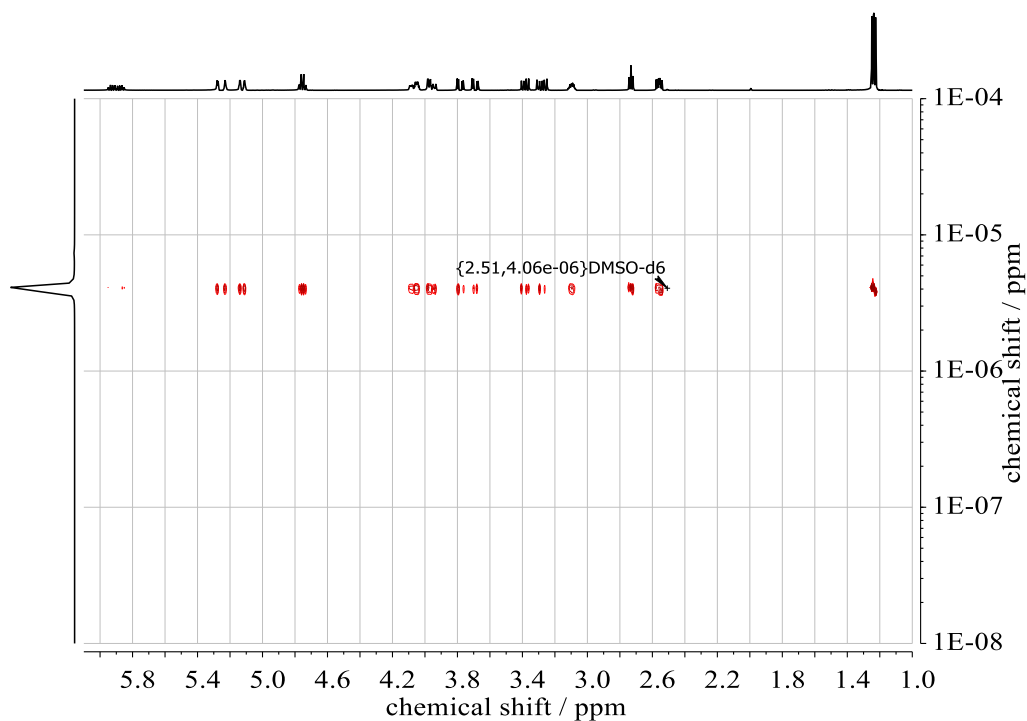
SI-Figure 6. ^{1}H DOSY NMR (400 MHz, DMSO-d_6) of EAGE monomer.
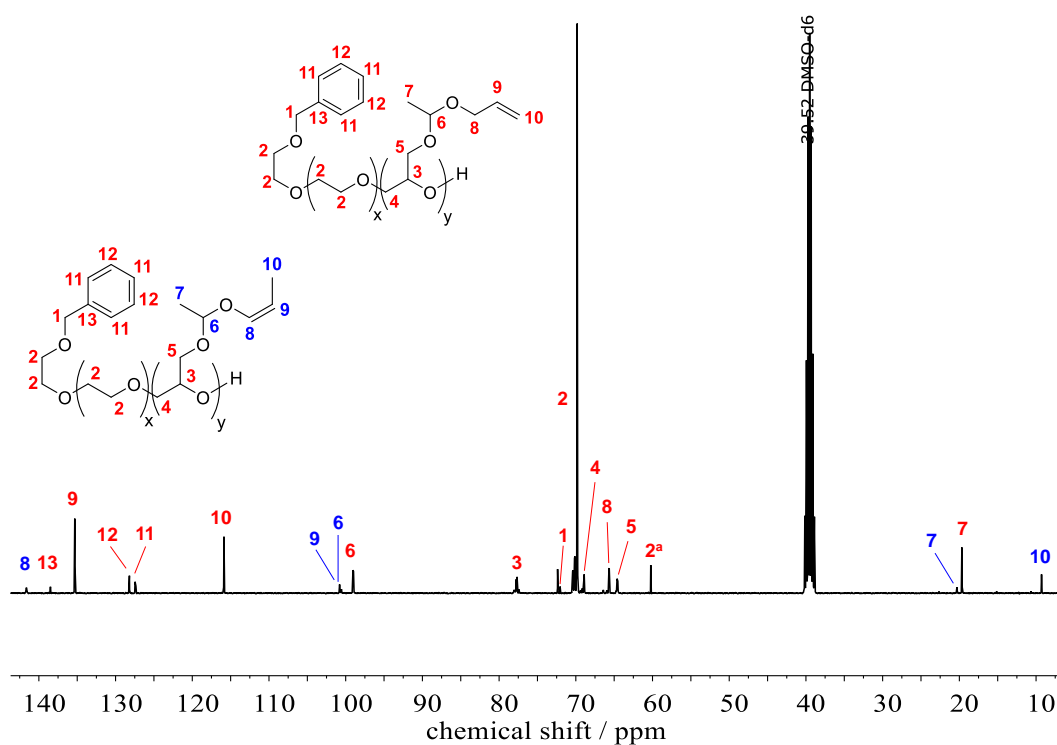
SI-Figure 7. ^{13}C NMR spectrum (100 MHz, DMSO-d_6) of PEG$_{86}$-*ran*-PEAGE$_{13}$ (entry 4, **Table 1**); upper structure: ally structure, lower structure: *cis*-prop-1-enyl isomer. [a]-**C**H$_2$-OH of chain ends.[1,2]
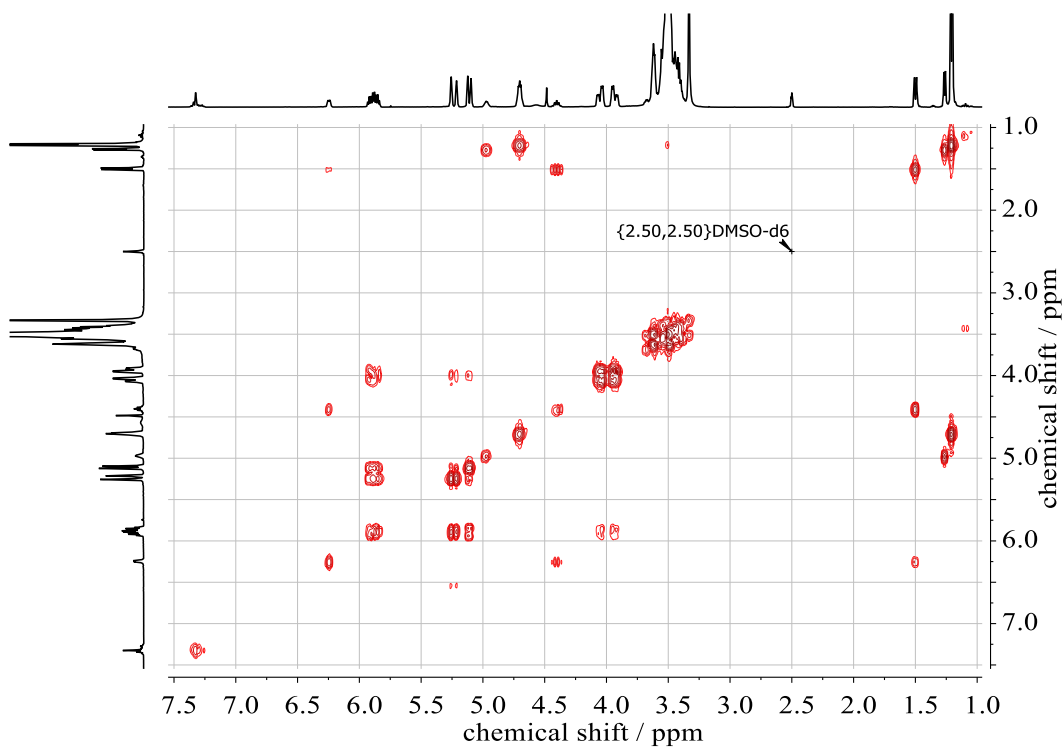
SI-Figure 8. ^{1}H, ^{1}H COSY NMR (400 MHz, DMSO-d_6) of PEG$_{86}$-*ran*-PEAGE$_{13}$ (entry 4, **Table 1**).
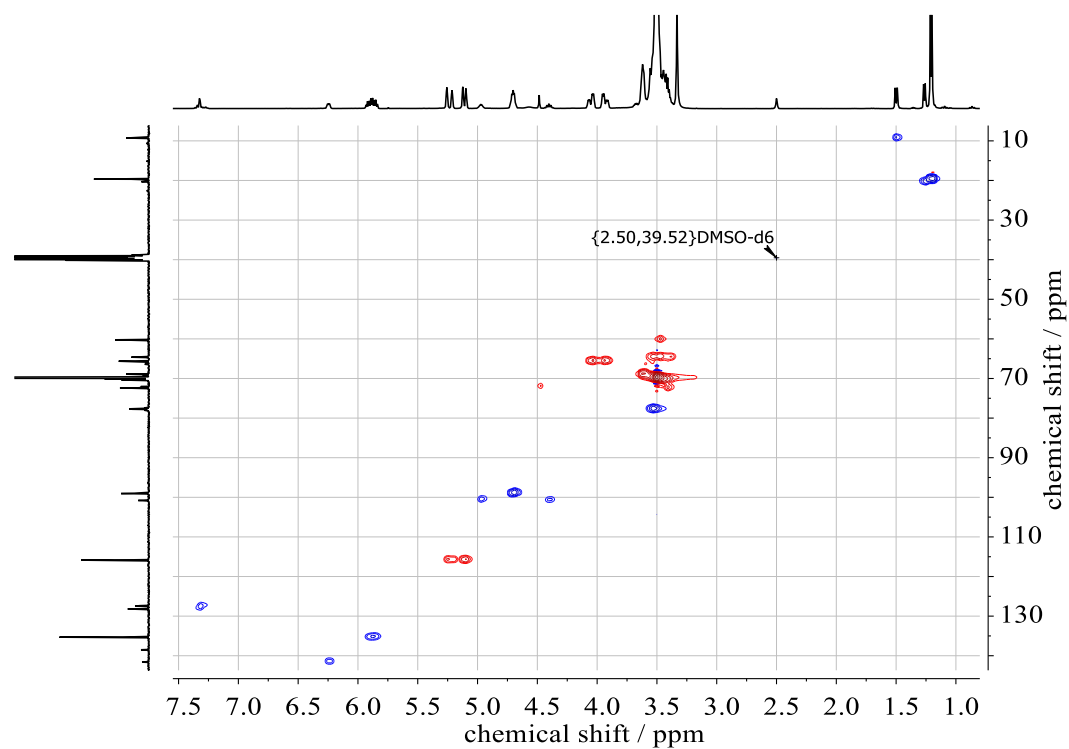
SI-Figure 9. ^{1}H, ^{13}C HSQC NMR of PEG$_{86}$-*ran*-PEAGE$_{13}$ (entry 4, **Table 1**) in DMSO-d_6. Color of the signals indicates the phase information (red: methine proton, blue: methylene protons).
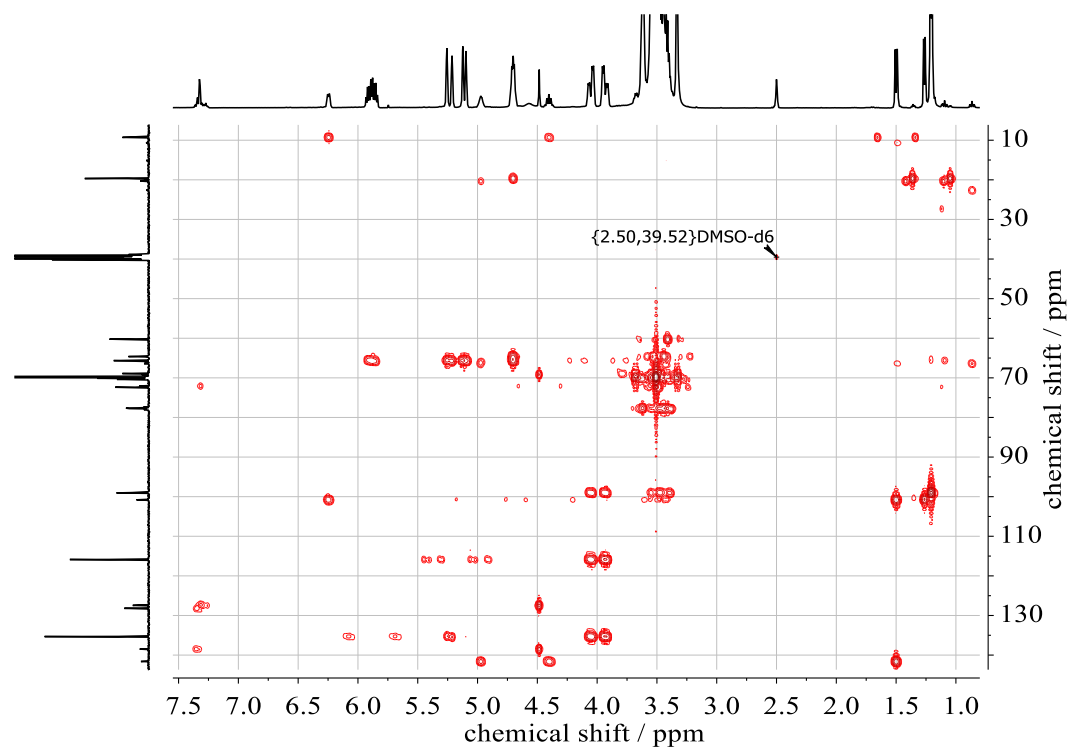
SI-Figure 10. ^{1}H, ^{13}C HMBC NMR of PEG$_{86}$-*ran*-PEAGE$_{13}$ (entry 4, **Table 1**) in DMSO-d_6.
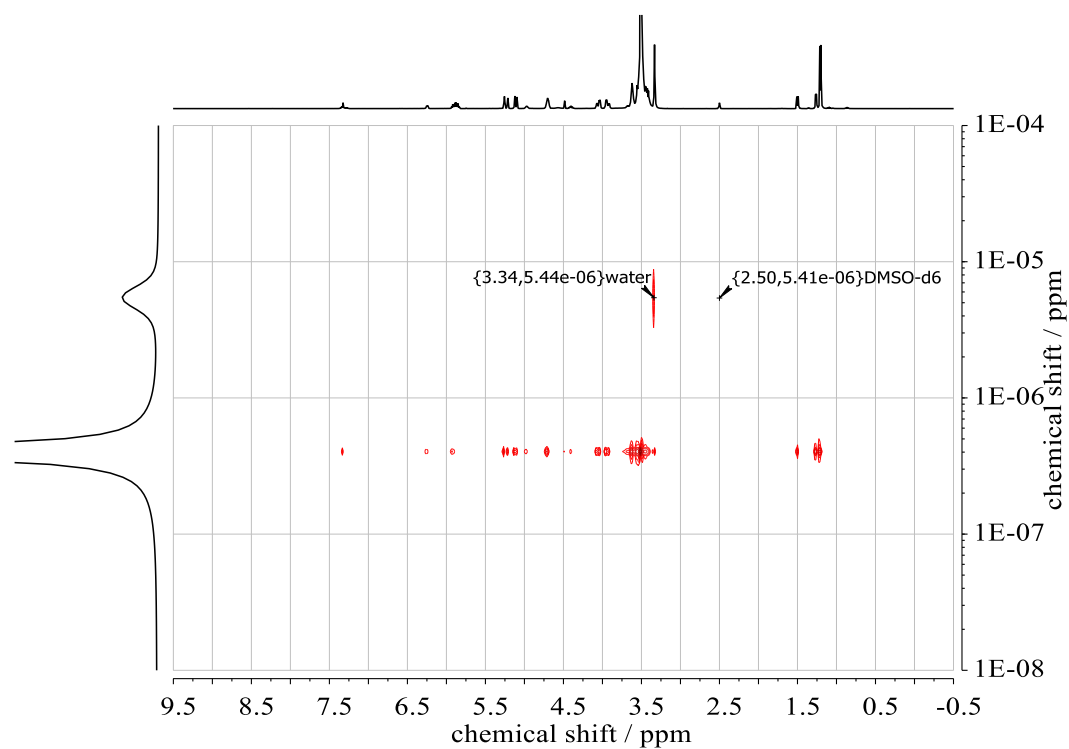
SI-Figure 11. ^{1}H DOSY NMR spectrum (400 MHz, DMSO-d_6) of PEG$_{86}$-*ran*-PEAGE$_{13}$ (entry 4, **Table 1**).
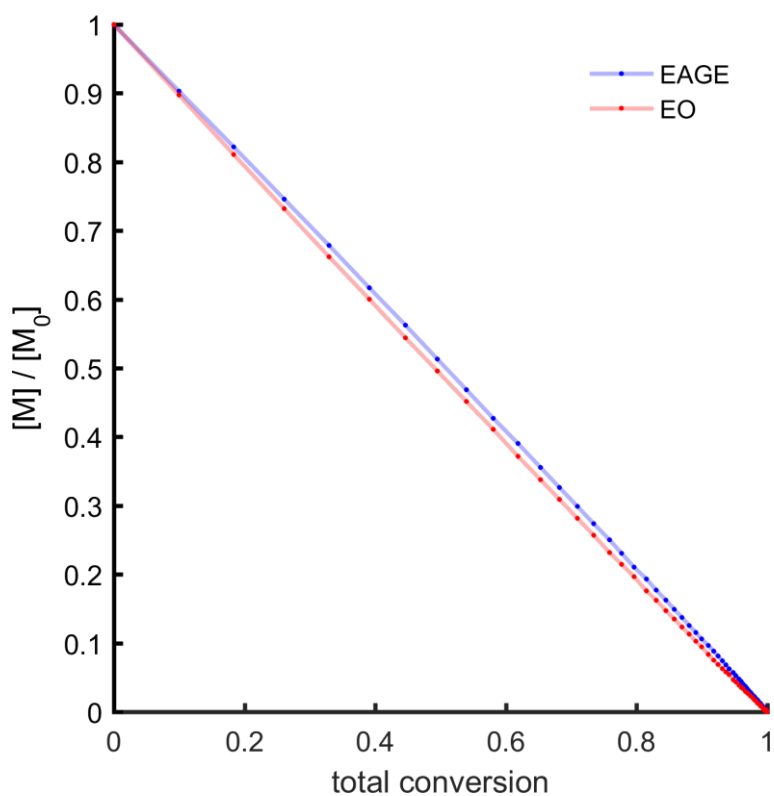
SI-Figure 12. Concentration of the comonomers EO and EAGE plotted versus the conversion.
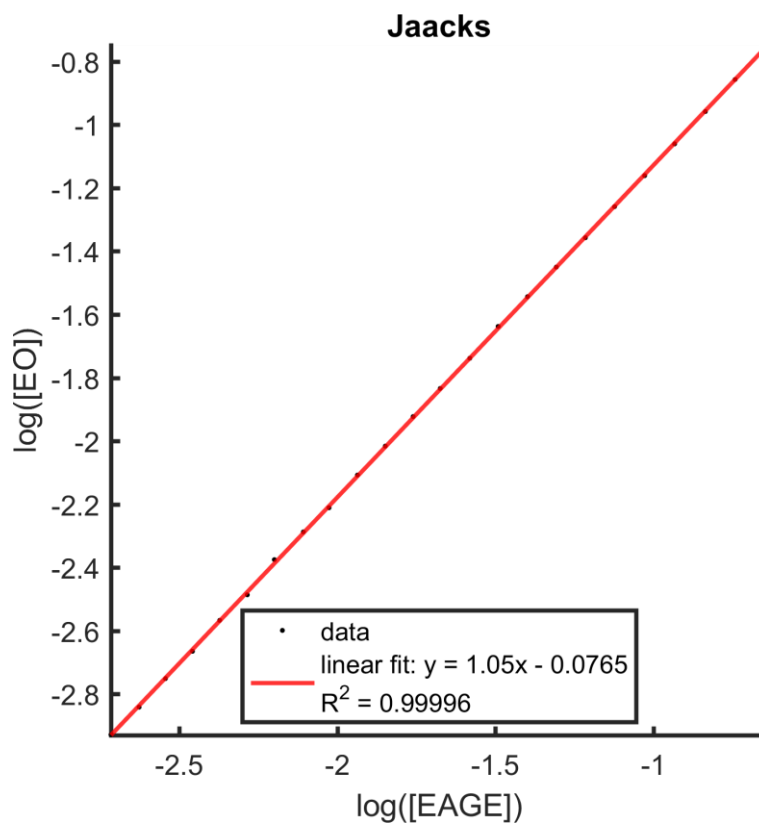
SI-Figure 13. Ideal (Jaacks) fit for determination of reactivity ratios of the EAGE/EO copolymerization in DMSO-d_6 at 55 °C.
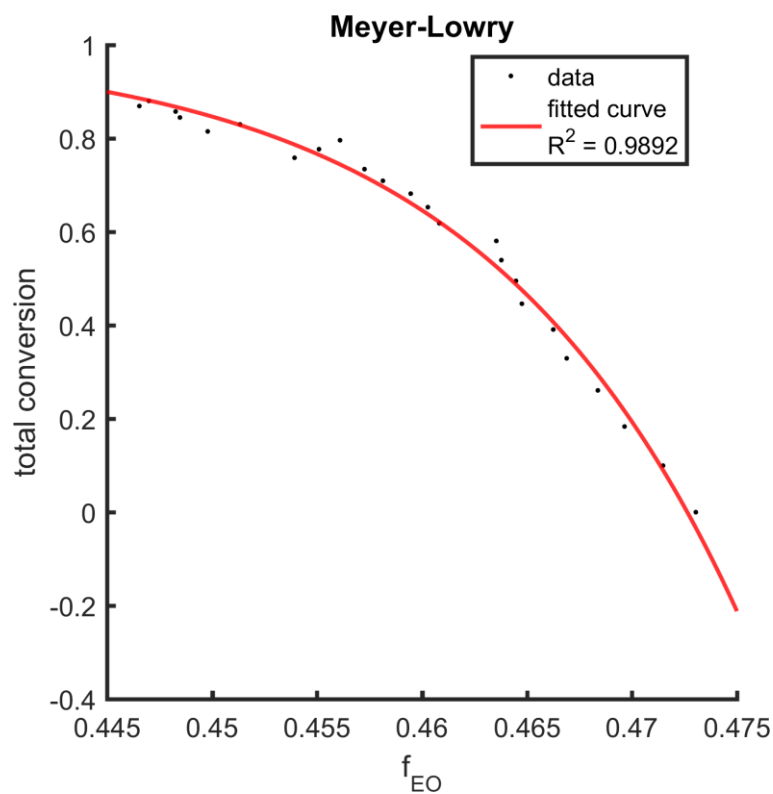
SI-Figure 14. Meyer-Lowry fit for determination of reactivity ratios of the EAGE/EO copolymerization in DMSO-d_6 at 55 °C.
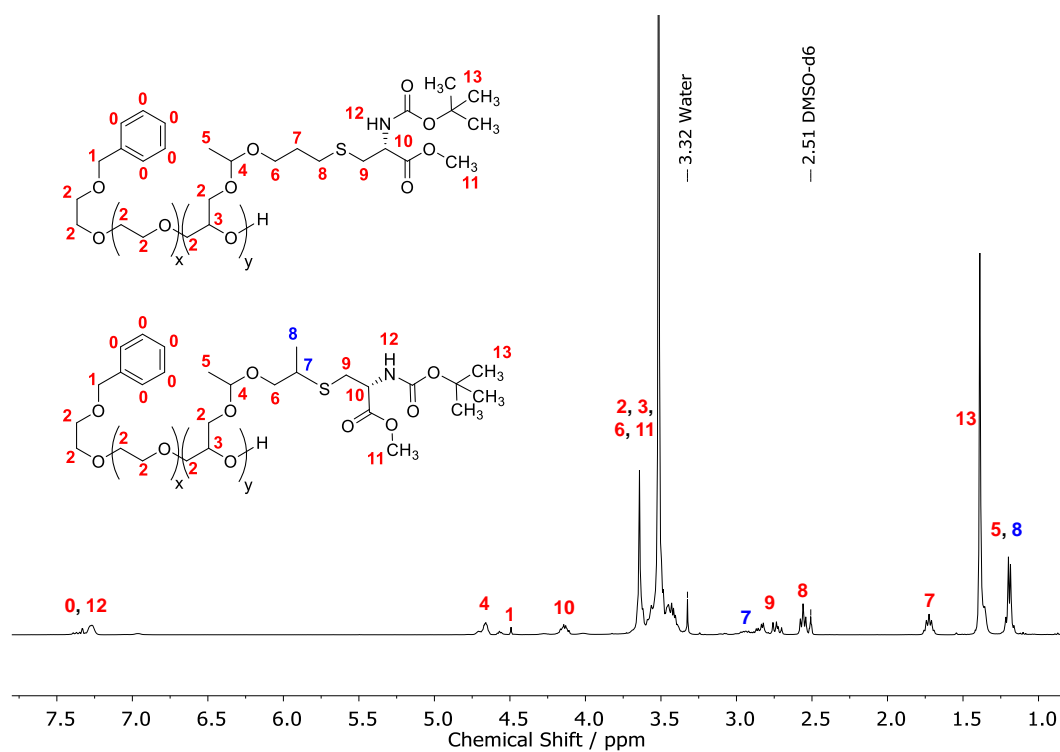
SI-Figure 15. ^{1}H NMR spectrum (400 MHz, DMSO-*d₆*) of BCCME functionalized PEG₈₆-*ran*-PEAGE₁₃.
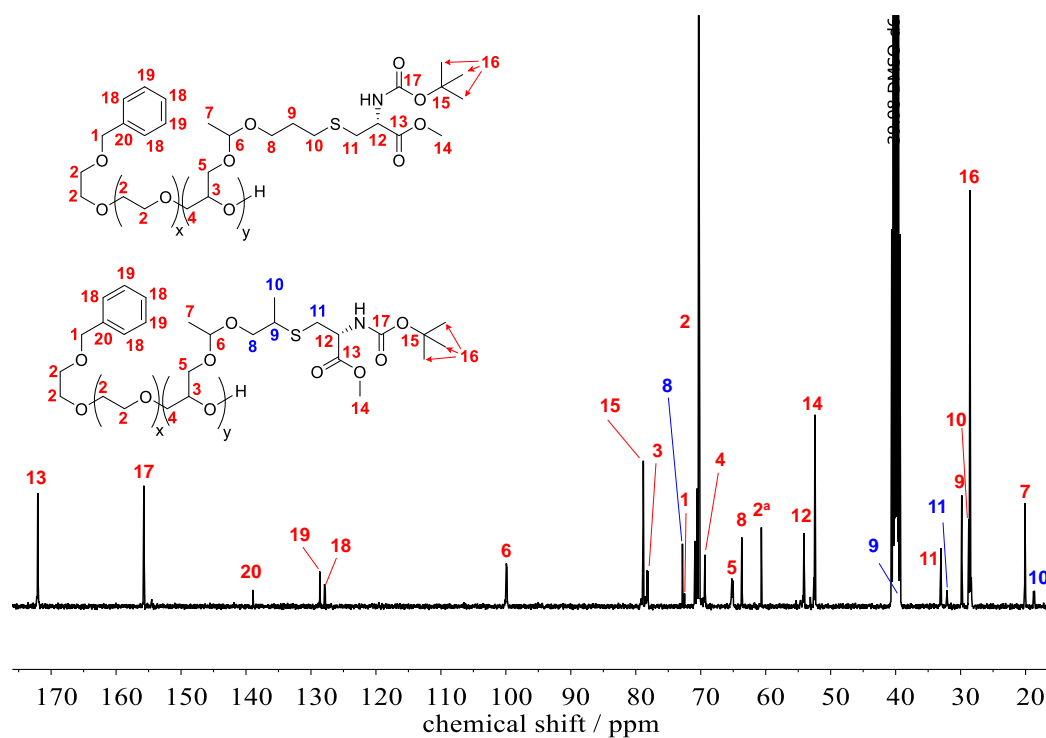
SI-Figure 16. ^{13}C NMR spectrum (400 MHz, DMSO-*d₆*) of BCCME-modified PEG₈₆-*ran*-PEAGE₁₃. [a]-**C**H₂-OH of chain ends.[1,2]
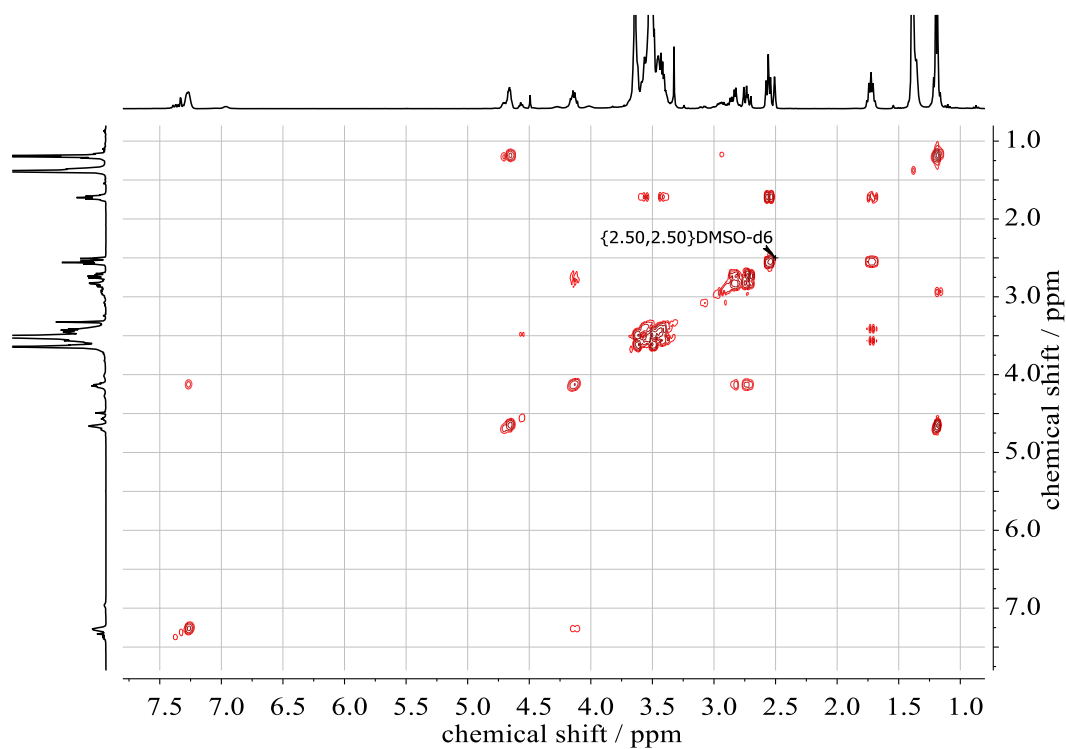
SI-Figure 17. ^{1}H, ^{1}H COSY NMR (400 MHz, DMSO-d_6) of BCCME-modified PEG$_{86}$-*ran*-PEAGE$_{13}$.
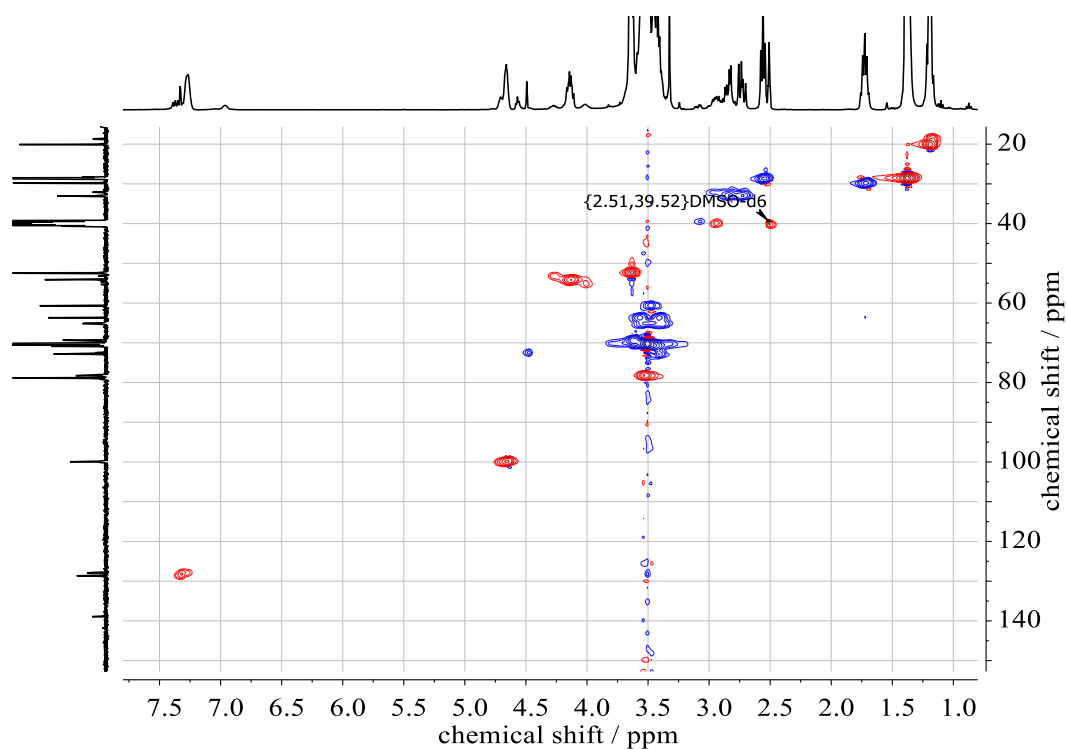
SI-Figure 18. ^{1}H, ^{13}C HSQC NMR of BCCME-modified PEG$_{86}$-*ran*-PEAGE$_{13}$ in DMSO-d_6. Color of the signals indicates the phase information (red: methine proton, blue: methylene protons).
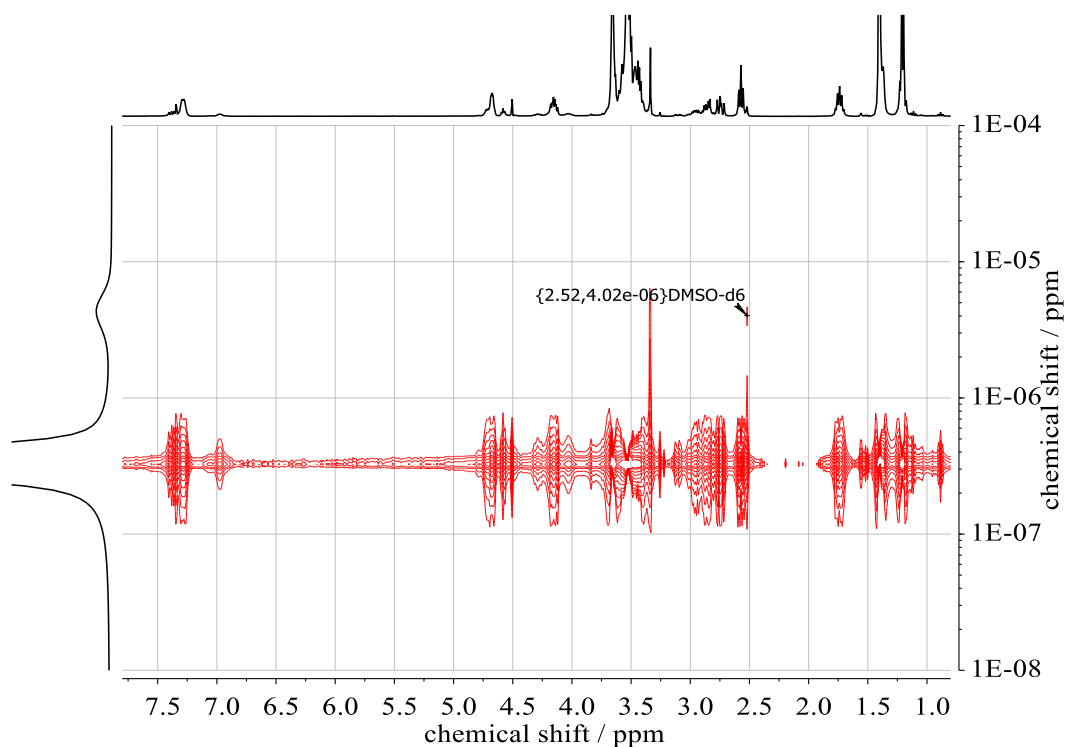
SI-Figure 19. ^{1}H DOSY NMR spectrum (400 MHz, DMSO-d_6) of BCCME-modified PEG$_{86}$-*ran*-PEAGE$_{13}$.
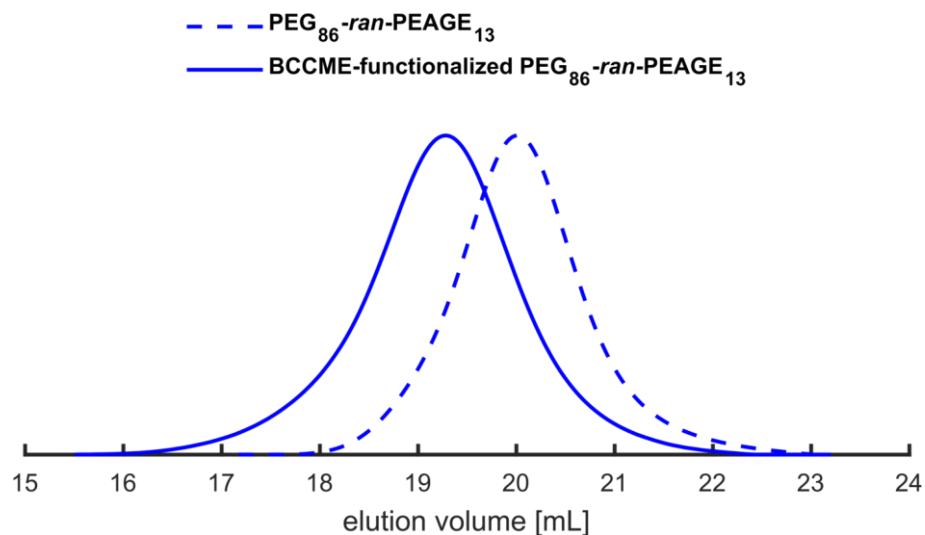
SI-Figure 20. SEC traces of precursor PEG$_{86}$-*ran*-PEAGE$_{13}$ (entry 4, **Table 1**) and BCCME-modified copolymer before and after thiol-ene click reaction (before: M_n = 2,500 g mol^{-1}, $Đ$ = 1.12; after: M_n = 3,600 g mol^{-1}, $Đ$ = 1.17).
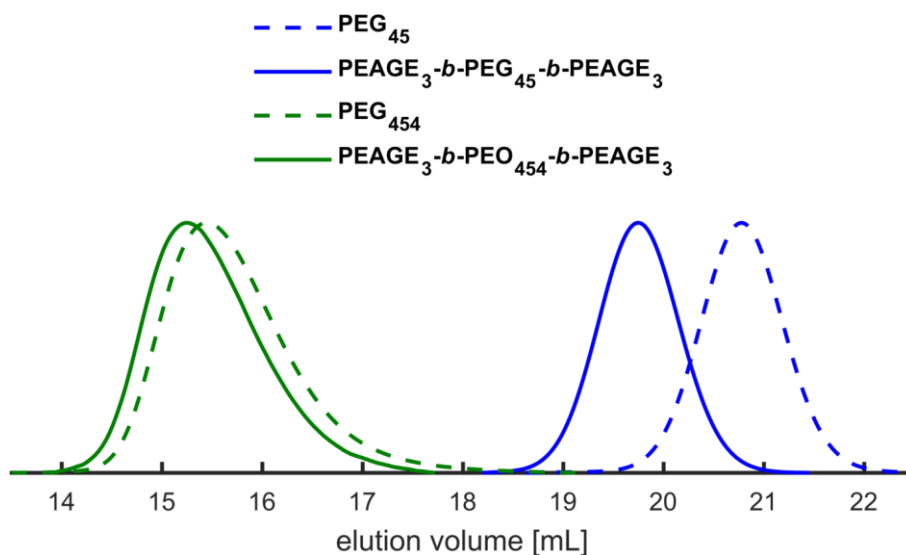
SI-Figure 21. Shift of the SEC traces of PEAGE$_3$-*b*-PEG$_{45}$-*b*-PEAGE$_3$ (entry 1, **Table 4**), PEAGE$_3$-*b*-PEG$_{455}$-*b*-PEAGE$_3$ (entry 5, **Table 4**) and the respective unfunctionalized PEG macroinitiators as exemplary representation.
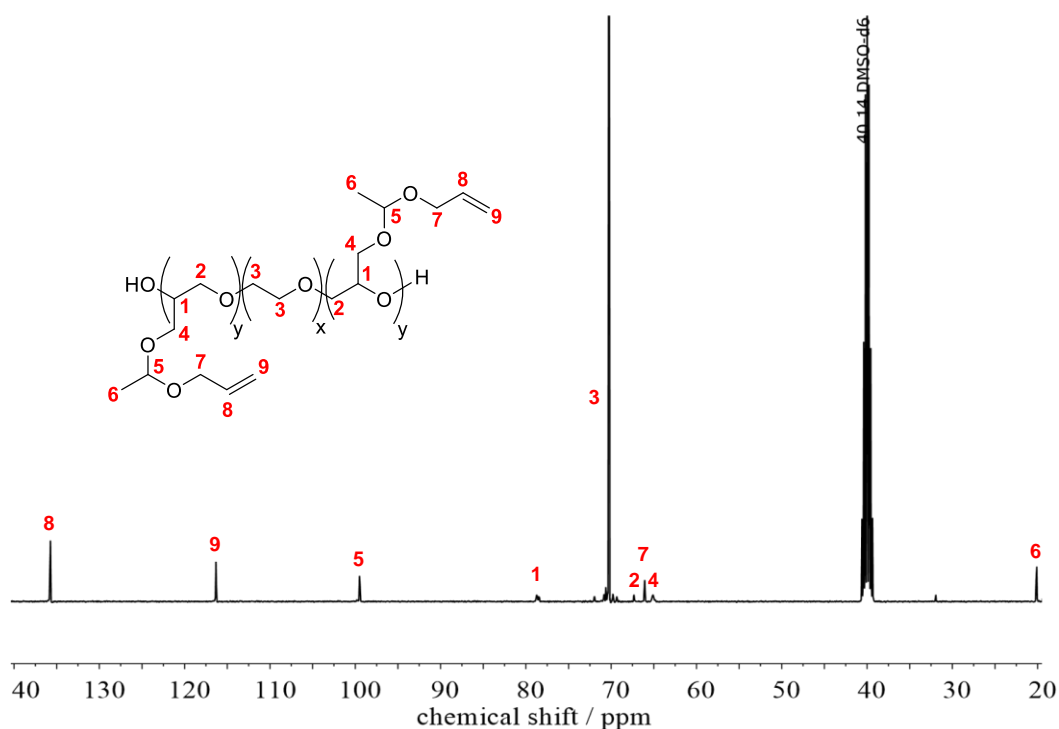
SI-Figure 22. ^{13}C NMR spectrum (100 MHz, DMSO-d_6) of PEAGE$_3$-*b*-PEG$_{45}$-*b*-PEAGE$_3$ (entry 1, **Table 4**).
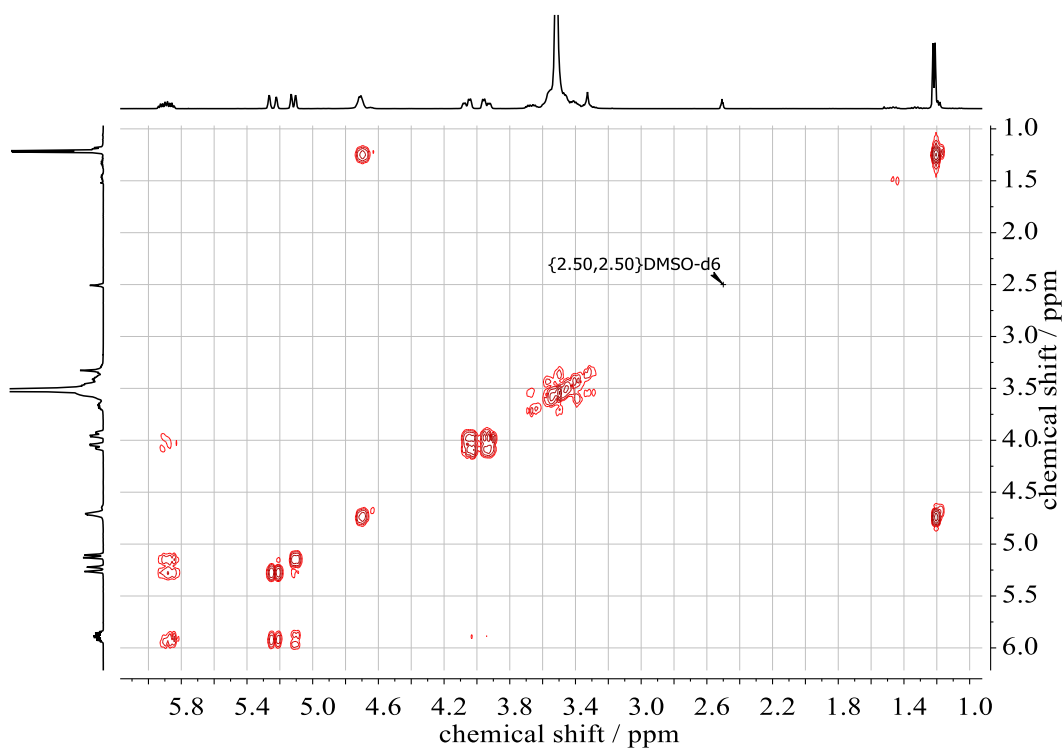
SI-Figure 23. ^{1}H, ^{1}H COSY NMR (400 MHz, DMSO-d_6) of PEAGE$_3$-b-PEG$_{45}$-b-PEAGE$_3$ (entry 1, **Table 4**).
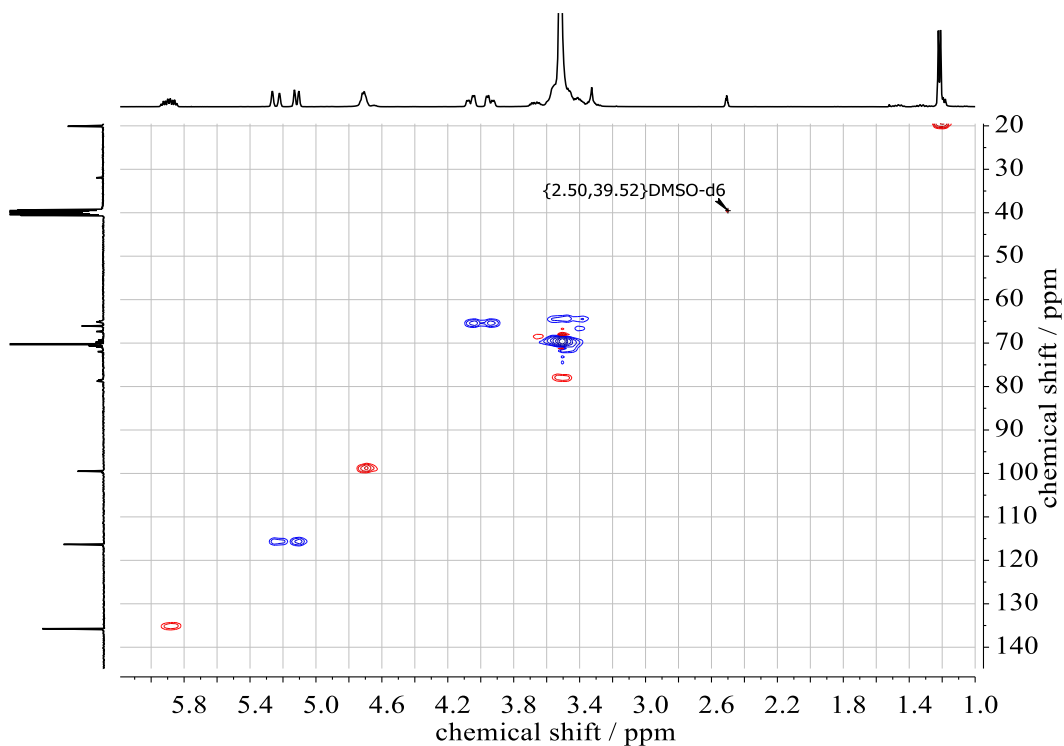
SI-Figure 24. ^{1}H, ^{13}C HSQC NMR of PEAGE$_3$-b-PEG$_{45}$-b-PEAGE$_3$ (entry 1, **Table 4**) in DMSO-d_6. Color of the signals indicates the phase information (red: methine proton, blue: methylene protons).
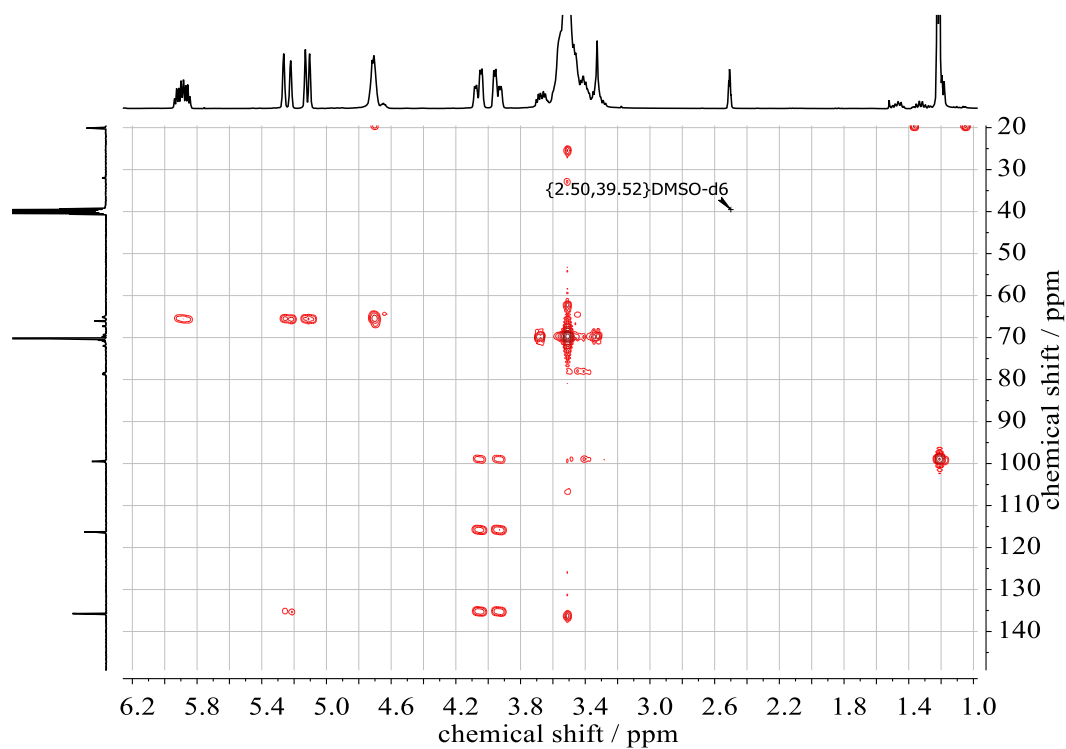
SI-Figure 25. ^{1}H, ^{13}C HMBC NMR of PEAGE$_3$-b-PEG$_{45}$-b-PEAGE$_3$ (entry 1, **Table 4**) in DMSO-d_6.
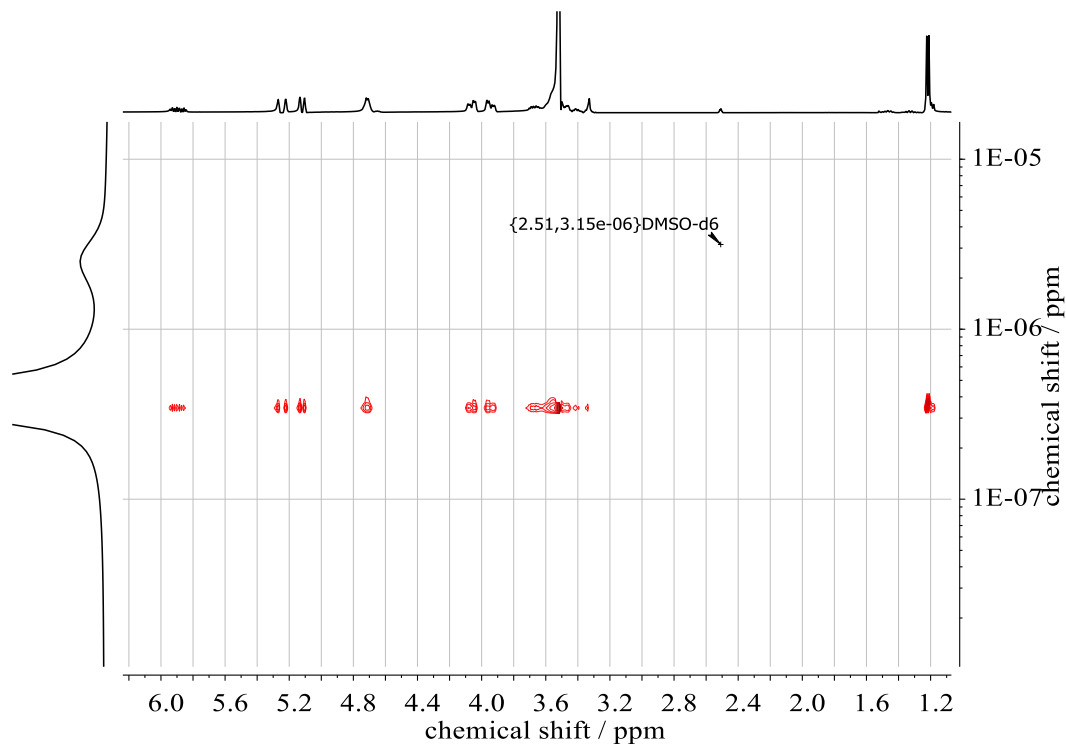
SI-Figure 26. ^{1}H DOSY NMR spectrum (400 MHz, DMSO-d_6) of PEAGE$_3$-b-PEG$_{45}$-b-PEAGE$_3$ (entry 1, **Table 4**).
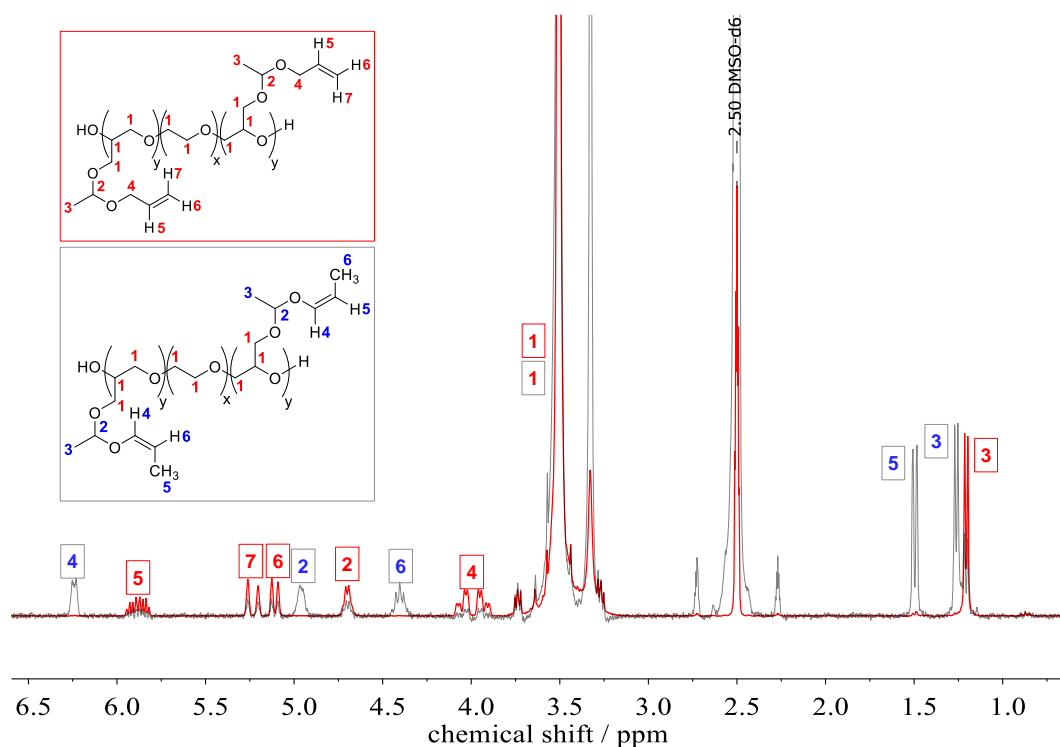
SI-Figure 27. Superimposed ^{1}H NMR spectra (400 MHz, DMSO-d_6) of PEAGE-b-PEG-b-PEAGE triblock copolymers, which were prepared in bulk (red spectrum) and in DMSO (black spectrum) without usage of crown ether.

SI-Table 1. Overview of approaches for the preparation of the acid-cleavable PEAGE-b-PEG-b-PEAGE hydrogels. The amount of PETMP thiols was always used equivalent to the amount of EAGE allyl double bonds.

No.	Composition[a]	w_{HMP}[b] / wt%	w_{PBS}[c] / wt%	t_{irrad}[d] / min
1	PEAGE$_3$-b-PEG$_{45}$-b-PEAGE$_3$	1.5	20	30
2	PEAGE$_3$-b-PEG$_{68}$-b-PEAGE$_3$	1.5	20	30
3	PEAGE$_4$-b-PEG$_{182}$-b-PEAGE$_4$	1.5	15	30
4	PEAGE$_4$-b-PEG$_{227}$-b-PEAGE$_4$	1.5	15	30
5	PEAGE$_3$-b-PEG$_{454}$-b-PEAGE$_3$	1.5	15	30

[a] Values calculated by ^{1}H NMR spectroscopy. [b] Mass fraction of photoinitiator HMP with respect to the total amount of polymer and thiol. As a stock solution, HMP was dissolved in absolute ethanol (10 wt%) and the required amounts were taken from of this solution. [c] Amount of polymer and thiol in PBS for crosslinking experiments. [d] Irradiation duration with the UV lamp
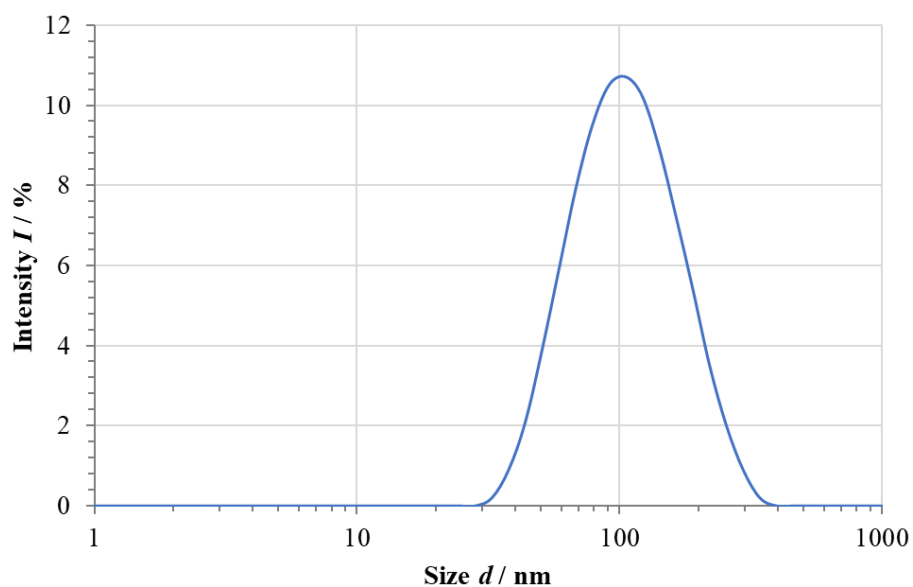
SI-Figure 28. Intensity based particle size distribution of PEAGE$_3$-b-PEG$_{45}$-b-PEAGE$_3$ (entry 1, **Table 4**): c = 5 g · L^{-1}, D_z = 105.1 nm, $Đ$ = 0.33.
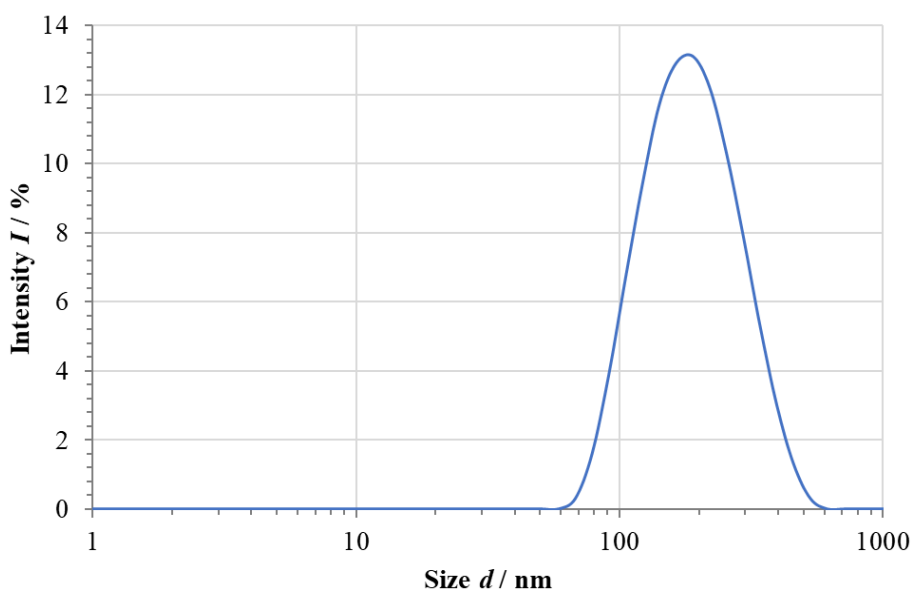
SI-Figure 29. Intensity based particle size distribution of PEAGE$_3$-b-PEG$_{68}$-b-PEAGE$_3$ (entry 2, **Table 4**): c = 5 g · L^{-1}, D_z = 170.7 nm, $Đ$ = 0.14.
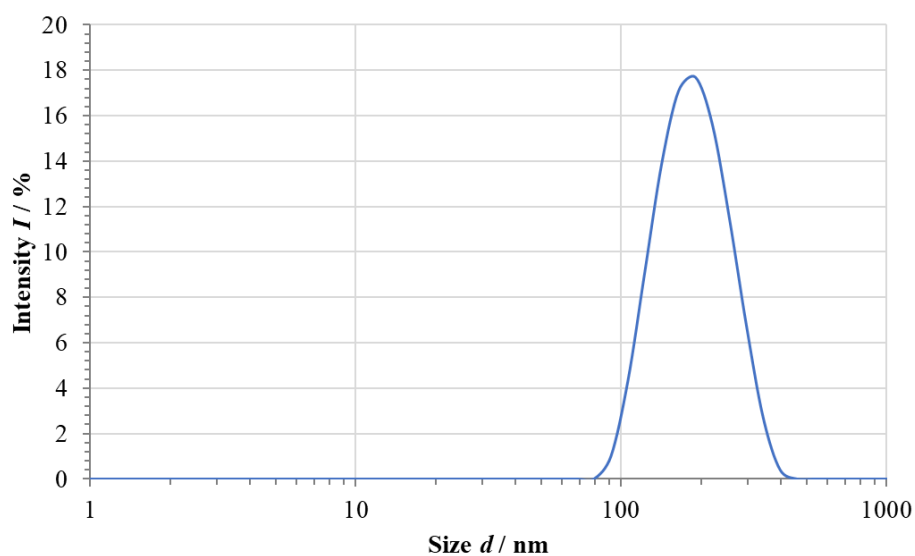
SI-Figure 30. Intensity based particle size distribution of PEAGE$_4$-b-PEG$_{182}$-b-PEAGE$_4$ (entry 3, **Table 4**): $c = 5$ g · L^{-1}, $D_z = 173.8$ nm, Đ $= 0.10$.
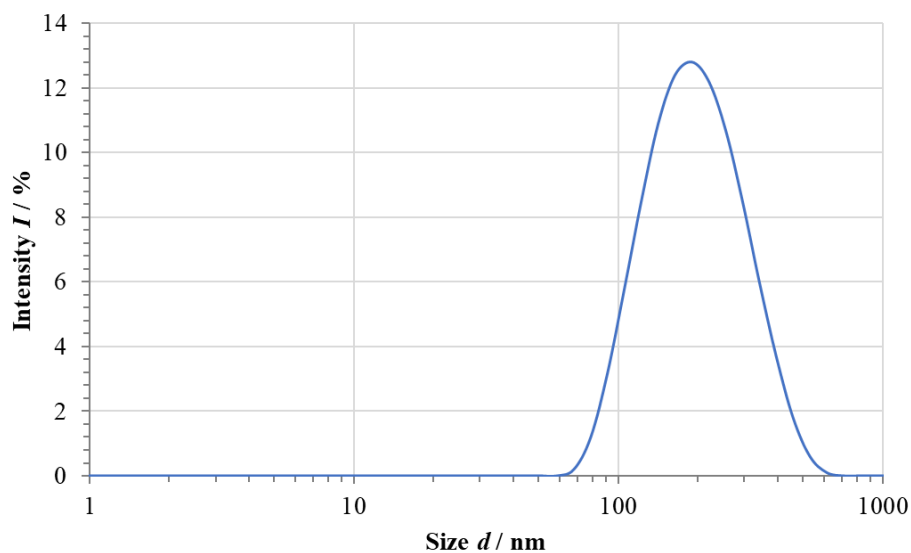
SI-Figure 31. Intensity based particle size distribution of PEAGE$_4$-b-PEG$_{227}$-b-PEAGE$_4$ (entry 4, **Table 4**): $c = 5$ g · L^{-1}, $D_z = 180.4$ nm, Đ $= 0.20$.
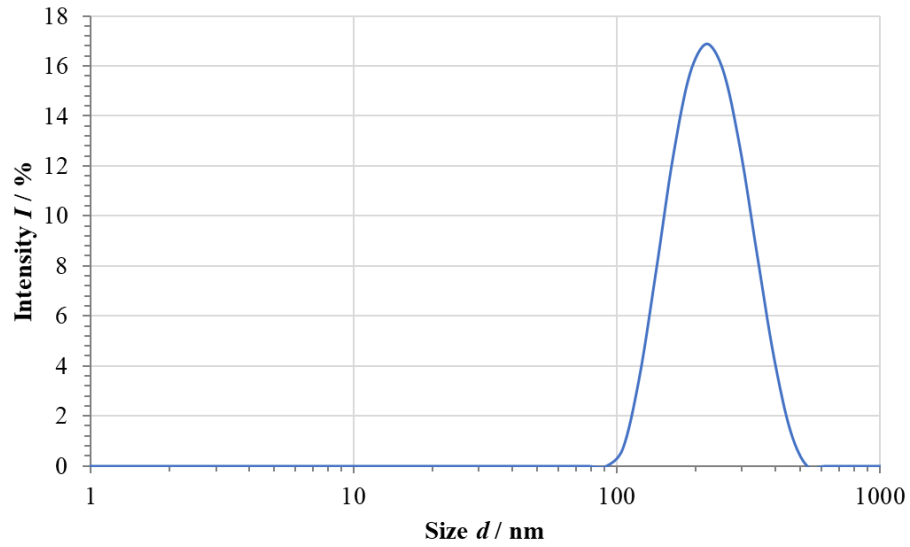
SI-Figure 32. Intensity based particle size distribution of PEAGE$_3$-b-PEG$_{454}$-b-EAGE$_3$ (entry 5, **Table 4**): $c = 5$ g $\cdot$ L^{-1}, $D_z = 192.1$nm, Đ $= 0.22$.

SI-Table 2. Rheological key figures: values for the shear deformations γ (before and after photogelation), angular frequencies ω and time of the crossover t_p.

No.	Composition[a]	γ_{bp}[b] / %	ω_{bp}[c] / rad s^{-1}	t_p[d] / s	γ_{ap}[b] / %
1	PEAGE$_3$-b-PEG$_{45}$-b-PEAGE$_3$	16	4	46	16
2	PEAGE$_3$-b-PEG$_{68}$-b-PEAGE$_3$	8	3	40	8
3	PEAGE$_4$-b-PEG$_{182}$-b-PEAGE$_4$	5	2	50	5
4	PEAGE$_4$-b-PEG$_{227}$-b-PEAGE$_4$	5	5	20	5
5	PEAGE$_3$-b-PEG$_{454}$-b-PEAGE$_3$	7	2	32	7

[a] Values calculated by ^{1}H NMR spectroscopy. [b] Shear deformation values, that were kept constant for frequency sweep and photogelation tests (Index "bp": before photogelation, index "ap": after photogelation). [c] Values for the angular frequency, which were kept constant for the photogelation tests. [d] Time between the turning on of the UV lamp and the moment of the crossover of G' and G''.
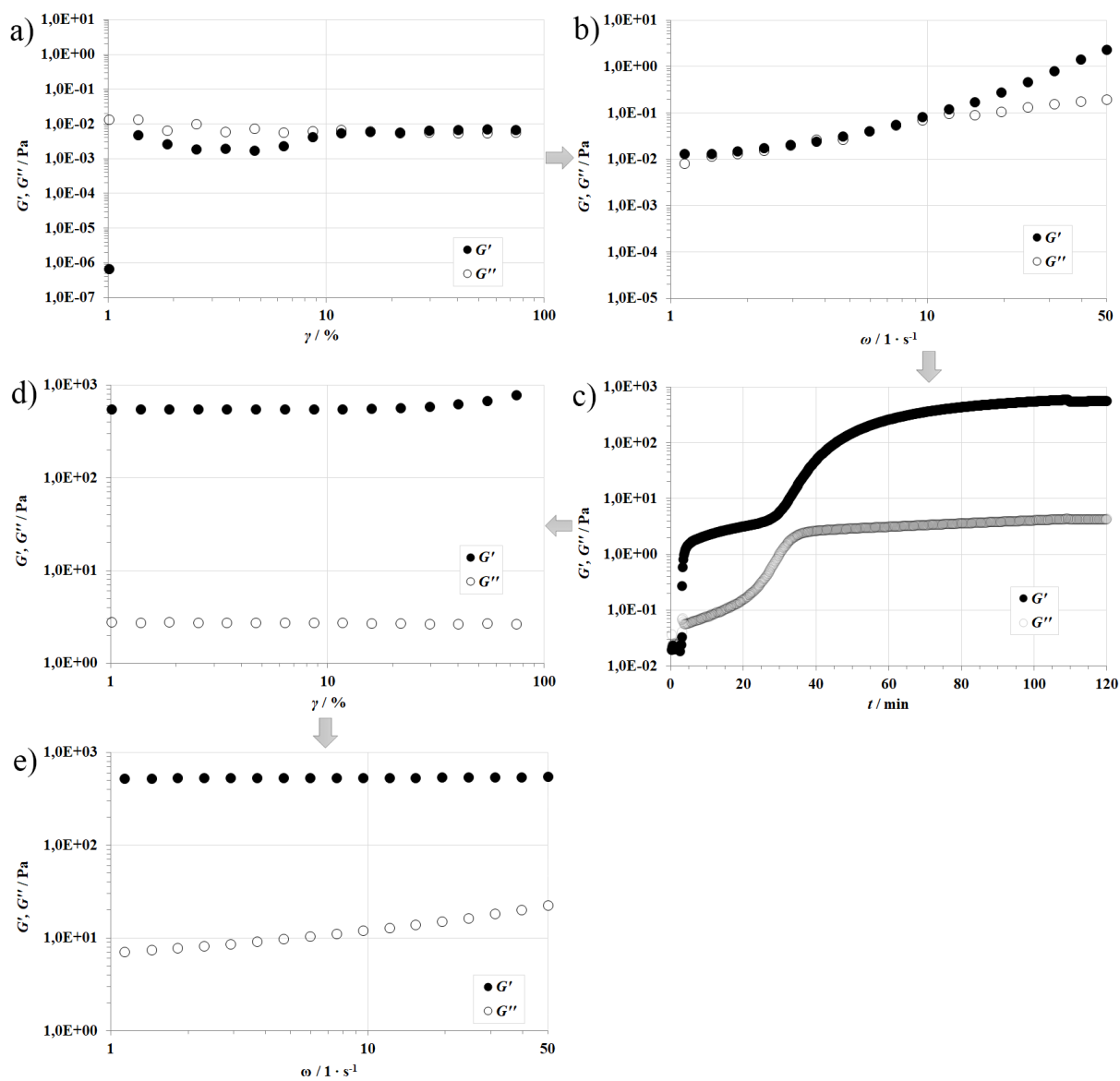
SI-Figure 33. Rheological investigation of $PEAGE_3$-b-PEG_{45}-b-$PEAGE_3$ (entry 1, **Table 4**): a) strain sweep before photogelation, b) frequency sweep before photogelation, c) photogelation, d) strain sweep after photogelation, e) frequency sweep after photogelation.
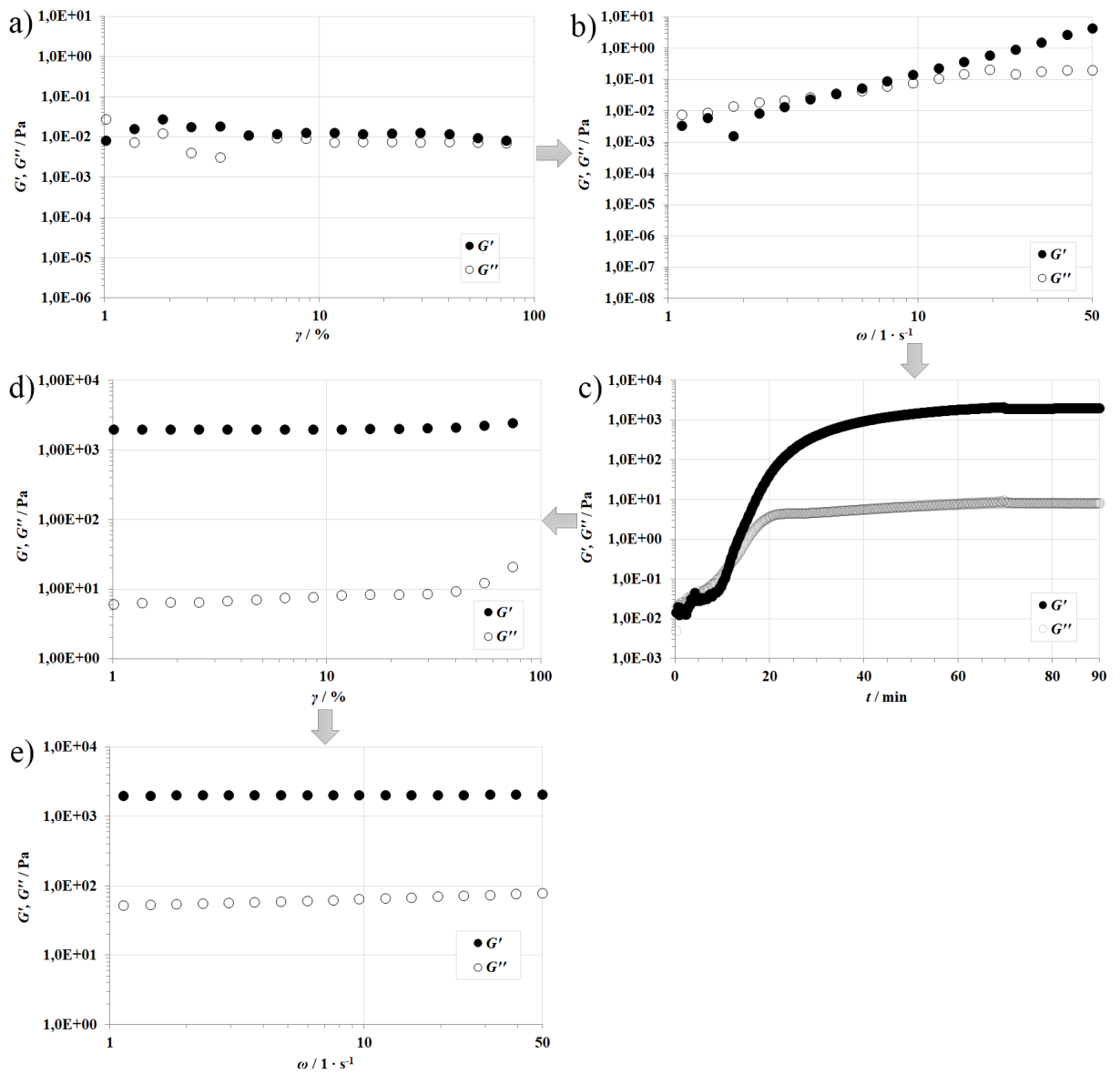
SI-Figure 34. Rheological investigation of PEAGE$_3$-b-PEG$_{68}$-b-PEAGE$_3$ (entry 2, **Table 4**): a) strain sweep before photogelation, b) frequency sweep before photogelation, c) photogelation, d) strain sweep after photogelation, e) frequency sweep after photogelation.
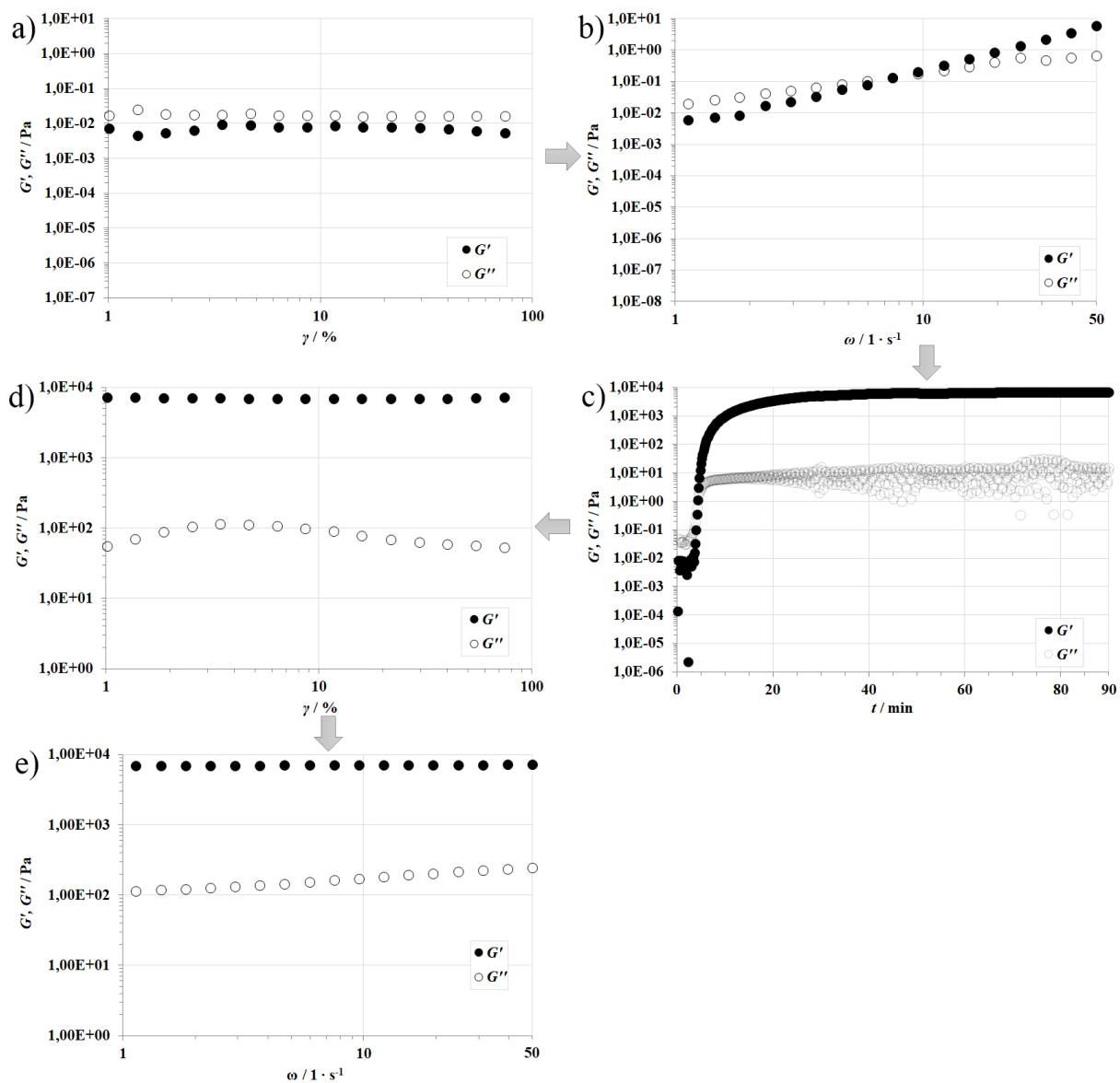
SI-Figure 35. Rheological investigation of $PEAGE_4$-b-PEG_{182}-b-$PEAGE_4$ (entry 3, **Table 4**): a) strain sweep before photogelation, b) frequency sweep before photogelation, c) photogelation, d) strain sweep after photogelation, e) frequency sweep after photogelation.
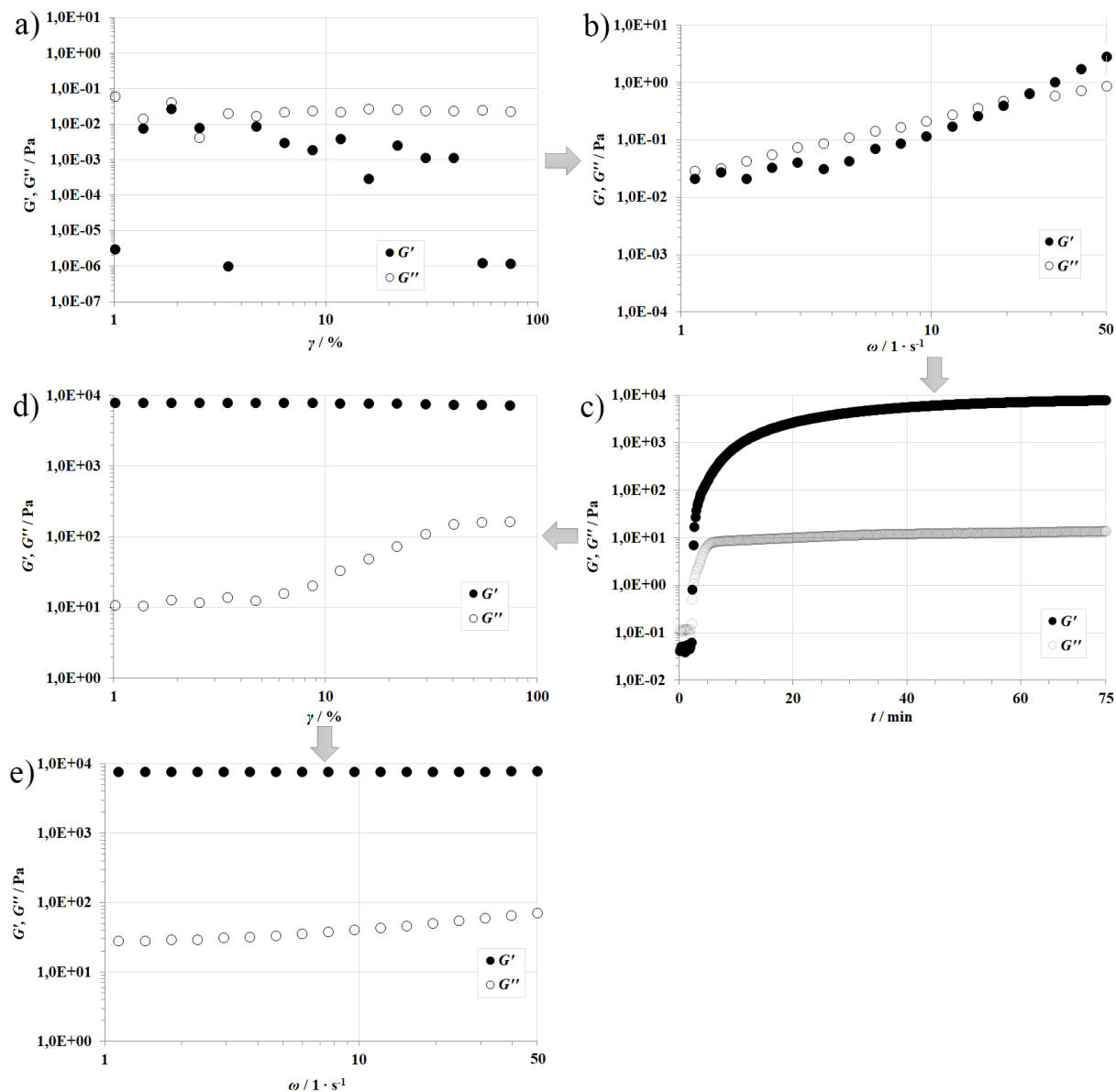
SI-Figure 36. Rheological investigation of $PEAGE_4$-*b*-PEG_{227}-*b*-$PEAGE_4$ (entry 4, Table 4): a) strain sweep before photogelation, b) frequency sweep before photogelation, c) photogelation, d) strain sweep after photogelation, e) frequency sweep after photogelation.

SI-REFERENCES

(1) Lee, B. F.; Wolffs, M.; Delaney, K. T.; Sprafke, J. K.; Leibfarth, F. A.; Hawker, C. J.; Lynd, N. A. Reactivity ratios, and mechanistic insight for anionic ring-opening copolymerization of epoxides. *Macromolecules* **2012**, *45*, 3722–3731, DOI: 10.1021/ma300634d.

(2) Herzberger, J.; Frey, H. Epicyanohydrin: Polymerization by Monomer Activation Gives Access to Nitrile-, Amino-, and Carboxyl-Functional Poly(ethylene glycol). *Macromolecules* **2015**, *48*, 8144–8153, DOI: 10.1021/acs.macromol.5b02178.

2.2. Ketone Dioxolane Glycidyl Ether: Synthesis of Multi-Ketone-Functional Poly(ethylene glycol) as a Promising Candidate for Bioconjugation and Reversible Hydrogels

Kamil Maciol[‡], Jan Blankenburg[‡,§], Moritz Urschbach[‡], Daniel Leibig[‡,§] and Holger Frey[‡,]*

[‡] Institute of Organic Chemistry, Johannes Gutenberg University Mainz, Duesbergweg 10-14, 55128 Mainz, Germany

[§]Graduate School Materials Science in Mainz, Staudinger Weg 9, 55128 Mainz, Germany

*E-Mail: hfrey@uni-mainz.de

To be submitted

ABSTRACT

Ketone-based polyethers are a promising candidate for biomedical applications and provide a versatile platform for post-polymerization modification reactions. We report the very first polyethers with incorporated aliphatic ketone units in a controlled manner synthesized by anionic ring-opening polymerization. Ketone dioxolane glycidyl ether (KDGE) copolymerized with ethylene oxide (EO) led to well-defined random copolymers with molecular weights up to 10,700 g mol^{-1} and dispersities below 1.2. In addition to a detailed characterization by SEC and NMR spectroscopy, thermal properties of both protected and deprotected copolymers were investigated. The copolymer microstructure was studied by real-time ^{1}H NMR kinetic analysis, revealing a random incorporation of KDGE moieties into the poly(ethylene glycol) backbone. As a model reaction for bioconjugation, the KDGE functionalities were deprotected *in-situ* and reacted with 2,4-dinitrophenylhydrazine forming hydrazone linkages. Triblock copolymer architectures were synthesized by polymerization of KDGE starting from bifunctional PEG macroinitiators. Molecular weights ranging from 7,300 g mol^{-1} to 23,500 g mol^{-1} ($Đ \leq 1.2$). The deprotected triblock copolymers were crosslinked by ketoxime ether formation using a difunctional alkoxyamine. Hydrogels were obtained with swelling ratios up to 3,200% and mesh sizes ranging from 10 nm to 20 nm. Addition of monofunctional alkoxyamine led to the dissolution of the gels.

TABLE OF CONTENTS GRAPHICS
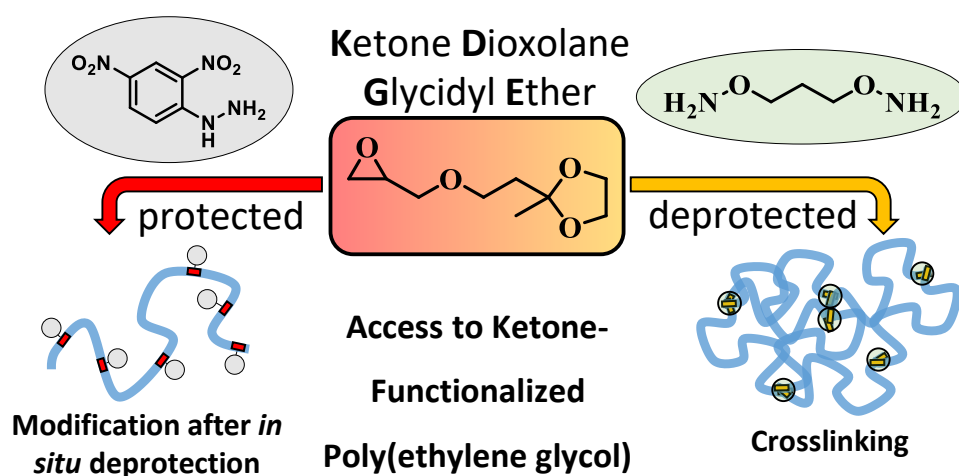
INTRODUCTION

Ketones are widely used in nature and occur, for instance as 4-(*p*-hydroxyphenyl)-2-butanone in raspberries, as *cis*-jasmone in jasmine beans or as *β*-damascenone in rose petals.[1] They provide the basis for a variety of chemical reactions. Carbon (Grignard reagents, cyanides, alkyne anions), oxygen (alcohols), or nitrogen (amines, hydrazines) nucleophiles can be reacted with these carbonyl groups through addition reactions.[2] The great importance of the Wittig reaction for the synthesis of organic compounds was the occasion for the award of the Nobel Prize in 1979, enabling the access to alkenes by reaction of ketones (and aldehydes) with ylides.[3] The diversity of ketones has also attracted the attention of polymer science. In many cases, this was realized via the reversible addition-fragmentation chain-transfer (RAFT) polymerization.[4–8] Bandyopadhyay *et al.* prepared a ketone-modified Z-group RAFT chain transfer agent for the synthesis of amphiphilic block copolymers for potential theranostic/biotechnological applications. Via this approach, polymer nanoparticle assemblies were formed by conjugation with hydrazides.[9] The specific control of the copolymer morphology of poly-(*N,N*-dimethylacrylamide) (PDMAC) copolymers with incorporated diacetone acrylamide (DAAM) is described in the work of Armes and co-worker, including a constructed phase diagram of the copolymers. Depending on the degree of polymerization and the ratio of DMAC to DAAM, defined spherical nanoparticles, anisotropic worms or polydisperse vesicles were detected.[10] Besides RAFT, there are also synthetic approaches via free radical polymerization[11], controlled nitroxide-mediated polymerization (NMP)[12] and post-polymerization modifications[13]. Yang and Weck presented the synthesis of an azide- and ketone-functionalized copolymer by ring-opening metathesis polymerization (ROMP). These functionalities could be addressed either selectively via 1,3-dipolar cycloaddition or hydrazone formation, but also simultaneously through combination of this post-polymerization modification reactions.[14]

Ketone-functional polymers provide an innovative basis for biomedical applications. In this regard, hydrazines and alkoxyamines are particularly suitable as coupling partners for ketones. Hydrazone formation from ketones and hydrazines play an important role in the field of drug delivery. Here, they are used as acid-labile cleavage site.[15] The cytostatic doxorubicin was linked in this manner to block copolymers, which subsequently served as pH sensitive micellar nanocarriers.[16,17] Zhao and co-workers developed a hydrazone-linked polymer-drug conjugate, which induced considerable cytotoxicity in HeLa cells.[18] Hydrazone crosslinks were also used to stabilize micelles, increasing their thermal and hydrolytic stability in comparison to non-

crosslinked micelles.[19] Hoare *et al.* pursued a completely different approach for the application of hydrazone linkages. They developed a fully injectable interpenetrating network, which comprised of thiosuccinimide-crosslinked poly(vinyl pyrrolidone) and thermoresponsive hydrazone-crosslinked poly(*N*-isopropylacrylamide).[20] The reaction of ketones with alkoxylamines to ketoxime ether is an elegant pathway for bioconjugation. Advantages include the possibility to perform these reactions in aqueous solution, the non-toxic by-product formation of water and the reversibility of reaction depending on conditions.[21] Such reactions have already been described in detail in the literature.[22–25] Recently, Sumerlin and co-workers, reported on a crosslinked keto-functional copolymer by oxime formation. As a result, self-healing hydrogels were obtained, which were studied in detail.[26] Hill *et al.* followed a different approach. By polymerizing phthalamides-protected *O*-(4-vinylbenzyl)-hydroxylamine via RAFT, they obtained protected hydroxylamine moieties in the polyethylene backbone. After deprotection, the oxime formation was investigated with model aldehydes and ketones.[27]

Surprisingly, ketone functionalities are rare in the field of aliphatic polyethers. One reason for this is the inability of free ketones to polymerize under the harsh conditions of the anionic ring-opening polymerization (AROP) and the necessity of protecting group chemistry. Only a benzophenone containing glycidyl ether is known, based on the work of Weinhart and co-workers.[28] However, this monomer can only be polymerized using the activated monomer strategy.[29,30] Besides the difficulties in the full removal of the amphiphilic initiator and aluminum-containing catalyst salts, there are ill-defined chain ends[31] caused by undesired initiations from side reactions. Moreover, the copolymerization of glycidyl ethers with ethylene oxide results in gradient- rather than random copoylmers.[32–34] Approaches exist to combine PEG and ketone moieties in hydrogels as crosslinkers. For this purpose, Cui *et al.* reacted 3,3′-dithiodipropionate hydrazide-modified hyaluronic acid (HA) with poly(ethylene glycol) dilevulinate to HA hydrogels, a promising candidates in bone tissue regeneration applications.[35] PEG in particular is the best-known aliphatic polyether and represents an ideal basis for biomedical applications.[36–41] This is attributable to the unique properties of PEG[42]: it has an exceptionally high water solubility in contrast to other aliphatic polyethers such as poly(oxymethylene) or poly(propylene oxide), which are insoluble in water.[43,44] Moreover, PEG exhibits an excellent biocompatibility due to its low immunogenicity and toxicity.[45] One of the limitations of PEG is the lack of functionality along the polyether backbone. Copolymerization of ethylene oxide with functional epoxide derivatives, glycidyl ethers or glycidyl amines provides an approach to multifunctional PEGs (*mf*-PEGs) and is usually the method of choice to overcome the known limitations of PEG.[46,47]

In this work, we present a strategy for the synthesis of ketone-functionalized polyether architectures with the novel ketone dioxolane glycidyl ether (KDGE) monomer. The synthesis of random PEG-*ran*-PKDGE copolymers by anionic ring-opening polymerization (**Scheme 1A**) is described. In a model bioconjugation reaction, the ketone moieties were *in-situ* deprotected and addressed by hydrazone linkages. Additionally, PKDGE-*b*-PEG-*b*-PKDGE triblock copolymers (**Scheme 1B**) were also prepared. After removal of the dioxolane protecting groups, reversible hydrogels were prepared.
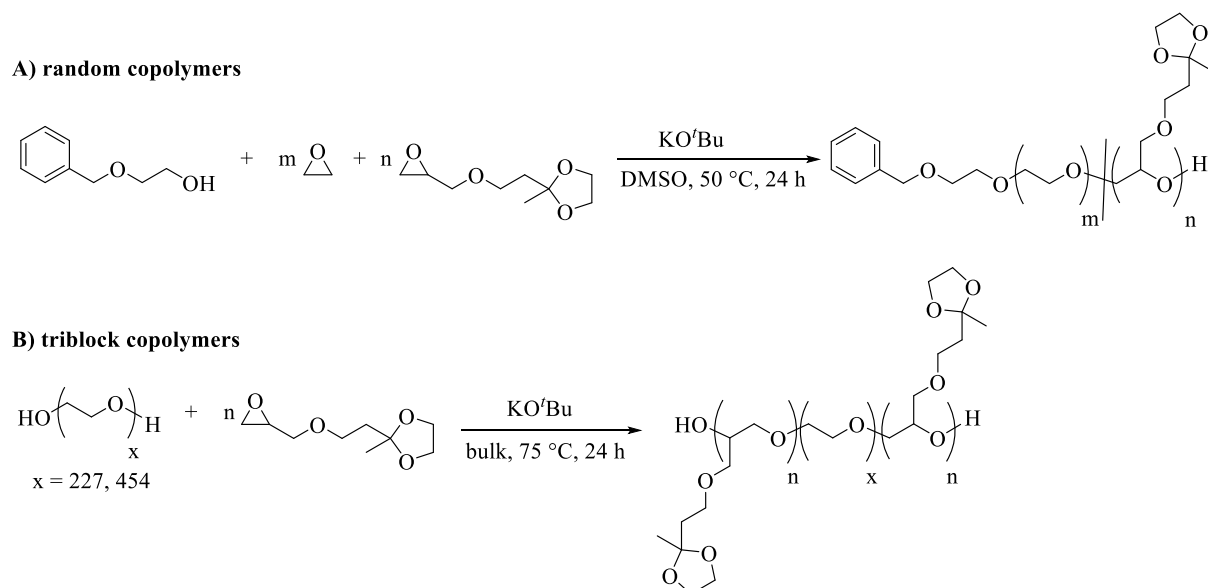
Scheme 1. Strategies for the synthesis of two polyether architectures. A) Random PEG-*ran*-PKDGE copolymers. B) PKDGE-*b*-PEG-*b*-PKDGE triblock copolymers.

EXPERIMENTAL PART

Terminology. Protected ketone dioxolane glycidyl ether units are abbreviated as KDGE units, deprotected units as KGE (ketone glycidyl ether).

Instrumentation. ^{1}H NMR (400 MHz), ^{13}C NMR (100 MHz) and 2D NMR spectra were measured on a Bruker Avance II 400 (5 mm BBFO Z-gradient and ATM, SampleXPress 60 auto sampler). Real-time ^{1}H NMR (400 MHz) kinetics were recorded on a Bruker Avance III HD 400 spectrometer (5 mm BBFO SmartProbe with Z-gradient and ATM, SampleXPress 60 auto sampler). For internal referencing, the residual protons of the deuterated solvents were used.

For SEC measurements in DMF (containing 1 g L^{-1} lithium bromide) an Agilent 1,100 Series was used at 50 °C, equipped with HEMA columns (300/ 100/ 40 Å porosity) provided by Polymer Standards Service (PSS) and UV (254 nm) and RI detectors. The determined molecular weights refer to poly(ethylene oxide) standards by PSS.

Thermal properties were investigated on a Perkin Elmer DSC 8,500 in sealed aluminum crucibles under a nitrogen atmosphere. The measurements were performed in the temperature range of -95 °C to 95 °C and were measured in two cycles with heating and cooling rates of 20 K min^{-1} and 10 K min^{-1}. For evaluation the second heating curve was used.

Materials. All reagents and solvents were purchased from commercial distributors (Sigma-Aldrich, Acros Organics, TCI, abcr, etc.) and used without further purification unless noted otherwise. Orange Scientific was the manufacturer of the dialysis membranes, which consisted of regenerated cellulose (*MWCO* = 1,000 g mol^{-1}). Deuterated DMSO-d_6, (CD_3)$_2$CO and C$_6D_6$ were purchased from Deutero GmbH. Generally, initiator solutions were dried by azeotropic distillation of benzene and a small amount of THF. KDGE was dried over CaH$_2$ and freshly distilled prior to use.

Monomer synthesis: ketone dioxolane glycidyl ether (KDGE). Epichlorohydrin (8.9 ml, 113 mmol, 3 equiv) was added to freshly ground NaOH (1.82 g, 45 mmol, 1 eqiv). The mixture was cooled in an ice bath and 4.7 mL (37.8 mmol, 1 eqiv) 3,3-ethylenedioxy-1-butanol (according to Deslongchamps *et al.*[48]) was added slowly under vigorous stirring. Further epichlorohydrin was added to lower the viscosity of the reaction mixture. After stirring for 5 days at room temperature, the mixture was diluted with diethyl ether (30 mL) and the solid was filtered off. The filtrate was washed twice with saturated NaHCO$_3$ (2 · 30 mL), water

(2 · 30 mL), brine (2 · 30 mL) and dried over NaSO$_4$. The crude product was concentrated under reduced pressure and the final product was distilled *in vacuo* to give KDGE as a colorless liquid in yields of 70%. For more details, see **SI-Scheme 1**. ^{1}H NMR (400 MHz, C$_6$D$_6$): δ (ppm) = 3.61–3.45 (6H, m, C$H_{2, \text{glycidyl ether}}$ and -O-CH_2-CH_2-O-). 3.37 (1H, dd, C$H_{2, \text{glycidyl ether}}$, J = 11.4, 3.0 Hz), 3.07 (1H, dd, C$H_{2 \text{ glycidyl ether}}$, J = 11.4, 5.9 Hz), 2.85–2.81 (1H, m, CH_{epoxide}), 2.32 (1H, dd, C$H_{2, \text{epoxide}}$, J = 5.7, 4.1 Hz), 2.19 (1H, dd, C$H_{2, \text{epoxid}}$, J = 5.3, 2.7 Hz), 1.97 (2H, t, CH_2, J = 7.2 Hz), 1.27 (3H, t, CH_3, J = 7.2 Hz). ^{13}C NMR (100 MHz, C$_6$D$_6$): δ (ppm) = 109.02 (-CH$_2$-CCH$_3$-(O-CH$_2$)$_2$), 71.98 (CH$_{2, \text{glycidyl ether}}$), 67.70 (C$H_{2, \text{glycidyl ether}}$), 64.57 (-O-CH$_2$-CH$_2$-O-), 50.71 (CH$_{\text{epoxide}}$), 43.62 (CH$_{2, \text{epoxide}}$), 39.38 (CH$_2$), 24.61 (CH$_3$).

Copolymer synthesis: poly(ethylene oxide)-ran-poly(ketone dioxolane glycidyl ether) (PEG-ran-PKDGE). As an example, the synthesis of PEG$_{197}$-*ran*-PKDGE$_{11}$ (entry 1, **Table 1**) is described here. All other random copolymers and PKDGE homopolymer were synthesized in a similar manner. 2-(Benzyloxy)ethanol (0.014 mL, 9.86 · 10^{-2} mmol, 1 equiv) and potassium *tert*-butoxide (KO^{t}Bu) (0.010 g, 8.87 · 10^{-2} mmol, 0.9 equiv) were placed in a 100 mL Schlenk flask and dissolved in a mixture of 5 mL benzene and 1 mL THF. The mixture was stirred at 60 °C for 30 minutes. Subsequent, the flask was evacuated overnight to remove the solvents and traces of water. Then, the flask was filled with argon and 10 mL of dry DMSO were added. The solution was cooled to -70 °C and KDGE (0.19 mL, 9.86 · 10^{-1} mmol, 10 equiv) was injected via syringe through a septum. Afterwards, the flask was evacuated and EO (0.83 mL, 18.16 mmol, 185 equiv) was introduced to the reactor. The mixture was left to stir at 60 °C for 24 hours. The copolymerization was terminated with 1 mL of MeOH. Subsequent, the solution was diluted with dichloromethane (DCM) (50 mL) and washed five times with saturated NaHCO$_3$ solution (10 mL). DCM was removed under reduced pressure and the mixture was dialyzed against MeOH : DCM (3 : 2). The copolymer was dried under reduced pressure. The final yield was 90%.

Sample preparation for real-time ^{1}H NMR kinetic studies. 0.03 mL (0.20 mmol, 1 equiv) 2-(Benzyloxy)ethanol and 0.02 g (0.18 mmol, 0.9 equiv) KO^{t}Bu were dissolved in 1 mL THF and 3 mL benzene and stirred at 60 °C for 30 minutes. To remove the solvents, the mixture was evacuated overnight. The flask was filled with argon and 1 mL DMSO-d_6 was added. 0.1 mL of this solution was transferred to a Norell S-5-400 VT-7 NMR tube, which was previously evacuated three times and filled with argon. After cooling the initiator solution to -70 °C, KDGE (0.06 mL, 0.30 mmol, 15 equiv) and 0.5 mL DMSO-d_6 were added. Then, the NMR

tube was evacuated and EO was introduced to the NMR tube under external cooling (-70 °C). The measurement was performed at 60 °C in a preheated NMR spectrometer. ^{1}H NMR spectra were recorded every 2 minutes for the first hour, for the following three hours every 5 minutes and finally for fourteen hours every 10 minutes. The number of scans per measurement was 16 over the whole course of the measurement.

Post-polymerization modification: hydrazone formation. The reaction was carried out analogously to the synthesis protocol in the *Organikum*.[49] In the first step, a solution of 0.4 g 2,4-dinitrophenylhydrazin, 2 mL H_2SO_4, 3 mL H_2O and 10 mL EtOH was prepared. Then, 0.1 g PKDGE$_{27}$ (entry 5, **Table 1**) was dissolved in 1.1 mL EtOH and the ethanolic solution was slowly added dropwise to the hydrazine solution. The precipitated orange solid was filtered off and washed with water and EtOH. After dialysis in a mixture of MeOH : DCM (3 : 2), the modified polymer was dried *in vacuo*, resulting in yields of 89%.

Triblock copolymer synthesis: poly(ketone dioxolane glycidyl ether)-block-poly(ethylene glycol)-block-poly(ketone dioxolane glycidyl ether) (PKDGE-b-PEG-b-PKDGE). The synthesis of PKDGE$_4$-*b*-PEG$_{136}$-*b*-PKDGE$_4$ (entry 1, **Table 2**) is used as an example hereafter. PEG$_{136}$ (1.6 g, 0.27 mmol, 1 equiv) and KO^{t}Bu (0.054 g, 0.48 mmol, 1.8 equiv) were dissolved in 5 mL benzene and 1 ml of dry THF in a Schlenk flask. The mixture was heated for 30 minutes at 60 °C. Afterwards, the solvents were removed under reduced pressure. The solid was liquified at 75 °C, freshly dried KDGE (0.50 ml, 2.67 mmol, 10 equiv) was added and the reaction mixture was stirred at 75 °C overnight. The polymerization was terminated by addition of 1 mL of methanol and the product was purified by dialysis with MeOH : DCM (3 : 2). After removal of the solvents, the polymer was isolated to give yields of 95%.

Removal of the dioxolane protecting group. The corresponding polymer (1 g) was dissolved in a mixture of acetone (20 mL) and 10 mL methanolic HCl (5% (w/v)) and stirred at room temperature for 15 minutes. The solution was concentrated to a volume of 10 mL and diluted with DCM (50 mL). The organic phase was washed with saturated NaCl solution (30 mL each) until the aqueous phase showed a pH value of 7. The organic phase was dried over MgSO$_4$. Next, the deprotected polymer was precipitated in *n*-hexanes and the residue was dried *in vacuo*, leading to quantitative yields.

Hydrogels: preparation and crosslinking. PKDGE-*b*-PEG-*b*-PKDGE (0.05 g) was dissolved in PBS buffer in an Eppendorf tube. A defined amount of a stock solution of *O,O′*-1,3-propanediylbishydroxylamine dihydrochloride in PBS buffer was added (see **Table 5** for the

total concentration of PBS solutions). Ketone to alkoxyamine group ratio was $1.2 : 1$ for all approaches. After homogenization, the hydrogels were mechanically shaken on the shaker plate for 48 hours. The Eppendorf tube was frozen in liquid nitrogen and the solidified hydrogel was loosened by gentle tapping. To test the swelling properties, the resulting hydrogels were transferred into PBS buffer filled screw-capped glasses. The hydrogels were equilibrated for 24 hours. Then, the hydrogel was weighed after removing excess water. This procedure was repeated three times and the average value was calculated. Dry weights of the hydrogels were ascertained by lyophilization after removal of the water.

Hydrogels: characterization. The following equation was used to calculate the swelling ratio SR[50]:

$$\text{Swelling ratio } (SR) = \frac{W_s - W_d}{W_d} \tag{1}$$

where W_s is the average weight of the swollen hydrogel and W_d is the weight of the dry hydrogel. In order simplify the following calculations, the deprotected KGE units were neglected and the triblock copolymers were considered as pure PEG chains. **Equation 2** was used for the determination of the volume swelling ratio Q_v:

$$\text{Volume swelling ratio } (Q_v) = 1 + \frac{\rho_p}{\rho_s} \cdot (Q_m - 1) \tag{2}$$

where ρ_p is the density of PEG ($\rho_p = 1.12 \text{ g mL}^{-1}$)[51] and ρ_s the density of water ($\rho_s = 1 \text{ g mL}^{-1}$). Mass swelling Q_m was calculated from the ratio of W_s to W_d.

The molecular weight between the crosslinks M_c was calculated based on a modified Flory-Rehner theory[52] according to Merrill and Peppas.[53,54] This modification applies to hydrogels prepared in solutions:[55]

$$\frac{1}{M_c} = \frac{2}{M_n} - \frac{\left(\frac{\bar{v}}{V_1}\right) \cdot \left[\ln(1 - v_{2,s}) + v_{2,s} + \chi_1 \cdot v_{2,s}^2\right]}{v_{2,r} \cdot \left[(v_{2,s})^{\frac{1}{3}} - \left(\frac{1}{2} \cdot v_{2,s}\right)\right]} \tag{3}$$

Here, M_n, is the average molecular weight of the triblock copolymers determined by ^{1}H NMR spectroscopy and $\bar{v}$ the specific volume of the polymers, which is defined as $\frac{\rho_s}{\rho_p}$. The polymer volume fraction $v_{2,s}$ in the swollen hydrogel is equivalent to the reciprocal value of Q_v. V_1 is the

molar volume of water (18 mL mol^{-1}) and χ_1 is the PEG-solvent interaction parameter with a value of $\chi_1 = 0.426$.[56]

The equation of Canal and Peppas[57] was used for the calculation of the mesh size ξ:

$$\xi = v_{2,s}^{-\frac{1}{3}} \cdot \left(2 \cdot C_n \cdot \frac{M_c}{M_r} \right)^{\frac{1}{2}} \cdot l \tag{4}$$

Here, C_n is the characteristic ratio of PEG ($C_n = 4.0$), M_r is the molecular weight of the repeating unit (44.05 g mol^{-1} for PEG) and l is the average bond length (0.154 nm).[56]

RESULTS AND DISCUSSION

A.   Synthesis of KDGE monomer and its polymerization.

Ketone dioxolane glycidyl ether. The dioxolane-containing alcohol 3,3-ethylenedioxy-1-butanol was deliberately chosen for the synthesis of the ketone dioxolane glycidyl ether (KDGE). Cyclic protecting groups show a substantially higher resistance to hydrolysis than acyclic protecting groups representatives. The comparison of the relative hydrolysis rates of the dioxolane protecting group with aryl ketals clarifies that dimethyl ketals hydrolyze about 2,800 times- and diethyl ketals even 24,100 times faster than the analogue five-membered ring ketals.[58] This results in a very long storage life of the KDGE monomer under appropriate conditions (> 1 year).

Starting from 3,3-ethylenedioxy-1-butanol (**SI-Scheme 1**), KDGE was prepared in a one-step reaction with epichlorohydrin (**Scheme 2**).
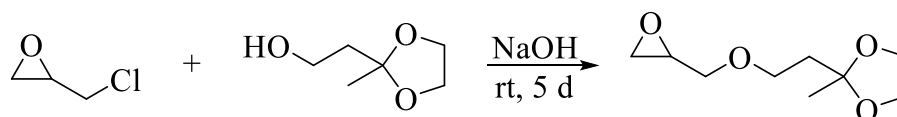
Scheme 2. Synthesis of ketone dioxolane glycidyl ether (KDGE) monomer.

It is known in literature, that in the presence of bases and phase transfer catalysts, epichlorohydrin tends to form *trans*-3-chloroallyl 2,3-epoxypropyl ether.[59,60] This by-product cannot be removed by distillation, but only via column chromatographic methods in the case of KDGE (**SI-Figure 2**). Therefore, the use of phase transfer catalysts was omitted. In general, a correlation between the reaction time and yield was observed. The maximum was reached after about 5 days at 70%. **Figure 1** shows the ^{1}H NMR spectrum of KDGE (^{13}C NMR and 2D NMR spectra are included in the Supporting Information, **SI-Figures 3−6**).
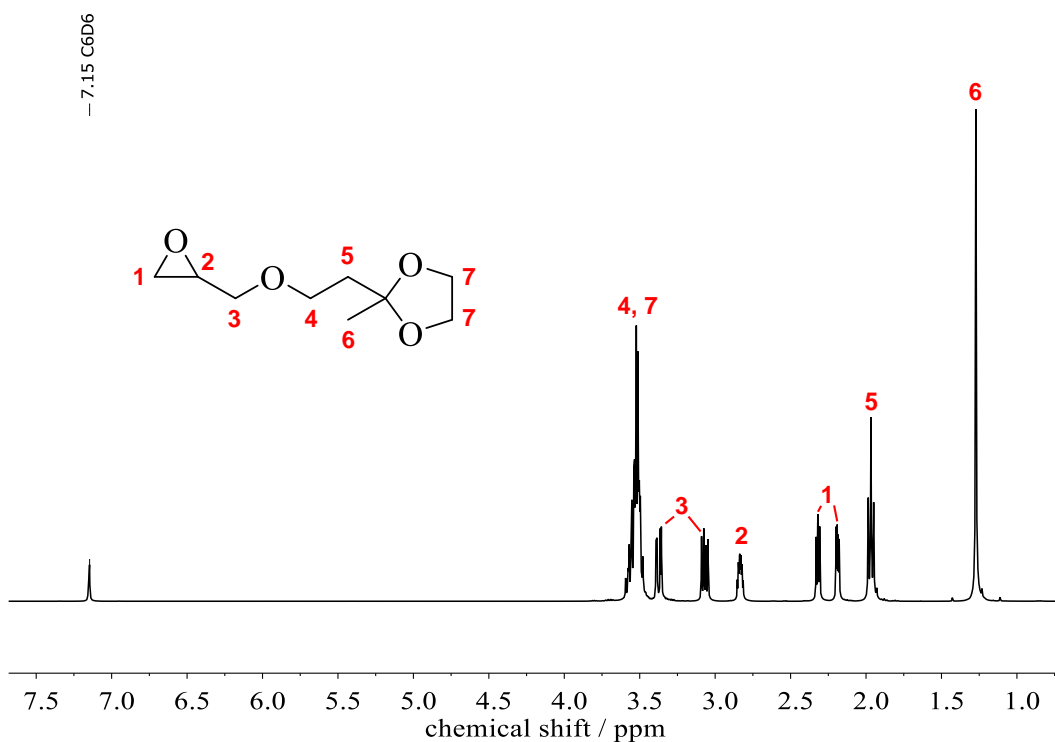
Figure 1. ^{1}H NMR spectrum (400 MHz, C$_6$D$_6$) of KDGE monomer.

Based on KDGE, two different polyether architectures were synthesized (**Scheme 1**): random copolymers with ethylene oxide (EO) and triblock copolymers using three differently sized PEG macroinitiators (M_n = 6,000 / 10,000 / 20,000 g mol^{-1}).

Random PEG-ran-PKDGE copolymers. EO and KDGE were copolymerized by anionic ring-opening polymerization (AROP) and were studied in detail. The use of 2-(benzyloxy)ethanol has the advantage that its isolated methylene group in the ^{1}H NMR spectrum (**SI-Figure 7**) can be used to determine the absolute molecular weights (^{13}C NMR and 2D NMR spectra can be found in the Supporting Information, **SI-Figures 8−11**). Using DMSO as a solvent allowed a successful copolymerization of KDGE and EO in all ratios. The quantitative removal of the solvent was possible with a combination of liquid-liquid extraction and dialysis.

SEC studies revealed well-defined and monomodal molecular weight distributions (**Figure 2**).
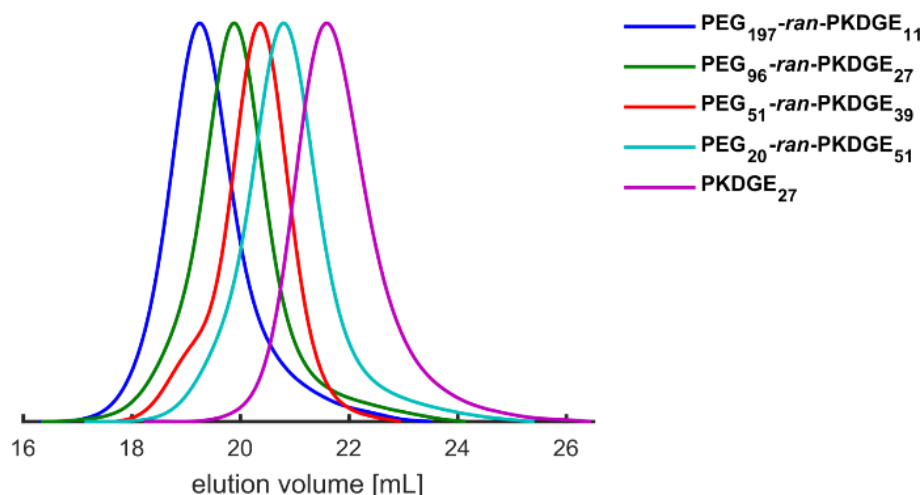
Figure 2. SEC traces (DMF, PEG-standard, RI detector) of random PEG-*ran*-PKDGE copolymers (entries 1−4, **Table 1**) and PKDGE$_{27}$ homopolymer (entry 5, **Table 1**).

Summarized analytic results of the synthesized statistical PEG-*ran*-PKDGE copolymers are given in **Table 1**. The amount of KDGE in the monomer mixtures was varied between 5 mol% and 100 mol%. Molecular weights determined by ^{1}H NMR spectroscopy coincide with the theoretical values and range from 5,200 g mol^{-1} to 10,700 g mol^{-1} with dispersities (*Đ*) below 1.2. The minimal deviations between the values are due to weighing errors. It is noticeable that the molecular weights determined by SEC differ greatly from the theoretical and NMR values. The deviation increases the more KDGE is incorporated. This can be attributed to the PEG-standard used for the calibration in the SEC measurements. By incorporation of comonomers such as KDGE, the hydrodynamic radii of the copolymers behave differently in comparison to pure PEG homopolymers, resulting in the deviation in the determined molecular weights.

Table 1. Overview of synthesized PEG-*ran*-PKDGE copolymers and PKDGE homopolymer.

No.	Composition[a]	KDGE / mol%[a]	M_n^{th} / g mol^{-1}	M_n^{b} / g mol^{-1}	M_n^{a} / g mol^{-1}	*Đ*
1	PEG$_{197}$-*ran*-PKDGE$_{11}$	5	10,000	5,100	10,700	1.19
2	PEG$_{96}$-*ran*-PKDGE$_{27}$	22	10,000	4,000	9,400	1.20
3	PEG$_{51}$-*ran*-PKDGE$_{39}$	43	10,200	3,600	9,700	1.12
4	PEG$_{20}$-*ran*-PKDGE$_{51}$	72	10,200	2,600	10,400	1.19
5	PKDGE$_{27}$	100	5,100	1,700	5,200	1.15

[a] Values calculated by ^{1}H NMR spectroscopy. [b] Determined by SEC in DMF (PEG-standard).

To gain a deeper understanding of the copolymerization of EO and KDGE in terms of the microstructure, real-time ^{1}H NMR kinetic measurements were performed. A random

incorporation of the glycidyl ether and EO was expected.[61–63] The reaction conditions of the ^{1}H NMR kinetics characterization were analogous to the synthetic approaches. KDGE and EO were copolymerized at 60 °C in deuterated DMSO in an NMR tube. For the evaluation of the results the decreasing monomer signals of EO at 2.6 ppm and of KDGE at 3.1 ppm were used (**Figure 3**).
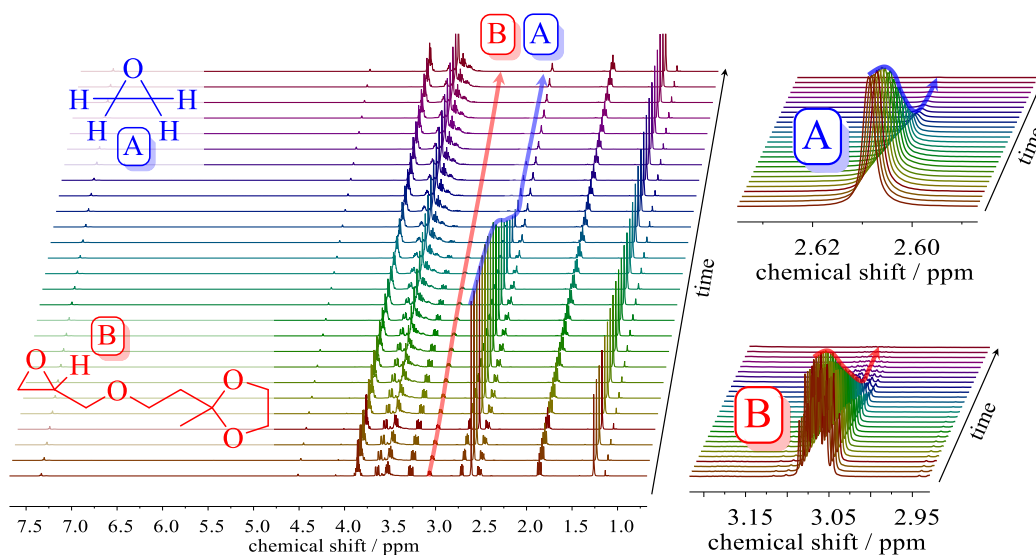
Figure 3. Stacked ^{1}H NMR spectra (400 MHz, 60 °C, DMSO-d_6) for the copolymerization of KDGE and EO including a zoom of relevant areas for evaluation.

Comparing the decreasing monomer concentration versus the total conversion, it is noticeable that the decrease of the curves is uniform for both monomers, indicating a nearly random incorporation of KDGE in the polyether backbone (**SI-Figure 12**). Based on the kinetic data, the reactivity ratios were determined according to the Jaacks[64] (**SI-Figure 13**) and Meyer-Lowry[65] (**SI-Figure 14**) method. These are $r_{\text{KDGE},J} = 0.74$ for KDGE and $r_{EO,J} = 1.35$ for EO, respectively $r_{\text{KDGE},M\text{-}L} = 0.66$ and $r_{EO,\,M\text{-}L} = 1.28$. The reactivity ratios imply a slightly preferred incorporation of EO in the polyether backbone resulting in an almost random incorporation of the comonomers with a weak gradient. Niederer *et al.* observed analogues for the copolymerization of EO and catechol acetonide glycidyl ether (CAGE) and attributed this to steric hindrance.[60] **Figure 4** illustrates the nearly random composition of the synthesized PEG-*ran*-PKDGE copolymer. The color gradient is a simulation based on the reactivity ratios according to Meyer-Lowry, while the colorless dots are directly derived from measurement points from the ^{1}H NMR kinetics.
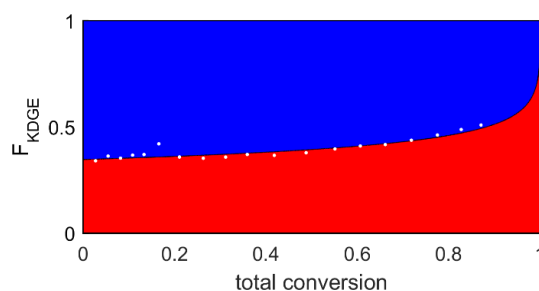
Figure 4. Simulated PEG-*ran*-PKDGE copolymer composition plotted versus total conversion of KDGE and EO. White dots represent are directly derived from measurement data. The color gradient was simulated using reactivity ratios according to Meyer-Lowry.

PKDGE-b-PEG-b-PKDGE triblock copolymers. For the crosslinking experiments, which will be discussed in the next section, a series of PKDGE-*b*-PEG-*b*-PKDGE triblock copolymers was prepared. Various PEG macroinitiators ($M_{n,PEG}$ = 6,000 / 10,000 / 20,000 g mol^{-1}) deprotonated by KO^{t}Bu were used for this purpose. The reactions were performed in bulk at 75 °C. ^{1}H NMR studies clearly demonstrate the presence of KDGE units (**Figure 5**). The use of defined PEG macroinitiators and the isolated methylene-, methyl-, and dioxolane moieties outside the polyether backbone allowed the determination of the absolute molecular weights from the spectra. For the evaluation, the signals of the KDGE methylene unit at 1.8 ppm were compared with the polyether signal at 3.5 ppm after the subtraction of the superimposed monomer units. An overview of the most important key data is given in **Table 2**. Associated ^{13}C NMR and 2D NMR spectra are available in the Supporting Information (**SI-Figures 15−18**).
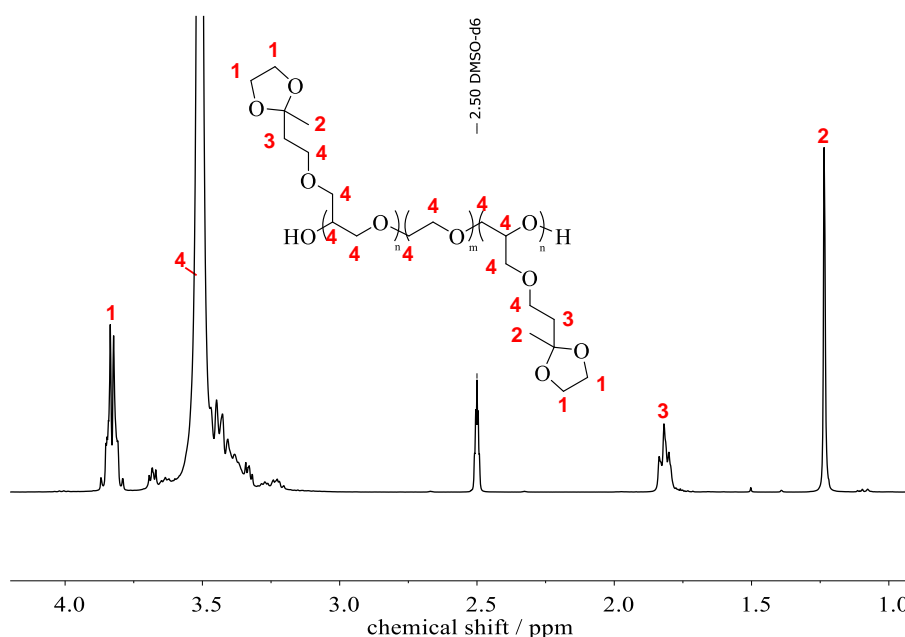
Figure 5. ^{1}H NMR spectrum (400 MHz, DMSO-d_6) of PKDGE$_4$-*b*-PEG$_{136}$-*b*-PKDGE$_4$ (entry 1, **Table 2**).

SEC analyses of the triblock copolymers show a narrow and well-defined molecular mass distribution (**Figure 6**). The comparison with the pure PEG macroinitiators confirmed the successful functionalization of the chains ends with KDGE (**SI-Figure 19**).
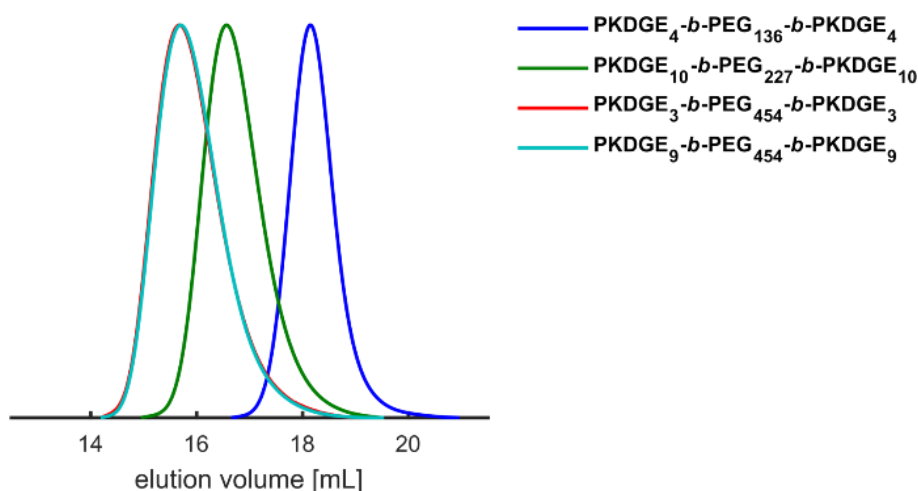
Figure 6. SEC traces (DMF, PEG-standard, RI detector) of PKDGE-*b*-PEG-*b*-PKDGE triblock copolymers (entries 1−4, **Table 2**).

Generally, a maximum of 10 units KDGE were incorporated per primary PEG hydroxyl group. The amount of KDGE varies depending on the selected initiator between 1 mol% and 8 mol%.

Table 2. Overview of synthesized PKDGE-*b*-PEG-*b*-PKDGE triblock copolymers.

No.	Composition[a]	KDGE / mol%[a]	M_n^{th} / g mol^{-1}	M_n^{b} / g mol^{-1}	M_n^{a} / g mol^{-1}	Đ
1	PKDGE$_4$-*b*-PEG$_{136}$-*b*-PKDGE$_4$	5	7,100	6,900	7,300	1.05
2	PKDGE$_{10}$-*b*-PEG$_{227}$-*b*-PKDGE$_{10}$	8	13,800	11,500	13,800	1.11
3	PKDGE$_3$-*b*-PEG$_{454}$-*b*-PKDGE$_3$	1	21,900	23,600	21,100	1.16
4	PKDGE$_9$-*b*-PEG$_{454}$-*b*-PKDGE$_9$	4	23,800	22,100	23,500	1.20

[a] Values calculated by ^{1}H NMR spectroscopy. [b] Determined by SEC in DMF (PEG-standard).

Release of ketone units by removal of the dioxolane protecting groups. As mentioned above, dioxolane protecting groups are relatively stable to hydrolysis. Experiments with acidic resins like Dowex® were not effective. Instead, the dioxolane protecting groups were cleaved in an acid-catalyzed exchange dioxolanation (**SI-Scheme 2**).[67,68] For this purpose, the copolymers were quantitatively deprotected with methanolic HCl in acetone. The successful reaction step for the transformation of PEG$_{197}$-*ran*-PKDGE$_{11}$ (entry 1, **Table 1**) to PEG$_{197}$-*ran*-PKGE$_{11}$ (entry 1, **Table 3**) is exemplified in **Figure 7**, while **SI-Figures 20−24** show the corresponding complete assigned ^{1}H NMR, ^{13}C NMR and 2D NMR spectra. It can clearly be seen that the

dioxolane protecting group was quantitatively removed at 3.8 ppm after acid treatment. Furthermore, a significant shift of the carbonyl methyl- and methylene groups is observed due to the changed chemical environment. The successful removal process is particularly evident in the comparison of the ^{13}C NMR spectra considering the ketal carbon at 108 ppm (**SI-Figure 8**), which can be found downfield at 207 ppm as carbonyl carbon (**SI-Figure 21**). Analogous observations can be made for the PKGE-*b*-PEG-*b*-PKGE triblock copolymers, whose NMR spectra are found in the Supporting Information (**SI-Figures 25−29**).
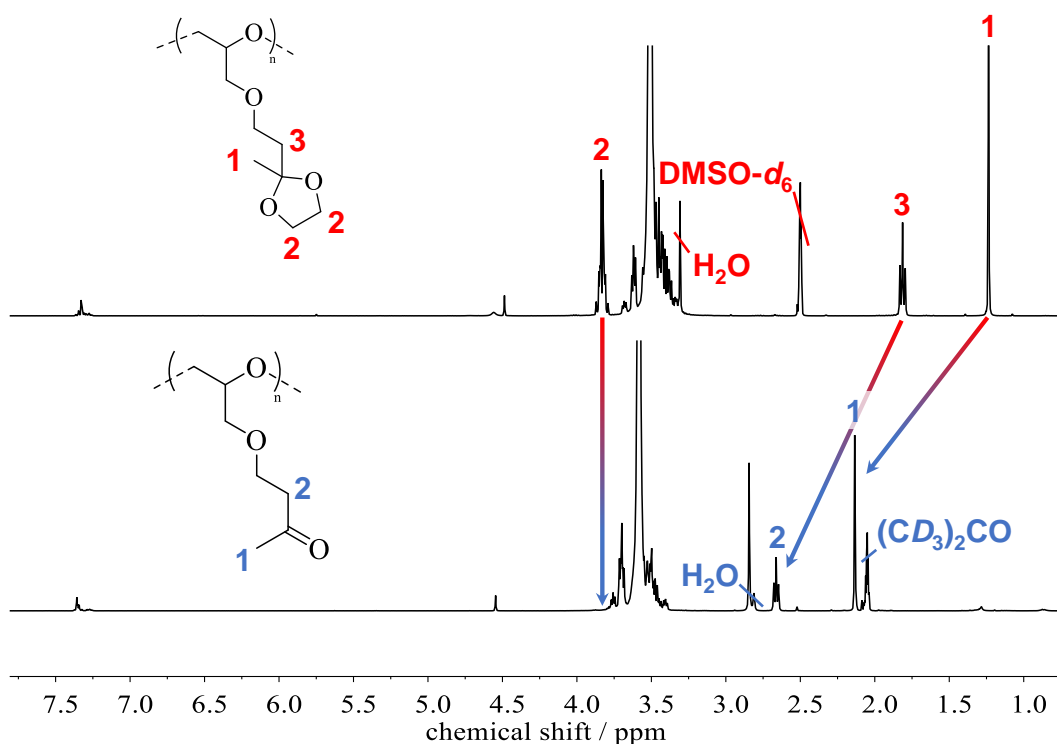
Figure 7. ^{1}H NMR spectra of protected PEG$_{197}$-*ran*-PKDGE$_{11}$ (entry 1, **Table 1**) (top, 400 MHz, DMSO-d_6) and deprotected PEG$_{197}$-*ran*-PKGE$_{11}$ (entry 1, **Table 3**) (bottom, 400 MHz, (CD_3)$_2$CO).

SEC characteristics are summarized in **Table 3**. Here, it is evident that the removal of the protective group has almost no influence on the dispersities. Interestingly, the trends in measured molar masses for the different polyether architectures behave in opposite directions. While the M_ns of the random copolymers (entries 1−5**, Table 3**) increase almost constantly compared to their protected species, they decrease slightly for the triblock copolymers (entries 6−9**, Table 3**). This effect is due to the different microstructure of the polymers.

Table 3. Overview of deprotected random PEG-*ran*-PKGE copolymers, PKGE homopolymer and PKGE-*b*-PEG-*b*-PKGE triblock copolymers.

No.	Composition[a]	M_n[b] / g mol^{-1}	Đ
1	PEG$_{197}$-*ran*-PKGE$_{11}$	6,700	1.16
2	PEG$_{96}$-*ran*-PKGE$_{27}$	5,500	1.08
3	PEG$_{51}$-*ran*-PKGE$_{39}$	2,800	1.12
4	PEG$_{20}$-*ran*-PKGE$_{51}$	3,200	1.14
5	PKGE$_{27}$	2,100	1.11
6	PKGE$_4$-*b*-PEG$_{136}$-*b*-PKGE$_4$	6,800	1.06
7	PKGE$_{10}$-*b*-PEG$_{227}$-*b*-PKGE$_{10}$	11,300	1.13
8	PKGE$_3$-*b*-PEG$_{454}$-*b*-PKGE$_3$	22,200	1.28
9	PKGE$_9$-*b*-PEG$_{454}$-*b*-PKGE$_9$	20,300	1.26

[a] Values calculated by ^{1}H NMR spectroscopy. [b] Determined by SEC in DMF (PEG-standard, RI detector).

Though it is counterintuitive, graphically, this effect (shown in **Figure 8** for a polymer selection) turns out to be much more pronounced for the random copolymers.
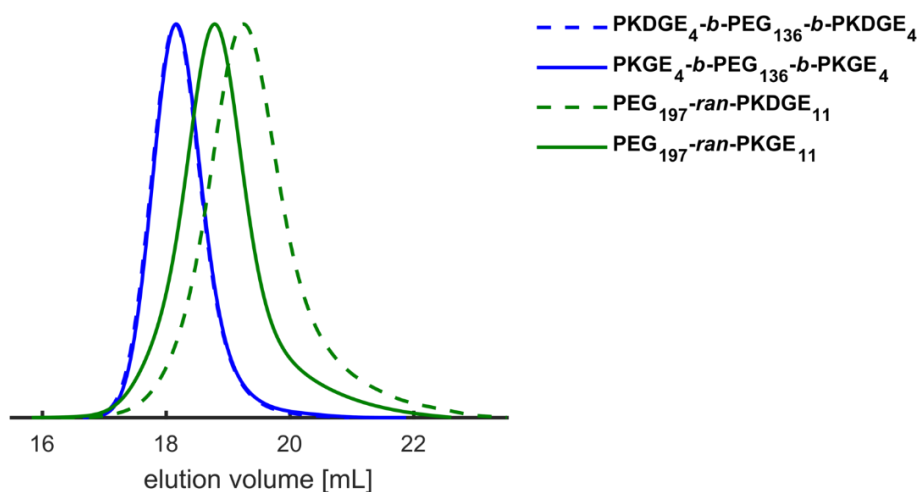
Figure 8. Selected SEC traces (DMF, PEG-standard, RI detector) of PKGE$_4$-*b*-PEG$_{136}$-*b*-PKGE$_4$ (entry 6, **Table 3**), PEG$_{197}$-*ran*-PKGE$_{11}$ (entry 1, **Table 3**) and their protected precursors.

Thermal properties of random and triblock copolymers. **Figure 9** shows the glass transition temperatures (T_gs) of the random PEG-*ran*-PKDGE copolymers before and after deprotection. Before removal of the dioxolane protecting groups, the T_gs move between from -55 °C

to -43 °C, after removal from -56 °C to -51 °C. It turns out, that the T_gs are lowered by the free ketone moieties. The trend is most pronounced for the homopolymer. This can be ascribed to the removal of the bulky dioxolane protecting groups, resulting in a decrease of the main chain stiffness and thus in an increase of its mobility.[66] Generally similar conclusions can be drawn for the triblock copolymers. The T_gs of PKGE-b-PEG-b-PKGE triblock copolymers are in the most cases lower than the values for the protected precursors. Possible reasons for the deviation are metrological nature, since the temperature difference is marginal. In the direct comparison of the triblock copolymers, it is noticeable that the T_g of PKDGE$_4$-b-PEG$_{136}$-b-PKDGE$_4$ (entry 1, **Table 2**) is generally higher than that of PKDGE$_{10}$-b-PEG$_{227}$-b-PKDGE$_{10}$ (entry 2, **Table 2**). This is due to the fact that second sample contains 3 mol% more KDGE, which increase the mobility of the polymer chains here. For PKDGE$_3$-b-PEG$_{454}$-b-PKDGE$_3$ (entry 3, **Table 2**), a sudden increase of 10 °C can be observed, since only about 1 mol% KDGE is incorporated here. In contrast, PKDGE$_9$-b-PEG$_{454}$-b-PKDGE$_9$ (entry 4, **Table 2**) contains about 4 mol% KDGE, causing the T_g to sink again. These general findings also apply to the respective deprotected species. As the KDGE and KGE moieties are not numerous, phase separation did not occur and consequently no second T_g was observed for the triblock copolymers.
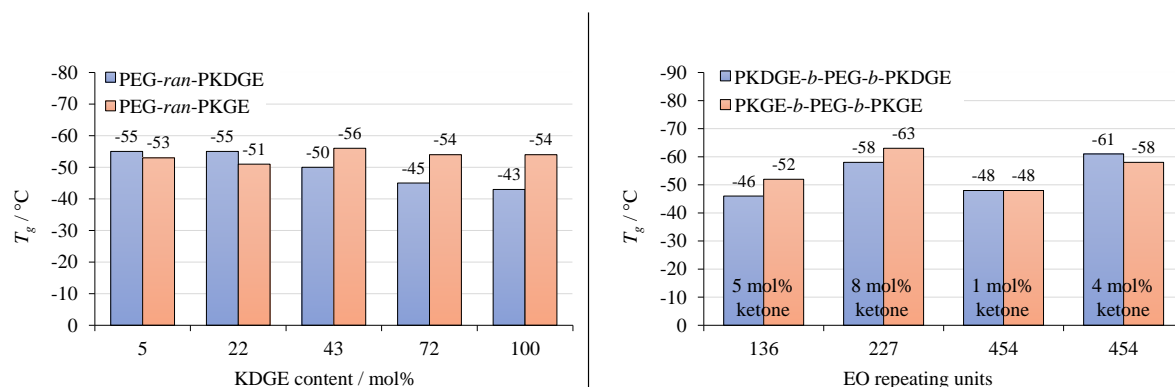
Figure 9. Comparison of the T_gs before and after removal of the dioxolane protecting groups. Left: random PEG-ran-PKDGE and PEG-ran-PKGE copolymers including homopolymer. Right: PKDGE-b-PEG-b-PKDGE and PKGE-b-PEG-b-PKGE triblock copolymers.

A melting point (T_m) can only be observed for the random copolymer with the smallest amount of KDGE/ KGE (5 mol%). For PEG$_{197}$-ran-PKDGE$_{11}$ (entry 1, **Table 4**) T_m is 35 °C and increases after removal of the dioxolane protecting group to 39 °C. We propose, firstly, that this is attributable to the increased compactness of the pendant KDE side chains caused by the removal of the sterically demanding protecting groups. Secondly, dipole-dipole interactions may also contribute here. From **Table 4** it can be seen that the T_ms of the PKDGE-b-PEG-b-

PKDGE triblock copolymers are almost unaffected by deprotection. For PKGE$_9$-b-PEG$_{454}$-b-PKGE$_9$ (entry 5, **Table 4**) and its protected precursor, a slight increase of the melting temperature can be observed, which can be traced back to the above-mentioned aspects for the statistical copolymer.

Table 4. Melting temperatures T_ms and -enthalpies ΔH of protected and deprotected KDGE-containing polymers.

No.	Composition[a]	$T_{m, prot.}$[b] / °C	ΔH[b] / J g^{-1}	$T_{m, depr.}$[c] / °C	ΔH[c] / J g^{-1}
1	PEG$_{197}$-ran-PKDGE$_{11}$	35	66	39	81
2	PKDGE$_4$-b-PEG$_{136}$-b-PKDGE$_4$	49	107	50	94
3	PKDGE$_{10}$-b-PEG$_{227}$-b-PKDGE$_{10}$	53	108	54	110
4	PKDGE$_3$-b-PEG$_{454}$-b-PKDGE$_3$	61	135	59	97
5	PKDGE$_9$-b-PEG$_{454}$-b-PKDGE$_9$	54	112	59	112

[a] Values calculated by ^{1}H NMR spectroscopy. [b] T_ms and ΔH values for KDGE-containing polymers. [c] T_ms and ΔH values for KGE-containing polymers.

B.   Post-polymerization modification and hydrogel formation.

As described above, ketones represent a versatile functional group for a variety of subsequent post-polymerization reactions. Generally, nucleophilic reagents are useful reactants for functionalization. These nucleophiles can be for instance amines (imine/enamine formation), alcohols (acetal formation) or phosphorus ylides (Wittig reaction).[67] In the following, two model reactions for the transformation of the ketone moieties are shown: on the one hand the *in-situ* deprotection and reaction of the pendant ketone functionalities with 2,4-dinitrophenylhydrazine (2,4-DNPH), on the other hand, the crosslinking of deprotected KGE units by using O,O'-1,3-propanediylbishydroxylamine dihydrochloride (1,3-PDBH) (**Scheme 3**).
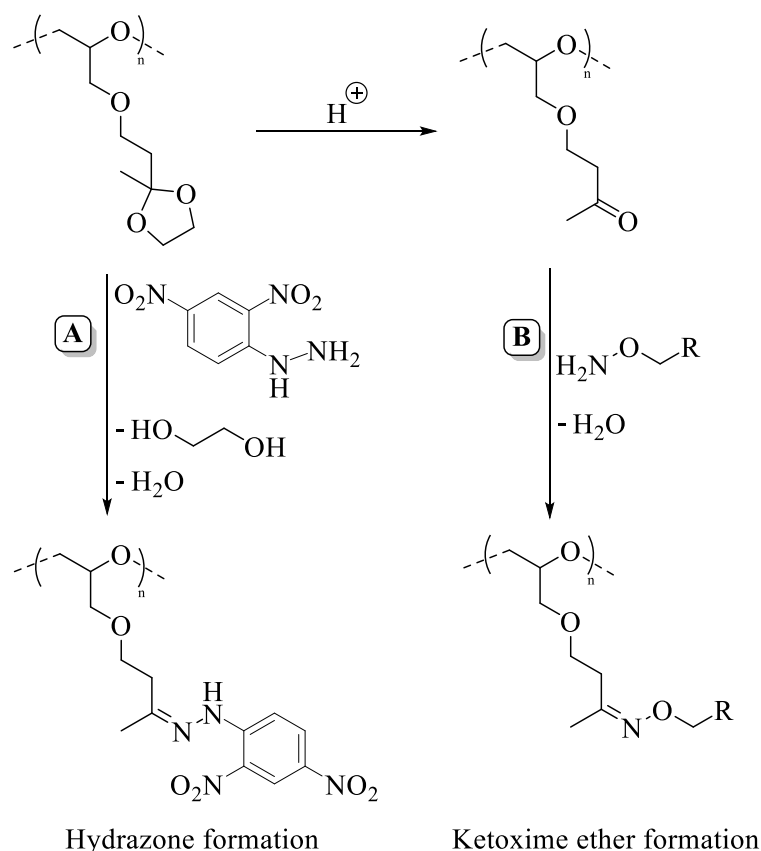
Scheme 3. Post-polymerization modification of KDGE moieties. A) Phenylhydrazone formation by *in-situ* deprotection and reaction of dioxolane-protected ketone groups with 2,4-DNPH. B) Ketoxime ether formation by reaction of the free ketone groups with 1,3-PDBH.

Nucleophilic addition of 2,4-dinitrophenylhydrazine (2,4-DNPH). 2,4-DNPH was directly attached to the KDGE units without a separate deprotection step to study the polymers as potential drug carriers (**Scheme 3A**). In order to see a difference as large as possible between the precursor and the modified polymer, homopolymer PKDGE$_{27}$ (entry 5, **Table 1**) was used for this purpose. After the ethanolic homopolymer solution was added to the acidic 2,4-DNPH solution, an intense orange solid precipitated. For purification, the product was washed several times with water and ethanol and subsequently dialyzed against MeOH/ DCM (1 : 1). The comparison of the SEC traces shows a significant increase in the molecular mass of approximately 2,300 g mol^{-1} after phenylhydrazone formation (**Figure 10**). Additionally, the SEC trace of the modified homopolymer is shifted uniformly and still narrowly distributed without any perceptible broadening of the dispersity ($Đ = 1.17$), indicating a quantitative conversion of the KDGE moieties.
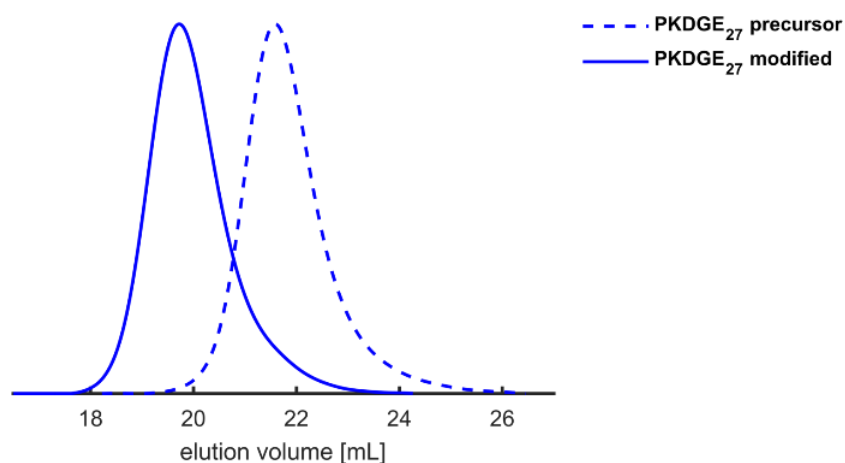
Figure 10. SEC traces (DMF, PEG-standard, RI detector) of precursor $PKDGE_{27}$ (entry 5, **Table 1**) and 2,4-DNPH-modified homopolymer (before: $M_{n, SEC}$ = 1,700 g mol^{-1}, $Đ$ = 1.15; after: $M_{n, SEC}$ = 4,000 g mol^{-1}, $Đ$ = 1.17).

The findings are in line with the ^{1}H NMR spectrum of the 2,4-DNPH modified $PKDGE_{27}$ (entry 5, **Table 1**) in **Figure 11**. The signals of phenylhydrazone groups are clearly recognizable (11.3−7.8 ppm). Further, it is known that *E*- and *Z* isomers are formed by reacting dinitrophenylhydrazines with asymmetrical ketones.[68] In the present case, a ratio of 2 : 1 (*E* : *Z*) was found. Additional spectra are given in the Supporting Information (**SI-Figures 30−31**).
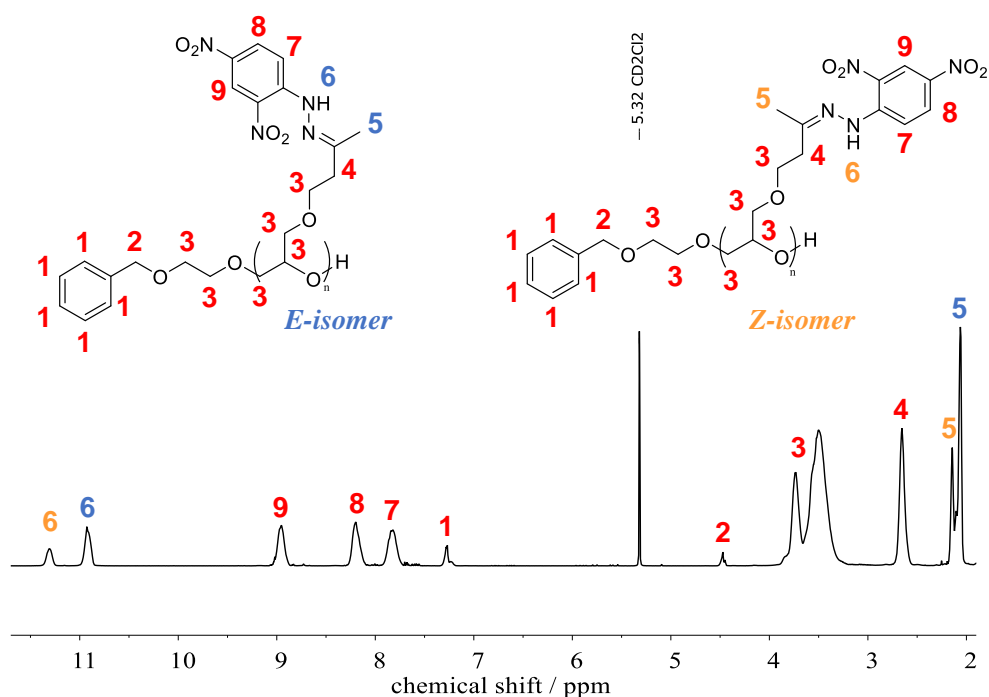
Figure 11. ^{1}H NMR spectrum (400 MHz, CD_2Cl$_2$) of 2,4-DNPH modified $PKDGE_{27}$ containing *E/Z*-isomers.

Nucleophilic addition of O,O'-1,3-Propanediyldifunctional alkoxyamine dihydrochloride (1,3-PDBH). For further investigations especially in potential biomedical applications, deprotected PKDGE-*b*-PEG-*b*-PKDGE triblock copolymers were crosslinked with 1,3-PDBH (**Scheme 3B**) and the obtained hydrogels were studied in detail. On the one hand the influence of the PEG block size was analyzed and on the other hand the number of functional, crosslinkable ketone groups. To ensure an adequate, mechanical stability of the hydrogels, they were crosslinked for two days on the mechanical shaker (**Figure 12A−B**). Subsequently, the crosslinked hydrogels were removed from the tube and placed in water for further swelling. In the last step, the swelling ratio *SR* (**Equation 1**) was determined. In general, it was observed that the water uptake reached a maximum at a ratio of [ketone] : [alkoxyamine] = 1.2 : 1, which is why this ratio was chosen as standard. For the individual approaches, the mass fraction of the triblock copolymer had to be individually adjusted. Otherwise, the hydrogels dissolved during the swelling process in water. The results are summarized in **Table 5**.

Table 5. Parameters for network formation of the PKDGE-*b*-PEG-*b*-PKDGE triblock copolymers, including their swelling ratio *SR*, their molecular weight between crosslinks M_c and the calculated mesh sizes ξ.

No.	Composition[a]	w^a / wt%	SR / %	M_c / g mol^{-1}	ξ / nm
1	PKGE$_{10}$-*b*-PEG$_{227}$-*b*-PKGE$_{10}$	50	1,100 ± 10	4,300	9.5
2	PKGE$_3$-*b*-PEG$_{454}$-*b*-PKGE$_3$	40	3,200 ± 200	9,300	19.9
3	PKGE$_9$-*b*-PEG$_{454}$-*b*-PKGE$_9$	40	2,800 ± 150	9,800	19.6

[a] Here, the mass fraction *w* is defined as the sum of the respective triblock and 1,3-PDBH in water.

There are generally two trends observable. On the one hand, the smaller the number of EO repeating units in each triblock, the more concentrated the initial solution must be before crosslinking. On the other hand, is conspicuous that the hydrogel of PKGE$_{10}$-*b*-PEG$_{227}$-*b*-PKGE$_{10}$ (entry 1, **Table 5**) absorbs about a third less water in comparison to hydrogels based on PEG$_{454}$ (entries 2−3, **Table 5**). The reason for this is, firstly, the higher crosslinking density due to the larger quantity of KGE units (8 mol% vs. 1/4 mol%) and secondly, the smaller mesh size due to the initiator size (PEG$_{227}$ vs. PEG$_{454}$).[69] While the other two samples (entries 2−3, **Table 5**) formed clear gels in water, the gel of PKGE$_{10}$-*b*-PEG$_{227}$-*b*-PKGE$_{10}$ (entry 1, **Table 5**) remained very cloudy, which is illustrated in **SI-Figure 32**. For the same reason the difference in *SR*s of PKGE$_3$-*b*-PEG$_{454}$-*b*-PKGE$_3$ (entry 2, **Table 5**) and PKGE$_9$-*b*-PEG$_{454}$-*b*-PKGE$_9$

(entry 3, **Table 5**) hydrogels can be explained. The latter has three times as many KGE units, resulting in an increased crosslink density and decreased water absorbency. The results are in line with the calculated mesh sizes ξ of gels ranging from 9.5 nm to 19.9 nm.
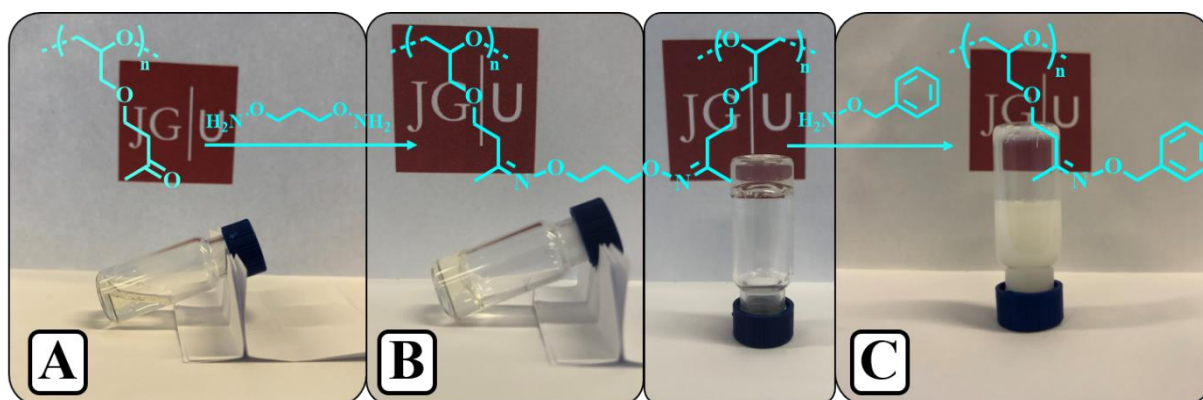
Figure 12. Hydrogel synthesis via ketoxime ether formation followed by cleavage through transoximination. A) Deprotected PKGE-*b*-PEG-*b*-PKGE dissolved in water. B) Hydrogel formation after addition of 1,3-PDBH. C) Cleavage of the crosslinks by addition of monofunctional BHA.

Finally, the reversibility of ketoxime ether formation was studied. For this purpose, monofunctional *O*-benzylhydroxylamine (BHA) was added to the crosslinked hydrogel depicted in **Figure 12B**. Within an hour, it could be observed that the gel slowly liquefied. After 24 hours the transition to a cloudy liquid was completed (**Figure 12C**). The turbidity is caused by the immiscibility of the BHA modified triblock copolymers, which aggregate in the aqueous solution. The hydrophobic benzyl groups are shielded by the PEG chains. In combination with the repulsion of the aggregates by repulsive steric interaction, this effect inhibits coalescence.[70]

CONCLUSION

In this work, we introduced the novel monomer ketone dioxolane glycidyl ether (KDGE), which possess both a protected, aliphatic carbonyl group and an epoxide functionality. The anionic ring-opening polymerization (AROP) of KDGE permitted the access to multi-ketone-functional polyether architectures.

Random PEG-*ran*-PKDGE copolymers were obtained through the anionic ROP of ethylene oxide (EO) and KDGE. The amount of KDGE was varied between 5 mol% and 100 mol% with molecular weights in the range of 5,200 g mol^{-1} to 10,700 g mol^{-1} ($Đ \leq 1.2$). Real-time ^{1}H NMR kinetic studies revealed a nearly ideally random incorporation of KDGE and EO with reactivity ratios of $r_{KDGE} = 0.7$ and $r_{EO} = 1.3$. Post-polymerization modification with 2,4-dinitrophenylhydrazine was achieved by *in-situ* deprotection of the pendant KDGE side chains, resulting in hydrazone-linked polymer-model drug conjugates. Examination of the thermal properties demonstrated marginal differences between protected (T_g = -55 °C to -43 °C) and deprotected (T_g = -56 °C to -51 °C) (co-)polymers, which can be attributed to the bulky dioxolane protecting groups of the ketone funtionalities.[66]

PKDGE-*b*-PEG-*b*-PKDGE triblock copolymers of various comonomer compositions were successfully obtained by AROP, using differently sized PEG macroinitiators (PEG$_{136}$, PEG$_{227}$ and PEG$_{454}$). The KDGE incorporation rate was varied between 1 mol% and 8 mol% with molecular weights up to 23,500 g mol^{-1} and $Đ$ less than 1.2. The triblock copolymers were deprotected and examined in detail by NMR, SEC and DSC measurements. Free ketone units of the PKGE-*b*-PEG-*b*-PKGE triblock copolymers were successfully crosslinked by reaction with a difunctional alkoxyamine via ketoxime ether formation, resulting in reversible hydrogels. The water uptake varied between 1,100% and 3,200% with mesh sizes of 10 nm to 20 nm, depending on the size of the PEG macroinitiator and amount of KGE groups. Regarding potential self-healing applications, the reversibility of the oxime formation was demonstrated through addition of a monofunctional hydroxylamine.

The successful incorporation of ketone functionalities along the polyether backbone provides the ideal building block for a variety of potential biomedical applications such as bioconjugation.

ACKNOWLEDGEMENT

REFERENCES

(1) *Fortschritte der Chemie Organischer Naturstoffe / Progress in the Chemistry of Organic Natural Products;* Gottlieb, O. R.; Herrmann, K.; Murray, R. D. H.; Ohloff, G.; Pattenden, G.; Herz, W.; Grisebach, H.; Kirby, G. W., Eds.; Fortschritte der Chemie Organischer Naturstoffe / Progress in the Chemistry of Organic Natural Products 35; Springer: Vienna, 1978.

(2) Brown, W. H.; Iverson, B. L.; Anslyn, E. V.; Foote, C. S. *Organic chemistry*, 7th edition; Wadsworth Cengage Learning: Australia, Belmont, CA, 2014.

(3) Wittig, G.; Schöllkopf, U. Über Triphenyl-phosphin-methylene als olefinbildende Reagenzien (I. Mitteil. *Chem. Ber.* **1954**, *87*, 1318–1330, DOI: 10.1002/cber.19540870919.

(4) Cheng, C.; Sun, G.; Khoshdel, E.; Wooley, K. L. Well-Defined Vinyl Ketone-Based Polymers by Reversible Addition−Fragmentation Chain Transfer Polymerization. *J. Am. Chem. Soc.* **2007**, *129*, 10086–10087, DOI: 10.1021/ja073541y.

(5) Zhou, W.; Qu, Q.; Xu, Y.; An, Z. Aqueous Polymerization-Induced Self-Assembly for the Synthesis of Ketone-Functionalized Nano-Objects with Low Polydispersity. *ACS Macro Lett.* **2015**, *4*, 495–499, DOI: 10.1021/acsmacrolett.5b00225.

(6) Mukherjee, S.; Bapat, A. P.; Hill, M. R.; Sumerlin, B. S. Oximes as reversible links in polymer chemistry: dynamic macromolecular stars. *Polym. Chem.* **2014**, *5*, 6923–6931, DOI: 10.1039/C4PY01282H.

(7) Krasia, T.; Soula, R.; Börner, H. G.; Schlaad, H. Controlled synthesis of homopolymers and block copolymers based on 2-(acetoacetoxy)ethyl methacrylate via RAFT radical polymerisation. *Chem. Commun.* **2003**, 538–539, DOI: 10.1039/b212634f.

(8) Tang, X.; Han, J.; Zhu, Z.; Lu, X.; Chen, H.; Cai, Y. Facile synthesis, sequence-tuned thermoresponsive behaviours and reaction-induced reorganization of water-soluble keto-polymers. *Polym. Chem.* **2014**, *5*, 4115–4123, DOI: 10.1039/C4PY00146J.

(9) Bandyopadhyay, S.; Xia, X.; Maiseiyeu, A.; Mihai, G.; Rajagopalan, S.; Bong, D. Z-Group ketone chain transfer agents for RAFT polymer nanoparticle modification via hydrazone conjugation. *Macromolecules* **2012**, *45*, 6766–6773, DOI: 10.1021/ma301536f.

(10) Byard, S. J.; Williams, M.; McKenzie, B. E.; Blanazs, A.; Armes, S. P. Preparation and Cross-Linking of All-Acrylamide Diblock Copolymer Nano-Objects via Polymerization-Induced Self-Assembly in Aqueous Solution. *Macromolecules* **2017**, *50*, 1482–1493, DOI: 10.1021/acs.macromol.6b02643.

(11) Patenaude, M.; Campbell, S.; Kinio, D.; Hoare, T. Tuning Gelation Time and Morphology of Injectable Hydrogels Using Ketone–Hydrazide Cross-Linking. *Biomacromolecules* **2014**, *15*, 781–790, DOI: 10.1021/bm401615d.

(12) Hepperle, J. A. M.; Luftmann, H.; Studer, A. Controlled nitroxide-mediated radical polymerization of methyl and phenyl vinyl ketone. *J. Polym. Sci. A Polym. Chem.* **2012**, *50*, 2150–2160, DOI: 10.1002/pola.25997.

(13) Kilic, S.; Michalik, S.; Wang, Y.; Johnson, J. K.; Enick, R. M.; Beckman, E. J. Effect of Grafted Lewis Base Groups on the Phase Behavior of Model Poly(dimethyl siloxanes) in CO 2. *Ind. Eng. Chem. Res.* **2003**, *42*, 6415–6424, DOI: 10.1021/ie030288b.

(14) Yang, S. K.; Weck, M. Modular Covalent Multifunctionalization of Copolymers. *Macromolecules* **2008**, *41*, 346–351, DOI: 10.1021/ma702052k.

(15) Haag, R. Supramolecular drug-delivery systems based on polymeric core-shell architectures. *Angew. Chem. Int. Ed.* **2004**, *43*, 278–282, DOI: 10.1002/anie.200301694.

(16) Bae, Y.; Fukushima, S.; Harada, A.; Kataoka, K. Design of Environment-Sensitive Supramolecular Assemblies for Intracellular Drug Delivery: Polymeric Micelles that are Responsive to Intracellular pH Change. *Angew. Chem.* **2003**, *115*, 4788–4791, DOI: 10.1002/ange.200250653.

(17) Prabaharan, M.; Grailer, J. J.; Pilla, S.; Steeber, D. A.; Gong, S. Amphiphilic multi-arm-block copolymer conjugated with doxorubicin via pH-sensitive hydrazone bond for tumor-targeted drug delivery. *Biomaterials* **2009**, *30*, 5757–5766, DOI: 10.1016/j.biomaterials.2009.07.020.

(18) Zhang, Y.; Gao, M.; Chen, C.; Wang, Z.; Zhao, Y. Residue cytotoxicity of a hydrazone-linked polymer–drug conjugate: implication for acid-responsive micellar drug delivery. *RSC Adv.* **2015**, *5*, 34800–34802, DOI: 10.1039/C5RA02097B.

(19) Shi, Y.; van Nostrum, C. F.; Hennink, W. E. Interfacially Hydrazone Cross-linked Thermosensitive Polymeric Micelles for Acid-Triggered Release of Paclitaxel. *ACS Biomater. Sci. Eng.* **2015**, *1*, 393–404, DOI: 10.1021/acsbiomaterials.5b00006.

(20) Gilbert, T.; Alsop, R. J.; Babi, M.; Moran-Mirabal, J.; Rheinstädter, M. C.; Hoare, T. Nanostructure of Fully Injectable Hydrazone-Thiosuccinimide Interpenetrating Polymer Network Hydrogels Assessed by Small-Angle Neutron Scattering and dSTORM Single-Molecule Fluorescence Microscopy. *ACS Appl. Mater. Interfaces* **2017**, *9*, 42179–42191, DOI: 10.1021/acsami.7b11637.

(21) Liu, J.; Li, R. C.; Sand, G. J.; Bulmus, V.; Davis, T. P.; Maynard, H. D. Keto-Functionalized Polymer Scaffolds As Versatile Precursors to Polymer Side Chain Conjugates. *Macromolecules* **2013**, *46*, 8–14, DOI: 10.1021/ma302183g.

(22) Seuyep Ntoukam, D. H.; Luinstra, G. A.; Theato, P. Postpolymerization modification of reactive polymers derived from vinylcyclopropane. III. Polymer sequential functionalization

using a combination of amines with alkoxyamines, hydrazides, isocyanates, or acyl halides. *J. Polym. Sci. A Polym. Chem.* **2014**, *52*, 2841–2849, DOI: 10.1002/pola.27311.

(23) Hang, H. C.; Bertozzi, C. R. Chemoselective Approaches to Glycoprotein Assembly. *Acc. Chem. Res.* **2001**, *34*, 727–736, DOI: 10.1021/ar9901570.

(24) Barrett, D. G.; Yousaf, M. N. Preparation of a class of versatile, chemoselective, and amorphous polyketoesters. *Biomacromolecules* **2008**, *9*, 2029–2035, DOI: 10.1021/bm800271f.

(25) Iha, R. K.; van Horn, B. A.; Wooley, K. L. Complex, degradable polyester materials via ketoxime ether-based functionalization: Amphiphilic, multifunctional graft copolymers and their resulting solution-state aggregates. *J. Polym. Sci. A Polym. Chem.* **2010**, *48*, 3553–3563, DOI: 10.1002/pola.24132.

(26) Mukherjee, S.; Hill, M. R.; Sumerlin, B. S. Self-healing hydrogels containing reversible oxime crosslinks. *Soft Matter* **2015**, *11*, 6152–6161, DOI: 10.1039/c5sm00865d.

(27) Hill, M. R.; Mukherjee, S.; Costanzo, P. J.; Sumerlin, B. S. Modular oxime functionalization of well-defined alkoxyamine-containing polymers. *Polym. Chem.* **2012**, *3*, 1758–1762, DOI: 10.1039/C1PY00451D.

(28) Stöbener, D. D.; Uckert, M.; Cuellar-Camacho, J. L.; Hoppensack, A.; Weinhart, M. Ultrathin Poly(glycidyl ether) Coatings on Polystyrene for Temperature-Triggered Human Dermal Fibroblast Sheet Fabrication. *ACS Biomater. Sci. Eng.* **2017**, *3*, 2155–2165, DOI: 10.1021/acsbiomaterials.7b00270.

(29) Billouard, C.; Carlotti, S.; Desbois, P.; Deffieux, A. "Controlled" High-Speed Anionic Polymerization of Propylene Oxide Initiated by Alkali Metal Alkoxide/Trialkylaluminum Systems. *Macromolecules* **2004**, *37*, 4038–4043, DOI: 10.1021/ma035768t.

(30) Brocas, A.-L.; Mantzaridis, C.; Tunc, D.; Carlotti, S. Polyether synthesis: From activated or metal-free anionic ring-opening polymerization of epoxides to functionalization. *Prog. Polym. Sci.* **2013**, *38*, 845–873, DOI: 10.1016/j.progpolymsci.2012.09.007.

(31) Sakakibara, K.; Nakano, K.; Nozaki, K. Regio-controlled ring-opening polymerization of perfluoroalkyl-substituted epoxides. *Chem. Commun.* **2006**, *0*, 3334–3336, DOI: 10.1039/b606693c.

(32) Herzberger, J.; Leibig, D.; Liermann, J. C.; Frey, H. Conventional Oxyanionic versus Monomer-Activated Anionic Copolymerization of Ethylene Oxide with Glycidyl Ethers: Striking Differences in Reactivity Ratios. *ACS Macro Lett.* **2016**, *5*, 1206–1211, DOI: 10.1021/acsmacrolett.6b00701.

(33) Herzberger, J.; Leibig, D.; Langhanki, J.; Moers, C.; Opatz, T.; Frey, H. "Clickable PEG" via anionic copolymerization of ethylene oxide and glycidyl propargyl ether. *Polym. Chem.* **2017**, *8*, 1882–1887, DOI: 10.1039/C7PY00173H.

(34) Müller, S. S.; Moers, C.; Frey, H. A Challenging Comonomer Pair: Copolymerization of Ethylene Oxide and Glycidyl Methyl Ether to Thermoresponsive Polyethers. *Macromolecules* **2014**, *47*, 5492–5500, DOI: 10.1021/ma501280k.

(35) Cui, N.; Qian, J.; Liu, T.; Zhao, N.; Wang, H. Hyaluronic acid hydrogel scaffolds with a triple degradation behavior for bone tissue engineering. *Carbohydr. Polym.* **2015**, *126*, 192–198, DOI: 10.1016/j.carbpol.2015.03.013.

(36) Herzberger, J.; Niederer, K.; Pohlit, H.; Seiwert, J.; Worm, M.; Wurm, F. R.; Frey, H. Polymerization of Ethylene Oxide, Propylene Oxide, and Other Alkylene Oxides: Synthesis, Novel Polymer Architectures, and Bioconjugation. *Chem. Rev.* **2016**, *116*, 2170–2243, DOI: 10.1021/acs.chemrev.5b00441.

(37) Dingels, C.; Schömer, M.; Frey, H. Die vielen Gesichter des Poly(ethylenglykol)s. *Chem. unserer Zeit* **2011**, *45*, 338–349, DOI: 10.1002/ciuz.201100551.

(38) *Poly(ethylene glycol): Chemistry and Biological Applications;* Harris, J. M.; Zalipsky, S., Eds.; ACS symposium series 680; American Chemical Society: Washington, 1997.

(39) Kodera, Y. Pegylation of proteins and bioactive substances for medical and technical applications. *Prog. Polym. Sci.* **1998**, *23*, 1233–1271, DOI: 10.1016/S0079-6700(97)00033-6.

(40) Pelegri-O'Day, E. M.; Lin, E.-W.; Maynard, H. D. Therapeutic Protein–Polymer Conjugates: Advancing Beyond PEGylation. *J. Am. Chem. Soc.* **2014**, *136*, 14323–14332, DOI: 10.1021/ja504390x.

(41) Knop, K.; Hoogenboom, R.; Fischer, D.; Schubert, U. S. Poly(ethylene glycol) in Drug Delivery: Pros and Cons as Well as Potential Alternatives. *Angew. Chem. Int. Ed.* **2010**, *49*, 6288–6308, DOI: 10.1002/anie.200902672.

(42) Bailey, F. E.; Koleske, J. V. *Poly(ethylene oxide)*; Academic Press: New York, 1976.

(43) Klein, R.; Wurm, F. R. Aliphatic Polyethers: Classical Polymers for the 21st Century. *Macromol. Rapid Commun.* **2015**, *36*, 1147–1165, DOI: 10.1002/marc.201500013.

(44) Kjellander, R.; Florin, E. Water structure and changes in thermal stability of the system poly(ethylene oxide)–water. *J. Chem. Soc., Faraday Trans. 1* **1981**, *77*, 2053, DOI: 10.1039/f19817702053.

(45) Fruijtier-Pölloth, C. Safety assessment on polyethylene glycols (PEGs) and their derivatives as used in cosmetic products. *Toxicology* **2005**, *214*, 1–38, DOI: 10.1016/j.tox.2005.06.001.

(46) Obermeier, B.; Wurm, F.; Mangold, C.; Frey, H. Multifunctional Poly(ethylene glycol)s. *Angew. Chem. Int. Ed. (English)* **2011**, *50*, 7988–7997, DOI: 10.1002/anie.201100027.

(47) Mangold, C.; Wurm, F.; Frey, H. Functional PEG-based polymers with reactive groups via anionic ROP of tailor-made epoxides. *Polym. Chem.* **2012**, *3*, 1714, DOI: 10.1039/c2py00489e.

(48) Deslongchamps, P.; Bélanger, A.; Berney, D. J. F.; Borschberg, H.-J.; Brousseau, R.; Doutheau, A.; Durand, R.; Katayama, H.; Lapalme, R.; Leturc, D. M. *et al.* The total synthesis of (+)-ryanodol. Part II. Model studies for rings B and C of (+)-anhydroryanodol. Preparation of a key pentacyclic intermediate. *Can. J. Chem.* **1990**, *68*, 127–152, DOI: 10.1139/v90-022.

(49) Becker, H. G. O.; Beckert, R. *Organikum: Organisch-chemisches Grundpraktikum*, 23., vollst. überarb. und aktualisierte Aufl.; Wiley VCH: Weinheim, 2009.

(50) Peter, M.; Tayalia, P. An alternative technique for patterning cells on poly(ethylene glycol) diacrylate hydrogels. *RSC Adv.* **2016**, *6*, 40878–40885, DOI: 10.1039/C6RA08852J.

(51) Elbert, D. L.; Pratt, A. B.; Lutolf, M. P.; Halstenberg, S.; Hubbell, J. A. Protein delivery from materials formed by self-selective conjugate addition reactions. *J. Control. Release* **2001**, *76*, 11–25, DOI: 10.1016/S0168-3659(01)00398-4.

(52) Flory, P. J.; Rehner, J. Statistical Mechanics of Cross-Linked Polymer Networks II. Swelling. *J. Chem. Phys.* **1943**, *11*, 521–526, DOI: 10.1063/1.1723792.

(53) Bray, J. C.; Merrill, E. W. Poly(vinyl alcohol) hydrogels. Formation by electron beam irradiation of aqueous solutions and subsequent crystallization. *J. Appl. Polym. Sci.* **1973**, *17*, 3779–3794, DOI: 10.1002/app.1973.070171219.

(54) Peppas, N. A.; Merrill, E. W. Crosslinked poly(vinyl alcohol) hydrogels as swollen elastic networks. *J. Appl. Polym. Sci.* **1977**, *21*, 1763–1770, DOI: 10.1002/app.1977.070210704.

(55) Slaughter, B. V.; Khurshid, S. S.; Fisher, O. Z.; Khademhosseini, A.; Peppas, N. A. Hydrogels in regenerative medicine. *Adv. Mater. (Weinheim, Ger.)* **2009**, *21*, 3307–3329, DOI: 10.1002/adma.200802106.

(56) Merrill, E. W.; Dennison, K. A.; Sung, C. Partitioning and diffusion of solutes in hydrogels of poly(ethylene oxide). *Biomaterials* **1993**, *14*, 1117–1126, DOI: 10.1016/0142-9612(93)90154-T.

(57) Canal, T.; Peppas, N. A. Correlation between mesh size and equilibrium degree of swelling of polymeric networks. *J. Biomed. Mater. Res.* **1989**, *23*, 1183–1193, DOI: 10.1002/jbm.820231007.

(58) Li, S.; Dory, Y. L.; Deslongchamps, P. On the relative rate of hydrolysis of a series of ketals and their proton affinities. *Isr. J. Chem.* **2000**, *40*, 209–215, DOI: 10.1560/QRH5-Q3N0-0XA6-PT9Y.

(59) Gu, X.-P.; Ikeda, I.; Okahara, M. Stereoselective Formation of Allyl Ethers by Reaction of Epoxides with Organic Chlorides under Liquid-Solid Phase-Transfer Catalysis. *Bull. Chem. Soc. Jpn.* **1987**, *60*, 667–672, DOI: 10.1246/bcsj.60.667.

(60) Niederer, K.; Schüll, C.; Leibig, D.; Johann, T.; Frey, H. Catechol Acetonide Glycidyl Ether (CAGE): A Functional Epoxide Monomer for Linear and Hyperbranched Multi-Catechol Functional Polyether Architectures. *Macromolecules* **2016**, *49*, 1655–1665, DOI: 10.1021/acs.macromol.5b02441.

(61) Obermeier, B.; Frey, H. Poly(ethylene glycol-co-allyl glycidyl ether)s: a PEG-based modular synthetic platform for multiple bioconjugation. *Bioconjugate Chem.* **2011**, *22*, 436–444, DOI: 10.1021/bc1004747.

(62) Mangold, C.; Dingels, C.; Obermeier, B.; Frey, H.; Wurm, F. PEG-based Multifunctional Polyethers with Highly Reactive Vinyl-Ether Side Chains for Click-Type Functionalization. *Macromolecules* **2011**, *44*, 6326–6334, DOI: 10.1021/ma200898n.

(63) Mangold, C.; Wurm, F.; Obermeier, B.; Frey, H. "Functional Poly(ethylene glycol)": PEG-Based Random Copolymers with 1,2-Diol Side Chains and Terminal Amino Functionality. *Macromolecules* **2010**, *43*, 8511–8518, DOI: 10.1021/ma1015352.

(64) Jaacks, V. A novel method of determination of reactivity ratios in binary and ternary copolymerizations. *Makromol. Chem.* **1972**, *161*, 161–172, DOI: 10.1002/macp.1972.021610110.

(65) Meyer, V. E.; Lowry, G. G. Integral and differential binary copolymerization equations. *J. Polym. Sci. A Gen. Pap.* **1965**, *3*, 2843–2851, DOI: 10.1002/pol.1965.100030811.

(66) Koltzenburg, S.; Maskos, M.; Nuyken, O. *Polymer Chemistry*; Springer Berlin Heidelberg: Berlin, Heidelberg, 2017.

(67) McMurry, J. E. *Organic chemistry*, 7th ed.; Thomson Brooks/Cole: Australia, Canada, 2008.

(68) Faramarz Tayyari, S.; L. Speakman, J.; B. Arnold, M.; Cai, W.; Behforouz, M. A comprehensive investigation of variations in melting ranges and NMR data of 2,4-dinitrophenylhydrazine derivatives. *J. Chem. Soc., Perkin Trans. 2* **1998**, 2195, DOI: 10.1039/a705101h.

(69) Stocke, N. A.; Zhang, X.; Hilt, J. Z.; DeRouchey, J. E. Transport in PEG-Based Hydrogels: Role of Water Content at Synthesis and Crosslinker Molecular Weight. *Macromol. Chem. Phys.* **2017**, *218*, 1600340, DOI: 10.1002/macp.201600340.

(70) Buchold, D. *Ein Beitrag zur Darstellung komplexer nanoskaliger Cyanide und Oxide sowie nanoskaliger Hohlkugeln in w/o-Mikroemulsionen*, 1st ed.; Cuvillier Verlag: Göttingen, 2007.

Supporting Information

Ketone Dioxolane Glycidyl Ether: Synthesis of Multi-Ketone-Functional Poly(ethylene glycol) as a Promising Candidate for Bioconjugation and Reversible Hydrogels

Kamil Maciol[‡], Jan Blankenburg[‡,§], Moritz Urschbach[‡], Daniel Leibig[‡,§] and Holger Frey[‡,]*

[‡] Institute of Organic Chemistry, Johannes Gutenberg University Mainz, Duesbergweg 10-14, 55128 Mainz, Germany

[§]Graduate School Materials Science in Mainz, Staudinger Weg 9, 55128 Mainz, Germany

*E-Mail: hfrey@uni-mainz.de

To be submitted
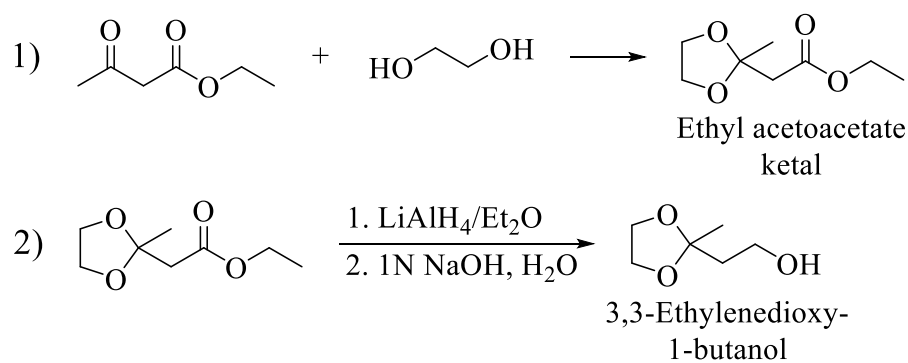
SI-Scheme 1. Strategy for the synthesis of ketone dioxolane glycidyl ether (KDGE) monomer (first two reaction steps).
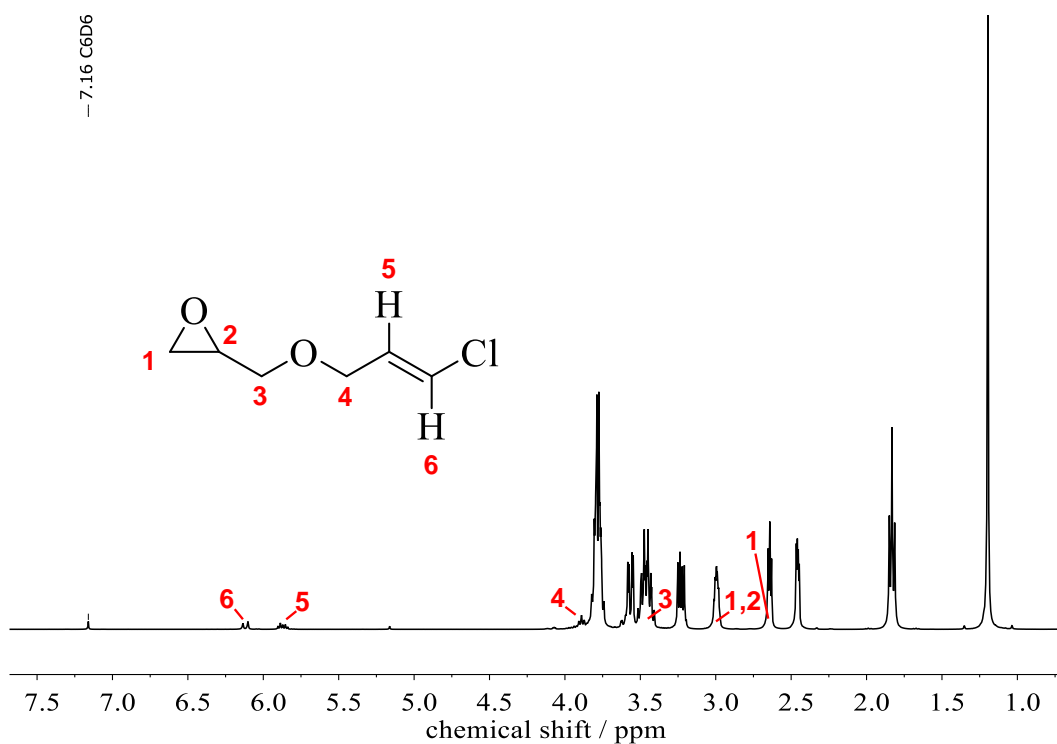
SI-Figure 2. ^{1}H NMR spectrum (400 MHz, C$_6$D$_6$) of KDGE and side product *trans*-3-chloroallyl 2,3-epoxypropyl ether (~ 7 mol%) after usage of phase-transfer catalyst.
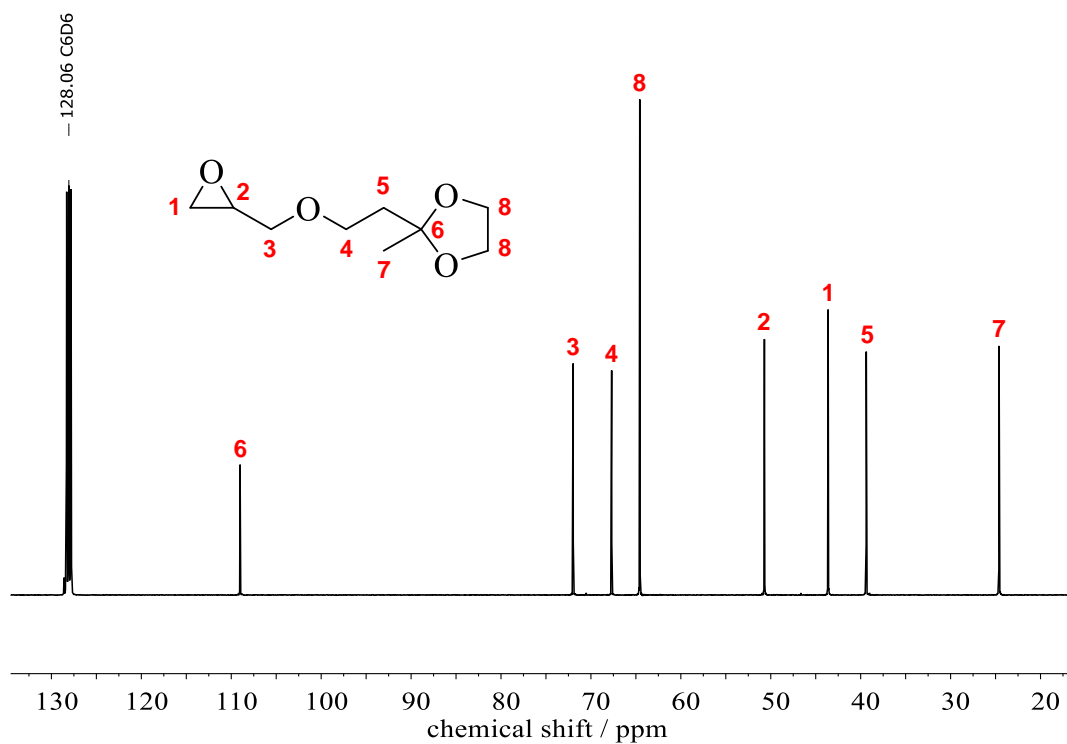
SI-Figure 3. ^{13}C NMR spectrum (100 MHz, C$_6$D$_6$) of KDGE monomer.
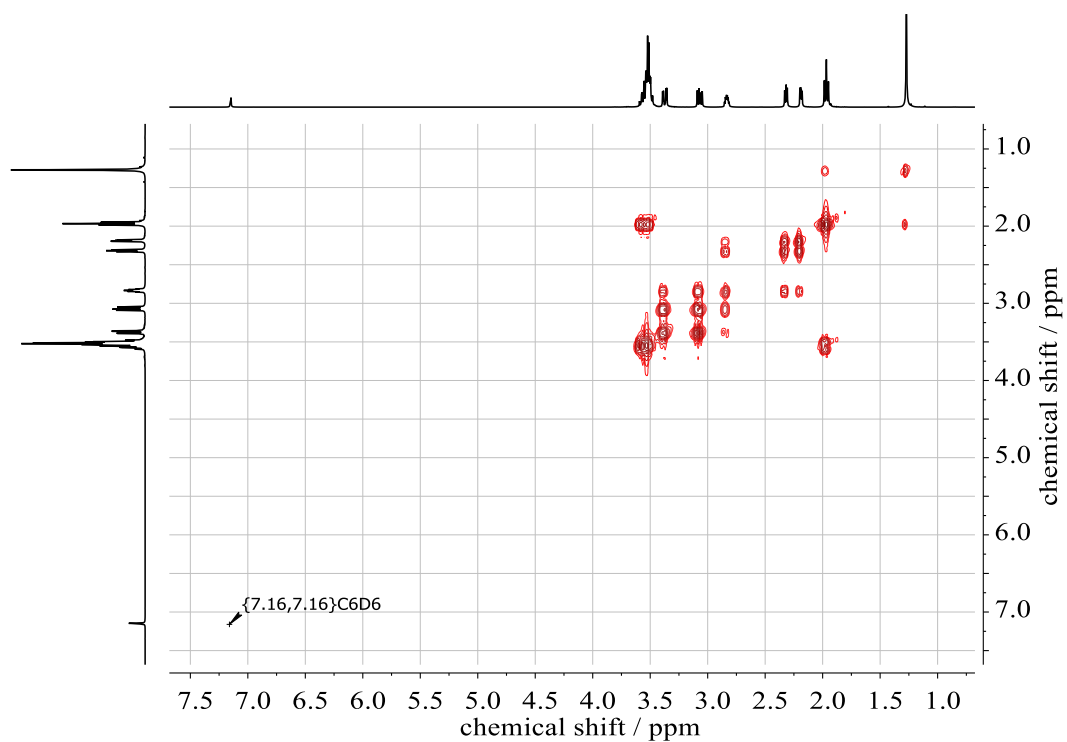
SI-Figure 4. ^{1}H, ^{1}H COSY NMR (400 MHz, C$_6$D$_6$) of KDGE monomer.
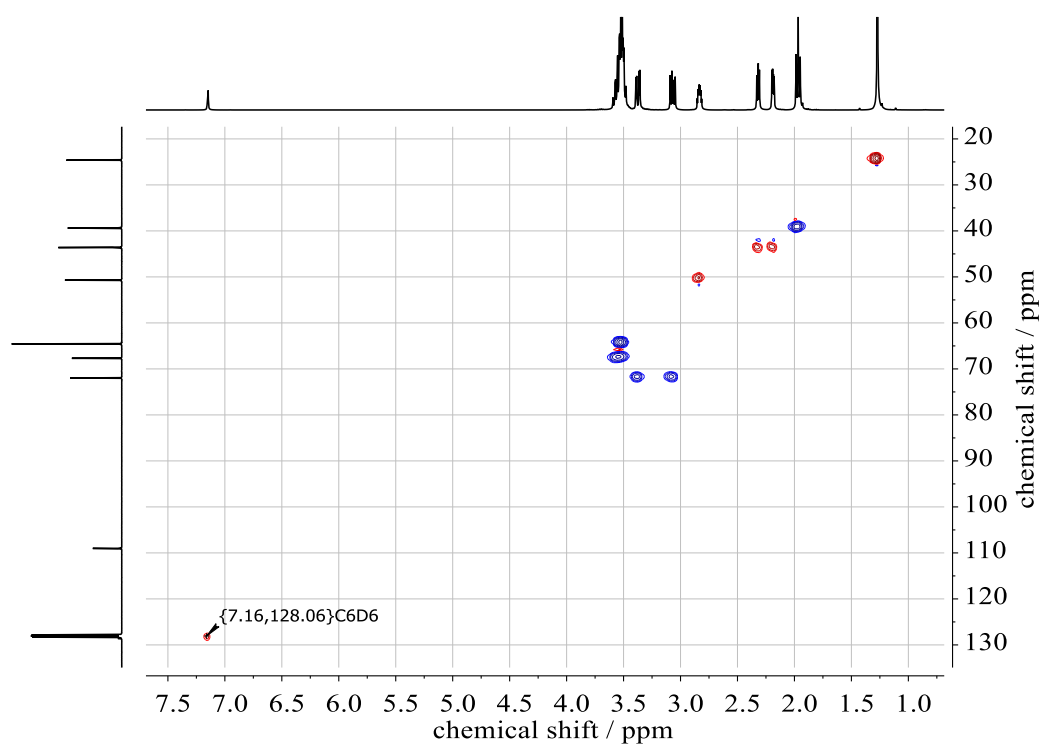
SI-Figure 5. ^{1}H, ^{13}C HSQC NMR of KDGE monomer in C$_6$D$_6$. Color of the signals indicates the phase information (red: methine proton, blue: methylene protons).
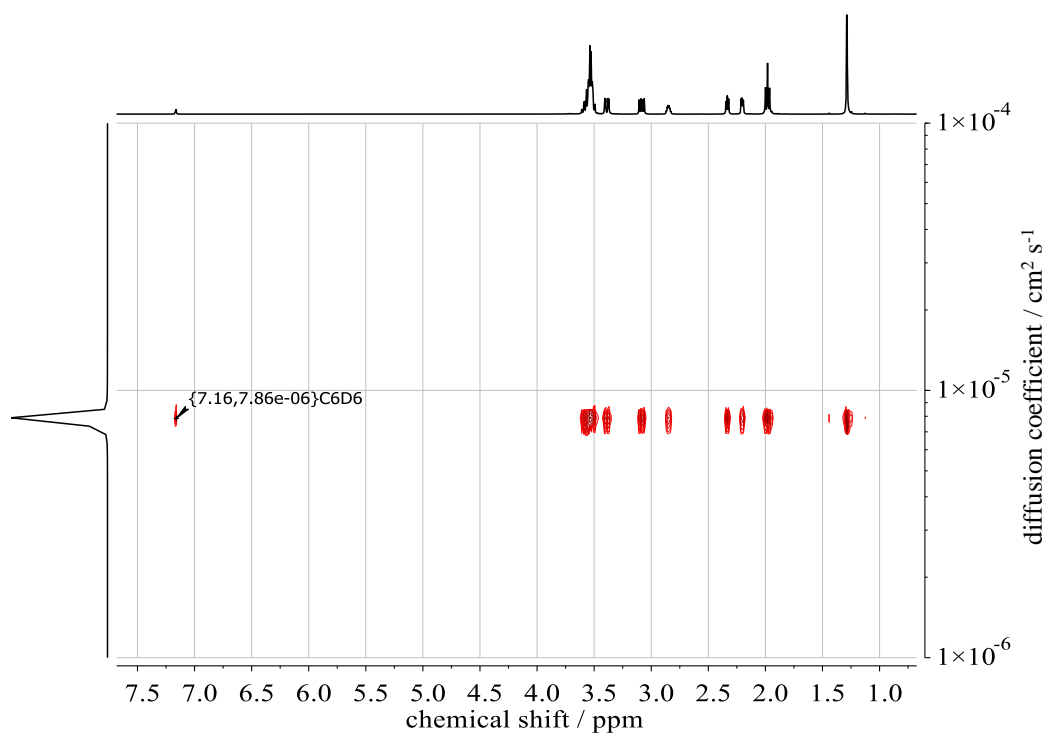
SI-Figure 6. ^{1}H DOSY NMR (400 MHz, C$_6$D$_6$) of KDGE monomer.
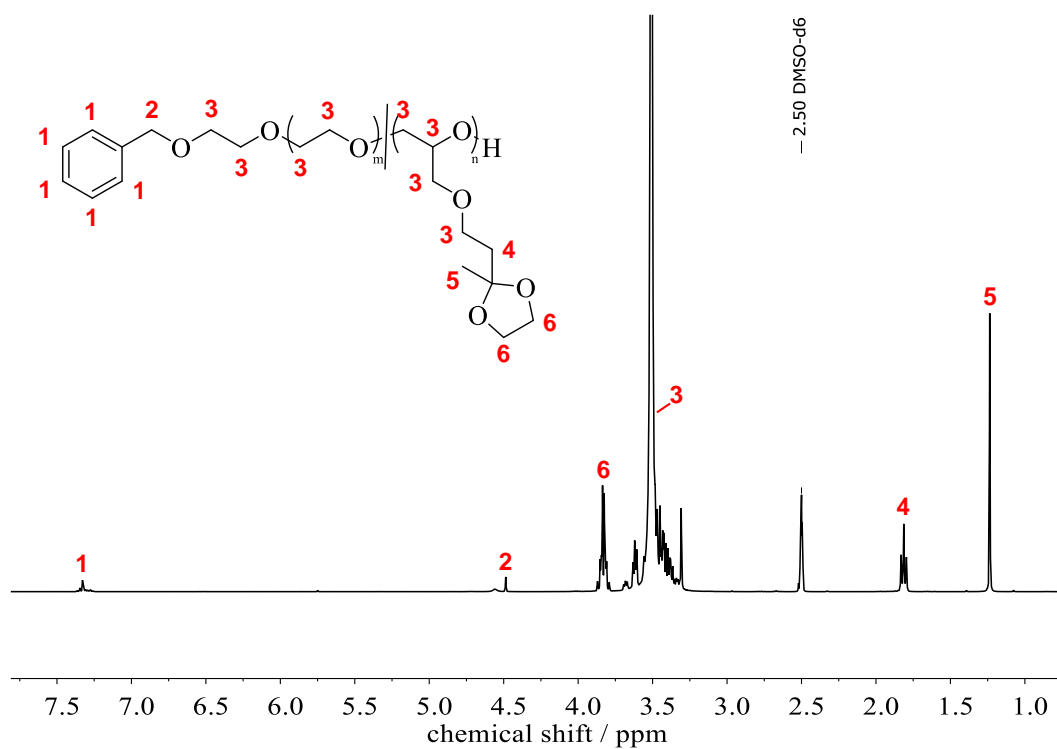
SI-Figure 7. ^{1}H NMR spectrum (400 MHz, DMSO-d_6) of PEG$_{197}$-*ran*-PKDGE$_{11}$ (entry 1, **Table 1**).
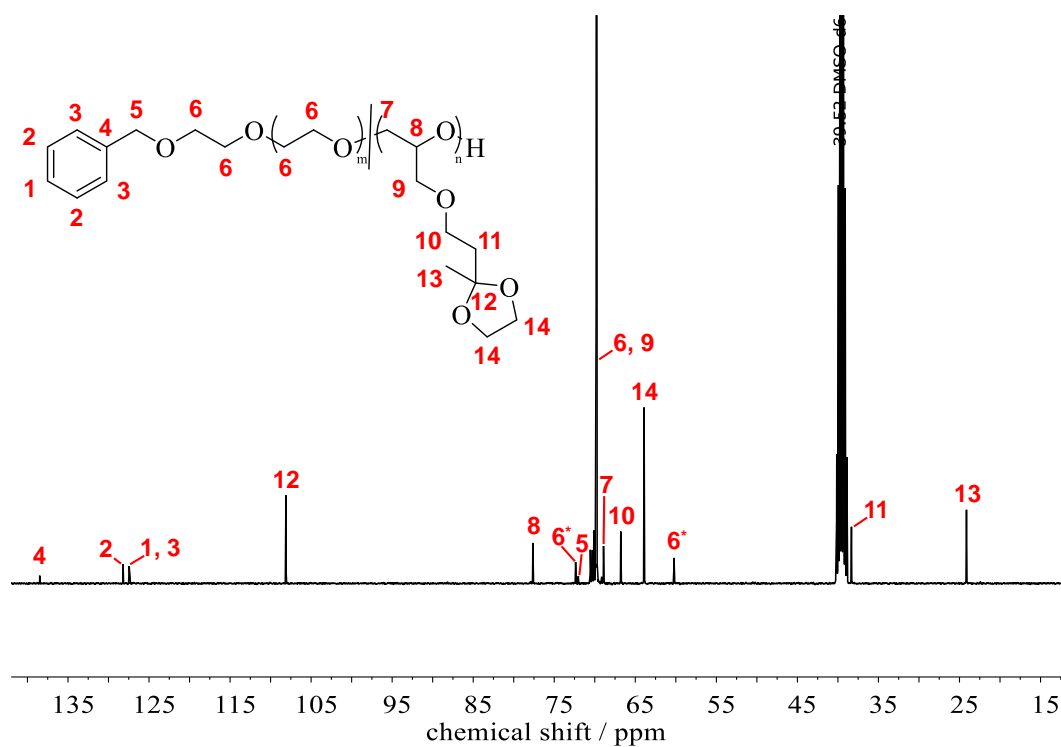
SI-Figure 8. ^{13}C NMR spectrum (100 MHz, DMSO-d_6) of PEG$_{197}$-*ran*-PKDGE$_{11}$ (entry 1, **Table 1**).
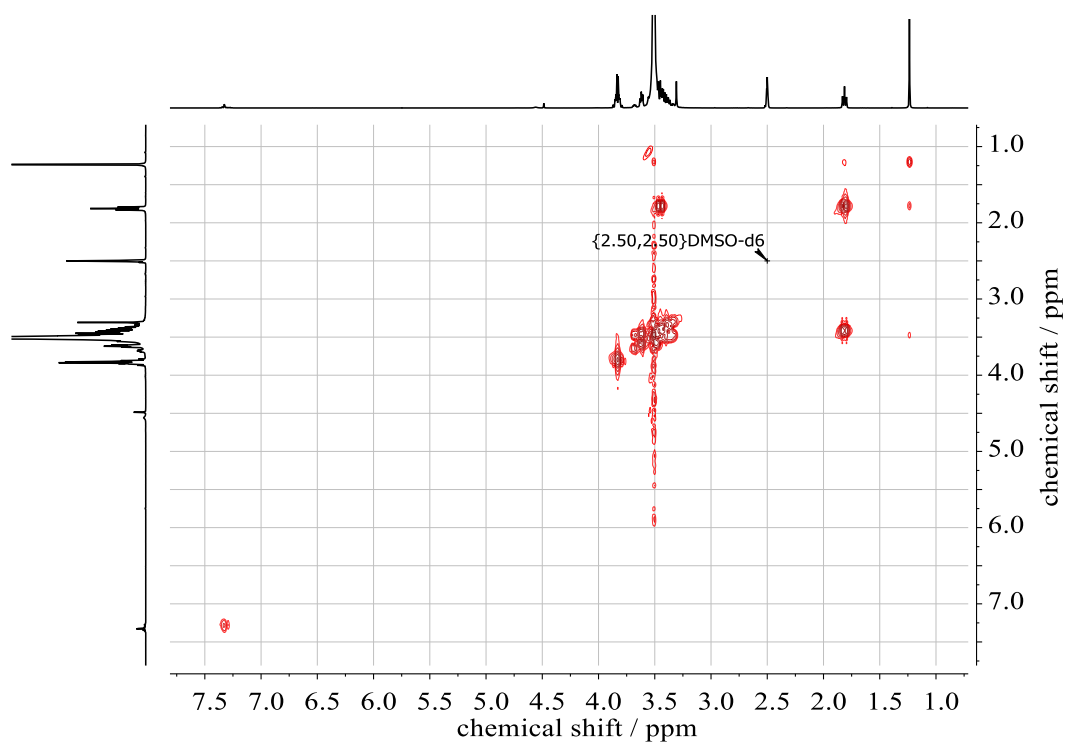
SI-Figure 9. ^{1}H, ^{1}H COSY NMR (400 MHz, DMSO-d_6) of PEG$_{197}$-*ran*-PKDGE$_{11}$ (entry 1, **Table 1**).
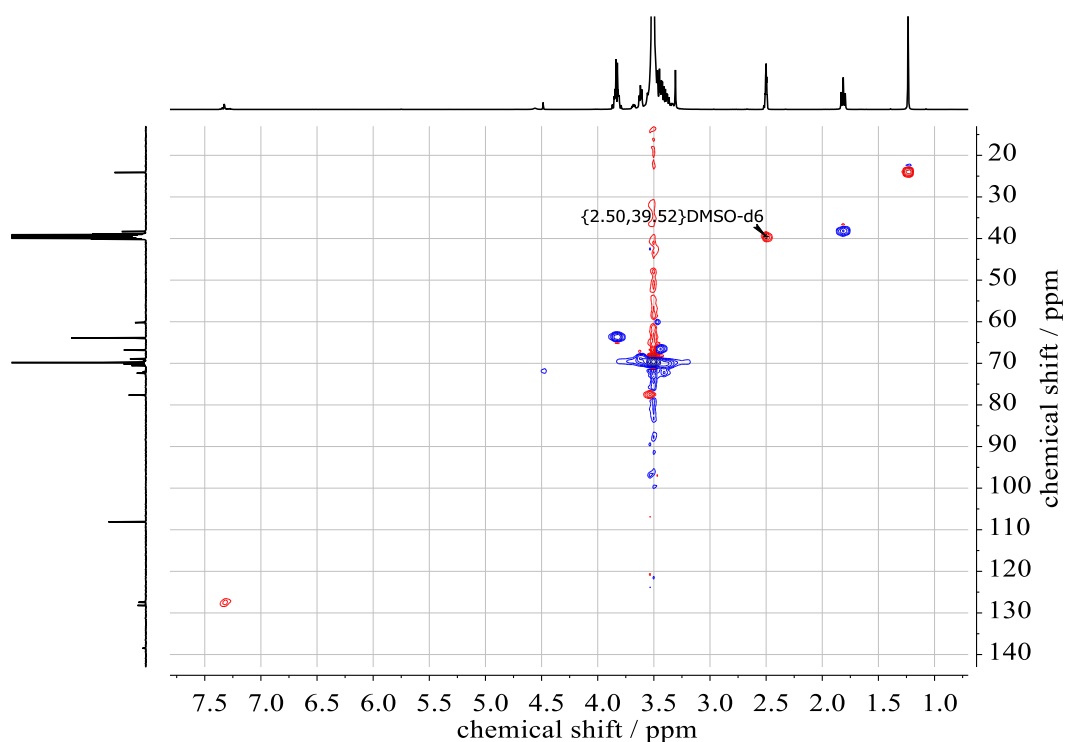
SI-Figure 10. ^{1}H, ^{13}C HSQC NMR of PEG$_{197}$-*ran*-PKDGE$_{11}$ (entry 1, **Table 1**) in DMSO-d_6. Color of the signals indicates the phase information (red: methine proton, blue: methylene protons).
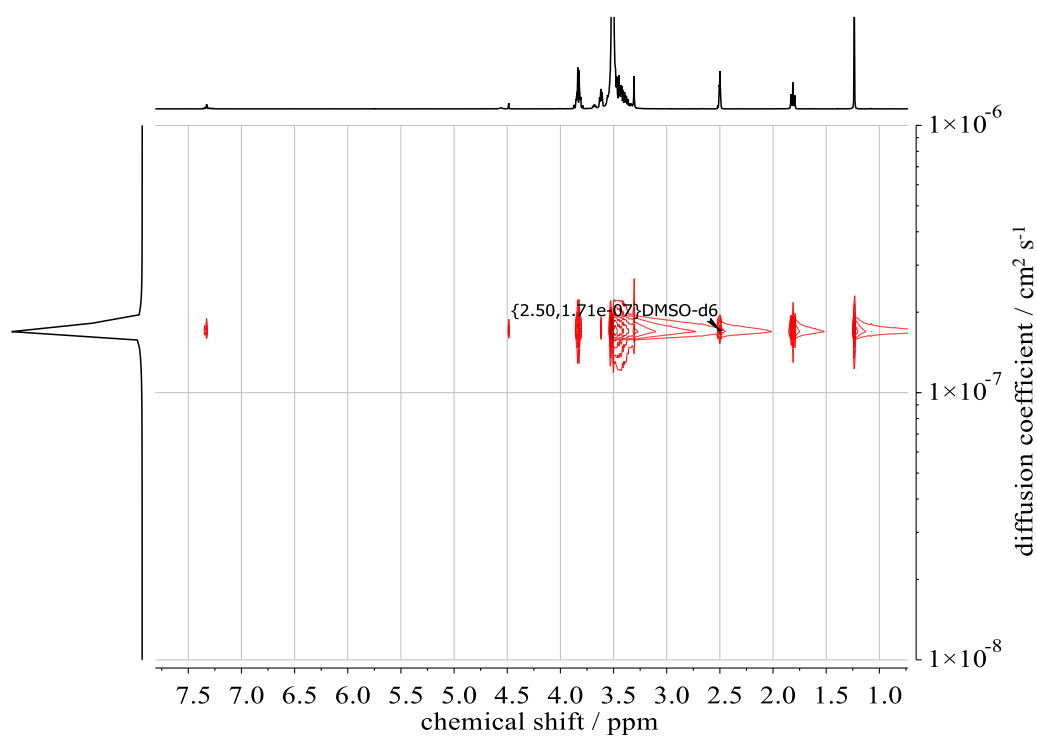
SI-Figure 11. ^{1}H DOSY NMR (400 MHz, DMSO-d_6) of PEG$_{197}$-*ran*-PKDGE$_{11}$ (entry 1, **Table 1**).
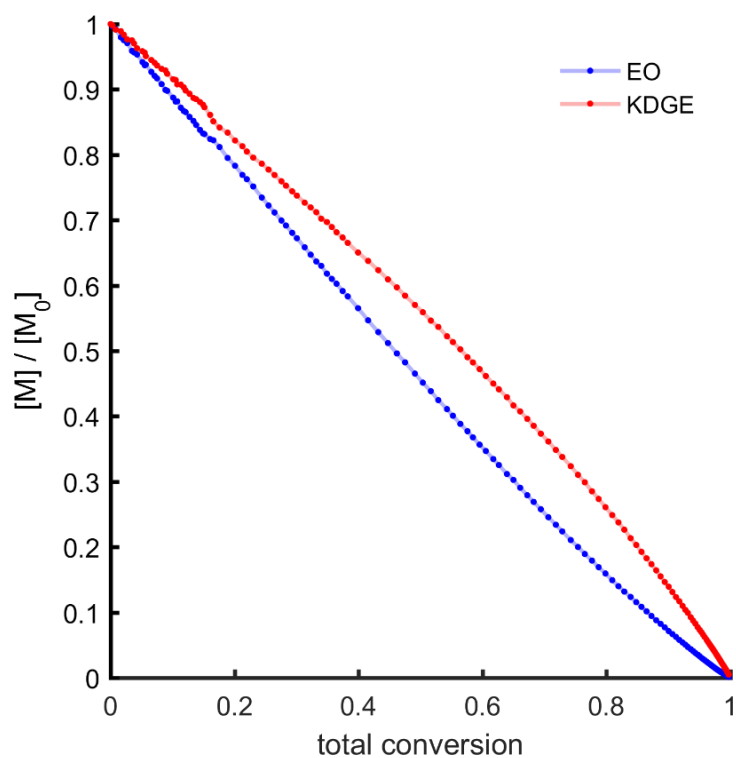
SI-Figure 12. Concentration of the comonomers KDGE and EO plotted versus the conversion.
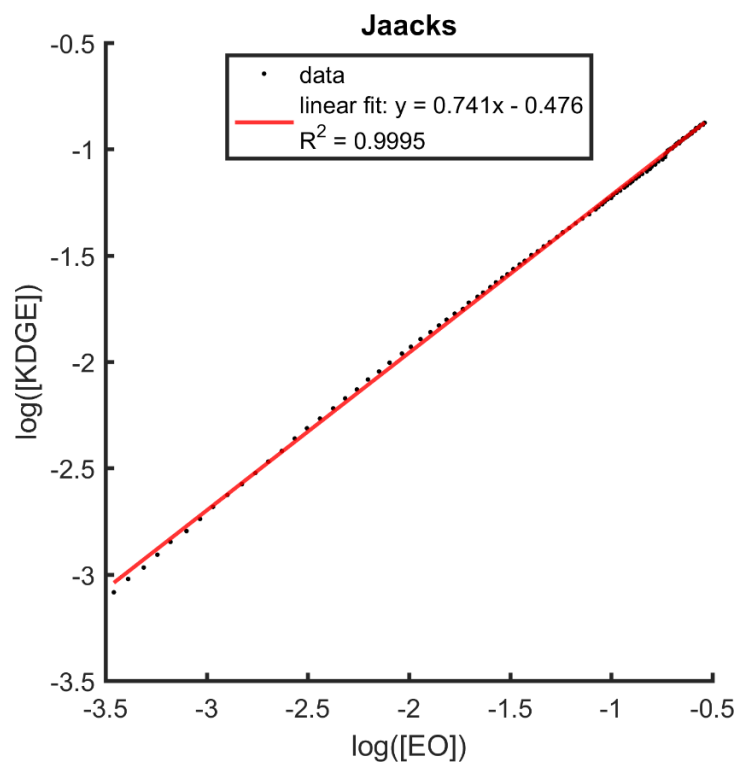
SI-Figure 13. Jaacks fit for determination of reactivity ratios of the copolymerization of KDGE and EO in DMSO-d_6 at 60 °C.
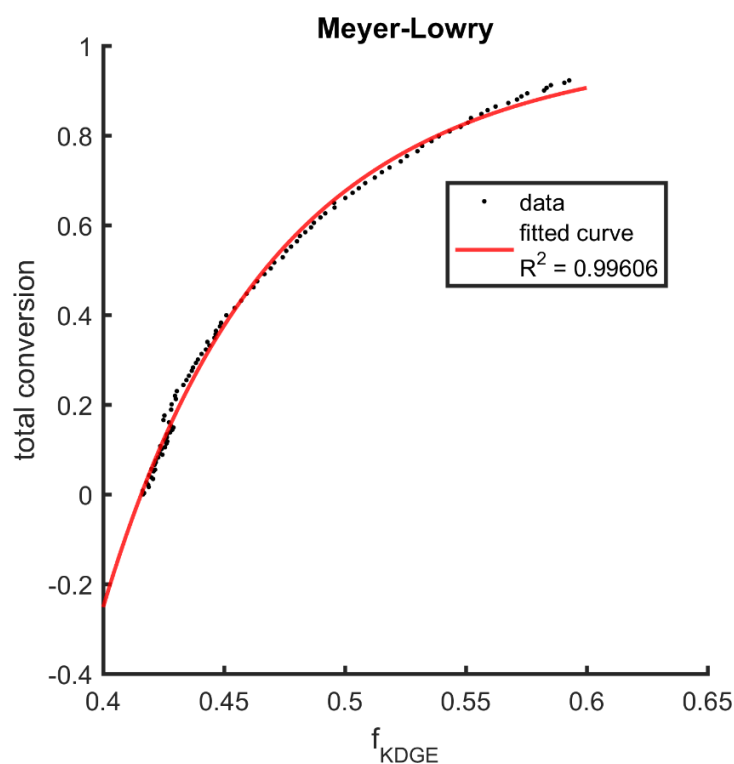
SI-Figure 14. Meyer-Lowry fit for determination of reactivity ratios of the copolymerization of KDGE and EO in DMSO-d_6 at 60 °C.
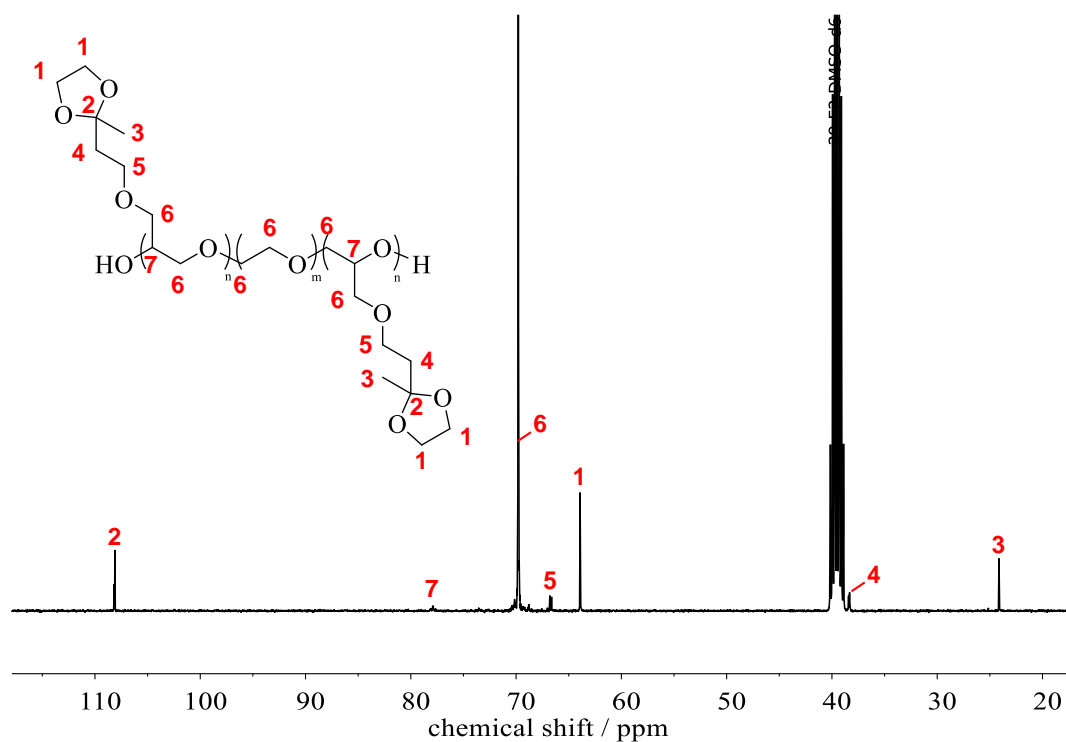
SI-Figure 15. ^{13}C NMR spectrum (100 MHz, DMSO-d_6) of PKDGE$_4$-b-PEG$_{136}$-b-PKDGE$_4$ (entry 1, **Table 2**).
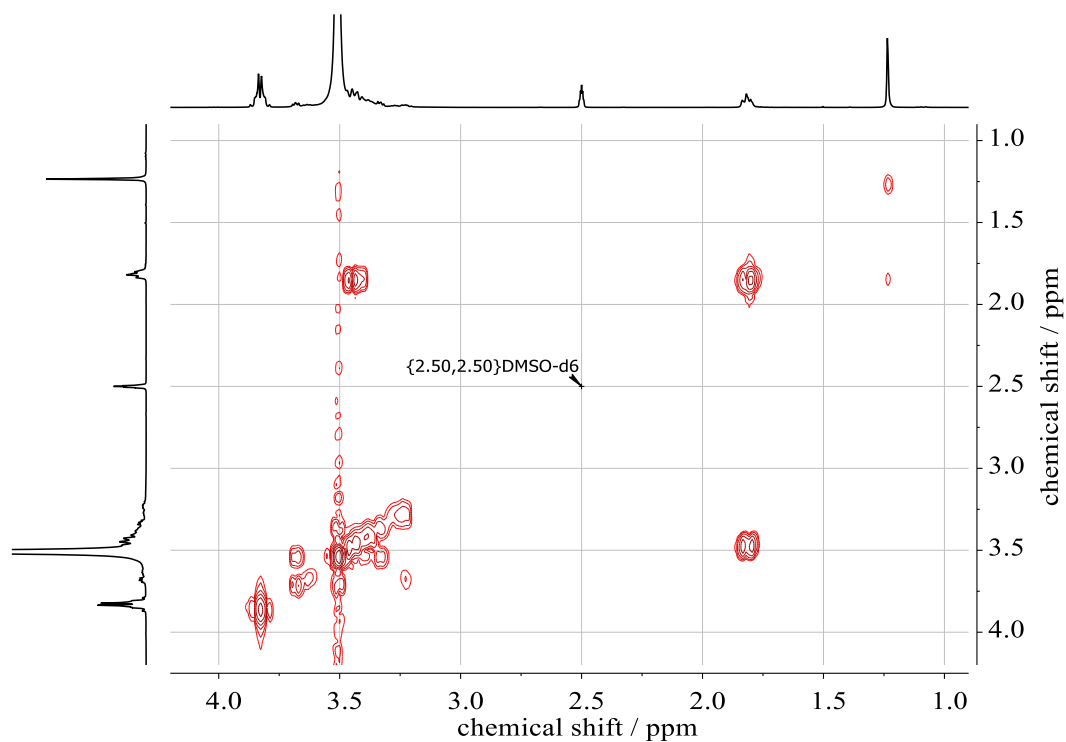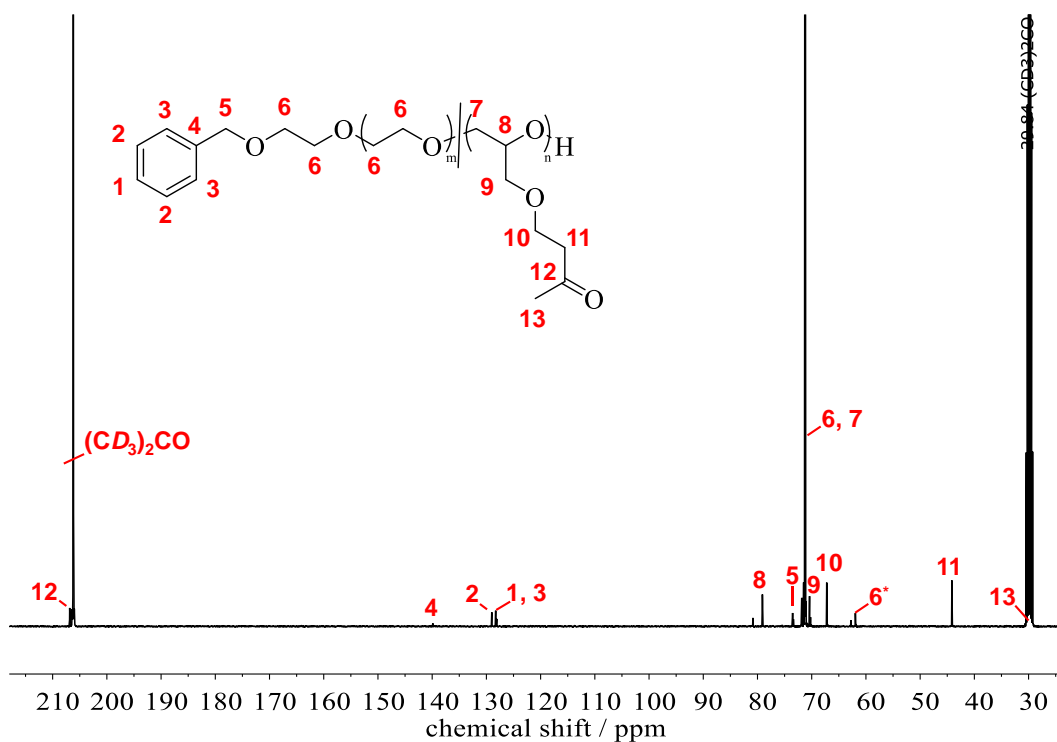

SI-Figure 16. ^{1}H, ^{1}H COSY NMR spectrum (400 MHz, DMSO-d_6) of PKDGE$_4$-b-PEG$_{136}$-b-PKDGE$_4$ (entry 1, **Table 2**).
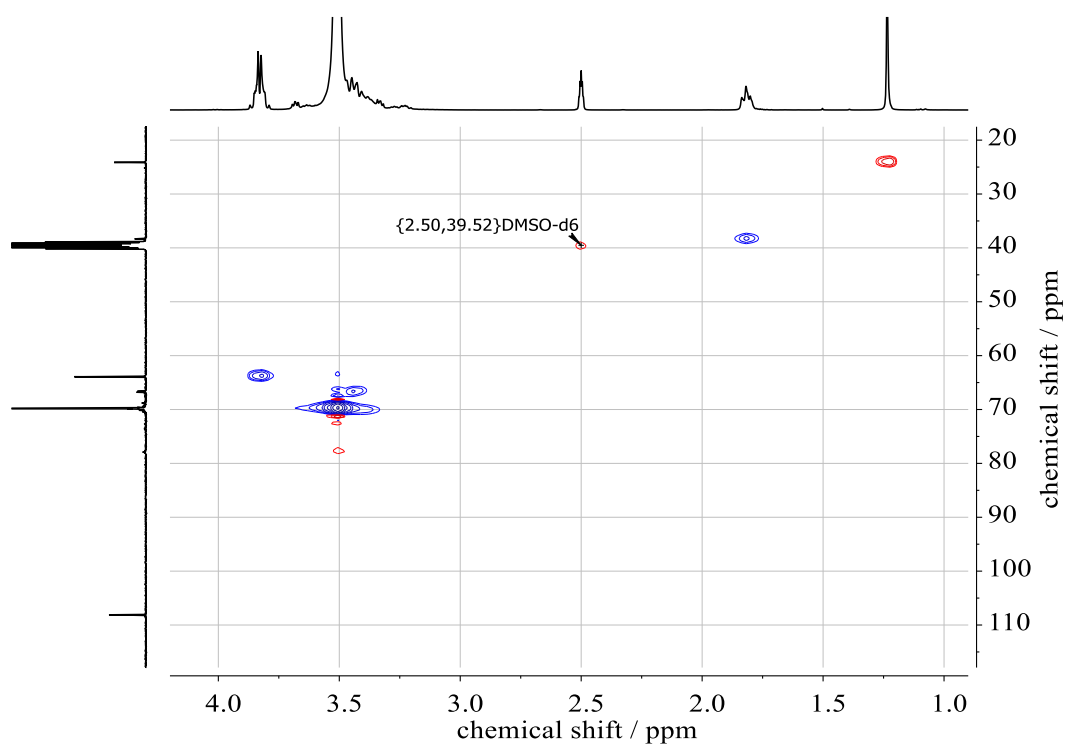
SI-Figure 17. ^{1}H, ^{13}C HSQC NMR spectrum (400 MHz, DMSO-d_6) of PKDGE$_4$-b-PEG$_{136}$-b-PKDGE$_4$ (entry 1, **Table 2**).
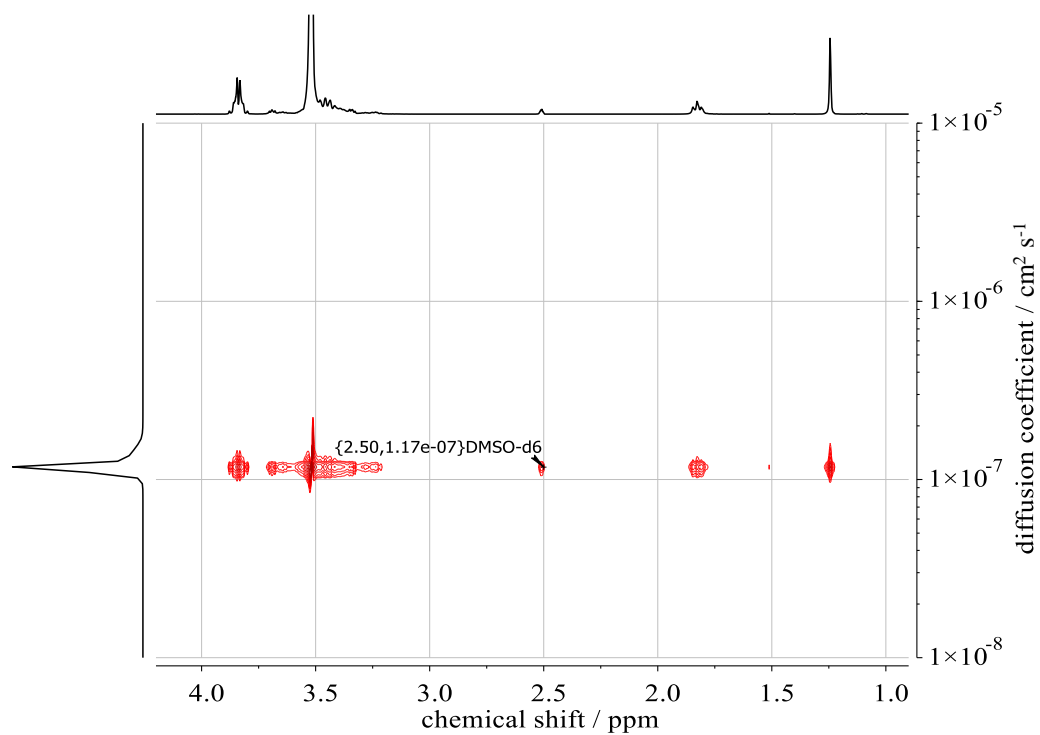
SI-Figure 18. ^{1}H DOSY NMR spectrum (400 MHz, DMSO-d_6) of PKDGE$_4$-b-PEG$_{136}$-b-PKDGE$_4$ (entry 1, **Table 2**).
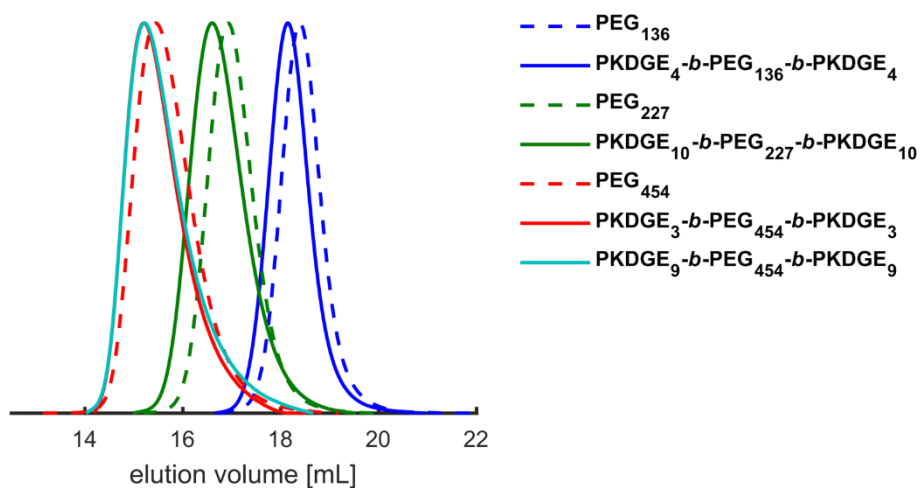
SI-Figure 19. SEC traces (DMF, PEG-standard, RI detector) of PKDGE-*b*-PEG-*b*-PKDGE triblock copolymers (entries 1−4, **Table 2**) and the respective unfunctionalized PEG macroinitiators.
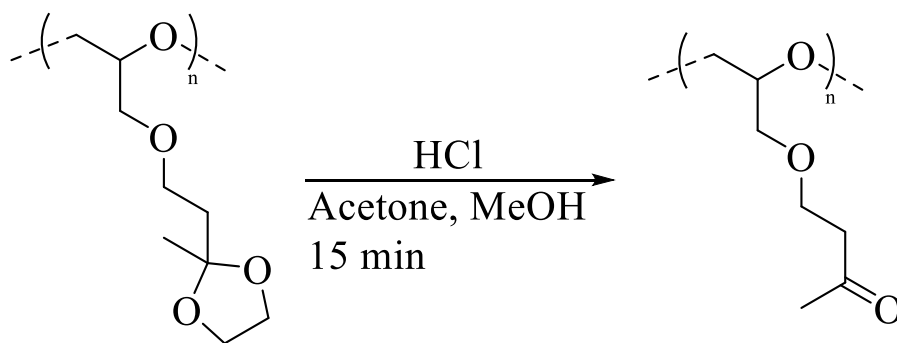
SI-Scheme 2. Removal of the dioxolane protecting groups with methanolic HCl in acetone to generate free ketone groups.
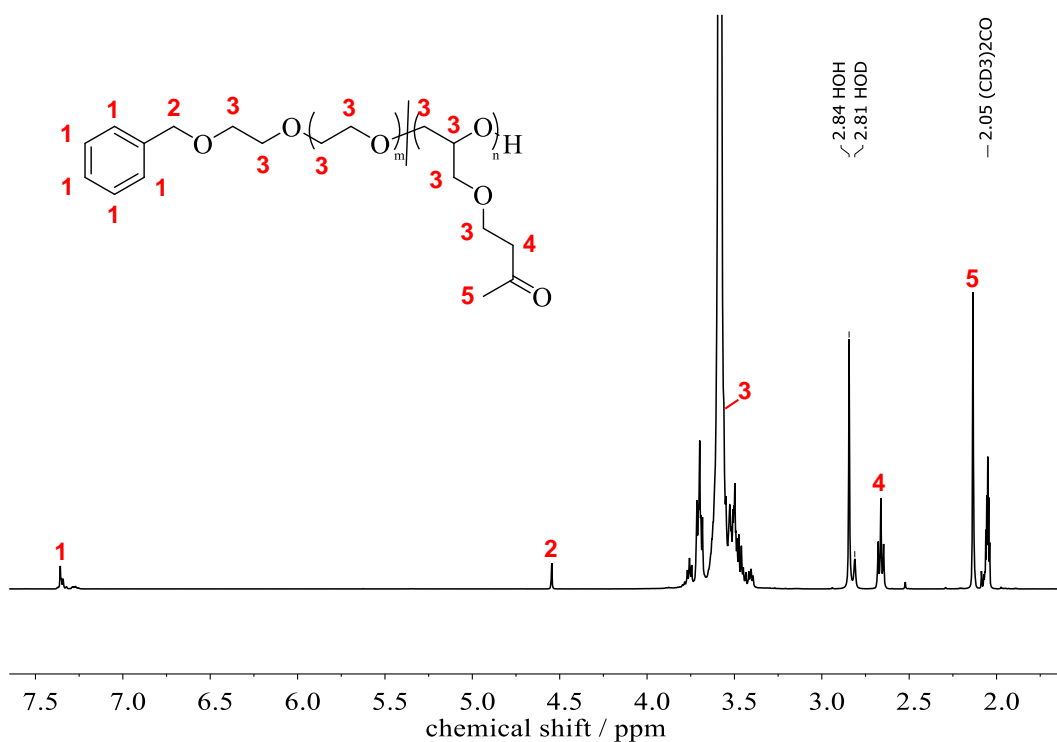
SI-Figure 20. ^{1}H NMR spectrum (400 MHz, (CD_3)$_2$CO) of PEG$_{197}$-*ran*-PKGE$_{11}$ (entry 1, **Table 3**).

SI-Figure 21. ^{13}C NMR spectrum (400 MHz, (CD_3)$_2$CO) of PEG$_{197}$-*ran*-PKGE$_{11}$ (entry 1, **Table 3**).
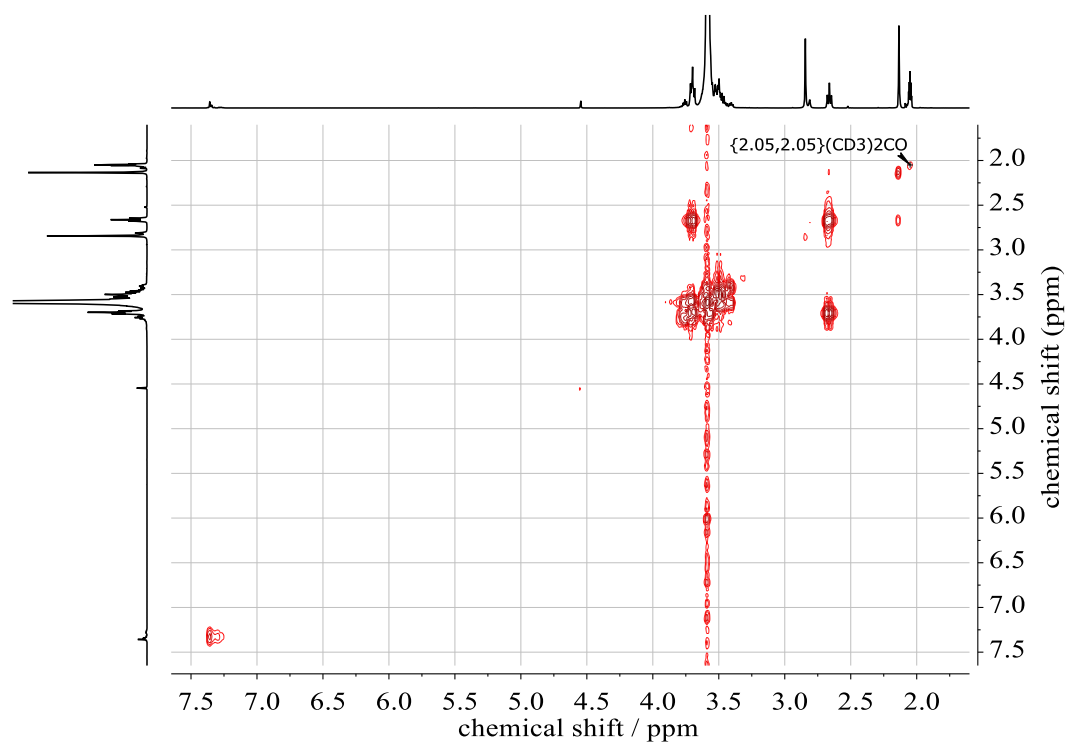
SI-Figure 22. ^{1}H, ^{1}H COSY NMR spectrum (400 MHz, (CD_3)$_2$CO) of PEG$_{197}$-*ran*-PKGE$_{11}$ (entry 1, **Table 3**).
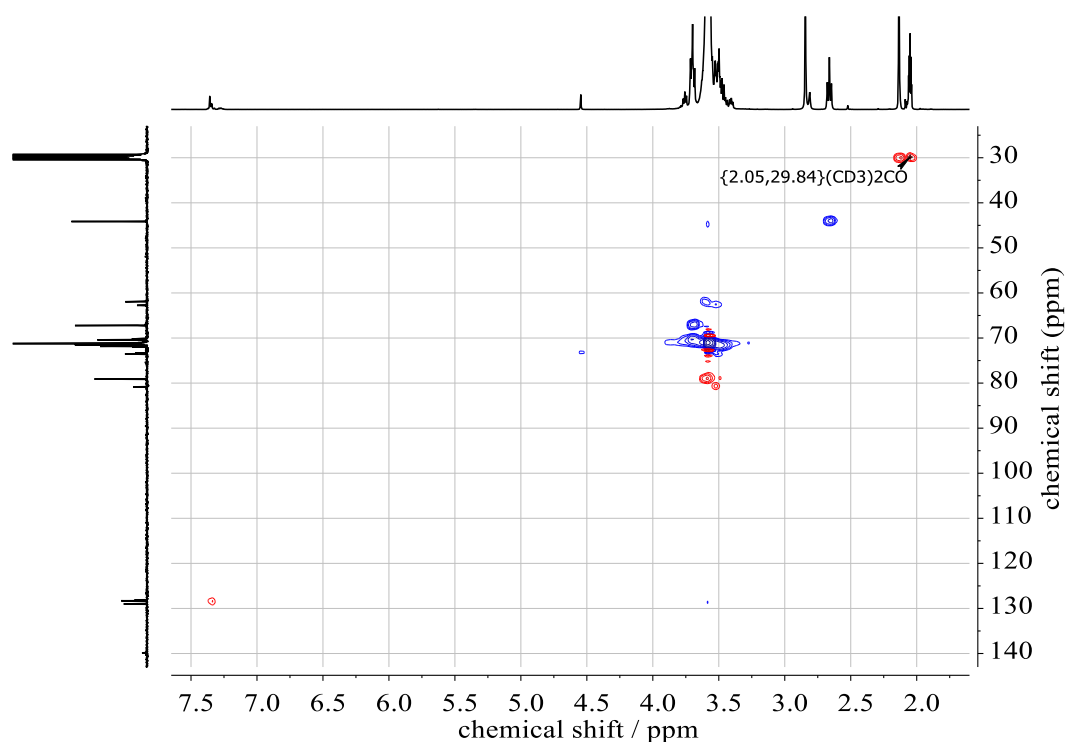
SI-Figure 23. ^{1}H, ^{13}C HSQC NMR of PEG$_{197}$-*ran*-PKGE$_{11}$ (entry 1, **Table 3**) in (CD_3)$_2$CO Color of the signals indicates the phase information (red: methine proton, blue: methylene protons).
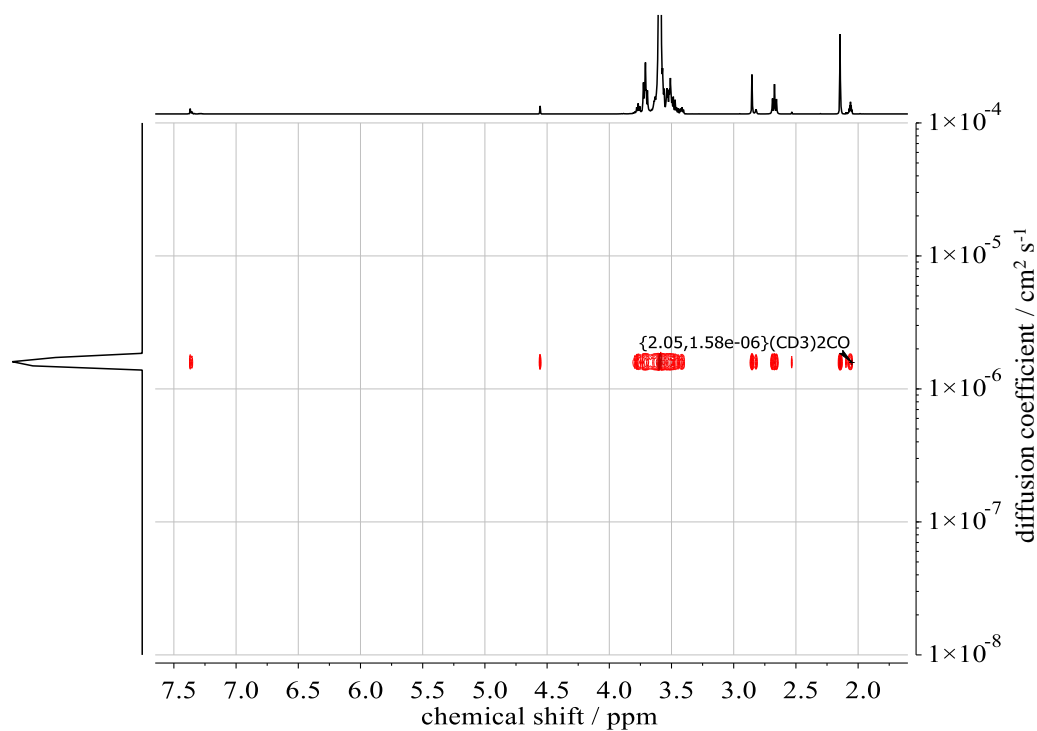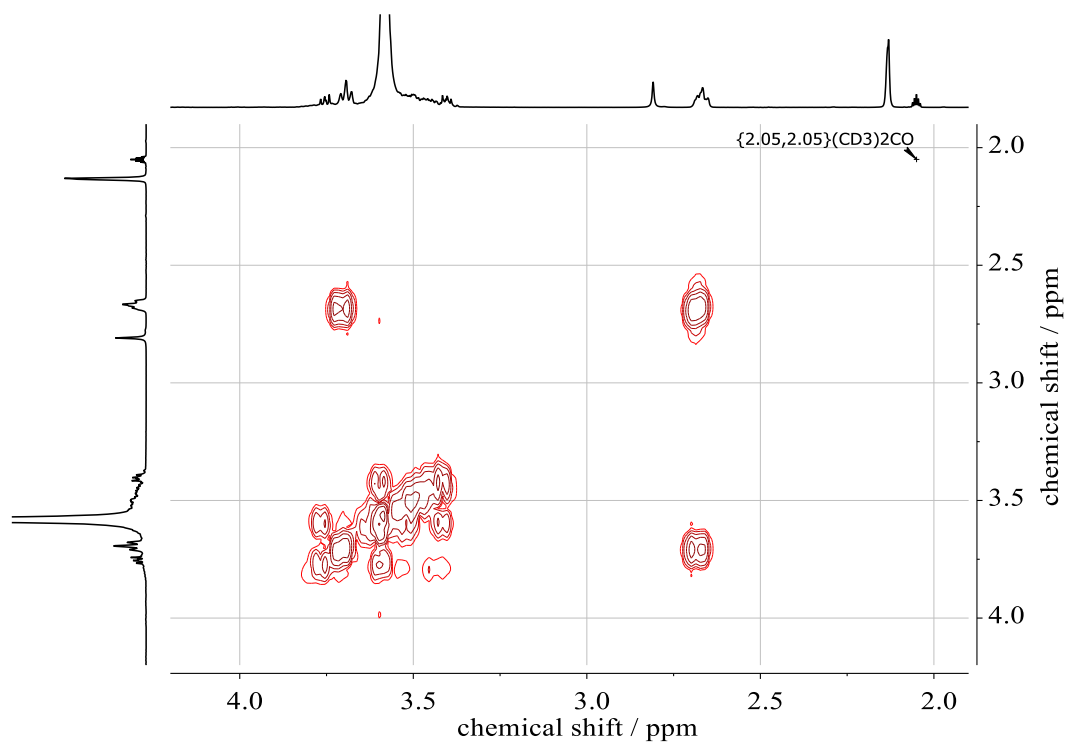
SI-Figure 24. ^{1}H DOSY NMR spectrum (400 MHz, (CD_3)$_2$CO) of PEG$_{197}$-*ran*-PKGE$_{11}$ (entry 1, **Table 3**).
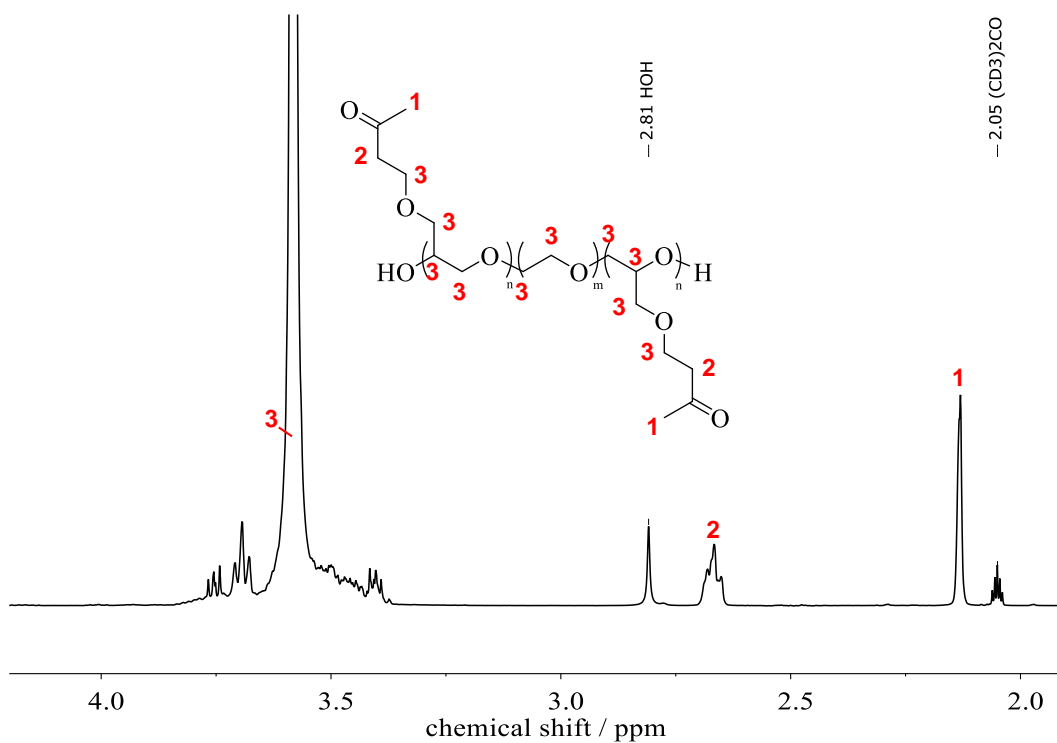
SI-Figure 25. ^{1}H NMR spectrum (100 MHz, (CD_3)$_2$CO) of PKGE$_4$-*b*-PEG$_{136}$-*b*-PKGE$_4$ (entry 6, **Table 3**).
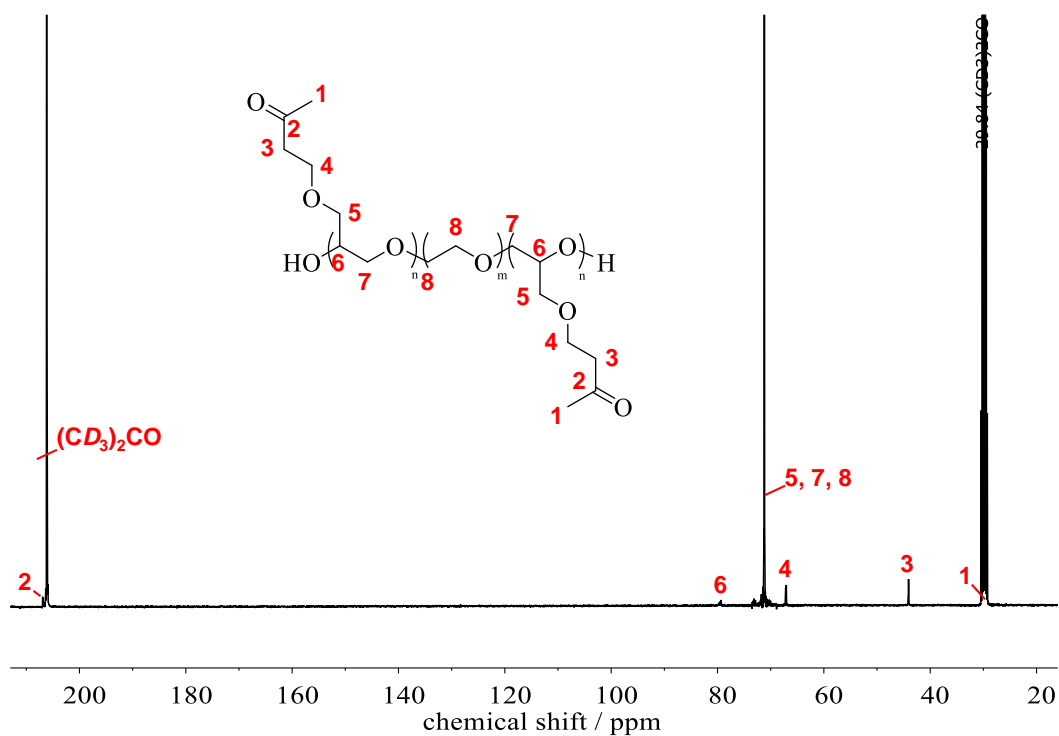
SI-Figure 26. ^{13}C NMR spectrum (100 MHz, $(CD_3)_2CO$) of PKGE$_4$-*b*-PEG$_{136}$-*b*-PKGE$_4$ (entry 6, **Table 3**).

SI-Figure 27. ^{1}H, ^{1}H COSY NMR spectrum (400 MHz, $(CD_3)_2CO$) of PKGE$_4$-*b*-PEG$_{136}$-*b*-PKGE$_4$ (entry 6, **Table 3**).
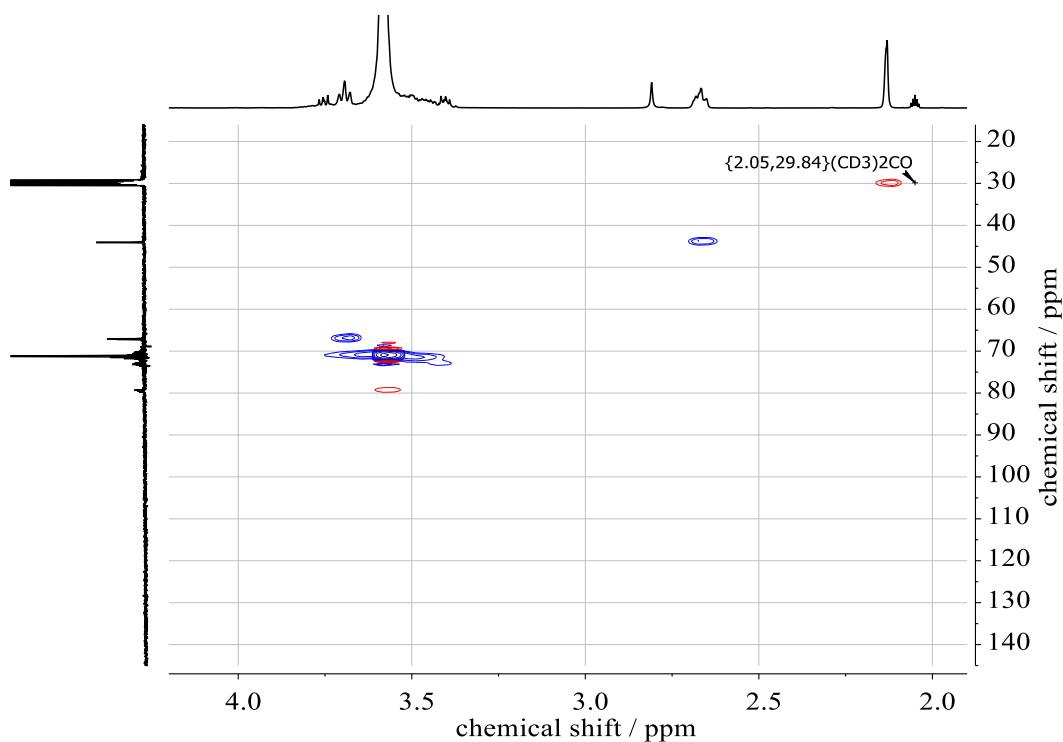
SI-Figure 28. ^{1}H, ^{13}C HSQC NMR of PKGE$_4$-*b*-PEG$_{136}$-*b*-PKGE$_4$ (entry 6, **Table 3**) in (C*D*$_3$)$_2$CO Color of the signals indicates the phase information (red: methine proton, blue: methylene protons).
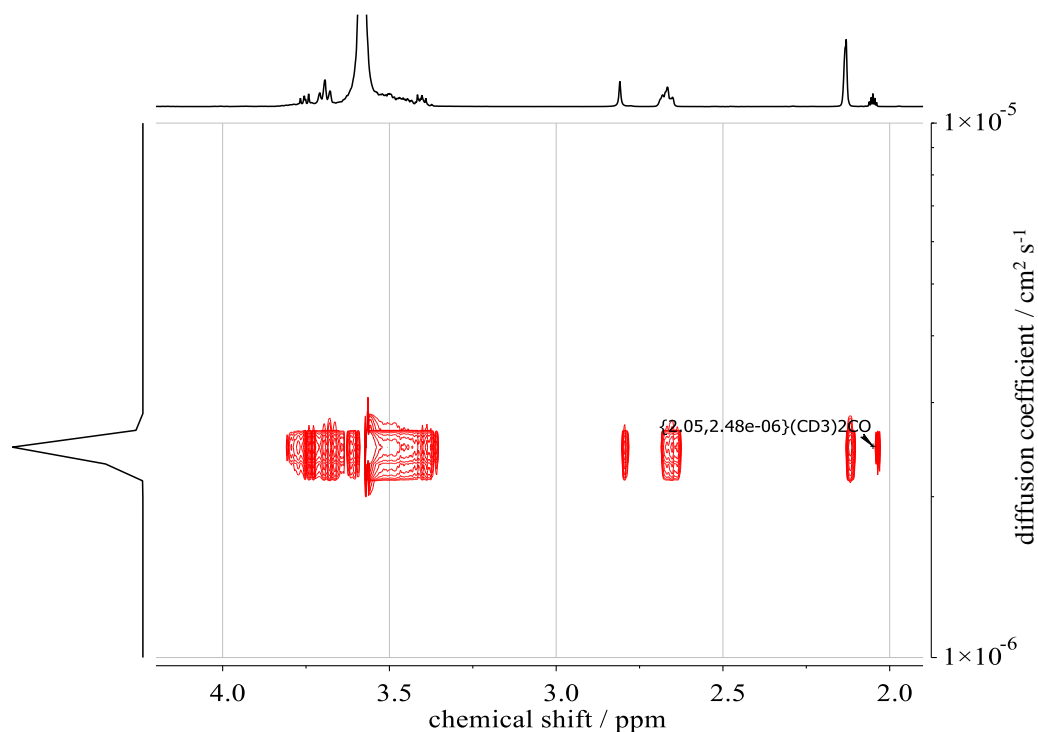
SI-Figure 29. ^{1}H DOSY NMR spectrum (400 MHz, (C*D*$_3$)$_2$CO) of PKGE$_4$-*b*-PEG$_{136}$-*b*-PKGE$_4$ (entry 6, **Table 3**).
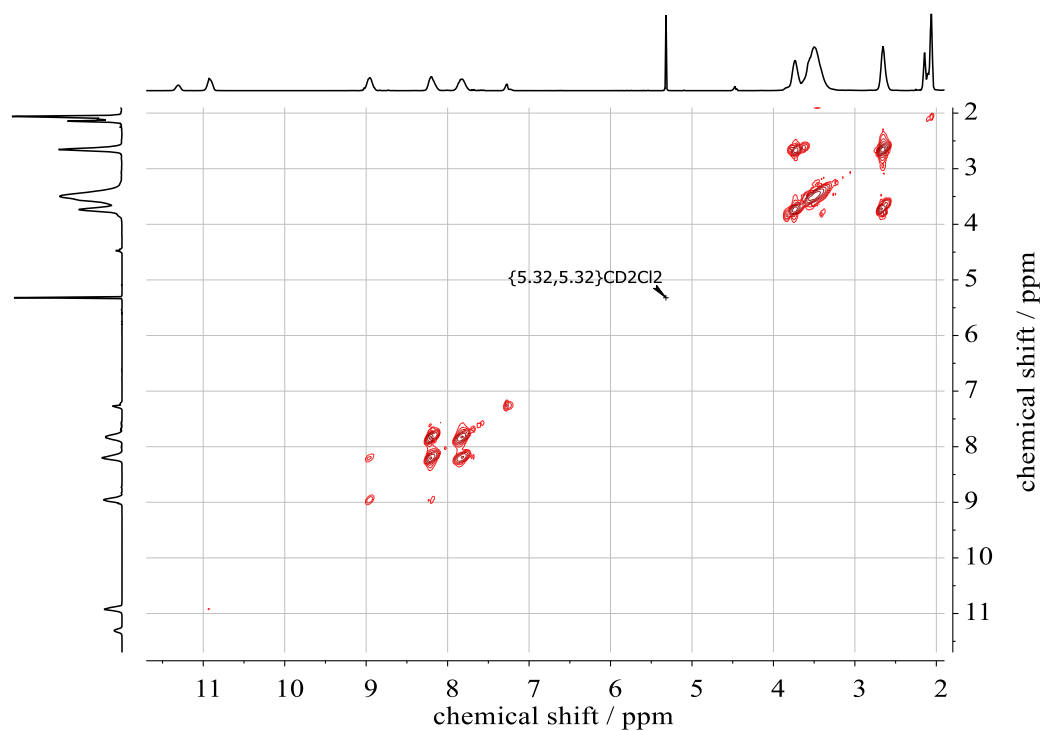
SI-Figure 30. ^{1}H, ^{1}H COSY NMR spectrum (400 MHz, CD_2Cl$_2$) of 2,4-DNPH modified PKDGE$_{27}$.
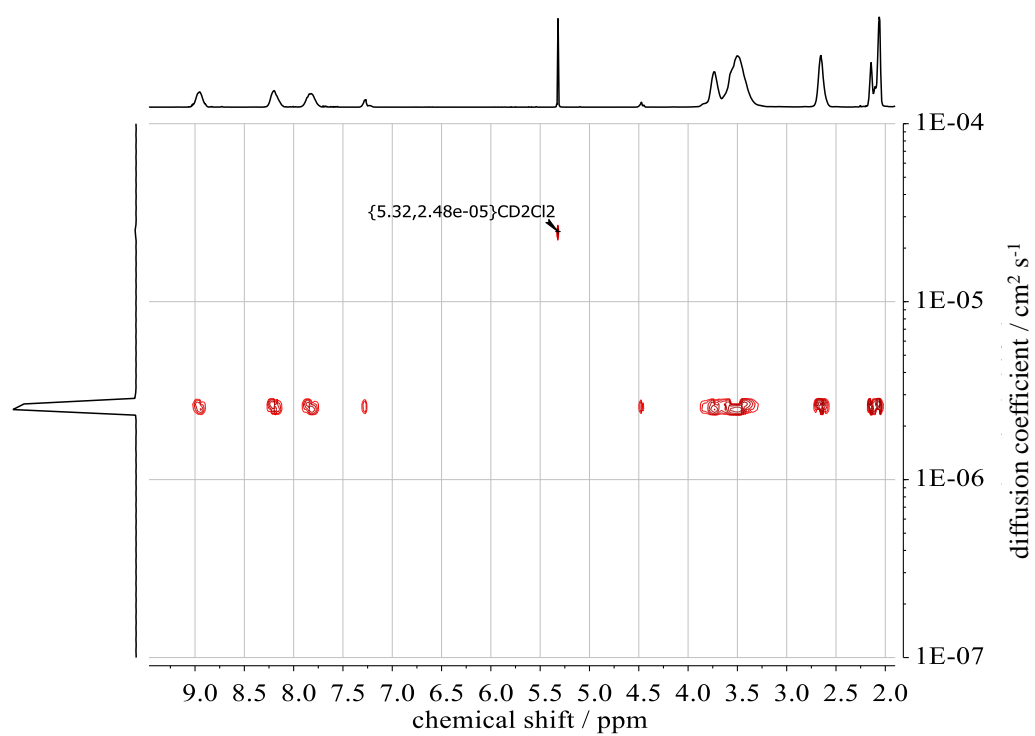
SI-Figure 31. ^{1}H DOSY NMR spectrum (400 MHz, CD_2Cl$_2$) of 2,4-DNPH modified PKDGE$_{27}$.
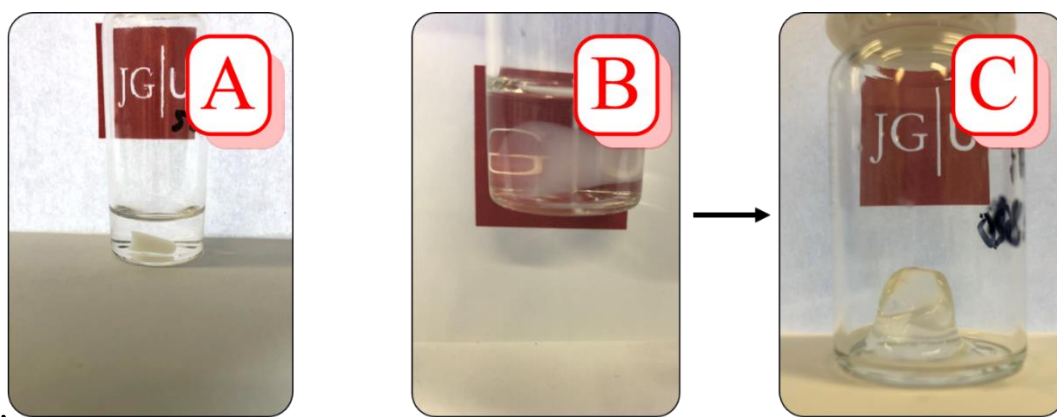
SI-Figure 32. Comparison of hydrogels: A) cloudy gel prepared of PKGE$_{10}$-b-PEG$_{227}$-b-PKGE$_{10}$ (entry 1, **Table 5**) in water. B) Typical appearance of the gels of PKGE$_3$-b-PEG$_{454}$-b-PKGE$_3$ (entry 2, **Table 5**) and PKGE$_9$-b-PEG$_{454}$-b-PKGE$_9$ (entry 3, **Table 5**) in water. C) Characteristic appearance of hydrogel from B) (entries 2−3, **Table 5**) without water

2.3. Glycidyl Cinnamate: Copolymerization with Glycidyl Ethers, *in-situ* NMR Kinetics and Photocrosslinking

Kamil Maciol[a], Sandra Schüttner[a], Jan Blankenburg[a,b], Tobias Johann[a,c], Holger Frey [a,*]

[a] Institute of Organic Chemistry, Johannes Gutenberg University Mainz, Duesbergweg 10-14, 55128 Mainz, Germany

[b] Graduate School Materials Science in Mainz, Staudinger Weg 9, 55128 Mainz, Germany

[c] Max Planck Graduate Center with the Johannes Gutenberg University, Staudinger Weg 6, 55128 Mainz, Germany

*E-Mail: hfrey@uni-mainz.de

ABSTRACT

The copolymerization of glycidyl cinnamate as a hitherto non-polymerizable photoreactive epoxide monomer to aliphatic polyether copolymers is described, using the monomer-activated epoxide ring-opening polymerization. Ethoxyethyl glycidyl ether (EEGE) and glycidyl cinnamate (GC) were copolymerized via monomer-activated anionic ring-opening polymerization. Triisobutylaluminum (i-Bu$_3$Al) was used as a catalyst and tetraoctylammonium bromide (NOctBr$_4$) as an initiator. The amount of GC was varied from 3 mol% to 100 mol% with apparent molecular weights in the range of 2,600 g mol^{-1} to 4,600 g mol^{-1} and polydispersities ($Đ$) below 1.35. The reaction kinetics of glycidyl esters with glycidyl ethers in general has hardly been investigated to date. Studies of the microstructure by in-$situ$ ^{1}H NMR kinetics characterization indicated a gradient-like distribution of EEGE and GC (reactivity ratios: $r_{EEGE} = 0.2$; $r_{GC} = 2.9$). A tentative explanation relies on different bond lengths in the respective epoxide rings, as suggested by density functional theory (DFT) calculations. Mild and selective cleavage of the acetal protecting groups of EEGE was achieved using the acidic ionic resin Dowex$^®$, leaving the GC ester bonds intact ($M_n = 1,900−3,700$ g mol^{-1}, $Đ < 1.35$). Thermal properties of the copolymers were investigated by differential scanning calorimetry (DSC), revealing T_gs between -60 °C for P(EEGE-co-GC), respectively -13 °C for P(G-co-GC) copolymers to 21 °C for the PGC homopolymer. P(G-co-GC) copolymers were crosslinked by UV irradiation and hydrogels were obtained. Characterization of the hydrogels was performed by analyzing the swelling ratio ($SR = 79–220\%$) and infrared spectroscopy to prove successful photocrosslinking.

TABLE OF CONTENTS GRAPHICS
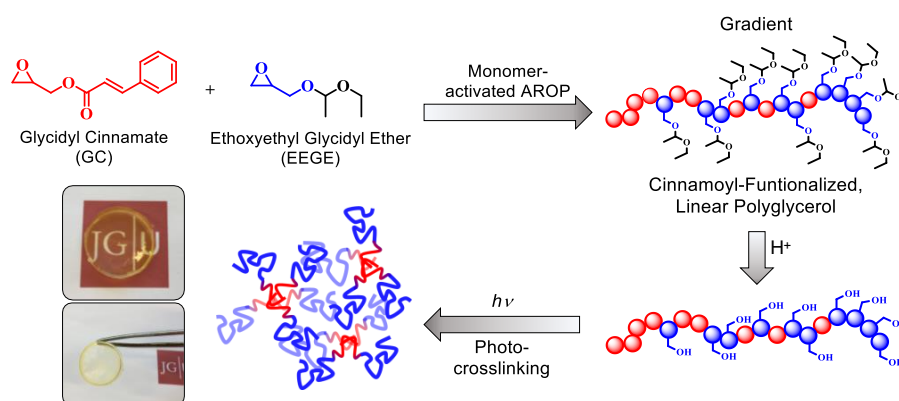
INTRODUCTION

Crosslinkable monomer units are widely used, for instance acrylates and methacrylates, and are described in detail in the literature.[1–3] In a recent work, Sumerlin and co-workers described the synthesis of photoreversible hydrogels derived from coumarin-containing polyacrylates.[4] However, polyether structures bearing reactive or polymerizable monomer units have only been studied to a very limited extent. In this context, glycidyl esters represent a very interesting platform to generate photocrosslinked polymer networks. Glycidyl esters with a variety of substituents are known.[5–9] The reason that this class of compounds has hardly been explored to date with respect to ring-opening polymerization are the harsh, basic conditions of the conventional oxyanionic polymerization[10,11], which lead to saponification of the glycidyl esters. Consequently, one has to resort to other polymerization mechanisms, such as the monomer-activated anionic ring-opening polymerization (AROP), pioneered by Carlotti and Deffieux[12–18] with the copolymerization of glycidyl methacrylate (GMA)[19]. Alternatively, these polymer architectures are also accessible by coordination-insertion polymerization, albeit resulting in broader molecular mass distributions.[20]

Glycidyl cinnamate (GC) is the glycidyl ester of cinnamic acid and possesses both a reactive double bond and an epoxide function.[21,22] As a photocrosslinkable monomer, the glycidyl ester of cinnamic acid is of particular interest, since it represents a bifunctional monomer. GC possesses a polymerizable epoxide moiety and a photosensitive cinnamoyl group. Cinnamic acid derivatives undergo a [2 + 2] photocycloaddition, isomerization, or a photo-Fries rearrangement under UV irradiation.[23–26] Previous access to the cinnamoyl groups in polyethers was achieved by post-polymerization modification, since the harsh conditions of an AROP would cleave the ester structure. Trzebicka *et al.* modified linear poly(ethylene oxide)-*b*-polyglycerol *lin*P(EO-*b*-G) block copolymers using cinnamic acid to nanogels synthesized by UV irradiation.[27] The photoreactivity of the cinnamic acid moiety was already used in various photoresponsive polymer structures like polyvinyl cinnamic acid ester (PVCm), which was the first synthesized photopolymer to be used as negative-tone photoresist.[24,28,29] Application for drug delivery systems was demonstrated by Shi *et al.* with the synthesis of degradable, photoresponsive nanoparticles. Starting from 3,4-dihydroxycinnamic acid (3,4DHCA), 4-hydroxycinnamic acid (4HCA) and dithiothreitol (DTT), photoresponsive PCA-*graft*-DTT nanoparticles were prepared, in which protein encapsulation was achieved during nanoparticle formation.[30]

Polyglycerol represents a highly biocompatible and hydrophilic material.[31,32] Both linear and branched polyglycerols are water-soluble and show structural similarity to poly(ethylene glycol) (PEG), but are not restricted in their number of functional groups at the polyether backbone.[33] The direct AROP of glycidol is not suitable for the synthesis of *lin*PG due to the inimer (initiator-monomer) structure of glycidol, which leads to branching.[34] The use of suitable protecting groups allows the formation of linear polyether structures. Ethoxyethyl glycidyl ether (EEGE)[35] is common for the synthesis of *lin*PG, capitalizing on the acetal moiety as a base-stable protecting group.[36–40] Each hydroxyl group of *lin*PG offers an anchor point for the introduction of various functional groups by post-polymerization modification, which renders the polymer interesting for biomedical application.[41] Potential applications for *lin*PG include the use for drug delivery systems or bioconjugation with proteins ("PGylation")[42], coatings for gold surfaces[43,44] or star-shaped macroinitiators for star block copolymers with core-shell structure[33,45].

In this work, we describe the statistical copolymerization of EEGE and GC. To the best of our knowledge, the anionic polymerization of GC has not been described to date. However, the conventional AROP is not suitable for the polymerization of GC, since cleavage of the ester moiety cannot be avoided under basic reaction conditions. However, employing the monomer-activated AROP, *lin*P(G-*co*-GC) copolymers were synthesized under mild conditions. **Scheme 1** shows the synthetic strategy for the copolymerization of EEGE and GC. The copolymers were characterized with regard to selective cleavage of the acetal groups of EEGE as well as thermal properties and microstructure of the copolymers. In addition, photocrosslinking and photochemical synthesis of polyglycerol hydrogels were studied.
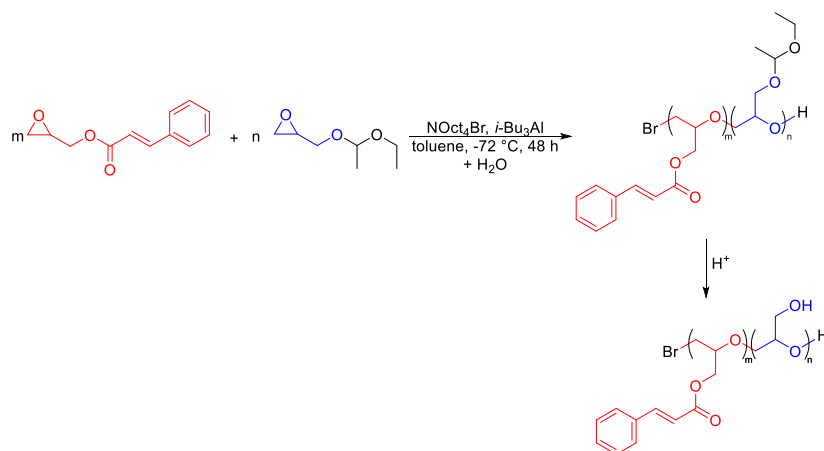
Scheme 1. Synthesis of P(G-*co*-GC) via the monomer activation technique by copolymerization of EEGE and GC and subsequent acidic cleavage of the protecting groups.

EXPERIMENTAL PART

Terminology. Linear polyglycerol is hereafter abbreviated as PG.

Instrumentation. ^{1}H NMR spectra (400 MHz or 600 MHz) were recorded on a Bruker Avance II 400 or Bruker Avance III 600 spectrometer. All spectra are referenced internally to residual proton signals of the deuterated solvent. *In-situ* ^{1}H NMR kinetics were measured on a Bruker Avance III HD 400 spectrometer equipped with a 5 mm BBFO SmartProbe (Z-gradient probe) and an ATM as well as a SampleXPress 60 auto sampler. Size exclusion chromatography (SEC) measurements were performed on an Agilent 1,100 Series, equipped with a Polymer Standards Service (PSS) HEMA column (300/ 100/ 40 Å porosity), RI and UV (275 nm) detector. Dimethylformamide (containing 1 g L^{-1} of lithium bromide) was used as a solvent at 50 °C and poly(ethylene glycol) standards provided by PSS were employed for calibration. Differential scanning calorimetry (DSC) measurements were performed on a Perkin Elmer 8,500 in a temperature range from -80 °C to 80 °C, using heating and cooling rates of 20 K min^{-1} (first cycle) and 10 K min^{-1} (second cycle). For evaluation, the data points of the second heating cycle were used. IR spectra were recorded on a Nicolet iS10 Fourier transform infrared spectrometer (Thermo Fisher Scientific) with attenuated total reflection.

Density functional theory (DFT) calculations. Quantum mechanical calculations were carried out with the ORCA 3.0.2 software suite.[46] All structures were optimized using the B3LYP DFT hybrid functional with geometrical counterpoise correction (gCP)[47] and dispersion correction (D3)[48,49] using def2-TZVP[50,51] as basis set and RIJK-COSX[52] as approximation. In all cases frequency analysis was performed and no imaginary frequency was detected.

Reagents. Chemicals and solvents were purchased from commercial suppliers (Acros, Sigma-Aldrich, Fisher Scientific, Alfa Aesar) and used without prior purification, unless otherwise stated. Deuterated solvents were obtained from Deutero GmbH. Triisobutylaluminum (*i*-Bu$_3$Al, 1.1 M solution in toluene, Acros Organics) and toluene (99.85%, Acros Organics) were used without further purification. Tetraoctylammonium bromide (NOct$_4$Br, 98%, TCI) was azeotropically dried with benzene overnight under reduced pressure. Glycidyl cinnamate (GC) was purified by stirring over CaH$_2$ and distillation. Ethoxyethyl glycidyl ether (EEGE) was synthesized according to Fitton *et al.*[35] and dried analogously. Dialysis membranes (regenerated cellulose, *MWCO* = 1,000 g mol^{-1}) were obtained from Orange Scientific.

Monomer synthesis (glycidyl cinnamate). Glycidyl cinnamate (GC) was prepared in a two-step synthesis. For the preparation of potassium cinnamate (PC), cinnamic acid (2 g, 13 mmol,

1 equiv) was dissolved in THF (20 mL) in a round-bottom flask and heated to 30 °C. Under stirring freshly ground potassium hydroxide (0.8 g, 13 mmol, 1 equiv) was added to the reaction solution. After one hour, the solvent was removed *in vacuo*. Yield: quantitative.

The second reaction step was performed according to a slightly modified procedure of Rusu *et al.*.[21] PC (1.5 g, 8 mmol, 1.0 equiv) and epichlorohydrin (7.9 mL, 101 mmol, 12.5 equiv) were placed in a reaction flask. Subsequently, tetrabutylammonium bromide (130 mg, 0.4 mmol, 0.05 equiv) was added and the reaction mixture was stirred at reflux at 115 °C for 3.5 h. The clear, orange, solution was diluted with dichloromethane (40 mL) and potassium chloride was filtered off. After washing twice with a saturated, aqueous $NaHCO_3$ solution (100 mL), the organic phase was dried over $MgSO_4$ and concentrated using a rotary evaporator. By distillation of the orange solution under reduced pressure, the product was isolated as a colorless, viscous liquid. Yield: 85%. ^{1}H NMR (400 MHz, CDCl$_3$): δ (ppm) = 2.67 (dd, 1H, H_a), 2.84 (t, 1H, H_a), 3.26 (m, 1H, H_b), 4.02 (dd, 1H, H_c), 4.53 (dd, 1H, H_c), 6.45 (d, 1H, H_d), 7.35 (m, 3H, Hf, H_h), 7.50 (m, 2H, H_g), 7.71 (d, 1H, H_e). ^{13}C NMR (100 MHz, CDCl$_3$): δ (ppm) = 44.64 (C_a), 49.43 (C_b), 65.04 (C_c), 117.30 (C_e), 128.11 (C_i), 128.88 (C_h), 130.44 (C_j), 134.16 (C_g), 145.50 (C_f), 166.49 (C_d).

P(EEGE-co-GC) – Copolymerization of EEGE and GC. The described protocol was performed in analogy to the literature procedure for the polymerization of EEGE according to Carlotti and Deffieux[17] and refers to sample P(EEGE$_{0.17}$-*co*-GC$_{0.83}$) (entry 2, **Table 1**). Tetraoctylammonium bromide (0.1 g, 0.09 mmol, 1 equiv) was freeze-dried with benzene (3 mL) in a Schlenk tube. Anhydrous toluene (5 mL) and the dried monomers GC (0.7 mL, 3.84 mmol, 42 equiv) and EEGE (0.1 mL, 0.91 mmol, 10 equiv) were added to the initiator via syringe under argon atmosphere. After cooling to -72 °C with an ethanol/dry ice bath, the polymerization was initiated by injection of the catalyst *i*-Bu$_3$Al (0.4 mL, 0.41 mmol, 4.5 equiv), resulting in a strong yellow color that decreased during the reaction. The reaction mixture was allowed to warm up slowly to room temperature. Termination was carried out after 48 h by addition of Milli-Q water (1 mL). Al(OH)$_3$ precipitated as a white solid, which was removed by filtration. The polymer solution was concentrated *in vacuo*. For purification, the copolymer was dissolved in dichloromethane and dialyzed against dichloromethane/methanol (3 : 2) for 24 h. Drying under vacuum afforded the copolymer in yields of 90%. ^{1}H NMR (600 MHz, CDCl$_3$): δ (ppm) = 1.15 (br, H_o), 1.22 (br, H_l), 3.36–4.01 (br, H_g, H_h, H_i, H_j, H_k, H_n), 4.32 (br, H_f), 4.70 (s, H_m), 6.43 (br, H_e), 7.30–7.45 (br, H_a, H_b, H_c), 7.64 (br, H_d). ^{13}C NMR (150 MHz, CDCl$_3$): δ (ppm) = 15.28 (C_q), 19.80 (C_n), 60.99 (C_p), 63.71 (C_h, C_j, C_l), 69.51 (C_m),

77.74 (C_i, C_k), 99.81 (C_o), 117.69 (C_f), 128.17–128.85 (C_b, C_c), 130.33 (C_a), 134.25 (C_d), 145.20 (C_e), 166.69 (C_g).

P(G-co-GC) – Selective deprotection of P(EEGE-co-GC): Removal of the acetal protecting group under acidic conditions was performed by using the ion exchange resin Dowex® 50WX8. For this purpose, the copolymer was dissolved in a methanol/toluene mixture (2 : 1, 20 wt%) and Dowex® was added. In order to shift the reaction equilibrium, the volatile by-products (acetaldehyde and ethanol) were removed under reduced pressure for 12 h at 30 °C. The resin residue was filtered and the polymer was dried *in vacuo*. Yield: 90% to quantitative.^{1}H NMR (600 MHz, CDCl3): δ (ppm) = 3.48–3.97 (br, H_g, H_h, H_i, H_j, H_k), 4.34 (br, H_f), 6.43 (br, H_e), 7.30–7.45 (br, H_a, H_b, H_c), 7.60 (br, H_d).^{13}C NMR (150 MHz, C*D*Cl$_3$): δ (ppm) = 63.62 (C_h, C_j, C_l), 69.72 (C_m), 77.74 (C_i, C_k), 117.61 (C_f), 128.21–128.91 (C_b, C_c), 130.37 (C_a), 134.22 (C_d), 145.28 (C_e), 166.75 (C_g).

Sample preparation for in-situ ^1H NMR kinetic studies. In the first step the initiator tetraoctylammonium bromide (NOct$_4$Br, 50 mg) was dried in a Schlenk tube by dissolving it in 2 mL benzene and stirring under vacuum for 30 min at 60 °C. After removing the solvent under vacuum for 24 h, 0.5 mL dry toluene-d_8 were added. A Norell S-5-400-VT-7 NMR tube was evacuated overnight and filled with argon. 0.1 mL of the initiator solution (NOct$_4$Br, 1 equiv) was added in the NMR tube, followed by 0.55 mL toluene-d_8. Glycidyl cinnamate (GC) and ethoxyethyl glycidyl ether (EEGE) were dried over CaH$_2$ and distilled under reduced pressure. 47 µL GC (15 equiv) and 40 µL EEGE (15 equiv) were placed in the NMR tube. After cooling with an acetone/dry ice bath for 20 min, 83 µL *i*-Bu$_3$Al solution (1.1 M in toluene, 5 equiv) was injected via syringe. The NMR tube was sealed with a Teflon stop-cock and shaken vigorously in order to homogenize the solution before placing the tube in the NMR spectrometer with the probe gas flow adjusted to -20 °C. When a stable temperature in the probe head was reached (~10 min, $\Delta T = 0.1$ K), the first spectrum was recorded. Sample spinning was turned off. Spectra were recorded with 16 scans at intervals of two minutes during the entire measurement. The measurement was stopped at full conversion (~2 h). SEC data of the isolated P(EEGE$_{0.50}$-*co*-GC$_{0.50}$) copolymer are shown in **SI-Figure 1**.

Crosslinking by UV irradiation and study of swelling behavior. Crosslinking experiments were performed in small PTFE pans (∅ = 20 mm). For this purpose, an ethanolic P(G-*co*-GC) solution ($c = 140$ g L^{-1}) was transferred into the pans. The pans were covered with a quartz glass slide in order to avoid contamination and rapid evaporation of the solvent. For the irradiation,

a UV lamp was used, into which UV tubes with wavelengths of 312 nm and 364 nm were installed. After 180 min, the crosslinked hydrogel films were removed from the pans.

For the study of the swelling properties, the hydrogels were placed in water for 48 h in Milli-Q water in order to reach equilibrium swelling. Subsequently, the swollen hydrogels were removed and weighed after removal surface adsorbed water by Kimwipes®. Then, the hydrogels were allowed to swell in water again for 1 h and the process was repeated three times to determine the standard deviation. Swelling ratio (*SR*) was determined using the following expression:[53]

$$SR = \left(\frac{w_s - w_d}{w_d} \right) \cdot 100 \tag{1}$$

where w_s and w_d are the weights of the swollen and dry hydrogels, respectively. The mass swelling (*Q_m*) was calculated according to:[53]

$$Q_m = \frac{w_s}{w_d} \tag{2}$$

RESULTS AND DISCUSSION

A. Synthesis of GC monomer.

The preparation of glycidyl cinnamate was performed by esterification of epichlorohydrin with cinnamic acid, which was converted into an activated nucleophile with KOH. Compared to the literature, the yield could be increased by approximately 17%, which is due to a higher amount of phase transfer catalyst and longer reaction times employed.[21] In general, GC is readily storable in the refrigerator (4 °C) and shows high storage stability. Temperatures of 150 °C and a pressure of $1 \cdot 10^{-3}$ mbar are required for the distillation. For the corresponding ^{1}H NMR, ^{13}C NMR and 2D NMR spectra, see **SI-Figures 2–5**.

B. Synthesis of P(EEGE-*co*-GC) copolymers, characterization, *in-situ* ^{1}H NMR kinetics, deprotection and thermal properties.

Copolymerization of EEGE and GC. The synthesis of the copolymers was performed employing an initiator/catalyst system consisting of tetraoctylammonium bromide (NOct$_4$Br) as an initiator and triisobutylaluminum *i*-Bu$_3$Al as a catalyst. The catalyst was used in excess (**Scheme 2**),[17] because besides the "ate"-complex formation with NOct$_4$Br, *i*-Bu$_3$Al acts simultaneously as a monomer activator. Since the initiator/catalyst ratio influences the propagation rate and molecular weight distributions, the ratio has to be adjusted specifically for each monomer system. Full removal of the catalyst and the hydrolyzed initiator residues represents a critical issue. There are different approaches in literature.[54,55] In our work, by termination with Milli-Q water, *i*-Bu$_3$Al was transformed into the amphoteric aluminum hydroxide and removed by filtration. Subsequent dialysis in dichloromethane/methanol (3 : 2) removed the residues of the initiator.
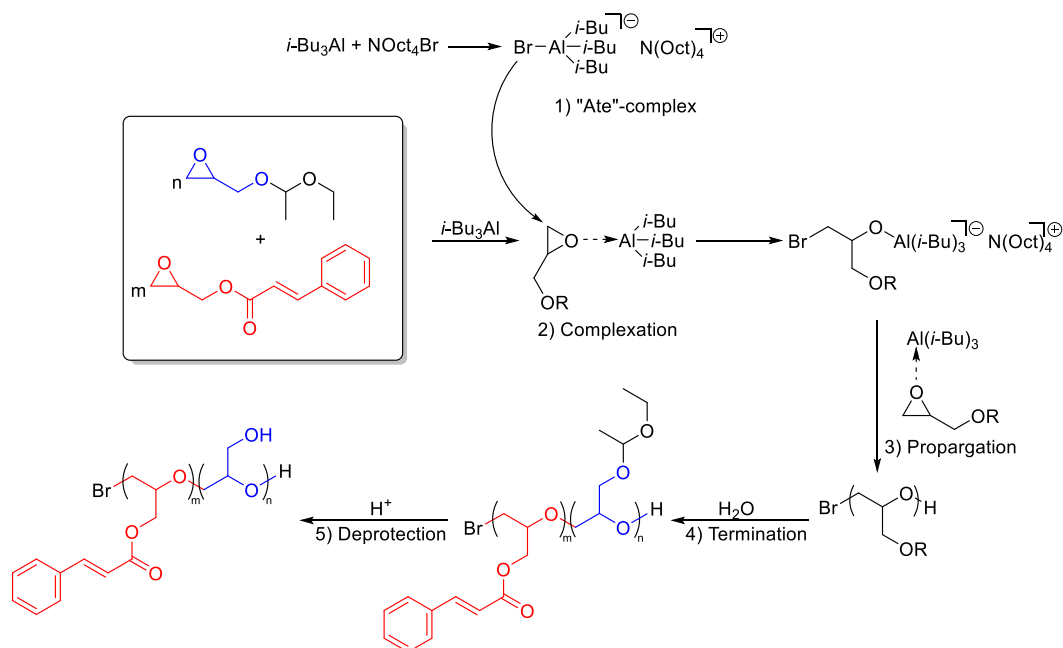
Scheme 2. Reaction mechanism for the copolymerization of EEGE and GC initiated by NOct$_4$Br: 1) formation of the "ate"-complex 2) activation of the monomers by complexation and nucleophilic attack of bromide 3) chain growth 4) termination by addition of water 5) acidic cleavage of the acetals.

Table 1 summarizes the data obtained by SEC (DMF, PEG standards) for the series of copolymers prepared of GC. Molar masses between 2,200 g mol^{-1} and 4,600 g mol^{-1} were obtained with polydispersities (Đ) between 1.09 and 1.34. The SEC traces of all P(EEGE-*co*-GC) copolymers and the PGC homopolymer (**Figure 1**) display monomodal molecular weight distributions. GC was incorporated in any desired ratio. All batches were targeted molecular weights of 10,000 g mol^{-1}. The main reason for the discrepancies of the molecular weights is the SEC calibration, carried out using PEG standards, which only gives exact values for pure PEG. This finding is substantiated by a comparison with the literature. Schömer *et al.* targeted a PEEGE homopolymer of 7,500 g mol^{-1} and measured 2,700 g mol^{-1} despite full monomer conversion.[56] An analogous deviation of about 60% between the theoretical and molecular weight determined by SEC can be observed for sample P(EEGE$_{0.97}$-*co*-GC$_{0.03}$) (entry 8, **Table 1**), which shows the lowest content of GC. In general, the deviation increases with the amount of GC incorporated in the copolymers, since the hydrodynamic radii of the copolymers increasingly differ from that of pure PEG standards. The overlap of RI and UV signal proves homogeneous incorporation of GC and EEGE over the entire molecular weight distribution of the copolymers (**SI-Figure 6**).

The last column of **Table 1** indicates the catalyst/initiator ratio, which had to be adjusted for each copolymerization with different monomer ratios to provide optimal reaction conditions. For propylene oxide (PO), Carlotti *et al.* already showed that high catalyst-initiator ratios caused broadening of the molecular weight distributions and that no polymerization took place at a ratio ≤ 1.[12,57] The high amount of catalyst must be chosen according to the structure of the reactants. In general, with increasing oxygen content of the monomer structure, higher amounts of catalyst are required for the copolymerization due to interaction and complexation of the catalyst (**SI-Figure 7**).[17]

Table 1. Copolymerization of EEGE with GC using [i-Bu$_3$Al]/[NOct$_4$Br] (synthesis in toluene, -72°C).

No.	Copolymer composition[a]	Theoretical composition	$M_n^{(th)}$ (g mol^{-1})	M_n^b (g mol^{-1})	$Đ^b$	[i-Bu$_3$Al]/ [NOct$_4$Br]
1	PGC	0 : 100	10,000	2,600	1.19	4.5
2	P(EEGE$_{0.17}$-co-GC$_{0.83}$)	19 : 81	10,000	2,200	1.20	4.5
3	P(EEGE$_{0.27}$-co-GC$_{0.73}$)	30 : 70	10,100	2,300	1.34	5.0
4	P(EEGE$_{0.70}$-co-GC$_{0.30}$)	69 : 31	10,200	4,600	1.21	4.5
5	P(EEGE$_{0.81}$-co-GC$_{0.19}$)	80 : 20	10,100	3,800	1.19	4.5
6	P(EEGE$_{0.84}$-co-GC$_{0.16}$)	85 : 15	10,100	3,400	1.09	5.0
7	P(EEGE$_{0.92}$-co-GC$_{0.08}$)	92 : 8	10,700	4,500	1.28	5.0
8	P(EEGE$_{0.97}$-co-GC$_{0.03}$)	96 : 4	10,100	4,400	1.11	5.0

[a] Obtained from ^{1}H NMR spectra. [b] Determined by SEC measurements in DMF (RI detector, PEG standards).

In the absence of a functional initiator, only the incorporation ratios can be determined via ^{1}H NMR, but no molecular weights. Monomer incorporation was in good agreement with the monomer ratios employed (**Table 1**). Characteristic signals at 6.4 ppm (proton of GC double bond) and 4.7 ppm (methine proton of EEGE) from the ^{1}H NMR spectrum (**Figure 1**) were used for the evaluation. Additional inverse gated ^{13}C NMR and 2D NMR spectra are given in the Supporting Information (**SI-Figures 8−10**).
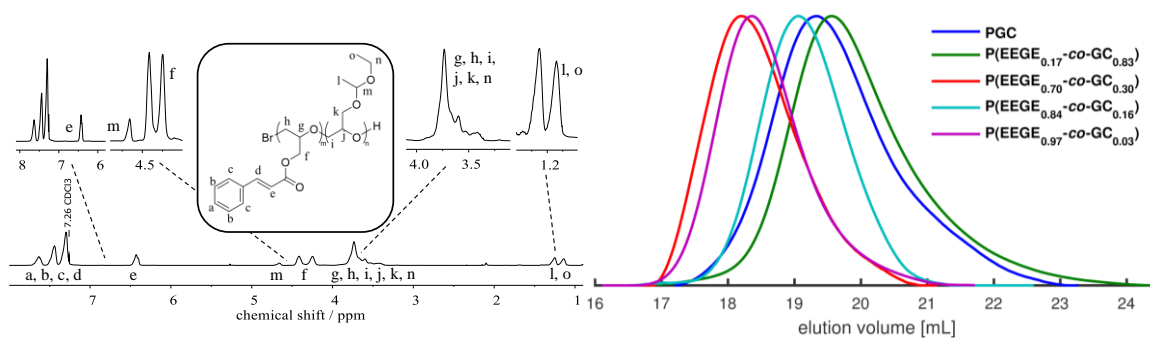
Figure 1. ^{1}H NMR spectrum (600 MHz, CDCl$_3$) of P(EEGE$_{0.84}$-co-GC$_{0.16}$) (entry 6, **Table 1**) and SEC traces (DMF, PEG standards) of selected P(EEGE-co-GC) copolymers and PGC homopolymer.

*Kinetics. In-situ* ^{1}H NMR spectroscopy has become an established method for the investigation of monomer gradients in living copolymerizations. We recently presented *in-situ* NMR studies of the monomer-activated AROP to elucidate the microstructure of copolymers.[58,59] This method is advantageous, since the copolymerization takes place undisturbed in the NMR tube without the need for external manipulation, for instance by removal of samples. In this manner, possible contamination by oxygen or traces of water is avoided. In addition, the safety aspect is not negligible, since *i*-Bu$_3$Al is pyrophoric and reacts violently in air. In the case of copolymerization with the gaseous, toxic, carcinogenic and mutagenic EO, this technique can also prevent possible contamination of the environment by undissolved gas, which could occur when drawing samples for kinetic studies.[60] To the best of our knowledge, the reaction kinetics of glycidyl esters with glycidyl ethers in general has not been investigated to date via real-time ^{1}H NMR spectroscopy. The monomer distribution in copolymers is highly dependent on the chemical nature of the monomers for the monomer-activated anionic ring-opening copolymerization. The copolymerization of different glycidyl ethers results in a random monomer sequence,[59,61] while the copolymerization of EO and glycidyl ethers provides strongly tapered copolymer structures with a preferred incorporation of EO in case of monomer activation by *i*-Bu$_3$Al.[58] The same applies to the copolymerization of glycidyl ethers and propylene oxide (PO). In this case behaves analogously to EO.[17] Comparing now the reactivity ratios of EO and PO, a higher reactivity of EO can be observed.[57]

Relying on the integrals of the signals for the proton of the GC double bond (6.4 ppm) and the methylene protons of EEGE (3.1 ppm), the decrease of the monomer concentrations was monitored (**Figure 2**) via *in-situ* ^{1}H NMR kinetics at -20 °C in toluene-d_8.
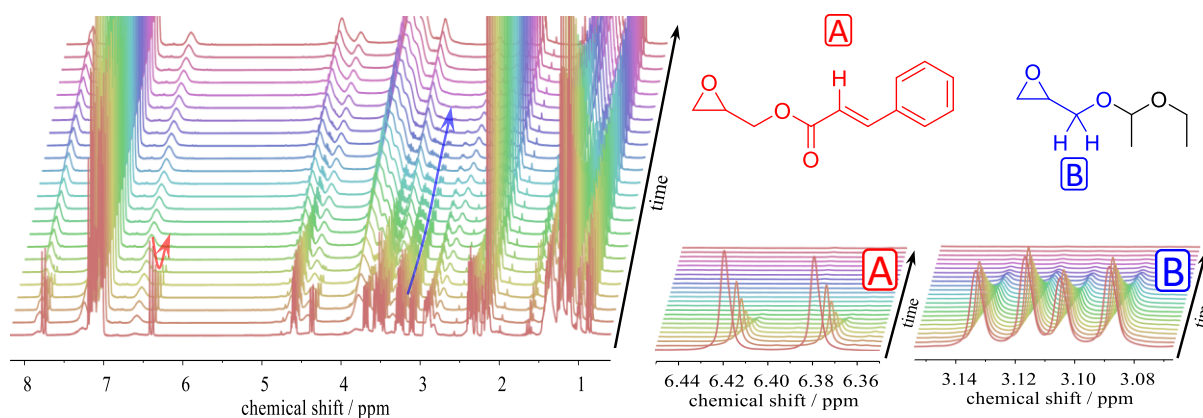
Figure 2. ^{1}H NMR spectra for copolymerization of EEGE and GC in toluene-d_8 at -20 °C employing the monomer activation method, including a zoom of relevant areas of the spectrum for evaluation (right).

The decrease of the monomer signals can be directly translated to their incorporation into the copolymer chains formed, since no transfer or termination reactions occur. **Figure 3a** illustrates the concentration of EEGE and GC plotted vs. total conversion, indicating a gradient structure of the copolymers.
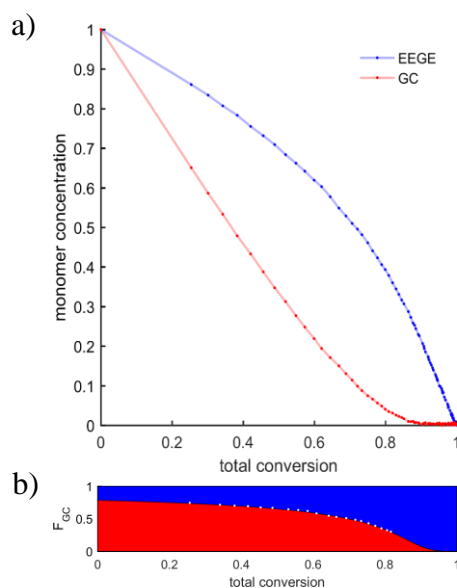
Figure 3. Top (a): monomer concentration plotted vs. total monomer conversion determined by ^{1}H NMR spectroscopy in toluene-d_8 at -20 °C, applying the monomer-activated AROP. Blue line: conversion of EEGE, red curve: conversion of GC. Bottom (b): simulation of P(EEGE-*co*-GC) microstructure based on the reactivity ratios determined from Kelen-Tüdős method, white points represent measured data points.

On the basis of the data obtained *in-situ*, reactivity ratios were determined by various known evaluation methods: Meyer-Lowry[62], Mayo-Lewis[63], Fineman-Ross[64] and Kelen-Tüdős[65]

(**Table 2**). These methods can be categorized according to the use of the differential form of the Mayo-Lewis equation or the integrated Meyer-Lowry form. Using the Mayo-Lewis equation, the collected data must be converted into differentials to evaluate the reactivity ratios. The Meyer-Lowry equation can be directly fitted to the data of the monomer composition shift for the full conversion range.

Table 2. Copolymerization reactivity ratios for the monomer-activated AROP of EEGE and GC in toluene at -20 °C, initiated with $NOct_4Br$ and i-Bu_3Al as catalyst.

Method	r_{EEGE}	r_{GC}	Type
Meyer-Lowry	0.21	2.72	integral
Mayo-Lewis	0.24	2.86	
Fineman-Ross	0.24	3.00	differential
Kelen-Tüdős	0.23	2.92	

The corresponding fits are given in the Supporting Information (**SI-Figures 11−14**). All methods provide similar reactivity ratios ($r_{EEGE} = 0.2$; $r_{GC} = 2.9$) and demonstrate the preferred incorporation of GC. Based on these reactivity ratios, the average monomer distribution along the polymer chains can be calculated.[66] The result is shown in **Figure 3b**, revealing a gradient-like microstructure. The reactivity ratios are consistent with a work by Labbé *et al.* who were able to prove that glycidyl methacrylate (GMA) incorporates faster than glycidyl methyl ether (GME) ($r_{GME} = 0.37$; $r_{GMA} = 1.24$).[19]

As an explanation for the EEGE/GC reactivity ratios, steric influence can be ruled out, since GC is incorporated preferentially, despite the bulky side group. Instead, the pronounced gradient must be due to the chemical nature of the monomers. To correlate the reactivity ratios to the molecular structure of EEGE and GC, quantum mechanical calculations (B3LYP-D3-gCP/def2-TZVP//B3LYP-D3-gCP/def2-TZVP) were performed. As a simplified model, the bond length of the epoxide C-O bond was investigated, which is attacked during propagation to form the backbone (for coordinates, see **SI-Table 1−3**). In the case of EEGE, this bond is slightly longer (143.4 pm) compared to GC (142.9 pm) or EO (142.8 pm). This leads to an increased ring strain towards the site for nucleophilic attack in GC compared to EEGE. Furthermore, the bond lengths in EO and GC show only slight differences, thus similar ring strain and reactivity can be expected. In a previous report of our group, a gradient was observed for EO and EEGE copolymerized via monomer-activated AROP ($r_{EO} = 8.00$; $r_{EEGE} = 0.125$).[58] From the calculated ring geometries, GC can be expected to show similar reactivity as EO

(**Figure 4**), which is considerably more reactive in the monomer-activated copolymerization than EEGE. This is in line with our findings regarding gradient type copolymerization of EEGE and GC.
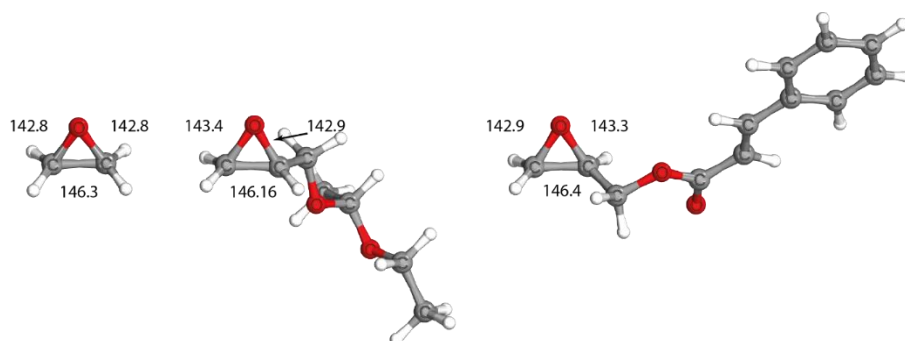
Figure 4. Determined bond lengths (in pm) for EO, EEGE and GC via DFT calculations.

Removal of the acetal protective groups to release the free hydroxyl groups. Cleavage of the acetal group subsequent to the polymerization without affecting the GC ester bonds is not trivial. For this purpose, the acidic ion exchange resin Dowex® 50WX8 was used for deprotection. Quantitative removal of the protective groups was achieved by using a methanol/toluene mixture and reduced pressure. Continuous removal of the cleavage products acetaldehyde and ethanol resulted in shifting of the reaction equilibrium towards the product side. As a consequence, a drastic difference in the polarity of the samples could be observed. While all the protected samples of **Table 1** were only soluble in organic solvents such as dichloromethane, the deprotected samples 11−15 (**Table 3**) could be dissolved in water, which is crucial for the preparation of the hydrogels discussed below.

Table 3 gives the SEC data for all deprotected P(G-*co*-GC) copolymers. Molecular weights are in the range of 1,900 to 3,700 g mol^{-1} with Đ below 1.35.

Table 3. Characterization data of deprotected polyglycerol copolymers.

No.[a]	Copolymer composition[b]	Theoretical composition	$M_n^{(th)}$ (g·mol^{-1})	M_n^c (g·mol^{-1})	$Đ^c$
9[(2)]	P(G$_{0.18}$-co-GC$_{0.82}$)	19 : 81	9,300	1,900	1.25
10[(3)]	P(G$_{0.29}$-co-GC$_{0.71}$)	30 : 70	8,900	2,200	1.33
11[(4)]	P(G$_{0.70}$-co-GC$_{0.30}$)	69 : 31	7,100	3,500	1.32
12[(5)]	P(G$_{0.81}$-co-GC$_{0.19}$)	80 : 20	6,400	3,700	1.21
13[(6)]	P(G$_{0.86}$-co-GC$_{0.14}$)	85 : 15	6,100	2,400	1.30
14[(7)]	P(G$_{0.92}$-co-GC$_{0.08}$)	92 : 8	6,000	3,300	1.34
15[(8)]	P(G$_{0.98}$-co-GC$_{0.02}$)	96 : 4	5,400	3,600	1.21

[a] Exponent specifies precursor from **Table 1**. [b] Obtained from ^{1}H NMR spectra. [c] Determined by SEC measurements in DMF (RI detector, PEG standards).

A superposition of selected SEC traces of P(G-co-GC) copolymers is shown in **Figure 5** and demonstrates the monomodal distributions obtained. In direct comparison, all individual elugrams are shifted in comparison to the precursors. The successful deprotection is also evidenced by the ^{1}H NMR spectrum, shown for the deprotected P(G$_{0.18}$-co-GC$_{0.82}$) (entry 9, **Table 3**) copolymer in **Figure 5**. The typical signals of the acetal protecting group at 4.7 ppm and 1.2 ppm are absent, confirming quantitative cleavage. In addition, all characteristic signals of glycidyl cinnamate are still present. The Supporting Information includes additional ^{13}C NMR and 2D NMR spectra (**SI-Figures 15−17**).
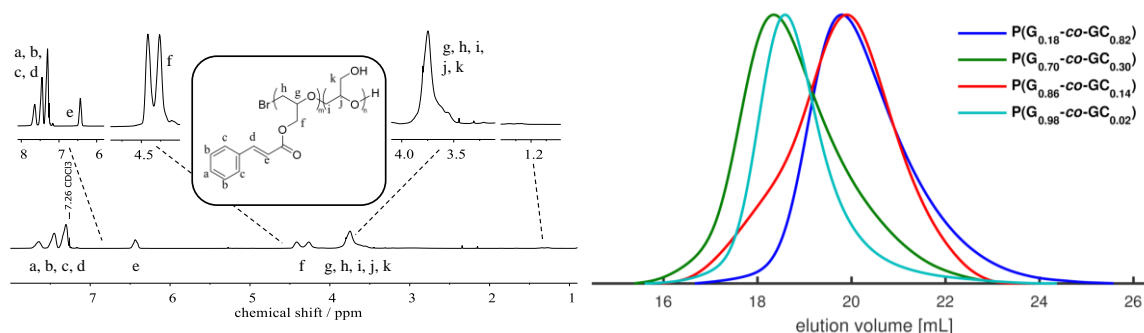
Figure 5. ^{1}H NMR spectra (600 MHz, CDCl$_3$) of P(G$_{0.18}$-co-GC$_{0.82}$) (entry 9, **Table 3**) and SEC traces (DMF, PEG standards) of selected P(G-co-GC) copolymers.

Thermal properties. Thermal properties of the copolymers were investigated by differential scanning calorimetry (DSC). **Table 4** documents the thermal characteristics for both P(EEGE-co-GC) and the deprotected P(G-co-GC) copolymers as well as PGC homopolymer, which were determined from the second heating curve (for DSC diagrams see **SI-Figure 18** and **SI-**
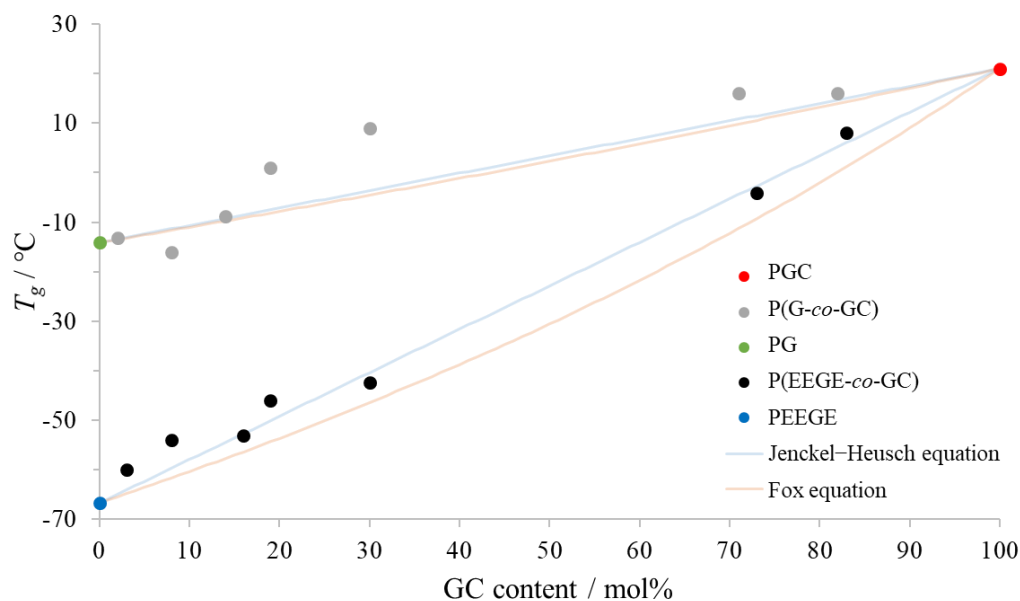
Figure 19). The glass transition temperatures (T_gs) vary in the range of -60 °C (entry 8, **Table 4**) for protected copolymers and -13 °C (entry 15, **Table 4**) after deprotection, to 21 °C (entry 1, **Table 4**). The values increase with increasing amount of GC. As expected, due to the generally atactic structure of the copolymers, amorphous materials were obtained and no melting points were observed.

Table 4. Thermal properties of P(EEGE-*co*-GC) / P(G-*co*-GC) copolymers and PGC homopolymer.

No.[a]	Copolymer composition[b]	T_g / °C
1	PGC	21
2	P(EEGE$_{0.17}$-*co*-GC$_{0.83}$)	8
3	P(EEGE$_{0.27}$-*co*-GC$_{0.73}$)	-4
4	P(EEGE$_{0.70}$-*co*-GC$_{0.30}$)	-42
5	P(EEGE$_{0.81}$-*co*-GC$_{0.19}$)	-46
6	P(EEGE$_{0.84}$-*co*-GC$_{0.16}$)	-53
7	P(EEGE$_{0.92}$-*co*-GC$_{0.08}$)	-54
8	P(EEGE$_{0.97}$-*co*-GC$_{0.03}$)	-60
9[(2)]	P(G$_{0.18}$-*co*-GC$_{0.82}$)	16
10[(3)]	P(G$_{0.29}$-*co*-GC$_{0.71}$)	16
11[(4)]	P(G$_{0.70}$-*co*-GC$_{0.30}$)	9
12[(5)]	P(G$_{0.81}$-*co*-GC$_{0.19}$)	1
13[(6)]	P(G$_{0.86}$-*co*-GC$_{0.14}$)	-9
14[(7)]	P(G$_{0.92}$-*co*-GC$_{0.08}$)	-16
15[(8)]	P(G$_{0.98}$-*co*-GC$_{0.02}$)	-13

[a] Exponent specifies precursor 2−8. [b] Obtained from ^{1}H NMR spectra.

In **Figure 6**, the linear relationship between the glass transition temperature of the acetal protected P(EEGE-*co*-GC) copolymers, the deprotected P(G-*co*-GC) copolymers and the PGC homopolymer are plotted as a function of their GC content. Please note that the T_gs, of PEEGE and PG homopolymers were taken from literature and amount to -67 °C[56] and -14 °C[67], respectively. The T_gs of the copolymers are within these limits. The nearly linear trend for the P(EEGE-*co*-GC) copolymers demonstrates the effect of the incorporation of the comonomers EEGE and GC, supporting the absence of a very pronounced gradient structure.

Figure 6. Glass transition temperatures of P(EEGE-*co*-GC)/P(G-*co*-GC) copolymers and PG/PEEGE/PGC homopolymers as a function of the GC content, including fits for the modified Jenckel-Heusch (blue curve) and Fox equation (red curve).

The systematic increase of the glass transition with increasing GC content is due to the substituent effects. Bulky side chains, such as the sterically demanding cinnamic acid ester groups impede mobility of the main chain and thus lead to an increase of the T_g.[68] Upon release of the hydroxyl groups, a general increase of the T_gs in the series of P(G-*co*-GC) copolymers is observed ($\Delta T_{8 \rightarrow 15} = 47$ °C), which is due to hydrogen bond interaction.[69] This effect becomes smaller with increasing GC content ($\Delta T_{2 \rightarrow 9} = 8$ °C), since the large, sterically demanding GC side groups have the major impact on the molecular mobility here.

For evaluation, the linear plot of Fox equation[70] (**3**) and the simple, linear combination based on the empirical Jenckel-Heusch equation[71] (**4**) were used:

$$\frac{1}{T_g} = \frac{x_{EEGE/G}}{T_{g_{PEEGE/PG}}} + \frac{x_{GC}}{T_{g_{PGC}}} \tag{3}$$

$$T_g = x_{EEGE/G} \cdot T_{g_{PEEGE/PG}} + x_{GC} \cdot T_{g_{PGC}} \tag{4}$$

Here, x is the mole fraction of the monomer units EEGE/G and GC, whereas $T_{g_{PEEGE/PG}}$ and $T_{g_{PGC}}$ correspond to the respective homopolymer. These equations here represent a simplified approach, which does not take specific interaction terms into account.[72] Direct comparison

demonstrates that the measured T_g values for the protected P(EEGE-*co*-GC) copolymers coincide very well with the course of the Fox and modified Jenckel-Heusch equation. Thus, the glass transitions can be predicted for arbitrary P(EEGE-*co*-GC) copolymer compositions, using these equations. For the deprotected P(G-*co*-GC) copolymers, a positive deviation from the course of the fits is observed, which reaches its maximum at a composition of 40–50 mol% GC. This behavior can be attributed to interactions and the considerations of the chemical nature of the comonomers.[73] As a consequence of the hydrogen bonding between the ester function of GC and the hydroxyl groups of the glycerol moieties, the free volume of the copolymers decreases, resulting in a reduction of the chain mobility that translates to higher T_gs.[74,75]

C.   Photocrosslinking of P(G-*co*-GC) copolymers.

Polyether copolymers with cinnamic acid functionality possess intriguing potential for the use as photosensitive materials.[76–80] The reactive double bond in the cinnamic acid side chain permits photodimerization, and thus crosslinking of the copolymers is possible, as shown in **SI-Figure 20**. In general, photocrosslinking of cinnamate derivatives requires UV radiation with $\lambda > 280$ nm (here 312 nm and 365 nm).[29,79,81] As a result, cinnamate units exhibit a substantial advantage, since no auxiliary reagents such as photoinitiators are required for crosslinking. The following section discusses the photodimerization-based crosslinking of the synthesized P(G-*co*-GC) copolymers by employing UV irradiation, resulting in hydrogel formation.[82,83]

Direct crosslinking via photodimerization in water failed, which could be attributed to the gradient-like microstructure of the copolymers that could lead to shielding of the insoluble glycidyl cinnamate units by the polar polyglycerol chains. A series of experiments were performed, varying both the concentration and UV irradiation times. Finally, the use of ethanol as a solvent turned out to be the best option, since also P(G-*co*-GC) copolymers possessing a GC content below 30% were soluble. The copolymers were successfully photocrosslinked while the solvent evaporated slowly. For successful formation of hydrogels, the GC content in the copolymer must exceed 2 mol% (cf. entry 15, **Table 5**). After irradiation of the soft and adhesive ("sticky") starting material, a non-sticky hydrogel was formed. Striking differences in the material properties of the hydrogels were observed depending on the amount of GC in the copolymers employed. While photocrosslinking of P(G$_{0.92}$-*co*-GC$_{0.08}$) (entry 14, **Table 3**) resulted in a yellow, elastic material, the hydrogels with higher amount of GC were brittle.

To confirm the successful photodimerization, IR spectroscopy was conducted as a qualitative method due to the insolubility of the hydrogels. **SI-Figure 21** shows the superimposed, normalized IR spectra of the P(G-*co*-GC) hydrogels. In particular, the wave number range of 1,800 to 1,600 cm^{-1} demonstrates successful crosslinking of the P(G-*co*-GC) copolymers. In the case of the non-crosslinked polymers, the unsaturated ester carbonyl band appears at $v_{C=O} = 1{,}709$ cm^{-1}, and the C=C stretching mode at $v_{C=C} = 1{,}636$ cm^{-1} (**Figure 7**). The IR spectrum of the corresponding hydrogel shows a strong decrease of the C=C stretching mode caused by the photodimerization and a shift of the carbonyl band to 1,731 cm^{-1}. According to Coleman *et al.*, the shift between the unsaturated C=O and the saturated carbonyl stretching band is the consequence of the formation of saturated C−C crosslinks from the cinnamoyl double bonds (cf. **SI-Figure 20**).[84]
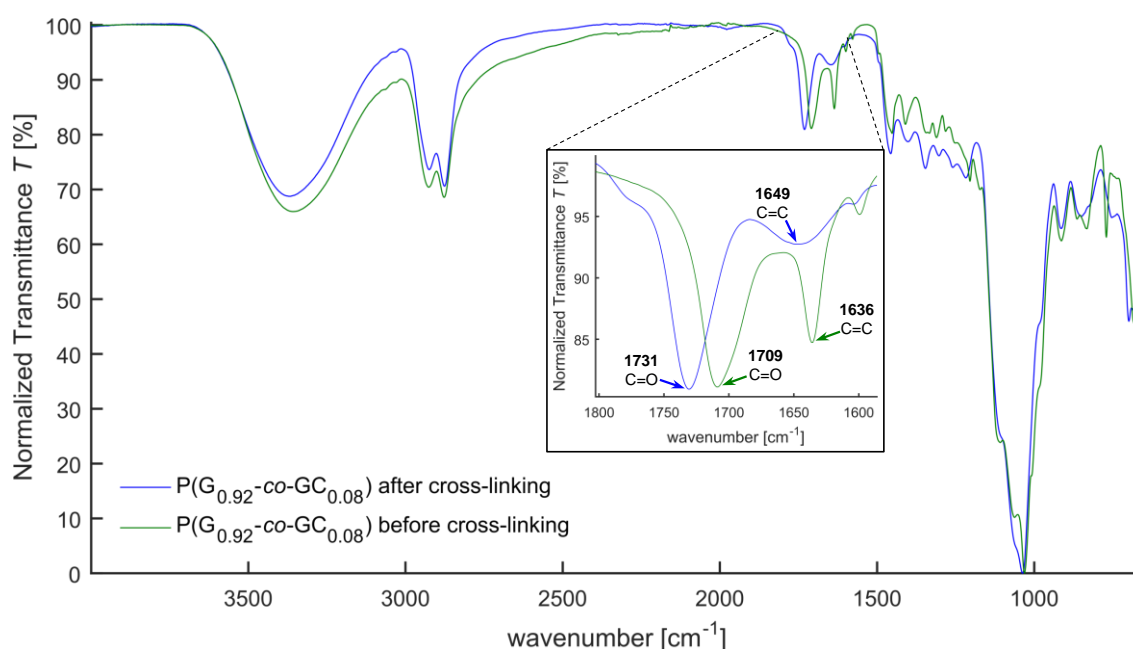
Figure 7. Normalized IR Spectra of P(G$_{0.92}$-*co*-GC$_{0.08}$) (entry 14, **Table 3**) before and after photocrosslinking, including a zoom in on the GC double bond region.

For the characterization of the hydrogels, the equilibrium swelling ratio (*SR*, **Equation 1**, see Experimental) and mass swelling (*Q$_m$*, **Equation 2**, see Experimental) were examined. **Table 5** summarizes the *SR* and *Q$_m$* results for the P(G-*co*-GC) hydrogels.

Table 5. Swelling behavior of the P(G-*co*-GC) hydrogels.

No.[a]	Copolymer composition[b]	SR / %	Q_m
11$^{(4)}$	P(G$_{0.70}$-*co*-GC$_{0.30}$)	79	1.8
12$^{(5)}$	P(G$_{0.81}$-*co*-GC$_{0.19}$)	172	2.7
13$^{(6)}$	P(G$_{0.86}$-*co*-GC$_{0.14}$)	175	2.8
14$^{(7)}$	P(G$_{0.92}$-*co*-GC$_{0.08}$)	220	3.2
15$^{(8)}$	P(G$_{0.98}$-*co*-GC$_{0.02}$)	-	-

[a] Exponent specifies precursor. [b] Obtained from ^{1}H NMR spectra.

The *SR* was calculated using **Equation 1** and varies from 220% to 79%. However, the mass swelling (**Equation 2**) decreases from 3.2 to 1.8, which is illustrated in the Supporting Information (**SI-Figure 22**). As expected, with increasing the GC content the water uptake decreases due to the increase of crosslink density. The hydrogels exhibit rather low water uptake compared to PEG hydrogels.[85–88] This behavior is tentatively attributed to the microstructure of the P(G-*co*-GC) copolymers. According to the *in-situ* ^{1}H NMR kinetic measurements the copolymer chains show a gradient-like distribution and consequently no uniformly distributed GC units. A large water uptake capacity requires rather long hydrophilic segments, leading to a large mesh size.[89] Instead, the crosslinks are concentrated in the GC-rich segments due to the gradient, resulting in a decreased mesh size and in reduced water uptake.[90].

CONCLUSION

In this work, we presented the copolymerization of glycidyl cinnamate (GC) and ethoxyethyl glycidyl ether (EEGE), capitalizing on the monomer-activated AROP. The results demonstrate that such reactive glycidyl esters as a hardly studied class of epoxide monomers are amenable to ring-opening polymerization reactions, if the monomer activation technique is employed. The amount of incorporated GC in the polymers was varied from 3 mol% to 100 mol% by using an excess of triisobutylaluminum (i-Bu$_3$Al) as a catalyst in combination with tetraoctylammonium bromide (NOct$_4$Br) as an initiator. The obtained P(EEGE-co-GC) copolymers showed apparent molecular weights ranging from 2,600 g mol^{-1} to 4,600 g mol^{-1}, with dispersities ($Đ$) below 1.35. Detailed characterization of the microstructure using *in-situ* ^{1}H NMR kinetics demonstrated a gradient in the incorporation of the comonomers ($r_{EEGE} = 0.2$; $r_{GC} = 2.9$). DFT calculations confirmed similar ring strain of GC and EO, for which a strong monomer gradient in the monomer-activated copolymerization with EEGE was recently demonstrated by our group.[58]

Selective cleavage of the acetal protecting groups, avoiding ester hydrolysis of the GC units was achieved by using Dowex® ion exchange resin. The molecular weights of the resulting deprotected P(G-co-GC) copolymers varied from 1,900 g mol^{-1} to 3,700 g mol^{-1}, while the dispersities $Đ$ were in the range of 1.21 to 1.34. An investigation of the thermal properties demonstrated the effect of hydrogen bonds of the P(G-co-GC) copolymers. The glass transition temperatures (T_gs) ranged between -13 °C (deprotected polyethers) and -60 °C (protected polymers) to 21 °C for the PGC homopolymer. Photocrosslinking via UV irradiation led to hydrogels with a water uptake capacity of up to 220%. When gradually increasing the GC content and thus the crosslink density, the expected decrease of the swelling ratio was observed.

These characteristics render P(G-co-GC) copolymers interesting candidates for biomedical applications, particularly since these hydrogels are accessible without the addition of further crosslinking agents.[91] Obviously, the results of this work are of a general nature for the polymerization and copolymerization of the hitherto scarcely studied monomer class of glycidyl esters. By esterification of carboxylic acids with glycidol, a vast variety of different substituents is conveniently accessible, enhancing the structural diversity of polyethers.

ACKNOWLEDGEMENT

REFERENCES

(1) Ouchi, M.; Terashima, T.; Sawamoto, M. Transition metal-catalyzed living radical polymerization: toward perfection in catalysis and precision polymer synthesis. *Chem. Rev.* **2009**, *109*, 4963–5050, DOI: 10.1021/cr900234b.

(2) Coessens, V.; Pintauer, T.; Matyjaszewski, K. Functional polymers by atom transfer radical polymerization. *Prog. Polym. Sci.* **2001**, *26*, 337–377, DOI: 10.1016/S0079-6700(01)00003-X.

(3) Matyjaszewski, K.; Tsarevsky, N. V. Nanostructured functional materials prepared by atom transfer radical polymerization. *Nat. Chem.* **2009**, *1*, 276–288, DOI: 10.1038/nchem.257.

(4) Kabb, C. P.; O'Bryan, C. S.; Deng, C. C.; Angelini, T. E.; Sumerlin, B. S. Photoreversible Covalent Hydrogels for Soft-Matter Additive Manufacturing. *ACS Appl. Mater. Interfaces* **2018**, *10*, 16793–16801, DOI: 10.1021/acsami.8b02441.

(5) Martínez, P.-A.; Cádiz, V.; Serra, A.; Mantecón, A. Curing of new trimellitimide glycidyl ester derivatives with aromatic diamines. *Angew. Makromol. Chemie* **1985**, *136*, 159–175, DOI: 10.1002/apmc.1985.051360112.

(6) Atta, A. M.; Mansour, R.; Abdou, M. I.; Sayed, A. M. Epoxy resins from rosin acids: synthesis and characterization. *Polym. Adv. Technol.* **2004**, *15*, 514–522, DOI: 10.1002/pat.507.

(7) Yu, H.; Wang, L.; Huo, J.; Ding, J.; Tan, Q. Synthesis and curing behavior of a novel ferrocene-based epoxy compound. *J. Appl. Polym. Sci.* **2008**, *110*, 1594–1599, DOI: 10.1002/app.28584.

(8) Huang, K.; Liu, Z.; Zhang, J.; Li, S.; Li, M.; Xia, J.; Zhou, Y. Epoxy monomers derived from tung oil fatty acids and its regulable thermosets cured in two synergistic ways. *Biomacromolecules* **2014**, *15*, 837–843, DOI: 10.1021/bm4018929.

(9) El-Ghazawy, R. A.; El-Saeed, A. M.; Al-Shafey, H. I.; Abdul-Raheim, A.-R. M.; El-Sockary, M. A. Rosin based epoxy coating: Synthesis, identification and characterization. *Eur. Polym. J.* **2015**, *69*, 403–415, DOI: 10.1016/j.eurpolymj.2015.06.025.

(10) Herzberger, J.; Niederer, K.; Pohlit, H.; Seiwert, J.; Worm, M.; Wurm, F. R.; Frey, H. Polymerization of Ethylene Oxide, Propylene Oxide, and Other Alkylene Oxides: Synthesis, Novel Polymer Architectures, and Bioconjugation. *Chem. Rev.* **2016**, *116*, 2170–2243, DOI: 10.1021/acs.chemrev.5b00441.

(11) Staudinger, H.; Lohmann, H. Über hochpolymere Verbindungen. 81. Mitteilung. Über eukolloides Polyäthylenoxyd. *Justus Liebigs Ann. Chem.* **1933**, *505*, 41–51, DOI: 10.1002/jlac.19335050104.

(12) Billouard, C.; Carlotti, S.; Desbois, P.; Deffieux, A. "Controlled" High-Speed Anionic Polymerization of Propylene Oxide Initiated by Alkali Metal Alkoxide/Trialkylaluminum Systems. *Macromolecules* **2004**, *37*, 4038–4043, DOI: 10.1021/ma035768t.

(13) Labbé, A.; Carlotti, S.; Billouard, C.; Desbois, P.; Deffieux, A. Controlled High-Speed Anionic Polymerization of Propylene Oxide Initiated by Onium Salts in the Presence of Triisobutylaluminum. *Macromolecules* **2007**, *40*, 7842–7847, DOI: 10.1021/ma070288d.

(14) Brocas, A.-L.; Mantzaridis, C.; Tunc, D.; Carlotti, S. Polyether synthesis: From activated or metal-free anionic ring-opening polymerization of epoxides to functionalization. *Prog. Polym. Sci.* **2013**, *38*, 845–873, DOI: 10.1016/j.progpolymsci.2012.09.007.

(15) Carlotti, S.; Labbé, A.; Rejsek, V.; Doutaz, S.; Gervais, M.; Deffieux, A. Living/Controlled Anionic Polymerization and Copolymerization of Epichlorohydrin with Tetraoctylammonium Bromide−Triisobutylaluminum Initiating Systems. *Macromolecules* **2008**, *41*, 7058–7062, DOI: 10.1021/ma801422c.

(16) Gervais, M.; Brocas, A.-L.; Deffieux, A.; Ibarboure, E.; Carlotti, S. Rapid and controlled synthesis of hydrophobic polyethers by monomer activation. *Pure Appl. Chem.* **2012**, *84,* DOI: 10.1351/PAC-CON-11-11-16.

(17) Gervais, M.; Brocas, A.-L.; Cendejas, G.; Deffieux, A.; Carlotti, S. Synthesis of Linear High Molar Mass Glycidol-Based Polymers by Monomer-Activated Anionic Polymerization. *Macromolecules* **2010**, *43*, 1778–1784, DOI: 10.1021/ma902286a.

(18) Cevada, E.; Roos, K.; Alvarez, F.; Carlotti, S.; Vázquez, F. High molar mass polyethers as defoamers of heavy crude oil. *Fuel* **2018**, *221*, 447–454, DOI: 10.1016/j.fuel.2018.02.136.

(19) Labbé, A.; Brocas, A.-L.; Ibarboure, E.; Ishizone, T.; Hirao, A.; Deffieux, A.; Carlotti, S. Selective Ring-Opening Polymerization of Glycidyl Methacrylate: Toward the Synthesis of Cross-Linked (Co)polyethers with Thermoresponsive Properties. *Macromolecules* **2011**, *44*, 6356–6364, DOI: 10.1021/ma201075n.

(20) Shen, H.; Chen, J.; Taha, M. Cross-linking and damping properties of poly(caprolactone-co-glycidyl methacrylate). *Polym. J.* **2014**, *46*, 598–608, DOI: 10.1038/pj.2014.29.

(21) Rusu, E., Comanita, E., Airinei, A. and Rusu, G. Photosensitive monomers and polymers derived from glycidyl cinnamate. *Iran. Polym. J.* **1998**, *7*, 157–162.

(22) Nishikubo, T.; Ichijyo, T.; Takaoka, T. Synthesis and Photosensitive Properties of Photocrosslinkable Poly(glicidyl cinnamate). *Nippon Kagaku Kaishi* **1973**, 35–39, DOI: 10.1246/nikkashi.1973.35.

(23) Sung, S.-J.; Cho, K.-Y.; Hah, H.; Lee, J.; Shim, H.-K.; Park, J.-K. Two different reaction mechanisms of cinnamate side groups attached to the various polymer backbones. *Polymer* **2006**, *47*, 2314–2321, DOI: 10.1016/j.polymer.2006.02.003.

(24) Egerton, P. L.; Pitts, E.; Reiser, A. Photocycloaddition in solid poly(vinyl cinnamate). The photoreactive polymer matrix as an ensemble of chromophore sites. *Macromolecules* **1981**, *14*, 95–100, DOI: 10.1021/ma50002a019.

(25) Creed, D.; Griffin, A. C.; Hoyle, C. E.; Venkataram, K. Chromophore aggregation and concomitant wavelength-dependent photochemistry of a main-chain liquid crystalline poly(aryl cinnamate). *J. Am. Chem. Soc.* **1990**, *112*, 4049–4050, DOI: 10.1021/ja00166a058.

(26) Chatani, S.; Kloxin, C. J.; Bowman, C. N. The power of light in polymer science: photochemical processes to manipulate polymer formation, structure, and properties. *Polym. Chem.* **2014**, *5*, 2187–2201, DOI: 10.1039/C3PY01334K.

(27) Jamróz-Piegza, M.; Wałach, W.; Dworak, A.; Trzebicka, B. Polyether nanoparticles from covalently crosslinked copolymer micelles. *J. Colloid Interface Sci.* **2008**, *325*, 141–148, DOI: 10.1016/j.jcis.2008.05.033.

(28) Murase, S.; Kinoshita, K.; Horie, K.; Morino, S.'y. Photo-optical Control with Large Refractive Index Changes by Photodimerization of Poly(vinyl cinnamate) Film. *Macromolecules* **1997**, *30*, 8088–8090, DOI: 10.1021/ma971077j.

(29) Ichimura, K.; Akita, Y.; Akiyama, H.; Kudo, K.; Hayashi, Y. Photoreactivity of Polymers with Regioisomeric Cinnamate Side Chains and Their Ability To Regulate Liquid Crystal Alignment. *Macromolecules* **1997**, *30*, 903–911, DOI: 10.1021/ma961225q.

(30) Shi, D.; Matsusaki, M.; Akashi, M. Photo-tunable protein release from biodegradable nanoparticles composed of cinnamic acid derivatives. *J. Control. Release* **2011**, *149*, 182–189, DOI: 10.1016/j.jconrel.2010.08.009.

(31) Thomas, A.; Müller, S. S.; Frey, H. Beyond poly(ethylene glycol): linear polyglycerol as a multifunctional polyether for biomedical and pharmaceutical applications. *Biomacromolecules* **2014**, *15*, 1935–1954, DOI: 10.1021/bm5002608.

(32) Dworak, A.; Slomkowski, S.; Basinska, T.; Gosecka, M.; Walach, W.; Trzebicka, B. Polyglycidol - how is it synthesized and what is it used for? *Polimery* **2013**, *58*, 641–649, DOI: 10.14314/polimery.2013.641.

(33) Keul, H.; Möller, M. Synthesis and degradation of biomedical materials based on linear and star shaped polyglycidols. *J. Polym. Sci. A Polym. Chem.* **2009**, *47*, 3209–3231, DOI: 10.1002/pola.23359.

(34) Wilms, D.; Stiriba, S.-E.; Frey, H. Hyperbranched polyglycerols: from the controlled synthesis of biocompatible polyether polyols to multipurpose applications. *Acc. Chem. Res.* **2010**, *43*, 129–141, DOI: 10.1021/ar900158p.

(35) Fitton, A. O.; Hill, J.; Jane, D. E.; Millar, R. Synthesis of Simple Oxetanes Carrying Reactive 2-Substituents. *Synthesis* **1987**, *1987*, 1140–1142, DOI: 10.1055/s-1987-28203.

(36) Halacheva, S.; Rangelov, S.; Tsvetanov, C. Poly(glycidol)-Based Analogues to Pluronic Block Copolymers. Synthesis and Aqueous Solution Properties. *Macromolecules* **2006**, *39*, 6845–6852, DOI: 10.1021/ma061040b.

(37) Dimitrov, P.; St. Rangelov; Dworak, A.; Haraguchi, N.; Hirao, A.; Tsvetanov, C.B. Triblock and Radial Star-Block Copolymers Comprised of Poly(ethoxyethyl glycidyl ether), Polyglycidol, Poly(propylene oxide) and Polystyrene Obtained by Anionic Polymerization Initiated by Cs Initiators. *Macromol. Symp.* **2004**, *215*, 127–140, DOI: 10.1002/masy.200451111.

(38) Wurm, F.; Nieberle, J.; Frey, H. Double-Hydrophilic Linear-Hyperbranched Block Copolymers Based on Poly(ethylene oxide) and Poly(glycerol). *Macromolecules* **2008**, *41*, 1184–1188, DOI: 10.1021/ma702308g.

(39) Mangold, C.; Wurm, F.; Obermeier, B.; Frey, H. Hetero-Multifunctional Poly(ethylene glycol) Copolymers with Multiple Hydroxyl Groups and a Single Terminal Functionality. *Macromol. Rapid Commun.* **2010**, *31*, 258–264, DOI: 10.1002/marc.200900472.

(40) Taton, D.; Le Borgne, A.; Sepulchre, M.; Spassky, N. Synthesis of chiral and racemic functional polymers from glycidol and thioglycidol. *Macromol. Chem. Phys.* **1994**, *195*, 139–148, DOI: 10.1002/macp.1994.021950111.

(41) Li, Z.; Chau, Y. Synthesis of linear polyether polyol derivatives as new materials for bioconjugation. *Bioconjugate Chem.* **2009**, *20*, 780–789, DOI: 10.1021/bc900036f.

(42) Wurm, F.; Dingels, C.; Frey, H.; Klok, H.-A. Squaric acid mediated synthesis and biological activity of a library of linear and hyperbranched poly(glycerol)-protein conjugates. *Biomacromolecules* **2012**, *13*, 1161–1171, DOI: 10.1021/bm300103u.

(43) Weinhart, M.; Grunwald, I.; Wyszogrodzka, M.; Gaetjen, L.; Hartwig, A.; Haag, R. Linear poly(methyl glycerol) and linear polyglycerol as potent protein and cell resistant alternatives to poly(ethylene glycol). *Chem. Asian J.* **2010**, *5*, 1992–2000, DOI: 10.1002/asia.201000127.

(44) Weinhart, M.; Becherer, T.; Haag, R. Switchable, biocompatible surfaces based on glycerol copolymers. *Chem. Commun.* **2011**, *47*, 1553–1555, DOI: 10.1039/c0cc04002a.

(45) Hans, M.; Gasteier, P.; Keul, H.; Moeller, M. Ring-Opening Polymerization of ε-Caprolactone by Means of Mono- and Multifunctional Initiators: Comparison of Chemical and Enzymatic Catalysis. *Macromolecules* **2006**, *39*, 3184–3193, DOI: 10.1021/ma052657g.

(46) Neese, F. The ORCA program system. *Wiley Interdiscip. Rev.-Comput. Mol. Sci.* **2012**, *2*, 73–78, DOI: 10.1002/wcms.81.

(47) Kruse, H.; Grimme, S. A geometrical correction for the inter- and intra-molecular basis set superposition error in Hartree-Fock and density functional theory calculations for large systems. *J. Chem. Phys.* **2012**, *136*, 154101, DOI: 10.1063/1.3700154.

(48) Grimme, S.; Ehrlich, S.; Goerigk, L. Effect of the damping function in dispersion corrected density functional theory. *J. Comput. Chem.* **2011**, *32*, 1456–1465, DOI: 10.1002/jcc.21759.

(49) Grimme, S.; Antony, J.; Ehrlich, S.; Krieg, H. A consistent and accurate ab initio parametrization of density functional dispersion correction (DFT-D) for the 94 elements H-Pu. *J. Chem. Phys.* **2010**, *132*, 154104, DOI: 10.1063/1.3382344.

(50) Schäfer, A.; Horn, H.; Ahlrichs, R. Fully optimized contracted Gaussian basis sets for atoms Li to Kr. *J. Chem. Phys.* **1992**, *97*, 2571–2577, DOI: 10.1063/1.463096.

(51) Weigend, F.; Ahlrichs, R. Balanced basis sets of split valence, triple zeta valence and quadruple zeta valence quality for H to Rn: Design and assessment of accuracy. *Phys. Chem. Chem. Phys.* **2005**, *7*, 3297–3305, DOI: 10.1039/b508541a.

(52) Neese, F.; Wennmohs, F.; Hansen, A.; Becker, U. Efficient, approximate and parallel Hartree–Fock and hybrid DFT calculations. A 'chain-of-spheres' algorithm for the Hartree–Fock exchange. *Chem. Phys.* **2009**, *356*, 98–109, DOI: 10.1016/j.chemphys.2008.10.036.

(53) Peter, M.; Tayalia, P. An alternative technique for patterning cells on poly(ethylene glycol) diacrylate hydrogels. *RSC Adv.* **2016**, *6*, 40878–40885, DOI: 10.1039/C6RA08852J.

(54) Meyer, J.; Keul, H.; Möller, M. Poly(glycidyl amine) and Copolymers with Glycidol and Glycidyl Amine Repeating Units: Synthesis and Characterization. *Macromolecules* **2011**, *44*, 4082–4091, DOI: 10.1021/ma200757v.

(55) Müller, S. S.; Moers, C.; Frey, H. A Challenging Comonomer Pair: Copolymerization of Ethylene Oxide and Glycidyl Methyl Ether to Thermoresponsive Polyethers. *Macromolecules* **2014**, *47*, 5492–5500, DOI: 10.1021/ma501280k.

(56) Schömer, M.; Frey, H. Water-Soluble "Poly(propylene oxide)" by Random Copolymerization of Propylene Oxide with a Protected Glycidol Monomer. *Macromolecules* **2012**, *45*, 3039–3046, DOI: 10.1021/ma300249c.

(57) Rejsek, V.; Sauvanier, D.; Billouard, C.; Desbois, P.; Deffieux, A.; Carlotti, S. Controlled Anionic Homo- and Copolymerization of Ethylene Oxide and Propylene Oxide by Monomer Activation. *Macromolecules* **2007**, *40*, 6510–6514, DOI: 10.1021/ma070450c.

(58) Herzberger, J.; Leibig, D.; Liermann, J. C.; Frey, H. Conventional Oxyanionic versus Monomer-Activated Anionic Copolymerization of Ethylene Oxide with Glycidyl Ethers:

Striking Differences in Reactivity Ratios. *ACS Macro Lett.* **2016**, *5*, 1206–1211, DOI: 10.1021/acsmacrolett.6b00701.

(59) Schubert, C.; Dreier, P.; Nguyen, T.; Maciol, K.; Blankenburg, J.; Friedrich, C.; Frey, H. Synthesis of linear polyglycerols with tailored degree of methylation by copolymerization and the effect on thermorheological behavior. *Polymer* **2017**, *121*, 328–339, DOI: 10.1016/j.polymer.2017.05.030.

(60) Obermeier, B.; Wurm, F.; Frey, H. Amino Functional Poly(ethylene glycol) Copolymers via Protected Amino Glycidol. *Macromolecules* **2010**, *43*, 2244–2251, DOI: 10.1021/ma902245d.

(61) Heinen, S.; Rackow, S.; Schäfer, A.; Weinhart, M. A Perfect Match: Fast and Truly Random Copolymerization of Glycidyl Ether Monomers to Thermoresponsive Copolymers. *Macromolecules* **2017**, *50*, 44–53, DOI: 10.1021/acs.macromol.6b01904.

(62) Meyer, V. E.; Lowry, G. G. Integral and differential binary copolymerization equations. *J. Polym. Sci. A Gen. Pap.* **1965**, *3*, 2843–2851, DOI: 10.1002/pol.1965.100030811.

(63) Mayo, F. R.; Lewis, F. M. Copolymerization. I. A Basis for Comparing the Behavior of Monomers in Copolymerization; The Copolymerization of Styrene and Methyl Methacrylate. *J. Am. Chem. Soc.* **1944**, *66*, 1594–1601, DOI: 10.1021/ja01237a052.

(64) Fineman, M.; Ross, S. D. Linear method for determining monomer reactivity ratios in copolymerization. *J. Polym. Sci.* **1950**, *5*, 259–262, DOI: 10.1002/pol.1950.120050210.

(65) Kelen, T.; Tüdos, F. Analysis of the Linear Methods for Determining Copolymerization Reactivity Ratios. I. A New Improved Linear Graphic Method. *J. Macromol. Sci., Chem.* **1975**, *9*, 1–27, DOI: 10.1080/00222337508068644.

(66) Skeist, I. Copolymerization: The Composition Distribution Curve. *J. Am. Chem. Soc.* **1946**, *68*, 1781–1784, DOI: 10.1021/ja01213a031.

(67) Osterwinter, C.; Schubert, C.; Tonhauser, C.; Wilms, D.; Frey, H.; Friedrich, C. Rheological Consequences of Hydrogen Bonding: Linear Viscoelastic Response of Linear Polyglycerol and Its Permethylated Analogues as a General Model for Hydroxyl-Functional Polymers. *Macromolecules* **2015**, *48*, 119–130, DOI: 10.1021/ma501674x.

(68) Singh, A.; Krogman, N. R.; Sethuraman, S.; Nair, L. S.; Sturgeon, J. L.; Brown, P. W.; Laurencin, C. T.; Allcock, H. R. Effect of side group chemistry on the properties of biodegradable L-alanine cosubstituted polyphosphazenes. *Biomacromolecules* **2006**, *7*, 914–918, DOI: 10.1021/bm050752r.

(69) Moers, C.; Wrazidlo, R.; Natalello, A.; Netz, I.; Mondeshki, M.; Frey, H. (1-Adamantyl)methyl glycidyl ether: a versatile building block for living polymerization. *Macromol. Rapid Commun.* **2014**, *35*, 1075–1080, DOI: 10.1002/marc.201400017.

(70) Fox, T. G. Influence of diluent of copolymer composition on the glass temperature of a polymer system. *Bull. Am. Phys. Soc.* **1956**, *1*, 123–125.

(71) Jenckel, E.; Heusch, R. Die Erniedrigung der Einfriertemperatur organischer Gläser durch Lösungsmittel. *Kolloid-Z.* **1953**, *130*, 89–105, DOI: 10.1007/BF01519799.

(72) Kwei, T. K. The effect of hydrogen bonding on the glass transition temperatures of polymer mixtures. *J. Polym. Sci. B Polym. Lett. Ed.* **1984**, *22*, 307–313, DOI: 10.1002/pol.1984.130220603.

(73) París, R.; La Fuente, J. L. de. Glass transition temperature of allyl methacrylate-n-butyl acrylate gradient copolymers in dependence on chemical composition and molecular weight. *J. Polym. Sci. B Polym. Phys.* **2007**, *45*, 1845–1855, DOI: 10.1002/polb.21180.

(74) Sanchis, A.; Prolongo, M. G.; Rubio, R. G.; Masegosa, R. M. Hydrogen-Bonded Polymer Blends. Blends Containing Poly(4-hydroxystyrene-co-4-methoxystyrene) Copolymers. *Polym. J.* **1995**, *27*, 10–20, DOI: 10.1295/polymj.27.10.

(75) Sanchis, A.; Prolongo, M. G.; Salom, C.; Masegosa, R. M. Melting behavior, miscibility, and hydrogen-bonded interactions of poly(ε-caprolactone)/poly(4-hydroxystyrene-co-methoxystyrene) blends. *J. Polym. Sci. B Polym. Phys.* **1998**, *36*, 95–104, DOI: 10.1002/(SICI)1099-0488(19980115)36:1<95:AID-POLB11>3.0.CO;2-9.

(76) Ni, Y.; Zheng, S. A Novel Photocrosslinkable Polyhedral Oligomeric Silsesquioxane and Its Nanocomposites with Poly(vinyl cinnamate). *Chem. Mater.* **2004**, *16*, 5141–5148, DOI: 10.1021/cm049463k.

(77) Assaid, I.; Bosc, D.; Hardy, I. Improvements of the Poly(vinyl cinnamate) Photoresponse in Order to Induce High Refractive Index Variations. *J. Phys. Chem. B* **2004**, *108*, 2801–2806, DOI: 10.1021/jp0306996.

(78) Guo, A.; Liu, G.; Tao, J. Star Polymers and Nanospheres from Cross-Linkable Diblock Copolymers. *Macromolecules* **1996**, *29*, 2487–2493, DOI: 10.1021/ma951354r.

(79) Gupta, P.; Trenor, S. R.; Long, T. E.; Wilkes, G. L. In Situ Photo-Cross-Linking of Cinnamate Functionalized Poly(methyl methacrylate- co -2-hydroxyethyl acrylate) Fibers during Electrospinning. *Macromolecules* **2004**, *37*, 9211–9218, DOI: 10.1021/ma048844g.

(80) Fertier, L.; Koleilat, H.; Stemmelen, M.?n.; Giani, O.; Joly-Duhamel, C.; Lapinte, V.; Robin, J.-J. The use of renewable feedstock in UV-curable materials ?: A new age for polymers and green chemistry. *Prog. Polym. Sci.* **2013**, *38*, 932–962, DOI: 10.1016/j.progpolymsci.2012.12.002.

(81) Shi, D.; Matsusaki, M.; Kaneko, T.; Akashi, M. Photo-Cross-Linking and Cleavage Induced Reversible Size Change of Bio-Based Nanoparticles. *Macromolecules* **2008**, *41*, 8167–8172, DOI: 10.1021/ma800648e.

(82) Yang, Q. Z.; Fan, C. J.; Yang, X. G.; Liao, L. Q.; Liu, L. J. Facile synthesis of biocompatible polyglycerol hydrogel based on epichlorohydrin. *J. Appl. Polym. Sci.* **2016**, *133*, 43451, DOI: 10.1002/app.43451.

(83) Salehpour, S.; Zuliani, C. J.; Dubé, M. A. Synthesis of novel stimuli-responsive polyglycerol-based hydrogels. *Eur. J. Lipid Sci. Technol.* **2012**, *114*, 92–99, DOI: 10.1002/ejlt.201100049.

(84) Coleman, M. M.; Hu, Y.; Sobkowiak, M.; Painter, P. C. Infrared characterization of poly(vinyl cinnamate) and its blends with poly(4-vinyl phenol) before and after UV exposure. *J. Polym. Sci. B Polym. Phys.* **1998**, *36*, 1579–1590, DOI: 10.1002/(SICI)1099-0488(19980715)36:9<1579:AID-POLB15>3.0.CO;2-2.

(85) Niederer, K.; Schüll, C.; Leibig, D.; Johann, T.; Frey, H. Catechol Acetonide Glycidyl Ether (CAGE): A Functional Epoxide Monomer for Linear and Hyperbranched Multi-Catechol Functional Polyether Architectures. *Macromolecules* **2016**, *49*, 1655–1665, DOI: 10.1021/acs.macromol.5b02441.

(86) Molina, I.; Li, S.; Martinez, M. B.; Vert, M. Protein release from physically crosslinked hydrogels of the PLA/PEO/PLA triblock copolymer-type. *Biomaterials* **2001**, *22*, 363–369, DOI: 10.1016/S0142-9612(00)00192-7.

(87) Kaga, S.; Yapar, S.; Gecici, E. M.; Sanyal, R. Photopatternable "Clickable" Hydrogels: "Orthogonal" Control over Fabrication and Functionalization. *Macromolecules* **2015**, *48*, 5106–5115, DOI: 10.1021/acs.macromol.5b01536.

(88) Cohn, D.; Stern, T.; González, M. F.; Epstein, J. Biodegradable poly(ethylene oxide)/poly(epsilon-caprolactone) multiblock copolymers. *J. Biomed. Mater. Res.* **2002**, *59*, 273–281.

(89) Bryant, S. J.; Bender, R. J.; Durand, K. L.; Anseth, K. S. Encapsulating chondrocytes in degrading PEG hydrogels with high modulus: engineering gel structural changes to facilitate cartilaginous tissue production. *Biotechnol. Bioeng.* **2004**, *86*, 747–755, DOI: 10.1002/bit.20160.

(90) Berger, J.; Reist, M.; Mayer, J. M.; Felt, O.; Peppas, N. A.; Gurny, R. Structure and interactions in covalently and ionically crosslinked chitosan hydrogels for biomedical applications. *Eur. J. Pharm. Biopharm.* **2004**, *57*, 19–34, DOI: 10.1016/S0939-6411(03)00161-9.

(91) Hoare, T. R.; Kohane, D. S. Hydrogels in drug delivery: Progress and challenges. *Polymer* **2008**, *49*, 1993–2007, DOI: 10.1016/j.polymer.2008.01.027.

Supporting Information

Glycidyl Cinnamate: Copolymerization with Glycidyl Ethers, *in-situ* NMR Kinetics and Photocrosslinking

*Kamil Maciol[a], Sandra Schüttner[a], Jan Blankenburg[a,b], Tobias Johann[a,c], Holger Frey [a,*]*

[a] Institute of Organic Chemistry, Johannes Gutenberg University Mainz, Duesbergweg 10-14, 55128 Mainz, Germany

[b] Graduate School Materials Science in Mainz, Staudinger Weg 9, 55128 Mainz, Germany

[c] Max Planck Graduate Center with the Johannes Gutenberg University, Staudinger Weg 6, 55128 Mainz, Germany

*E-Mail: hfrey@uni-mainz.de
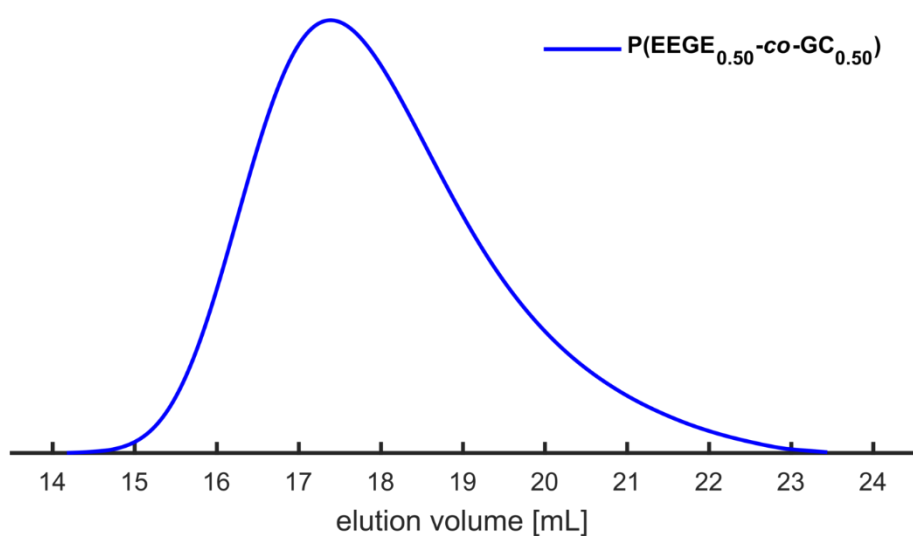
SI-Figure 1. SEC trace of *in-situ* ^{1}H NMR EEGE/GC copolymerization in toluene-d_8 at -20 °C, initiated with NOct$_4$Br and *i*-Bu$_3$Al as catalyst in a ratio of 1:5 (M_n = 4,800 g mol^{-1}, *Đ* = 1.57).
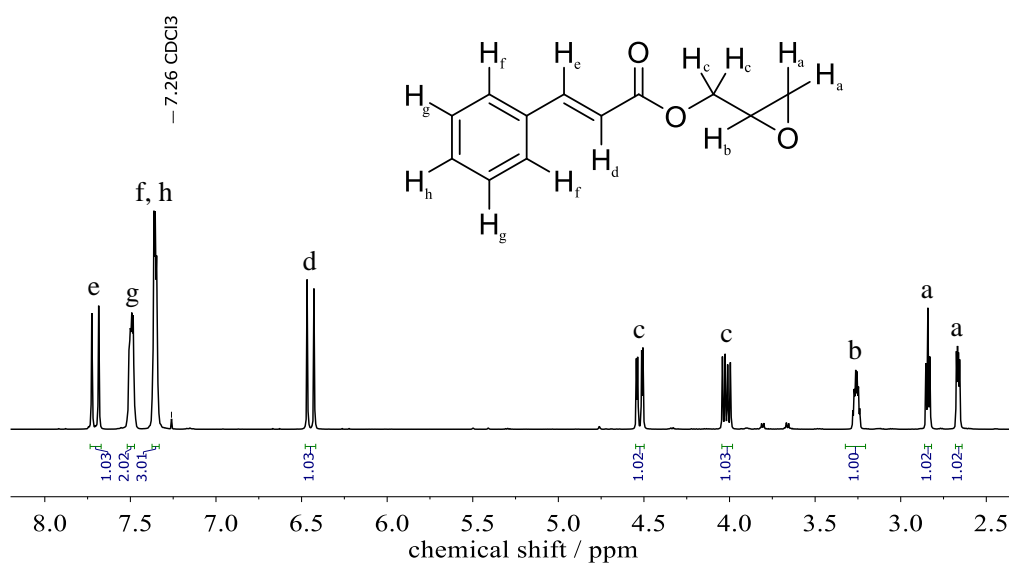
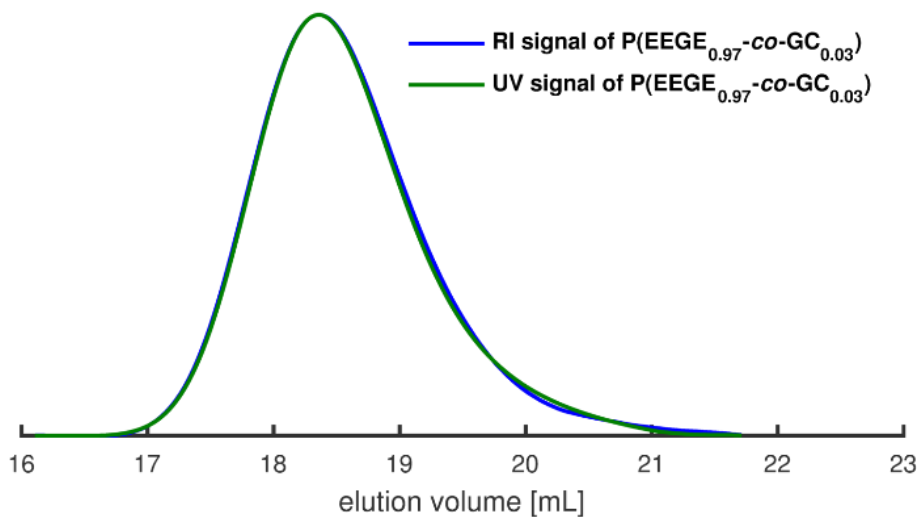**SI-Figure 2.** ^{1}H NMR spectrum (400 MHz, C*D*Cl$_3$) of GC monomer.
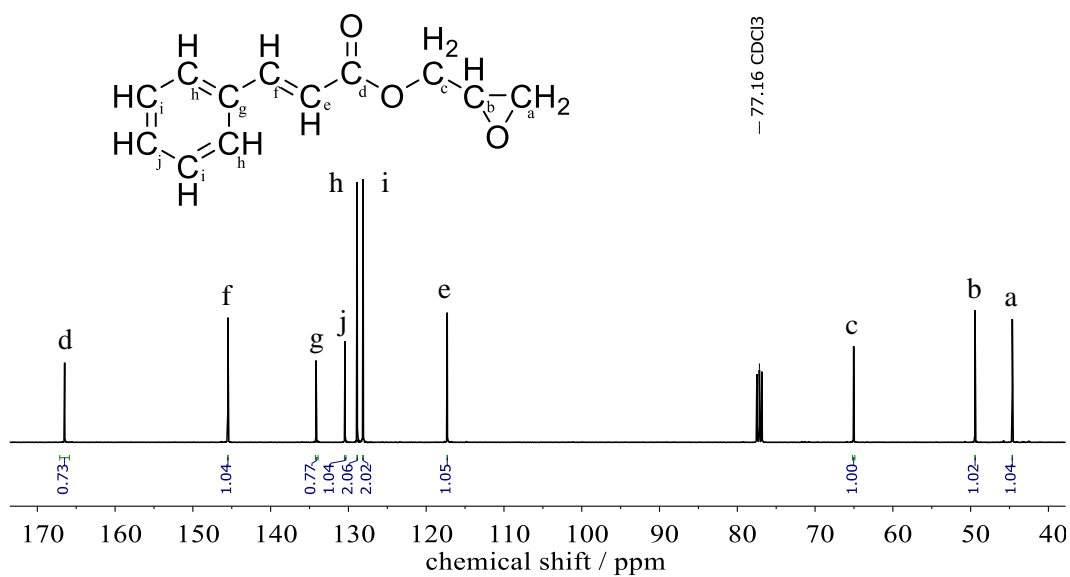
SI-Figure 3. Inverse gated ^{13}C NMR spectrum (100 MHz, C*D*Cl$_3$) of GC monomer.
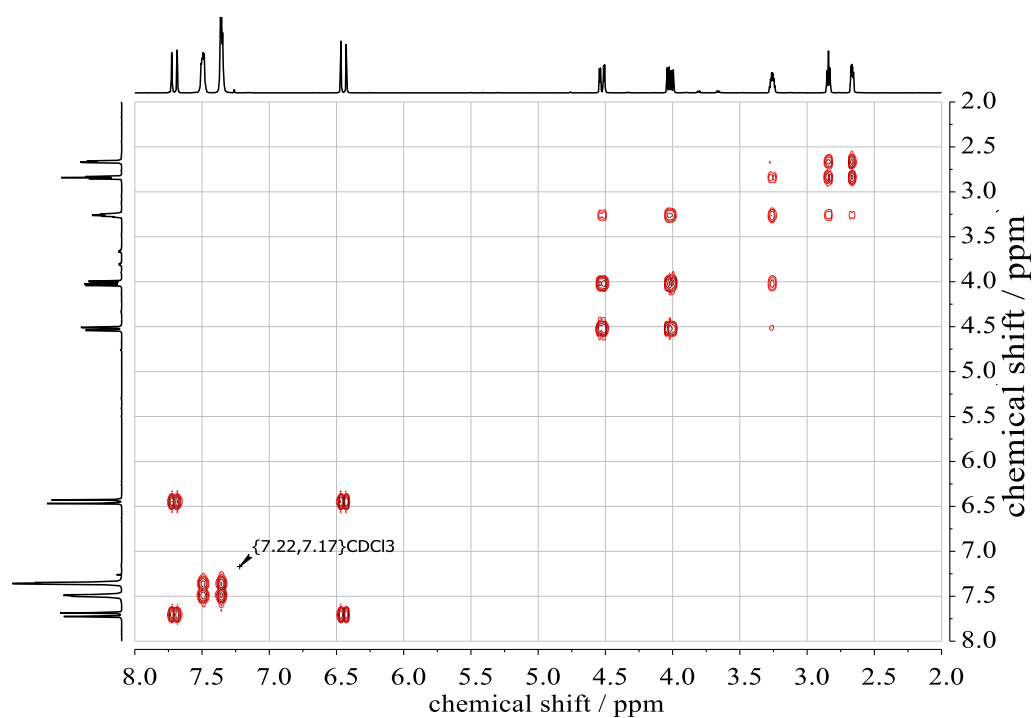
SI-Figure 4. ^{1}H, ^{1}H COSY NMR (400 MHz, C*D*Cl$_3$) of GC monomer.
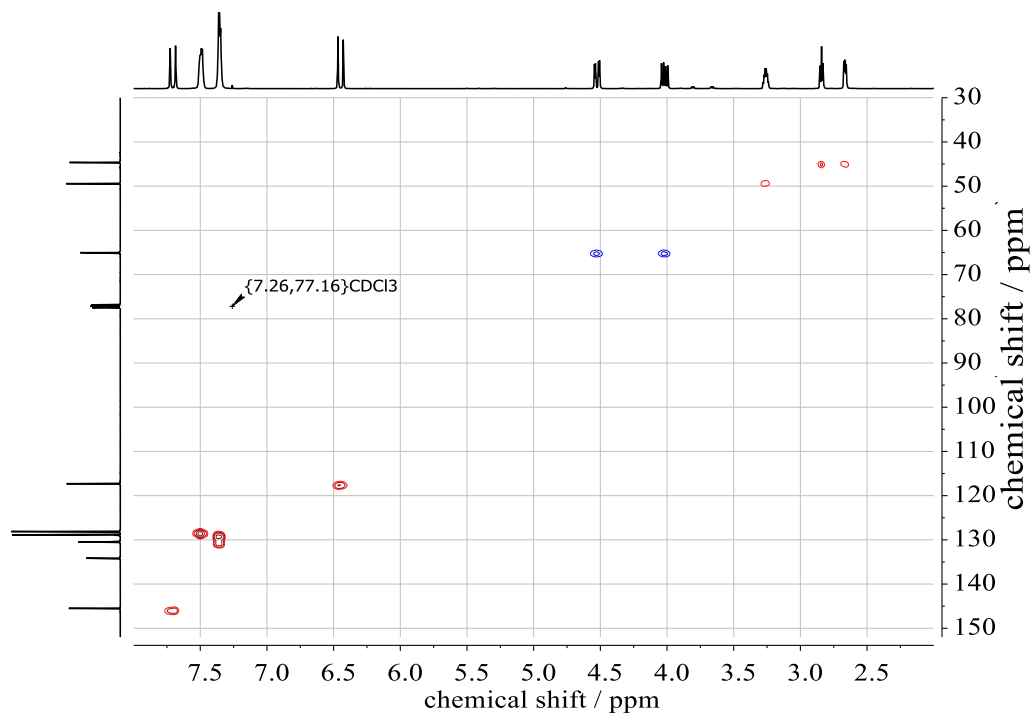
SI-Figure 5. ^{1}H, ^{13}C HSQC NMR of GC monomer in CDCl$_3$. Color of the signals indicates the phase information (red: methine proton, blue: methylene protons).

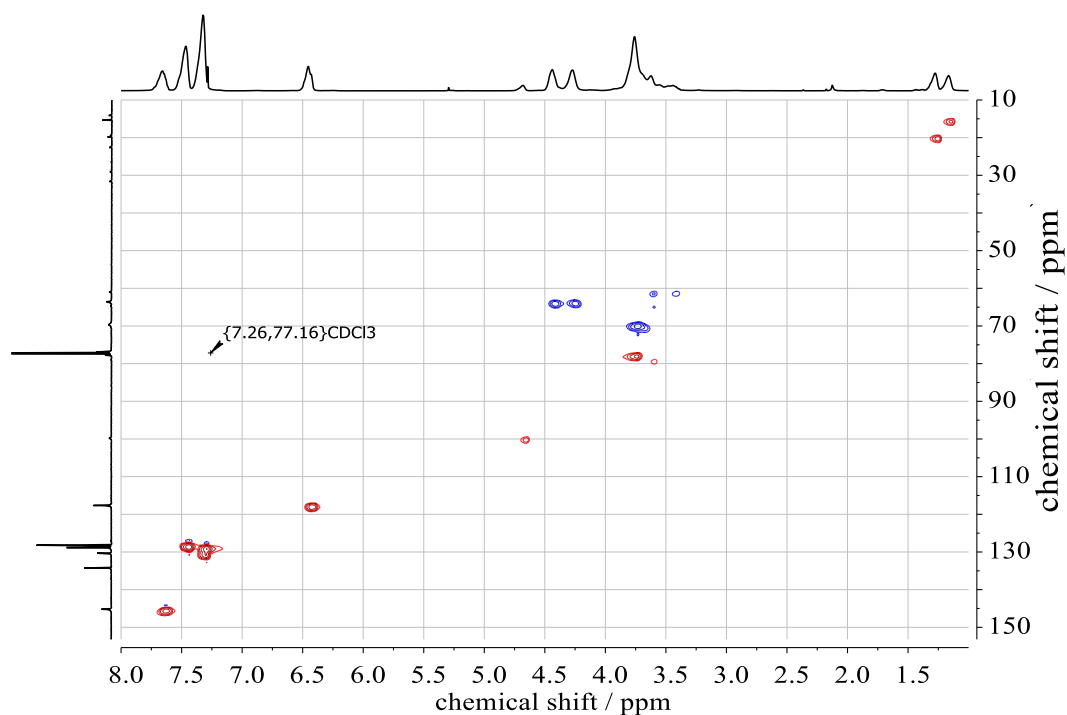**SI-Figure 6.** Superposition of RI and UV SEC traces (DMF, PEG standards) of P(EEGE$_{0.97}$-co-GC$_{0.03}$) (entry 8, **Table 1**).

**SI-Figure 7.** Complexation of *i*-Bu₃Al of PEEGE and PGC.

SI-Figure 8. Inverse gated ^{13}C NMR spectrum (150 MHz, C*D*Cl₃) of P(EEGE$_{0.84}$-*co*-GC$_{0.16}$) (entry 6, **Table 1**).
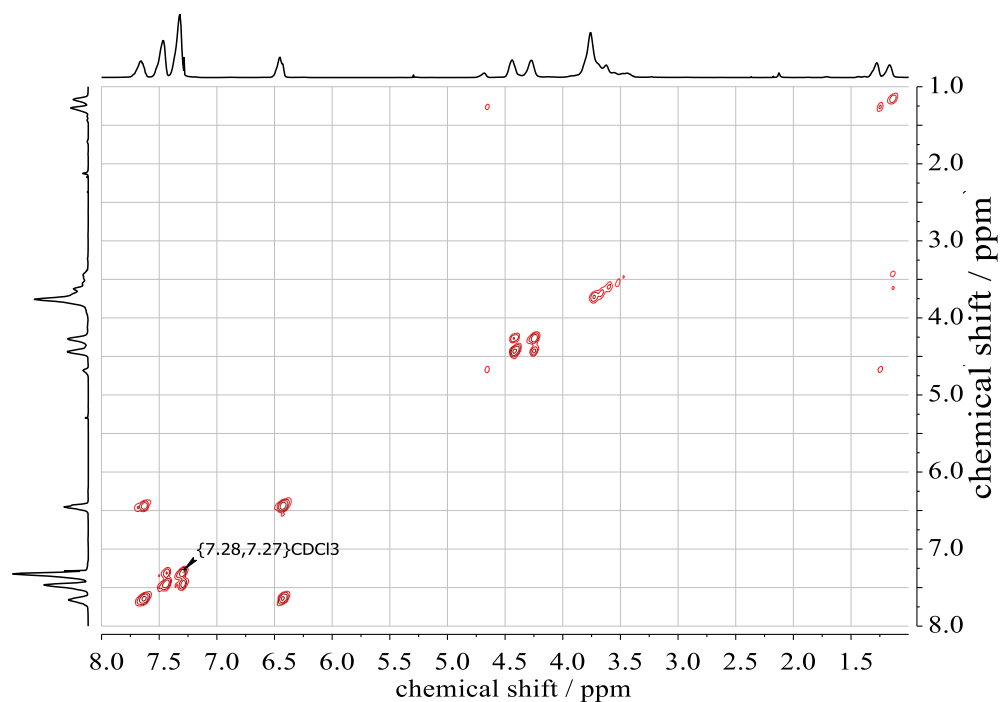
SI-Figure 9. ^{1}H, ^{1}H COSY NMR (600 MHz, CDCl$_3$) of P(EEGE$_{0.84}$-*co*-GC$_{0.16}$) (entry 6, **Table 1**).

SI-Figure 10. ^{1}H, ^{13}C HSQC NMR of P(EEGE$_{0.84}$-*co*-GC$_{0.16}$) (entry 6, **Table 1**) in CDCl$_3$. Color of the signals indicates the phase information (red: methyl / methine protons, blue: methylene protons).
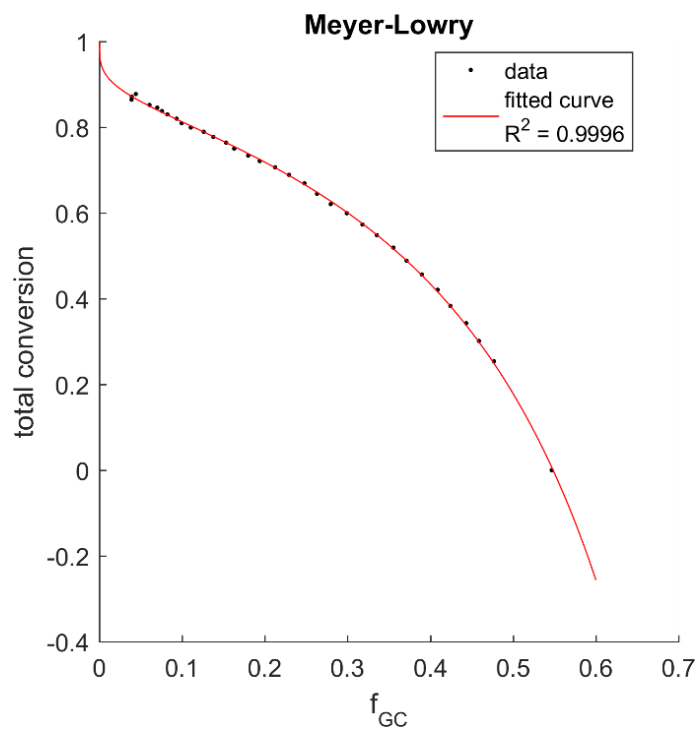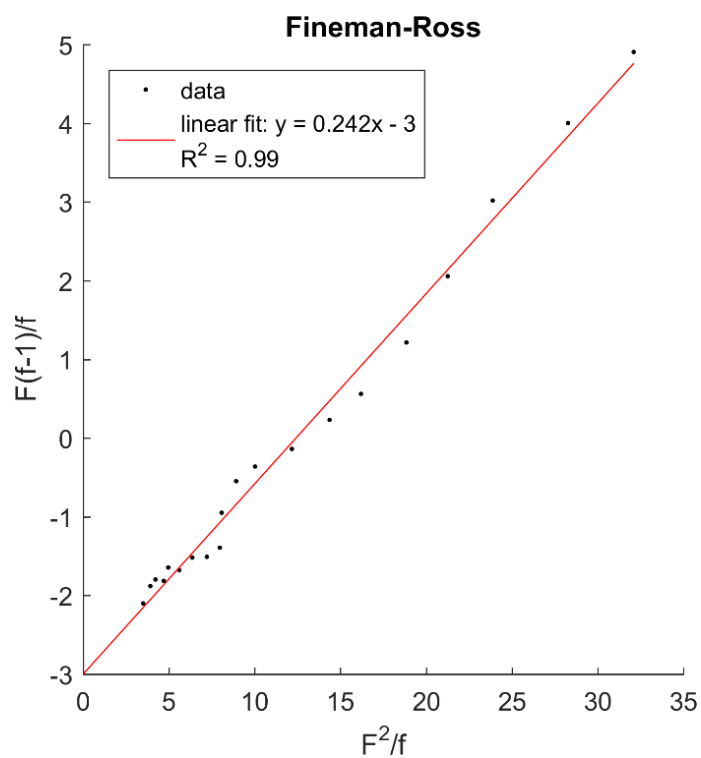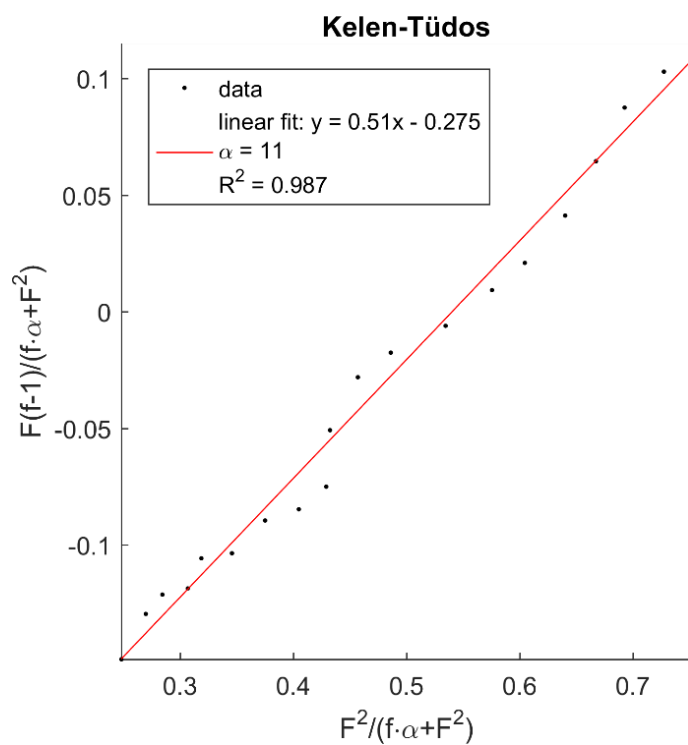
SI-Figure 11. Meyer-Lowry fit for determination of reactivity ratios of the EEGE/GC copolymerization.
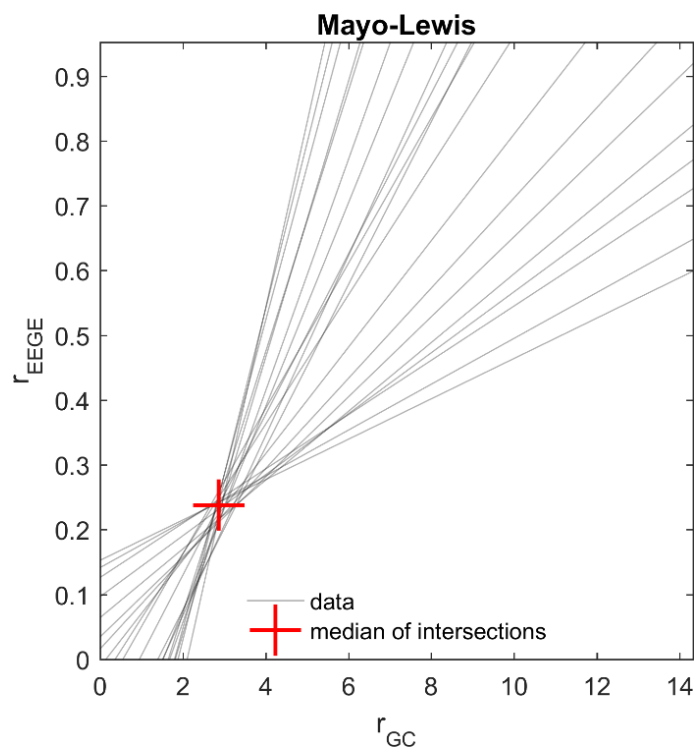
SI-Figure 12. Mayo-Lewis fit for determination of reactivity ratios of the EEGE/GC copolymerization.

SI-Figure 13. Fineman-Ross fit for determination of reactivity ratios of the EEGE/GC copolymerization.

SI-Figure 14. Kelen-Tüdős fit for determination of reactivity ratios of the EEGE/GC copolymerization.

**SI-Table 1.** Coordinates of EEGE determined by DFT calculations.

| Atom	*x-coordinate* / Å	*y-coordinate* / Å	*z-coordinate* / Å
C	0.69584981142474	0.84182649059141	-1.03107832274989
C	0.42981516495779	0.21584505479512	0.26257517591876
O	-0.12812296774754	1.49293957588247	-0.05453477669552
C	1.45880795221720	0.21325638344053	1.35976590845917
O	2.16677195136227	-1.00875156121085	1.28298101449223
C	3.02666777561716	-1.28337895116299	2.38702579090515
O	3.21348783973886	-2.65764414083924	2.46498997650405
C	4.38567036339129	-0.63573609258626	2.21012280384129
C	2.04801880911782	-3.40507129981717	2.81219289968290
C	2.44511658437132	-4.85949341043869	2.95450155567497
H	0.17305546222837	0.49261903789476	-1.91711502102055
H	1.66178696549529	1.30865834491411	-1.20650387103057
H	-0.29145578782194	-0.59808468382258	0.30545833376616
H	0.96044176506465	0.30890150646022	2.33632318786057
H	2.12092580710598	1.08059921940065	1.23562302828957
H	2.52718708007306	-0.91571177530558	3.30247398450397
H	4.85626768621454	-1.03009223937041	1.30778849674470
H	5.02160336040333	-0.85461194592223	3.06982857081610
H	4.28739932293439	0.44765469873491	2.11669141773896
H	1.28540790008215	-3.28056038353306	2.03706989583049
H	1.63764771061152	-3.01711913858508	3.75629480802924
H	2.85289196297729	-5.23788350293126	2.01456782068160
H	1.57415517409974	-5.46370249991122	3.22135791098450
H	3.20307230608072	-4.98054868667757	3.73172941077219

SI-Table 2. Coordinates of GC determined by DFT calculations.

| Atom	x-coordinate / Å	y-coordinate / Å	z-coordinate / Å
O	-0.63743073564652	1.15529059165816	0.02241995076104
C	-0.62173586316986	0.76400418923727	1.39626953789804
C	-1.20484670835902	-0.11160688515434	0.37781043256633
C	-0.46882829793232	-1.33105400167112	-0.09317985977775
O	-0.75730180385400	-1.62396215761769	-1.47236068990558
C	-1.89294714509388	-2.32045998774670	-1.71944074706016
C	-2.12673720832304	-2.56589140328495	-3.14926653268838
O	-2.63931832801341	-2.70248131511905	-0.84535192027636
C	-1.34126435906610	-2.10473931478058	-4.13167493731495
C	-1.51983453696762	-2.30095965591353	-5.56701755694803
C	-0.59916384887576	-1.71182802115374	-6.44321490772268
C	-0.71982033105174	-1.86330178354815	-7.81800182412858
C	-1.76672330942854	-2.61037331058614	-8.34408842467079
C	-2.69080074669560	-3.20409862776017	-7.48586521924545
C	-2.57029266422073	-3.05223886793990	-6.11464389996768
H	-1.27670859853479	1.32993327191481	2.05306479868901
H	0.36165709572494	0.53648267038497	1.80184299114385
H	-2.28711571483062	-0.15815989913302	0.29096645929856
H	-0.73239395660564	-2.19256226773700	0.52353479270632
H	0.60665926350744	-1.15752340905865	-0.06005760399875
H	-3.01597150925769	-3.15257184927557	-3.33994216640572
H	-0.47618057869667	-1.51528478298048	-3.84642134016552
H	0.21762053165213	-1.12803486533876	-6.03418646449563
H	0.00270253468236	-1.39838470575047	-8.47769527307597
H	-1.86508505084331	-2.73176005232042	-9.41599467931321
H	-3.50805765813041	-3.78795429617893	-7.89187090408974
H	-3.29676047196960	-3.52178926314585	-5.46397401181220

SI-Table 3. Coordinates of EO determined by DFT calculations.

| Atom	x-coordinate / Å	y-coordinate / Å	z-coordinate / Å
C	-5.31580396045005	0.27719546241736	0.04380125578157
C	-3.85555007036381	0.26289014833930	-0.04533378755923
O	-4.57367475955722	1.49666204477178	-0.00099855972908
H	-5.79699492011848	0.06301107826540	0.99345396308603
H	-5.90893046174849	0.06375792121888	-0.84045280077650
H	-3.37864572963725	0.03897063013281	-0.99490329451112
H	-3.26671009812471	0.03822271485447	0.83900322370834
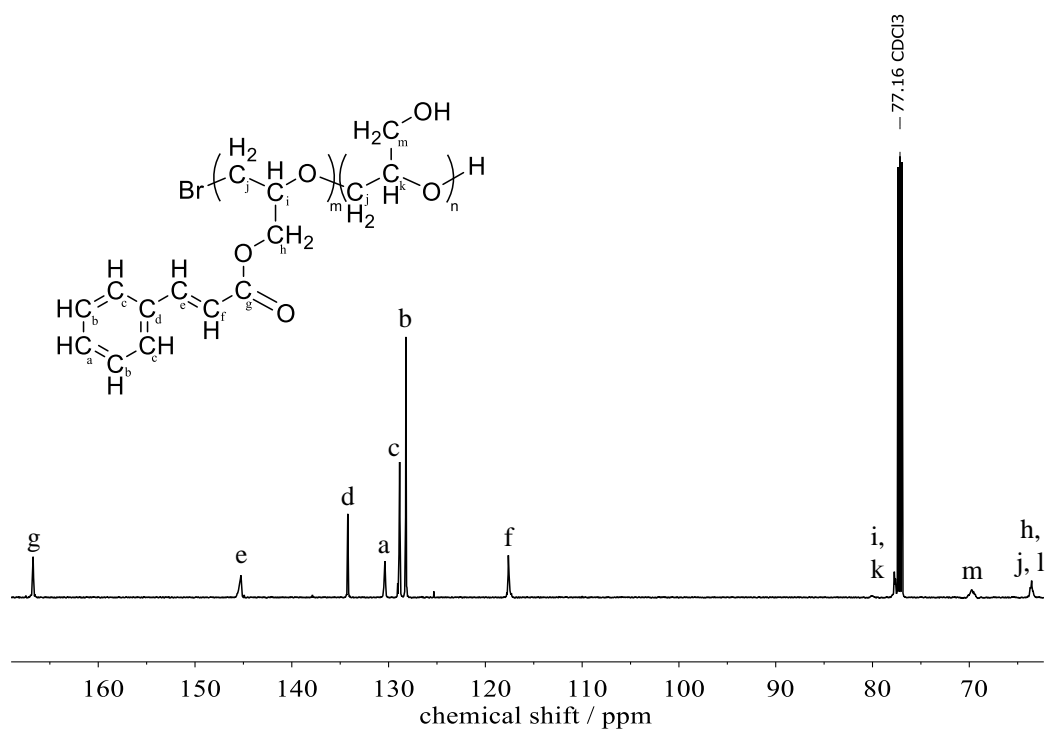
SI-Figure 15. Inverse gated ^{13}C NMR spectrum (150 MHz, CDCl$_3$) of P(G$_{0.18}$-co-GC$_{0.82}$) (entry 9, **Table 3**).
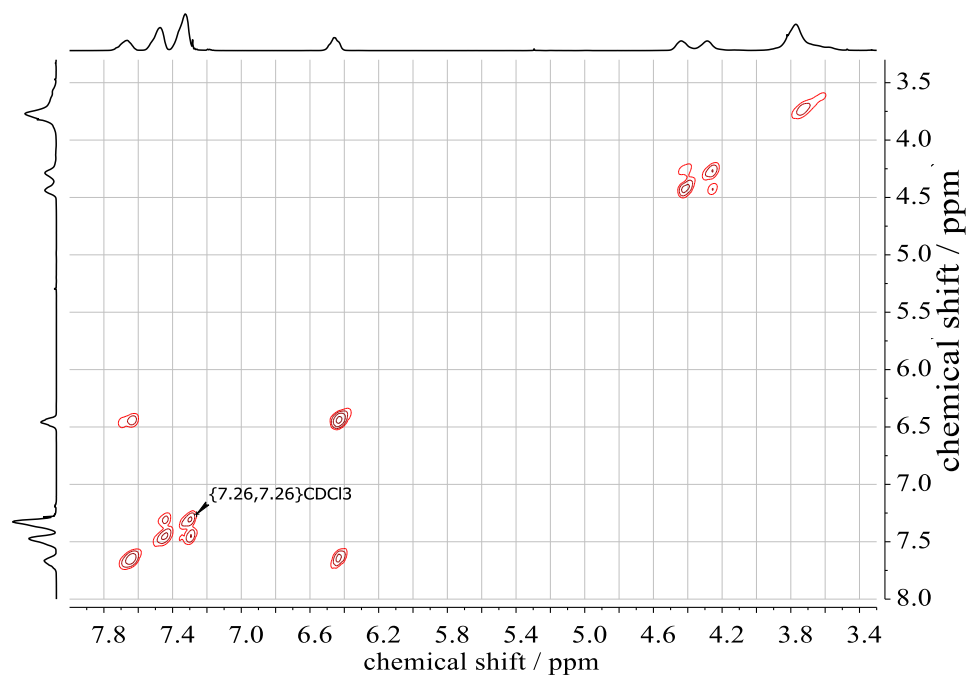
SI-Figure 16. ^{1}H, ^{1}H COSY NMR (600 MHz, C*D*Cl$_3$) of P(G$_{0.18}$-*co*-GC$_{0.82}$) (entry 9, **Table 3**).
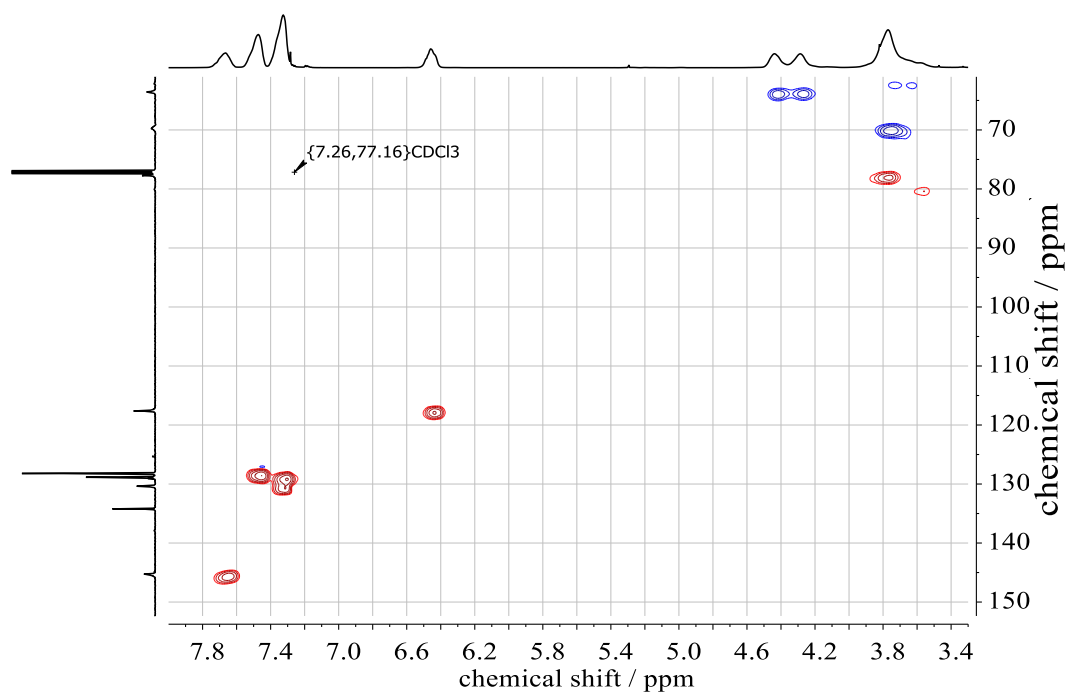
SI-Figure 17. ^{1}H, ^{13}C HSQC NMR of P(G$_{0.18}$-*co*-GC$_{0.82}$) (entry 9, **Table 3**) in C*D*Cl$_3$. Color of the signals indicates the phase information (red: methine protons, blue: methylene protons).
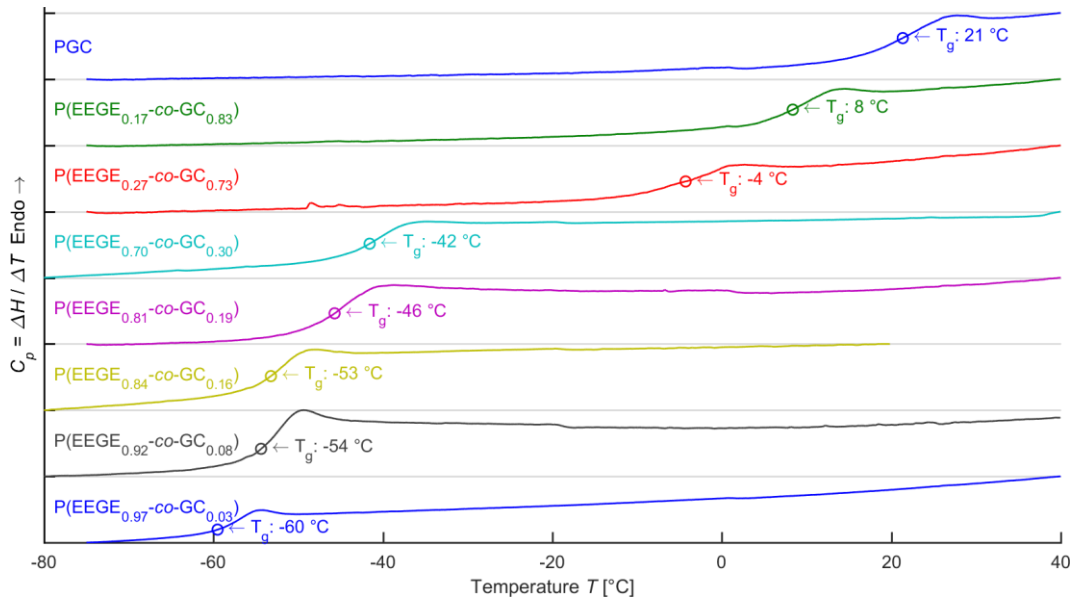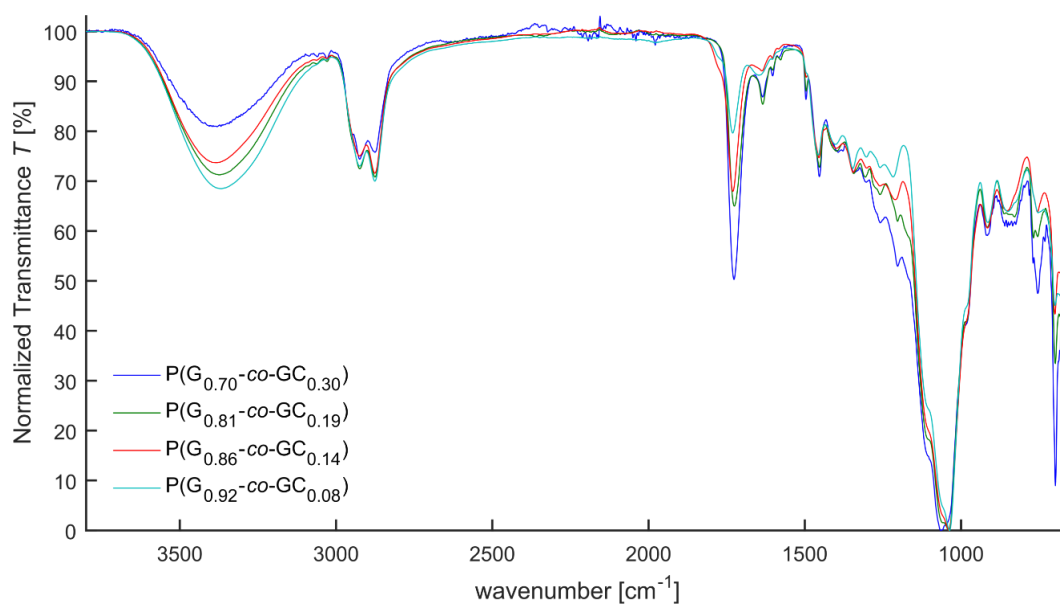
SI-Figure 18. DSC results for PGC homopolymer and P(EEGE-*co*-GC) copolymer samples (entries 1−8, **Table 1**).
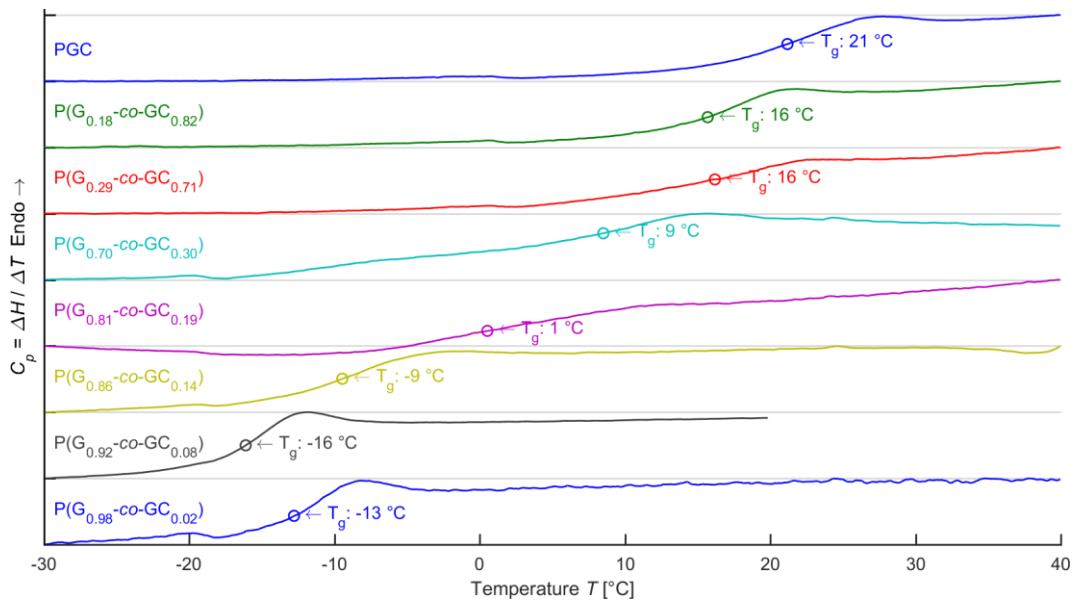
SI-Figure 19. DSC results for PGC homopolymer and P(G-*co*-GC) copolymer samples (entries 1 & 9−15, **Table 1**).
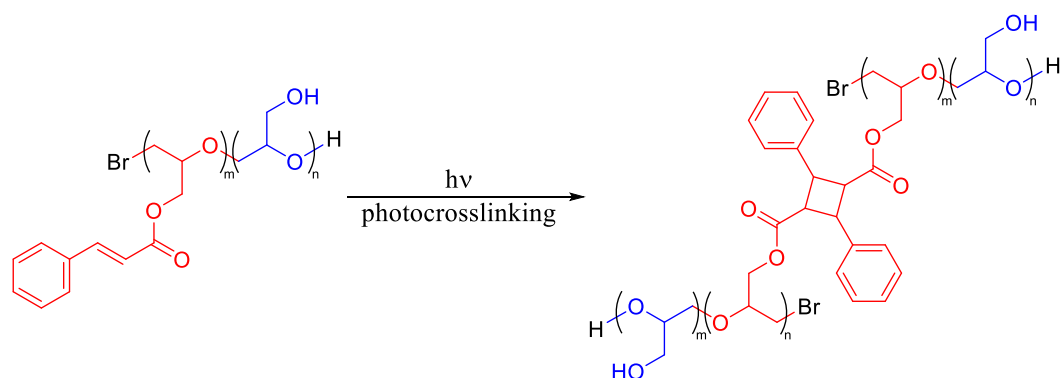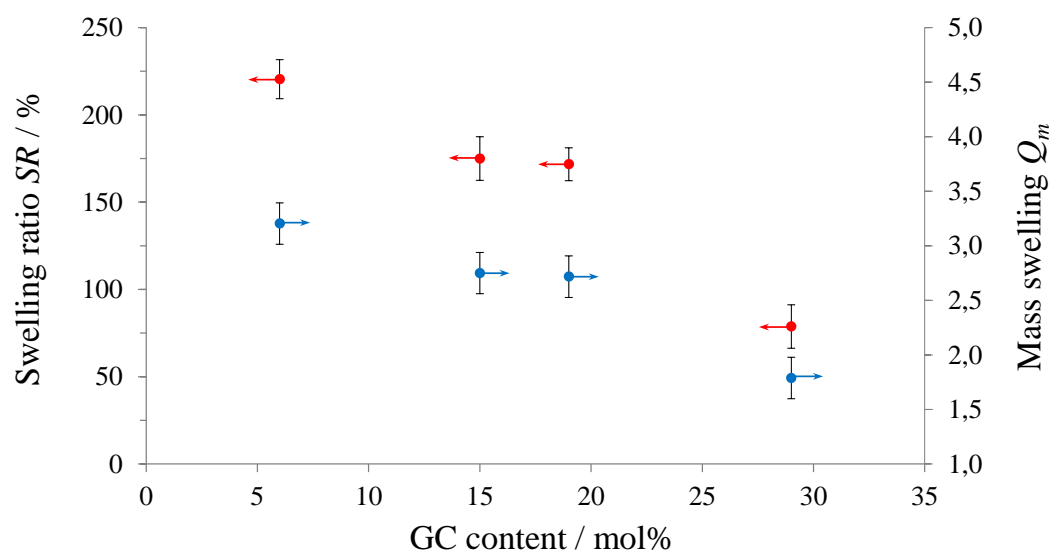
SI-Figure 20. Dimerization of P(G-*co*-GC) copolymers by photocrosslinking.

SI-Figure 21. Superimposed, normalized IR spectra of P(G-*co*-GC) hydrogels with various comonomer ratios.

SI-Figure 22. Swelling ratio (*SR*) of P(G-*co*-GC) copolymers as a function of GC content.

3. Preparation of Crosslinkable Micelles

3.1.   Ethoxy Butoxy Vinyl Glycidyl Ether: Reactive and Cleavable Multi-Vinyl Ether-Functional Poly(ethylene glycol)s for Drug Delivery Applications

Kamil Maciol[†], *Jan Blankenburg*[†,‡], *Karl Fischer*[§], *Matthias Bros*[∥], *Tassilo Gleede*[⊥], *Frederik R. Wurm*[⊥] and *Holger Frey*[†,*]

[†] Institute of Organic Chemistry, Johannes Gutenberg University Mainz, Duesbergweg 10-14, 55128 Mainz, Germany

[‡] Graduate School Materials Science in Mainz, Staudinger Weg 9, 55128 Mainz, Germany

[§] Institute of Physical Chemistry, Johannes Gutenberg-University Mainz, Duesbergweg 10-14, 55128 Mainz, Germany

[∥] Department of Dermatology, University Medical Center of the Johannes Gutenberg-University, Langenbeckstrasse 1, 55131 Mainz, Germany

[⊥] Max-Planck Institute for Polymer Research (MPI-P), Ackermannweg 10, D-55128 Mainz, Germany

*E-Mail: hfrey@uni-mainz.de

ABSTRACT

The novel bifunctional epoxide derivative ethoxy butoxy vinyl glycidyl ether (EBVGE) was developed to introduce both acid-cleavable acetal and reactive vinyl ether groups along the poly(ethylene glycol) (PEG) backbone. Anionic ring-opening polymerization (AROP) provided well-defined statistical PEG-*ran*-PEBVGE copolymers through copolymerization with ethylene oxide (EO) and *m*PEG-*b*-PEBVGE block copolymers using *m*PEG macroinitiators with systematically varied amount of EVBGE (2−100 mol%) in a molecular weight range of 2,600−11,700 g mol^{-1} ($Đ = M_w M_n^{-1} \leq 1.17$). Copolymerization kinetics by ^{1}H NMR spectroscopy proved an ideal, random incorporation of the comonomers with reactivity ratios of $r_{EO/EBVGE} = 1.0$. Studies of the thermal properties revealed glass transition temperatures (T_g) around -60 °C and melting points (T_m) between 33 °C and 53 °C. Besides the examination of the thermoresponsive behavior of the random copolymers, the self-assembly of the block copolymers into acid-degradable micelles in water was investigated. In this context, cytotoxicity was studied against mouse fibroblast L929 and human HEK-293T cells in the concentration range of 10−1,000 µg mL^{-1}, confirming excellent biocompatibility. Furthermore, core-crosslinking of the well-defined micelles by thiol-ene click chemistry and targeted cleavage under acidic conditions was examined using static- (SLS) and dynamic light scattering (DLS) and fluorescence correlation spectroscopy (FCS). Apart from the copolymers synthesized via AROP, EBVGE vinyl ether groups were reacted with maleic anhydride (MA) and *N*-phenylmaleimide (PM) by free-radical polymerization, demonstrating the bifunctionality of this monomer.

TABLE OF CONTENTS GRAPHICS
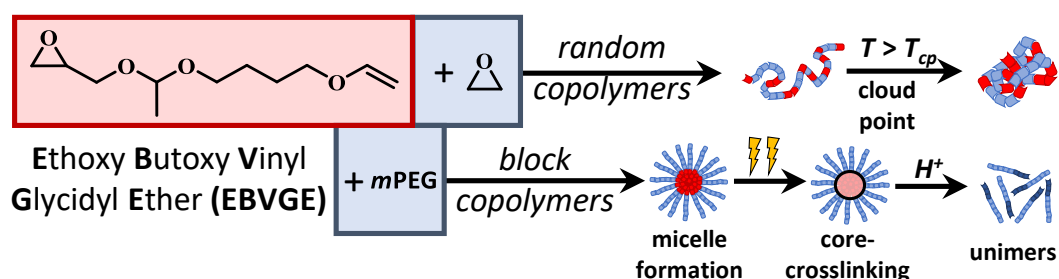
INTRODUCTION

In recent years, drug nanocarriers have become popular, since they permit to improve the pharmacological and pharmacogenetic properties of active ingredients.[1] Without suitable encapsulation and shielding, the therapeutic margin of a drug is often negatively influenced by the metabolism and the immune system.[2] A wealth of different materials has been established that are potentially suitable as nanocarriers: polymer-drug conjugates, polymeric micelles[3], dendrimers, liposomes, virus nanoparticles and carbon nanotubes.[4] Stimuli-responsive polymers also play an important role in this area in recent years. In the respective structures an external stimulus causes an abrupt change of the properties, which triggers the release of active ingredients in the targeted tissue. Stimuli can be physiological (pH change, redox potential, enzymatic activity) or of external nature (temperature, light, electric and magnetic fields, mechanical forces).[5] The system responds with abrupt changes in its properties, releasing the encapsulated active agent via precipitation, degradation, swelling or conformational changes.[6,7]

In this context, nanotechnology may well play a key role in the treatment of cancer in the future. Tumor tissue shows deficiencies in the vascular structure and also the lymphatic system due to their rapid cell growth. The resulting higher permeability of the tumor blood vessels compared to healthy tissue allows nanoparticles to diffuse more easily into the tumor tissue. Due to the deficient lymphatic system, nanoparticles accumulate in the tumor tissue, which is known as the enhanced permeation and retention (EPR) effect.[8] As a consequence of the overproduction of lactic acid, the extracellular pH in the tumor tissue is around 6.5, which can be exploited for cancer treatment by acid-labile nanoparticles.[9] Within the cells, the conditions are further tightened. Uptake of the nanoparticles into the cells takes place via endocytosis. The resulting endosomes fuse with lysosomes, which show a significantly reduced pH value (4−5) compared to the physiological conditions (7.4).[10] Consequently, acid-cleavable, polymeric micelles would be predestined for this application.[11–14]

Its outstanding biocompatibility and aqueous solubility renders poly(ethylene glycol) (PEG), also referred to as poly(ethylene oxide) (PEO), an excellent hydrophilic component for such micelles. PEG belongs to the class of aliphatic polyethers and can be synthesized by anionic ring-opening polymerization (AROP).[15] The low toxicity, immunogenicity and antigenicity are important properties of PEG compared to other polymers.[16–18] In addition to medicine, pharmaceutics and cosmetics, PEG-based polymers are broadly used as non-ionic surfactants and are even used for preservation.[19,20] Conventional PEG possesses only two functional groups (hydroxyl groups) on each chain end. For many applications, such as bioconjugation, specific

functional groups are required. By using appropriate initiators, endcapping- or functionalization reagents, these groups can be modified. In contrast, the copolymerization of EO with epoxide derivatives allows the introduction of functional groups into the polymer backbone, resulting in multi-functional PEGs.[21–26] In this manner, the properties of PEG can be tuned and expanded.

There are various approaches for the hydrophobic block. Recently, Kim *et al.* reported on the synthesis of acid-cleavable PEG-*b*-PTGE block copolymers, containing the novel hydrophobic, pH-responsive epoxide monomer tetrahydropyranyl glycidyl ether (TGE). In addition to a detailed characterization, they demonstrated that block copolymers containing the cyclic TGE moieties generally showed superior properties (stability, capacity, controllable degradation, etc.) compared to block copolymers with its acyclic analogue, ethoxyethyl glycidyl ether (EEGE).[27] In contrast, Yang *et al.* installed an acid-labile acetal cleavage site exactly between the hydrophilic PEG and the hydrophobic polylactide (PLA) block. Degradation could already be demonstrated at pH 6.5, which increased with decreasing pH value. Paclitaxel-loaded micelles showed an enhanced antitumor efficacy in *in vivo* and *in vitro* studies.[28] To enhance the stability of micelles, crosslinking is the means of choice.[29–31] In this regard, Zhong and co-workers crosslinked the micellar core by using photo-crosslinkable acryloyl groups in order to stabilize a diblock copolymer with acid-labile acetal moieties. Successful crosslinking was demonstrated in DLS studies. Additionally, the crosslinking had no significant influence on intracellular paclitaxel release.[32]

In this work, we present a novel bifunctional monomer for the synthesis of multi-functional PEGs: ethoxy butoxy vinyl glycidyl ether (EBVGE). EBVGE combines the acid lability of EEGE[33] or 1-(glycidyloxy)ethyl ethylene glycol ether (GEGE)[34] with a highly reactive vinyl group as in ethoxy vinyl glycidyl ether (EVGE)[35]. Random PEG-*ran*-PEBVGE copolymers were obtained by AROP from EBVGE and EO (**Scheme 1A**). In addition, we present the orthogonal copolymerization of electron-rich EBVGE vinyl ether groups with electron acceptors by free-radical copolymerization (**Scheme 1B**). *m*PEG-*b*-PEBVGE block copolymers were also synthesized and characterized in detail (**Scheme 1C**). In this context, we examined the self-assembly behavior of block copolymers in aqueous solution regarding their biocompatibility and their ability to form crosslinkable and pH-sensitive micelles.
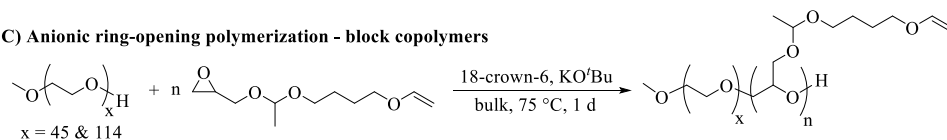
A) Anionic ring-opening polymerization - random copolymers

B) Free-radical copolymerization

X = O, N-Ph
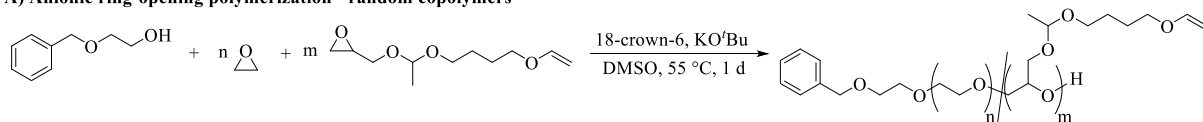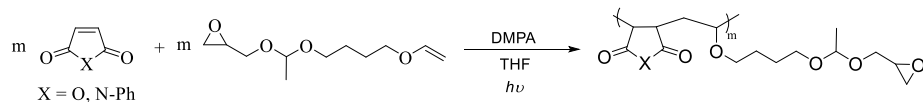
C) Anionic ring-opening polymerization - block copolymers

x = 45 & 114

Scheme 1. Synthetic route for different polymer architectures. A) Anionic copolymerization of EO and EBVGE yielding random PEG-*ran*-PEBVGE copolymers. B) Free-radical copolymerization of MA/PM and EBVGE. C) Synthesis of *m*PEG-*b*-PEBVGE block copolymers using *m*PEG macroinitiators.

EXPERIMENTAL PART

Materials. All chemicals and solvents were purchased from common suppliers such as Sigma-Aldrich, Acros Organics, Fluka or Roth. Unless otherwise stated, all chemicals were used without further purification. EBVGE was dried over CaH_2 and freshly distilled into a Schlenk tube, which was loaded with molecular sieve (3 Å). Suitable storage conditions (refrigerator, exclusion of light, inert gas) ensured that EBVGE could be kept stable and dry. After one year storage time the monomer was unchanged, which was evidenced by immediate polymerization without further purification procedures. Deuterated solvents were acquired from Deutero GmbH. Dialysis membranes (regenerated cellulose, $MWCO = 1,000$ g mol^{-1}) were obtained from Orange Scientific.

Instrumentation. ^{1}H NMR and ^{13}C NMR spectra, as well as two-dimensional spectra (COSY, HSQC, HMBC and DOSY) were recorded on a Bruker Avance II 400 (5 mm BBFO head with Z-gradient and ATM, SampleXPress 60 autosampler) at frequencies of 400 MHz (^{1}H) and 100 MHz (^{13}C). Chemical shifts (δ) are given in ppm and calibrated on an internal standard according to the residual proton signals of deuterated solvent. An Avance III HD 400 from Bruker was used for real-time ^{1}H NMR kinetic experiments, which was equipped with a 5 mm BBFO-SmartProbe (Z-gradient probe) and an ATM as well as a SampleXPress 60.

SEC measurements were conducted in DMF (containing 1 g L^{-1} lithium bromide as additive) on an Agilent 1,100 Series with a Polymer Standard Service (PSS) HEMA column (300/100/40 Å porosity), using RI and a UV (275 nm) detectors. The analyses were performed at a flow rate of 1 mL min^{-1} at 50 °C. All elugrams display the respective signal of the RI detector. Molecular weights were determined by calibration with linear PEG standards provided by PSS.

To determine the glass transition temperatures (T_gs) and melting points (T_ms), DSC curves were recorded using the Perkin Elmer 8,500 differential scanning calorimeter. Here, a temperature range of -90 °C to 100 °C was used with a heating rate of 20 K min^{-1} and a cooling rate of 10 K min^{-1}. A second heating cycle was performed at a heating rate of 10 K min^{-1}, which was used for evaluation.

Turbidity measurements for the quantification of the cloud points were performed on a JASCO V-640 spectrometer, equipped with a Jasco ETC-717 Peltier element. Here, the optical transmittance ($\lambda = 500$ nm) was measured using a quartz cuvette. The concentration of the

aqueous solution was 10 g L^{-1} at pH 7. The heating rate was 1 K min^{-1} within a temperature range of 10−90 °C.

Radical copolymerization and crosslinking experiments were performed via an UV lamp (XX-15B) from Ultra-Violet Products Ltd. The UV lamp was equipped with two UV tubes of the manufacturer Vilber Lourmat Deutschland GmbH of different wavelengths: 312 nm (T-15.M) and 365 nm (T-15.L).

The influence of block copolymers on the metabolic activity of cells was studied by MTT assays (Promega, Heidelberg, Germany). Mouse fibroblasts (L929) and human embryonic kidney cells (HEK-293T) were used as cell lines. 5,000 cells per well (100 µL) were seeded in 96-well cell culture plates. On the following day, the cells were incubated with different concentrations of *m*PEG-*b*-PEBVGE block copolymers (10–1,000 µg mL^{-1}). Negative controls were performed with 10% DMSO in medium. After the incubation period of 24 hours, MTT was introduced to each cell containing wells. Solubilization/stop solution was added after further incubated for 3-5 hours. The quantity of formed formazan was determined on an ELISA plate reader according to the manufacturer's protocol. Measured values shown in the histograms (**Figure 10**) are average values from at least three wells with corresponding standard error of the mean (SEM) as error. The results are normalized to the PBS control (10 vol%, corresponding to the highest block copolymer concentration of 1,000 µg mL^{-1}).

A DCAT 11 EC tensiometer (Dataphysics GmbH, Filderstadt, Germany) was used to measure the critical micelle concentration (CMC). The device was equipped with a TV 70 temperature control unit, a LDU 1/1 liquid dosing and refill unit and a Du Noüy ring RG 11. The ring was annealed with a Bunsen burner before the measurement. All solutions were stirred for 120 s with a stirring rate of 50%. After a rest period of 360 s, three surface tension measurements were recorded and averaged. For this purpose, an aqueous solution of *m*PEG$_{114}$-*b*-PEBVGE$_{13}$ (entry 6, **Table 4**) with a concentration of 2 g L^{-1} was used for the analysis. By plotting the surface tension against the surfactant concentration, the CMC could be determined by extrapolation of corresponding linear fitting curves at the intersection (**SI-Figure 29**).

Fluorescence correlation spectroscopy (FCS) measurements were performed using a Leica TCS SP8 AOBS SMD on a confocal microscope Leica DMi8CEL equipped with a HC PL APO 63x/1.20 W CORR CS2 water immersion objective optimized for FCS. Here, useable laser wavelengths of an argon-ion laser were 458, 476, 488, 496 and 514 nm (50 mW), with a DPSS-laser 561 nm (20 mW) or with a helium-neon laser 633 nm (10 mW). Two HyD detectors

(imaging) and one photomultiplier (PMT) tube for photon counting were employed. For FCS measurements the PicoHarp 300 Time-Correlated Single Photon Counting (TCSPC) module with the software SymPhoTime 64 (PicoQuant) for data evaluation was used. Low molar mass dyes used for calibration of the confocal volume were free Nile red in water ($D = 313.0 \ \mu m^2 \ s^{-1}$, $V_{eff} = 0.403$, $\kappa = 5.266$, $T = 293$ K) and free Rhodamine B in water ($D = 418.5 \ \mu m^2 \ s^{-1}$, $V_{eff} = 0.344$, $\kappa = 5.325$, $T = 293$ K) with 561 nm excitation at a concentration of 2−5 nM and detection wavelength of 571−700 nm. All FCS measurements were performed in FCS well plates (μ-Slide 8 well glass bottom by ibidi GmbH, ordering no. 80827) as aqueous solutions of identical dye concentrations for calibration (2−5 nM). mPEG$_{114}$-b-PEBVGE$_{13}$ (entry 6, **Table 4**) was used at a concentration of 1 g L^{-1} to ensure that its critical micelle concentration of 84.2 mg L^{-1} was always exceeded. 1 M hydrochloric acid was used for acidification to investigate the mechanism of dye release from the micelles. Data evaluation followed standard procedures provided with the SymPhoTime 64 software. The diffusion coefficients determined in the FCS measurements were used to calculate hydrodynamic radii using the Stokes-Einstein equation[36,37]:

$$R_H = \frac{k_B \cdot T}{6 \cdot \pi \cdot \eta \cdot D}$$

(1)

where k_B is the Boltzmann's constant $(1.38 \cdot 10^{-23} \ J \ K^{-1})$[38], T is the absolute temperature (293 K), η is the dynamic viscosity of water (1.0016 mPa)[39] and D is the diffusion coefficient.

Static (SLS) and dynamic light scattering (DLS) measurements were performed on an ALV spectrometer using aqueous solutions of the block copolymer mPEG$_{114}$-b-PEBVGE$_{13}$ (entry 6, **Table 4**) with a concentration of 2 g L^{-1}. The device was equipped with a goniometer and an ALV-5004 multiple-tau full-digital correlator (320 channels), which allows measurements over an angular range from 20° to 150°. A helium-neon laser operating at a laser wavelength of 632.8 nm was used as light source. For temperature-controlled measurements the light scattering instrument was equipped with a thermostat from JULABO GmbH. Diluted samples were filtered through PTFE membrane filters with a pore size of 0.45 μm (LCR syringe filters). Measurements were performed at 20 °C at different angles ranging from 30° to 150°.

A Malvern Zetasizer Nano ZS equipped with a Peltier-controlled thermostat was used to determine the particle sizes in the crosslinking studies of the micelles. Measurements were performed in disposable cuvettes from Brand GmbH & Co. KG. The measurement was conducted at a wavelength of 633 nm and a scattering angle of 173° at 25 °C. Samples were

filtered through a size of 0.45 µm LCR syringe filter to remove dust prior to measurement. Evaluation of the data were performed with Malvern Zetasizer series software v7.11.

Monomer synthesis (ethoxy butoxy vinyl glycidyl ether). The reaction protocol is inspired by the work of Fitton *et al.* on the synthesis of ethoxyethyl glycidyl ether (EEGE).[40] 1.8 mL (27.0 mmol, 1 equiv) Glycidol was added with 12.8 mL (81.0 mmol, 3 equiv) 1,4-butanediol divinyl ether (BDE) in a 100 mL flask and the mixture was cooled in an ice/water bath to 0 °C. The reaction was started by addition of 51 mg (0.3 mmol, 1 mol% with respect to glycidol, dissolved in 1 mL THF) *p*-toluenesulfonic acid monohydrate (*p*TSOH) and the mixture was allowed to warm up to room temperature. After four hours, *p*TSOH was removed by washing the solution three times (3 · 20 mL) with an aqueous solution of sodium bicarbonate $NaHCO_3$. After separating and drying of the organic phase over potassium carbonate K_2CO_3, excess of BDE was removed at 55 °C under reduced pressure. In the subsequent step, the temperature was raised and EBVGE was distilled at 84 °C and collected as a colorless liquid with a yield of 69%. ^{1}H NMR (400 MHz, $CDCl_3$): δ (ppm) = 6.40 (1H, dd, C$H_{\text{vinyl ether}}$, J = 14.4, 6.8 Hz), 4.70 (1H, p, CH_{acetal}, J = 5.4 Hz), 4.13 (1H, d, C$H_{2,\text{ vinyl ether}}$, J = 1.9 Hz), 4.09 (1H, d, C$H_{2,\text{ vinyl ether}}$, J = 1.9 Hz), 3.80–3.24 (6H, m, -O-CH_2-), 3.13–3.01 (1H, m, CH_{epoxide}), 2.74 (1H, ddd, C$H_{2,\text{ epoxide}}$, J = 5.4, 4.1, 1.4 Hz), 2.57 (1H, ddd, C$H_{2,\text{ epoxide}}$, J = 15.6, 5.1, 2.7 Hz), 1.75–1.55 (4H, m, -acetalO-CH$_2$-CH_2-CH_2-CH$_2$-O-), 1.26 (3H, dd, C$H_{3,\text{ acetal}}$, J = 6.2, 5.3 Hz). ^{13}C NMR (100 MHz, $CDCl_3$): δ (ppm) = 151.88 (C$H_{\text{vinyl ether}}$), 99.80 (CH_{acetal}), 86.28 (C$H_{2,\text{ vinyl ether}}$), 67.66 (-C$H_2$-O-CH=CH$_2$), 65.81–64.96 (-C$H_2$-O-$_{\text{acetal}}$), 50.81 (C$H_{\text{epoxide}}$), 44.50 (C$H_{2,\text{ epoxide}}$), 26.38 (-C$H_2$-CH$_2$-O-CH=CH$_2$), 25.94 (-C$H_2$-CH$_2$-CH$_2$-O-CH=CH$_2$), 19.60 (C$H_{3,\text{ acetal}}$).

Poly(ethylene glycol)-ran-poly(ethoxy butoxy vinyl glycidyl ether) (PEG-ran-PEBVGE). In the following, the described approach exemplifies the synthesis of sample PEG$_{16}$-*ran*-PEBVGE$_{44}$ (entry 4, **Table 1**). All other copolymers (entries 1−3, **Table 1**) and PEBVGE$_{31}$ homopolymer (entry 5, **Table 1**) were prepared in a similar fashion with correspondingly adapted ratios. 14.0 µL (0.1 mmol, 1 equiv) 2-(Benzyloxy)ethanol, 52.1 mg (0.2 mmol, 2 equiv) 18-crown-6 and 0.9 equiv (10 mg, 0.1 mmol) of potassium *tert*-butoxide (KO^{t}Bu) were introduced in a 100 mL Schlenk flask. In the next step, 1 mL THF and 6 mL benzene were added and the solution was stirred for 30 minutes in an inert argon atmosphere at 60 °C. Then, the solution was frozen and the flask was evacuated for 12 hours to remove traces of water. The flask was filled with argon and loaded with 10 mL of dry dimethyl sulfoxide (DMSO) and 0.9 mL (4.3 mmol, 44 equiv) of dried EBVGE. The solution was frozen with an ethanol cold bath (approximately -70 °C) and evacuated. In the subsequent step, 15 equiv (67.1 µL, 1.5 mmol) of

ethylene oxide (EO) were first condensed into an ampule to determine the volume and then into the reaction flask. After thawing, an oil bath preheated to 60 °C was placed under the flasks and the mixture was heated for 24 hours. The copolymerization was terminated by the addition of 1 mL methanol. To remove DMSO, 50 mL dichloromethane (DCM) was added, followed by five times washing with aqueous $NaHCO_3$ solution (5 · 20 mL) and subsequent dialysis against MeOH/DCM (3 : 2). To prevent hydrolysis of the cleavable EBVGE side groups, traces of $NaHCO_3$ were added to the dialysis solution. After drying under reduced pressure, PEG_{16}-*ran*-$PEBVGE_{44}$) was obtained as a viscous liquid with a yield of 80%.

Sample preparation for real-time ^1H NMR kinetics. To facilitate handling, an initiator stock solution was used. For this purpose, ten times of the required amount of 2-(benzyloxy)ethanol (23.3 µL, 0.2 mmol, 1 equiv), 18-crown-6 (86.8 mg, 0.3 mmol, 2 equiv) and KO^tBu (16.6 mg, 0.1 mmol, 0.9 equiv) were dissolved in 3 mL benzene and 0.5 mL THF and stirred for 30 minutes in an inert argon atmosphere at 60 °C. After the removal of the solvents overnight under reduced pressure, the initiator salt was dissolved in 1 mL dry DMSO-d_6. 0.1 mL of this solution and 50.8 µL (2.5 mmol, 15 equiv) of freshly dried EBVGE were transferred to a Norell S-5-400-VT-7 NMR tube, which was evacuated overnight and subsequently filled with argon. The solution was frozen in an ethanolic cold bath (-70 °C) and 0.5 mL dry DMSO-d_6 was added, which was also frozen. Once the NMR tube was evacuated, 29.8 µL (6.6 mmol, 40 equiv) EO was directly condensed into it. Then, the tube was sealed with a Teflon plug. After shaking for homogenization, the NMR tube was inserted into the preheated NMR spectrometer at 60 °C. When the temperature stabilized (~10 min, $\Delta T = 0.1$ K), the measurement was started. The sample rotation was turned off during the entire measurement period. Over a total period of six hours, two spectra were recorded each minute with one scan. A composition of PEG_{51}-*ran*-$PEBVGE_{29}$ was derived from the final ^1H NMR spectrum, which shows a quantitative conversion of comonomers. The associated SEC trace can be seen in **SI-Figure 1** ($M_n = 2,400$ g mol^{-1}; $Đ = 1.25$).

Poly(maleic anhydride-alt-ethoxy butoxy vinyl glycidyl ether) (P(MA-alt-EBVGE)). The free-radical copolymerization of MA and EBVGE described here (entry 1, **Table 3**) was performed analogously with *N*-phenylmaleimide (PM (entry 2, **Table 3**). 0.4 mL (1.8 mmol, 1 equiv) EBVGE was dissolved together with MA (0.3 g, 2.7 mmol, 1.5 equiv) and 20.2 mg (0.1 mmol, 3 wt% regarding to EBVGE and MA) of the photoinitiator 2,2-dimethoxy-2-phenylacetophenone (DMPA) in 10 mL of pure THF. The solution was degassed three times with the freeze-pump-thaw technique. Subsequently, the solution was stirred under irradiation

of UV light for two hours. The copolymer was precipitated in cold methanol and dialyzed against DCM. Typical yields were in the range of around 60%.

Methoxy poly(ethylene glycol)-block-poly(ethoxy butoxy vinyl glycidyl ether) (mPEG-b-PEBVGE). The synthesis for mPEG$_{45}$-b-PEBVGE$_{15}$ (entry 4, **Table 4**) is described below. All other block copolymers (entries 1−3/5−6, **Table 4**) were prepared with correspondingly adapted equivalents. 0.4 g (0.2 mmol, 1 equiv) mPEG$_{45}$ was mixed with 17.7 mg (0.2 mmol, 0.9 equiv) KO^{t}Bu and 92.5 mg (0.4 mmol, 2 equiv) 18-crown-6 in a flask and stirred in 6 mL of a mixture of benzene and THF (6 : 1) at 60 °C for 30 minutes. Then, the solution was frozen with liquid nitrogen and the flask was evacuated for 12 hours, allowing to warm up to room temperature. In the next step, the flask was filled with argon and 5 mL dry DMSO was injected into the flask via a syringe. The mixture was heated to 75 °C. After a homogeneous solution was formed, dried EBVGE (0.5 mL, 2.6 mmol, 15 equiv) was injected. After 24 hours, the polymerization was terminated by addition of 1 mL MeOH. For the removal of DMSO, 40 mL DCM was added and the solution was washed five times with aqueous NaHCO$_3$ solution (10 mL at a time). Subsequently, dialysis was performed against a mixture of DCM and MeOH (2 : 3). To prevent hydrolysis of the cleavable EBVGE side groups, traces of NaHCO$_3$ were added to the dialysis solution. Drying in vacuum led to typical yields over 80%.

Micelle preparation and crosslinking. Crosslinking experiments were divided into two different series (A: crosslinked micelles, B: non-crosslinked micelles) for comparability. Particle sizes were investigated in four environments: pure water, water with addition of a drop trifluoroacetic acid (TFA), pure methanol and methanol containing TFA (and traces of water). A) 34.0 µL ($8.9 \cdot 10^{-2}$ mmol) pentaerythritol tetrakis(3-mercaptopropionate) (PETMP) and 12.2 mg ($4.8 \cdot 10^{-2}$ mmol, 5 wt% regarding to EBVGE and PETMP) DMPA were dissolved in 1 mL of 2-methyltetrahydrofuran (MTHF). 0.1 mL of this solution was added to a solution of mPEG$_{114}$-b-PEBVGE$_{13}$ (entry 6, **Table 4**), containing 20 mg ($2.5 \cdot 10^{-3}$ mmol) of dissolved block copolymer in 0.1 mL MTHF. Subsequently, this mixture was slowly diluted with *Milli-Q water* to 20 mL, which corresponded to a surfactant concentration of 1 g L^{-1} containing 1% (v/v) MTHF. After 30 minutes of sonication, the solution was left to rest in a drying oven at 40 °C for 12 hours: Then, the solution was exposed to a UV lamp for two hours. Afterwards, the solution was filtered through a 0.45 µm LCR syringe filter. For aqueous experiments, two aliquots of 2 mL each were taken. Both were diluted with 2 mL Milli-Q water ($c = 0.5$ g L^{-1}), whereby a drop of TFA was added to one of the aliquots. For experiments in organic solvent, two aliquots (each 2 mL) were taken from the crosslinked stock solution and the *Milli-Q* water

was removed by lyophilization. Both aliquots were diluted with 4 mL MeOH ($c = 0.5$ g L^{-1}) after drying, whereby a drop of TFA and traces of Milli-Q water were added to one sample. Then, the samples were placed in a drying oven at 40 °C for 12 hours. B) Non-crosslinked micelles were prepared in the same way as described above, without the addition of PETMP/DMPA and irradiation with UV light.

RESULTS AND DISCUSSION

A.   Synthesis of KDGE monomer.

The drawbacks of our recently introduced acid-cleavable monomer ethoxy ally glycidyl ether (EAGE) was overcome by using a C4 spacer between the acetal group and the vinyl functionality.[41] As a consequence, EBVGE was copolymerized and incorporated in any ratio with ethylene oxide (EO), as the monomer no longer evaporates through the septum due to the higher boiling point during the copolymerization. In addition to a higher monomer yield, the starting materials are conveniently available commercially. Analogous to our EAGE work, the electrophilic addition of 1,4-butanediol divinyl ether (BDE) to glycidol was catalyzed by *p*-toluenesulfonic acid (*p*TSOH) (**Scheme 2**).
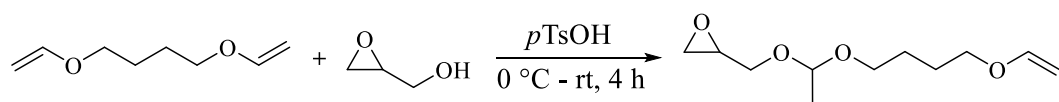
Scheme 2. Synthesis of EBVGE monomer.

It is important that BDE is used in excess due to its two equally reactive functionalities. Otherwise, reaction of the double electrophilic addition of glycidol to both vinyl ethers of BDE would significantly reduce the yield of the EBVGE monomer. Moreover, *p*TsOH must also be dissolved in an organic, unreactive solvent before addition to BDE and glycidol, as the catalyst is not soluble in the reagents. The catalyst can be removed by aqueous $NaHCO_3$ solution after the reaction. Under suitable conditions, the monomer can be kept for at least a year without degradation, which was evidenced by immediate polymerization without further purification procedures. Anhydrous conditions (for instance by addition of molecular sieve), exclusion of light and reduced temperatures are recommended. The analysis by ^{1}H NMR spectroscopy proves unequivocally the successful synthesis of EBVGE (**Figure 1**), which is further underpinned by additional NMR studies in **SI-Figures 2−6**.
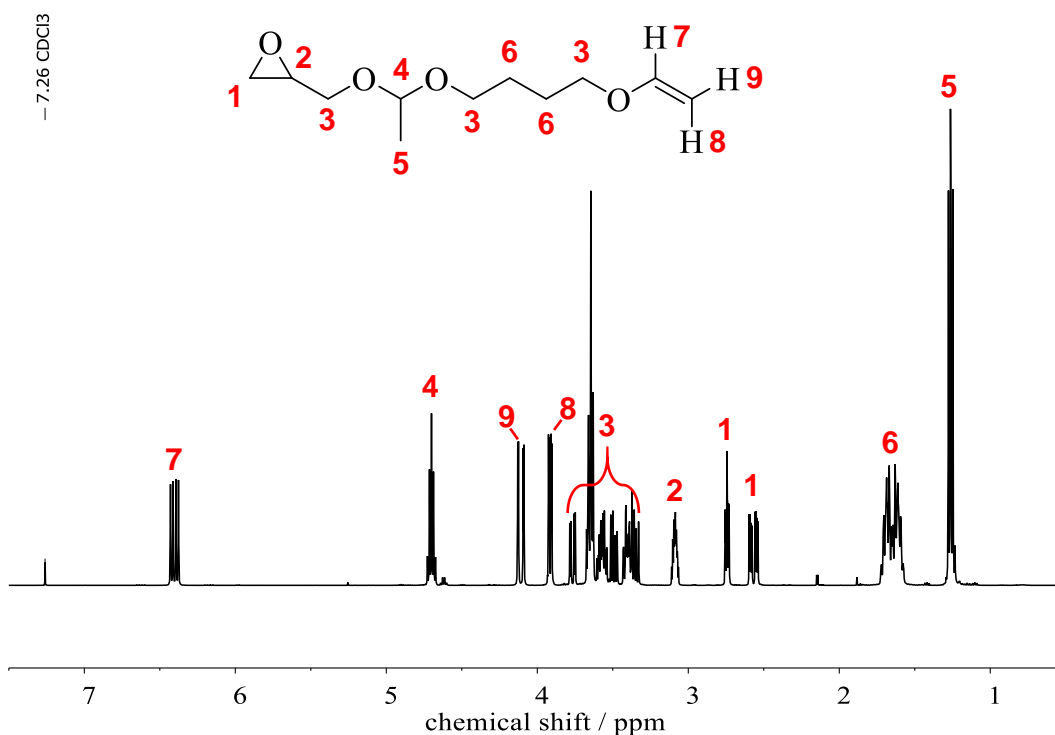
Figure 1. ^{1}H NMR spectrum (400 MHz, C*D*Cl$_3$) of EBVGE monomer.

B. Synthesis of random PEG-*ran*-PEBVGE copolymers, ^{1}H NMR kinetics and studies of the solution behavior.

It is well-known that crown ethers have a strong influence on the reaction rate of an alkoxide-based polymerization.[42,43] 18-Crown-6 in combination with potassium counterions enables the incorporation of glycidyl ethers into a polyether backbone in almost any ratio. Full conversion is only possible with the use of crown ethers in certain cases.[44,45] For the aforementioned reasons, this system was chosen. Best results for the copolymerization of EO and EBVGE were obtained in dimethyl sulfoxide as a solvent. Utilization of 2-(benzyloxy)ethanol as an initiator enabled the determination the absolute molecular weight from ^{1}H NMR spectra. The copolymerization conditions (elevated temperature, reaction times) were comparable to those already published in previous work.[23,46–49]

Ethoxy butoxy vinyl glycidyl ether (EBVGE) and ethylene oxide (EO) were copolymerized by anionic ring-opening polymerization (AROP), and a series of copolymers was prepared with systematically varied monomer ratios. **Figure 2** displays the recorded SEC traces of the copolymers and confirms their well-defined and narrow molecular weight distributions.
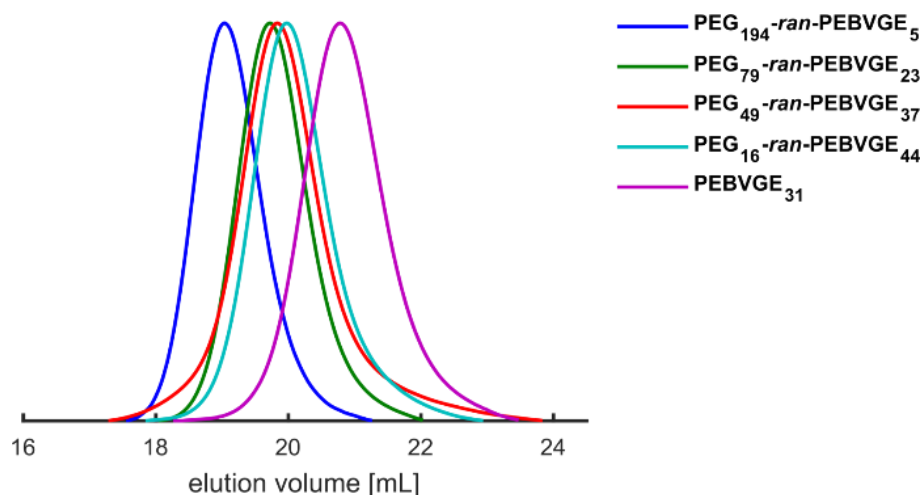
Figure 2. SEC traces (DMF, PEG-standard, RI detector) of all synthesized PEG-*ran*-PEBVGE copolymers (entries 1−4, **Table 1**) and PEBVGE$_{31}$ homopolymer (entry 5, **Table 1**).

The incorporation ratio of EBVGE was systematically varied between 2 mol% and 100 mol%. **Table 1** summarizes the complete synthesis results. Absolute molecular weights derived from ^{1}H NMR spectroscopy range between 6,700 g mol^{-1} and 10,200 g mol^{-1} with dispersities less than 1.18. The determined molecular weights obtained by NMR agree well with the theoretical values. A strong deviation of the SEC molecular weights from the theoretical values is noted. This effect increases with increasing incorporation ratio of the EBVGE moieties. In the case of PEBVGE$_{31}$ (entry 5, **Table 1**) homopolymer, it reaches a maximum deviation of 59%. The reason for this is the PEG-standard used for the SEC measurements. This has also been observed previously for other PEG copolymers with large side chains.[50] Due to the different hydrodynamic radii of PEG-*ran*-PEBVGE copolymers compared to pure PEG, the molecular weights obtained by SEC differ from the theoretical/calculated ones. In contrast to the recently reported EAGE monomer, the incorporation of more than 20 repeating units is possible for EBVGE.[41] This is attributable to the butoxy spacer, which raises the boiling point clearly above the polymerization temperature and thus prevents monomer diffusion through the septum.

**Table 1.** Overview of synthesized PEG-*ran*-PEBVGE copolymers and PEBVGE homopolymer.

No.	Composition[a]	M_n^{th} / g mol^{-1}	M_n^{b} / g mol^{-1}	M_n^{a} / g mol^{-1}	Đ
1	PEG$_{194}$-*ran*-PEBVGE$_5$	10,100	6,300	9,600	1.07
2	PEG$_{79}$-*ran*-PEBVGE$_{23}$	10,000	4,500	8,500	1.08
3	PEG$_{49}$-*ran*-PEBVGE$_{37}$	10,200	4,000	10,100	1.17
4	PEG$_{16}$-*ran*-PEBVGE$_{44}$	10,200	3,800	10,200	1.10
5	PEBVGE$_{31}$	6,500	2,700	6,700	1.10

[a] Values calculated by ^{1}H NMR spectroscopy. [b] Determined by SEC in DMF (PEG-standard).

Figure 3 shows the corresponding ^{1}H NMR spectrum of PEG$_{16}$-*ran*-PEBVGE$_{44}$ (entry 4, **Table 1**) including the complete assignment of all signals. As mentioned at the very beginning, the reliable molecular weights were calculated from the NMR spectra. For this purpose, the methylene group of the initiator (4.48 ppm) was used as a reference and compared with the integral of the isolated EBVGE acetal moieties (4.64 ppm) and the polyether backbone at 3.76–3.18 ppm. In the **SI-Figures 7−11** the associated ^{13}C NMR and 2D NMR spectra can be found.
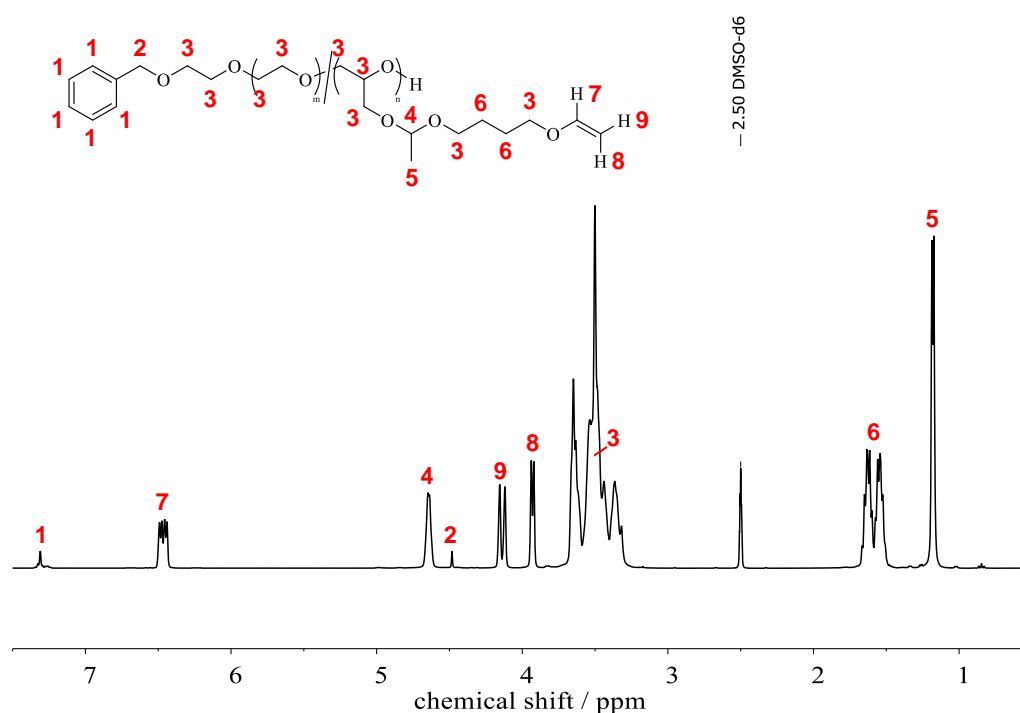
Figure 3. ^{1}H NMR spectrum (400 MHz, DMSO-d_6) of PEG$_{16}$-*ran*-PEBVGE$_{44}$ (entry 4, **Table 1**).

Real-time ^{1}H NMR kinetics was employed to examine the microstructure of PEG-*ran*-PEBVGE copolymers. In agreement with previous findings, a random incorporation of the glycidyl ether EBVGE and EO was assumed.[23,41,50–52] To verify this assumption, EBVGE and EO were copolymerized directly in an NMR tube at 60 °C and ^{1}H NMR spectra were recorded in narrow time intervals. Overlayed NMR kinetic spectra are shown in **Figure 4**. The integrals of the epoxide protons of EBVGE at 3.12–3.03 ppm (**Figure 4A**) and EO at 2.62 ppm (**Figure 4B**) were compared for evaluation. Considering the decreasing concentration of the comonomers with increasing polymerization time (**SI-Figure 12**), it can be observed that both monomers are consumed in an ideally random fashion. This clearly proves random incorporation of both monomers into the copolymers, as was generally observed before for other glycidyl ethers.[23,35,50]
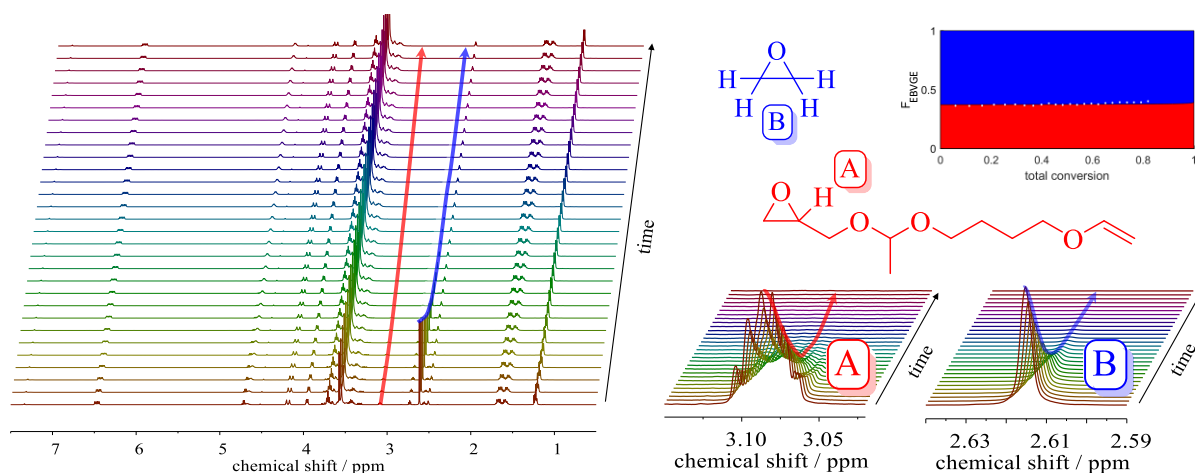
Figure 4. Left: Every 30th spectrum of the real-time ^{1}H NMR kinetics of the copolymerization of EBVGE and EO (400 MHz, 60 °C, DMSO-d_6). Right: Zoom of the characteristic monomer areas from the spectra used for the evaluation of the kinetic data and simulated copolymer composition as a function of the total monomer conversion. The color gradient was simulated based on the reactivity ratios according to Jaacks.[53] White dots are derived from real measurement points of the ^{1}H NMR kinetic studies.

To quantify the results, the reactivity ratios were calculated according to Jaacks.[53] As the comonomers are ideally randomly incorporated and no compositional shift is observed, other methods such as those of Meyer-Lowry[54] or Fineman-Ross[55] cannot be used. Reactivity ratios of $r_{EBVGE} = 0.99$ for EBVGE and $r_{EO} = 1.01$ for EO were determined from the measured data. The microstructure of the synthesized PEG$_{51}$-*ran*-PEBVGE$_{29}$ copolymer is graphically shown in **Figure 4** and was determined by means of these ratios.

Differential scanning calorimetry (DSC) was used to examine the thermal properties of PEG-*ran*-PEBVGE copolymers (entries 1−4, **Table 2**) and PEBVGE$_{31}$ homopolymer (entry 5, **Table 2**) more closely. All results are summarized in **Table 2**:

Table 2. Thermal properties of PEG-*ran*-PEBVGE copolymers and PEBVGE homopolymer.

No.	Composition[a]	mol% EBVGE	T_m / °C	ΔH / J g^{-1}	T_g / °C
1	PEG$_{194}$-*ran*-PEBVGE$_5$	2	44	87	-60
2	PEG$_{79}$-*ran*-PEBVGE$_{23}$	22	-	-	-63
3	PEG$_{49}$-*ran*-PEBVGE$_{37}$	43	-	-	-63
4	PEG$_{16}$-*ran*-PEBVGE$_{44}$	73	-	-	-63
5	PEBVGE$_{31}$	100	-	-	-64

[a] Values calculated by ^{1}H NMR spectroscopy

The glass transition (T_g) of pure PEG with a comparable molecular weight is -60 °C.[56] While PEBVGE$_{31}$ (entry 5, **Table 2**) homopolymer exhibits a slightly lower T_g of -64 °C, the T_gs of the copolymers (entries 1−4, **Table 2**) vary between these two values. This is attributable to the flexible side groups of the pendant EBVGE groups, which increase the free volume for the polymer chains.[57] A melting point (T_m) of 44 °C was only observed for PEG$_{194}$-*ran*-PEBVGE$_5$ (entry 1, **Table 2**). Since the real-time ^{1}H NMR kinetics showed an ideal, random incorporation of the comonomers, the average size of the PEG segments within the copolymer chains can thus be estimated. Crystallization of PEG homopolymer requires approximately 13 EO repeating units (PEG-600), whereas PEG-400 (9 EO units) is already a non-volatile liquid at room temperature.[58] Transferred to the copolymers shown here, PEG$_{194}$-*ran*-PEBVGE$_5$ (entry 1, **Table 2**) possesses PEG segments with an average length of 39 EO units, while PEG$_{79}$-*ran*-PEBVGE$_{23}$ (entry 2, **Table 2**) contains only 3 EO units on average and therefore ten EO repeat units less compared to PEG-600.

Thermal (and pH) responsiveness in a polymer is promising for instance in gene delivery and tissue engineering applications.[59] Schmaljohann wrote a very detailed and informative review on stimuli-responsive polymers in drug delivery applications.[6] By incorporating EBVGE into a polyether backbone, both stimuli can be combined in one copolymer. As only PEG$_{194}$-*ran*-PEBVGE$_5$ (entry 1, **Table 1**) was still water-soluble due to the low EBVGE mole fraction, this sample was examined in detail. **Figure 5** shows the results of turbidimetry to determine the cloud point (T_c):
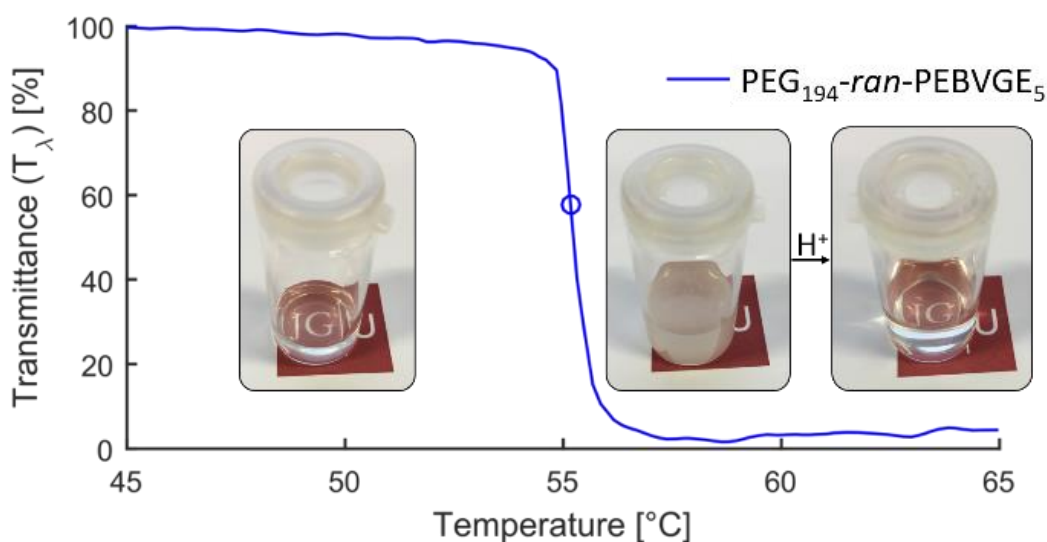
Figure 5. Temperature-dependent solution behavior of PEG$_{194}$-*ran*-PEBVGE$_5$ (entry 1, **Table 1**). Left: clear copolymer solution below the T_c. Middle: precipitated copolymer above the T_c. Right: irreversible cleavage of the hydrophobic side groups by acidification and the resulting re-solubilization of the polyether residues.

The T_c was defined as the turning point of the curve and is 55.2 °C. The left and middle pictures illustrate the drastic difference in the solution behavior. Acidification of the sample led to a clarification of the solution, which is shown in the picture on the right. This is caused by the cleavage of the hydrophobic pendant EVBGE groups, leading to the formation of the water-soluble linear polyglycerol copolymer PEG-*co*-PG and the soluble by-products acetaldehyde and 1,4-butanediol.
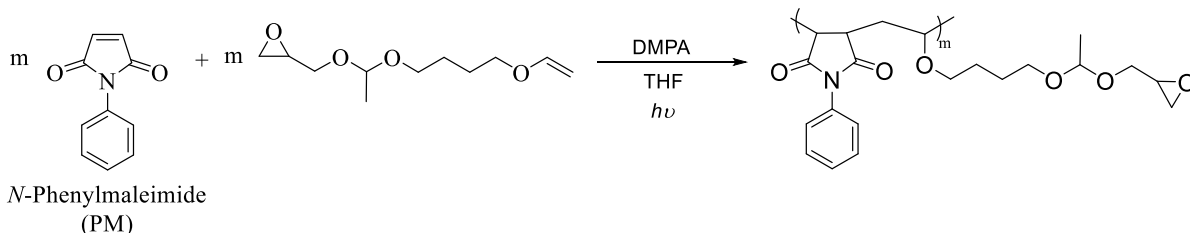
C.   Radical copolymerization of EBVGE.

Epoxy functionalities are highly relevant for industrial applications in the form of resins.[60] The mechanical properties and temperature resistance of uncured epoxy resins can be improved by crosslinking with polyfunctional primary amines as hardeners.[61] In this context, the bifunctional EBVGE monomer is a promising candidate, since the polymerization of its vinyl ether functionalities would provide access to acid degradable epoxy resins. However, vinyl ethers are well known for not homopolymerizing by free-radical polymerization. The reason for this is their electron donor nature due to their electron-rich double bond and the low stability of radicals formed.[62] In order to stabilize vinyl ethers, other methods, such as Friedel-Crafts-type catalysts, must normally be used. An elegant way to polymerize vinyl ethers under free-radical conditions is the polymerization with electron acceptors such as maleic anhydride.[63] To

demonstrate the radical copolymerization, EBVGE was copolymerized with MA and PM (**Scheme 3**).
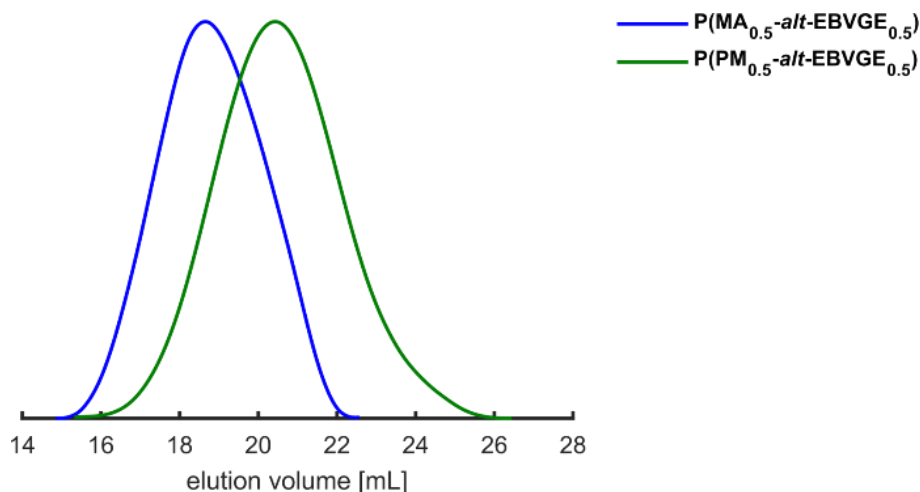
A) P(MA-*alt*-EBVGE)

Maleic anhydride
(MA)

B) P(PM-*alt*-EBVGE)
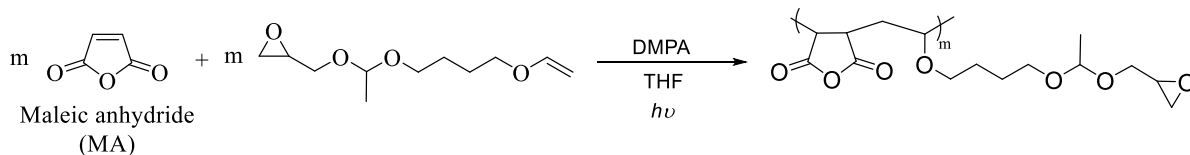
N-Phenylmaleimide
(PM)

Scheme 3. Copolymerization of EBVGE and maleic anhydride (MA, A) and *N*-phenylmaleimide (PM, B) via free-radical polymerization.

Figure 6 depicts the monomodal molecular weight distributions obtained from SEC measurements.

Figure 6. SEC traces (DMF, PS-standard, RI detector) of synthesized P(MA$_{0.5}$-*alt*-EBVGE$_{0.5}$) (entry 1, **Table 3**) and P(PM$_{0.5}$-*alt*-EBVGE$_{0.5}$) (entry 2, **Table 3**) copolymers.

Table 3 summarizes the overall synthesis results. The relative broad dispersities of 1.57 and 1.92 are common for free-radical polymerization. Molecular weights shown here are in the range of 3,400−9,200 g mol^{-1}, calibrated with polystyrene standards. The absence of integrable initiator signals prevented the determination of absolute molecular weights by NMR spectroscopy. Nevertheless, the comonomer ratios could be determined. The equimolar ratios

of the comonomers determined by NMR spectroscopy support at an alternating copolymerization of the donor-acceptor monomer pair described above, which has to be quantified by a precise investigation of the reaction kinetics. The thermal properties are fully in line with theoretical expectation. Due to the bulky side groups, the mobility of the main chain is generally limited. As a result, the T_gs are far above those of the random PEG-*ran*-PEBVGE copolymers. These effects are enhanced by the additional phenyl group in P(PM$_{0.5}$-*alt*-EBVGE$_{0.5}$) (entry 2, **Table 3**), leading to an increase of 60 °C compared to P(MA$_{0.5}$-*alt*-EBVGE$_{0.5}$) (entry 1, **Table 3**). A comparison of the T_g of P(MA$_{0.5}$-*alt*-EBVGE$_{0.5}$) (entry 1, **Table 3**) with poly(methyl vinyl ether-*alt*-maleic anhydride)s reveals differences of more than 100 °C.[64] This can be attributed to the flexible EBVGE side groups, increasing the mobility of the main chain. However, if a comparable structure like poly(dodecyl vinyl ether-*alt*-*N*-phenyl maleimide) is considered , the difference is only about 10 °C.[65]

Table 3. Synthesis results for the EBVGE-maleic anhydride (MA), respectively *N*-phenylmaleimide (PM) copolymers by free-radical polymerization.

No.	Composition[a]	M_n[b] / g mol^{-1}	Đ	T_g / °C
1	P(MA$_{0.5}$-*alt*-EBVGE$_{0.5}$)	9,200	1.57	26
2	P(PM$_{0.5}$-*alt*-EBVGE$_{0.5}$)	3,400	1.92	86

[a] Values calculated by ^{1}H NMR spectroscopy. [b] Determined by SEC in DMF (PS-standard).

The successful copolymerization was further proven by ^{1}H NMR spectroscopy, as shown in **Figure 7** for P(MA$_{0.5}$-*alt*-EBVGE$_{0.5}$) (entry 1, **Table 3**). In the ^{1}H NMR spectrum, all units were clearly identified and assigned, such as the acetal units (4.67 ppm) or the epoxy groups (3.08−2.56 ppm) of the EBVGE moieties. Corresponding ^{13}C NMR and 2D NMR spectra can be found in **SI-Figures 14−17**. The same applies to the spectra in **SI-Figures 18−22** of P(PM$_{0.5}$-*alt*-EBVGE$_{0.5}$) (entry 2, **Table 3**).
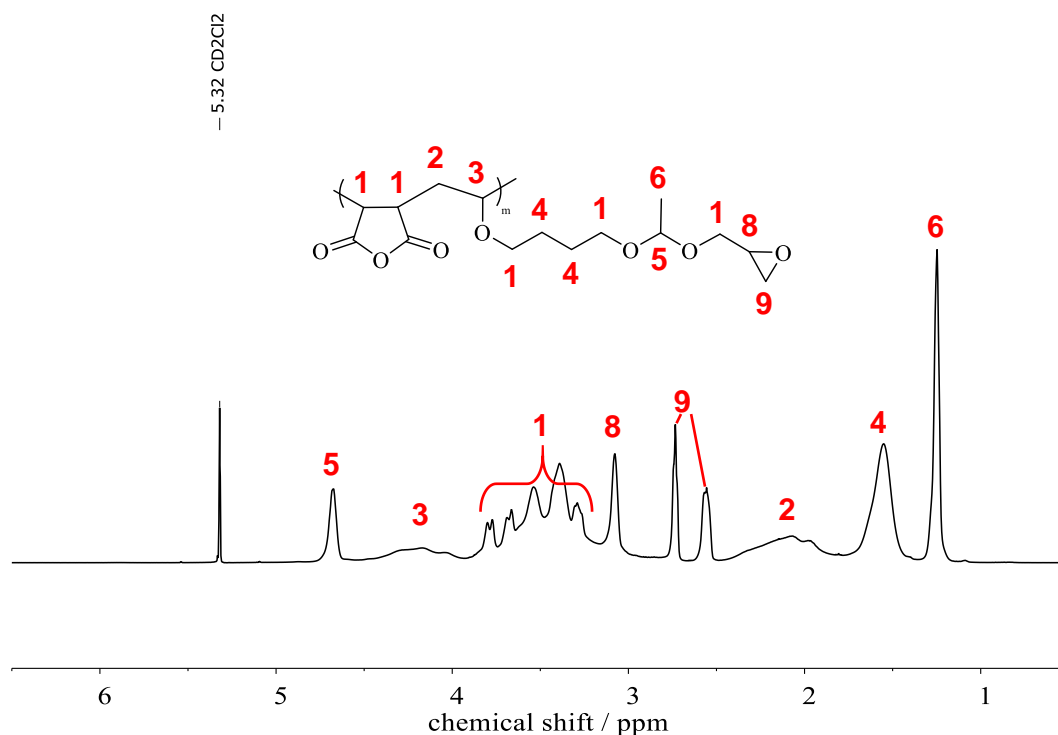
Figure 7. ^{1}H NMR spectrum (400 MHz, CD_2Cl$_2$) of P(MA$_{0.5}$-*alt*-EBVGE$_{0.5}$) (entry 1, **Table 3**).

D. Synthesis of *m*PEG-*b*-PEBVGE block copolymers, characterization and studies of the micellar behavior.

The stability of polymeric micelles is a major problem regarding their use for the transport of drugs. Thus, the dilution in the bloodstream or the interaction with plasma proteins such as albumin may lead to the dissolution of micellar structures.[66] In this context, the formation of pH-sensitive and crosslinkable micelles from mPEG-*b*-PEBVGE block copolymers is discussed in detail below. A series of well-defined block copolymers was prepared with systematically varied EBVGE mole fraction and macroinitiator size. The superimposed SEC traces of the *m*PEG$_{45}$-*b*-PEBVGE block copolymers including the pure macroinitiator *m*PEG$_{45}$ are shown in **Figure 8**, those for *m*PEG$_{114}$-*b*-PEBVGE$_{13}$ (entry 6, **Table 4**) and *m*PEG$_{114}$ are shown in **SI-Figure 23**.
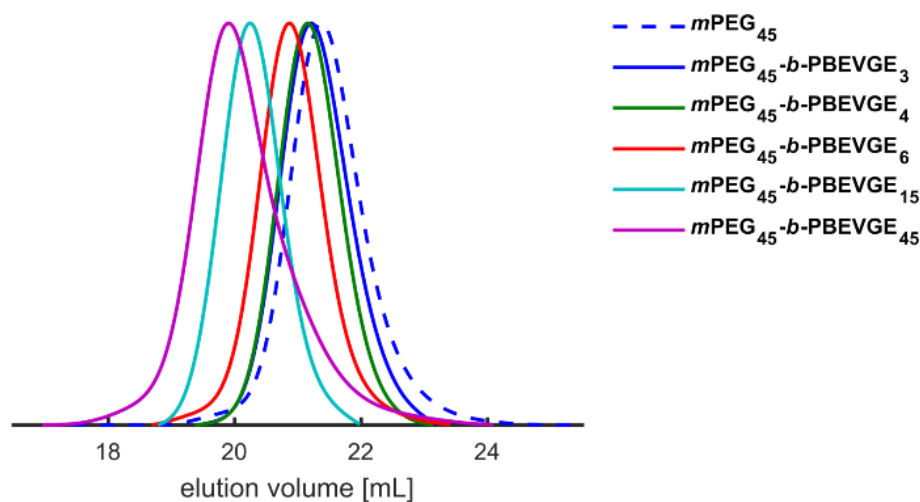
Figure 8. SEC traces (DMF, PEG-standard, RI detector) of all synthesized mPEG$_{45}$-b-PEBVGE block copolymers (entries 1−5, **Table 4**) and pure mPEG$_{45}$.

An overview of all samples can be found in **Table 4**. The molecular weights range from 2,600 g mol^{-1} to 11,700 g mol^{-1} with dispersities below 1.17. The deviation between the SEC and NMR molecular weights which was observed for the random PEG-ran-PEBVGE copolymers is also observed here. In analogy to the previous elaborations, the difference increases with increasing EBVGE incorporation ratio, due to the differing hydrodynamic radii of the functional block copolymers compared to the pure PEG standard. Within the error range, the desired comonomer ratios were generally achieved also for the block copolymers.

Table 4. Overview of synthesized mPEG-b-PEBVGE block copolymers.

No.	Composition[a]	M_n^{th} / g mol^{-1}	M_n^{b} / g mol^{-1}	M_n^{a} / g mol^{-1}	Đ
1	mPEG$_{45}$-b-PEBVGE$_3$	2,500	2,300	2,600	1.06
2	mPEG$_{45}$-b-PEBVGE$_4$	2,600	2,400	2,800	1.05
3	mPEG$_{45}$-b-PEBVGE$_6$	3,100	2,700	3,300	1.07
4	mPEG$_{45}$-b-PEBVGE$_{15}$	5,200	3,600	5,200	1.05
5	mPEG$_{45}$-b-PEBVGE$_{45}$	11,700	3,700	11,700	1.16
6	mPEG$_{114}$-b-PEBVGE$_{13}$	7,800	6,100	7,900	1.04

[a] Values calculated by ^{1}H NMR spectroscopy. [b] Determined by SEC in DMF (PEG-standard).

Figure 9 shows the ^{1}H NMR spectrum of mPEG$_{45}$-b-PEBVGE$_{15}$ (entry 4, **Table 4**). Further details are available in the Supporting Information (**SI-Figures 24−28**). Any characteristic signals, such as the acetal or double bond protons of the EBVGE units at 6.74−3.93 ppm, can

be uniquely assigned. The isolated methoxy unit at 3.24 ppm of the *m*PEG macroinitiator allows absolute molecular weights to be calculated (cf. **Table 4**). For this purpose, this signal was used as a reference and the integrals of the acetal proton (4.64 ppm) were compared with those of the polyether backbone (3.75–3.25 ppm). It is worth noting that the PEBVGE signals superimposed by the *m*PEG backbone have to be subtracted.
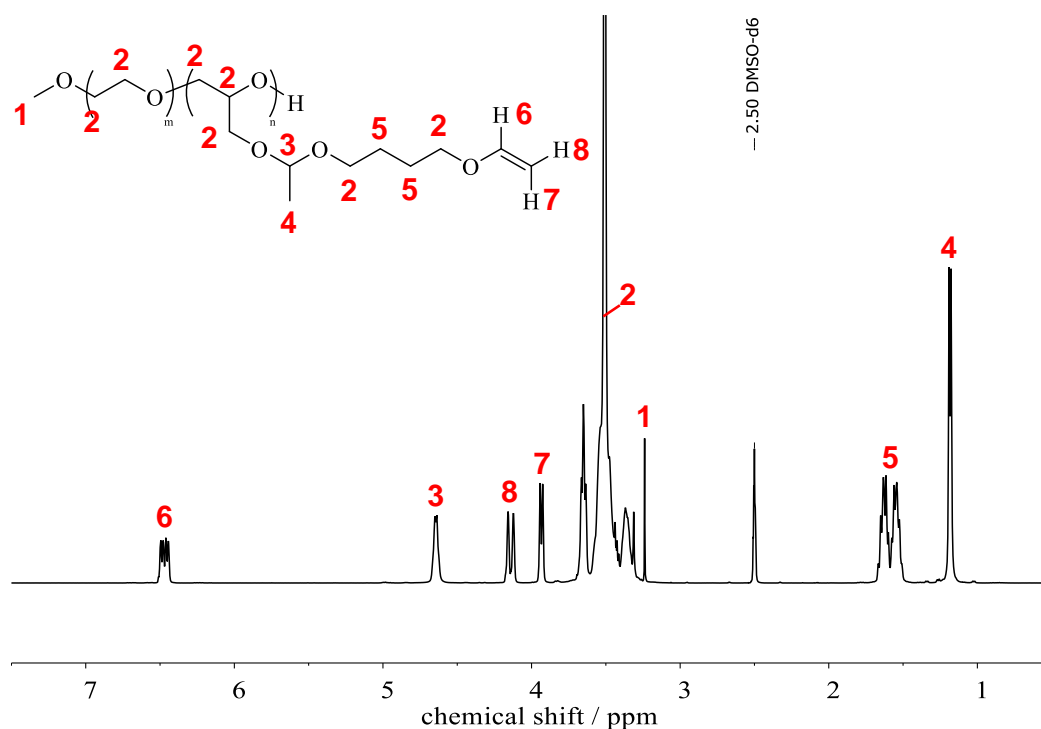
Figure 9. ^{1}H NMR spectrum (400 MHz, DMSO-d_6) of *m*PEG$_{45}$-*b*-PEBVGE$_{15}$ (entry 4, **Table 4**).

The examination of the thermal properties (**Table 5**) is also completely in line with the findings for the random PEG-*ran*-PEBVGE copolymers. T_gs vary between -61 °C and -64 °C. With the increasing amount of flexible pendant EBVGE groups, the mobility of the main chain increases, reducing the T_g. This is evident for both the *m*PEG$_{45}$-*b*-PEBVGE$_x$ (entries 1−5, **Table 5**) block copolymer series as well as for *m*PEG$_{45}$-*b*-PEBVGE$_{13}$ (entry 6, **Table 5**). T_ms vary in the range between 33 °C to 53 °C depending on the used *m*PEG macroinitiator size. With an increasing amount of EBVGE, T_m decreases, since the PEG crystal lattice is disturbed by the flexible PEBVGE side chains.[57]

Table 5. Thermal properties of *m*PEG-*b*-PEBVGE block copolymers.

No.	Composition[a]	mol% EBVGE	T_m / °C	ΔH / J g^{-1}	T_g / °C
1	*m*PEG$_{45}$-*b*-PEBVGE$_3$	5	49	118	-61
2	*m*PEG$_{45}$-*b*-PEBVGE$_4$	8	45	103	-61
3	*m*PEG$_{45}$-*b*-PEBVGE$_6$	12	45	93	-61
4	*m*PEG$_{45}$-*b*-PEBVGE$_{15}$	25	35	49	-64
5	*m*PEG$_{45}$-*b*-PEBVGE$_{45}$	50	33	28	-63
6	*m*PEG$_{114}$-*b*-PEBVGE$_{13}$	10	53	98	-64

[a] Values calculated by ^{1}H NMR spectroscopy

PEG is characterized by its excellent biocompatibility.[67] With regard to drug delivery applications, multi-functional PEGs have to retain this property. For this purpose, MTT assays were performed on the cell lines L929 and HEK-293T in the concentration range of 10-1,000 µg mL^{-1}. L929 cell line are mouse fibroblasts, HEK-293T cells originate from human embryonic kidney cells. Water-soluble *m*PEG$_{45}$ block copolymers with the lowest and highest amount of EBVGE (entries 1/4, **Table 4**) were used as test samples, as well as *m*PEG$_{114}$-*b*-PEBVGE$_{13}$ (entry 6, **Table 4**). The analysis was conducted after an incubation period of 24 hours. The results are given in **Figure 10**. Concerning the L929 cell line, none of the sample induced cytotoxicity up to a concentration of 1,000 µg mL^{-1}. All three samples show only minimal fluctuations below 5% around their respective mean value. The result is different for HEK-293T cells, which are more sensitive towards treatment with the different mPEG$_{45}$ block copolymers. Here, only *m*PEG$_{45}$-*b*-PEBVGE$_3$ (entry 1, **Table 4**) is biocompatible over the entire concentration range. At high concentrations of 500 µg mL^{-1}, the cells show a moderately decreased metabolic activity (< 80% of solvent control) for *m*PEG$_{45}$-*b*-PEBVGE$_{15}$ (entry 4, **Table 4**) and *m*PEG$_{114}$-*b*-PEBVGE$_{13}$ (entry 6, **Table 4**). Compared to the L929 cells, the relative standard deviation of 2% to 13% is also somewhat larger. In conclusion, *m*PEG-*b*-PEBVGE block copolymers with 5−25 mol% EBVGE are highly biocompatible.
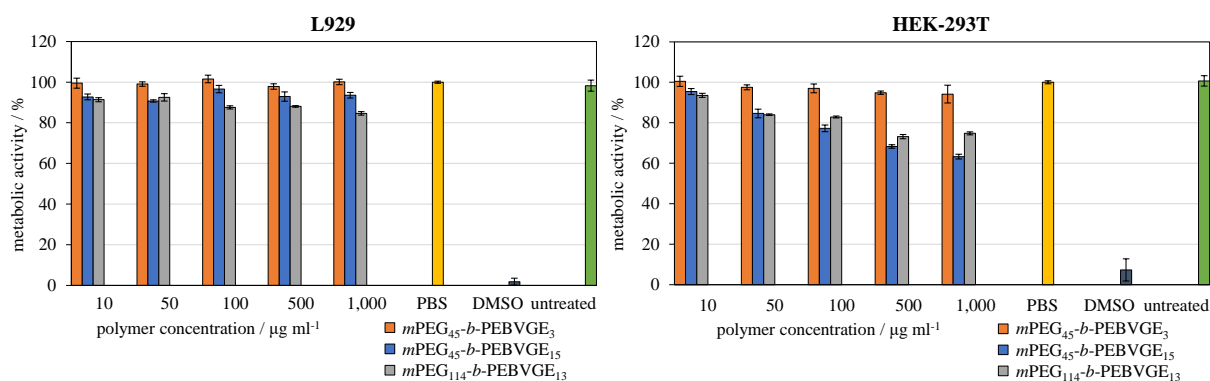
Figure 10. Overview of MTT assays for cell lines L929 (mouse fibroblasts) and HEK-293T (human embryonic kidney) tested with block copolymers mPEG$_{45}$-*b*-PEBVGE$_3$ (entry 1, **Table 4**), mPEG$_{45}$-*b*-PEBVGE$_{15}$ (entry 4, **Table 4**) and mPEG$_{114}$-*b*-PEBVGE$_{13}$ (entry 6, **Table 4**).

Amphiphilic *m*PEG-*b*-PEBVGE block copolymers tend to self-assemble in aqueous milieu. In terms of drug delivery applications, three aspects were studied: 1) analysis of the surfactant structure, 2) the cleavability of the EBVGE side chains from non-crosslinked *m*PEG-*b*-PEBVGE micelles and 3) crosslinking and the cleavage of the hydrophobic micellar core.
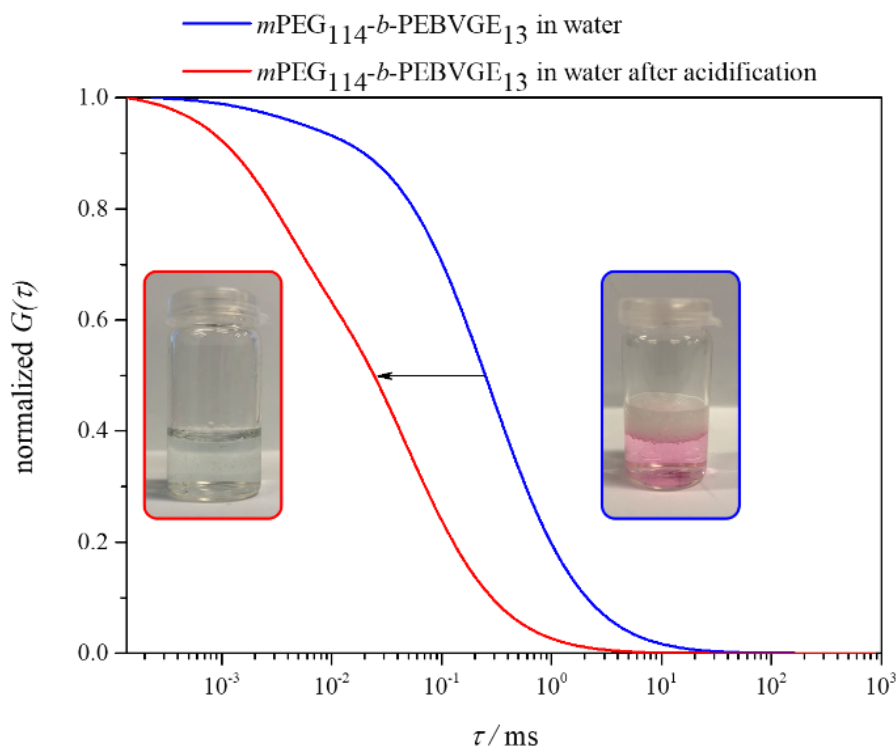
For this purpose, *m*PEG$_{114}$-*b*-PEBVGE$_{13}$ (entry 6, **Table 4**) was used as a model compound. At first, the critical micelle formation concentration was determined (84.2 mg L^{-1}), which is in the same order of magnitude as for other PEG block copolymers with similar degree of polymerization (**SI-Figure 29**).[23] The surfactant architecture was investigated for further characterization by static (SLS) and dynamic light scattering (DLS) (**SI-Figures 30−32**). An aqueous solution of pure *m*PEG$_{114}$-*b*-PEBVGE$_{13}$ (entry 6, **Table 4**) was examined and compared with aqueous solutions of the block copolymer loaded and subsequently crosslinked with the photoinitiator 2,2-dimethoxy-2-phenylacetophenone (DMPA) and the thiol pentaerythritol tetrakis(3-mercaptopropionate) (PETMP). As shown in **Table 6**, the hydrodynamic radius R_h increases by a factor of approximately four from 16 nm to 58 nm as result of the loading and crosslinking with PETMP and DMPA. In contrast, the differences of 3 nm between loaded (non-crosslinked) and crosslinked micelles are negligible. The characteristic ratio ρ provides information on the topology of the *m*PEG$_{114}$-*b*-PEBVGE$_{13}$ (entry 6, **Table 4**) particles. Interestingly, from a theoretical point of view, for pure aqueous solutions of the block copolymer a value of 1.0 is obtained, indicating a vesicle-like structure. A similar characteristic ratio was reported by Herzberger *et al.* for *m*PEG block copolymers with pendant di(*n*-alkyl)amine moieties.[68] Loaded and crosslinked micelles, on the other hand, are close to the expected value 0.75 for homogeneous spheres.[69] This distinction can be

attributed to the loading of the aggregates with PETMP and DMPA, since all other parameters were identical in all three approaches.

Table 6. Overview of hydrodynamic (R_h) and gyration radii (R_g) from static and dynamic light scattering for aqueous solutions of mPEG$_{114}$-b-PEBVGE$_{13}$ (entry 6, **Table 4**) ($c = 2$ g L^{-1}). ρ is the characteristic ratio and defined as $\rho = R_g R_h^{-1}$. Indices are as follows: u = unloaded, l = loaded, l + c = loaded and crosslinked.

$R_{h,\,u}$ / nm	$R_{g,\,u}$ / nm	ρ_u	$R_{h,\,l}$ / nm	$R_{g,\,l}$ / nm	ρ_l	$R_{h,\,l+c}$ / nm	$R_{g,\,l+c}$ / nm	ρ_{l+c}
15.7	16.1	1.0	61.0	48.0	0.8	58.2	40.6	0.7

Based on these findings, fluorescence correlation spectroscopy (FCS) measurements were used to investigate the solubilization of the hydrophobic, fluorescent dye Nil red as a model active substance by the non-crosslinked polymeric micelles ($c = 1$ g L^{-1}). In addition, the release by treatment with 1 M HCl was also investigated. **Figure 11** summarizes these results. Here, the normalized autocorrelation curves before and after the addition of HCl are depicted. All measurement curves can be found in the Supporting Information in **SI-Figures 33−36**. A significant decrease in the delay time τ after acidification was detected. Qualitatively, this process is exemplified by the two illustrations in **Figure 11**. Before acidification, the water-insoluble Nile red is solubilized by the hydrophobic core of mPEG$_{114}$-b-PEBVGE$_{13}$ (entry 6, **Table 4**) micelles, resulting in the pink solution color. By lowering the pH value, the EBVGE side arms are cleaved and the micelles irreversibly disassemble to their corresponding water-soluble mPEG$_{114}$-b-PG$_{13}$ block copolymers unimers and the soluble side products, leading to almost non-fluorescent aggregates (precipitation) of the dye.

Figure 11. Normalized autocorrelation curves of Nile red loaded mPEG$_{114}$-b-PEBVGE$_{13}$ (entry 6, **Table 4**) micelles including manual assay. Blue curve and illustration on the right side: before acidification. Red curve and illustration on the left side: after acidification.

These results are validated by evaluation of the fitting functions of the autocorrelation curves (**Table 7**). Encapsulation of the dye led to a longer diffusion. After acidification, D was increased the sixfold and correlated with pure Nile red in water. Thus, the encapsulation and release of the dye is clearly proven. Hydrodynamic radii R_h can be obtained from the Stokes-Einstein relation (**Equation 1**). Here, a significant decrease from 4.1 nm to 0.7 nm can be overserved as a consequence of the removal of the EBVGE side arms. This is contributed to the transition from micelles to unimers and the consequent release of Nile red.

Table 7. FCS results for Nile red (NR) labeled mPEG$_{114}$-b-PEBVGE$_{13}$ (BC, entry 6, **Table 4**) block copolymers: diffusion coefficients D and hydrodynamic radii R_hs before and after addition of 1 M HCl.

$D_{NR, H2O}$ / μm^2 s^{-1}	$D_{BC, H2O}$ / μm^2 s^{-1}	$D_{BC, H2O+HCl}$ / μm^2 s^{-1}	$R_{h, H2O}$ / nm	$R_{h, H2O+HCl}$ / nm
313.0	51.7	292.0	4.1	0.7

The successful photo-induced crosslinking of the micellar core was proven by DLS studies both in aqueous and organic media.[70–73] mPEG$_{114}$-b-PEBVGE$_{13}$ (entry 6, **Table 4**) was loaded with

PETMP and DMPA and crosslinked by irradiation with UV light using thiol-ene click chemistry. The hydrodynamic radii were compared in aqueous solutions of neutral and acidic pH. To prove the increased stability of the crosslinked micelles, non- and crosslinked aqueous solutions of mPEG$_{114}$-b-PEBVGE$_{13}$ (entry 6, **Table 4**) were freeze-dried, subsequently dissolved in neutral and acidic methanol and then investigated by DLS. The hydrodynamic radii were compared with R_h of mPEG$_{114}$-b-PEBVGE$_{13}$ (entry 6, **Table 4**) in water. The results are displayed in **Figure 12**.
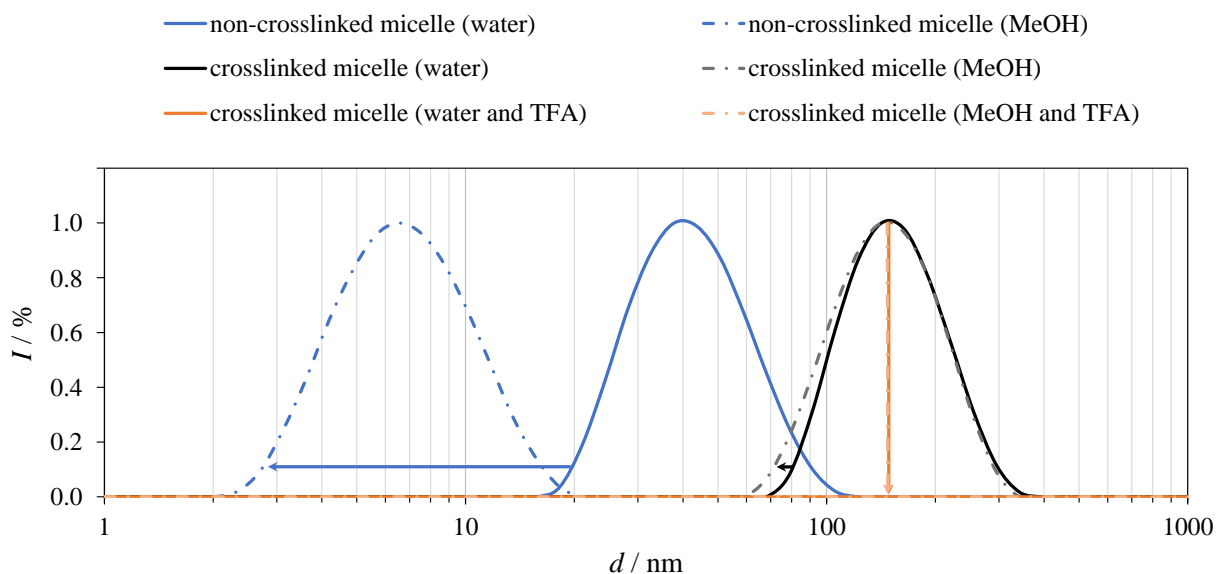
Figure 12. Particle size distribution based normalized intensity of mPEG$_{114}$-b-PEBVGE$_{13}$ (entry 6, **Table 4**) micelles in H$_2$O (solid) or MeOH (dashed) with c = 0.5 g L^{-1}. Blue curves: non-crosslinked micelles of pure block copolymer. Black curves: crosslinked micelles by using PETMP and DMPA. Orange lines: decomposed crosslinked micelles after acidification with TFA.

Disassembly of the non-crosslinked micelles into free unimers reduces R_h from 20 nm to 5 nm due the solvent change form water to methanol (**Figure 12**, blue plot). With 77 nm, R_h remains constant for the crosslinked micelles after changing the solvents, proving the successful particle stabilization (**Figure 12**, black plot). After adding trifluoroacetic acid (TFA), the crosslinked micelles disassemble irreversibly (**Figure 12**, orange plot). Consequently, no more scattering was observed in both H$_2$O and MeOH, indicating the absence of nanoparticles.

CONCLUSION

With this work, we opened a new avenue for the synthesis of multi-pH-responsive and vinyl ether-functional PEGs introducing the novel bifunctional monomer EBVGE that bears a vinyl ether group as well as an epoxide moiety. In addition, it is acid labile, permitting to cleave the side chains.

The anionic ring-opening (co)polymerization of EBVGE and EO allowed access to random PEG-*ran*-PEBVGE copolymers and to PEBVGE$_{31}$ homopolymer. These were obtained with dispersities up to 1.17 and molecular weights between 6,700−10,200 g mol^{-1}. EBVGE could be quantitatively incorporated into the polyether backbone in any ratio (2−100 mol%). *In-situ* NMR studies proved an ideally random incorporation of the copolymers ($r_{EO, EBVGE} = 1.0$). The T_gs were little influenced by copolymerization and remained in between that of pure PEG (-60 °C[56]) and PEBVGE$_{31}$ homopolymer (-64 °C). Only the copolymer with 2 mol% EBVGE showed a melting point T_m of 44 °C and also exhibited thermoresponsive behavior in water with a cloud point at 55 °C.

To demonstrate the bifunctional nature of the EBVGE monomer and the potential application as acid-cleavable epoxy resins, the free-radical copolymerization of electron-rich vinyl units from EBVGE monomer was accomplished by copolymerization with electron acceptors. Copolymers with maleic anhydride and *N*-phenylmaleimide resulted in molecular weights of 9,200 g mol^{-1} and 3,400 g mol^{-1} ($Đ < 2.0$; SEC). The polymers were further characterized by NMR spectroscopy and DSC measurements, revealing T_gs of 26 °C and 86 °C.

Well-defined *m*PEG-*b*-PEBVGE block copolymers with varying EBVGE content (5−50 mol%) were synthesized by using *m*PEG$_{45}$ and *m*PEG$_{114}$ macroinitiators. Molecular weights ranged between 2,600 g mol^{-1} and 11,700 g mol^{-1} ($Đ ≤ 1.16$). Studies of the thermal properties showed that T_gs almost overlapped with those of the PEG-*ran*-PEBVGE copolymers, but T_ms could be precisely tailored between 33−53 °C according to the amount of EBVGE. Detailed studies concerning micelle formation in aqueous solutions ($CMC = 84$ mg L^{-1}) were carried out as well, aiming at using the polymers for acid-labile micellar nanocarriers. In this context, their biocompatibility was investigated using MTT assays. Minor effects on the metabolic activity of L929 and HEK-293T cells were observed in concentration ranges up to 1,000 µg mL^{-1} depending on the PEBVGE block size. In general, *m*PEG-*b*-PEBVGE block copolymers with 5−25 mol% EBVGE were observed to be highly biocompatible. In-depth SLS and DLS studies were used to characterize the non- and core-crosslinked micelles, proving

increasing values for R_h (non-crosslinked: 16 nm, crosslinked: 58 nm) as a result of the loading with PETMP and DMPA. Crosslinking of the micelles in aqueous solution was conducted by thiol-ene click chemistry. FCS measurements confirmed the encapsulation of the dye Nile red by the non-crosslinked micelles, which could be released by acidification. The successful crosslinking of the micelle core was evidenced by DLS studies in aqueous and organic solvents. While the switch from water to methanol resulted in the transformation of the non-crosslinked micelles (R_h = 20 nm) to the unimers (R_h = 5 nm), the crosslinked micelles retained their shape ($R_{h,\,both}$ = 77 nm).

To sum up, this fundamental work has shown that the novel epoxide monomer EBVGE combines in a unique manner three features: (i) polymerization via the epoxide moiety; (ii) crosslinking or functionalization via the vinyl group and (iii) acid cleavability of the vinyl ether structure. Due to these characteristics, this bifunctional monomer is a promising candidate for micellar nanocarriers in nanomedicine.

ACKNOWLEDGEMENT

REFERENCES

(1) Tong, R.; Cheng, J. Anticancer Polymeric Nanomedicines. *Polymer Revs.* **2007**, *47*, 345–381, DOI: 10.1080/15583720701455079.

(2) Mura, S.; Nicolas, J.; Couvreur, P. Stimuli-responsive nanocarriers for drug delivery. *Nat. Mater.* **2013**, *12*, 991–1003, DOI: 10.1038/nmat3776.

(3) Cabral, H.; Miyata, K.; Osada, K.; Kataoka, K. Block Copolymer Micelles in Nanomedicine Applications. *Chem. Rev.* **2018**, *118*, 6844–6892, DOI: 10.1021/acs.chemrev.8b00199.

(4) Cho, K.; Wang, X.; Nie, S.; Chen, Z. G.; Shin, D. M. Therapeutic nanoparticles for drug delivery in cancer. *Clin. Cancer Res.* **2008**, *14*, 1310–1316, DOI: 10.1158/1078-0432.CCR-07-1441.

(5) Lu, Y.; Sun, W.; Gu, Z. Stimuli-responsive nanomaterials for therapeutic protein delivery. *J. Control. Release* **2014**, *194*, 1–19, DOI: 10.1016/j.jconrel.2014.08.015.

(6) Schmaljohann, D. Thermo- and pH-responsive polymers in drug delivery. *Adv. Drug Deliv. Rev.* **2006**, *58*, 1655–1670, DOI: 10.1016/j.addr.2006.09.020.

(7) Roy, D.; Cambre, J. N.; Sumerlin, B. S. Future perspectives and recent advances in stimuli-responsive materials. *Prog. Polym. Sci.* **2010**, *35*, 278–301, DOI: 10.1016/j.progpolymsci.2009.10.008.

(8) Matsumura, Y.; Maeda, H. A new concept for macromolecular therapeutics in cancer chemotherapy: mechanism of tumoritropic accumulation of proteins and the antitumor agent smancs. *Cancer Res.* **1986**, *46*, 6387–6392.

(9) *Layer-by-layer films for biomedical applications;* Picart, C.; Caruso, F.; Voegel, J.-C., Eds.; Wiley-VCH-Verl.: Weinheim, 2015.

(10) Haag, R. Supramolekulare Wirkstoff-Transportsysteme auf der Basis polymerer Kern-Schale-Architekturen. *Angew. Chem.* **2004**, *116*, 280–284, DOI: 10.1002/ange.200301694.

(11) Chen, W.; Meng, F.; Li, F.; Ji, S.-J.; Zhong, Z. pH-responsive biodegradable micelles based on acid-labile polycarbonate hydrophobe: synthesis and triggered drug release. *Biomacromolecules* **2009**, *10*, 1727–1735, DOI: 10.1021/bm900074d.

(12) Tang, R.; Ji, W.; Panus, D.; Palumbo, R. N.; Wang, C. Block copolymer micelles with acid-labile ortho ester side-chains: Synthesis, characterization, and enhanced drug delivery to human glioma cells. *J. Control. Release* **2011**, *151*, 18–27, DOI: 10.1016/j.jconrel.2010.12.005.

(13) Oishi, M.; Sasaki, S.; Nagasaki, Y.; Kataoka, K. pH-responsive oligodeoxynucleotide (ODN)-poly(ethylene glycol) conjugate through acid-labile beta-thiopropionate linkage:

preparation and polyion complex micelle formation. *Biomacromolecules* **2003**, *4*, 1426–1432, DOI: 10.1021/bm034164u.

(14) Huang, X.; Du, F.; Cheng, J.; Dong, Y.; Liang, D.; Ji, S.; Lin, S.-S.; Li, Z. Acid-Sensitive Polymeric Micelles Based on Thermoresponsive Block Copolymers with Pendent Cyclic Orthoester Groups. *Macromolecules* **2009**, *42*, 783–790, DOI: 10.1021/ma802138r.

(15) Staudinger, H.; Lohmann, H. Über hochpolymere Verbindungen. 81. Mitteilung. Über eukolloides Polyäthylenoxyd. *Justus Liebigs Ann. Chem.* **1933**, *505*, 41–51, DOI: 10.1002/jlac.19335050104.

(16) Herzberger, J.; Niederer, K.; Pohlit, H.; Seiwert, J.; Worm, M.; Wurm, F. R.; Frey, H. Polymerization of Ethylene Oxide, Propylene Oxide, and Other Alkylene Oxides: Synthesis, Novel Polymer Architectures, and Bioconjugation. *Chem. Rev.* **2016**, *116*, 2170–2243, DOI: 10.1021/acs.chemrev.5b00441.

(17) Harris, J. M. *Poly(Ethylene Glycol) Chemistry: Biotechnical and Biomedical Applications*; Springer US, 1992.

(18) Bailey, F. E. *Alkylene Oxides and Their Polymers*; Taylor & Francis, 1990.

(19) Knop, K.; Hoogenboom, R.; Fischer, D.; Schubert, U. S. Anwendung von Poly(ethylenglycol) beim Wirkstoff-Transport: Vorteile, Nachteile und Alternativen. *Angew. Chem.* **2010**, *122*, 6430–6452, DOI: 10.1002/ange.200902672.

(20) Dingels, C.; Schömer, M.; Frey, H. Die vielen Gesichter des Poly(ethylenglykol)s. *Chem. unserer Zeit* **2011**, *45*, 338–349, DOI: 10.1002/ciuz.201100551.

(21) Koyama, Y.; Umehara, M.; Mizuno, A.; Itaba, M.; Yasukouchi, T.; Natsume, K.; Suginaka, A. Synthesis of novel poly(ethylene glycol) derivatives having pendant amino groups and aggregating behavior of its mixture with fatty acid in water. *Bioconjugate Chem.* **1996**, *7*, 298–301, DOI: 10.1021/bc9600123.

(22) Obermeier, B.; Wurm, F.; Mangold, C.; Frey, H. Multifunctional Poly(ethylene glycol)s. *Angew. Chem. Int. Ed. (English)* **2011**, *50*, 7988–7997, DOI: 10.1002/anie.201100027.

(23) Herzberger, J.; Fischer, K.; Leibig, D.; Bros, M.; Thiermann, R.; Frey, H. Oxidation-Responsive and "Clickable" Poly(ethylene glycol) via Copolymerization of 2-(Methylthio)ethyl Glycidyl Ether. *J. Am. Chem. Soc.* **2016**, *138*, 9212–9223, DOI: 10.1021/jacs.6b04548.

(24) Rangelov, S. Synthesis and polymerization of novel oxirane bearing an aliphatic double chain moiety. *Polymer* **2001**, *42*, 4483–4491, DOI: 10.1016/S0032-3861(00)00826-0.

(25) Son, S.; Shin, E.; Kim, B.-S. Redox-Degradable Biocompatible Hyperbranched Polyglycerols: Synthesis, Copolymerization Kinetics, Degradation, and Biocompatibility. *Macromolecules* **2015**, *48*, 600–609, DOI: 10.1021/ma502242v.

(26) Wurm, F.; Nieberle, J.; Frey, H. Synthesis and Characterization of Poly(glyceryl glycerol) Block Copolymers. *Macromolecules* **2008**, *41*, 1909–1911, DOI: 10.1021/ma702458g.

(27) Song, J.; Palanikumar, L.; Choi, Y.; Kim, I.; Heo, T.-y.; Ahn, E.; Choi, S.-H.; Lee, E.; Shibasaki, Y.; Ryu, J.-H. *et al.* The power of the ring: a pH-responsive hydrophobic epoxide monomer for superior micelle stability. *Polym. Chem.* **2017**, *8*, 7119–7132, DOI: 10.1039/C7PY01613A.

(28) Xiao, L.; Huang, L.; Moingeon, F.; Gauthier, M.; Yang, G. pH-Responsive Poly(Ethylene Glycol)-block-Polylactide Micelles for Tumor-Targeted Drug Delivery. *Biomacromolecules* **2017**, *18*, 2711–2722, DOI: 10.1021/acs.biomac.7b00509.

(29) Wu, L.; Zou, Y.; Deng, C.; Cheng, R.; Meng, F.; Zhong, Z. Intracellular release of doxorubicin from core-crosslinked polypeptide micelles triggered by both pH and reduction conditions. *Biomaterials* **2013**, *34*, 5262–5272, DOI: 10.1016/j.biomaterials.2013.03.035.

(30) Ren, J.; Zhang, Y.; Zhang, J.; Gao, H.; Liu, G.; Ma, R.; An, Y.; Kong, D.; Shi, L. pH/sugar dual responsive core-cross-linked PIC micelles for enhanced intracellular protein delivery. *Biomacromolecules* **2013**, *14*, 3434–3443, DOI: 10.1021/bm4007387.

(31) Liu, S.; Weaver, J. V. M.; Save, M.; Armes, S. P. Synthesis of pH-Responsive Shell Cross-Linked Micelles and Their Use as Nanoreactors for the Preparation of Gold Nanoparticles. *Langmuir* **2002**, *18*, 8350–8357, DOI: 10.1021/la020496t.

(32) Wu, Y.; Chen, W.; Meng, F.; Wang, Z.; Cheng, R.; Deng, C.; Liu, H.; Zhong, Z. Core-crosslinked pH-sensitive degradable micelles: A promising approach to resolve the extracellular stability versus intracellular drug release dilemma. *J. Control. Release* **2012**, *164*, 338–345, DOI: 10.1016/j.jconrel.2012.07.011.

(33) Taton, D.; Le Borgne, A.; Sepulchre, M.; Spassky, N. Synthesis of chiral and racemic functional polymers from glycidol and thioglycidol. *Macromol. Chem. Phys.* **1994**, *195*, 139–148, DOI: 10.1002/macp.1994.021950111.

(34) Tonhauser, C.; Schüll, C.; Dingels, C.; Frey, H. Branched Acid-Degradable, Biocompatible Polyether Copolymers via Anionic Ring-Opening Polymerization Using an Epoxide Inimer. *ACS Macro Lett.* **2012**, *1*, 1094–1097, DOI: 10.1021/mz300265z.

(35) Mangold, C.; Dingels, C.; Obermeier, B.; Frey, H.; Wurm, F. PEG-based Multifunctional Polyethers with Highly Reactive Vinyl-Ether Side Chains for Click-Type Functionalization. *Macromolecules* **2011**, *44*, 6326–6334, DOI: 10.1021/ma200898n.

(36) Einstein, A. Über die von der molekularkinetischen Theorie der Wärme geforderte Bewegung von in ruhenden Flüssigkeiten suspendierten Teilchen. *Ann. Phys.* **1905**, *322*, 549–560, DOI: 10.1002/andp.19053220806.

(37) Stokes, G. G. On the Effect of the Internal Friction of Fluids on the Motion of Pendulums. *Trans. Cambridge Philos. Soc.* **1851**, *9*, 8.

(38) Mohr, P. J.; Newell, D. B.; Taylor, B. N. *Codata Recommended Values Of The Fundamental Physical Constants: 2014*.

(39) *Viscosity of water;* International Organization for Standardization (ISO), Ed.; ISO/TR Technical Report No. 3666; Geneva, 1998.

(40) Fitton, A. O.; Hill, J.; Jane, D. E.; Millar, R. Synthesis of Simple Oxetanes Carrying Reactive 2-Substituents. *Synthesis* **1987**, *1987*, 1140–1142, DOI: 10.1055/s-1987-28203.

(41) Maciol, K.; Linden, G.; Blankenburg, J.; Schmolke, W.; Seiffert, S.; Frey. H. Design of a Novel Epoxide Monomer for pH-Sensitive Poly(ethylene glycol) Hydrogels via Acid-Labile and Crosslinkable Allyl Side Groups. *Chapter 2.1.* **2018**.

(42) Ding, J.; Price, C.; Booth, C. Use of crown ether in the anionic polymerization of propylene oxide—1. Rate of polymerization. *Eur. Polym. J.* **1991**, *27*, 891–894, DOI: 10.1016/0014-3057(91)90028-M.

(43) Stolarzewicz, A.; Neugebauer, D.; Grobelny, Z. Influence of the kind of crown ether on the anionic polymerization of (phenoxymethyl)oxirane initiated by potassium tert-butoxide. *Macromol. Chem. Phys.* **1995**, *196*, 1301–1306, DOI: 10.1002/macp.1995.021960429.

(44) Blankenburg, J.; Wagner, M.; Frey, H. Well-Defined Multi-Amino-Functional and Stimuli-Responsive Poly(propylene oxide) by Crown Ether Assisted Anionic Ring-Opening Polymerization. *Macromolecules* **2017**, *50*, 8885–8893, DOI: 10.1021/acs.macromol.7b01324.

(45) Sato, K.; Sukegawa, T.; Oyaizu, K.; Nishide, H. Synthesis of Poly(TEMPO-Substituted Glycidyl Ether) by Utilizing t -BuOK/18-Crown-6 for an Organic Cathode-Active Material. *Macromol. Symp.* **2015**, *351*, 90–96, DOI: 10.1002/masy.201300224.

(46) Alkan, A.; Thomi, L.; Gleede, T.; Wurm, F. R. Vinyl ferrocenyl glycidyl ether: An unprotected orthogonal ferrocene monomer for anionic and radical polymerization. *Polym. Chem.* **2015**, *6*, 3617–3624, DOI: 10.1039/C5PY00404G.

(47) Mangold, C.; Obermeier, B.; Wurm, F.; Frey, H. From an epoxide monomer toolkit to functional PEG copolymers with adjustable LCST behavior. *Macromol. Rapid Commun.* **2011**, *32*, 1930–1934, DOI: 10.1002/marc.201100489.

(48) Pang, X.; Wang, G.; Jia, Z.; Liu, C.; Huang, J. Preparation of the amphiphilic macro-rings of poly(ethylene oxide) with multi-polystyrene lateral chains and their extraction for dyes. *J. Polym. Sci. A Polym. Chem.* **2007**, *45*, 5824–5837, DOI: 10.1002/pola.22333.

(49) Niederer, K.; Schüll, C.; Leibig, D.; Johann, T.; Frey, H. Catechol Acetonide Glycidyl Ether (CAGE): A Functional Epoxide Monomer for Linear and Hyperbranched Multi-Catechol

Functional Polyether Architectures. *Macromolecules* **2016**, *49*, 1655–1665, DOI: 10.1021/acs.macromol.5b02441.

(50) Tonhauser, C.; Alkan, A.; Schömer, M.; Dingels, C.; Ritz, S.; Mailänder, V.; Frey, H.; Wurm, F. R. Ferrocenyl Glycidyl Ether: A Versatile Ferrocene Monomer for Copolymerization with Ethylene Oxide to Water-Soluble, Thermoresponsive Copolymers. *Macromolecules* **2013**, *46*, 647–655, DOI: 10.1021/ma302241w.

(51) Alkan, A.; Gleede, T.; Wurm, F. R. Ruthenocenyl Glycidyl Ether: A Ruthenium-Containing Epoxide for Anionic Polymerization. *Organometallics* **2017**, *36*, 3023–3028, DOI: 10.1021/acs.organomet.7b00278.

(52) Obermeier, B.; Frey, H. Poly(ethylene glycol-co-allyl glycidyl ether)s: a PEG-based modular synthetic platform for multiple bioconjugation. *Bioconjugate Chem.* **2011**, *22*, 436–444, DOI: 10.1021/bc1004747.

(53) Jaacks, V. A novel method of determination of reactivity ratios in binary and ternary copolymerizations. *Makromol. Chem.* **1972**, *161*, 161–172, DOI: 10.1002/macp.1972.021610110.

(54) Meyer, V. E.; Lowry, G. G. Integral and differential binary copolymerization equations. *J. Polym. Sci. A Gen. Pap.* **1965**, *3*, 2843–2851, DOI: 10.1002/pol.1965.100030811.

(55) Fineman, M.; Ross, S. D. Linear method for determining monomer reactivity ratios in copolymerization. *J. Polym. Sci.* **1950**, *5*, 259–262, DOI: 10.1002/pol.1950.120050210.

(56) Bailey, F. E.; Koleske, J. V. *Poly(ethylene oxide)*; Academic Press: New York, 1976.

(57) Koltzenburg, S.; Maskos, M.; Nuyken, O. *Polymer Chemistry*; Springer Berlin Heidelberg: Berlin, Heidelberg, 2017.

(58) *Handbook of thermoplastics;* Olabisi, O.; Adewale, K. P., Eds., Second edition; CRC Press Taylor & Francis Group: Boca Raton, London, New York, 2016.

(59) Ward, M. A.; Georgiou, T. K. Thermoresponsive Polymers for Biomedical Applications. *Polymers* **2011**, *3*, 1215–1242, DOI: 10.3390/polym3031215.

(60) Jin, F.-L.; Li, X.; Park, S.-J. Synthesis and application of epoxy resins: A review. *J. Ind. Eng. Chem.* **2015**, *29*, 1–11, DOI: 10.1016/j.jiec.2015.03.026.

(61) Tillet, G.; Boutevin, B.; Ameduri, B. Chemical reactions of polymer crosslinking and post-crosslinking at room and medium temperature. *Prog. Polym. Sci.* **2011**, *36*, 191–217, DOI: 10.1016/j.progpolymsci.2010.08.003.

(62) Kharas, G. B.; Ajbani, H. Radical alternating copolymerization of vinyl ethers. *J. Polym. Sci. A Polym. Chem.* **1993**, *31*, 2295–2303, DOI: 10.1002/pola.1993.080310912.

(63) Odian, G. G. *Principles of polymerization*, 4. ed.; Wiley-Interscience: Hoboken, NJ, 2004.

(64) Chung, K. H.; Wu, C. S.; Malawer, E. G. Glass transition temperatures of poly(methyl vinyl ether-co-maleic anhydride) (PMVEMA) and poly(methyl vinyl ether-co-maleic acid) (PMVEMAC) and the kinetics of dehydration of PMVEMAC by thermal analysis. *J. Appl. Polym. Sci.* **1990**, *41*, 793–803, DOI: 10.1002/app.1990.070410326.

(65) Kohli, P.; Scranton, A. B.; Blanchard, G. J. Co-Polymerization of Maleimides and Vinyl Ethers: A Structural Study. *Macromolecules* **1998**, *31*, 5681–5689, DOI: 10.1021/ma980067v.

(66) Talelli, M.; Barz, M.; Rijcken, C. J.; Kiessling, F.; Hennink, W. E.; Lammers, T. Core-Crosslinked Polymeric Micelles: Principles, Preparation, Biomedical Applications and Clinical Translation. *Nano today* **2015**, *10*, 93–117, DOI: 10.1016/j.nantod.2015.01.005.

(67) Fruijtier-Pölloth, C. Safety assessment on polyethylene glycols (PEGs) and their derivatives as used in cosmetic products. *Toxicology* **2005**, *214*, 1–38, DOI: 10.1016/j.tox.2005.06.001.

(68) Herzberger, J.; Kurzbach, D.; Werre, M.; Fischer, K.; Hinderberger, D.; Frey, H. Stimuli-Responsive Tertiary Amine Functional PEGs Based on N,N -Dialkylglycidylamines. *Macromolecules* **2014**, *47*, 7679–7690, DOI: 10.1021/ma501367b.

(69) Schärtl, W. *Light scattering from polymer solutions and nanoparticle dispersions: With 16 tables*; Springer laboratory manuals in polymer science; Springer: Berlin, Heidelberg, 2007.

(70) Duong, H. T. T.; Nguyen, T. L. U.; Kumpfmüller, J.; Stenzel, M. H. Synthesis of Core–Shell Nanoparticles with Polystyrene Core and PEO Corona from Core-Crosslinked Micelles by the RAFT Process. *Aust. J. Chem.* **2010**, *63*, 1210, DOI: 10.1071/CH10127.

(71) Shiraishi, K.; Yusa, S.-i.; Ito, M.; Nakai, K.; Yokoyama, M. Photo Irradiation-Induced Core Crosslinked Poly(ethylene glycol)-block-poly(aspartic acid) Micelles: Optimization of Block Copolymer Synthesis and Characterization of Core Crosslinked Micelles. *Polymers* **2017**, *9*, 710, DOI: 10.3390/polym9120710.

(72) Hu, X.; Chen, X.; Wei, J.; Liu, S.; Jing, X. Core crosslinking of biodegradable block copolymer micelles based on poly(ester carbonate). *Macromol. Biosci.* **2009**, *9*, 456–463, DOI: 10.1002/mabi.200800158.

(73) Di Xiong; Zhang, R.; Luo, W.; Gu, H.; Peng, S.; Zhang, L. Hydrazone cross-linked micelles based on redox degradable block copolymer for enhanced stability and controlled drug release. *React. Funct. Polym.* **2017**, *119*, 64–74, DOI: 10.1016/j.reactfunctpolym.2017.08.003.

Supporting Information

Ethoxy Butoxy Vinyl Glycidyl Ether: Reactive and Cleavable Multi-Vinyl Ether-Functional Poly(ethylene glycol)s for Drug Delivery Applications

Kamil Maciol[†], *Jan Blankenburg*[†,‡], *Karl Fischer*[§], *Matthias Bros*[‖], *Tassilo Gleede*[⊥], *Frederik R. Wurm*[⊥] and *Holger Frey*[†,*]

[†] Institute of Organic Chemistry, Johannes Gutenberg University Mainz, Duesbergweg 10-14, 55128 Mainz, Germany

[‡] Graduate School Materials Science in Mainz, Staudinger Weg 9, 55128 Mainz, Germany

[§] Institute of Physical Chemistry, Johannes Gutenberg-University Mainz, Duesbergweg 10-14, 55128 Mainz, Germany

[‖] Department of Dermatology, University Medical Center of the Johannes Gutenberg-University, Langenbeckstrasse 1, 55131 Mainz, Germany

[⊥] Max-Planck Institute for Polymer Research (MPI-P), Ackermannweg 10, D-55128 Mainz, Germany

*E-Mail: hfrey@uni-mainz.de

SI-Figure 1. SEC trace of real-time ^{1}H NMR EO/EBVGE copolymerization in DMSO-d_6 at 60 °C (M_n = 2,400 g mol^{-1}, Đ = 1.25).
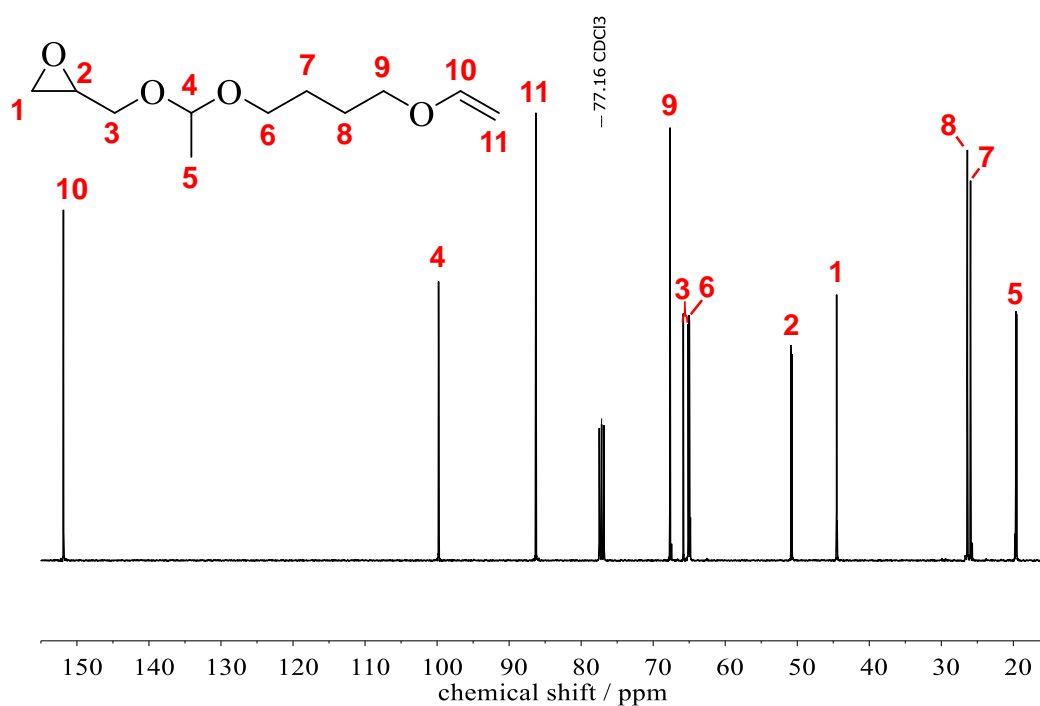
SI-Figure 2. ^{13}C NMR spectrum (100 MHz, C*D*Cl₃) of EBVGE monomer.
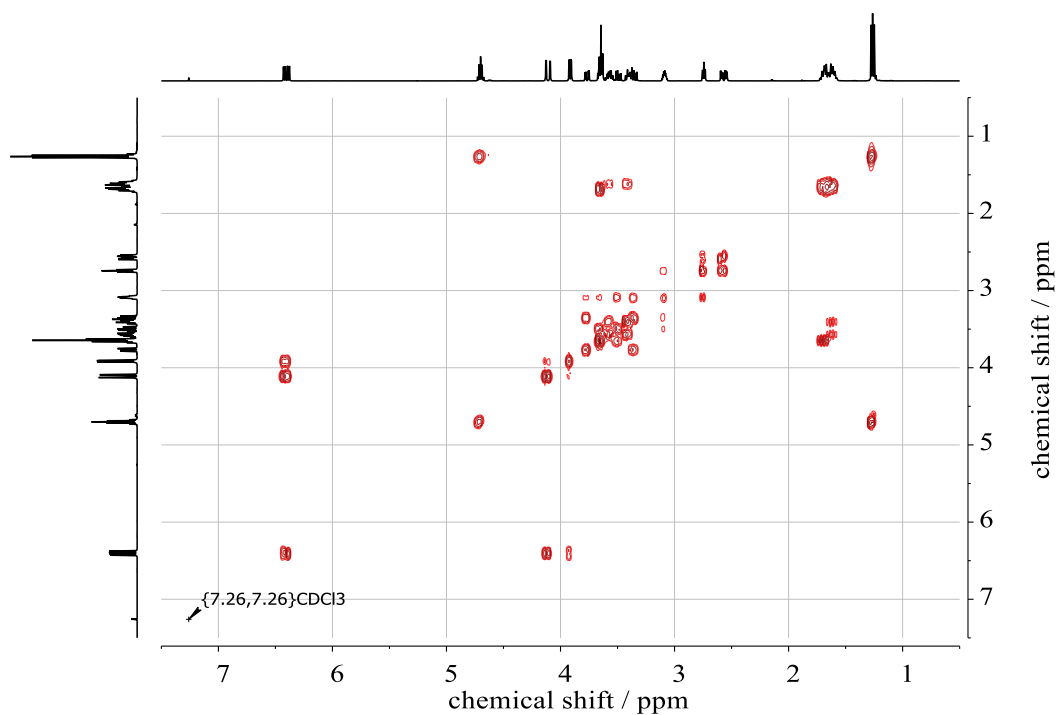
SI-Figure 3. ^{1}H, ^{1}H COSY NMR (400 MHz, C*D*Cl$_3$) of EBVGE monomer.
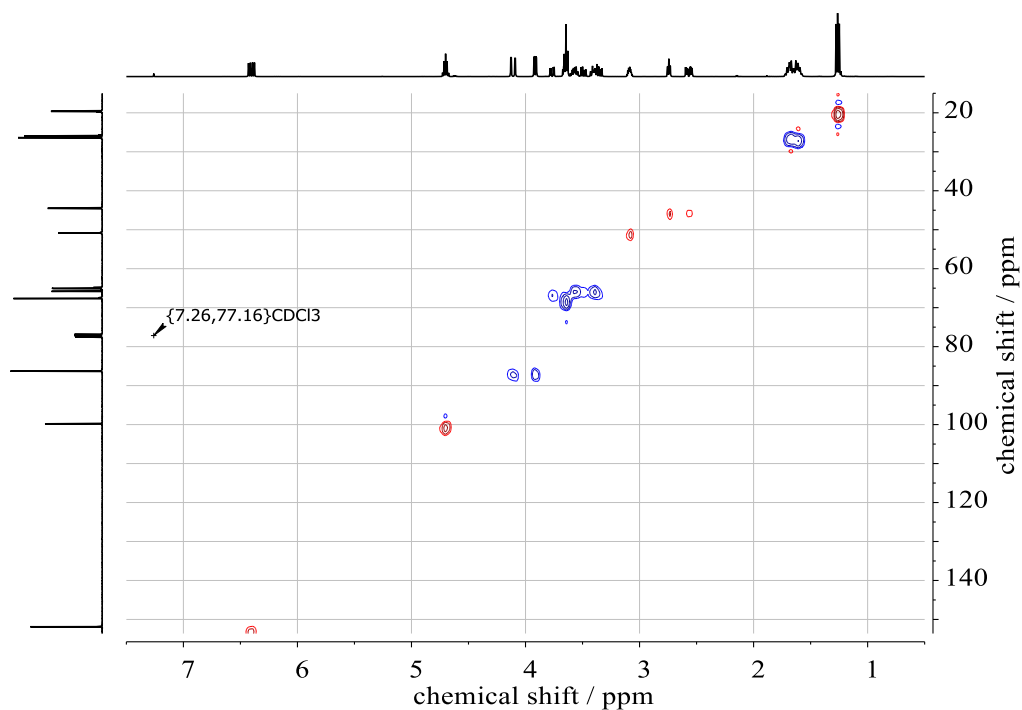
SI-Figure 4. ^{1}H, ^{13}C HSQC NMR of EBVGE monomer in C*D*Cl$_3$. Color of the signals indicates the phase information (red: methine proton, blue: methylene protons).
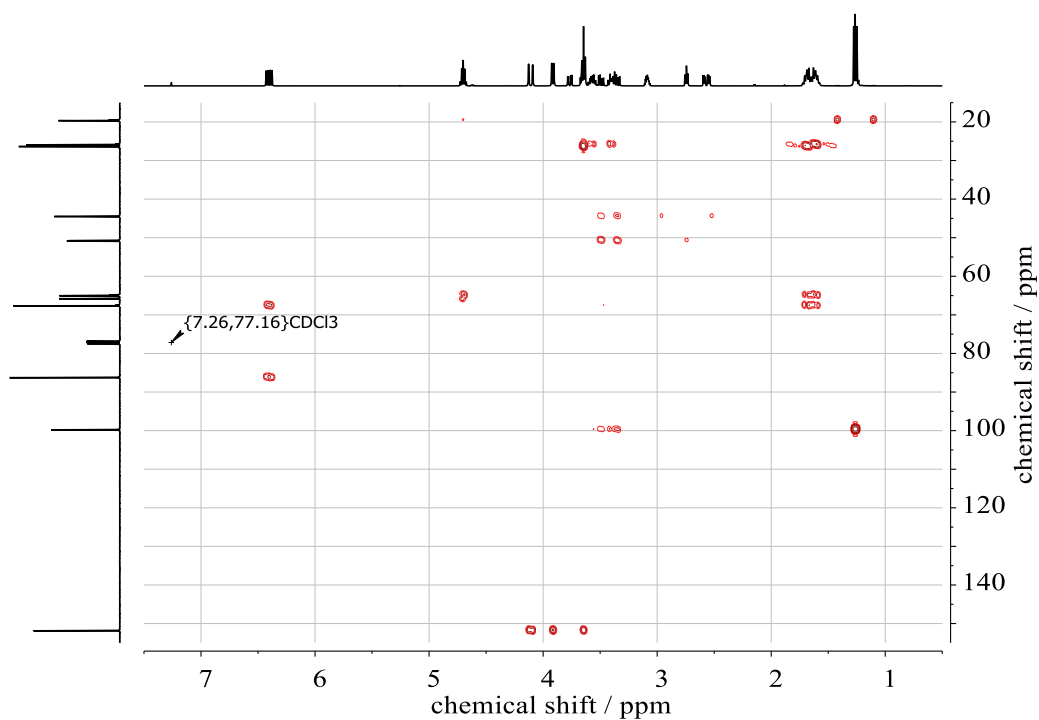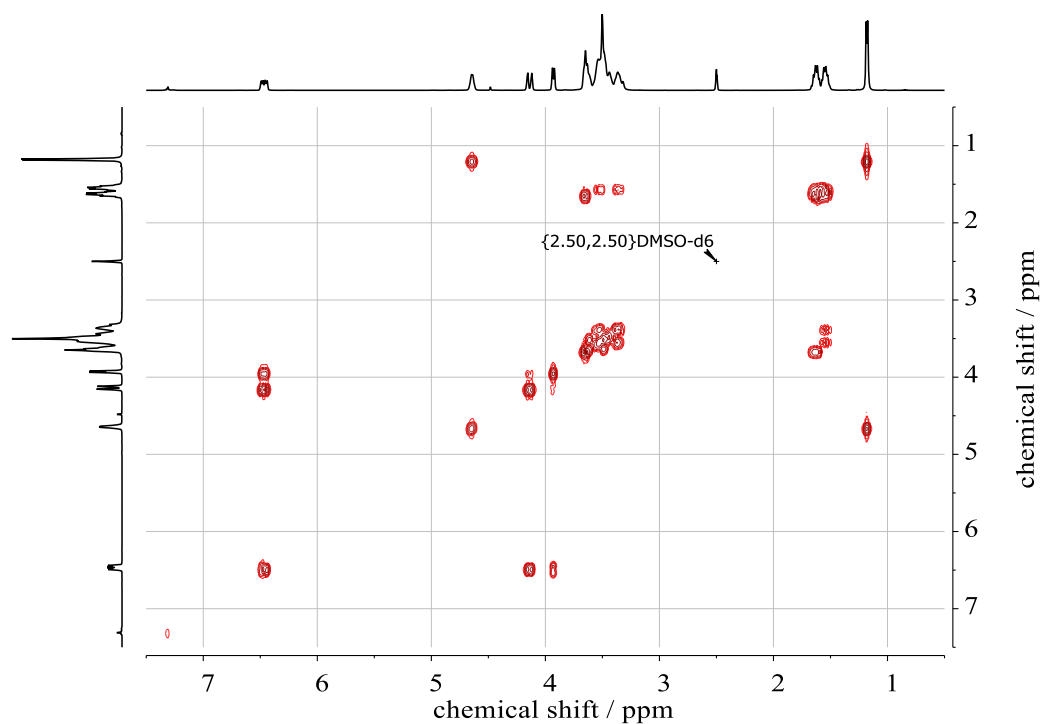
SI-Figure 5. ^{1}H, ^{13}C HMBC NMR of EBVGE monomer in C*D*Cl$_3$.
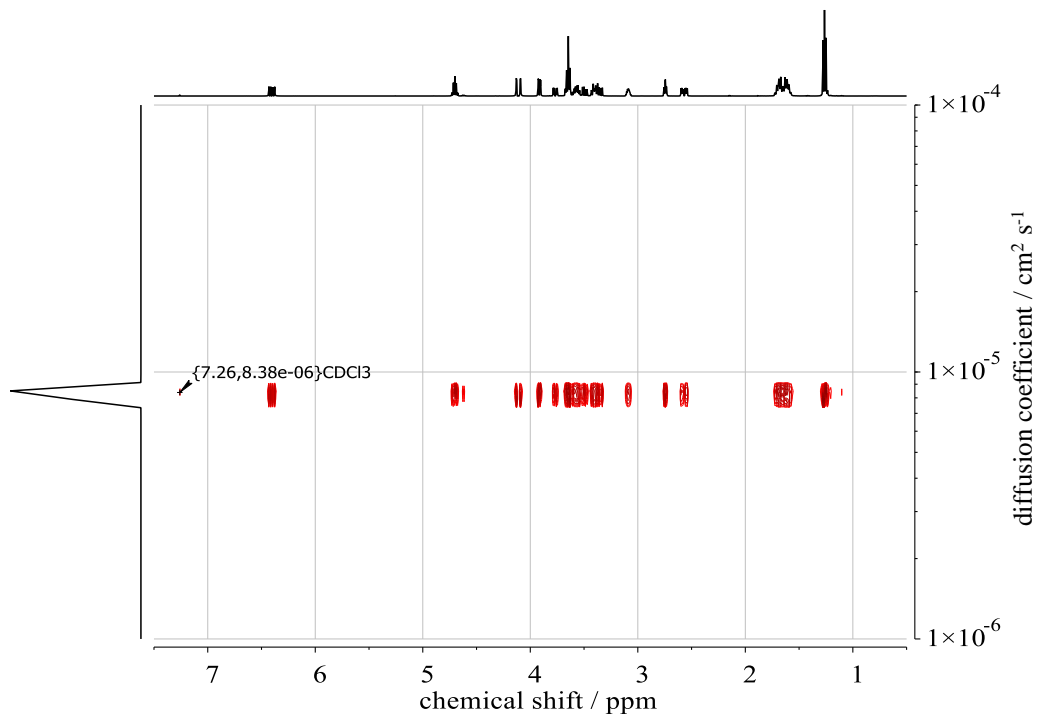
SI-Figure 6. ^{1}H DOSY NMR (400 MHz, C*D*Cl$_3$) of EBVGE monomer.
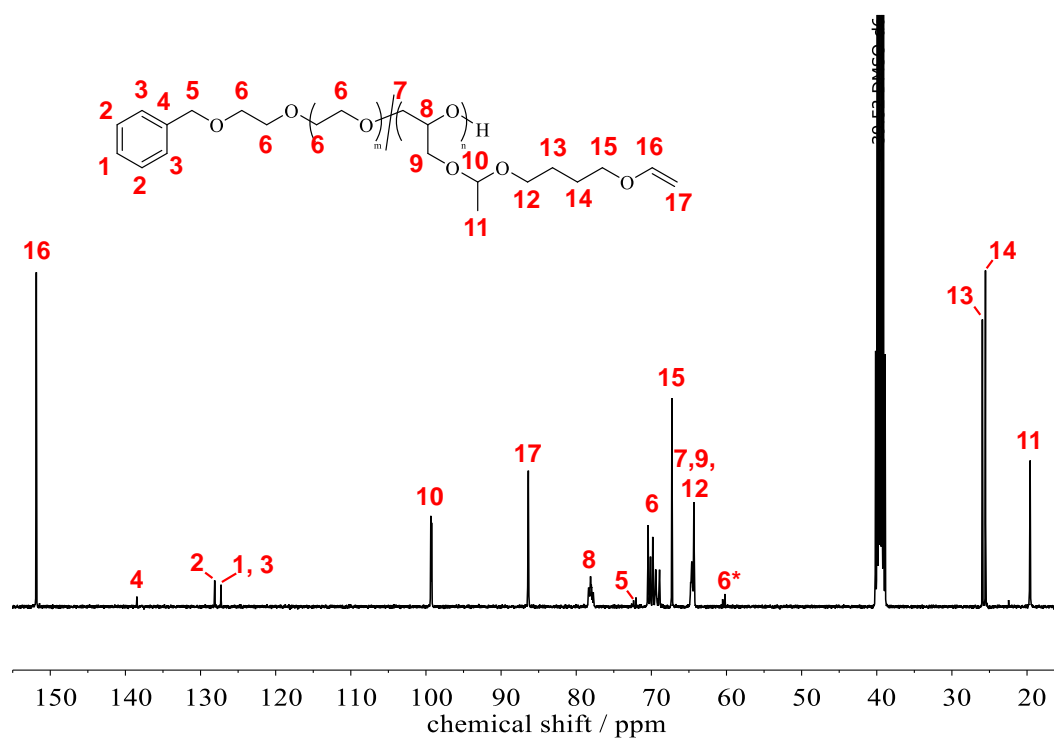
SI-Figure 7. ^{13}C NMR spectrum (100 MHz, DMSO-d_6) of PEG$_{16}$-*ran*-PEBVGE$_{44}$ (entry 4, **Table 1**).

**SI-Figure 8.** ^{1}H, ^{1}H COSY NMR (400 MHz, DMSO-d_6) of PEG$_{16}$-*ran*-PEBVGE$_{44}$ (entry 4, **Table 1**).
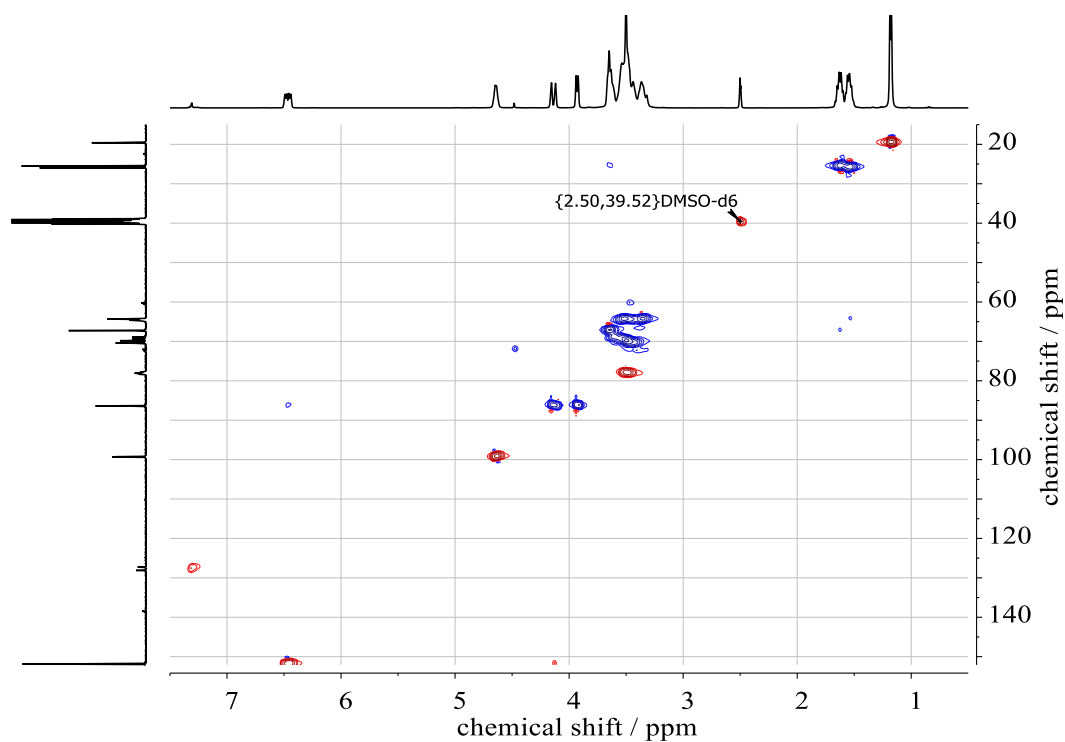
SI-Figure 9. ^{1}H, ^{13}C HSQC NMR of PEG$_{16}$-*ran*-PEBVGE$_{44}$ (entry 4, **Table 1**) in DMSO-d_6. Color of the signals indicates the phase information (red: methine proton, blue: methylene protons).
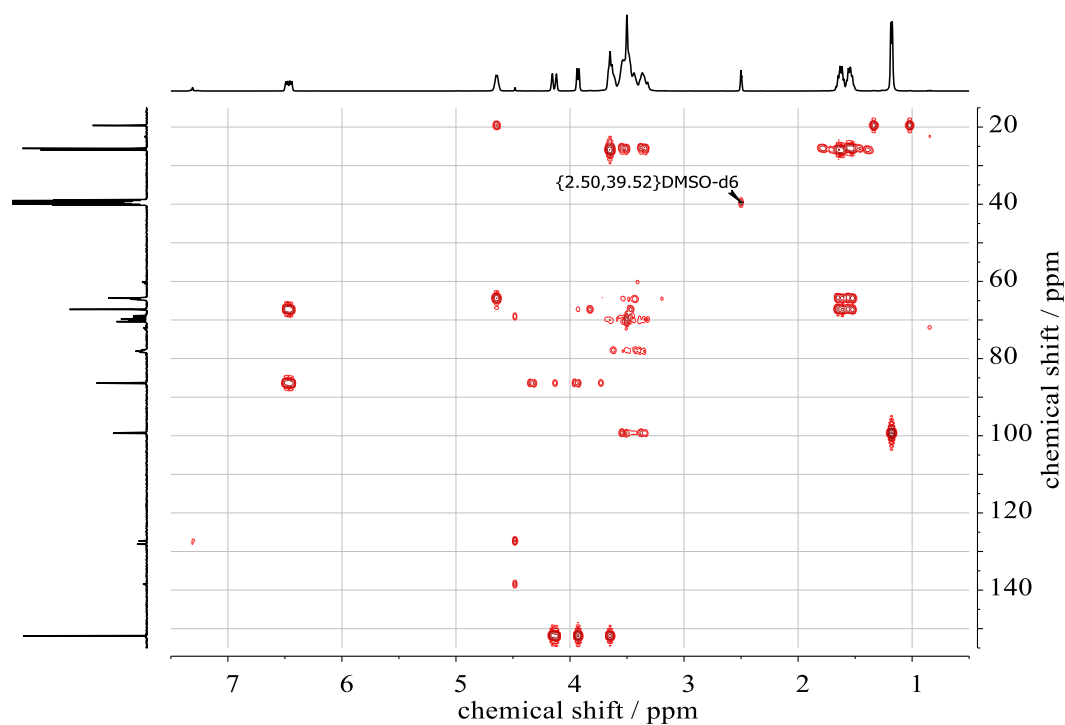
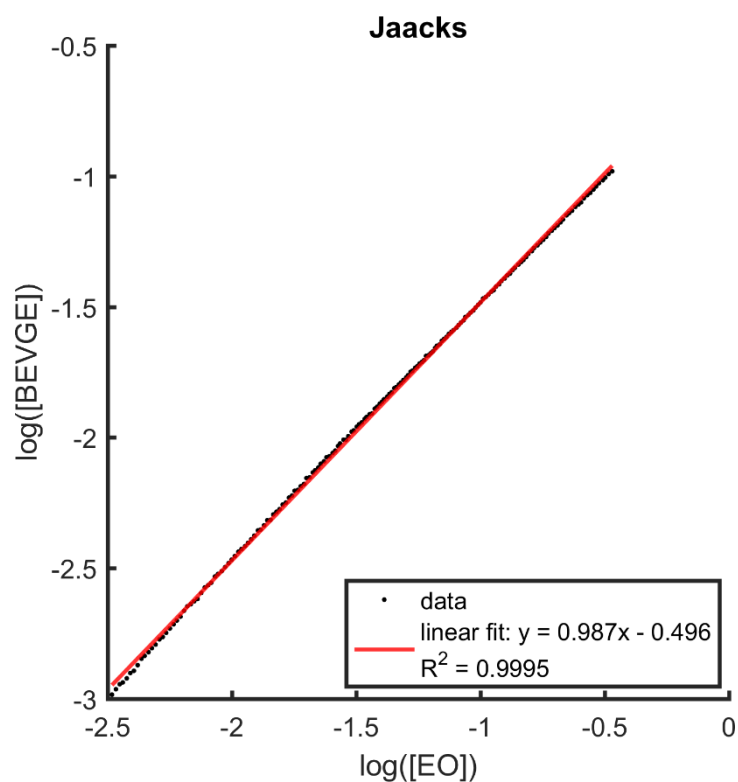**SI-Figure 10.** ^{1}H, ^{13}C HMBC NMR of PEG$_{16}$-*ran*-PEBVGE$_{44}$ (entry 4, **Table 1**) in DMSO-d_6.
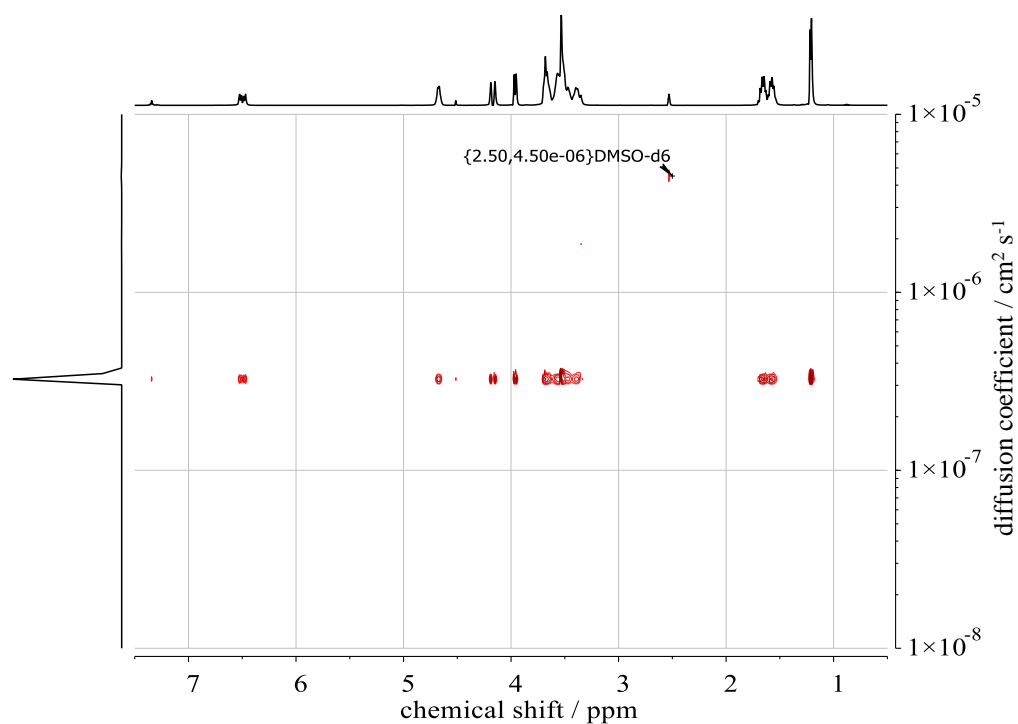
SI-Figure 11. ^{1}H DOSY NMR (400 MHz, DMSO-d_6) of PEG$_{16}$-*ran*-PEBVGE$_{44}$ (entry 4, Table 1).
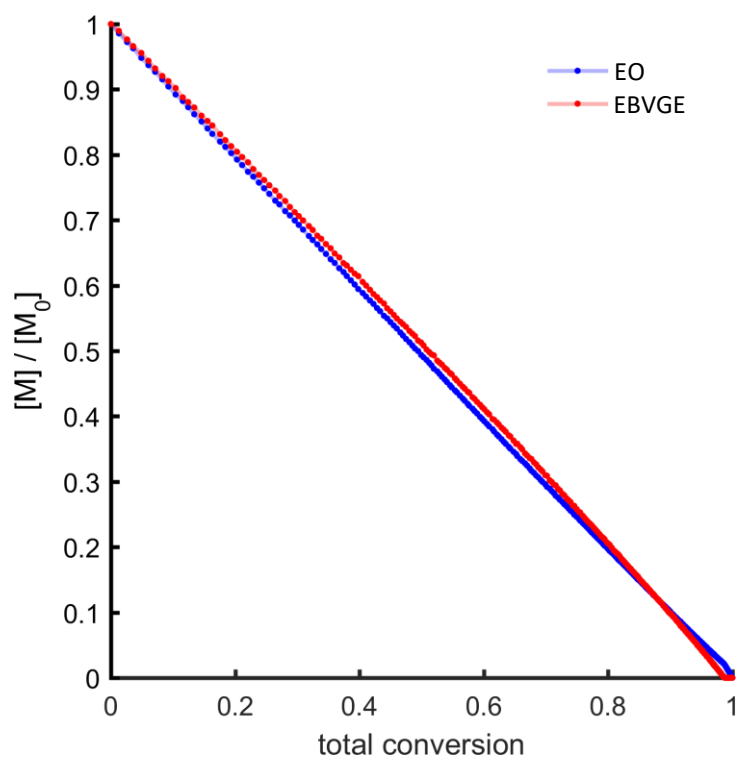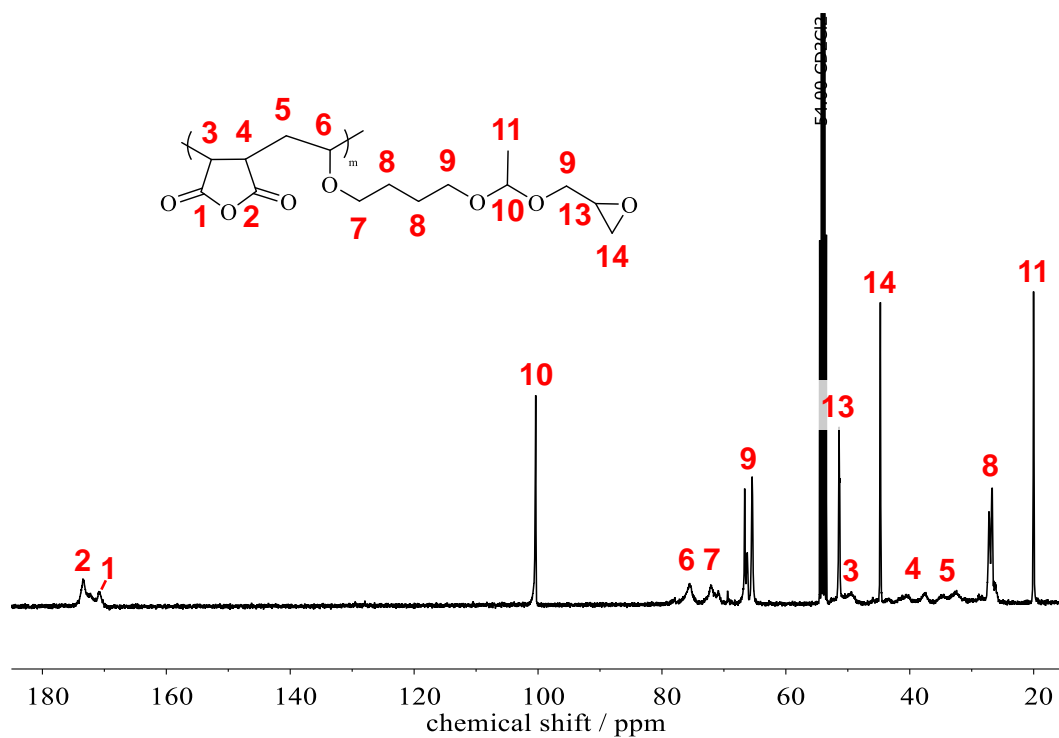

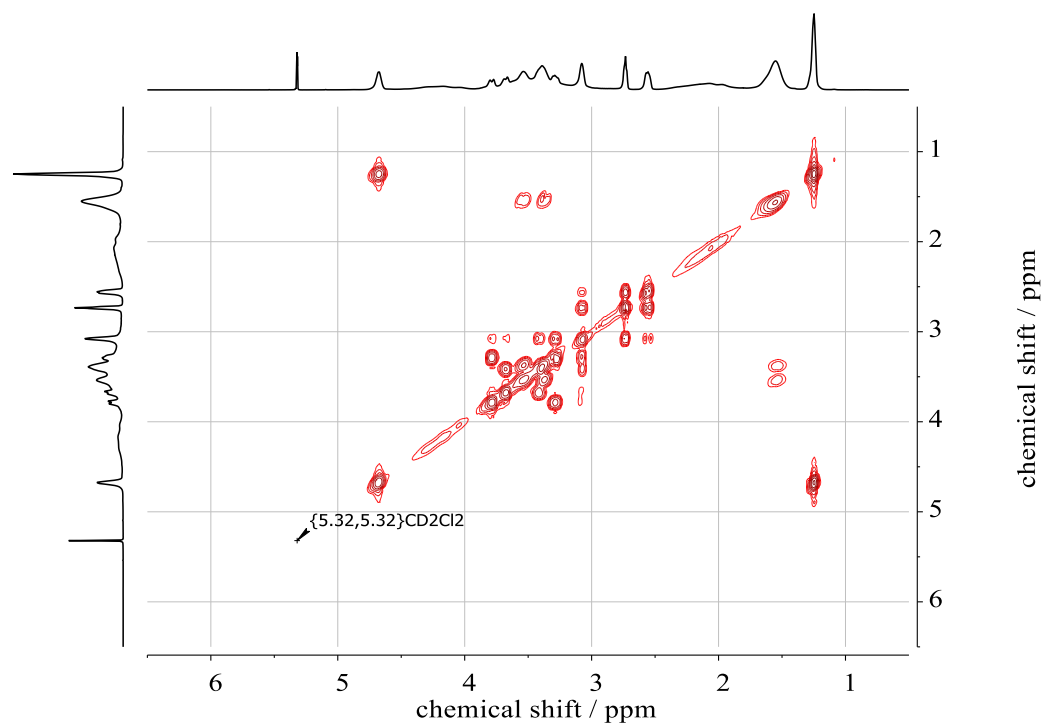**SI-Figure 12.** Concentration of the comonomers EBVGE and EO plotted versus the conversion.

SI-Figure 13. Jaacks fit for determination of reactivity ratios for the copolymerization of EBVGE and EO in DMSO-d_6 at 60 °C.
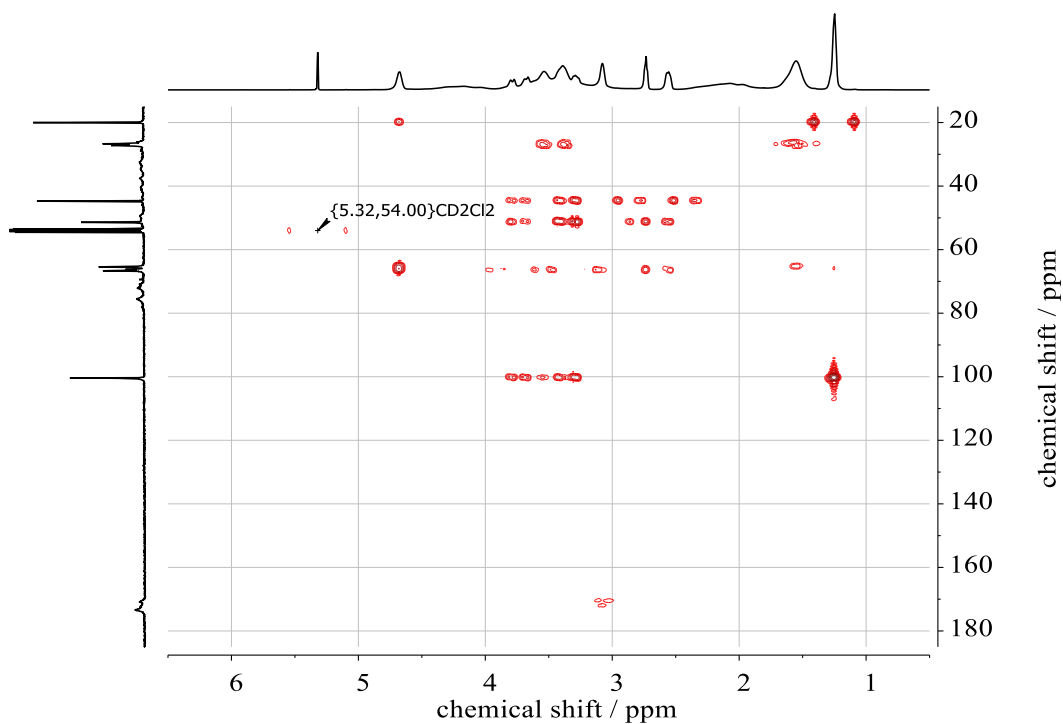

SI-Figure 14. ^{13}C NMR spectrum (100 MHz, CD_2Cl$_2$) of P(MA$_{0.5}$-*alt*-EBVGE$_{0.5}$) (entry 1, **Table 3**).

SI-Figure 15. ^{1}H, ^{1}H COSY NMR (400 MHz, CD_2Cl$_2$) of P(MA$_{0.5}$-*alt*-EBVGE$_{0.5}$) (entry 1, **Table 3**).
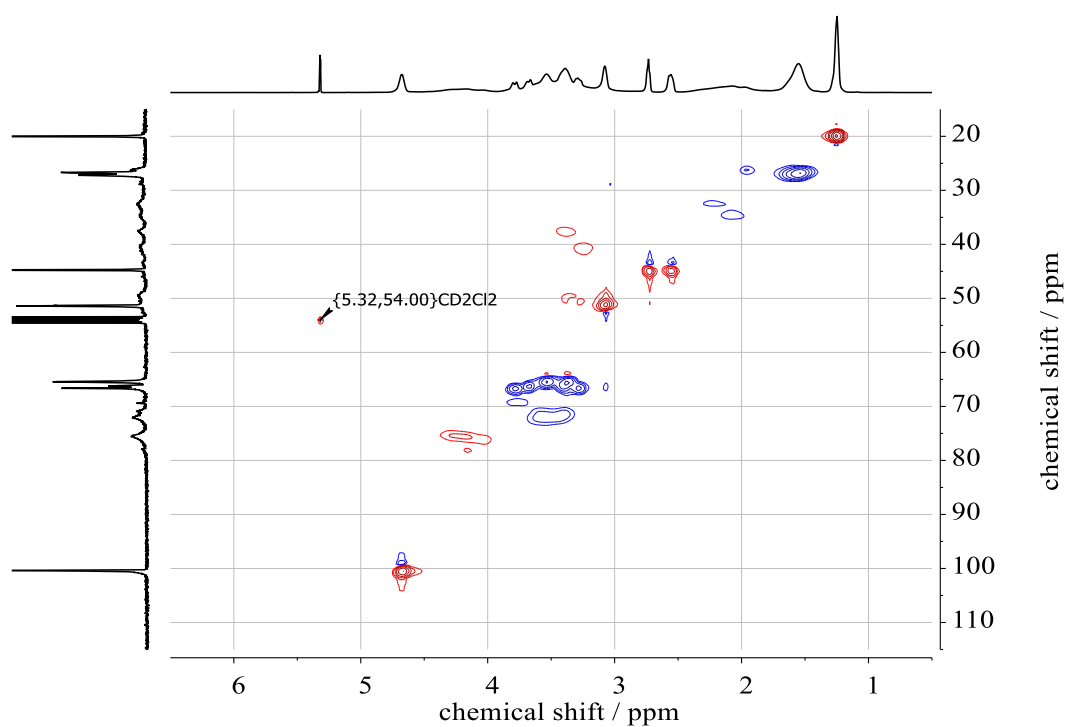
SI-Figure 16. ^{1}H, ^{13}C HSQC NMR of P(MA$_{0.5}$-*alt*-EBVGE$_{0.5}$) (entry 1, **Table 3**) in CD_2Cl$_2$. Color of the signals indicates the phase information (red: methine proton, blue: methylene protons).

SI-Figure 17. ^{1}H, ^{13}C HMBC NMR of P(MA$_{0.5}$-*alt*-EBVGE$_{0.5}$) (entry 1, **Table 3**) in CD_2Cl$_2$.
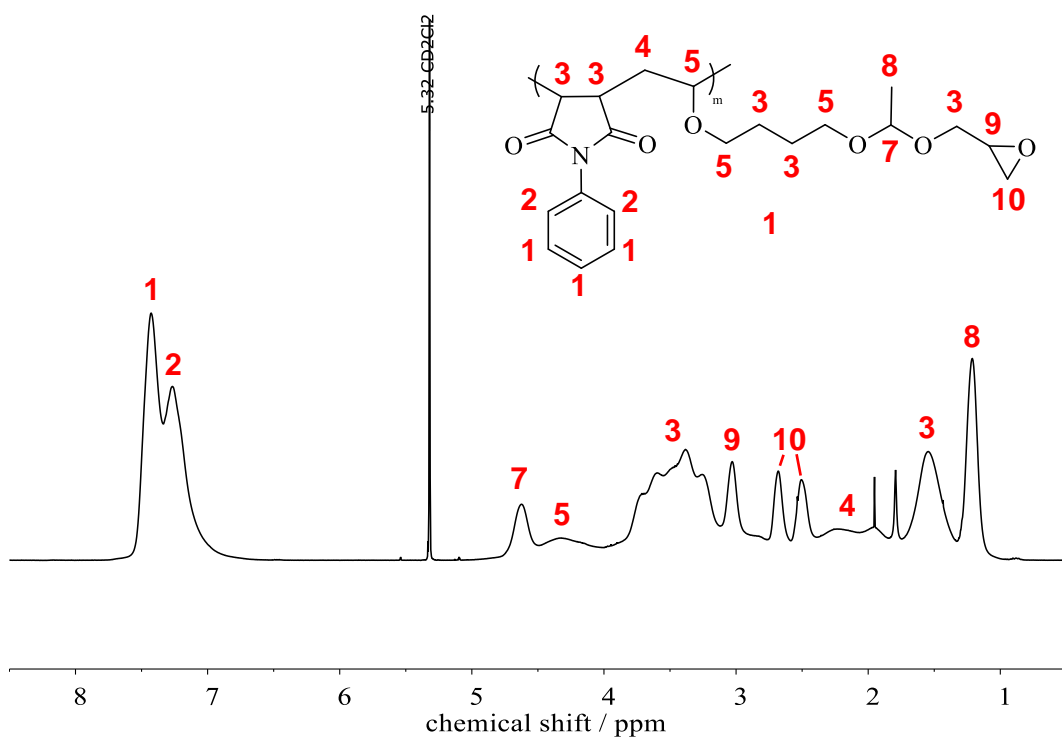
SI-Figure 18. ^{1}H NMR spectrum (400 MHz, CD_2Cl$_2$) of P(PM$_{0.5}$-*alt*-EBVGE$_{0.5}$) (entry 2, **Table 3**).
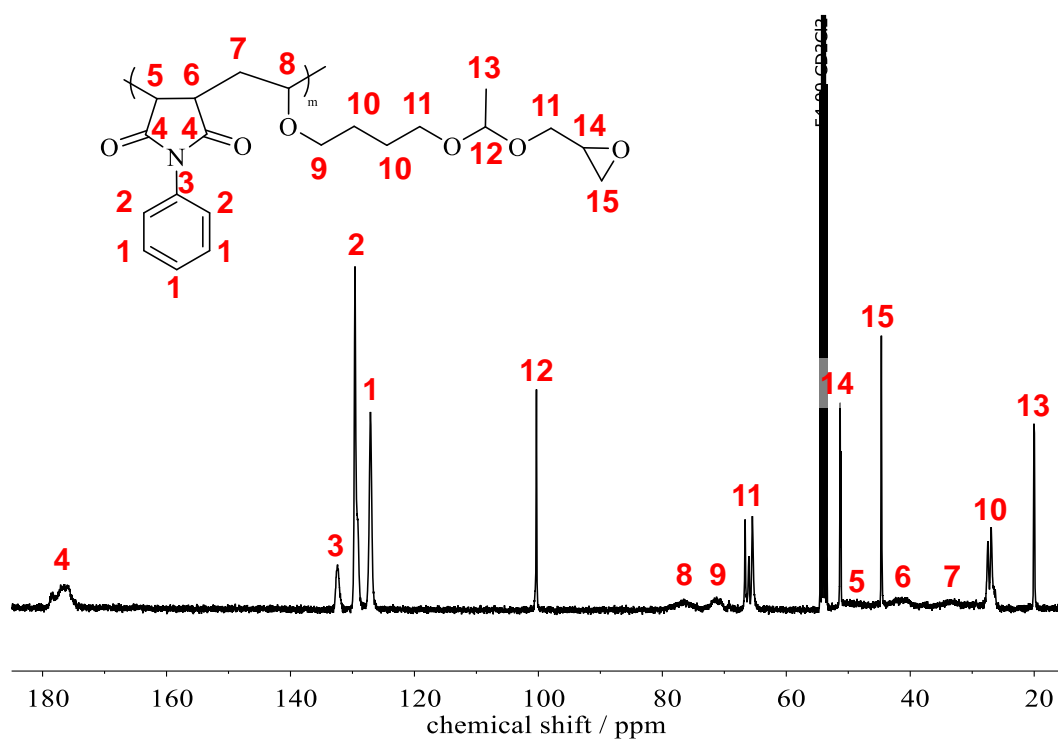
SI-Figure 19. ^{13}C NMR spectrum (100 MHz, CD_2Cl$_2$) of P(PM$_{0.5}$-*alt*-EBVGE$_{0.5}$) (entry 2, **Table 3**).
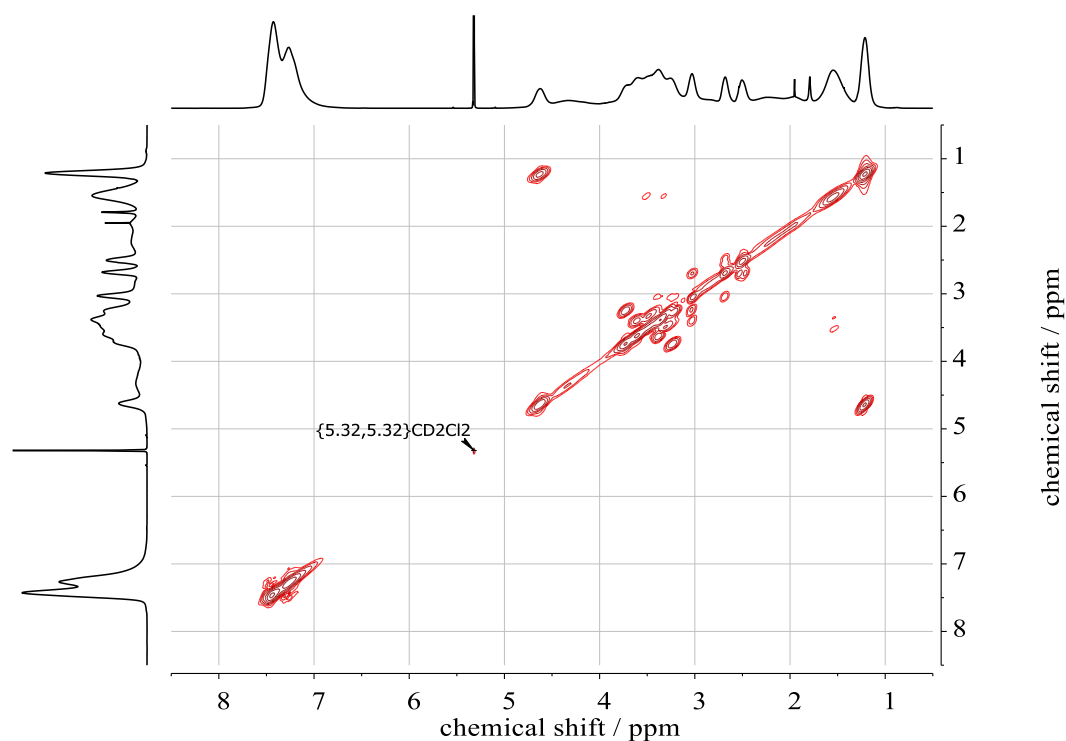
SI-Figure 20. ^{1}H, ^{1}H COSY NMR (400 MHz, CD_2Cl$_2$) of P(PM$_{0.5}$-*alt*-EBVGE$_{0.5}$) (entry 2, **Table 3**).
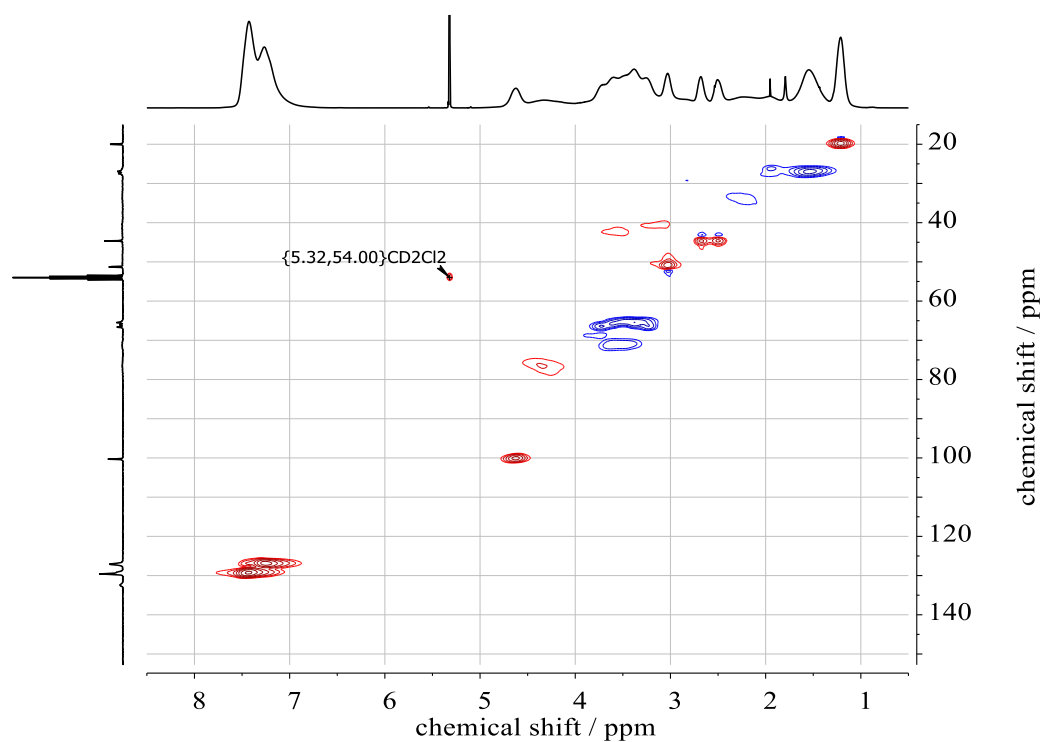
SI-Figure 21. ^{1}H, ^{13}C HSQC NMR of P(PM$_{0.5}$-*alt*-EBVGE$_{0.5}$) (entry 2, **Table 3**) in CD$_2$Cl$_2$. Color of the signals indicates the phase information (red: methine proton, blue: methylene protons).
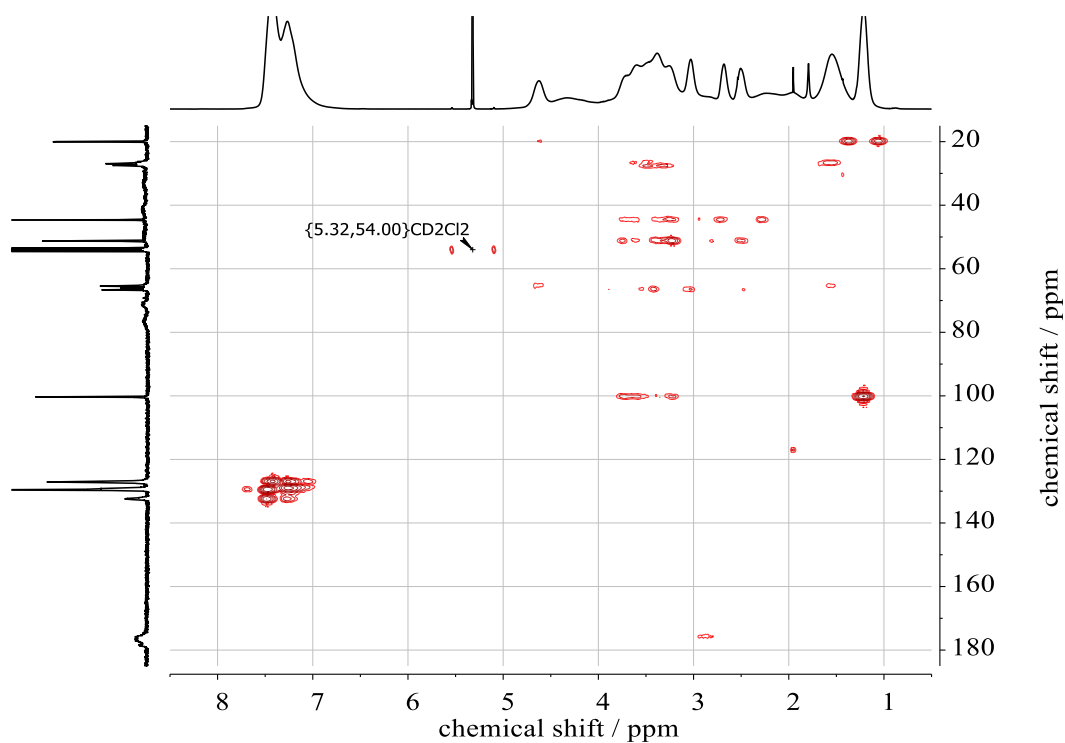
SI-Figure 22. ^{1}H, ^{13}C HMBC NMR of P(PM$_{0.5}$-*alt*-EBVGE$_{0.5}$) (entry 2, **Table 3**) in CD$_2$Cl$_2$.
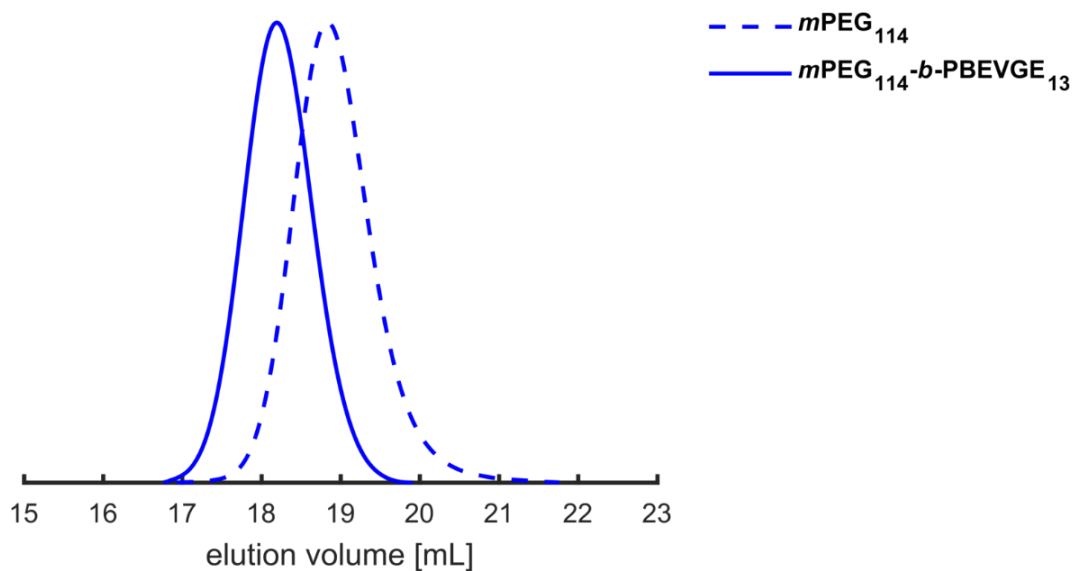
SI-Figure 23. SEC traces (DMF, PEG-standard, RI detector) of $mPEG_{114}$-b-PEBVGE$_{13}$ (entry 6, Table 4) and its macroinitiator $mPEG_{114}$.
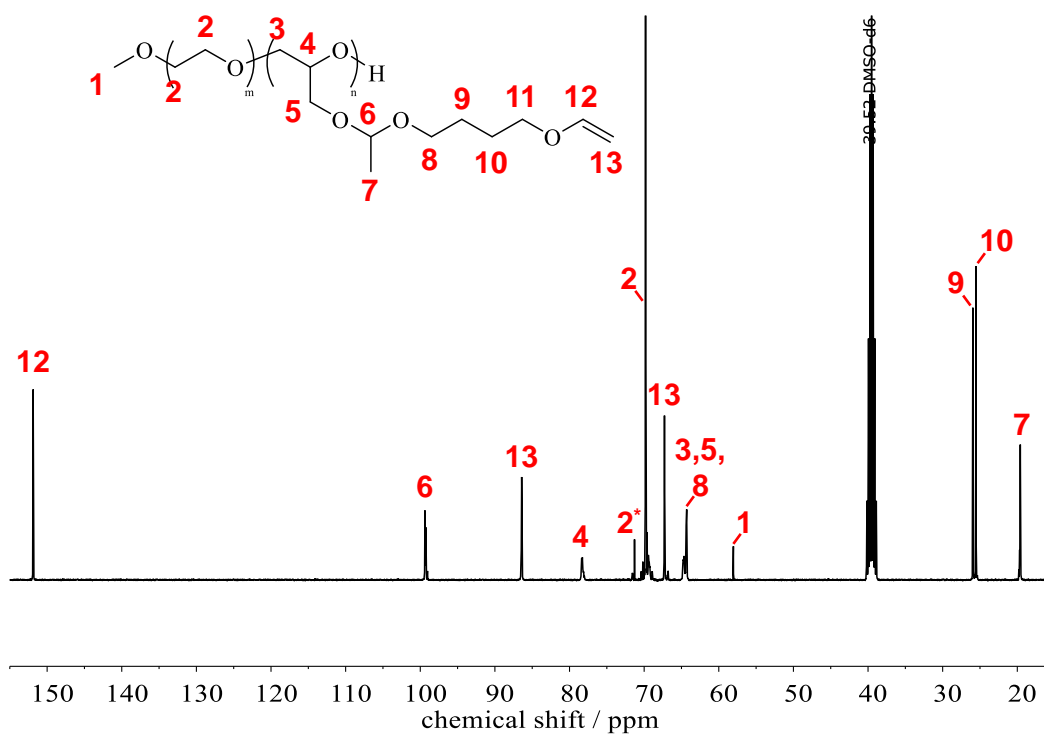
SI-Figure 24. ^{13}C NMR spectrum (400 MHz, DMSO-d_6) of $mPEG_{45}$-b-PEBVGE$_{15}$ (entry 4, Table 4).
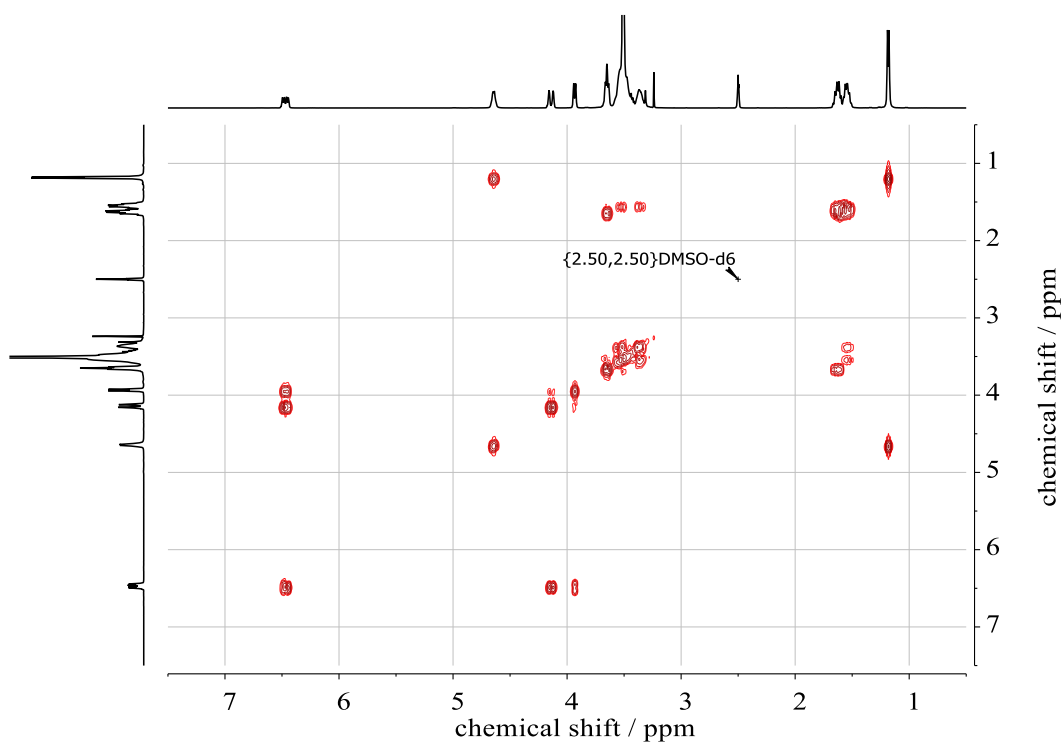
SI-Figure 25. ^{1}H, ^{1}H COSY NMR (400 MHz, DMSO-d_6) of mPEG$_{45}$-b-PEBVGE$_{15}$ (entry 4, **Table 4**).
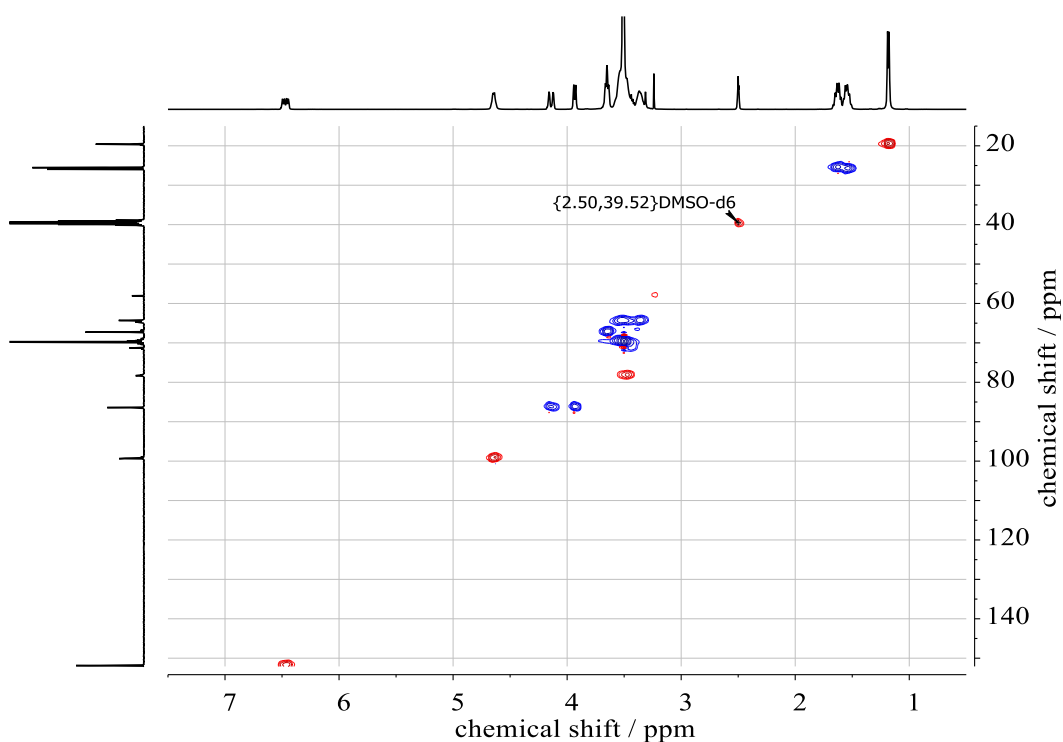
SI-Figure 26. ^{1}H, ^{13}C HSQC NMR of mPEG$_{45}$-b-PEBVGE$_{15}$ (entry 4, **Table 4**) in DMSO-d_6 Color of the signals indicates the phase information (red: methine proton, blue: methylene protons).
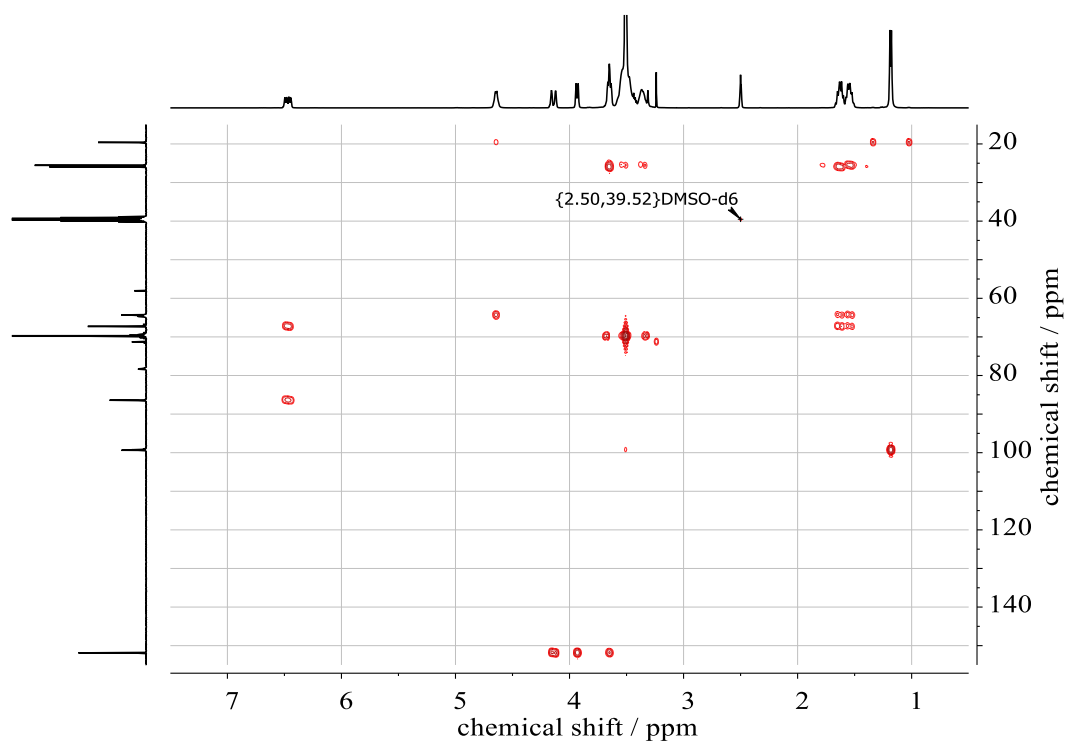
**SI-Figure 27.** ^{1}H, ^{13}C HMBC NMR (400 MHz, DMSO-d_6) of mPEG$_{45}$-b-PEBVGE$_{15}$ (entry 4, **Table 4**).
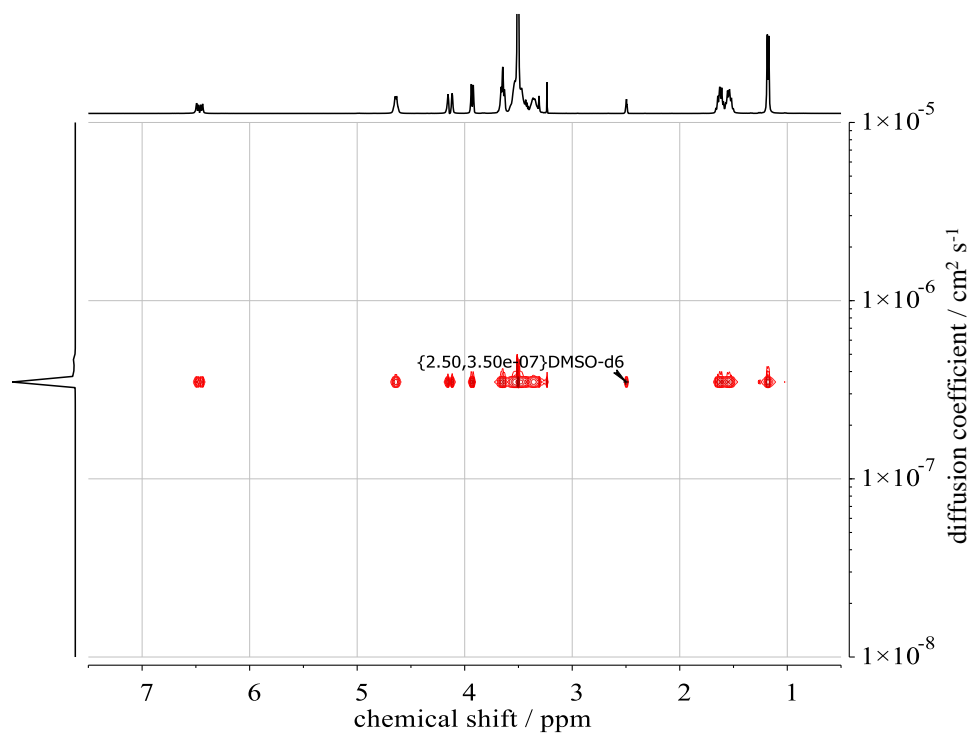
SI-Figure 28. ^{1}H DOSY NMR (400 MHz, DMSO-d_6) of mPEG$_{45}$-b-PEBVGE$_{15}$ (entry 4, **Table 4**).
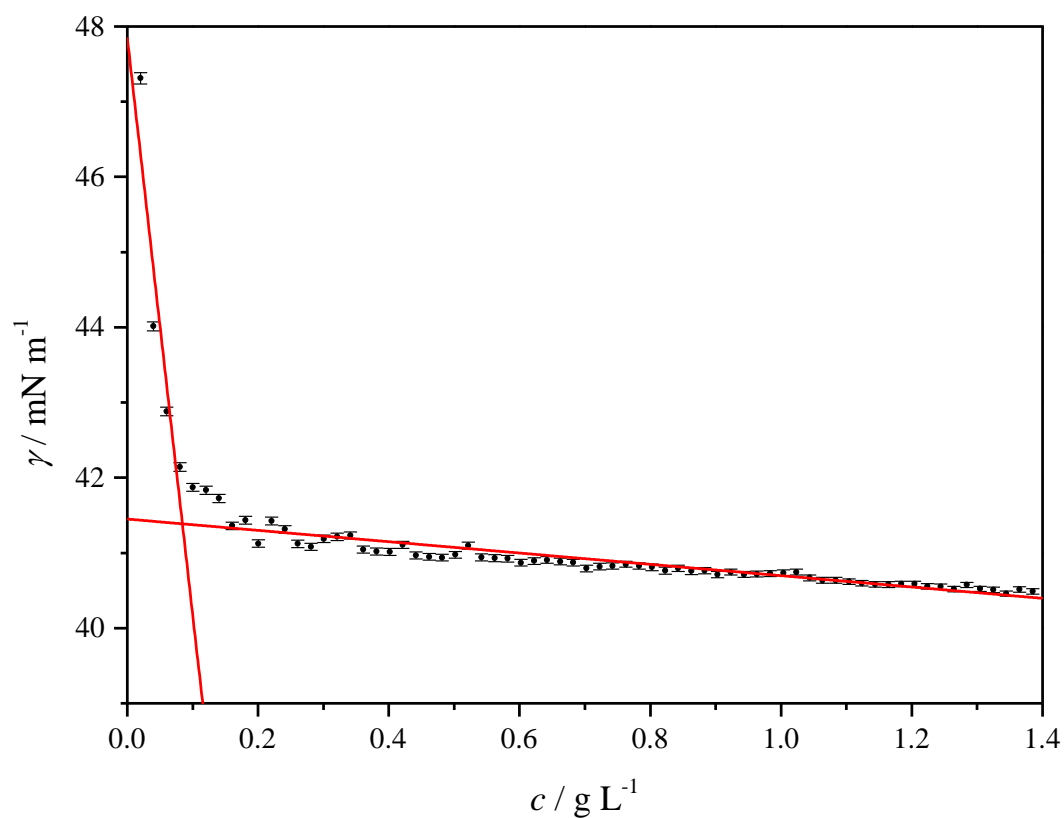
SI-Figure 29. Plot of surface tension γ vs. concentration c of aqueous surfactant solution of mPEG$_{114}$-b-PEBVGE$_{13}$ (entry 6, **Table 4**) including regression straight lines for determination of the critical micelle concentration ($CMC = 84.2$ mg L^{-1}).
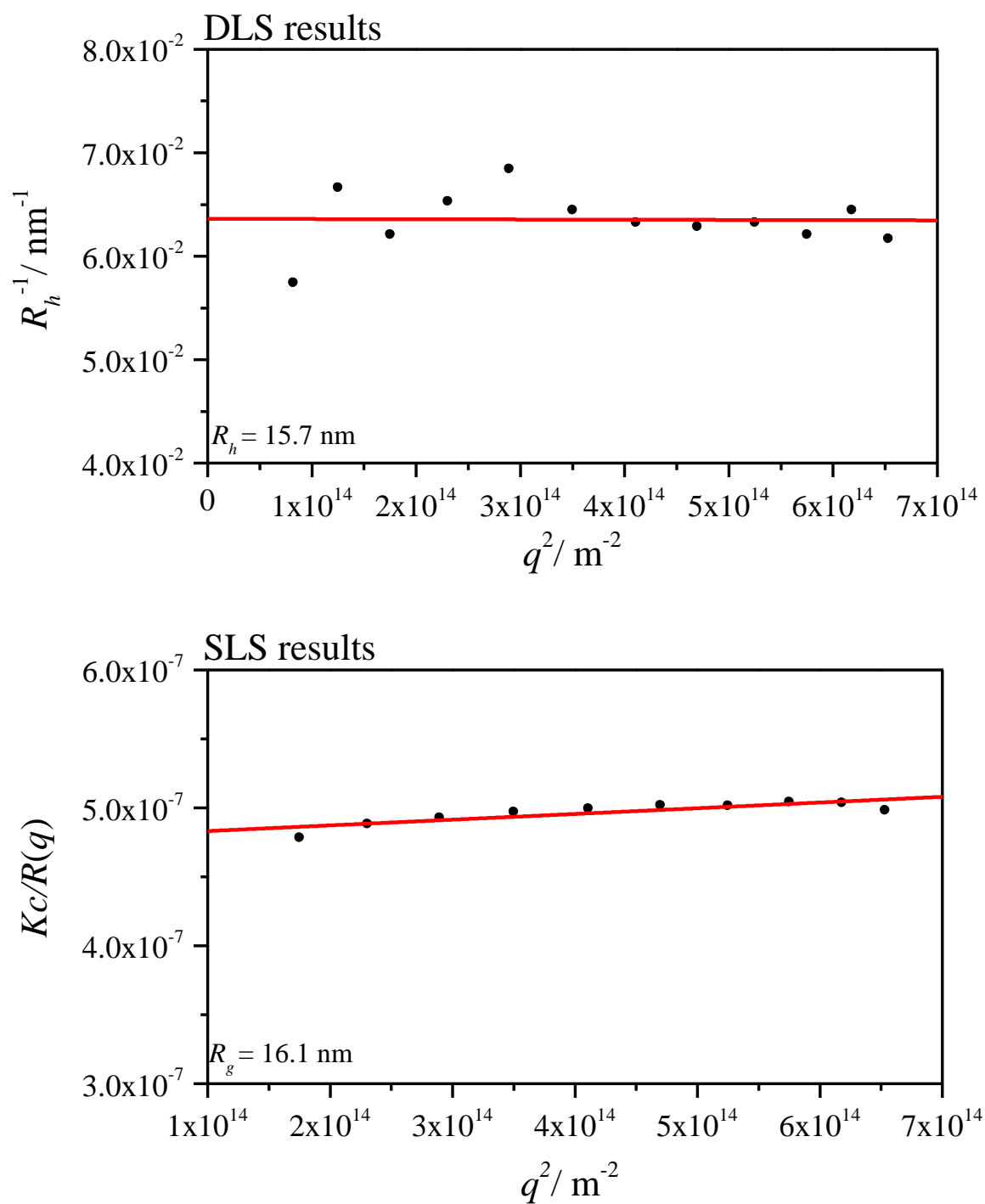
SI-Figure 30. DLS and SLS characterization of non-crosslinked mPEG$_{114}$-b-PEBVGE$_{13}$ (entry 6, **Table 4**) micelles in water ($c = 2$ g L^{-1}).
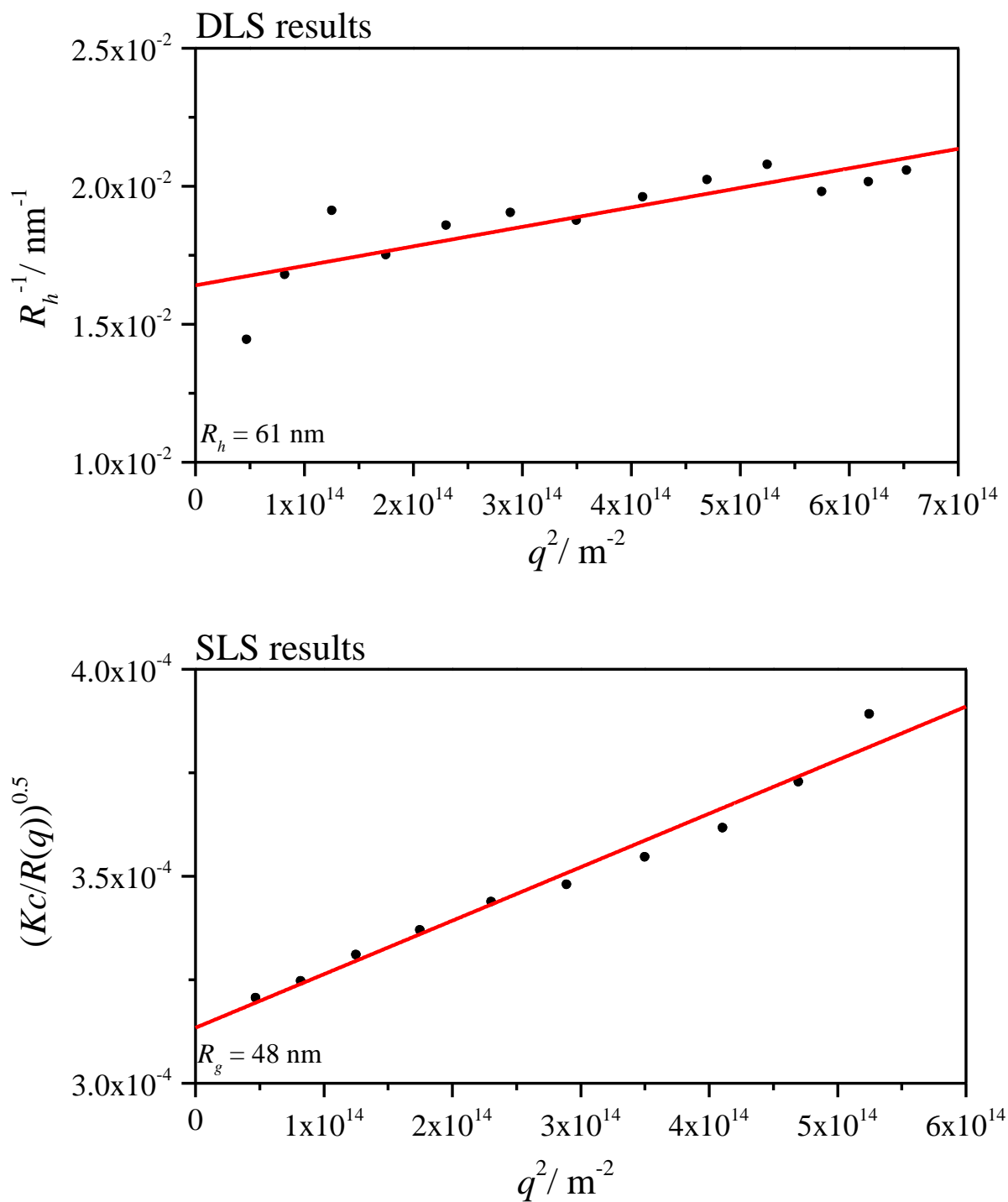
SI-Figure 31. DLS and SLS characterization of non-crosslinked and loaded (PETMP and DMPA) mPEG$_{114}$-b-PEBVGE$_{13}$ (entry 6, **Table 4**) micelles in water (c = 2 g L^{-1}).
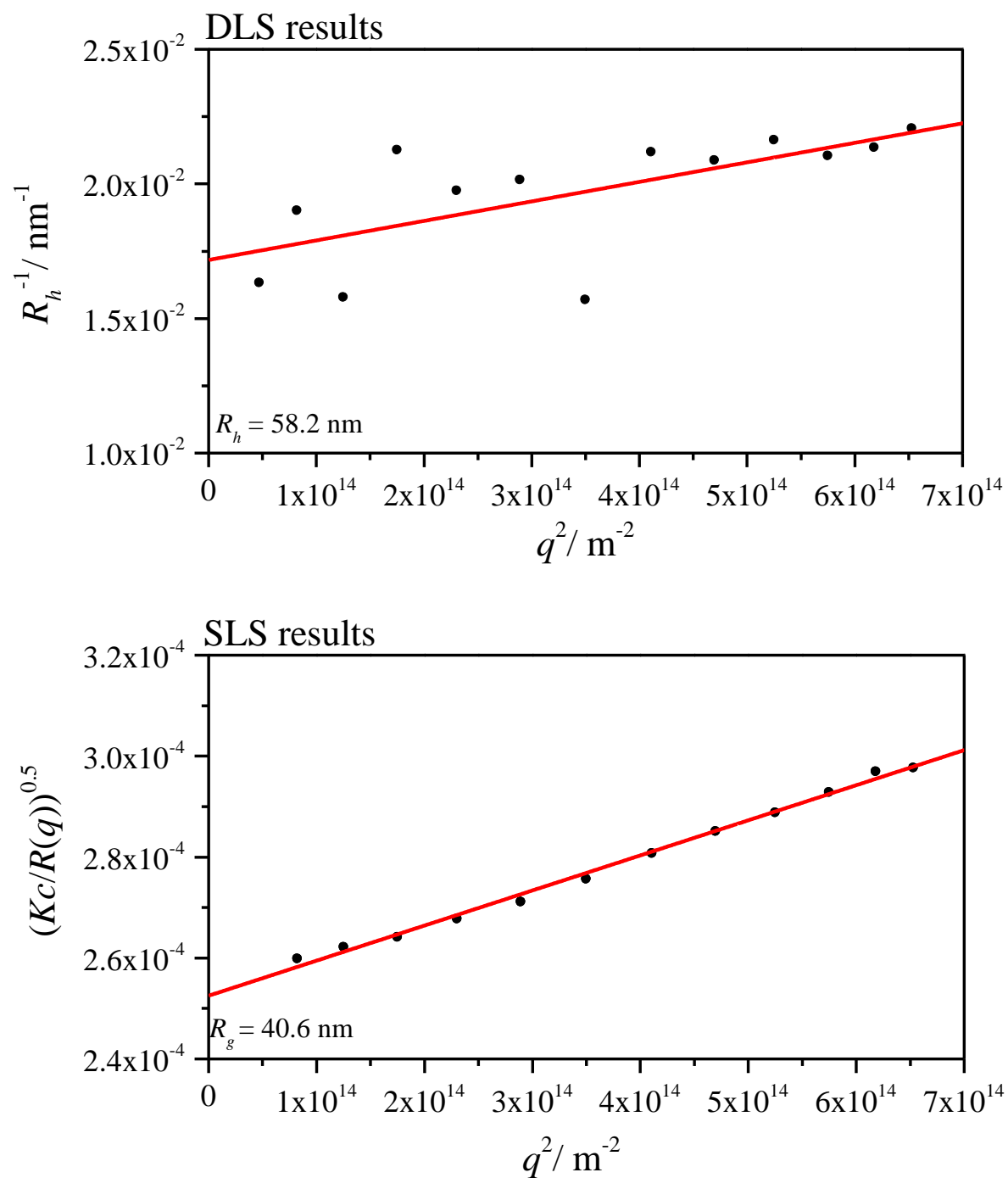
SI-Figure 32. DLS and SLS characterization of crosslinked mPEG$_{114}$-b-PEBVGE$_{13}$ (entry 6, **Table 4**) micelles in water ($c = 2$ g L^{-1}) by using PETMP and DMPA.
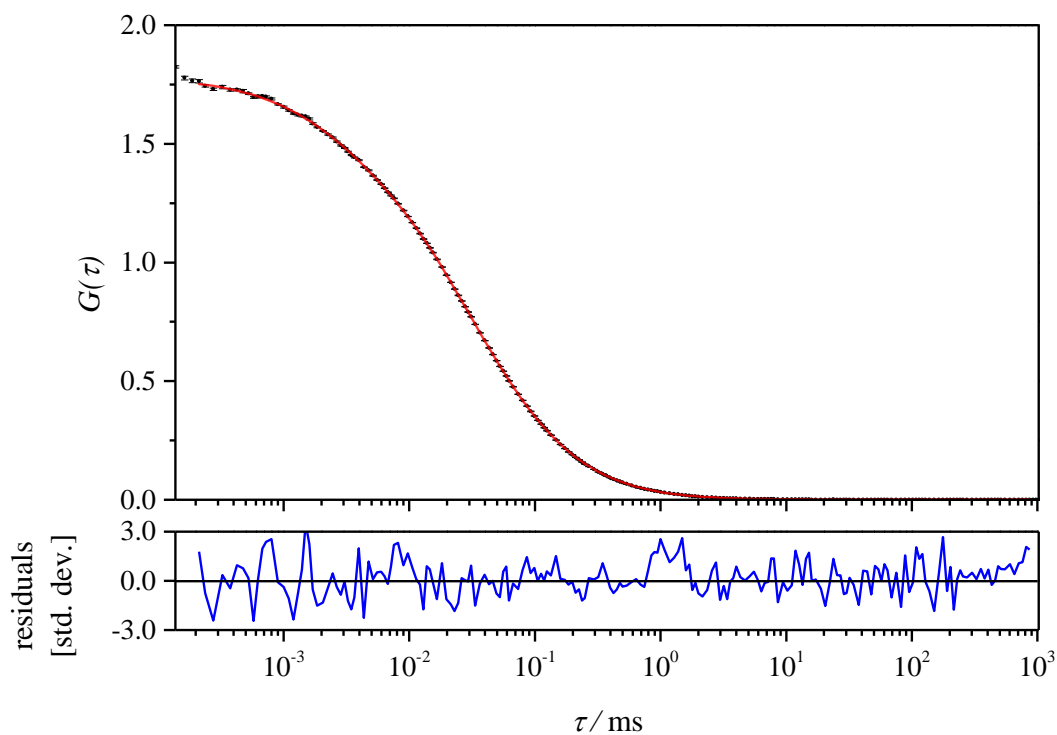
SI-Figure 33. Autocorrelation curve, fitting curve and residuals of free Rhodamine B in water ($D = 418.5\ \mu\text{m}^2\ \text{s}^{-1}$, $V_{eff} = 0.344$, $\kappa = 5.325$).
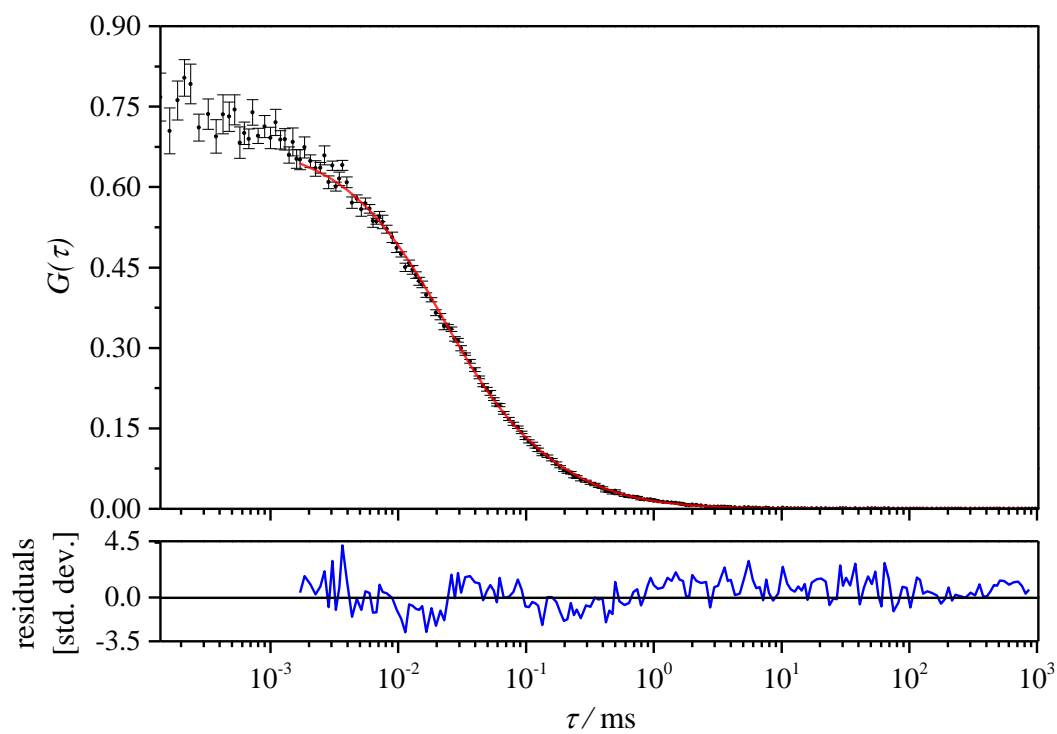
SI-Figure 34. Autocorrelation curve, fitting curve and residuals of free Nile red in water ($D = 313.0\ \mu\text{m}^2\ \text{s}^{-1}$, $V_{eff} = 0.403$, $\kappa = 5.266$).
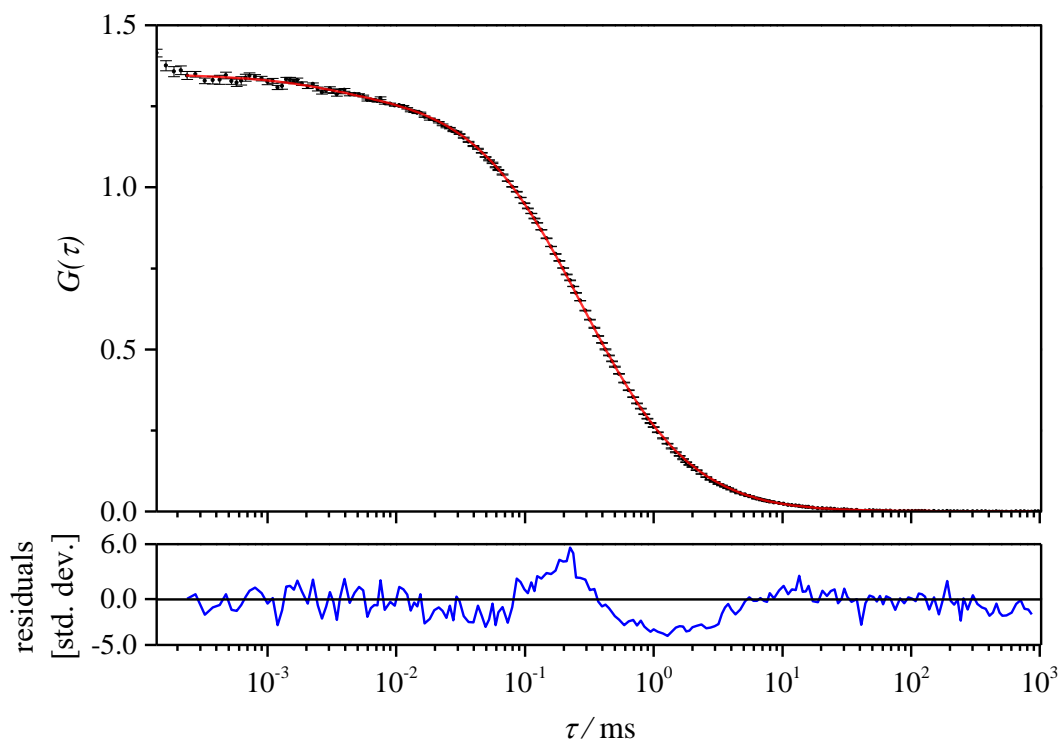
SI-Figure 35. Autocorrelation curve, fitting curve and residuals of mPEG$_{114}$-b-PEBVGE$_{13}$ (entry 6, **Table 4**) in water before acidification ($D = 51.7$ µm² s^{-1}, $V_{eff} = 0.403$, $\kappa = 5.266$).
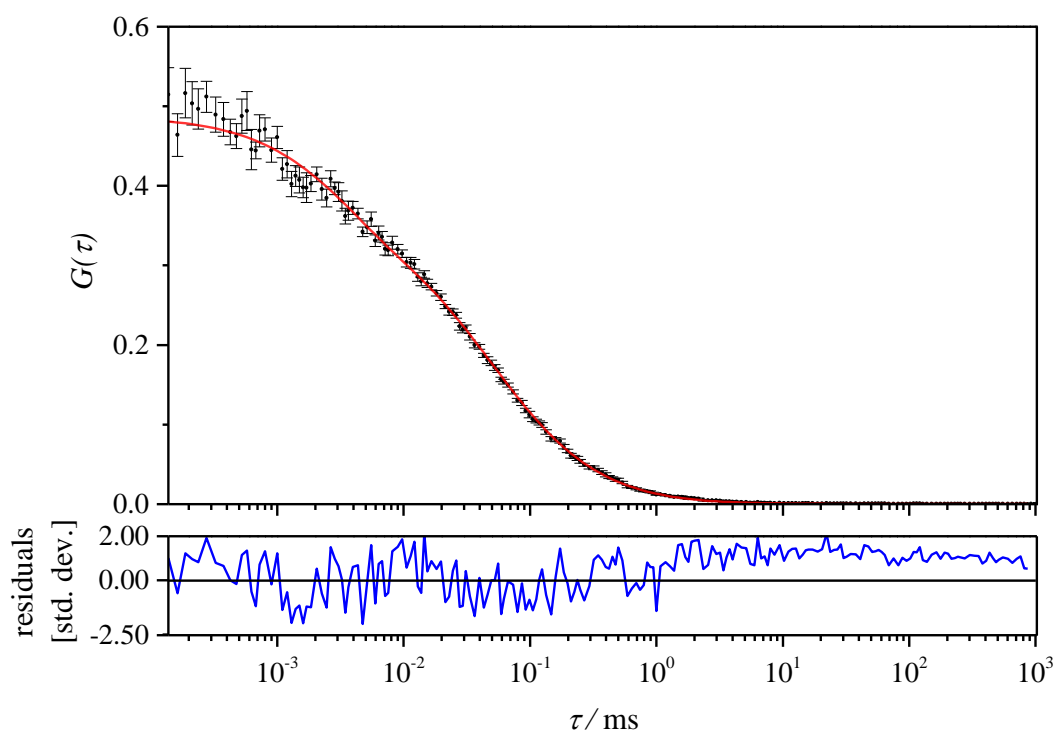
SI-Figure 36. Autocorrelation curve, fitting curve and residuals of mPEG$_{114}$-b-PEBVGE$_{13}$ (entry 6, **Table 4**) in water after acidification ($D = 292.0$ µm² s^{-1}, $V_{eff} = 0.403$, $\kappa = 5.266$).

3.2. Epoxy Undecane Methacrylate: A Symbiosis of Methacrylates and Poly(ethylene glycol)

Kamil Maciol[a], *Tatjana Dänzer*[a], *Jennifer Keth*[a], *Jan Blankenburg*[a,b] and *Holger Frey*[a,*]

[a] Institute of Organic Chemistry, Johannes Gutenberg University Mainz, Duesbergweg 10-14, 55128 Mainz, Germany

[b] Graduate School Materials Science in Mainz, Staudinger Weg 9, 55128 Mainz, Germany

*E-Mail: hfrey@uni-mainz.de

To be submitted

ABSTRACT

A novel methacrylate-containing alkyl epoxide is presented: epoxy undecane methacrylate (EUMA). This orthogonal monomer is prepared in a two-step reaction sequence and is suitable for both anionic and radical polymerization. Monomer-activated anionic ring-opening copolymerization of ethylene oxide (EO) and EUMA allowed access to multi-functional PEG-*grad*-PEUMA gradient copolymers with molecular weights up to 20,500 g mol^{-1}. Besides the detailed characterization via NMR spectroscopy and the investigation of thermal properties ($T_g \leq$ -57 °C, $T_m \leq$ 50 °C), the reaction kinetics were studied by real-time ^{1}H NMR spectroscopy and revealed reactivity ratios of $r_{EO} = 9.43$ and $r_{EUMA} = 0.10$. These strongly tapered copolymer structures were used for the preparation of crosslinkable micelles in aqueous solutions. The reversible addition-fragmentation chain transfer (RAFT) polymerization enabled the design of epoxide-bearing side chains along the methacrylate backbone by the copolymerization of EUMA with 2-hydroxyethyl methacrylate (HEMA) and methyl methacrylate (MMA). This approach led to well-defined copolymers with molecular weights ranging from 8,300−14,900 g mol^{-1}. For the formation of organogels, the pendant epoxide moieties were crosslinked with an amine curing agent. The formed networks exhibited a dichloromethane uptake of approximately 1,000%.

TABLE OF CONTENTS GRAPHICS
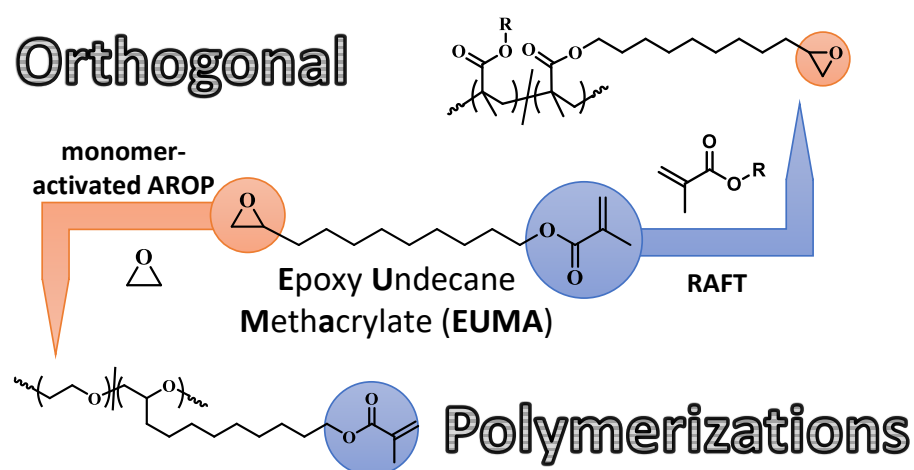
INTRODUCTION

The highly reactive double bond of methacrylates renders them, together with acrylates, to one of the most versatile and important class of monomers for the synthesis of polymers.[1–4] Owing to their properties, methacrylates would be eminent candidates as highly reactive side chains in a poly(ethylene glycol) (PEG) backbone for post-polymerization crosslinking reactions. PEG belongs to the class of polyethers and can be considered as the gold standard for many pharmaceutical and medical applications due to its excellent biocompatibility, very low toxicity and exceptional solubility in water.[5–10] The U.S. Food and Drug Administration (FDA) approved PEG as a polymer for medical use.[11] There are multiple routes for the synthesis of PEG by polymerization of the epoxide ethylene oxide (EO). Here, polymerization techniques such as anionic ring-opening polymerization (AROP)[12], monomer-activated polymerization[13] and cationic polymerization are included.[14,15]

Apart from numerous studies on the radical polymerization of the bifunctional monomer glycidyl methacrylate (GMA),[16–23] approaches already exist for the successful incorporation of pendant methacrylate groups in a polyether backbone via its epoxide functionality by cationic polymerization.[24–26] However, these polymerization techniques are limited due to transfer reactions.[27] In view of the harsh reaction conditions of the AROP, it is not surprising that there is nearly no literature on the direct polymerization of methacrylate-containing epoxide derivatives. Instead, post-polymerization modification such as end-group functionalization must be considered. In this context, there is a wealth of works about poly(ethylene glycol) dimethacrylate (PEGDMA).[28–31] Aside from numerous studies in the field of hydrogels, PEGDMA can also be used for the stabilization of poly(vinylidene fluoride-*co*-hexafluoropropylene) (PVDF-*co*-HFP) nanofibers[32] or as polymer electrolytes[33]. As recently reported, PEGDMA can be expanded with acetal[34,35] or ketal[36] cleavage sites to ensure the biodegradability of the polymer chains.

However, there is a possible solution for the direct incorporation of methacrylate moieties into a polyether backbone: the above-mentioned activated monomer method developed by Deffieux and Carlotti.[37] This method is based on a monomer-activated mechanism using an initiator/catalyst system. Organic salts such as tetraoctylammonium bromide (NOct$_4$Br) are used as initiators in combination with Lewis acid catalysts such as triisobutylaluminum (*i*Bu$_3$Al). As a result of monomer activation, polymerizations can be conducted under milder reaction conditions. In this manner, high molecular weight poly(propylene oxide) (PPO)[13] was achieved and monomers like epichlorohydrin (ECH)[38–40], epicyanohydrin (EPICH)[41], glycidyl

methyl ether (GME)[42–44] and fluoroalkyl glycidyl ethers[45,46] were polymerized, which is challenging or impossible under conventional AROP conditions.

In this work, we report on a novel methacrylate-containing epoxide derivative: epoxy undecane methacrylate (EUMA). This bifunctional monomer was selectively reacted via its epoxide and methacrylate functionality using anionic (**Scheme 1A**) and radical (**Scheme 1B**) polymerization techniques. As a result of the determined microstructure, the PEG-*grad*-PEUMA gradient copolymers were investigated regarding their self-assembly behavior. The radical copolymerization of EUMA led to poly(methacrylate)s with pendant epoxide groups, providing an ideal platform as organogels after crosslinking with amine curing agents. In addition, each type of copolymer was characterized and investigated in detail.

A) Monomer-activated anionic ring-opening polymerization
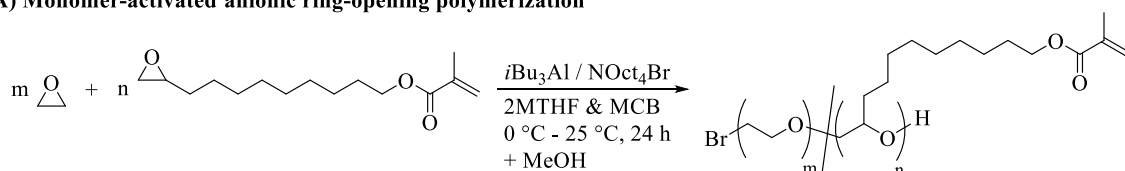
B) Reversible addition-fragmentation chain transfer polymerization
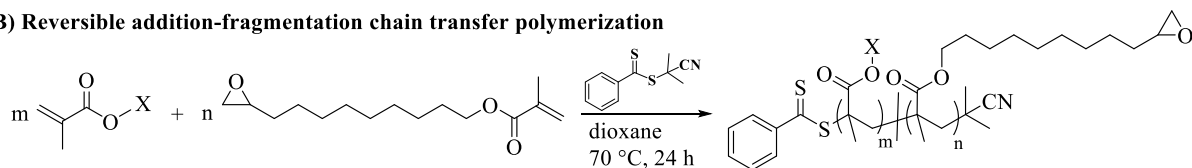
Scheme 1. Synthesis strategies for the monomer-activated anionic and the controlled radical copolymerization using the bifunctional epoxy undecane methacrylate (EUMA) monomer.

EXPERIMENTAL PART

Materials. Chemicals were purchased from general suppliers (Sigma-Aldrich, Acros Organics, Fluka, Carl Roth, etc.). Enzymatic transesterification of vinyl methacrylate was conducted with CALB (Lipase B from *Candida antarctica*, immobilized on Immobead 150, recombinant from *Aspergillus oryzae*), which was obtained from Sigma-Aldrich. Unless otherwise stated, all chemicals were used without further purification. Deuterated solvents were acquired by Deutero GmbH. Dialysis membranes (regenerated cellulose, $MWCO = 1,000$ g mol^{-1}) were purchased from Orange Scientific.

Instrumentation. ^{1}H NMR (400 MHz), ^{13}C NMR (100 MHz) and two-dimensional NMR spectra (COSY, HSQC, HMBC and DOSY) were recorded on a Bruker Avance II HD 400 spectrometer equipped with 5 mm BBFO-SmartProbe (Z-gradient) and an ATM as well as a SampleXPress 60 auto sampler. For real-time ^{1}H NMR kinetic studies a Bruker Avance III HD 400 (5 mm BBFO-SmartProbe with Z -gradient and ATM, SampleXPress 60 autosampler) was used. All recorded spectra were referenced internally to residual proton signals of the deuterated solvent.

SEC measurements were performed on an Agilent 1,100 Series equipped with a refractive index (RI) and ultraviolet (UV) detector. For measurements in DMF (containing 1 g L^{-1} LiBr as additive) HEMA columns (300/100/40 Å porosity) from Polymer Standards Service GmbH were used at 50 °C. For measurements in THF, the PSS column set SDV ($10^6/10^5/10^3$ Å porosity) was used at 30 °C. The flow rate was always 1.0 mL min^{-1}. The calibration was conducted with PEG and poly(methyl methacrylate) standards from PSS. All shown SEC traces show the signal of the RI detector.

A Perkin Elmer 8,500 was used to investigate the thermal properties (T_g, T_m) in a temperature range of -95 °C to 95 °C. The heating rate of the first cycle was 20 K min^{-1} as was the cooling rate. The second heating cycle was again conducted at 20 K min^{-1} and used for evaluation.

The critical micelle concentration (CMC) was determined using a DataPhysics DCAT 11 EC tensiometer equipped with a TV 70 temperature control unit, a LDU 1/1 and a Du Noüy ring RG 11, which was annealed with a burner before the measurement. The solutions were stirred for 120 s at a stirring rate of 50%. After a subsequent rest period of 10 s, the surface tension was measured and averaged three times. Aqueous solutions of PEG$_{0.96}$-*grad*-PEUMA$_{0.04}$ (entry 1, **Table 1**) with a concentration of 1 g L^{-1} were used for the measurement. The point of

intersection, which was obtained by extrapolation of the two linear regression lines, described the CMC (**SI-Figure 15**).

The self-assembly behavior of PEG-*grad*-PEUMA copolymers was analyzed by dynamic light scattering on a Malvern Zetasizer Nano ZS, whose measuring cell holder was equipped with a Peltier-controlled thermostat. As laser wavelength of 633 nm was used in combination with a scatter angle of 173°. Measurements were performed at a constant temperature of 25 °C either in disposable cuvettes from Brand GmbH & Co. KG (aqueous solutions) or in UV quartz cuvettes from Carl Roth GmbH + Co. KG (organic solutions). For the evaluation, the software Malvern Zetasizer Software 7.11 from Macromedia was used.

Transmission electron microscopy (TEM) images were recorded with a FEI Tecnai 12 microscope equipped with a LaB6-cathode (120 kV acceleration voltage, nominal magnification: 68,000; nominal underfocus: 0.5−1.5 mm). For sample preparation, carbon grids for TEM applications were negatively glow discharged at 25 mA for 30 s in an Emitech K100X glow discharge system. An aqueous solution of crosslinked PEG$_{0.96}$-*grad*-PEUMA$_{0.04}$ (entry 1, **Table 1**) micelles with a concentration of 50 mg L^{-1} was used for analysis. A droplet of the sample (5 µL) was placed on the grid and incubated for 30 s. The grid was dried with Whatman filter paper No. 4 by side-blotting.

10,11-Epoxyundecan-1-ol. The synthesis was performed in a slightly modified fashion to the protocol of Marshall and Sabatini and is shown in **SI-Figure 1**.[47] 8 g (47.0 mmol, 1 equiv) 10-undencen-1-ol was introduced in 50 mL benzene in a three-necked flask equipped with KPG stirrer and cooler and the solution was cooled with an ice bath to 0 °C. Then, 14.2 g (82.2 mmol, 1.4 equiv) *meta*-chloroperoxybenzoic acid (*m*-CPBA) was carefully added in portions to this solution. Residues of *m*-CPBA were flushed down with approximately 40 mL benzene. The solution was stirred for 24 h, allowing it to warm up to room temperature. Saturated NaHCO$_3$ solution was subsequently added until the precipitate had dissolved. The organic phase was separated and washed three times with NaHCO$_3$ solution (3 · 30 mL). Next, the organic phase was washed three times (3 · 30 mL) with aqueous sodium metabisulfite (Na$_2$S$_2$O$_5$) solution and in the last step again three times with NaHCO$_3$ solution (3 · 30 mL). After drying with Na$_2$SO$_4$, 10,11-epoxyundecan-1-ol was obtained with a yield of 92%.

Monomer synthesis: epoxy undecane methacrylate (EUMA). Synthesis of EUMA was conducted in the same fashion as recently reported by our group.[36] A mixture of 5 g (27.2 mmol, 1 equiv) 10,11-epoxyundecan-1-ol and 4.91 g (40.8 mmol, 1.5 equiv) vinyl methacrylate were

introduced in a 100 mL flask, containing 100 mg CALB and a small amount of hydroquinone (HQ). 50 mL benzene and traces of water were added to this mixture. The mixture was stirred for 2 days at 50 °C under exclusion of light. Subsequent, the mixture was concentrated under reduced pressure. Purification of the product was achieved by flash chromatography on silica gel in a mixture of dichloromethane (DCM) and pentane (1 : 4) containing traces of HQ. In the last step, solvents and the residues of vinyl methacrylate were removed under reduced pressure. After filtration over neutral aluminum oxide (AlOx), EUMA was isolated as a yellowish oil in yields of 62%. The monomer was stored unstabilized over molecular sieve (3 Å) in an argon-filled flask at temperatures of -20 °C to -30 °C, at which EUMA crystallized. ^{1}H NMR (400 MHz, CD_2Cl$_2$): δ (ppm) = 6.05 (1H, m, C=CH_2), 5.53 (1H, p, C=CH_2, J = 1.7 Hz), 4.10 (2H, t, -CH_2-OCO-, J = 6.7 Hz), 2.84 (1H, m, CH_{epoxide}), 2.67 (1H, dd, C$H_{2,\,\text{epoxid}}$, J = 5.2, 4.0 Hz), 2.39 (1H, dd, C$H_{2,\,\text{epoxid}}$, J = 5.1, 2.7 Hz), 1.91 (3H, t, H$_2$C=CCH_3, J = 1.3 Hz), 1.65 (2H, p, -CH_2-CH$_2$-OCO-, J = 6.8 Hz), 1.54–1.14 (14H, m, C$H_{2,\,\text{alkyl chain}}$). ^{13}C NMR (100 MHz, C$_6$$D_6$): δ (ppm) = 167.74 (C=O), 137.33 (C=CH$_2$), 125.20 (C=CH$_2$), 65.25 (-CH$_2$-OCO-), 52.61 (CH$_{\text{epoxide}}$), 47.27 (CH$_{2,\,\text{epoxide}}$), 33.11 (H$_2$COCH-CH$_2$), 30.05–26.56 (CH$_{2,\,\text{alkyl chain}}$), 18.66 (H$_2$C=C$CH_3$).

Poly(ethylene glycol)-grad-poly(epoxy undecane methacrylate) (PEG-grad-PEUMA). The following approach refers to sample PEG$_{0.96}$-*grad*-PEUMA$_{0.04}$ (entry 1, **Table 1**). PEG$_{0.91}$-*grad*-PEUMA$_{0.09}$ (entry 2, **Table 1**) was synthesized in the same fashion with adapted equivalents. 64 mg (0.1 mmol, 1 equiv) Tetraoctylammonium bromide (NOct$_4$Br) was dissolved in 5 mL benzene and dried overnight in vacuum at room temperature. Afterwards, dried EUMA (0.25 mL, 1.0 mmol, 8 equiv) and 12 mL of a 1 : 1 mixture of dry 2-methyltetrahydrofuran (2MTHF) and chlorobenzene (MCB) were introduced to the flask. When the mixture was cooled to approximately -70 °C with a liquid nitrogen/ethanol cooling bath, 1.2 mL (24.0 mmol, 205 equiv) ethylene oxide (EO) was condensed into an ampule for volumetric determination and afterwards into the flask. After switching to an ice bath, the flask was carefully filled with argon and polymerization was started by adding 0.4 mL (4 equiv) *i*Bu$_3$Al. The reaction mixture was stirred for 24 h and allowed to warm up to room temperature, before termination with 1 mL methanol. For purification, the solution was concentrated, precipitated five times in a mixture of diethyl ether and pentane (1 : 4) and subsequently dialyzed against MeOH/DCM (3 : 2). To prevent crosslinking side reactions, traces of HQ were added in each step. After drying in a vacuum, PEG$_{0.96}$-*grad*-PEUMA$_{0.04}$ (entry 1, **Table 1**) was obtained as a slightly brownish solid with a yield of 69%.

Sample preparation for real-time ^{1}H NMR kinetics. To ensure a safe handling with EO for ^{1}H NMR kinetic measurements, a special NMR tube equipped with a valve was used (Norell S-5-400-VT-7). In the first step, a stock solution of NOct$_4$Br in toluene-d_8 was prepared for an easier handling. For this purpose, ten times the required initiator quantity (0.1 g, 0.18 mmol) was weighed, dissolved in 2 mL benzene and dried overnight under reduced pressure. Next, the residue was dissolved in 1 mL toluene-d_8. Using a liquid nitrogen/ethanolic cooling bath, the NMR tube was cooled to approximately -70 °C and a small amount (~32 µL, 0.64 mmol, 35 equiv) of EO was condensed. The tube was then filled with argon and 0.1 mL (1 equiv) of the initiator solution and 41 µL (0.16 mmol, 9 equiv) EUMA were injected under continuous cooling. Afterwards, 0.8 mL toluene-d_8 and the catalyst iBu$_3$Al (50 µL, 0.05 mmol, 3 equiv) were introduced. Before the kinetic measurement was started, the so prepared NMR tube was shaken strongly for homogenization and then transferred to the pre-cooled ($T = 0$ °C) NMR spectrometer. After stabilization of the thermal parameters (~10 min, $\Delta T = 0.1$ K) the measurement was started automatically. Two spectra were recorded per minute with one scan each and sample spinning switched off.

Poly(hydroxyethyl methacrylate-co-epoxy undecane methacrylate) (P(HEMA-co-EUMA)). The synthesis of P(HEMA$_{126}$-co-EUMA$_9$) (entry 1, **Table 3**) is described below. All other radical copolymers were similarly performed with adapted monomer ratios. 14 mg (0.06 mmol, 1 equiv) of the RAFT agent 2-cyano-2-propyl benzodithioate was dissolved together with 0.1 mL (0.39 mmol, 6 equiv) EUMA, 0.9 mL (7.47 mmol, 117 equiv) HEMA and 1 mg (0.01 mmol, 0.2 equiv) azobisisobutyronitrile in 1.5 mL dioxane in a Schlenk tube. After three freeze-pump-thaw cycles, the solution was stirred at 70 °C for 24 h. The polymerization was terminated by ventilation of the Schlenk tube with air and rapid cooling. For purification, the copolymer was precipitated five times in cold diethyl ether (respectively methanol for P(MMA-co-EUMA) copolymers). After drying in a vacuum oven, P(HEMA$_{126}$-co-EUMA$_9$) (entry 1, **Table 3**) was obtained as reddish solid in a yield of 81%.

Micelle preparation. PEG$_{0.96}$-$grad$-PEUMA$_{0.04}$ (entry 1, **Table 1**) was used as surfactant for the self-assembly examinations since it was still water soluble. For the removal of possible insoluble particles, 18 mg of the copolymer was dissolved in 2 mL THF, filtered (0.45 µm, LCR syringe filters) and dried with a stream of nitrogen. The residue was used to prepare two solutions: **A**) 1 mg of the residue was dissolved in 0.2 mL THF and slowly diluted with 20 mL Milli-Q water. The solution was immersed in an ultrasonic bath for 30 min and then placed on a mechanical shaking plate for 24 h. **B**) A photoinitiator stock solution was prepared for the

crosslinking of PEG$_{0.96}$-*grad*-PEUMA$_{0.04}$ (entry 1, **Table 1**). For this purpose, 2 mg 2,2-dimethoxy-2-phenylacetophenone was dissolved in 10 mL THF. At the same time, 1 mg PEG$_{0.96}$-*grad*-PEUMA$_{0.04}$ (entry 1, **Table 1**) was dissolved in 0.1 mL THF and subsequent mixed with 0.1 mL of the photoinitiator stock solution described above. The preparation of the micelles was analogous to **A**). Afterwards, the solution was exposed to UV light for one hour to crosslink the micellar core. For the experiments in organic medium and the determination of dry weights, the water was removed by lyophilization.

Crosslinking of a P(MMA-co-EUMA) copolymer and investigation of the swelling behavior. Copolymer P(MMA$_{91}$-*co*-EUMA$_5$) (entry 4, **Table 3**) was chosen as model compound in combination with *m*-phenylenediamine as curing agent. 50 mg of the copolymer was mixed with 1.2 mg amine and dissolved in a mixture of 2MTHF (1 mL) and DCM (0.1 mL) in an Eppendorf reaction vessel. Then, the solution was placed in a drying oven (70−80 °C) for 48 h, where the solvent slowly evaporated and the crosslinking started. Characterization was conducted by swelling studies in DCM. For this purpose, the organogel was placed in 5 mL DCM for 24 h to reach its equilibrium state. After removal of the excess solvent, the weight of the swollen gel was determined. The procedure was repeated three times, whereby the reswelling time between the individual measurements was 90 minutes. The solvent uptake (*SU*) was determined as follows:

$$SU = \left(\frac{w_s - w_d}{w_d}\right) \cdot 100 \qquad (1)$$

where w_s and w_d are the weights of the swollen and dry organogel.

RESULTS AND DISCUSSION

A.   Synthesis of EUMA monomer.

Epoxy undecane methacrylate (EUMA) was synthesized in two steps from 10-undecen-1-ol. In the first step, the terminal ethenyl group of the alkenol was converted with *meta*-chloroperoxybenzoic acid (*m*-CPBA) to the corresponding epoxide in a Prilezhaev reaction (**SI-Figure 1**).[48] Subsequently, the enzyme-catalyzed transesterification of vinyl methacrylate with the alcohol group was conducted with *Candida antarctica* lipase B (CALB), as shown in **Scheme 2**.[49]
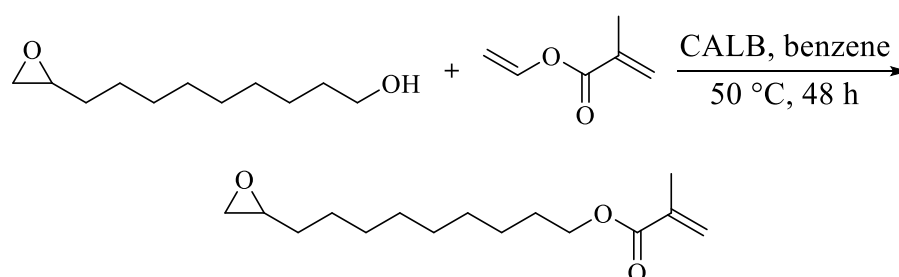
Scheme 2. Synthesis protocol for the preparation of the orthogonal monomer epoxy undecane methacrylate (EUMA).

The use of benzene as solvent greatly facilitates the purification in both the first and second reaction step. If the dichloromethane (DCM) is used as solvent for the epoxidation of 10-undecen-1-ol, a milky solution was obtained by quenching excess *m*-CPBA with aqueous $Na_2S_2O_5$. Here, the separation of the phases took at least 24 h instead of several minutes in case of benzene. Similar to DCM, benzene can also be easily removed quantitatively under reduced pressure at room temperatures, which is crucial for the prevention of crosslinking side reactions in the purification of EUMA. Moreover, the use of hydroquinone (HQ) as inhibitor instead of butylated hydroxytoluene (BHT) is also essential in the transesterification reaction step. ^{1}H NMR (**SI-Figure 2**) studies showed that BHT could not be separated from the monomer by filtration via aluminum oxide (AlOx).

EUMA was obtained as a yellowish oil, which can be stored at temperatures around -20 °C without stabilization. **Figure 1** displays the ^{1}H NMR spectrum of the monomer including complete assignment of the signals. Further spectra (^{13}C NMR and 2D NMR spectra) can be found in Supporting Information **SI-Figures 3−6**.
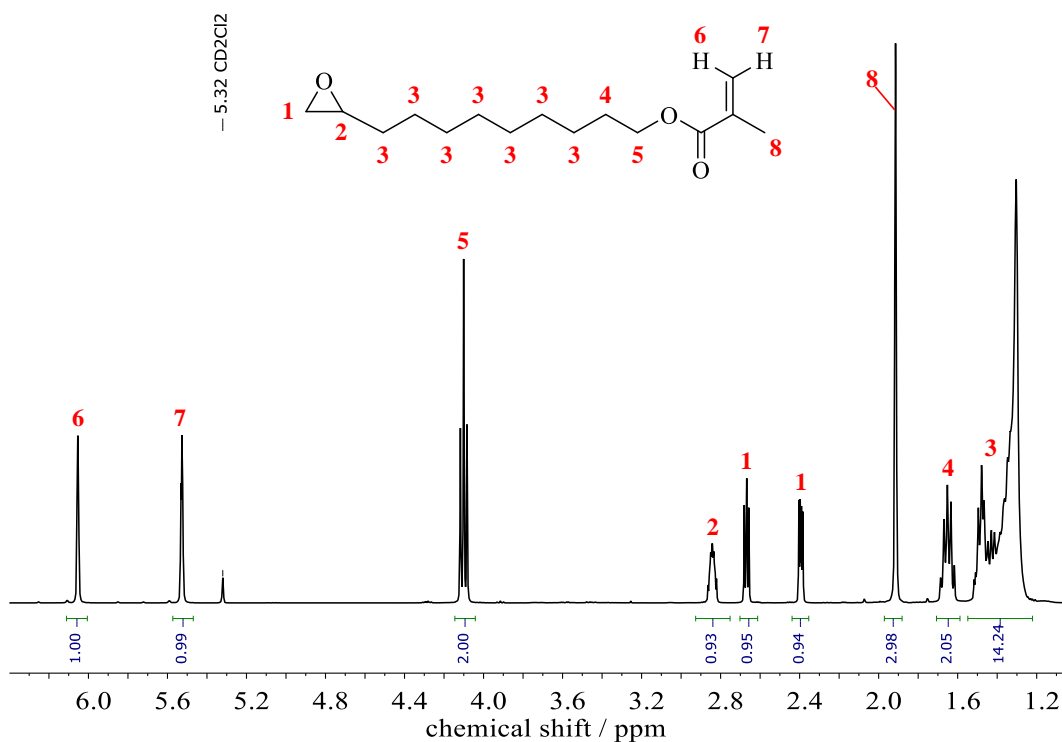
Figure 1. ^{1}H NMR spectrum (400 MHz, CD_2Cl$_2$) of EUMA monomer.

B.   Monomer-activated anionic ring-opening of EO and EUMA.

EUMA was copolymerized with ethylene oxide (EO) via its epoxide functionality using the activated monomer method. This technique involves an initiator/catalyst system consisting of tetraoctylammonium bromide (NOct$_4$Br) as initiator and triisobutylaluminum (*i*Bu$_3$Al) as catalyst. The latter is used in excess, whereby one equivalent of the catalyst forms an "ate" complex with NOct$_4$Br and excess catalyst acts as monomer activator. The initiation step is a nucleophile attack of the "ate" complex at the activated monomer. Here, the bromide ion of NOct$_4$Br initiates the polymerization and the monomer is inserted followed by further propagation. This mechanism is depicted in **Scheme 3**.
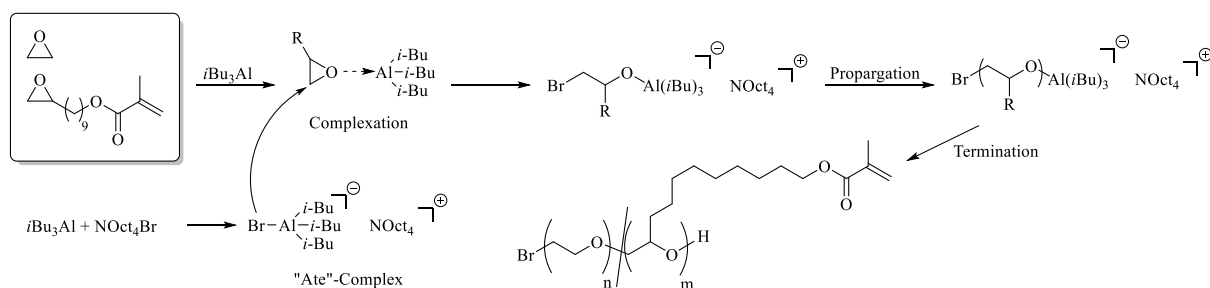
Scheme 3. Reaction mechanism for the monomer-activated anionic copolymerization of EO and EUMA initiated by NOct$_4$Br: formation of the "ate" complex, activation of the monomers by complexation, nucleophilic attack of bromide, chain growth and termination by addition of methanol.

EUMA was specifically incorporated into the polyether backbone at low incorporation rates to guarantee water solubility. The copolymerizations were conducted in iBu$_3$Al quantities of 4 equivalents. In contrast to toluene as the "standard solvent" for the activated monomer method, a mixture of 2-methyltetrahydrofuran (2MTHF) and chlorobenzene (MCB) was applied. For EUMA as well as for experiments with glycidyl methacrylate as model compound, a gelation of the reaction mixture was observed during the copolymerization which could not be dissolved again, indicating crosslinking side reactions. This observation was not made in the mixture mentioned above. The most important key data are summarized in **Table 1**.

Table 1 Copolymerization of EO with EUMA using [iBu$_3$Al]/[NOct$_4$Br] in a mixture of 2MTHF and MCB (0 °C).

No.	Copolymer composition[a]	Theoretical composition	$M_n^{(th)}$ / g mol^{-1}	M_n^b / g mol^{-1}	$Đ^b$
1	PEG$_{0.96}$-*grad*-PEUMA$_{0.04}$	95:5	11,100	19,600	1.65
2	PEG$_{0.91}$-*grad*-PUMA$_{0.09}$	90:10	10,200	20,500	1.33

[a] Obtained from ^{1}H NMR spectra. [b] Determined by SEC measurements in THF (RI detector, PEG standards).

Molecular weights of PEG-*grad*-PEUMA gradient copolymers are about 20,000 g mol^{-1} with dispersities of less than 1.7. It is striking that the molecular weights determined from the SEC deviate strongly from the theoretical molecular weight, which is due to the used PEG standards and the associated different hydrodynamic radii. While monomodal distributions were obtained in THF (**Figure 2**), multimodal distributions were observed in DMF (**SI-Figure 7**), as a result

of the aggregation of the PEG-*grad*-PEUMA copolymers in polar solvents. By only evaluating the main signals, almost the targeted theoretical molecular weights are obtained.
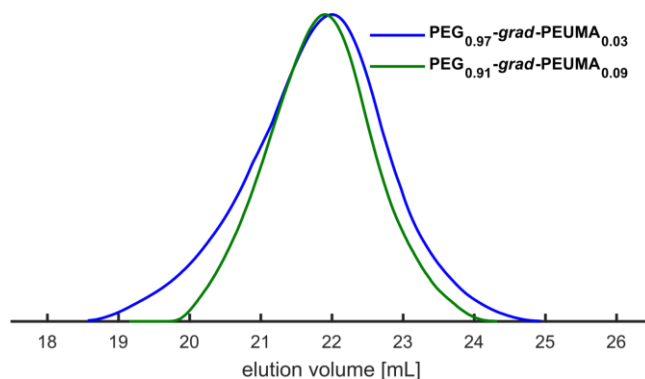
Figure 2. SEC traces (THF, PEG standards) of PEG-*grad*-PEUMA copolymers (entries 1−2, **Table 1**).

Figure 3 shows the ^{1}H NMR spectrum of PEG$_{0.96}$-*grad*-PEUMA$_{0.04}$ (entry 1, **Table 1**) including the complete assignment of the signals. ^{13}C NMR spectra, as well as the two-dimensional NMR investigations can be found in **SI-Figures 8−12**. Due to the absence of an integrable initiator signal, only ratios can be determined from the NMR spectra. The ratio corresponds almost to the target ratio of 95:5 for PEG$_{0.96}$-*grad*-PEUMA$_{0.04}$ (entry 1, **Table 1**). The methylene signal at 1.64 ppm was compared with the signal of the polyether backbone at 3.58 ppm after subtraction of the overlapping EUMA protons.
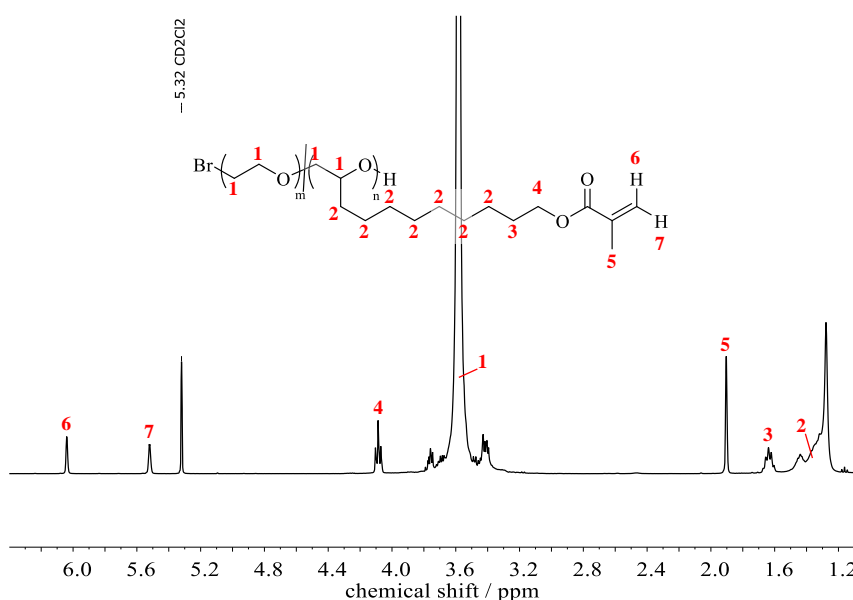
Figure 3. ^{1}H NMR spectrum of PEG$_{0.96}$-*grad*-PEUMA$_{0.04}$ (entry 1, **Table 1**) (400 MHz, CD_2Cl$_2$).

As already shown in previous works, real-time ^{1}H NMR spectroscopy is excellently suited to investigate the microstructure of copolymers, thus also being used here.[43,50–52] For this purpose, the copolymerization was carried out in an NMR tube similar to the approaches in the flask and ^{1}H NMR spectra were recorded at defined intervals. Due to lack of availability, toluene-d_8 was used as solvent instead of the mixture of 2MTHF and MCB. As described above, the copolymerization in toluene is very demanding and sensitive with regard to the used iBu$_3$Al catalyst quantities. Excessive quantities led to the gelation of the entire reaction solution during the copolymerization, caused by crosslinking side reactions. Three equivalents of iBu$_3$Al proved to be the means of choice in terms of reaction time and controllability for the kinetic studies. In addition, it was found that copolymerization only starts at 0 °C, whereas at -20 °C almost no polymerization took place. A similar observation was also made by Herzberger et al. in the case of the copolymerization of EO and ethoxyethyl glycidyl ether (EEGE).[50] The evaluation was based on the signals at 2.16 ppm for EO and 2.83 ppm for EUMA. A selection of the recorded ^{1}H NMR spectra with an enlargement of the relevant areas is shown in **Figure 4**.
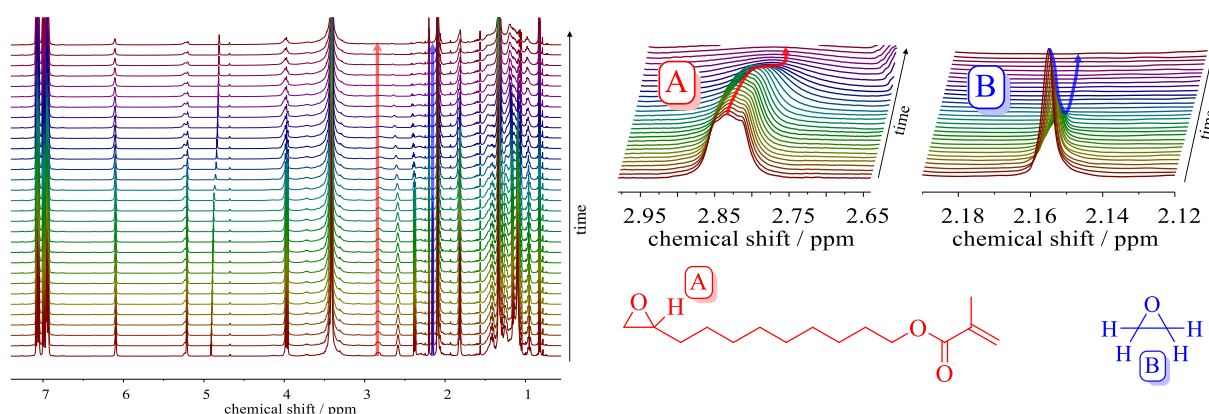
Figure 4. Selection of superimposed ^{1}H NMR spectra (400 MHz) from the copolymerization of EO and EUMA in toluene-d_8. Areas relevant for the evaluation are shown as an enlargement.

The consideration of the decrease in EO and EUMA monomer concentrations during copolymerization clearly indicates the formation of a relatively hard gradient within the PEG-$grad$-PEUMA copolymers (**Figure 5**, top). This is also proved by the quantitative evaluation of the ^{1}H NMR kinetic data. The reactivity ratios were determined by fits of the Jaacks[53] ($r_{EO} = 9.49$, $r_{EUMA} = 0.10$) and the Meyer-Lowry[54] ($r_{EO} = 9.43$, $r_{EUMA} = 0.10$) equations. The respective plots can be found in the Supporting Information (**SI-Figures 13−14**). Assuming a living-like character, these results indicate a pronounced tapered copolymer structure. While there are almost exclusively rich EO segments in the area of the initiator, the chain ends consist of rich EUMA segments. Similar observations were made for the copolymers of EO and

glycidyl propargyl ether (GPgE) and PO using the monomer activation technique.[51,55] On the basis of reactivity ratios according to Meyer-Lowry, the microstructure of the PEG-*grad*-PEUMA copolymers was simulated, emphasizing the above findings once again (**Figure 5**, bottom).[56]
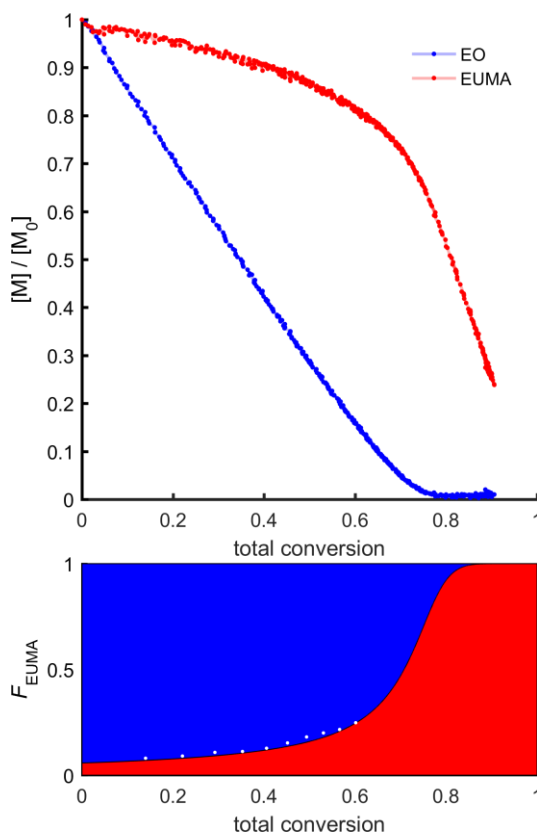
Figure 5. Top: concentration of comonomers EO (blue) and EUMA (red) plotted against total monomer conversion. Bottom: simulated PEG-*grad*-PEUMA copolymer composition plotted versus total conversion of EO and EUMA. The color gradient was simulated with the reactivity ratios according to Meyer-Lowry, whereas the white points are derived directly from the measured data.

Thermal properties of PEG-*grad*-PEUMA copolymers were studied by dynamic differential calorimetry (DSC) measurements and are given in **Table 2**. Glass transition temperatures (T_gs) of both copolymers are almost identical with approximately -57 °C and are in the order of magnitude of pure PEG with a similar molecular weight.[57] In contrast, there is a difference in the melting points (T_ms). These values are between 43 °C and 50 °C. The long flexible EUMA alkyl side chains interfere with the PEG crystal lattice, resulting in a decrease of the T_ms.

Table 2. Thermal properties of PEG-*grad*-PEUMA copolymers.

No.	Copolymer composition[a]	T_m / °C	ΔH / J g^{-1}	T_g / °C
1	PEG$_{0.96}$-*grad*-PEUMA$_{0.04}$	50	66	-57
2	PEG$_{0.91}$-*grad*-PEUMA$_{0.09}$	43	68	-58

[a] Obtained from ^{1}H NMR spectra.

Since the copolymerization of EO and EUMA led to a pronouncedly tapered block microstructure consisting of hydrophilic PEG and hydrophobic PEUMA regions, the surfactant properties of the PEG-*grad*-PEUMA were examined in detail. In this context, the crosslink-ability of the hydrophobic, reactive EUMA micelle core was a central point. For this purpose, PEG$_{0.96}$-*grad*-PEUMA$_{0.04}$ (entry 1, **Table 1**) was used, which was still water soluble. Higher amounts of incorporated EUMA (> 4 mol%) in the copolymers no longer allowed a quantitative dissolution in water. In this context, the critical micelle formation concentration (CMC) was determined at 6.1 mg L^{-1} first (**SI-Figure 15**). The detection of a CMC further verifies the found copolymer tapered block microstructure by the ^{1}H NMR kinetic experiment. The hydrophobic, poorly water-soluble dye Nile red was used as model compound to study and visualize the encapsulation behavior of the PEG$_{0.96}$-*grad*-PEUMA$_{0.04}$ (entry 1, **Table 1**) micelles. While undissolved Nile red was present at the bottom of the reaction vessel in the blank sample containing pure Milli-Q water (**Figure 6a**), the dye was encapsulated and mobilized by the micelles, resulting in homogeneous discoloration of the aqueous solution (**Figure 6b**).
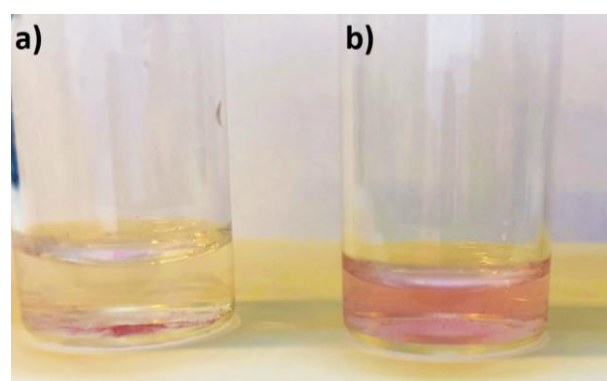
Figure 6. Solubilization of Nile red in PEG$_{0.96}$-*grad*-PEUMA$_{0.04}$ (entry 1, **Table 1**) micelles. a) Blank sample with pure Milli-Q water and Nile red. b) Aqueous solution of PEG$_{0.96}$-*grad*-PEUMA$_{0.04}$ (entry 1, **Table 1**) including Nile red. The color change of the aqueous solution demonstrates the encapsulation of the dye.

In order to increase the stability of the micelles, the hydrophobic EUMA core was crosslinked. For this purpose, the micelles were loaded with the photoinitiator 2,2-dimethoxy-2-phenylacetophenone and afterwards exposed to UV light. To proof the extended stability, the water was removed via lyophilization and the (non-)crosslinked micelles were redissolved in THF, which is suitable for the dissolution of both EO and EUMA moieties. The crosslinking of the EUMA methacrylate groups inside the micelle core was investigated via dynamic light scattering (DLS) and transmission electron microscopy (TEM). **Figure 7** displays the distribution of the $PEG_{0.96}$-*grad*-$PEUMA_{0.04}$ (entry 1, **Table 1**) micelles in water and in THF. The particle radius of the non-crosslinked micelles was 59 nm. Due to the loading with the photoinitiator, the diameter increased to 197 nm. The removal of water by lyophilization and the re-dissolving in THF had a drastic effect on the size of the micelles. No defined distribution was observed for the non-crosslinked $PEG_{0.96}$-*grad*-$PEUMA_{0.04}$ (entry 1, **Table 1**). Even within each run during the measurement, the distribution changed, indicating a very dynamic system. In contrast, only swelling was observed in case of the crosslinked micelles ($r_H = 743$ nm), as reported in literature for PEG-based core-crosslinked pH-sensitive degradable micelles.[58] After the removal of the organic solvent and the dissolution of the crosslinked micelles in water again, the particle radius (82 nm) was approximately the same as the non-crosslinked $PEG_{0.96}$-*grad*-$PEUMA_{0.04}$ (entry 1, **Table 1**) micelles.
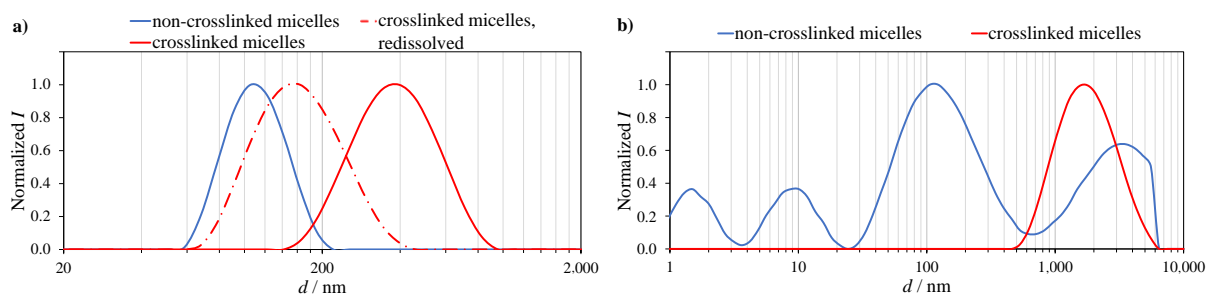
Figure 7. Distributions of non-crosslinked (blue) and crosslinked (red) $PEG_{0.96}$-*grad*-$PEUMA_{0.04}$ (entry 1, **Table 1**) micelles in Milli-Q water (a) and in THF (b) measured by DLS. The micelle concentration was constant at 50 mg L^{-1}.

In contrast to these results, the TEM results in **Figure 8** of the crosslinked $PEG_{0.96}$-*grad*-$PEUMA_{0.04}$ (entry 1, **Table 1**) micelles show a different picture regarding the particle size. For two different evaluation areas, a diameter of approximately 9 nm was obtained for the spherical micelles, which is significantly smaller compared to the results of the DLS measurements. The reason for this is the nature of both measurement methods. In DLS, hydrodynamic diameters are derived from an equivalent hard sphere with the same diffusivity as the micelles.[59] Here,

the micelle size also includes the hydration shell around the micelle. In addition, larger micelles are also given more weight, as the scattering intensity (I) increases with the particle radius (R) as $I \sim R^6$. Consequently, the values obtained by DLS are greater than those of the TEM measurements.
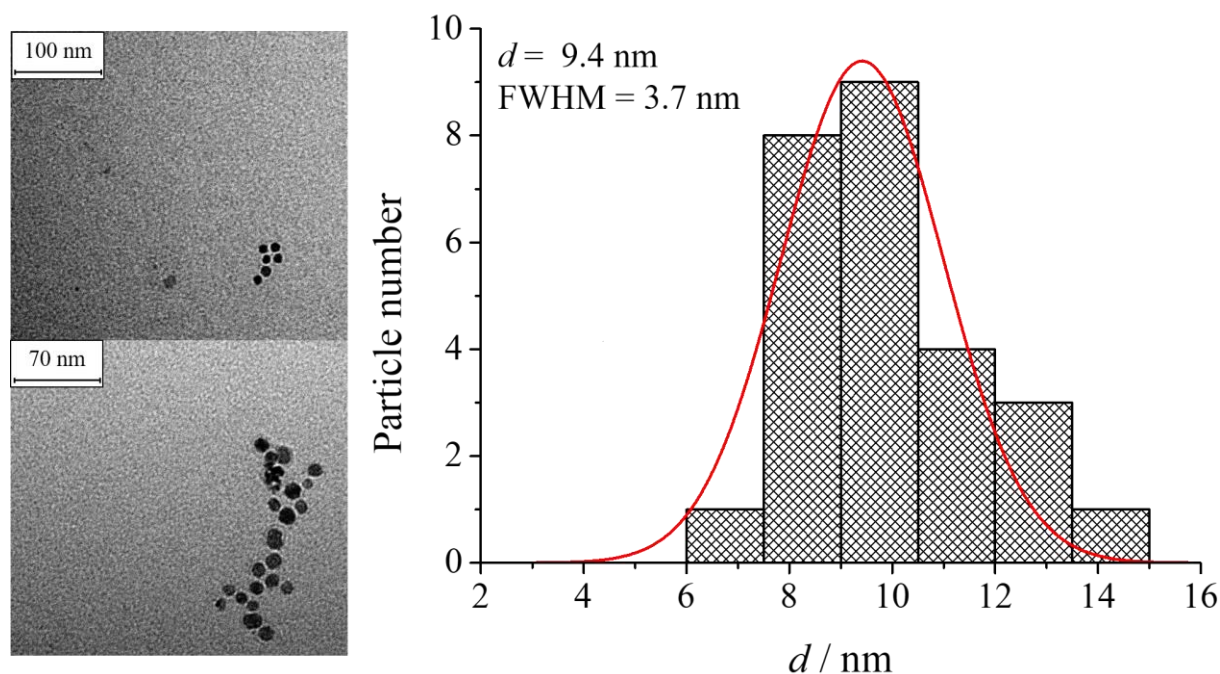
Figure 8. TEM images of two different sections and corresponding distribution of crosslinked PEG$_{0.96}$-*grad*-PEUMA$_{0.04}$ (entry 1, **Table 1**) micelles including most important key data.

C.   RAFT Copolymerization of methacrylates and EUMA.

RAFT (reversible addition-fragmentation chain transfer) polymerization is a relatively new method established by the CSIRO group in 1998.[60] This controlled radical polymerization technique enables the synthesis of polymers with controllable molecular weights and narrow distributions.[61–63] Using the RAFT polymerization technique, a series of EUMA-containing copolymers with methyl methacrylate (MMA) and 2-hydroxyethyl methacrylate (HEMA) were prepared, with the key data summarized in **Table 3**.

Table 3 Overview of synthesized P(HEMA-*co*-EUMA) and P(MMA-*co*-EUMA) copolymers including SEC data and thermal properties.

No.	Copolymer composition[a]	EUMA / mol%	M_n[a] / g mol^{-1}	M_n[b] / g mol^{-1}	$Đ$[b]	T_g / °C
1	P(HEMA$_{126}$-*co*-EUMA$_9$)	7	14,900	5,300	1.23	87
2	P(HEMA$_{70}$-*co*-EUMA$_5$)	7	8,300	3,800	1.37	76
3	P(MMA$_{85}$-*co*-EUMA$_{10}$)	11	11,000	9,100	1.15	76
4	P(MMA$_{91}$-*co*-EUMA$_5$)	6	10,500	9,000	1.14	87

[a] Obtained from ^{1}H NMR spectra. [b] Determined by SEC measurements in THF (RI detector, PMMA standards).

EUMA was incorporated up to 11 mol% and copolymers with molecular weights in the range of 8,300−14,900 g mol^{-1} and moderate dispersities (1.14−1.37) were obtained. The explanation for the deviation of the SEC molecular weights described in the previous section is also valid here and can be traced back to the PMMA standards. The SEC traces in **Figure 9** show a monomodal shape, confirming the well-controllable character of the polymerization.
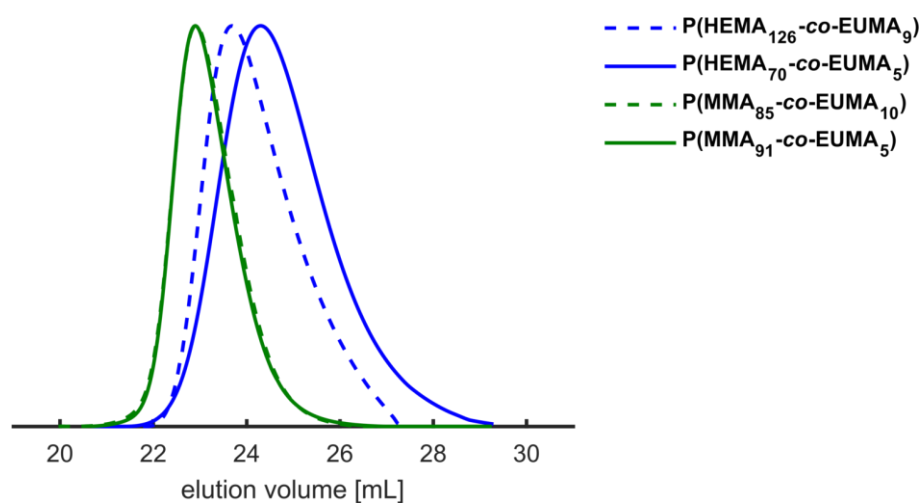
Figure 9. SEC traces (THF, PMMA-standards) of P(HEMA-*co*-EUMA) (entries 1−2, **Table 3**) and P(MMA-*co*-EUMA) (entries 3−4, **Table 3**) copolymers.

In contrast to the PEG-*grad*-PEUMA (entries 1−2, **Table 1**) copolymers synthesized via the monomer-activated anionic polymerization, the number of comonomer units and the absolute molecular weights can be determined from the NMR spectra. **Figure 10** shows the ^{1}H NMR spectrum of P(HEMA$_{70}$-*co*-EUMA$_5$) (entry 2, **Table 3**). The signals for the EUMA epoxide groups at 2.86−2.42 ppm and the HEMA methylene groups at 3.89−3.57 ppm are clearly visible. By normalization to the signals of the chain transfer agent in the aromatic region

(7.82−7.46 ppm), the repeating units were determined on the basis of the signals of the EUMA epoxide methine group at 2.86 ppm and HEMA methylene group at 3.57 ppm. Other spectra (^{13}C NMR and 2D NMR) can be found in the Supporting Information in the **SI-Figures 16−20**, as well as those for the MMA-containing copolymers (**SI-Figures 21−26**), as shown exemplarily for P(MMA$_{91}$-*co*-EUMA$_5$) (entry 4, **Table 3**).
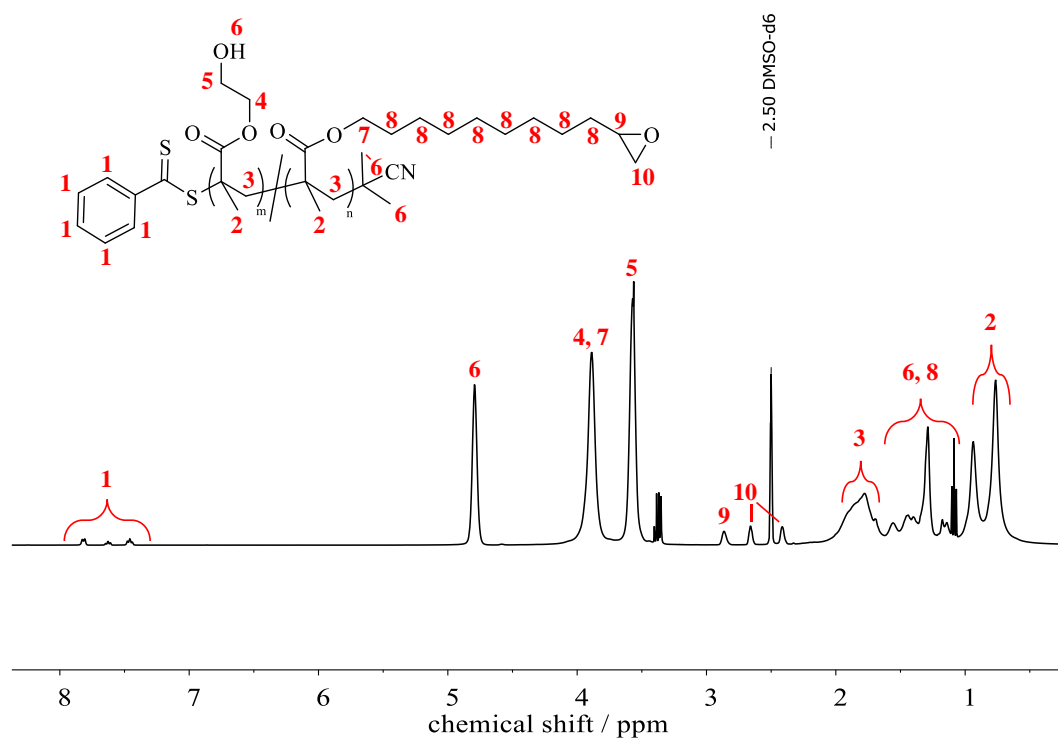
Figure 10. ^{1}H NMR spectrum (400 MHz, DMSO-d_6) of P(HEMA$_{70}$-*co*-EUMA$_5$) (entry 2, **Table 3**).

The analysis of the thermal properties provides two insights. Firstly, according to the Flory-Fox equation[64], the T_gs shift with decreasing molecular weight to lower temperatures, which can be observed for the P(HEMA-*co*-EUMA) (entries 1−2, **Table 3**) copolymers. Here, the T_gs sink from 87 °C to 76 °C as a result of the decrease in molecular weight by approximately 6,600 g mol^{-1}. Secondly, the alkyl side chains of the EUMA moieties act as flexible chain elements and consequently increase the mobility of the polymer main chain, thus reducing the T_gs of the P(MMA-*co*-EUMA) (entries 3−4, **Table 3**) from 87 °C to 76 °C with increasing amount of EUMA.[27]

Epoxy resins play an important role in the field of adhesives. Their synthesis is based on a nucleophilic substitution curing reaction of epoxide-containing precursors and amines. This principle was applied to prepare organogels by ring-opening of the pendant epoxide groups of

the EUMA side chains. Copolymer P(MMA$_{91}$-*co*-EUMA$_5$) (entry 4, **Table 3**) was used as a model compound in combination with *m*-phenylenediamine. The copolymer, which was previously soluble in DCM, had become insoluble because of the crosslinking, as can be seen in **SI-Figure 27**. According to **Equation 1**, the solvent uptake (*SU*) of DCM was determined. In this context, an uptake of $1,000 \pm 10\%$ dichloromethane was determined, proving the successful formation of an organogel.

CONCLUSION

The successful synthesis of epoxy undecane methacrylates (EUMA) yielded a storage-stable and in handling unproblematic, bifunctional monomer. EUMA was used for orthogonal anionic and radical polymerizations. The epoxide units were reacted by monomer-activated anionic ring-opening polymerization using the initiator/catalyst system $NOct_4Br/iBu_3Al$, whereas reversible addition-fragmentation chain transfer (RAFT) polymerization was employed for the methacrylate functionalities.

The latter was used for the preparation of organogels. For this purpose, EUMA was copolymerized with methyl methacrylate (MMA) leading to well-defined structures with molecular weights up to 11,000 g mol^{-1}. Subsequently, the pendant epoxide groups were reacted with a primary amine curing agent. Furthermore, hydrophilic copolymers ($M_n = 8,300−14,900$ g mol^{-1}) were obtained by copolymerization of EUMA and 2-hydroxyethyl methacrylates (HEMA), which were also characterized in detail.

The anionic copolymerization of EUMA with EO via the monomer-activated technique led to water-soluble PEG-*grad*-PEUMA copolymers of molecular weights up to 20,500 g mol^{-1}. Due to their gradient structure, as demonstrated by real-time ^{1}H NMR kinetics ($r_{EO} = 9.43$, $r_{EUMA} = 0.10$), PEG-*grad*-PEUMA surfactants were obtained directly in a one-pot synthesis. As a result of the crosslinking of the micelle cores, a significant improvement in the particle stability was achieved and proved by DLS studies.

By virtue of its bifunctionality, EUMA unites the world of polyethers and polymethacrylates and thus opens up a wide variety of potential applications, such as hydro- and organogels, drug delivery or scaffolds for tissue engineering. We believe that this novel monomer is a very interesting candidate for these biomedical applications.

ACKNOWLEDGEMENT

REFERENCES

(1) Matyjaszewski, K.; Xia, J. Atom Transfer Radical Polymerization. *Chem. Rev.* **2001**, *101*, 2921–2990, DOI: 10.1021/cr940534g.

(2) Kamigaito, M.; Ando, T.; Sawamoto, M. Metal-Catalyzed Living Radical Polymerization. *Chem. Rev.* **2001**, *101*, 3689–3746, DOI: 10.1021/cr9901182.

(3) Hawker, C. J.; Bosman, A. W.; Harth, E. New Polymer Synthesis by Nitroxide Mediated Living Radical Polymerizations. *Chem. Rev.* **2001**, *101*, 3661–3688, DOI: 10.1021/cr990119u.

(4) Coessens, V.; Pintauer, T.; Matyjaszewski, K. Functional polymers by atom transfer radical polymerization. *Prog. Polym. Sci.* **2001**, *26*, 337–377, DOI: 10.1016/S0079-6700(01)00003-X.

(5) Herzberger, J.; Niederer, K.; Pohlit, H.; Seiwert, J.; Worm, M.; Wurm, F. R.; Frey, H. Polymerization of Ethylene Oxide, Propylene Oxide, and Other Alkylene Oxides: Synthesis, Novel Polymer Architectures, and Bioconjugation. *Chem. Rev.* **2016**, *116*, 2170–2243, DOI: 10.1021/acs.chemrev.5b00441.

(6) Fruijtier-Pölloth, C. Safety assessment on polyethylene glycols (PEGs) and their derivatives as used in cosmetic products. *Toxicology* **2005**, *214*, 1–38, DOI: 10.1016/j.tox.2005.06.001.

(7) Dingels, C.; Schömer, M.; Frey, H. Die vielen Gesichter des Poly(ethylenglykol)s. *Chem. unserer Zeit* **2011**, *45*, 338–349, DOI: 10.1002/ciuz.201100551.

(8) Knop, K.; Hoogenboom, R.; Fischer, D.; Schubert, U. S. Poly(ethylene glycol) in Drug Delivery: Pros and Cons as Well as Potential Alternatives. *Angew. Chem. Int. Ed.* **2010**, *49*, 6288–6308, DOI: 10.1002/anie.200902672.

(9) Klein, R.; Wurm, F. R. Aliphatic Polyethers: Classical Polymers for the 21st Century. *Macromol. Rapid Commun.* **2015**, *36*, 1147–1165, DOI: 10.1002/marc.201500013.

(10) Dimitrov, I.; Tsvetanov, C. B. High-Molecular-Weight Poly(ethylene oxide). In *Polymer science: A comprehensive reference*; Matyjaszewski, K., Möller, M., Eds.; Elseiver: Amsterdam, 2012; pp 551–569.

(11) Alconcel, S. N. S.; Baas, A. S.; Maynard, H. D. FDA-approved poly(ethylene glycol)–protein conjugate drugs. *Polym. Chem.* **2011**, *2*, 1442, DOI: 10.1039/c1py00034a.

(12) Staudinger, H.; Lohmann, H. Über hochpolymere Verbindungen. 81. Mitteilung. Über eukolloides Polyäthylenoxyd. *Justus Liebigs Ann. Chem.* **1933**, *505*, 41–51, DOI: 10.1002/jlac.19335050104.

(13) Billouard, C.; Carlotti, S.; Desbois, P.; Deffieux, A. "Controlled" High-Speed Anionic Polymerization of Propylene Oxide Initiated by Alkali Metal Alkoxide/Trialkylaluminum Systems. *Macromolecules* **2004**, *37*, 4038–4043, DOI: 10.1021/ma035768t.

(14) Brzezińska, K.; Szymański, R.; Kubisa, P.; Penczek, S. Activated monomer mechanism in cationic polymerization, 1. Ethylene oxide, formulation of mechanism. *Makromol. Chem., Rapid Commun.* **1986**, *7*, 1–4, DOI: 10.1002/marc.1986.030070101.

(15) Penczek, S.; Kubisa, P.; Szymański, R. Activated monomer propagation in cationic polymerizations. *Makromol. Chem., Macromol. Symp.* **1986**, *3*, 203–220, DOI: 10.1002/masy.19860030116.

(16) Teng, C.-C.; Ma, C.-C. M.; Lu, C.-H.; Yang, S.-Y.; Lee, S.-H.; Hsiao, M.-C.; Yen, M.-Y.; Chiou, K.-C.; Lee, T.-M. Thermal conductivity and structure of non-covalent functionalized graphene/epoxy composites. *Carbon* **2011**, *49*, 5107–5116, DOI: 10.1016/j.carbon.2011.06.095.

(17) Han, E.; Stuen, K. O.; La, Y.-H.; Nealey, P. F.; Gopalan, P. Effect of Composition of Substrate-Modifying Random Copolymers on the Orientation of Symmetric and Asymmetric Diblock Copolymer Domains. *Macromolecules* **2008**, *41*, 9090–9097, DOI: 10.1021/ma8018393.

(18) Xu, F. J.; Cai, Q. J.; Li, Y. L.; Kang, E. T.; Neoh, K. G. Covalent immobilization of glucose oxidase on well-defined poly(glycidyl methacrylate)-Si(111) hybrids from surface-initiated atom-transfer radical polymerization. *Biomacromolecules* **2005**, *6*, 1012–1020, DOI: 10.1021/bm0493178.

(19) Nyström, D.; Lindqvist, J.; Ostmark, E.; Hult, A.; Malmström, E. Superhydrophobic bio-fibre surfaces via tailored grafting architecture. *Chem. Commun.* **2006**, 3594–3596, DOI: 10.1039/b607411a.

(20) Grubbs, R. B.; Dean, J. M.; Broz, M. E.; Bates, F. S. Reactive Block Copolymers for Modification of Thermosetting Epoxy. *Macromolecules* **2000**, *33*, 9522–9534, DOI: 10.1021/ma001414f.

(21) Webster, O. W.; Hertler, W. R.; Sogah, D. Y.; Farnham, W. B.; RajanBabu, T. V. Group-transfer polymerization. 1. A new concept for addition polymerization with organosilicon initiators. *J. Am. Chem. Soc.* **1983**, *105*, 5706–5708, DOI: 10.1021/ja00355a039.

(22) Krishnan, R.; Srinivasan, K. S. V. Controlled/"Living" Radical Polymerization of Glycidyl Methacrylate at Ambient Temperature. *Macromolecules* **2003**, *36*, 1769–1771, DOI: 10.1021/ma025637c.

(23) Hork, D.; Shapoval, P. Reactive poly(glycidyl methacrylate) microspheres prepared by dispersion polymerization. *J. Polym. Sci. A Polym. Chem.* **2000**, *38*, 3855–3863, DOI: 10.1002/1099-0518(20001101)38:21<3855:AID-POLA20>3.0.CO;2-2.

(24) Lu, Q.; Fang, J.; Yang, J.; Miao, R.; Wang, J.; Nuli, Y. Novel cross-linked copolymer gel electrolyte supported by hydrophilic polytetrafluoroethylene for rechargeable lithium batteries. *J. Membr. Sci.* **2014**, *449*, 176–183, DOI: 10.1016/j.memsci.2013.08.029.

(25) Huang, W.; Zhou, Y.; Yan, D. Direct synthesis of amphiphilic block copolymers from glycidyl methacrylate and poly(ethylene glycol) by cationic ring-opening polymerization and supramolecular self-assembly thereof. *J. Polym. Sci. A Polym. Chem.* **2005**, *43*, 2038–2047, DOI: 10.1002/pola.20688.

(26) Karagoz, B.; Bicak, N. Novel photocurable polyethers with methacrylate pendant groups. *Eur. Polym. J.* **2008**, *44*, 106–112, DOI: 10.1016/j.eurpolymj.2007.10.005.

(27) Koltzenburg, S.; Maskos, M.; Nuyken, O. *Polymer Chemistry*; Springer Berlin Heidelberg: Berlin, Heidelberg, 2017.

(28) Bryant, S. J.; Anseth, K. S. Controlling the spatial distribution of ECM components in degradable PEG hydrogels for tissue engineering cartilage. *J. Biomed. Mater. Res. A* **2003**, *64*, 70–79, DOI: 10.1002/jbm.a.10319.

(29) Yu, Q.; Zeng, F.; Zhu, S. Atom Transfer Radical Polymerization of Poly(ethylene glycol) Dimethacrylate. *Macromolecules* **2001**, *34*, 1612–1618, DOI: 10.1021/ma001665o.

(30) Hirayama, Y.; Kase, Y.; Tanihara, N.; Sumiyama, Y.; Kusuki, Y.; Haraya, K. Permeation properties to CO2 and N2 of poly(ethylene oxide)-containing and crosslinked polymer films. *J. Membr. Sci.* **1999**, *160*, 87–99, DOI: 10.1016/S0376-7388(99)00080-0.

(31) Lin-Gibson, S.; Jones, R. L.; Washburn, N. R.; Horkay, F. Structure−Property Relationships of Photopolymerizable Poly(ethylene glycol) Dimethacrylate Hydrogels. *Macromolecules* **2005**, *38*, 2897–2902, DOI: 10.1021/ma0487002.

(32) Zhao, L.; Zhang, H.; Li, X.; Zhao, J.; Zhao, C.; Yuan, X. Modification of electrospun poly(vinylidene fluoride- co -hexafluoropropylene) membranes through the introduction of poly(ethylene glycol) dimethacrylate. *J. Appl. Polym. Sci.* **2009**, *111*, 3104–3112, DOI: 10.1002/app.29374.

(33) Shaplov, A. S.; Vlasov, P. S.; Armand, M.; Lozinskaya, E. I.; Ponkratov, D. O.; Malyshkina, I. A.; Vidal, F.; Okatova, O. V.; Pavlov, G. M.; Wandrey, C. *et al.* Design and synthesis of new anionic "polymeric ionic liquids" with high charge delocalization. *Polym. Chem.* **2011**, *2*, 2609, DOI: 10.1039/c1py00282a.

(34) Pohlit, H.; Bellinghausen, I.; Schömer, M.; Heydenreich, B.; Saloga, J.; Frey, H. Biodegradable pH-Sensitive Poly(ethylene glycol) Nanocarriers for Allergen Encapsulation and Controlled Release. *Biomacromolecules* **2015**, *16*, 3103–3111, DOI: 10.1021/acs.biomac.5b00458.

(35) Schröder, R.; Pohlit, H.; Schüler, T.; Panthöfer, M.; Unger, R. E.; Frey, H.; Tremel, W. Transformation of vaterite nanoparticles to hydroxycarbonate apatite in a hydrogel scaffold: relevance to bone formation. *J. Mater. Chem. B* **2015**, *3*, 7079–7089, DOI: 10.1039/C5TB01032B.

(36) Pohlit, H.; Leibig, D.; Frey, H. Poly(Ethylene Glycol) Dimethacrylates with Cleavable Ketal Sites: Precursors for Cleavable PEG-Hydrogels. *Macromol. Biosci.* **2017**, *17,* DOI: 10.1002/mabi.201600532.

(37) Labbé, A.; Brocas, A.-L.; Ibarboure, E.; Ishizone, T.; Hirao, A.; Deffieux, A.; Carlotti, S. Selective Ring-Opening Polymerization of Glycidyl Methacrylate: Toward the Synthesis of Cross-Linked (Co)polyethers with Thermoresponsive Properties. *Macromolecules* **2011**, *44*, 6356–6364, DOI: 10.1021/ma201075n.

(38) Carlotti, S.; Labbé, A.; Rejsek, V.; Doutaz, S.; Gervais, M.; Deffieux, A. Living/Controlled Anionic Polymerization and Copolymerization of Epichlorohydrin with Tetraoctylammonium Bromide−Triisobutylaluminum Initiating Systems. *Macromolecules* **2008**, *41*, 7058–7062, DOI: 10.1021/ma801422c.

(39) Lundberg, P.; Lee, B. F.; van den Berg, S. A.; Pressly, E. D.; Lee, A.; Hawker, C. J.; Lynd, N. A. Poly(ethylene oxide)-co-(methylene ethylene oxide): A hydrolytically-degradable poly(ethylene oxide) platform. *ACS Macro Lett.* **2012**, *1*, 1240–1243, DOI: 10.1021/mz300477t.

(40) Meyer, J.; Keul, H.; Möller, M. Poly(glycidyl amine) and Copolymers with Glycidol and Glycidyl Amine Repeating Units: Synthesis and Characterization. *Macromolecules* **2011**, *44*, 4082–4091, DOI: 10.1021/ma200757v.

(41) Herzberger, J.; Frey, H. Epicyanohydrin: Polymerization by Monomer Activation Gives Access to Nitrile-, Amino-, and Carboxyl-Functional Poly(ethylene glycol). *Macromolecules* **2015**, *48*, 8144–8153, DOI: 10.1021/acs.macromol.5b02178.

(42) Müller, S. S.; Moers, C.; Frey, H. A Challenging Comonomer Pair: Copolymerization of Ethylene Oxide and Glycidyl Methyl Ether to Thermoresponsive Polyethers. *Macromolecules* **2014**, *47*, 5492–5500, DOI: 10.1021/ma501280k.

(43) Schubert, C.; Dreier, P.; Nguyen, T.; Maciol, K.; Blankenburg, J.; Friedrich, C.; Frey, H. Synthesis of linear polyglycerols with tailored degree of methylation by copolymerization and the effect on thermorheological behavior. *Polymer* **2017**, *121*, 328–339, DOI: 10.1016/j.polymer.2017.05.030.

(44) Heinen, S.; Rackow, S.; Schäfer, A.; Weinhart, M. A Perfect Match: Fast and Truly Random Copolymerization of Glycidyl Ether Monomers to Thermoresponsive Copolymers. *Macromolecules* **2017**, *50*, 44–53, DOI: 10.1021/acs.macromol.6b01904.

(45) Sakakibara, K.; Nakano, K.; Nozaki, K. Regioregular Polymerization of Fluorine-Containing Epoxides. *Macromolecules* **2007**, *40*, 6136–6142, DOI: 10.1021/ma070428j.

(46) Sakakibara, K.; Nakano, K.; Nozaki, K. Regio-controlled ring-opening polymerization of perfluoroalkyl-substituted epoxides. *Chem. Commun.* **2006**, *0*, 3334–3336, DOI: 10.1039/b606693c.

(47) Marshall, J. A.; Sabatini, J. J. An outside-in approach to adjacent bistetrahydrofuran annonaceous acetogenins with C2 core symmetry. Total synthesis of asimicin and a C32 analogue. *Org. Lett.* **2006**, *8*, 3557–3560, DOI: 10.1021/ol061352z.

(48) Prileschajew, N. Oxydation ungesättigter Verbindungen mittels organischer Superoxyde. *Ber. Dtsch. Chem. Ges.* **1909**, *42*, 4811–4815, DOI: 10.1002/cber.190904204100.

(49) Sen, S.; Puskas, J. E. Green polymer chemistry: enzyme catalysis for polymer functionalization. *Molecules* **2015**, *20*, 9358–9379, DOI: 10.3390/molecules20059358.

(50) Herzberger, J.; Leibig, D.; Liermann, J. C.; Frey, H. Conventional Oxyanionic versus Monomer-Activated Anionic Copolymerization of Ethylene Oxide with Glycidyl Ethers: Striking Differences in Reactivity Ratios. *ACS Macro Lett.* **2016**, *5*, 1206–1211, DOI: 10.1021/acsmacrolett.6b00701.

(51) Herzberger, J.; Leibig, D.; Langhanki, J.; Moers, C.; Opatz, T.; Frey, H. "Clickable PEG" via anionic copolymerization of ethylene oxide and glycidyl propargyl ether. *Polym. Chem.* **2017**, *8*, 1882–1887, DOI: 10.1039/C7PY00173H.

(52) Maciol, K.; Schüttner, S.; Blankenburg, J.; Johann, T.; Frey, H. Glycidyl cinnamate: copolymerization, NMR kinetics and photocrosslinking. *Chapter 2.3*. **2018**.

(53) Jaacks, V. A novel method of determination of reactivity ratios in binary and ternary copolymerizations. *Makromol. Chem.* **1972**, *161*, 161–172, DOI: 10.1002/macp.1972.021610110.

(54) Meyer, V. E.; Lowry, G. G. Integral and differential binary copolymerization equations. *J. Polym. Sci. A Gen. Pap.* **1965**, *3*, 2843–2851, DOI: 10.1002/pol.1965.100030811.

(55) Rejsek, V.; Sauvanier, D.; Billouard, C.; Desbois, P.; Deffieux, A.; Carlotti, S. Controlled Anionic Homo- and Copolymerization of Ethylene Oxide and Propylene Oxide by Monomer Activation. *Macromolecules* **2007**, *40*, 6510–6514, DOI: 10.1021/ma070450c.

(56) Blankenburg, J.; Wagner, M.; Frey, H. Well-Defined Multi-Amino-Functional and Stimuli-Responsive Poly(propylene oxide) by Crown Ether Assisted Anionic Ring-Opening Polymerization. *Macromolecules* **2017**, *50*, 8885–8893, DOI: 10.1021/acs.macromol.7b01324.

(57) Bailey, F. E.; Koleske, J. V. *Poly(ethylene oxide)*; Academic Press: New York, 1976.

(58) Wu, Y.; Chen, W.; Meng, F.; Wang, Z.; Cheng, R.; Deng, C.; Liu, H.; Zhong, Z. Core-crosslinked pH-sensitive degradable micelles: A promising approach to resolve the extracellular stability versus intracellular drug release dilemma. *J. Control. Release* **2012**, *164*, 338–345, DOI: 10.1016/j.jconrel.2012.07.011.

(59) Makhlouf, A. S. H.; Abu-Thabit, N. Y. *Stimuli Responsive Polymeric Nanocarriers for Drug Delivery Applications: Types and Triggers*; Woodhead Publishing Series in Biomaterials Ser; Elsevier Science & Technology: San Diego, 2018.

(60) Chiefari, J.; Chong, Y. K.; Ercole, F.; Krstina, J.; Jeffery, J.; Le, T. P. T.; Mayadunne, R. T. A.; Meijs, G. F.; Moad, C. L.; Moad, G. *et al.* Living Free-Radical Polymerization by Reversible Addition−Fragmentation Chain Transfer: The RAFT Process. *Macromolecules* **1998**, *31*, 5559–5562, DOI: 10.1021/ma9804951.

(61) Moad, G.; Rizzardo, E.; Thang, S. H. Radical addition–fragmentation chemistry in polymer synthesis. *Polymer* **2008**, *49*, 1079–1131, DOI: 10.1016/j.polymer.2007.11.020.

(62) Perrier, S.; Takolpuckdee, P. Macromolecular design via reversible addition-fragmentation chain transfer (RAFT)/xanthates (MADIX) polymerization. *J. Polym. Sci. A Polym. Chem.* **2005**, *43*, 5347–5393, DOI: 10.1002/pola.20986.

(63) Braunecker, W. A.; Matyjaszewski, K. Controlled/living radical polymerization: Features, developments, and perspectives. *Prog. Polym. Sci.* **2007**, *32*, 93–146, DOI: 10.1016/j.progpolymsci.2006.11.002.

(64) Fox, T. G.; Flory, P. J. Second-Order Transition Temperatures and Related Properties of Polystyrene. I. Influence of Molecular Weight. *J. Appl. Phys.* **1950**, *21*, 581–591, DOI: 10.1063/1.1699711.

Supporting Information

Epoxy Undecane Methacrylate: A Symbiosis of Methacrylates and Poly(ethylene glycol)

Kamil Maciol[a], *Tatjana Dänzer*[a], *Jennifer Keth*[a], *Jan Blankenburg*[a,b] and *Holger Frey*[a,*]

[a] Institute of Organic Chemistry, Johannes Gutenberg University Mainz, Duesbergweg 10-14, 55128 Mainz, Germany

[b] Graduate School Materials Science in Mainz, Staudinger Weg 9, 55128 Mainz, Germany

*E-Mail: hfrey@uni-mainz.de

To be submitted
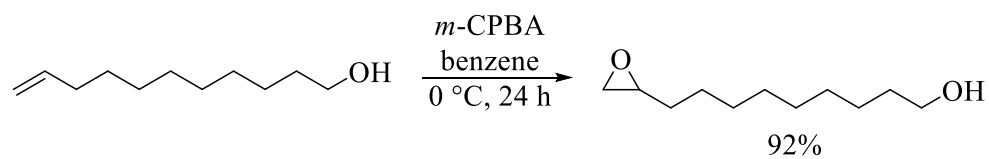
SI-Figure 1. Preparation of the starting compound 10,11-epoxyundecan-1-ol for the synthesis of epoxy undecane methacrylate (EUMA) monomer.
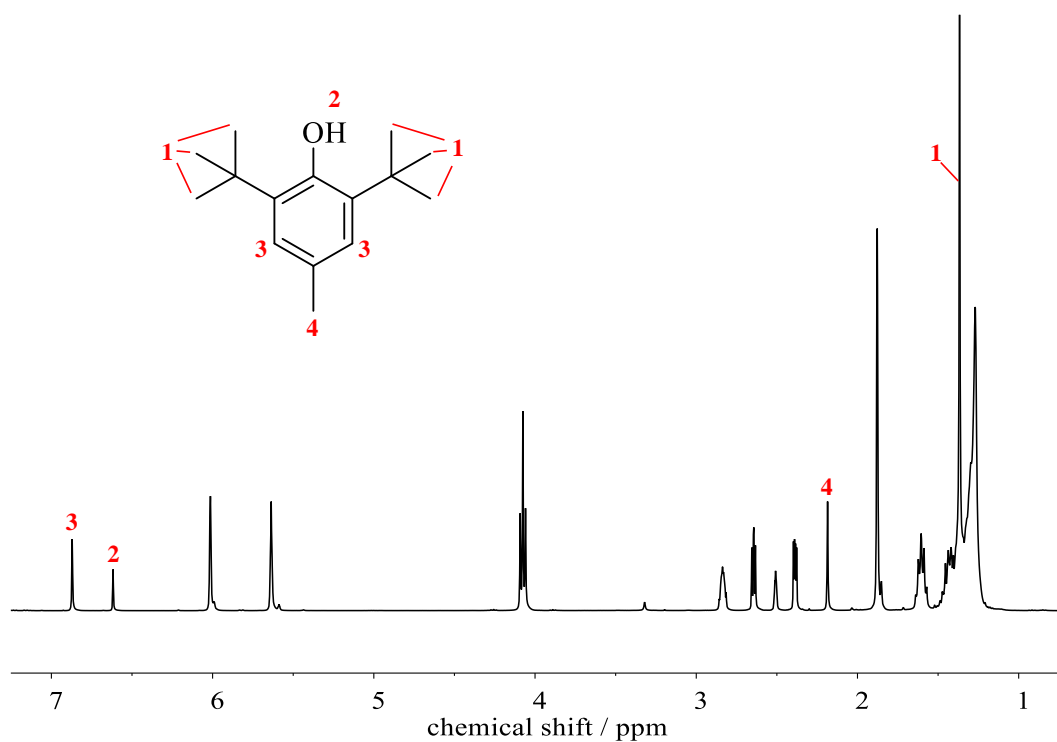
SI-Figure 2. ^{1}H NMR spectrum (400 MHz, DMSO-d_6) of an unsuccessful attempt to remove BHT from EUMA using AlOx.
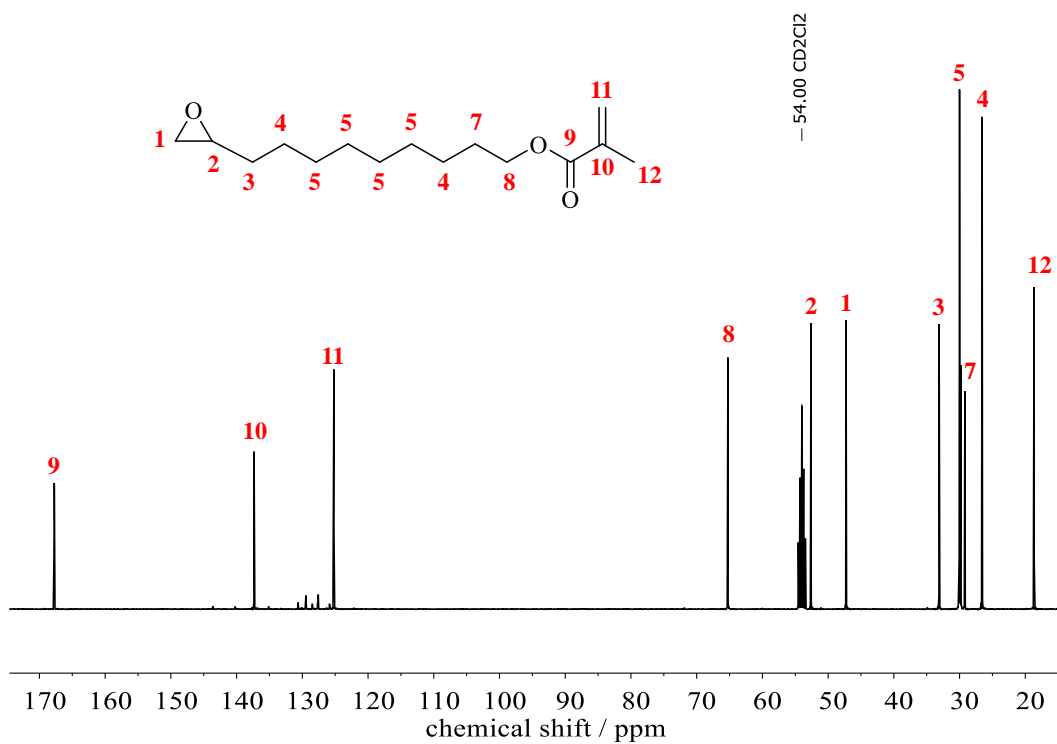
SI-Figure 3. ^{13}C NMR spectrum (100 MHz, CD_2Cl$_2$) of EUMA monomer.
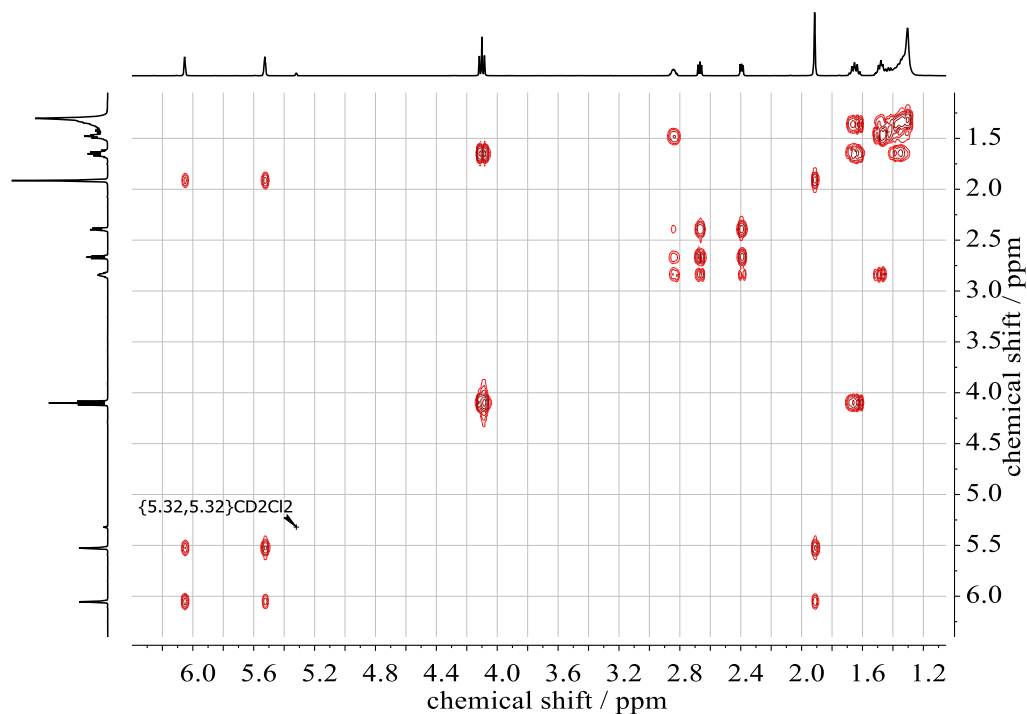
SI-Figure 4. ^{1}H, ^{1}H COSY NMR (400 MHz, CD_2Cl$_2$) of EUMA monomer.
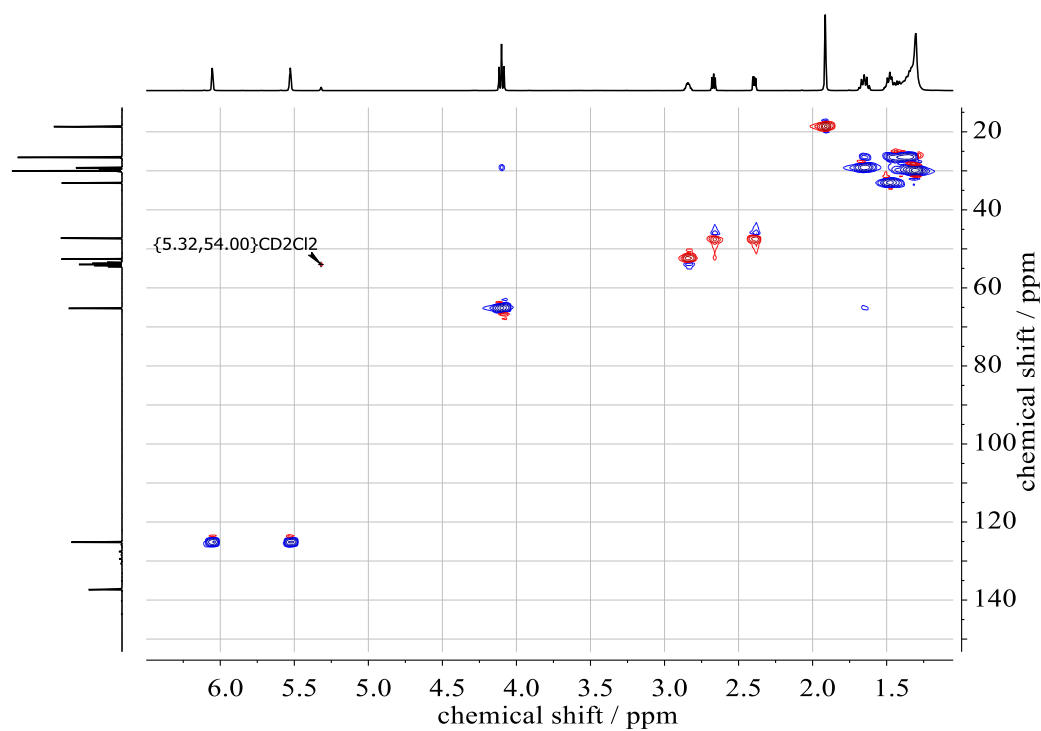
SI-Figure 5. ^{1}H, ^{13}C HSQC NMR of EUMA monomer in CD_2Cl$_2$. Color of the signals indicates the phase information (red: methine proton, blue: methylene protons).
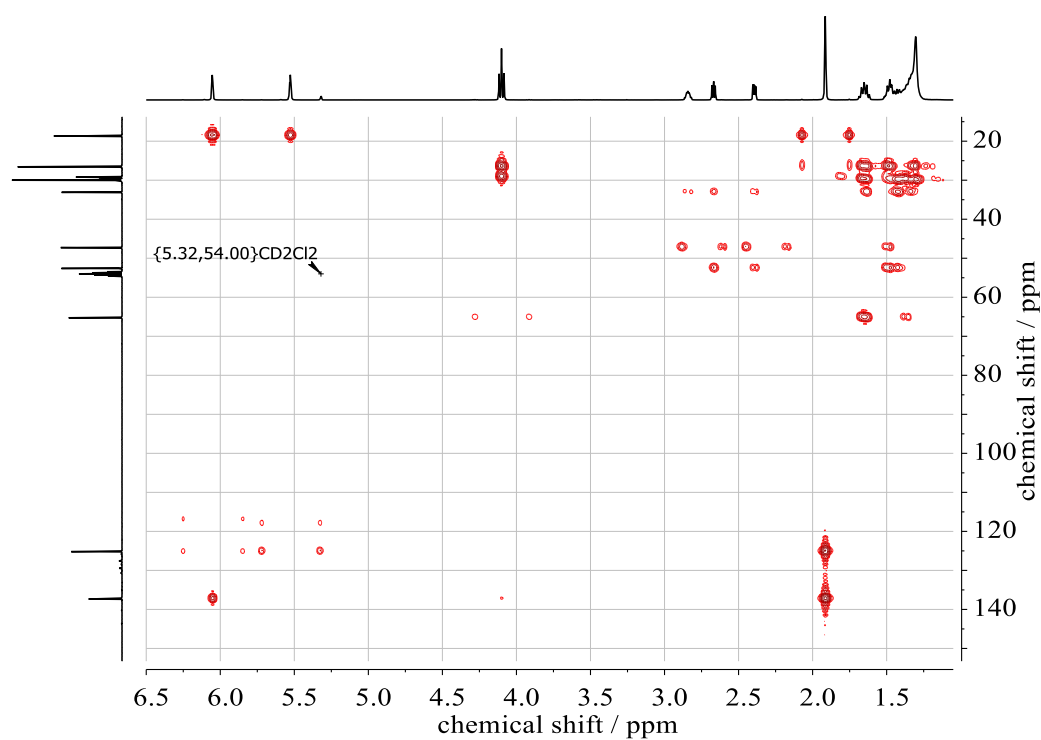
SI-Figure 6. ^{1}H, ^{13}C HMBC NMR of EUMA monomer in CD_2Cl$_2$.
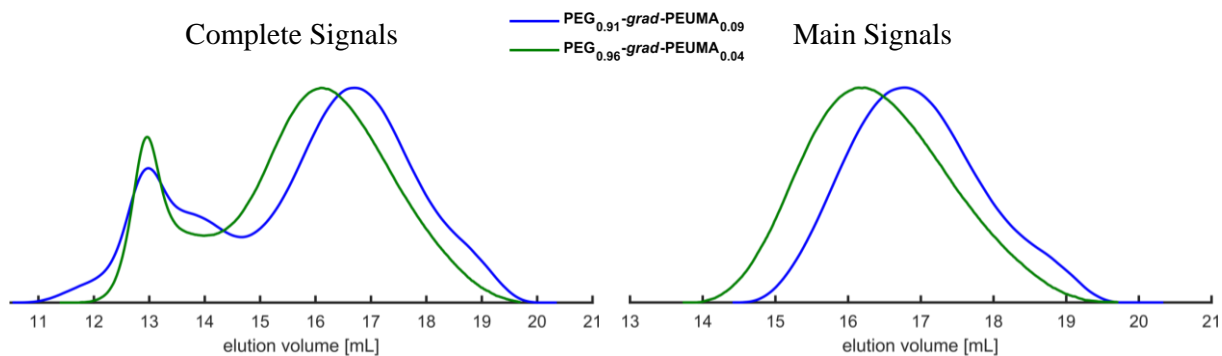
SI-Figure 7. SEC traces of PEG-*grad-P*EUMA copolymers (entries 1−2, **Table 1**) in DMF showing the formation of aggregates. Characteristics of the main signals are: $M_n = 12,600$ g mol^{-1} with $Đ = 1.28$ for PEG$_{0.96}$-*grad*-PEUMA$_{0.04}$ (entry 1, **Table 1**) and $M_n = 9,900$ g mol^{-1} with $Đ = 1.24$ for PEG$_{0.91}$-*grad*-PEUMA$_{0.09}$ (entry 2, **Table 1**).
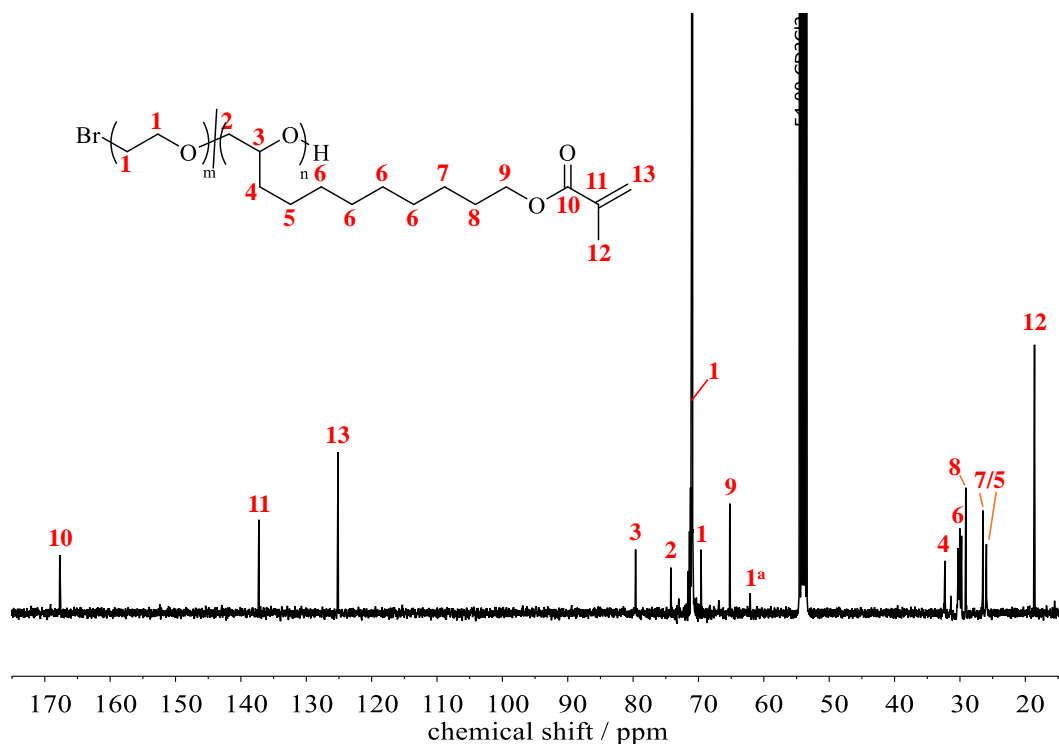
SI-Figure 8. ^{13}C NMR spectrum (100 MHz, CD_2Cl$_2$) of PEG$_{0.96}$-*grad*-PEUMA$_{0.04}$ (entry 1, **Table 1**). ^{a}-$\underline{C}$H$_2$-OH of chain ends.
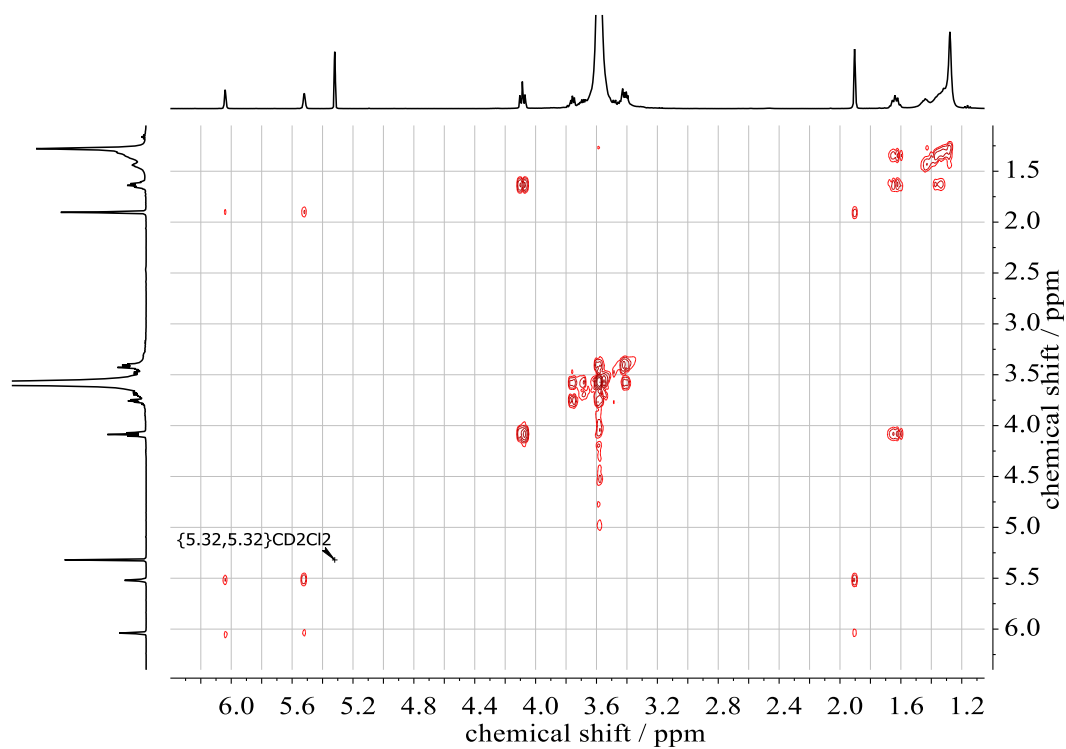
SI-Figure 9. ^{1}H, ^{1}H COSY NMR (400 MHz, CD_2Cl$_2$) of PEG$_{0.96}$-*grad*-PEUMA$_{0.04}$ (entry 1, **Table 1**).
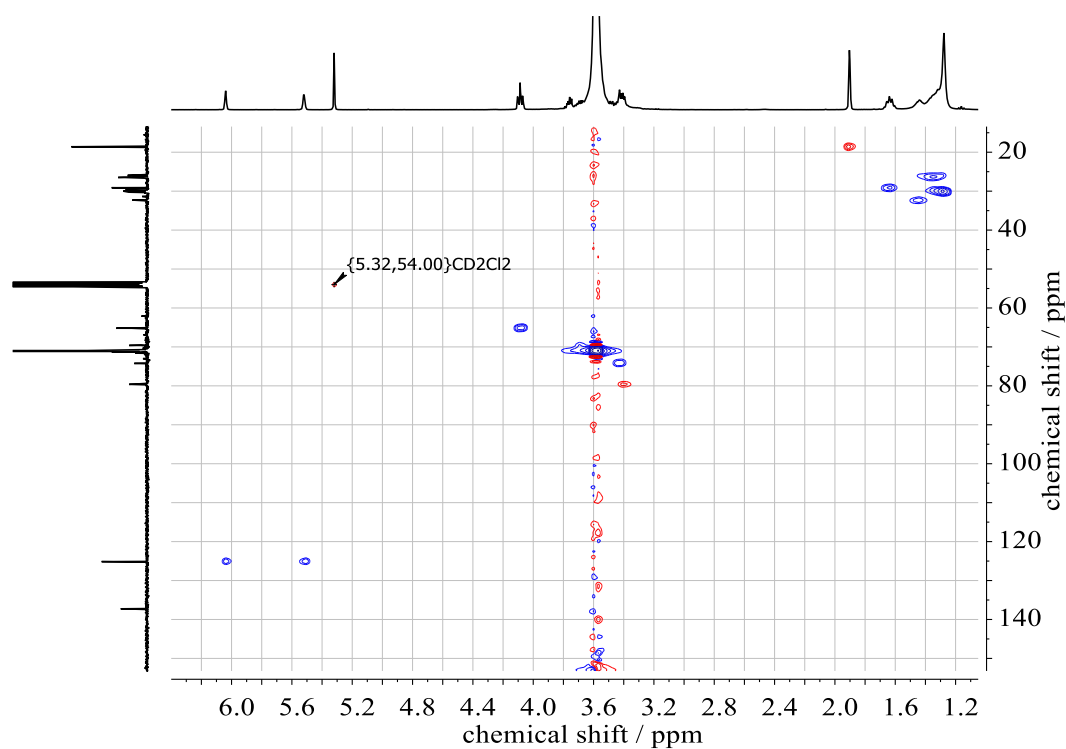
SI-Figure 10. ^{1}H, ^{13}C HSQC NMR of PEG$_{0.96}$-*grad*-PEUMA$_{0.04}$ (entry 1, **Table 1**) in CD_2Cl$_2$. Color of the signals indicates the phase information (red: methine proton, blue: methylene protons).
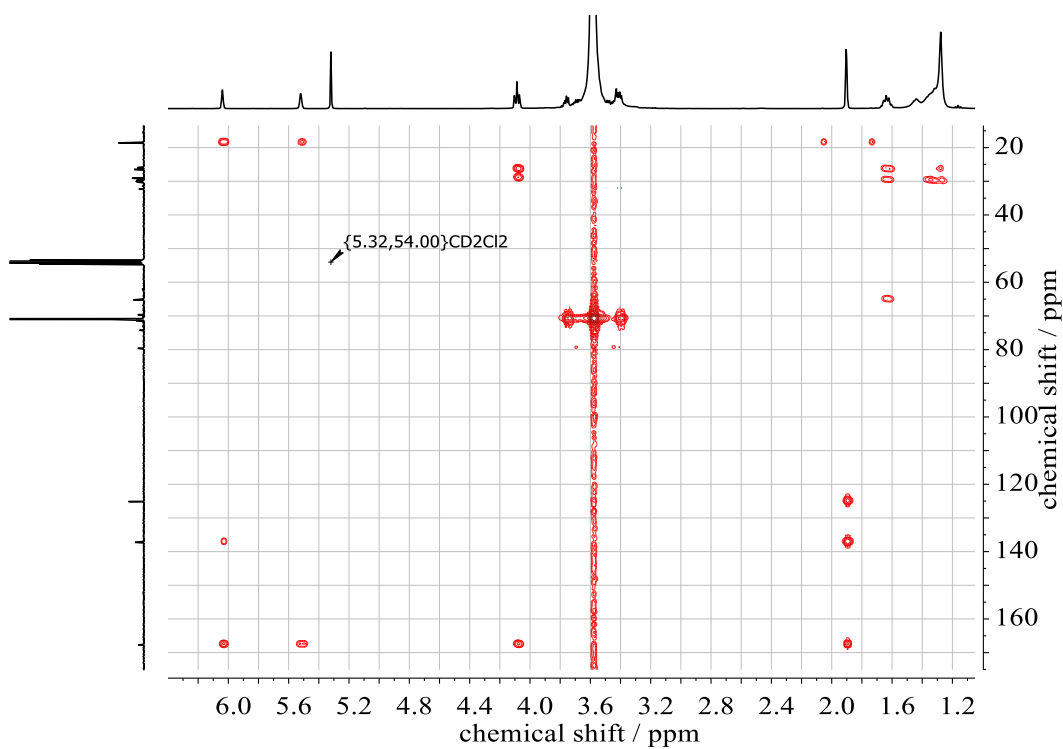
SI-Figure 11. ^{1}H, ^{13}C HMBC NMR of PEG$_{0.96}$-*grad*-PEUMA$_{0.04}$ (entry 1, **Table 1**) in CD_2Cl$_2$.
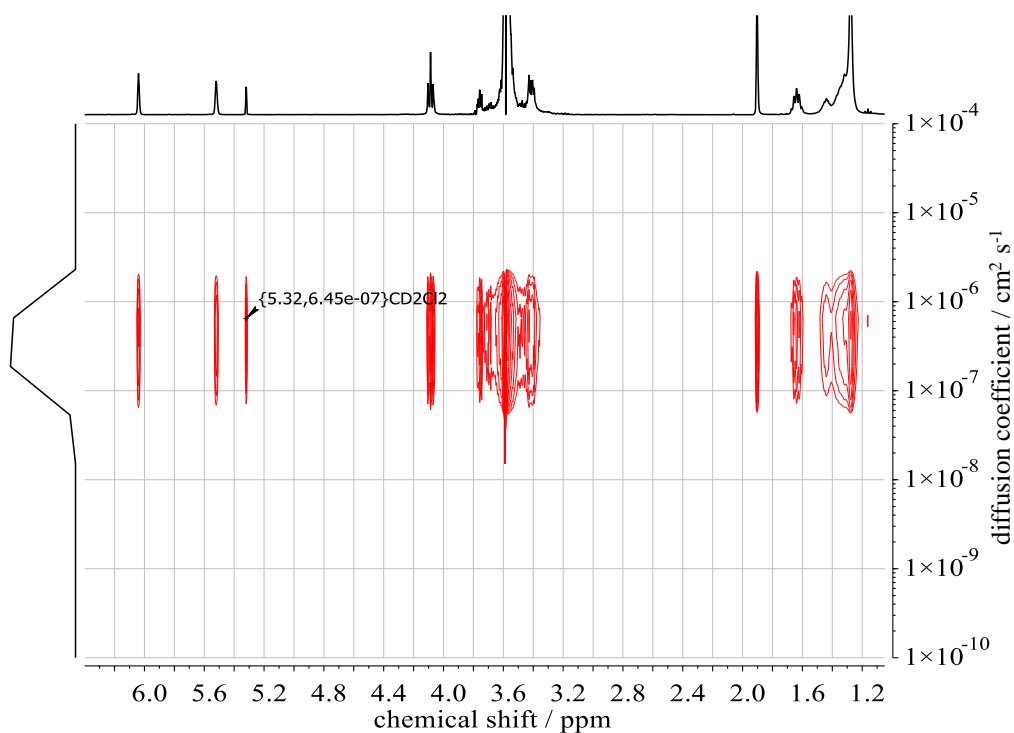
SI-Figure 12. ^{1}H DOSY NMR (400 MHz, CD_2Cl$_2$) of PEG$_{0.96}$-*grad*-PEUMA$_{0.04}$ (entry 1, **Table 1**).
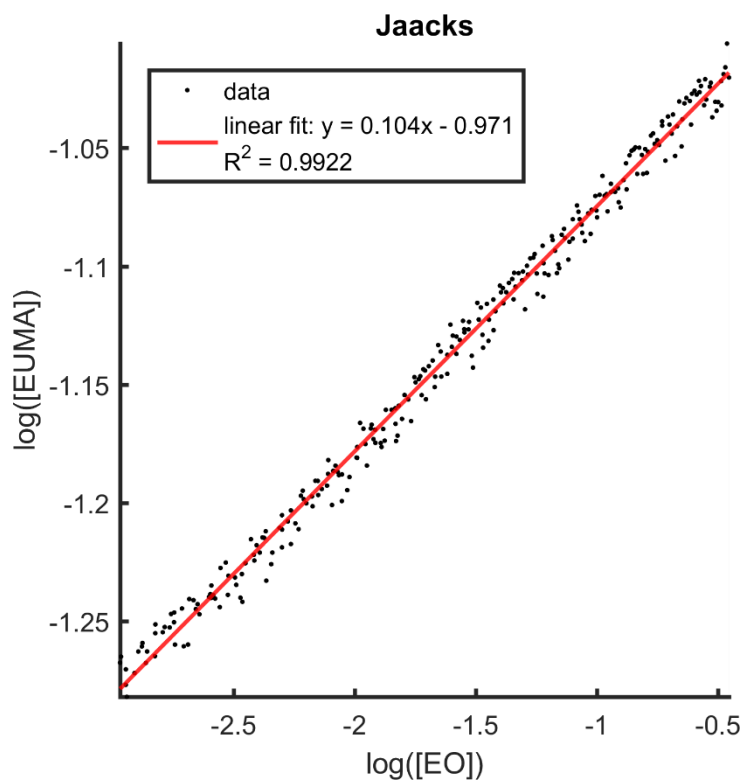
SI-Figure 13. Jaacks fit for determination of reactivity ratios of the copolymerization of EO and EUMA via the activated monomer strategy in toluene-d_8.
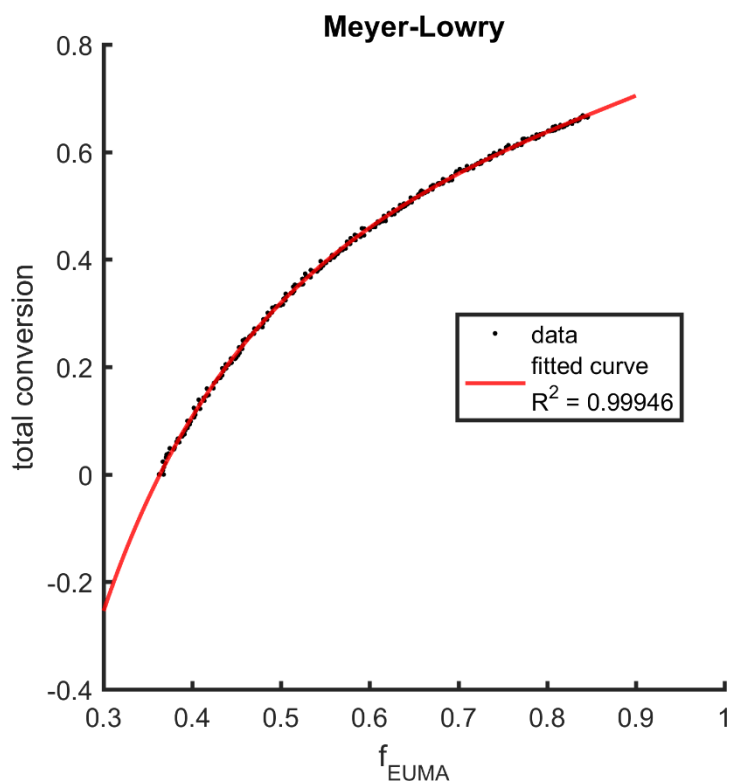
SI-Figure 14. Meyer-Lowry fit for determination of reactivity ratios of the copolymerization of EO and EUMA via the activated monomer strategy in toluene-d_8.
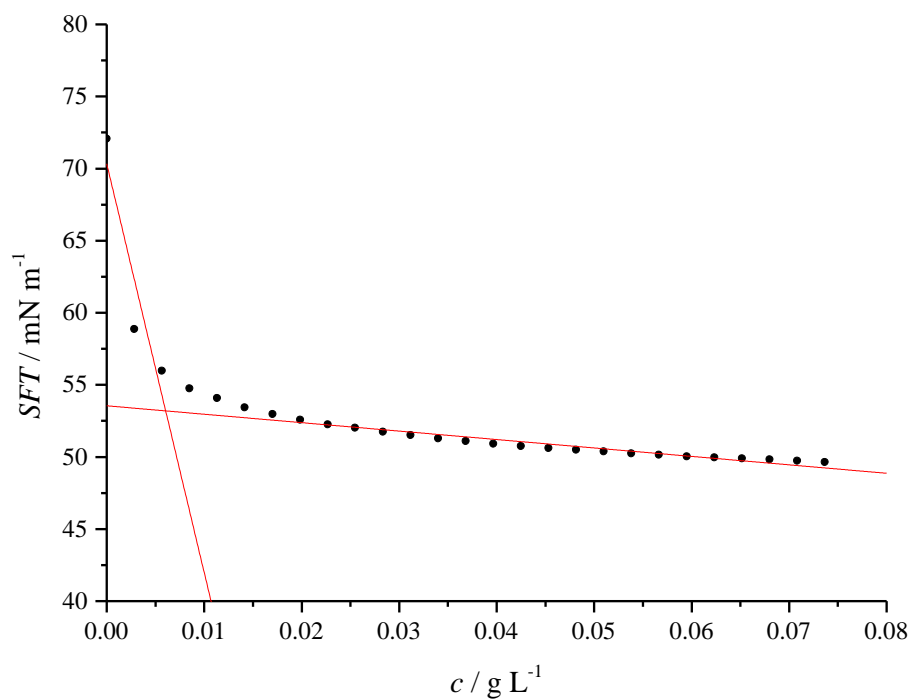
SI-Figure 15. Plot of surface tension vs. concentration of aqueous surfactant solution of PEG$_{0.96}$-*grad*-PEUMA$_{0.04}$ (entry 1, **Table 1**) including regression straight lines for determination of the critical micelle concentration (*CMC* = 6.1 mg L^{-1}).
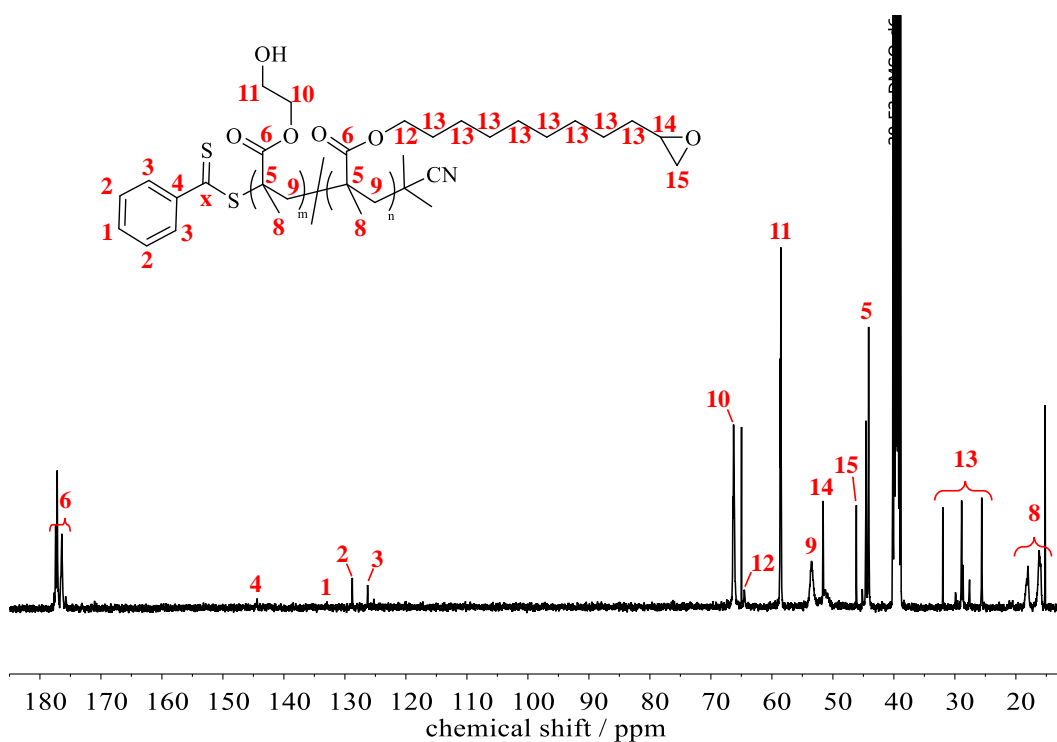
SI-Figure 16. ^{13}C NMR spectrum (100 MHz, DMSO-d_6) of P(HEMA$_{70}$-*co*-EUMA$_5$) (entry 2, **Table 3**).
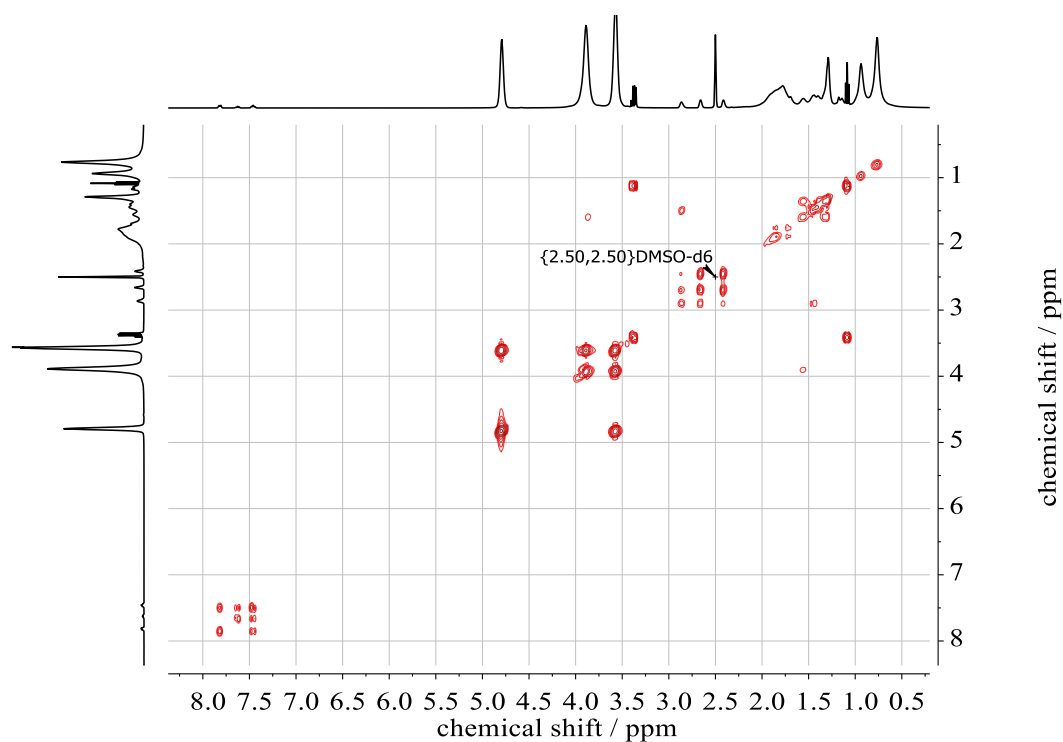
SI-Figure 17. ^{1}H, ^{1}H COSY NMR (400 MHz, DMSO-d_6) of P(HEMA$_{70}$-*co*-EUMA$_5$) (entry 2, **Table 3**).
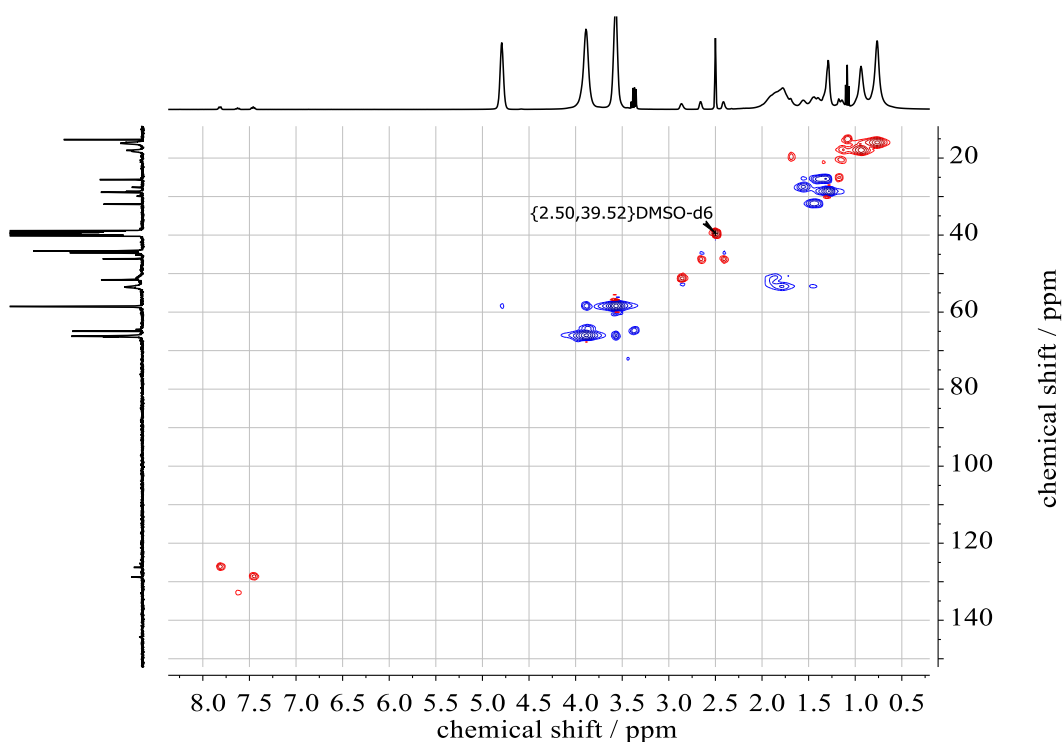
SI-Figure 18. ^{1}H, ^{13}C HSQC NMR of P(HEMA$_{70}$-*co*-EUMA$_5$) (entry 2, **Table 3**) in DMSO-d_6. Color of the signals indicates the phase information (red: methine proton, blue: methylene protons).
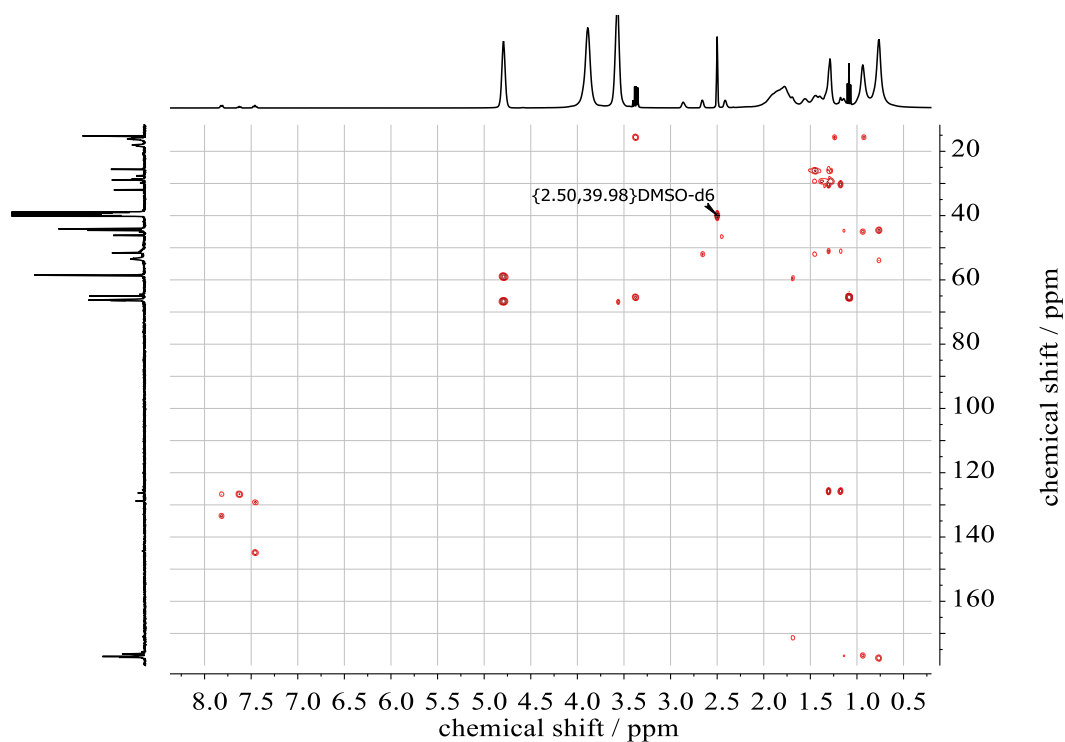
SI-Figure 19. ^{1}H, ^{13}C HMBC NMR of P(HEMA$_{70}$-*co*-EUMA$_5$) (entry 2, **Table 3**) in DMSO-d_6.
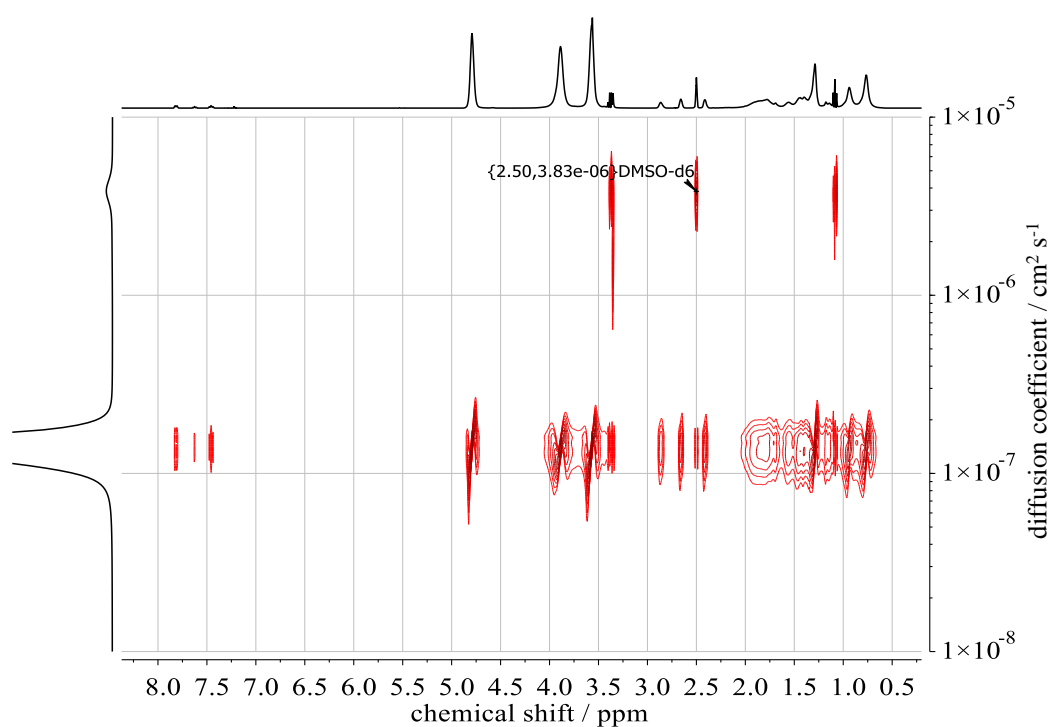
SI-Figure 20. ^{1}H DOSY NMR (400 MHz, DMSO-d_6) of P(HEMA$_{70}$-*co*-EUMA$_5$) (entry 2, Table 3).
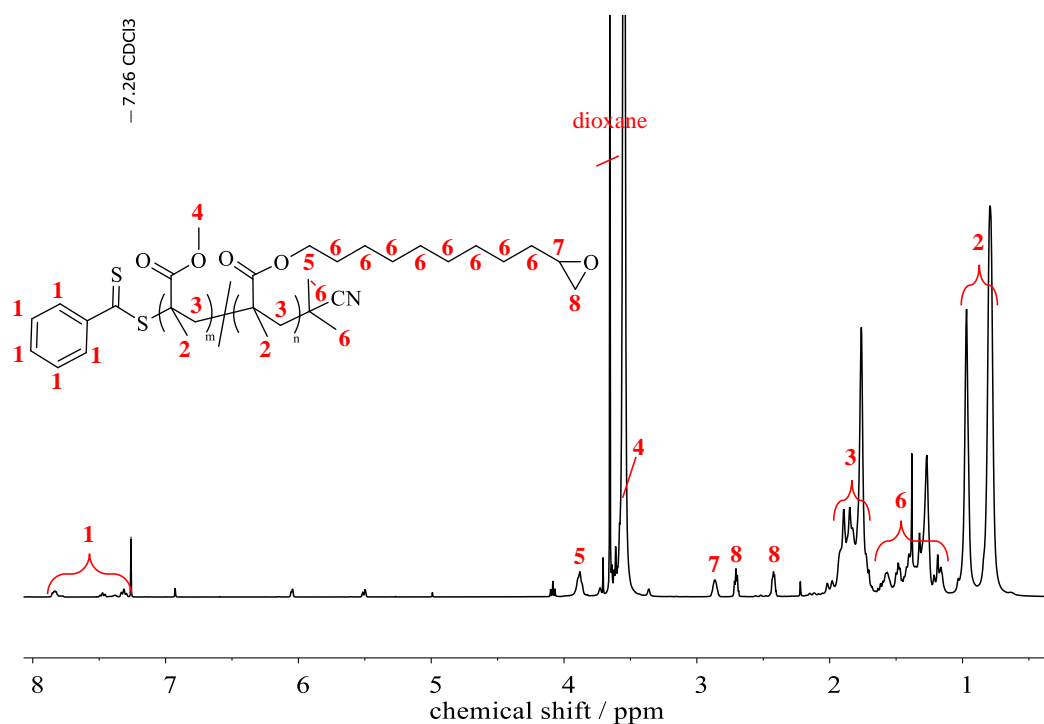
SI-Figure 21. ^{1}H NMR spectrum of P(MMA$_{91}$-*co*-EUMA$_5$) (entry 4, **Table 3**) (400 MHz, CDCl$_3$).
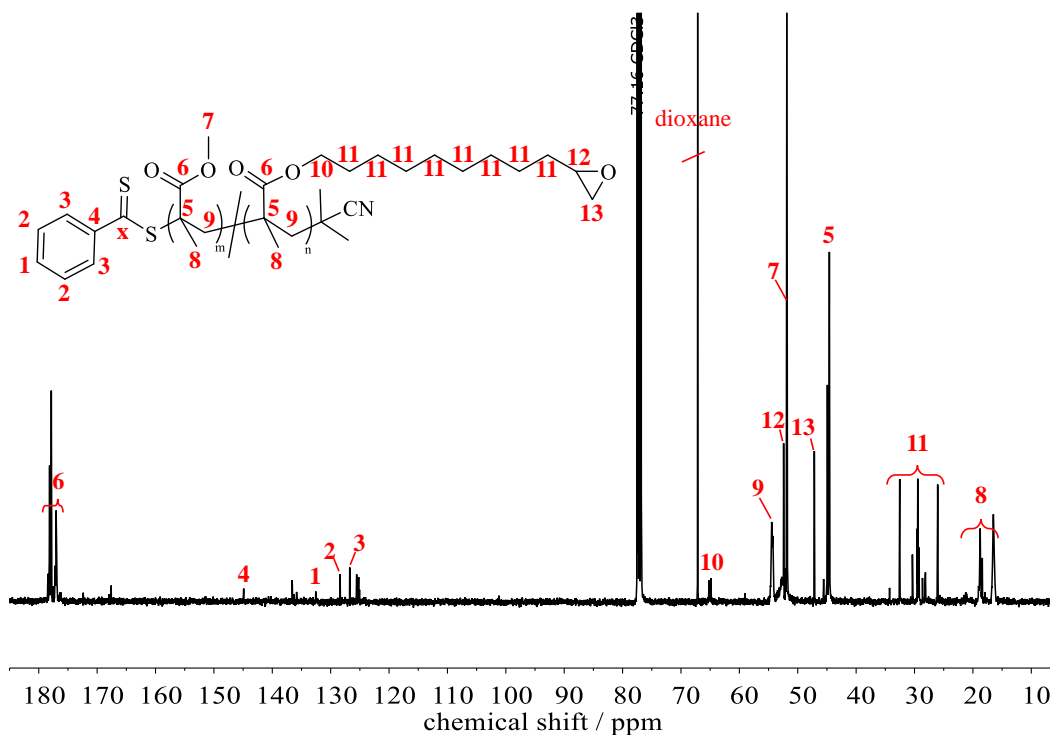
SI-Figure 22. ^{13}C NMR spectrum (100 MHz, CDCl$_3$) of P(MMA$_{91}$-*co*-EUMA$_5$) (entry 4, **Table 3**).
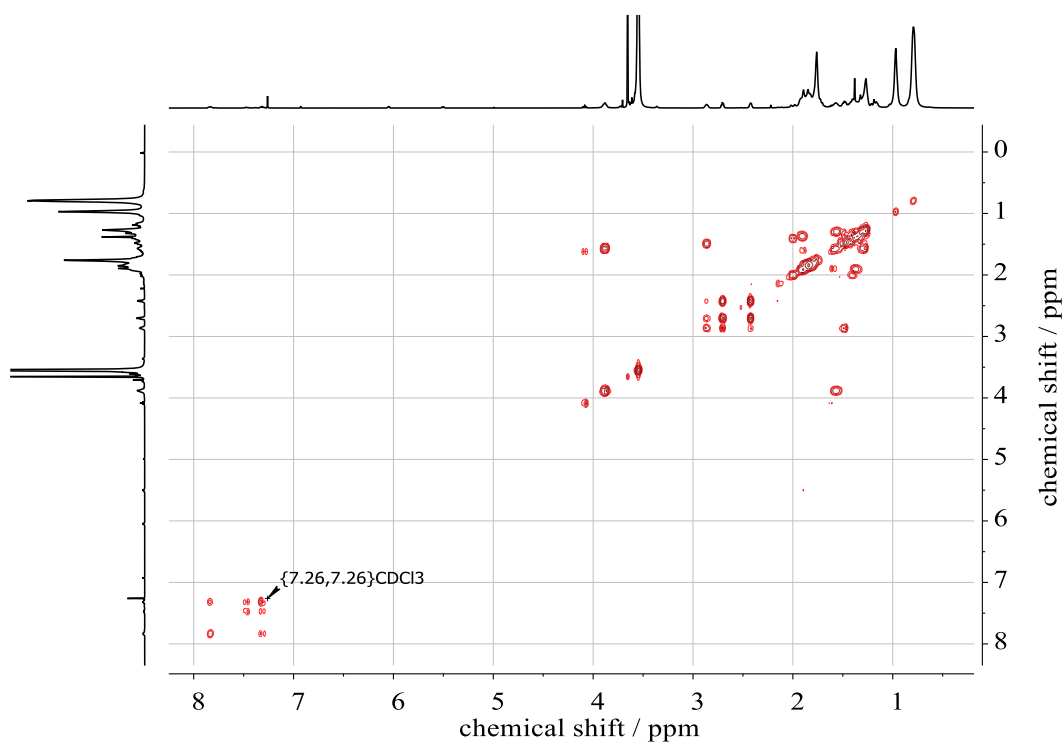
SI-Figure 23. ^{1}H, ^{1}H COSY NMR (400 MHz, CDCl$_3$) of P(MMA$_{91}$-*co*-EUMA$_5$) (entry 4, **Table 3**).
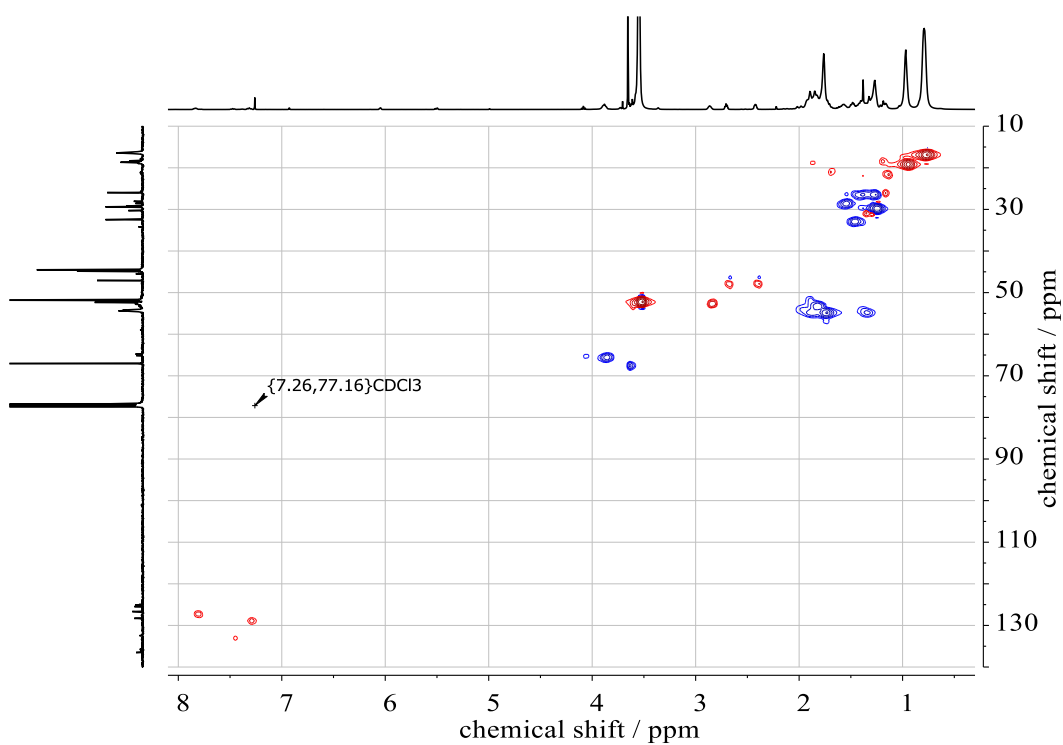
SI-Figure 24. ^{1}H, ^{13}C HSQC NMR of P(MMA$_{91}$-*co*-EUMA$_5$) (entry 4, **Table 3**) in CDCl$_3$. Color of the signals indicates the phase information (red: methine proton, blue: methylene protons).
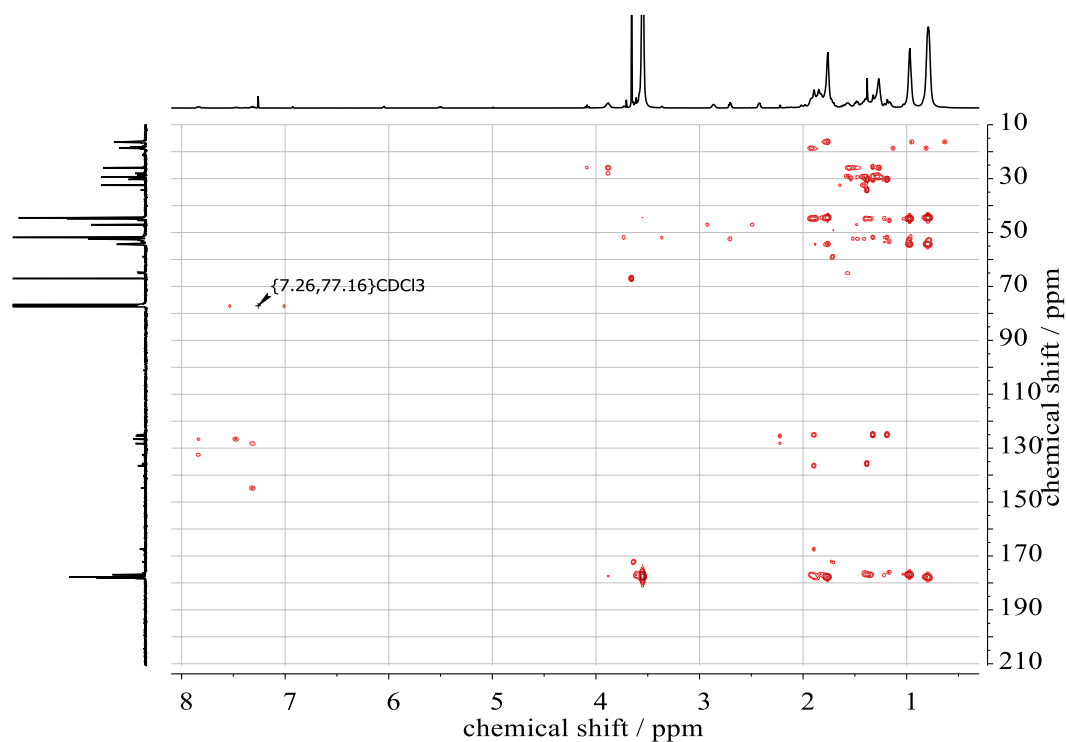
SI-Figure 25. ^{1}H, ^{13}C HMBC NMR of P(MMA$_{91}$-*co*-EUMA$_5$) (entry 4, **Table 3**) in C*D*Cl$_3$.
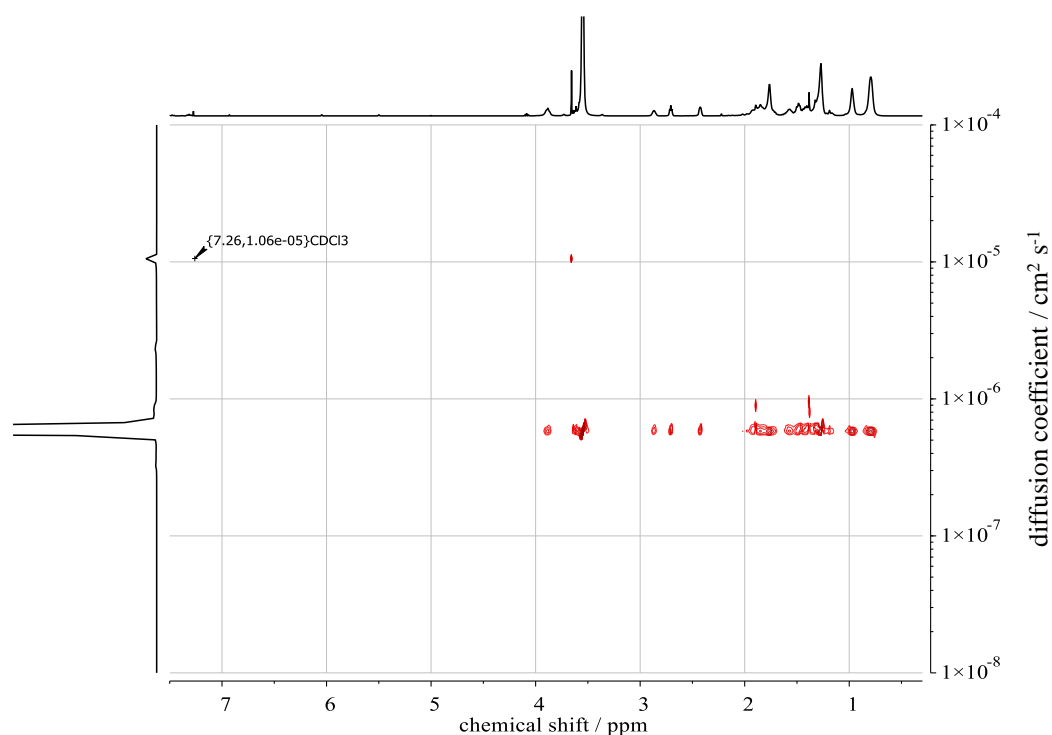
SI-Figure 26. ^{1}H DOSY NMR (400 MHz, C*D*Cl$_3$) of P(MMA$_{91}$-*co*-EUMA$_5$) (entry 4, **Table 3**).

SI-Figure 27. Organogel of crosslinked P(MMA$_{91}$-*co*-EUMA$_5$) (entry 4, **Table 3**) during swelling in DCM.

4.   Preparation of Surface Coatings

4.1. Synthesis of Perfluoroalkyl-Bearing Polyether, Their Characterization and Application as Coating for Glass Slides

Kamil Maciol[a] and Holger Frey[a,]*

[a] Institute of Organic Chemistry, Johannes Gutenberg University Mainz, Duesbergweg 10-14, 55128 Mainz, Germany

*E-Mail: hfrey@uni-mainz.de

To be submitted

ABSTRACT

The introduction of perfluoroalkyl chains into a poly(ethylene glycol) backbone was achieved by the copolymerization of the commercially available fluoroalkyl glycidyl ether 3,3,4,4,5,5,6,6,7,7,8,8,8-tridecafluorooctyl glycidyl ether (TDFOGE) using the monomer activation technique according to Carlotti and Deffieux. Methyltriphenylphosphonium bromide (MePPh$_3$Br) served as initiator in combination with triisobutylaluminum (*i*-Bu$_3$Al) as catalyst. TDFOGE (10−97 mol%) was co- and terpolymerized with catechol acetonide glycidyl ether (CAGE, 2−4 mol%) and allyl glycidyl ether (AGE, 46−98 mol%), respectively ethoxyethyl glycidyl ether (EEGE, 48−97 mol%). Terpolymers with molecular weights between 8,700 and 17,200 g mol^{-1} and narrow distribution ($M_w M_n^{-1} < 1.28$) were synthesized. AGE units were addressed by thiol-ene click chemistry, introducing amino and carboxyl groups. Furthermore, EEGE units could be selectively deprotected before the catechol moieties, resulting in linear polyglycerol structures. Characterization was conducted by SEC measurements and NMR spectroscopy. Thermal properties were investigated by differential scanning calorimetry (DSC), revealing a linear relationship between glass transition temperatures (T_gs) and TDFOGE incorporation rates ($T_{g, PAGE polymers}$ = -55 °C to -71 °C, $T_{g, linPG polymers}$ = -32 °C to -2 °C). CAGE unites served as adhesive anchor for the coating of surfaces after the removal of the acetonide protective groups. Glass slides were coated with the perfluoroalkyl-bearing polymers, leading to contact angles of up to 120°.

TABLE OF CONTENTS GRAPHICS
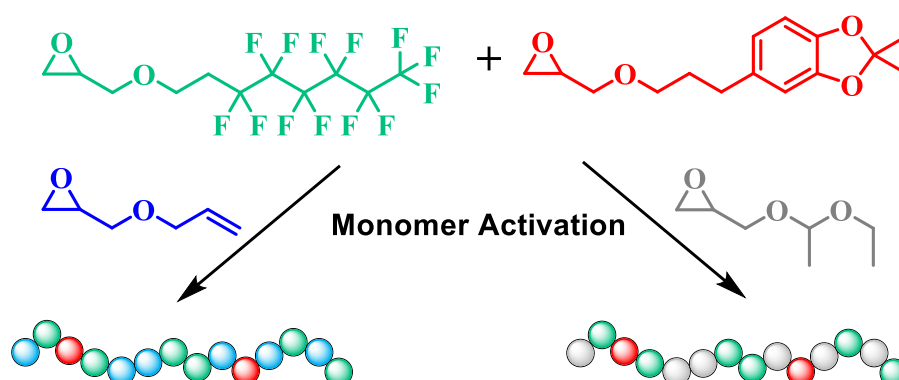
INTRODUCTION

Organofluorine compounds exhibit special properties, which can be attributed to the carbon-fluorine bond.[1,2] As a consequence of the strong polarization, the C-F bond is one of the strongest bonds in organic chemistry, resulting in bonding energies up to 546 kJ mol^{-1}.[3,4] Consequently, organofluorine compounds show a very high thermal stability.[5] Characteristic is also their chemical resistance. The most significant property of fluorine compounds is their extremely low surface energy, due to their low polarizability.[6] The anionic ring-opening polymerization (AROP) makes it possible to synthesize defined and narrowly distributed polymers.[7,8] Accordingly, it would be extremely interesting to transfer these unusual properties of fluorocarbons to polyethers and thus prepare polymers with a defined structure and a low polydispersity. Such polymers could be used for instance as emulsifiers for fluorine-containing active ingredients in medicine. The use of fluorine-containing surfactants for the stabilization of the volatile anesthetic Sevoflurane has already been reported in the literature.[9] Another field of applications are fuel membranes, sealings and electronic devices. Ameduri *et al.* published here very detailed review articles.[10–12] By combining with other glycidyl ether derivatives, additional properties can be modeled. Thus, by copolymerizing fluoroalkyl-containing glycidyl ethers with glycidyl propargyl ether (GPE), dyes could be attached to the alkyne bonds by azide-alkyne click chemistry and biological processes can be studied.[13,14] Due to the anti-stick and anti-corrosive properties of the fluorine groups, coatings of surfaces are very interesting and it would be desirable to transfer these properties to polyethers.[15] However, the oxyanionic polymerization has the disadvantages, that CH-acidic or less reactive compounds cannot be polymerized under these harsh conditions, which applies to perfluoroalkyl-substituted glycidyl ethers. Thanks to the monomer activation according to Carlotti and Deffieux, polymerization under mild reaction conditions is possible due to the low temperatures and the use of weak nucleophiles.[16] This broadened the spectrum of monomers for the AROP, which could not be polymerized under classical conditions. For example, high molecular weight poly(propylene oxide) (PPO)[17] and aliphatic polyethers based on glycidyl methyl ether (GME)[18,19] or epicyanohydrin (EPICH)[20] were obtained in this manner.

3,3,4,4,5,5,6,6,7,7,8,8,8-Tridecafluorooctyl glycidyl ether (TDFOGE) is a glycidyl ether derivative bearing a fluoroalkyl group. In general, there are only a few publications on the direct polymerization of fluorine-containing glycidyl ethers. Fluorinated thermoplastic polyurethane elastomers were prepared based on a fluorine-containing polyether, which was synthesized by cationic polymerization from a fluoroalkyl glycidyl ether.[21] Especially 3,3,3-trifluoro-1,2-

epoxypropane (TFEP) and its copolymers were the focus of attention.[22] Sakakibara *et al.* synthesized a variety of homopolymers from various fluoroalkyl glycidyl ethers including TDFOGE by using the monomer activation technique.[23,24]

In this work, novel polyether co- and terpolymers were prepared in a one-step synthesis based on the fluoroalkyl glycidyl ether TDFOGE. Activated monomer polymerization technique was used, allowing a mild polymerization under reduced temperatures (-20 °C to 25 °C). To the best of our knowledge, TDFOGE has never been co- and terpolymerized before. Just homopolymers were synthesized hitherto.[23] TDFOGE was terpolymerized with catechol acetonide glycidyl ether (CAGE) and allyl glycidyl ether (AGE), respectively ethoxyethyl glycidyl ether (EEGE) (**Scheme 1**). Protecting groups were released selectively without affecting the polyether backbone. The extraordinary properties of fluoropolymers are a central point in the present work. Therefore, these polymers are highly interesting for surface modifications. Here, we examined this point more closely via contact angle measurements.
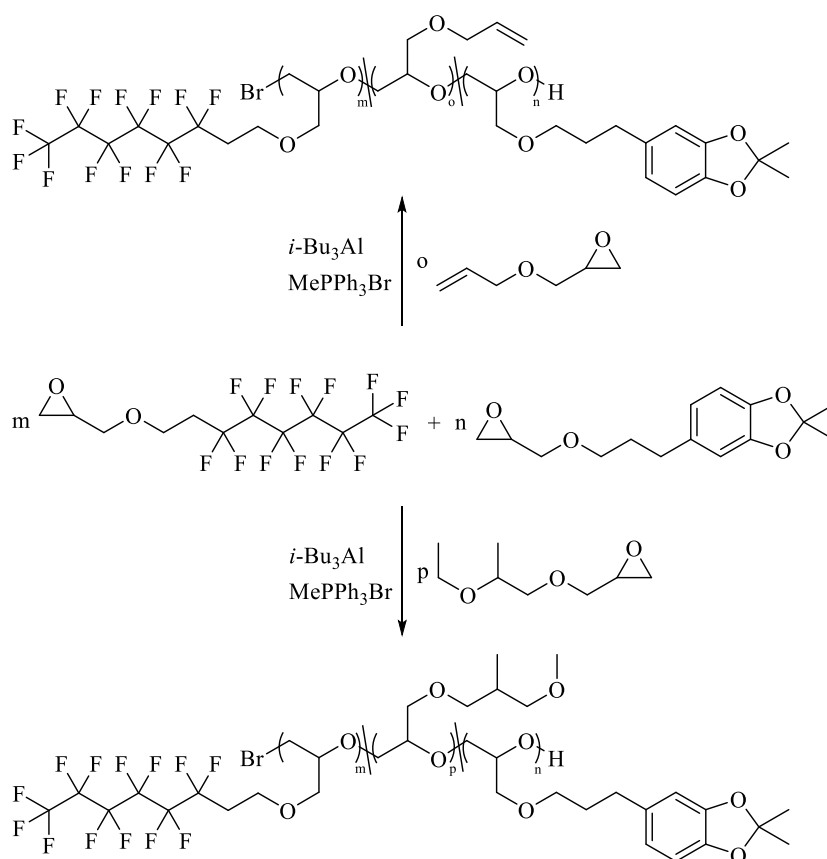
Scheme 1. Synthetic route for the terpolymerization of TDFOGE and CAGE with AGE (top) or EEGE (bottom) via the activated monomer method.

EXPERIMENTAL PART

Terminology. According to the literature, poly(catechol acetonide glycidyl ether) (PCAGE) is designated as poly(catechol glycidyl ether) P(CaGE) after the release of the acetonide protecting group.[25] Poly(ethoxyethyl glycidyl ether) PEEGE is hereinafter referred to as linear polyglycerol (*lin*PG) after deprotection.[26] The name "terpolymer" is used for P(AGE-*co*-TDFOGE-*co*-CAGE) (entries 2−6, **Table 1**) and *lin*P(G-*co*-TDFOGE-*co*-CAGE) (entries 2−6, **Table 3**) structures. The term "copolymers" refers to samples P(AGE$_{0.98}$-*co*-CAGE$_{0.02}$) (entry 1, **Table 1**), *lin*P(G$_{0.97}$-*co*-CAGE$_{0.03}$) (entry 1, **Table 3**) and P(TDFOGE$_{0.97}$-*co*-CAGE$_{0.03}$) (entry 7, **Table 1**). "Polymers" generally relates to co- and terpolymers.

Instrumentation. ^{1}H NMR (400 MHz), ^{13}C NMR (100 MHz), ^{19}F NMR (377 MHz) and 2D NMR spectra were recorded on a Bruker Avance III HD (400 MHz, 5 mm BBFO-SmartProbe with Z-gradient and ATM, SampleXPress 60 sample changer) and referenced internally to the proton signal of the deuterated solvent. Size exclusion chromatography (SEC) were conducted with Polymer Standards Service (PSS) SDV columns (100/1,000/10,000 Å porosity) and tetrahydrofuran (THF) as eluent at 25 °C, using a RI and UV (275 nm) detector. Calibration was carried out using poly(ethylene glycol) standards provided by PSS. Differential scanning calorimetry (DSC) measurements were performed under a nitrogen atmosphere using a PerkinElmer DSC 8,500 in the temperature range of -90 °C to 30 °C. Hereby, heating rates of 20 K min^{-1} and 10 K min^{-1} were used for the first and the second heating run, respectively. The values of the second heating cycle were applied for analysis. Contact angle measurements were performed on a Contact Angle System OCA 20 (DataPhysics Instruments GmbH), using Milli-Q water as probe liquid. For analysis, the software SCA 20 was used. For the post-polymerization modification via thiol-ene click reaction, the UV lamp XX-15B (Ultra-Violet Products Ltd) was used, which consisted of two UV tubes (model T-15.M: 312 nm; T-15.L: 365 nm) provided by Vilber Lourmat Deutschland GmbH.

Materials. Triisobutylaluminium (*i*-Bu$_3$Al, 1.1 M solution in toluene, Acros Organics) was used without further purification. Methyltriphenylphosphonium bromide (MePPh$_3$Br, 98%, Acros Organics) was azeotropically dried with benzene overnight under reduced pressure. Toluene was dried over sodium and stored under reduced pressure. 3,3,4,4,5,5,6,6,7,7,8,8,8-Tridecafluorooctyl glycidyl ether (TDFOGE, >96%, TCI) and allyl glycidyl ether (AGE, 99%, Acros Organics) were freshly dried over CaH$_2$ and distilled under reduced pressure prior to use. Ethoxyethyl glycidyl ether (EEGE) was synthesized according to Fitton *et al.*[27] and purified by stirring over CaH$_2$ and subsequent distillation. Catechol acetonide glycidyl ether (CAGE) was

synthesized according to Niederer *et al.*[25] and azeotropically dried with benzene overnight under reduced pressure. Ethylene oxide (EO, ≥99,5%, Sigma-Aldrich) was used as received. Dialysis membranes (regenerated cellulose, $MWCO = 1,000$ g mol^{-1}) were obtained from Orange Scientific.

Polymer synthesis. A general synthesis is described for P(AGE$_{0.87}$-*co*-TDFOGE$_{0.11}$-*co*-CAGE$_{0.02}$) (entry 2, **Table 1**). Other AGE as well as EEGE approaches were performed analogously with correspondingly adjusted equivalents. MePPh$_3$Br (1 equiv) was dried in a flask with benzene overnight under reduced pressure. The flask was filled with argon, followed by the addition of dried CAGE (4 equiv), AGE (86 equiv), TDFOGE (10 equiv) and 10 mL anhydrous toluene via syringe. Then, the mixture was cooled using an ice/salt bath (-20 °C) and the polymerization was initiated by the careful addition of *i*-Bu$_3$Al (3 equiv). The reaction was allowed to slowly warm up to room temperature and stirred for 24 h. Subsequently, the reaction was stopped by addition of 1 mL methanol. For purification, a dialysis was conducted in a methanol/dichloromethane (DCM) mixture (3 : 2) using regenerated cellulose ($MWCO = 1,000$ g mol^{-1}). In order to prevent excessive foaming during the removal of the solvent, the solution was frozen with liquid nitrogen and the solvents were removed under reduced pressure for 20 h. Typical yields: 60−80%.

Removal of the protecting groups. For AGE containing polymers, 1 mL water, 1 mL acetonitrile and 5 mL trifluoroacetic acid (TFA) were added to 1 g polymer. The solution was stirred at 500 mbar and 40 °C. After two hours, CHCl$_3$ was added and the organic layer was neutralized by washing with saturated NaHCO$_3$ solution. Removal of the solvent under reduced pressure at room temperature led to a quantitative yield.

For EEGE containing polymers, the procedure was analogous. By applying this approach, both acetonide (CAGE) and ethoxyethyl (EEGE) protecting groups were cleaved simultaneously. Here, dialysis (regenerated cellulose, $MWCO = 1,000$ g mol^{-1}) in a methanol/DCM mixture (3 : 2) was used for purification.

Polymer modification: thiol-ene functionalization. The respective terpolymer was dissolved in methanol/dichloromethane mixture (1 : 1) and 10 equiv thiol per AGE double bond were added. In order to achieve a quantitative conversion, the literature procedure was optimized by using 1 wt% DMPA instead of 0.1 wt%.[28] After three freeze-pump-thaw cycles, the mixture was irradiated with an UV lamp for 2 h. For purification, the modified terpolymer was dialyzed

against methanol/DCM (1 : 1) using regenerated cellulose ($MWCO = 1,000$ g mol^{-1}) and dried under reduced pressure.

Sample preparation for contact angle measurements. Contact angles were measured by the sessile drop method wherein the static contact angle measurement was used. Since the static contact angle is time-dependent due to sedimentation and evaporation, the measurement was started five seconds after dropping and repeated until a consistent value was reached to guarantee identical conditions. For the coating of the glass slides, the polymers (100 mg) were dissolved in 2 mL dichloromethane. The glass slides were immersed in these solutions, which were previously placed for 12 h in concentrated hydrochloric acid, cleaned with isopropanol and dried overnight in a vacuum oven (40 °C). The coated glass slides were removed from the polymer solutions after 24 h and washed with DCM to remove excess polymer, which did not adhere to the surface. After drying for 24 h at room temperature under reduced pressure, the so prepared slides were used for the contact angle measurements.

RESULTS AND DISCUSSION

A. Synthesis and characterization of P(AGE-*co*-TDFOGE-*co*-CaGE).

The monomer-activated anionic ring-opening polymerization (AROP) according to Carlotti and Deffieux and co-workers represents an important alternative to the conventional AROP.[16,17,29] An organic salt such as MePPh₃Br is used as initiator, which is combined with an excess of a Lewis acid (*i*-Bu₃Al). The initiator reacts with the catalyst, forming an "ate" complex.[30] Excess catalyst activates the monomer by complexation, resulting in an increased electrophilic reactivity towards nucleophiles. Chain growth occurs due to insertion of further monomers. Termination of the reaction is performed by addition of protic solvents such as MeOH. Consequently, a polymerization under mild reaction conditions is possible via the activated monomer technique. The mechanism is displayed in **Scheme 2**.
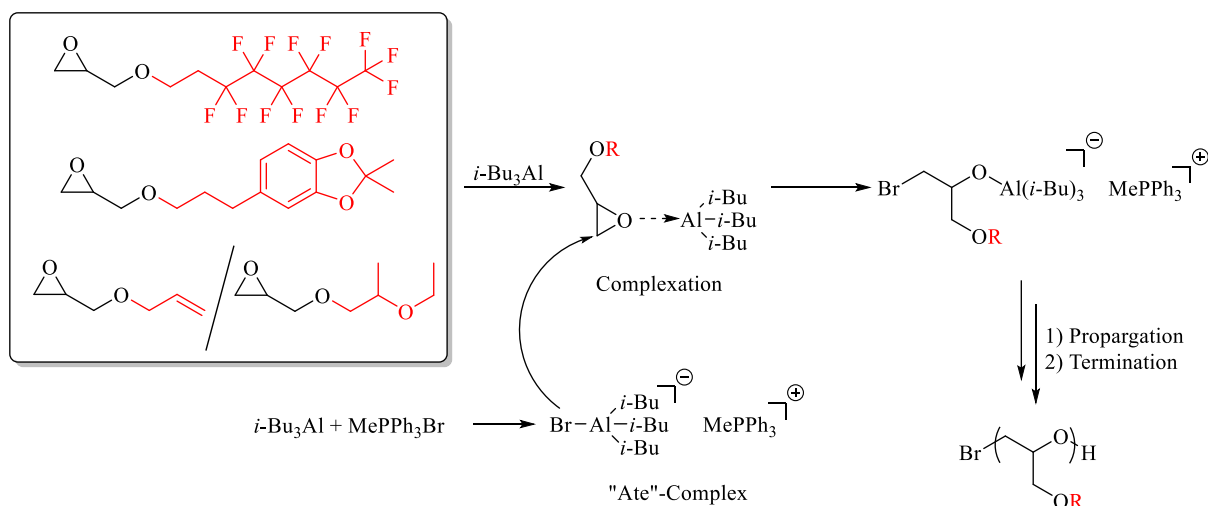
Scheme 2. Terpolymerization of TDFOGE, CAGE and AGE, respectively EEGE initiated by MePPh₃Br and catalyzed by *i*-Bu₃Al.

AGE was co- and terpolymerized with TDFOGE and CAGE via the monomer-activated AROP. The polymers were addressed on the one hand by thiol-ene click chemistry and on the other hand used as coatings for glass surfaces after removal of the acetonide protecting group. **Table** 1 summarizes the SEC results for deprotected co- and terpolymers of AGE, TDFOGE and CAGE

Table 1. Terpolymerization of AGE, TDFOGE and CAGE. Initiated with a [i-Bu$_3$Al]/[MePPh$_3$Br] ratio of 3 : 1 in toluene (T = -20 °C).

No.	Composition[a]	Theoretical composition	$M_n^{(th)}$ (g mol^{-1})	M_n^{b} (g mol^{-1})	$Đ$
1	P(AGE$_{0.98}$-co-CaGE$_{0.02}$)	97:0:3	12,400	12,800	1.19
2	P(AGE$_{0.87}$-co-TDFOGE$_{0.11}$-co-CaGE$_{0.02}$)	86:10:4	15,600	8,700	1.28
3	P(AGE$_{0.79}$-co-TDFOGE$_{0.19}$-co-CaGE$_{0.02}$)	78:19:3	18,300	13,400	1.21
4	P(AGE$_{0.63}$-co-TDFOGE$_{0.35}$-co-CaGE$_{0.02}$)	67:29:4	21,700	14,700	1.11
5	P(AGE$_{0.58}$-co-TDFOGE$_{0.40}$-co-CaGE$_{0.02}$)	58:39:3	24,800	17,200	1.10
6	P(AGE$_{0.46}$-co-TDFOGE$_{0.52}$-co-CaGE$_{0.02}$)	48:49:3	27,200	13,700	1.17
7	P(TDFOGE$_{0.97}$-co-CaGE$_{0.03}$)[c]	0:97:3	42,700	42,600	1.19

[a] Values calculated by ^{1}H NMR spectroscopy. [b] Determined by SEC in THF (RI detector, PEG standards). [c] Determined by SEC in HFIP (RI detector, PMMA standards).

The molecular weights are in a range between 8,700 g mol^{-1} and 42,600 g mol^{-1} with dispersities ($Đ = M_w M_n^{-1}$) of less than 1.28. The discrepancy between $M_n^{(th)}$ and M_n is attributed to the PEG calibration. Especially higher amounts of TDFOGE cause a decrease of the measured molecular weights as a consequence of the strongly deviating hydrodynamic radii of terpolymers (cf. entry 6, **Table 1**). Similar observations were made by Obermeier *et al.* for P(EO-*co*-AGE) copoylmers.[31] SEC measurements revealed a narrow and monomodal distribution (**Figure 1**). For P(TDFOGE$_{0.97}$-*co*-CaGE$_{0.03}$) (entry 7, **Table 1**) see Supporting Information **Figure S1**. The successful co- and terpolymerization is additionally supported by the fact that the RI and UV signal distribution are superimposable (**Figure S2**).
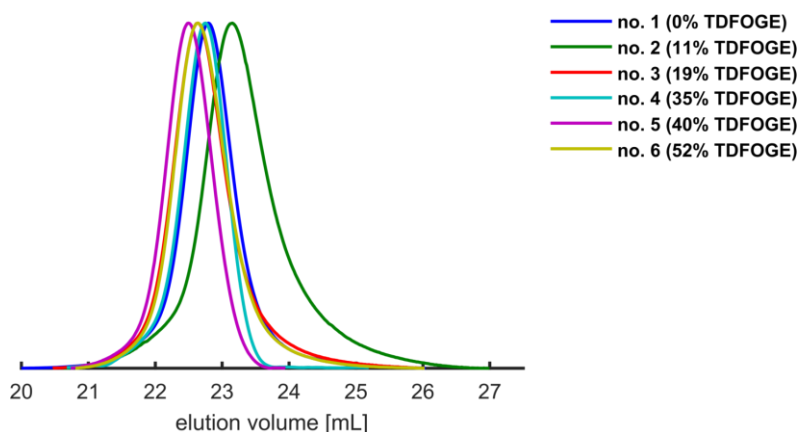
Figure 1. SEC traces (THF, PEG standards) of P(AGE-*co*-TDFOGE-*co*-CaGE) (entries 2−6, **Table 1**) terpolymers with a varied amount of TDFOGE and P(AGE$_{0.98}$-*co*-CaGE$_{0.02}$) (entry 1, **Table 1**) copolymer.

Incorporation rates were calculated from ^{1}H NMR spectra, which is shown exemplified for protected P(AGE$_{0.46}$-*co*-TDFOGE$_{0.52}$-*co*-CAGE$_{0.02}$) (entry 6, **Table 1**) in **Figure 2**. For this purpose, the signals of the methylene groups of the AGE (5.3–5.1 ppm), TDFOGE (2.4–2.3 ppm) and CAGE (2.6–2.5 ppm) moieties were compared, giving the ratio showed in **Table 1**. The isomerization of the AGE double bonds reported by Lee *et al.* was not observed, which can be attributed to the mild polymerization conditions in combination with the absence of potassium ions and polar solvents such as DMSO.[32]
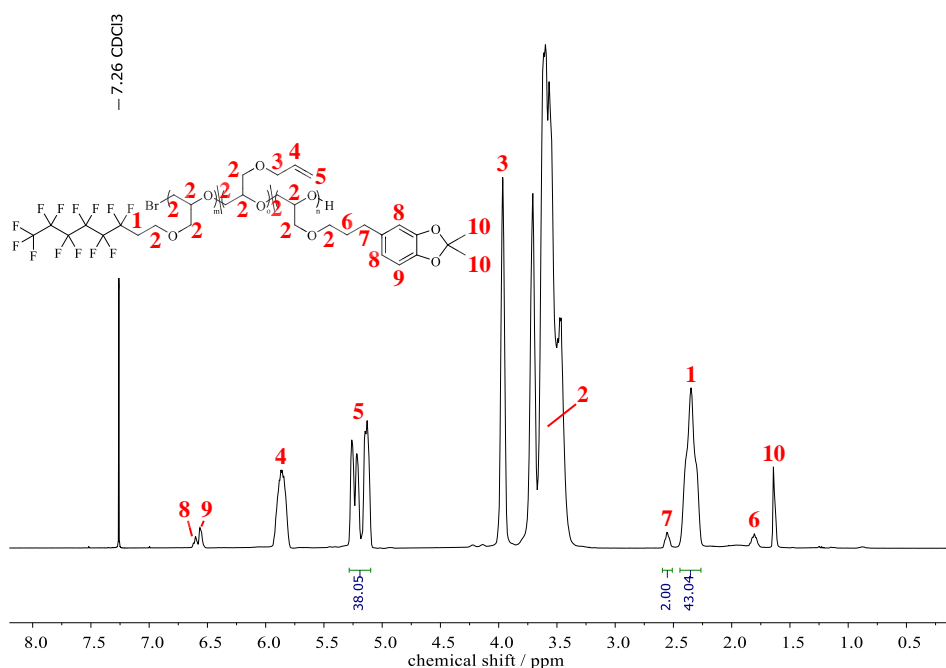
Figure 2. ^{1}H NMR spectrum (400 MHz, C*D*Cl$_3$) of protected P(AGE$_{0.46}$-*co*-TDFOGE$_{0.52}$-*co*-CAGE$_{0.02}$) (entry 6, **Table 1**).

In contrast to literature, the quantitative removal of the protecting group was not successful using hydrochloric acid.[25] Instead, an excess of trifluoroacetic acid (TFA) in acetonitrile was used (**Figure S3**). By extraction with aqueous $NaHCO_3$ solution, TFA could be removed from the AGE-containing terpolymers. Quantitative conversion for the removal of the acetonide protecting groups was monitored by ^{1}H NMR spectroscopy according to the absence of the signal of the acetonide protecting group at 1.6 ppm. **Figure 3** shows the ^{1}H NMR spectra before and after removal of the acetonide protecting groups of the AGE-containing terpolymers (^{13}C NMR, ^{19}F NMR and 2D NMR spectra are available in the Supporting Information, **Figures S4–7**). In the lower spectrum, no signal can be seen at 1.6 ppm. Instead, a change in the aromatic region can be observed, due to the release of the catechol hydroxyl functions.
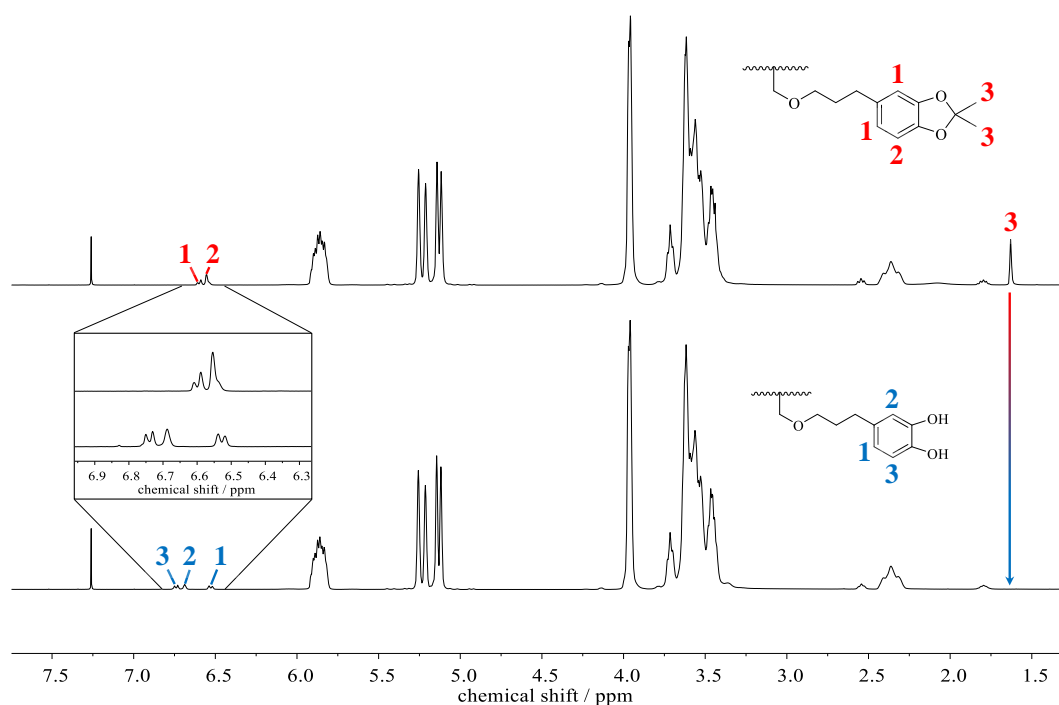
Figure 3. ^{1}H NMR spectra (400 MHz, C*D*Cl₃) of precursor P(AGE$_{0.79}$-*co*-TDFOGE$_{0.19}$-*co*-CAGE$_{0.02}$) (entry 3, **Table 1**) before (top) and after (bottom) acidic removal of the acetonide protecting groups.

Post-Polymerization Modification via Thiol-ene Click Chemistry. Thiol-ene coupling (TEC) is a powerful tool to modify double bonds with any desired functionality. For example, free amines cannot be polymerized in the AROP, since initiation by the amine would occur.[33] By using TEC, functional groups can be applied directly without resorting to protecting group chemistry. Common methods for functionalizing of the pendant AGE moieties are based on the

use of radical initiators such as *N,N*-azobisisobutyronitrile (AIBN) or photoinitiators such as 2,2-dimethoxy-2-phenylacetophenone (DMPA).[34]

Two different commercially available thiols were used for the modification of the precursor P(AGE-*co*-TDFOGE-*co*-CaGE) (**Scheme 3**).
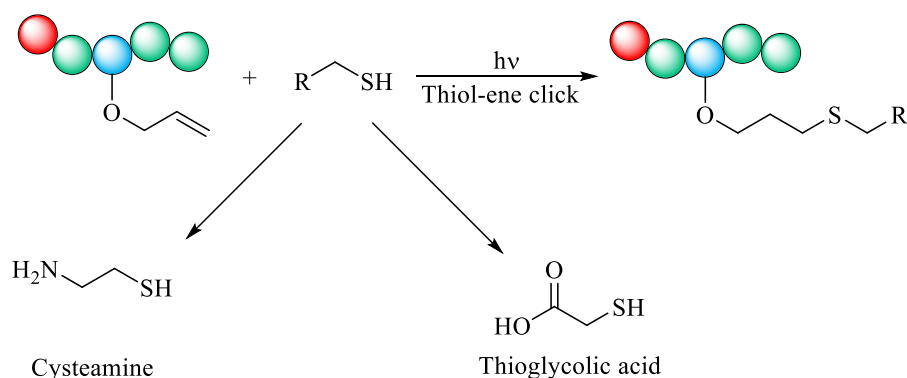
Scheme 3. Thiol-ene modification of P(AGE-*co*-TDFOGE-*co*-CaGE) precursors with thiols.

Based on of P(AGE$_{0.79}$-*co*-TDFOGE$_{0.19}$-*co*-CaGE$_{0.02}$) (entry 3, **Table 1**), cysteamine hydrochloride (CA) was attached to the AGE double bonds. Thioglycolic acid (TA) was used for P(AGE$_{0.58}$-*co*-TDFOGE$_{0.40}$-*co*-CaGE$_{0.02}$) (entry 5, **Table 1**). The results of the SEC analysis are given in **Table 2**.

Table 2. Synthesized derivatives of P(AGE-co-TDFOGE-co-CaGE) terpolymers by thiol-ene coupling.

No.	Composition	R-SH[a]	M_n[b] (g mol^{-1})	$Đ$[b]	M_n[c] (g mol^{-1})	$Đ$[c]
A	P(AGE$_{0.79}$-*co*-TDFOGE$_{0.19}$-*co*-CaGE$_{0.02}$)	CA	13,400	1.21	N/A	N/A
B	P(AGE$_{0.58}$-*co*-TDFOGE$_{0.40}$-*co*-CaGE$_{0.02}$)	TA	17,200	1.10	11,900	1.17

[a] CA = cysteamine hydrochloride, TA = thioglycolic acid. [b] Data for P(AGE-*co*-TDFOGE-*co*-CaGE) precursors, determined by SEC (THF, RI detector, PEG standards). [c] Data for functional derivatives, determined by SEC (THF, RI detector, PEG standards).

The combination of the hydrophobic perfluoroalkyl chains with very polar substances such as CA or TA expands the field of application. In this regard, the use in the area of microarrays is conceivable.[35] For CA-functionalized P(AGE$_{0.79}$-*co*-TDFOGE$_{0.19}$-*co*-CaGE$_{0.02}$) (entry A, **Table 2**), SEC analysis was not successful due to the insolubility of the modified polymer in

THF. SEC analysis for the TA-modified P(AGE$_{0.58}$-*co*-TDFOGE$_{0.40}$-*co*-CaGE$_{0.02}$) (entry B, **Table 2**) showed a shift of the traces compared to the unmodified precursors (**Figure S8**). A molecular weight difference of approximately 5,300 g mol^{-1} was observed here with nearly no change in the polydispersity. ^{1}H NMR spectroscopy proved a quantitative functionalization of the AGE double bonds, which is here exemplified for the TEC modification with thioglycolic acid (**Figure 4**). The characteristic signals of allyl units at 4.0 ppm, 5.2 ppm and 5.9 ppm disappeared after the modification and signals for the introduced thiol functionalities were observed. The corresponding COSY NMR spectrum for TA, as well as ^{1}H NMR and COSY NMR spectra for CA are given in the Supporting Information in **Figures S9–11**.
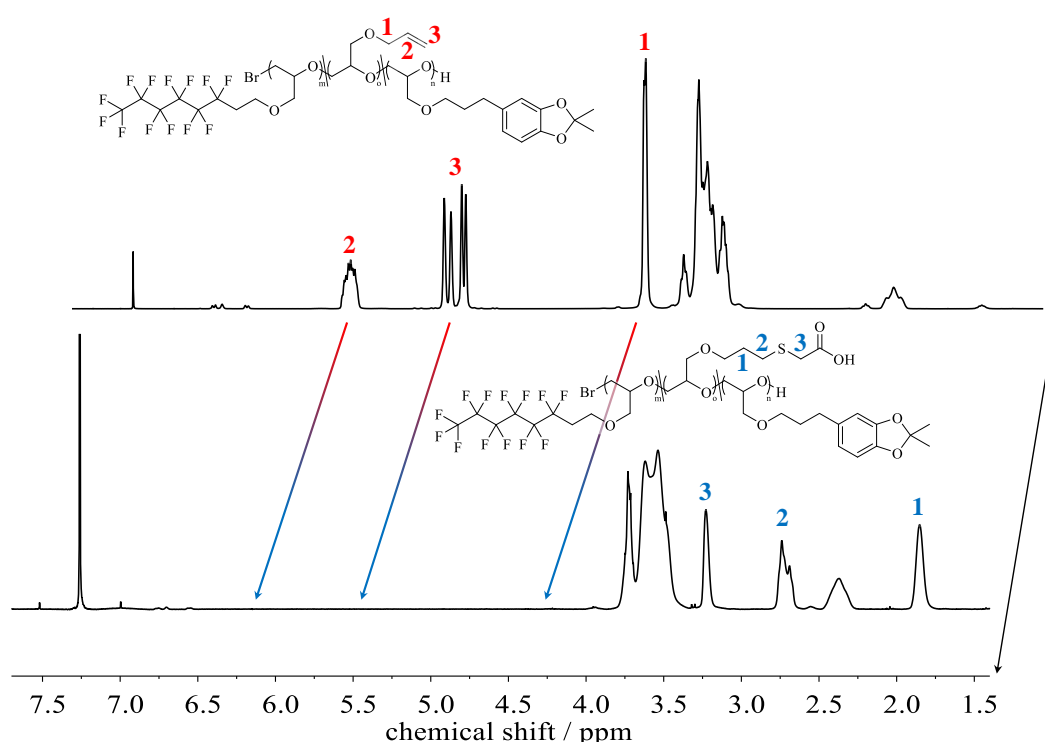
Figure 4. Relevant sections of ^{1}H NMR spectra (400 MHz, C*D*Cl$_3$) of precursor P(AGE$_{0.58}$-*co*-TDFOGE$_{0.40}$-*co*-CaGE$_{0.02}$) (entry 5, **Table 1**) and TA-functionalized derivative (entry B, **Table 2**).

B.   Synthesis of *lin*P(G-*co*-TDFOGE-*co*-CaGE).

In order to obtain direct access to hydrophilic-hydrophobic structures, EEGE was terpolymerized with TDFOGE and CAGE. Such structures are interesting as antibacterial surfaces.[36] Beside the thermal properties, the surface properties of the polymers were in the foreground. SEC analysis of the multi-functional *lin*PGs revealed molecular weights in a range

of 11,900−14,500 g mol^{-1} with $Đ$ up to 1.26. Here, the discrepancy between theoretical and measured values also increases with higher TDFOGE incorporation. This can be attributed to the PEG calibration analogous to the AGE-based terpolymers.[37] **Table 3** summarizes the compositions, molecular weights and polydispersities.

Table 3. Terpolymerization of EEGE, TDFOGE and CAGE. Initiated with a [i-Bu$_3$Al]/[MePPh$_3$Br] ratio of 3 : 1 in toluene (T = -20 °C).

No.	Composition^a	Theoretical composition	$M_n^{(th)}$ (g mol^{-1})	M_n^b (g mol^{-1})	$Đ$
1	linP(G$_{0.97}$-co-CaGE$_{0.03}$)	97:0:3	15,400	12,900	1.19
2	linP(G$_{0.87}$-co-TDFOGE$_{0.10}$-co-CaGE$_{0.03}$)	88:9:3	18,400	11,900	1.24
3	linP(G$_{0.77}$-co-TDFOGE$_{0.19}$-co-CaGE$_{0.04}$)	78:19:3	21,100	13,400	1.26
4	linP(G$_{0.67}$-co-TDFOGE$_{0.31}$-co-CaGE$_{0.02}$)	68:29:3	23,900	12,100	1.19
5	linP(G$_{0.58}$-co-TDFOGE$_{0.39}$-co-CaGE$_{0.03}$)	58:39:3	26,500	13,200	1.15
6	linP(G$_{0.48}$-co-TDFOGE$_{0.50}$-co-CaGE$_{0.02}$)	48:49:3	29,700	14,500	1.15

^{a} Values calculated by ^{1}H NMR spectroscopy. ^{b} Determined by SEC in THF (RI detector, PEG standards).

All SEC traces displayed monomodal polymer distributions (**Figure 5**). In addition, RI and UV signal of the distribution were superimposable, demonstrating a uniform incorporation of the comonomers (**Figure S12**).
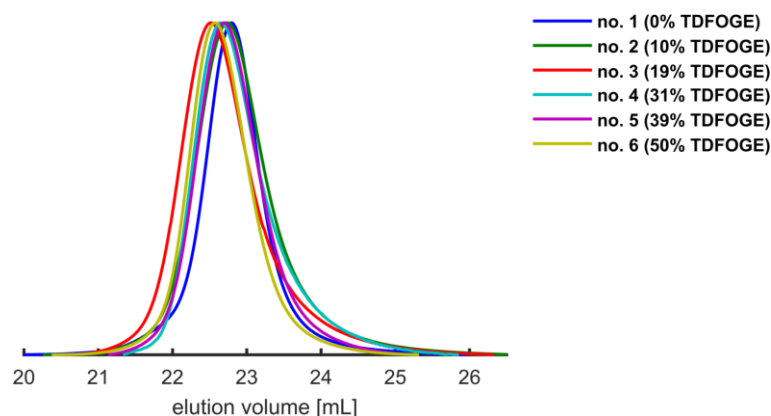
Figure 5. SEC traces (THF, PEG standards) of *lin*P(G-*co*-TDFOGE-*co*-CaGE) (entries 2−6, **Table 3**) terpolymers with varied amount of TDFOGE and *lin*P(G$_{0.97}$-*co*-CaGE$_{0.03}$) (entry 1, **Table 3**) copolymer.

The incorporation ratios of the *lin*PG-containing polymers were obtained from the ^{1}H NMR spectra of the respective protected species. Signals at 1.3–1.2 ppm (EEGE), 2.3 ppm (TDFOGE) and 2.6–2.5 ppm (CAGE) were used for evaluation (**Figure 6**). Minor catalyst residues in the range of 3–2 ppm could be identified despite dialysis in a methanol/dichloromethane (DCM) mixture (3 : 2).
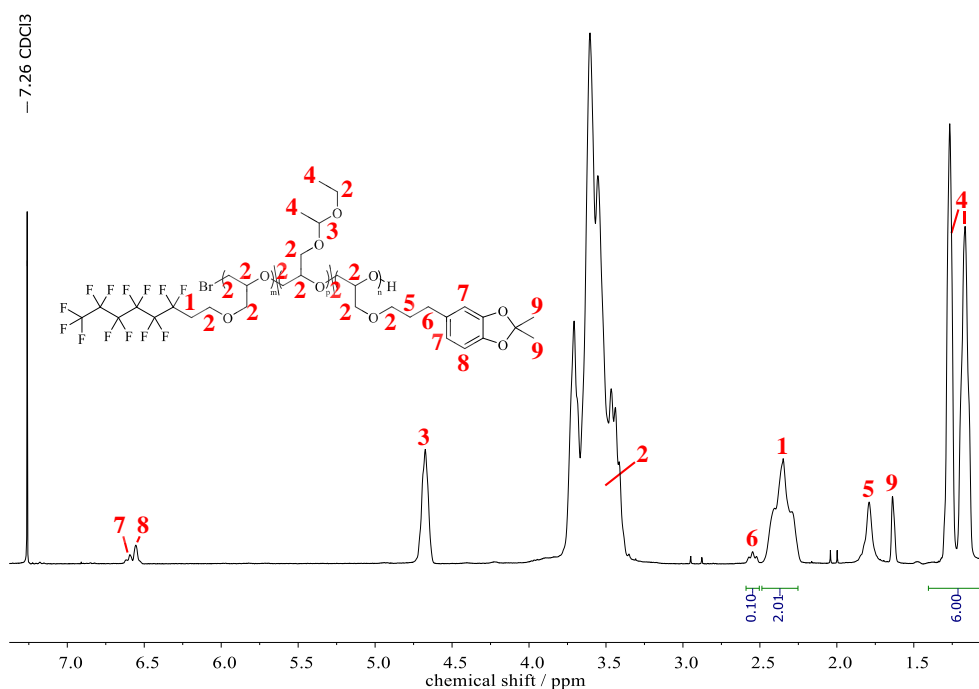
Figure 6. ^{1}H NMR spectrum (400 MHz, C*D*Cl$_3$) of protected P(EEGE$_{0.48}$-*co*-TDFOGE$_{0.50}$-*co*-CAGE$_{0.02}$) (entry 6, **Table 3**).

In order to use the catechol functionalities as an adhesive anchor for the coating of glass slides, the acetonide group must be removed quantitatively. The EEGE/CAGE-containing polymers distinguish the particular characteristic that the ethoxyethyl acetal protecting groups can be removed selectively before the acetonide groups to release linear glycerol units with free hydroxyl groups.[38] ^{1}H NMR studies proofed that the ethoxyethyl acetal protecting groups were quantitatively removed by using 1 M hydrochloric acid at 60 °C over a period of 24 h (**Figure 7**, middle). Characteristic signals of EEGE at 4.7 and 1.2 ppm disappeared, while the signal of the acetonide protecting group at 1.6 ppm was left. By using TFA for two hours at 40 °C under reduced pressure, the removal of the acetonide protecting groups took place (**Figure 7**). Assigned ^{1}H NMR, ^{13}C NMR, ^{19}F NMR and 2D NMR spectra can be found in the Supporting Information (**Figures S13–17**). In contrast to the AGE-containing terpolymers, *lin*PG-based polymers are water-soluble, especially those with a high amount of linear glycerol moieties. Therefore, these polymers were dialyzed in contrast to the AGE-containing polymers
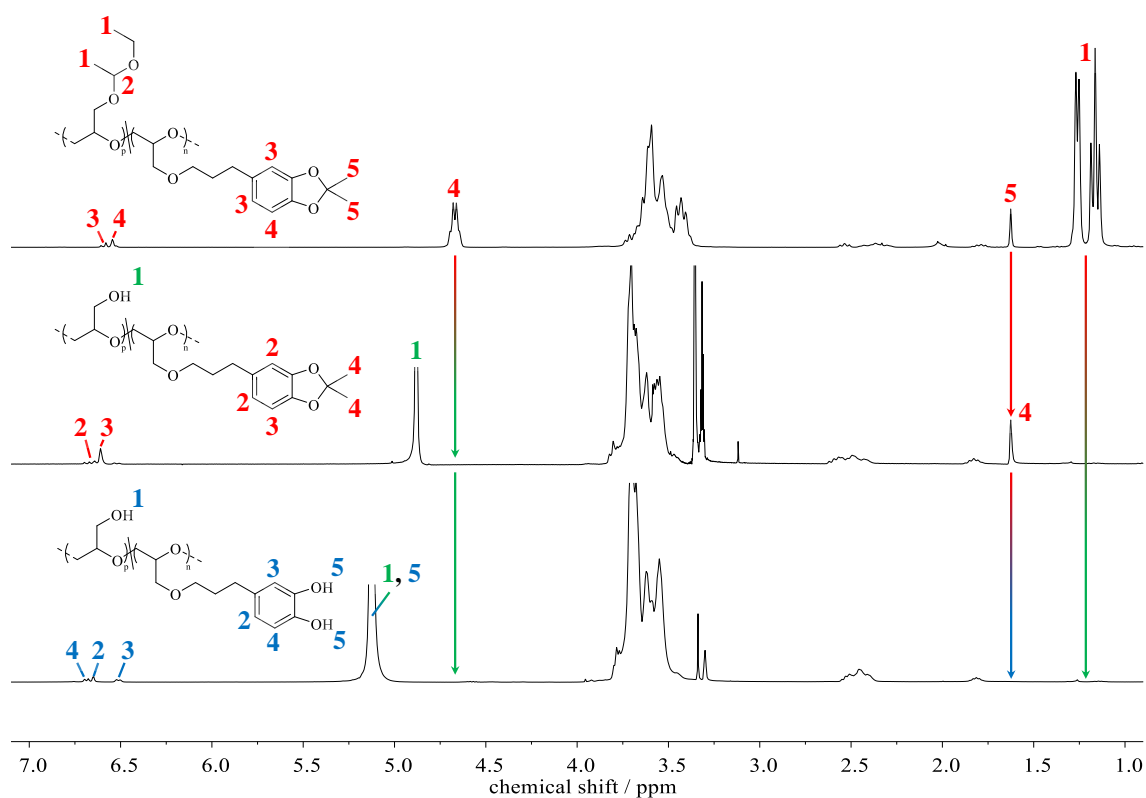
Figure 7. ^{1}H NMR spectra (400 MHz) of precursor P(EEGE$_{0.87}$-*co*-TDFOGE$_{0.10}$-*co*-CAGE$_{0.03}$) (entry 2, **Table 3**) before (top, C*D*Cl$_3$) and after acidic treatment with hydrochloric acid (middle, C*D*$_3$O*D*), respectively trifluoroacetic acid (bottom, C*D*$_3$O*D*).

C. Thermal properties

Conclusions can be drawn about structural properties of the polymers by the characterization of the thermal properties, whereby parameters such as the melting points, the heat capacities and the glass transitions can be analyzed. As a result of the lack of tacticity and the bulky substituents, no melting points and hence no crystalline domains were observed neither for the AGE, nor for the linear glycerol-containing polymers. Determined glass transition temperatures (T_gs) obtained by differential scanning calorimetric measurements (DSC) are listed in **Table 4**.

Table 4. Thermal properties of P(AGE-*co*-TDFOGE-*co*-CaGE) and *lin*P(G-*co*-TDFOGE-*co*-CaGE) terpolymers, including corresponding copolymers.

No.	Composition[a]	T_g (°C)
1	P(AGE$_{0.98}$-*co*-CaGE$_{0.02}$)	-71
2	P(AGE$_{0.87}$-*co*-TDFOGE$_{0.11}$-*co*-CaGE$_{0.02}$)	-69
3	P(AGE$_{0.79}$-*co*-TDFOGE$_{0.19}$-*co*-CaGE$_{0.02}$)	-65
4	P(AGE$_{0.63}$-*co*-TDFOGE$_{0.35}$-*co*-CaGE$_{0.02}$)	-60
5	P(AGE$_{0.58}$-*co*-TDFOGE$_{0.40}$-*co*-CaGE$_{0.02}$)	-60
6	P(AGE$_{0.46}$-*co*-TDFOGE$_{0.52}$-*co*-CaGE$_{0.02}$)	-55
7	P(TDFOGE$_{0.97}$-*co*-CaGE$_{0.03}$)	-44
8	*lin*P(G$_{0.48}$-*co*-TDFOGE$_{0.50}$-*co*-CaGE$_{0.02}$)	-32
9	*lin*P(G$_{0.58}$-*co*-TDFOGE$_{0.39}$-*co*-CaGE$_{0.03}$)	-24
10	*lin*P(G$_{0.67}$-*co*-TDFOGE$_{0.31}$-*co*-CaGE$_{0.02}$)	-15
11	*lin*P(G$_{0.77}$-*co*-TDFOGE$_{0.19}$-*co*-CaGE$_{0.04}$)	-8
12	*lin*P(G$_{0.87}$-*co*-TDFOGE$_{0.10}$-*co*-CaGE$_{0.03}$)	-2
13	*lin*P(G$_{0.97}$-*co*-CaGE$_{0.03}$)	-2

[a] Values calculated by ^{1}H NMR spectroscopy.

P(AGE-*co*-TDFOGE-*co*-CaGE) terpolymers show T_gs between -69 °C and -55 °C (entries 2–6, **Table 4**). For the copolymer P(AGE$_{0.98}$-*co*-CaGE$_{0.02}$) (entry 1, **Table 4**) the T_g is -71 °C, which is in agreement with the literature value of PAGE homopolymer (T_g = -77 °C).[39,40] For P(TDFOGE$_{0.97}$-*co*-CaGE$_{0.03}$) (entry 7, **Table 4**) a glass transition of -44 °C was detected. Thermal properties of TDFOGE-containing polymers have not been analyzed yet. The more flexible AGE units increase the free volume of the polymer chain. Consequently, the T_gs

decrease with increasing amount of AGE. On the other side, the "stiffer" perfluoroalkyl chains of TDFOGE cause a hindrance to the binding rotation of the main chain, resulting in an increase of the T_gs.[41,42] For *lin*PG homopolymer, literature values for T_g move in a range of -8 °C and -27 °C depending on the molecular weight.[43] Measured T_gs for *lin*PG-containing co- and terpolymers are in a range between -2 °C and -32 °C (entries 8–13, **Table 4**). With growing number of linear glycerol moieties, T_gs increase steadily. Due to polar glycerol substituents, hydrogen bonds are formed, whereby the bond rotation is hindered, resulting in an increase of the T_gs. **Figures 8−9** graphically depict the glass transitions depending on the amount of TDFOGE, both for AGE and *lin*PG-containing terpolymers (DSC heating curve as flowcharts available in the Supporting Information, **Figures S18−19**). The almost linear course of the T_gs represents a nearly ideal behavior for amorphous polymers, indicating a random incorporation of the comonomers along the polyether backbone.[44] This is noteworthy, since access to random copolymers via the monomer activation technique is only guaranteed through the copolymerization of glycidyl ether derivatives.[45,46] In contrast, the copolymerization with ethylene oxide leads to strongly tapered copolymer structures.[47]
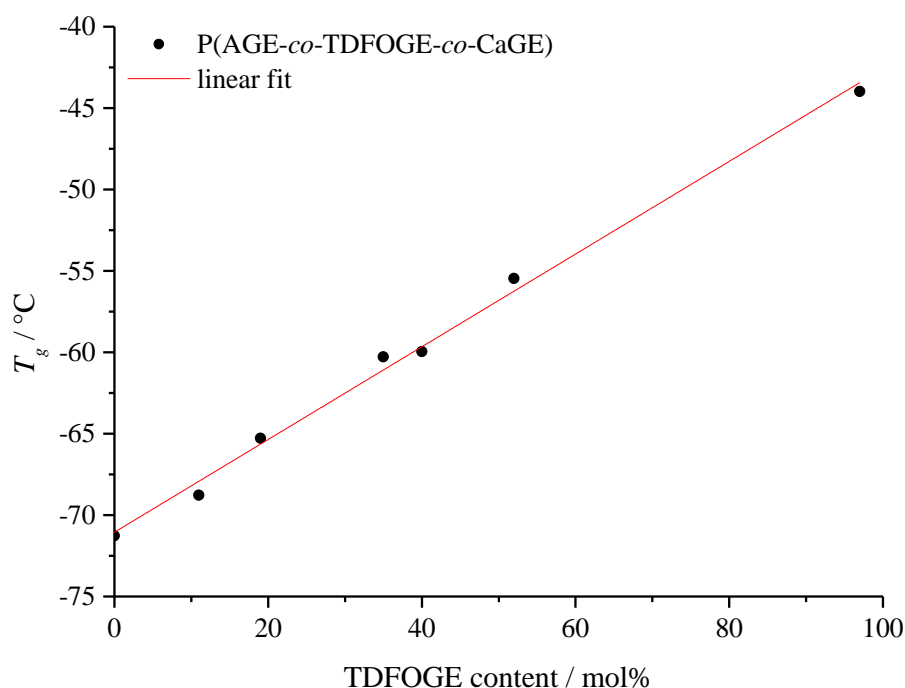
Figure 8. Glass transition temperature vs. TDFOGE content in P(AGE-*co*-TDFOGE-*co*-CaGE) terpolymers (entries 2–6, **Table 4**) and corresponding copolymers (entries 1/7, **Table 4**).
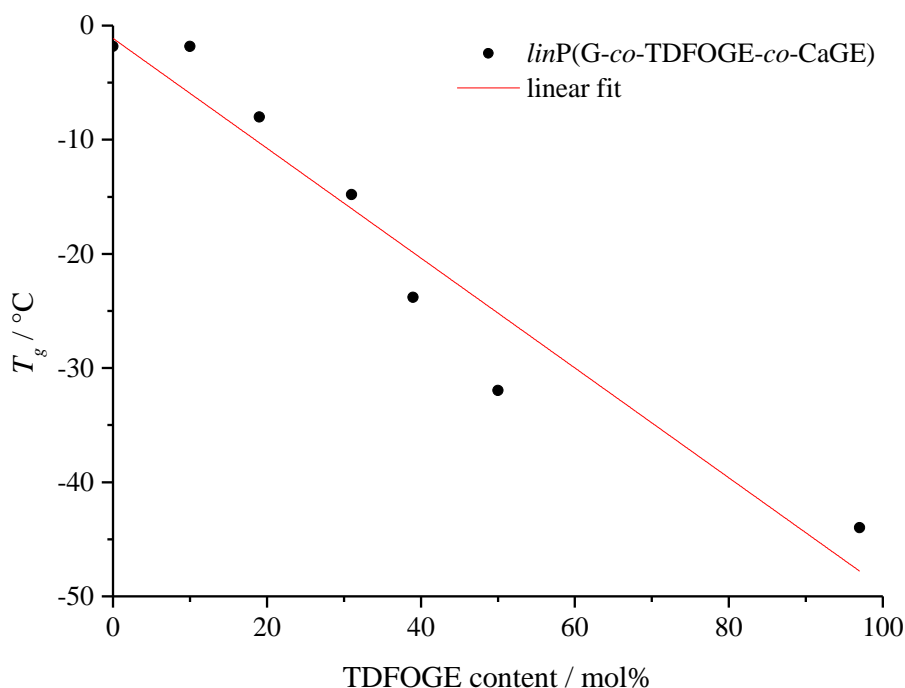
Figure 9. Glass transition temperature vs. TDFOGE content in *lin*P(G-*co*-TDFOGE-*co*-CaGE) terpolymers (entries 8–12, **Table 4**) and corresponding copolymers (entries 7/13, **Table 4**).

D.   Surface properties

Each polymer has a specific wettability. To determine this intrinsic wettability, contact angle measurements can be measured by placing a drop of water on the surface, which was coated with the corresponding polymer. In general, differentiation is made between hydrophobic and hydrophilic surfaces. Surfaces are considered to be hydrophobic, if the contact angle is greater than 90° against water.[48] Besides high contact angles, characteristics of a hydrophobic surface are low adhesion, low wettability and a small free surface energy, while hydrophilic surfaces represents the opposite.[49]

In order to determine the influence of the perfluoroalkyl chains on the surface properties of the polymers, contact angle measurements were performed. The deprotected CaGE units served as an adhesive anchor for the coating of glass slides. In **Figure 10** the contact angles were plotted against the amount of incorporated TDFOGE.
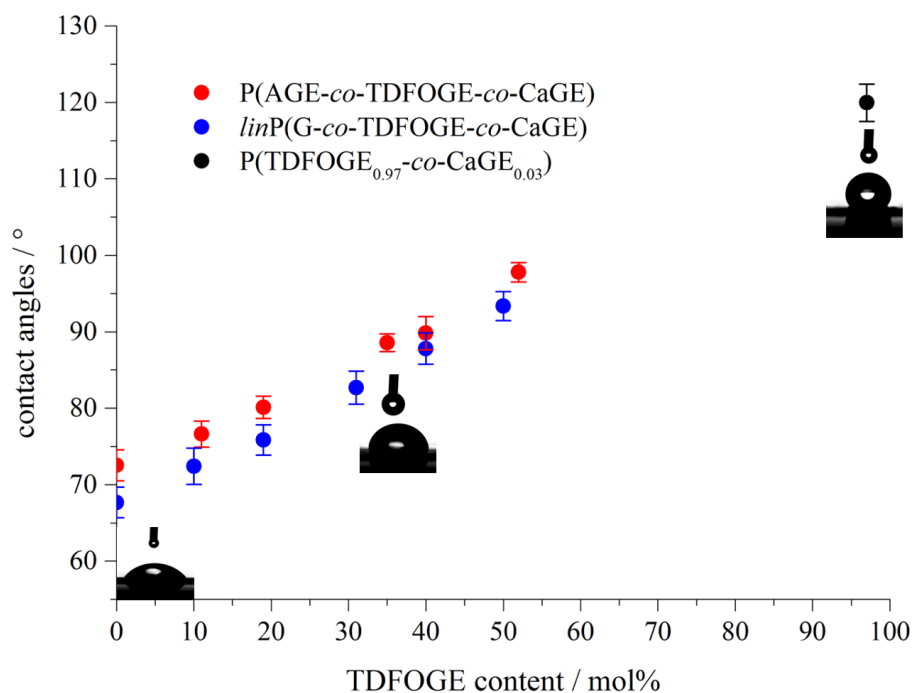
Figure 10. Contact angles of the AGE and *lin*PG-containing polymers coated on glass slides. Note: 0 mol% TDFOGE corresponds to the two copolymers P(AGE$_{0.98}$-co-CaGE$_{0.02}$) (entry 1, **Table 1**) and *lin*P(G$_{0.97}$-*co*-CaGE$_{0.03}$) (entry 1, **Table 3**).

A significant change in the contact angles was observed. Due to the increasing amount of TDFOGE, the contact angles increased constantly. In case of untreated glass slides, the contact angle was 55° and increased to the maximum value of 120° for P(TDFOGE$_{0.97}$-*co*-CaGE$_{0.03}$) (entry 7, **Table 1**). Literature values for PTDFOGE are unknown. Comparable materials, such as PTFE show contact angles for water of 112−117°.[50] Values of the terpolymers were between these limits. The fluoroalkyl substituents are responsible for the sharp increase. They are characterized by a low polarizability and thus a low surface energy. Due to the non-stick properties of the surface, water can hardly adhere here. Contact angles of P(AGE-*co*-TDFOGE-*co*-CaGE) were on average higher than the values of *lin*P(G-*co*-TDFOGE-*co*-CaGE). This is in line with expectations, since the free hydroxyl groups of the linear glycerol units increase the hydrophilicity.

CONCLUSION

Motivated by the special anti-adhesive surface properties of fluoropolymers, the monomer activating technique was used for the co- and terpolymerization of 3,3,4,4,5,5,6,6,7,7,8,8,8-tridecafluorooctyl glycidyl ether (TDFOGE). To the best of our knowledge P(AGE-*co*-TDFOGE-*co*-CAGE) and *lin*P(G-*co*-TDFOGE-*co*-CAGE) terpolymers were synthesized for the first time. Based on the initiator/catalyst system [*i*-Bu$_3$Al]/[MePPh$_3$Br] (3 : 1), terpolymers were obtained with molecular weights between 8,700−17,200 g mol^{-1} and dispersities up to 1.28. The incorporation rate of CAGE was kept constant at 2−4 mol%, whereby the amount of TDFOGE was varied between 0−97 mol%, which was proofed by ^{1}H NMR analysis. Glass transition temperatures (T_gs) were adjustable between -69 °C and -55 °C for AGE-, respectively -2 °C and -32 °C for *lin*PG-containing terpolymers and indicated a random distribution of the comonomers along the polymer backbone. P(AGE-*co*-TDFOGE-*co*-CAGE) terpolymers were addressed by thiol-ene click chemistry, whereby amino and carboxyl groups were introduced. It could be shown for the *lin*PG-based polymers, that the pendant, linear glycerol units could be selectively released from the catechol units. The catechol functionalities served as adhesive anchors for the coating of glass slides after the release of the acetonide protecting groups. Investigations of surface properties revealed both a successful coating and a correlation between anti-adherent behavior towards water and amount of TDFOGE. Contact angles could be varied up to 120°.

Due to their non-stick properties, fluoropolymers are very interesting as coating protection against biological contamination. For instance, adhesive forces of marine life are caused by secretion of proteins or glycoproteins of hydrophilic or hydrophobic nature.[51] Both linear poly(glycerol)s, as well as TEC modified poly(ally glycidyl ether)s and fluoropolymers show antifouling properties.[52,53] By combining hydrophilic and hydrophobic properties, they would be a promising candidates as non-stick coating.[36]

In summary, the incorporation of organofluorine compounds into an aliphatic polyether backbone provokes exceptional properties.

REFERENCES

(1) O'Hagan, D. Understanding organofluorine chemistry. An introduction to the C-F bond. *Chem. Soc. Rev.* **2008**, *37*, 308–319, DOI: 10.1039/b711844a.

(2) Banks, R. E.; Smart, B. E.; Tatlow, J. C. *Organofluorine Chemistry: Principles and Commercial Applications*; Springer US, 2013.

(3) Lemal, D. M. Perspective on fluorocarbon chemistry. *J. Org. Chem.* **2004**, *69*, 1–11, DOI: 10.1021/jo0302556.

(4) Blanksby, S. J.; Ellison, G. B. Bond dissociation energies of organic molecules. *Acc. Chem. Res.* **2003**, *36*, 255–263, DOI: 10.1021/ar020230d.

(5) O'Hagan, D. Organofluorine chemistry: synthesis and conformation of vicinal fluoromethylene motifs. *J. Org. Chem.* **2012**, *77*, 3689–3699, DOI: 10.1021/jo300044q.

(6) Kirsch, P. *Modern Fluoroorganic Chemistry: Synthesis, Reactivity, Applications*; Wiley, 2013.

(7) Staudinger, H.; Lohmann, H. Über hochpolymere Verbindungen. 81. Mitteilung. Über eukolloides Polyäthylenoxyd. *Justus Liebigs Ann. Chem.* **1933**, *505*, 41–51, DOI: 10.1002/jlac.19335050104.

(8) Nuyken, O.; Pask, S. Ring-Opening Polymerization—An Introductory Review. *Polymers* **2013**, *5*, 361–403, DOI: 10.3390/polym5020361.

(9) Fast, J. P.; Perkins, M. G.; Pearce, R. A.; Mecozzi, S. Fluoropolymer-based emulsions for the intravenous delivery of sevoflurane. *Anesthesiology* **2008**, *109*, 651–656, DOI: 10.1097/ALN.0b013e31818630ff.

(10) Souzy, R.; Ameduri, B. Functional fluoropolymers for fuel cell membranes. *Prog. Polym. Sci.* **2005**, *30*, 644–687, DOI: 10.1016/j.progpolymsci.2005.03.004.

(11) Ameduri, B. From vinylidene fluoride (VDF) to the applications of VDF-containing polymers and copolymers: recent developments and future trends. *Chem. Rev.* **2009**, *109*, 6632–6686, DOI: 10.1021/cr800187m.

(12) Améduri, B.; Boutevin, B.; Kostov, G. Fluoroelastomers: synthesis, properties and applications. *Prog. Polym. Sci.* **2001**, *26*, 105–187, DOI: 10.1016/S0079-6700(00)00044-7.

(13) Schüll, C.; Gieshoff, T.; Frey, H. One-step synthesis of multi-alkyne functional hyperbranched polyglycerols by copolymerization of glycidyl propargyl ether and glycidol. *Polym. Chem.* **2013**, *4*, 4730–4736, DOI: 10.1039/c3py00707c.

(14) Binder, W. H.; Sachsenhofer, R. 'Click' Chemistry in Polymer and Materials Science. *Macromol. Rapid Commun.* **2007**, *28,* DOI: 10.1002/marc.200600625.

(15) Yamamoto, H.; Hiyama, T.; Kanie, K.; Kusumoto, T.; Morizawa, Y.; Shimzu, M. *Organofluorine Compounds: Chemistry and Applications*; Springer Berlin Heidelberg, 2013.

(16) Brocas, A.-L.; Mantzaridis, C.; Tunc, D.; Carlotti, S. Polyether synthesis: From activated or metal-free anionic ring-opening polymerization of epoxides to functionalization. *Prog. Polym. Sci.* **2013**, *38*, 845–873, DOI: 10.1016/j.progpolymsci.2012.09.007.

(17) Billouard, C.; Carlotti, S.; Desbois, P.; Deffieux, A. "Controlled" High-Speed Anionic Polymerization of Propylene Oxide Initiated by Alkali Metal Alkoxide/Trialkylaluminum Systems. *Macromolecules* **2004**, *37*, 4038–4043, DOI: 10.1021/ma035768t.

(18) Labbé, A.; Carlotti, S.; Deffieux, A.; Hirao, A. Controlled Polymerization of Glycidyl Methyl Ether Initiated by Onium Salt/Triisobutylaluminum and Investigation of the Polymer LCST. *Macromol. Symp.* **2007**, *249-250*, 392–397, DOI: 10.1002/masy.200750409.

(19) Müller, S. S.; Moers, C.; Frey, H. A Challenging Comonomer Pair: Copolymerization of Ethylene Oxide and Glycidyl Methyl Ether to Thermoresponsive Polyethers. *Macromolecules* **2014**, *47*, 5492–5500, DOI: 10.1021/ma501280k.

(20) Herzberger, J.; Frey, H. Epicyanohydrin: Polymerization by Monomer Activation Gives Access to Nitrile-, Amino-, and Carboxyl-Functional Poly(ethylene glycol). *Macromolecules* **2015**, *48*, 8144–8153, DOI: 10.1021/acs.macromol.5b02178.

(21) Jia, R.-P.; Zong, A.-X.; He, X.-Y.; Xu, J.-Y.; Huang, M.-s. Synthesis of newly fluorinated thermoplastic polyurethane elastomers and their blood compatibility. *Fibers Polym.* **2015**, *16*, 231–238, DOI: 10.1007/s12221-015-0231-6.

(22) Trischler, F. D.; Hollander, J. Preparation of fluorine-containing polyethers. *J. Polym. Sci. A-1 Polym. Chem.* **1967**, *5*, 2343–2349, DOI: 10.1002/pol.1967.150050913.

(23) Sakakibara, K.; Nakano, K.; Nozaki, K. Regio-controlled ring-opening polymerization of perfluoroalkyl-substituted epoxides. *Chem. Commun.* **2006**, *0*, 3334–3336, DOI: 10.1039/b606693c.

(24) Sakakibara, K.; Nakano, K.; Nozaki, K. Regioregular Polymerization of Fluorine-Containing Epoxides. *Macromolecules* **2007**, *40*, 6136–6142, DOI: 10.1021/ma070428j.

(25) Niederer, K.; Schüll, C.; Leibig, D.; Johann, T.; Frey, H. Catechol Acetonide Glycidyl Ether (CAGE): A Functional Epoxide Monomer for Linear and Hyperbranched Multi-Catechol Functional Polyether Architectures. *Macromolecules* **2016**, *49*, 1655–1665, DOI: 10.1021/acs.macromol.5b02441.

(26) Taton, D.; Le Borgne, A.; Sepulchre, M.; Spassky, N. Synthesis of chiral and racemic functional polymers from glycidol and thioglycidol. *Macromol. Chem. Phys.* **1994**, *195*, 139–148, DOI: 10.1002/macp.1994.021950111.

(27) Fitton, A. O.; Hill, J.; Jane, D. E.; Millar, R. Synthesis of Simple Oxetanes Carrying Reactive 2-Substituents. *Synthesis* **1987**, *1987*, 1140–1142, DOI: 10.1055/s-1987-28203.

(28) Feldman, K. E.; Martin, D. C. Functional Conducting Polymers via Thiol-ene Chemistry. *Biosensors* **2012**, *2*, 305–317, DOI: 10.3390/bios2030305.

(29) Deffieux, A.; Carlotti, S.; Desbois, P. New Perspectives in Living/Controlled Anionic Polymerization. *Macromol. Symp.* **2005**, *229*, 24–31, DOI: 10.1002/masy.200551104.

(30) Carlotti, S.; Desbois, P.; Billouard, C.; Deffieux, A. Reactivity control in anionic polymerization of ethylenic and heterocyclic monomers through formation of 'ate' complexes. *Polym. Int.* **2006**, *55*, 1126–1131, DOI: 10.1002/pi.1981.

(31) Obermeier, B.; Frey, H. Poly(ethylene glycol-co-allyl glycidyl ether)s: a PEG-based modular synthetic platform for multiple bioconjugation. *Bioconjugate Chem.* **2011**, *22*, 436–444, DOI: 10.1021/bc1004747.

(32) Lee, B. F.; Kade, M. J.; Chute, J. A.; Gupta, N.; Campos, L. M.; Fredrickson, G. H.; Kramer, E. J.; Lynd, N. A.; Hawker, C. J. Poly(allyl glycidyl ether)-A versatile and functional polyether platform. *J. Polym. Sci. A Polym. Chem.* **2011**, *49*, 4498–4504, DOI: 10.1002/pola.24891.

(33) Mosquet, M.; Chevalier, Y.; Le Perchec, P.; Guicquero, J.-P. Synthesis of poly(ethylene oxide) with a terminal amino group by anionic polymerization of ethylene oxide initiated by aminoalcoholates. *Macromol. Chem. Phys.* **1997**, *198*, 2457–2474, DOI: 10.1002/macp.1997.021980808.

(34) Campos, L. M.; Killops, K. L.; Sakai, R.; Paulusse, J. M. J.; Damiron, D.; Drockenmuller, E.; Messmore, B. W.; Hawker, C. J. Development of Thermal and Photochemical Strategies for Thiol−Ene Click Polymer Functionalization. *Macromolecules* **2008**, *41*, 7063–7070, DOI: 10.1021/ma801630n.

(35) Feng, W.; Li, L.; Ueda, E.; Li, J.; Heißler, S.; Welle, A.; Trapp, O.; Levkin, P. A. Surface Patterning via Thiol-Yne Click Chemistry: An Extremely Fast and Versatile Approach to Superhydrophilic-Superhydrophobic Micropatterns. *Adv. Mater. Interfaces* **2014**, *1*, 1400269, DOI: 10.1002/admi.201400269.

(36) Weinman, C. J.; Gunari, N.; Krishnan, S.; Dong, R.; Paik, M. Y.; Sohn, K. E.; Walker, G. C.; Kramer, E. J.; Fischer, D. A.; Ober, C. K. Protein adsorption resistance of anti-biofouling block copolymers containing amphiphilic side chains. *Soft Matter* **2010**, *6*, 3237, DOI: 10.1039/b925114f.

(37) Schömer, M.; Frey, H. Water-Soluble "Poly(propylene oxide)" by Random Copolymerization of Propylene Oxide with a Protected Glycidol Monomer. *Macromolecules* **2012**, *45*, 3039–3046, DOI: 10.1021/ma300249c.

(38) Thomas, A.; Bauer, H.; Schilmann, A.-M.; Fischer, K.; Tremel, W.; Frey, H. The "Needle in the Haystack" Makes the Difference: Linear and Hyperbranched Polyglycerols with a Single Catechol Moiety for Metal Oxide Nanoparticle Coating. *Macromolecules* **2014**, *47*, 4557–4566, DOI: 10.1021/ma5003672.

(39) Sunder, A.; Türk, H.; Haag, R.; Frey, H. Copolymers of Glycidol and Glycidyl Ethers: Design of Branched Polyether Polyols by Combination of Latent Cyclic AB 2 and ABR Monomers. *Macromolecules* **2000**, *33*, 7682–7692, DOI: 10.1021/ma992166u.

(40) Alkan, A.; Natalello, A.; Wagner, M.; Frey, H.; Wurm, F. R. Ferrocene-Containing Multifunctional Polyethers: Monomer Sequence Monitoring via Quantitative 13 C NMR Spectroscopy in Bulk. *Macromolecules* **2014**, *47*, 2242–2249, DOI: 10.1021/ma500323m.

(41) *Fluoropolymers 2: Properties;* Hougham, G.; Cassidy, P. E.; Johns, K.; Davidson, T., Eds.; Topics in Applied Chemistry; Kluwer Academic Publishers: Boston, MA, 2002.

(42) Heijboer, J. Modulus and damping of polymers in relation to their structure. *Br. Polym. J.* **1969**, *1,* DOI: 10.1002/pi.4980010102.

(43) Wurm, F.; Nieberle, J.; Frey, H. Double-Hydrophilic Linear-Hyperbranched Block Copolymers Based on Poly(ethylene oxide) and Poly(glycerol). *Macromolecules* **2008**, *41*, 1184–1188, DOI: 10.1021/ma702308g.

(44) Sperling, L. H. *Introduction to Physical Polymer Science*; Wiley, 2015.

(45) Heinen, S.; Rackow, S.; Schäfer, A.; Weinhart, M. A Perfect Match: Fast and Truly Random Copolymerization of Glycidyl Ether Monomers to Thermoresponsive Copolymers. *Macromolecules* **2017**, *50*, 44–53, DOI: 10.1021/acs.macromol.6b01904.

(46) Schubert, C.; Dreier, P.; Nguyen, T.; Maciol, K.; Blankenburg, J.; Friedrich, C.; Frey, H. Synthesis of linear polyglycerols with tailored degree of methylation by copolymerization and the effect on thermorheological behavior. *Polymer* **2017**, *121*, 328–339, DOI: 10.1016/j.polymer.2017.05.030.

(47) Herzberger, J.; Leibig, D.; Liermann, J. C.; Frey, H. Conventional Oxyanionic versus Monomer-Activated Anionic Copolymerization of Ethylene Oxide with Glycidyl Ethers: Striking Differences in Reactivity Ratios. *ACS Macro Lett.* **2016**, *5*, 1206–1211, DOI: 10.1021/acsmacrolett.6b00701.

(48) Drelich, J.; Chibowski, E.; Meng, D. D.; Terpilowski, K. Hydrophilic and superhydrophilic surfaces and materials. *Soft Matter* **2011**, *7*, 9804, DOI: 10.1039/c1sm05849e.

(49) Jung, Y. C.; Bhushan, B. Contact angle, adhesion and friction properties of micro-and nanopatterned polymers for superhydrophobicity. *Nanotechnology* **2006**, *17*, 4970, DOI: 10.1088/0957-4484/17/19/033.

(50) Law, K. Y.; Zhao, H. *Surface Wetting: Characterization, Contact Angle, and Fundamentals*; Springer International Publishing, 2015.

(51) Gudipati, C. S.; Greenlief, C. M.; Johnson, J. A.; Prayongpan, P.; Wooley, K. L. Hyperbranched fluoropolymer and linear poly(ethylene glycol) based amphiphilic crosslinked networks as efficient antifouling coatings: An insight into the surface compositions, topographies, and morphologies. *J. Polym. Sci. A Polym. Chem.* **2004**, *42*, 6193–6208, DOI: 10.1002/pola.20466.

(52) Brady, R. F.; Bonafede, S. J.; Schmidt, D. L. Self-assembled water-borne fluoropolymer coatings for marine fouling resistance. *Surf. Coat. Int.* **1999**, *82*, 582–585, DOI: 10.1007/BF02692670.

(53) Kang, T.; Banquy, X.; Heo, J.; Lim, C.; Lynd, N. A.; Lundberg, P.; Oh, D. X.; Lee, H.-K.; Hong, Y.-K.; Hwang, D. S. *et al.* Mussel-Inspired Anchoring of Polymer Loops That Provide Superior Surface Lubrication and Antifouling Properties. *ACS Nano* **2016**, *10*, 930–937, DOI: 10.1021/acsnano.5b06066.

Supporting Information

Synthesis of Perfluoroalkyl-Bearing Polyether, Their Characterization and Application as Coating for Glass Slides

Kamil Maciol[a] and Holger Frey[a,]*

[a] Institute of Organic Chemistry, Johannes Gutenberg University Mainz, Duesbergweg 10-14, 55128 Mainz, Germany

*E-Mail: hfrey@uni-mainz.de

To be submitted
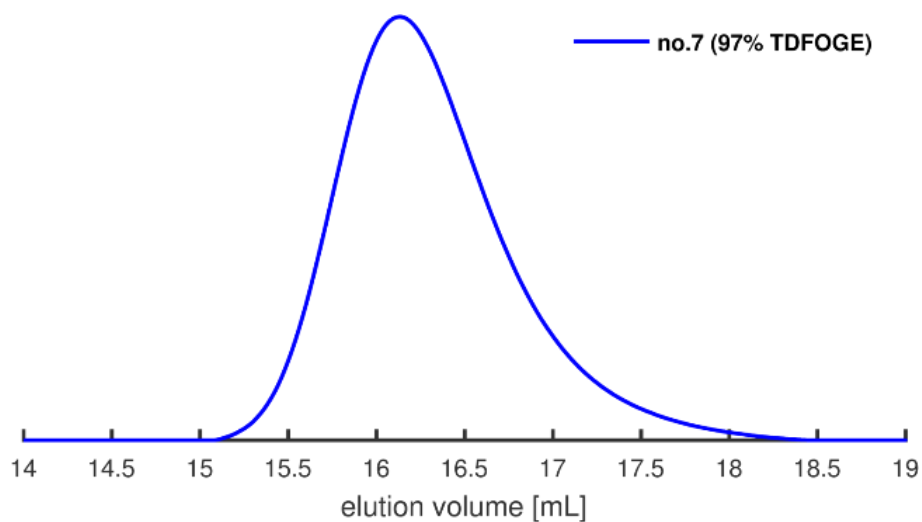
Figure S1. SEC trace (HFIP, PMMA standards) of P(TDFOGE$_{0.97}$-*co*-CaGE$_{0.03}$) (entry 7, **Table 1**).
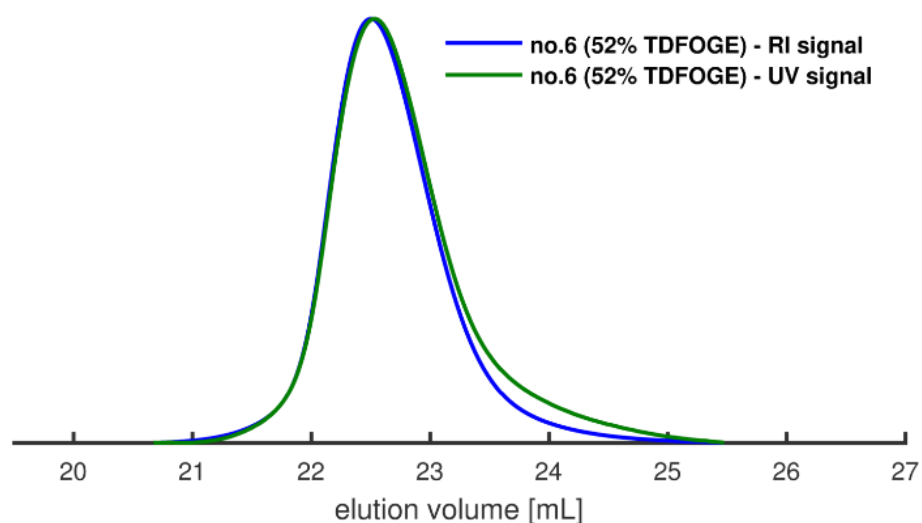
Figure S2. SEC traces (THF, PEG standards) of superimposed RI (blue) and UV (green) signals of of P(AGE$_{0.46}$-*co*-TDFOGE$_{0.52}$-*co*-CaGE$_{0.02}$) (entry 6, **Table 1**).
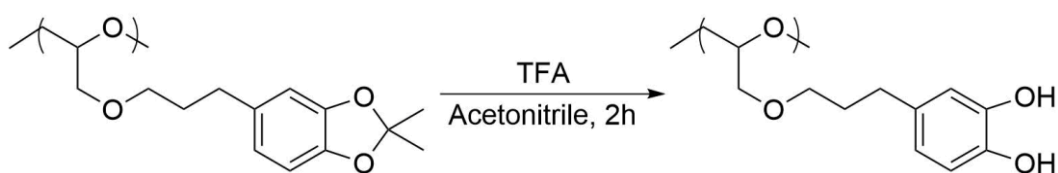
Figure S3. Removal of acetonide protecting group.
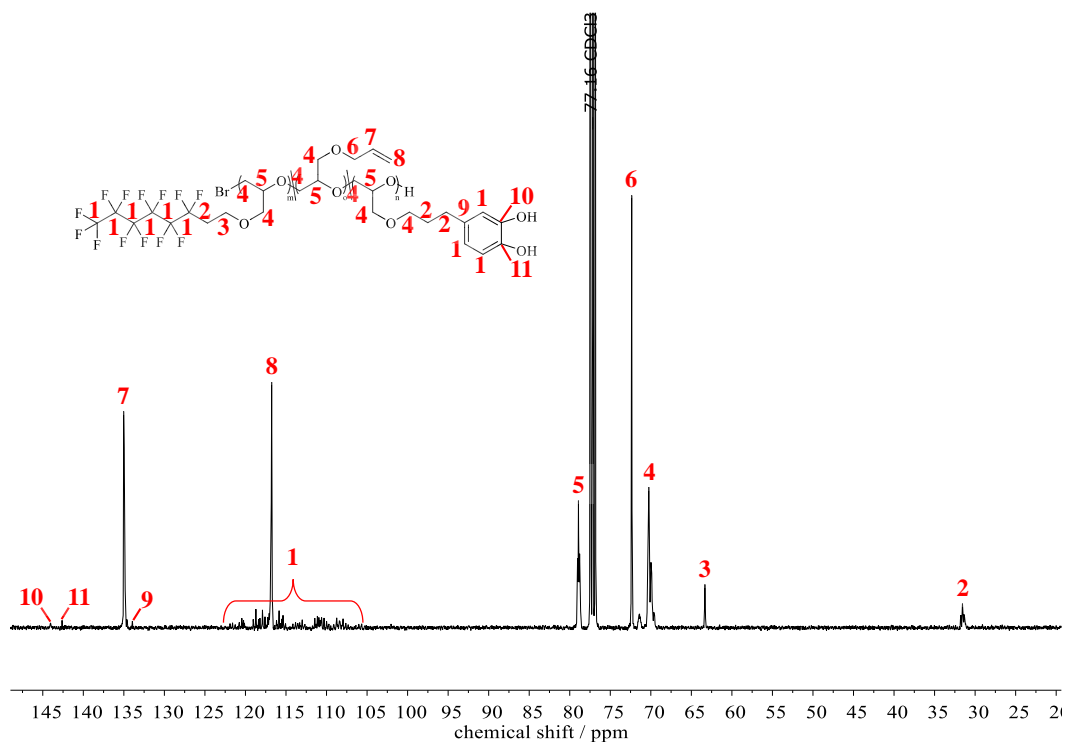
Figure S4. ^{13}C NMR spectrum (100 MHz, C*D*Cl$_3$) of P(AGE$_{0.79}$-*co*-TDFOGE$_{0.19}$-*co*-CaGE$_{0.02}$) (entry 3, **Table 1**) after the removal of acetonide protecting groups.
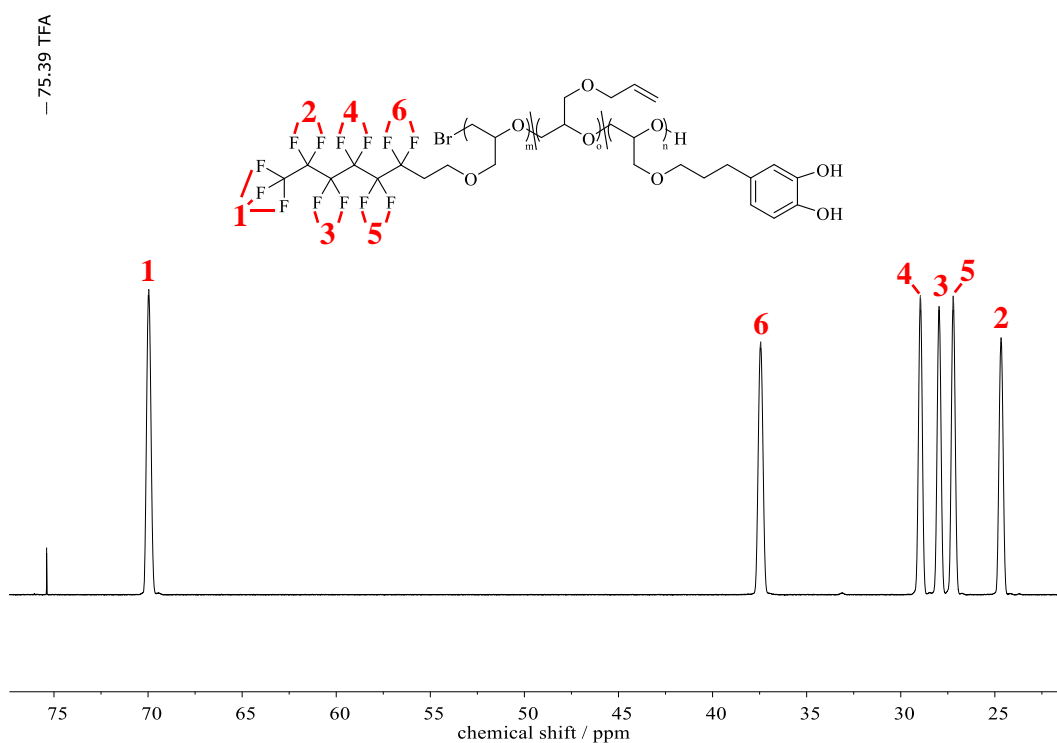
Figure S5. ^{19}F NMR spectrum (377 MHz, C*D*Cl$_3$) of P(AGE$_{0.79}$-*co*-TDFOGE$_{0.19}$-*co*-CaGE$_{0.02}$) (entry 3, **Table 1**) after the removal of acetonide protecting groups. TFA was added to C*D*Cl$_3$ as external reference and set to -75.39 ppm according to Tian and co-workers.[1] Assignment of signals is based on literature.[2]
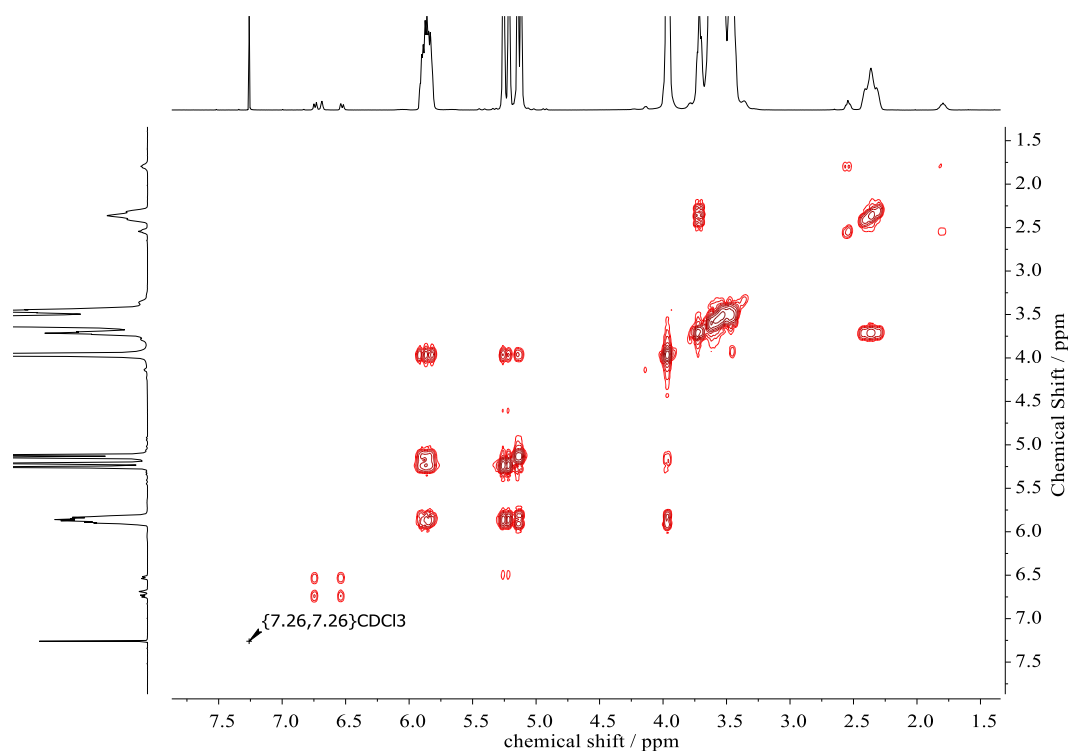
Figure S6. ^{1}H, ^{1}H COSY NMR spectrum (400 MHz, C*D*Cl$_3$) of P(AGE$_{0.79}$-*co*-TDFOGE$_{0.19}$-*co*-CaGE$_{0.02}$) (entry 3, **Table 1**) after the removal of acetonide protecting groups.
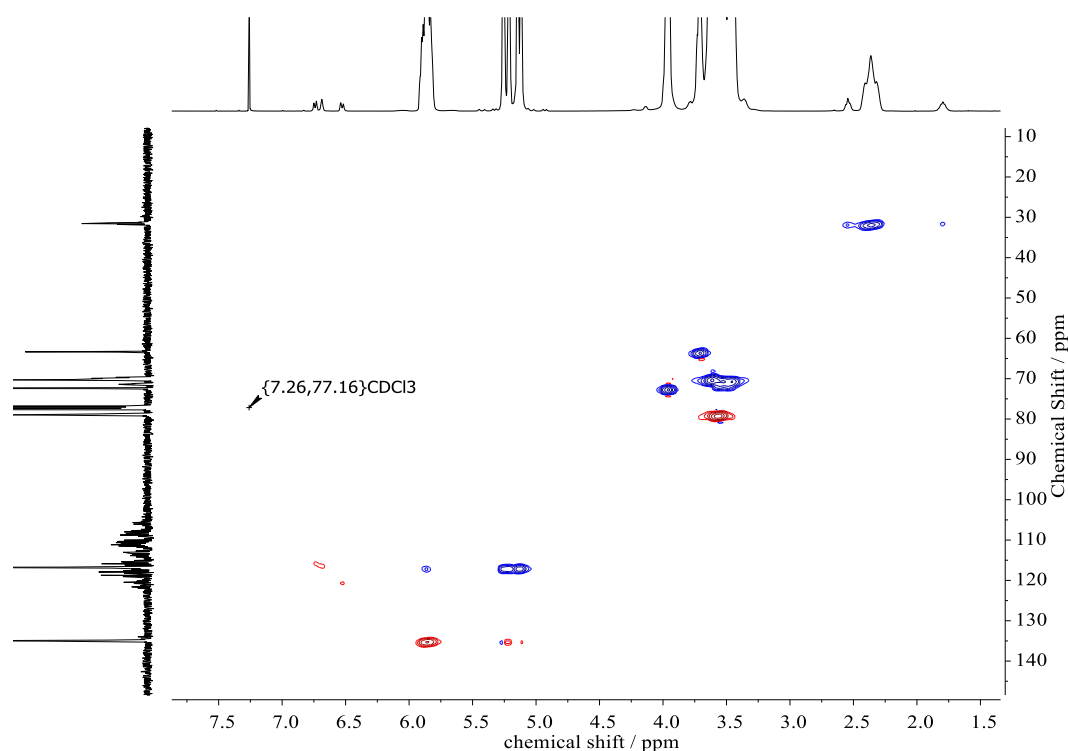
Figure S7. ^{1}H, ^{13}C HSQC NMR spectrum (400 MHz, C*D*Cl$_3$) of P(AGE$_{0.79}$-*co*-TDFOGE$_{0.19}$-*co*-CaGE$_{0.02}$) (entry 3, **Table 1**) after the removal of acetonide protecting groups. Color of the signals indicates the phase information (red: methine proton, blue: methylene protons).
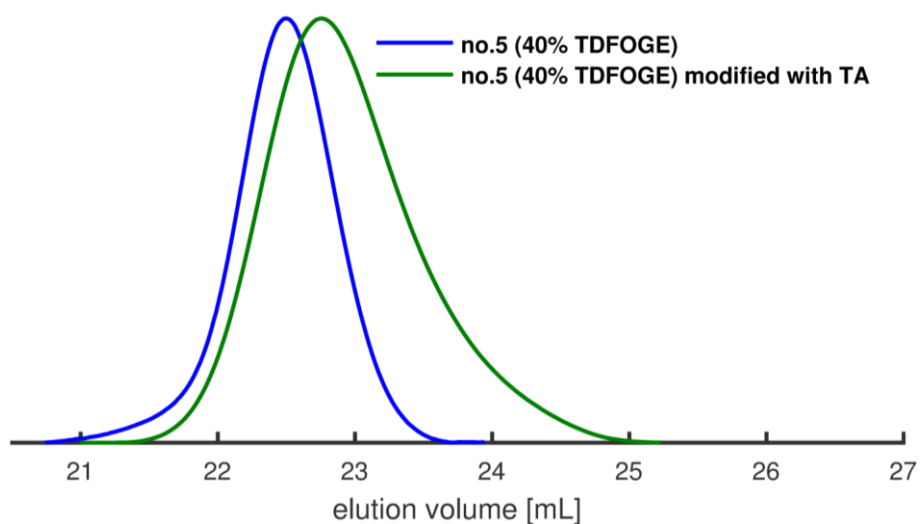
Figure S8. SEC traces (THF, PEG standards) of precursor P(AGE$_{0.58}$-*co*-TDFOGE$_{0.40}$-*co*-CaGE$_{0.02}$) (blue, entry 5, **Table 1**) and thioglycolic acid-functionalized derivative (green, entry B, **Table 2**).
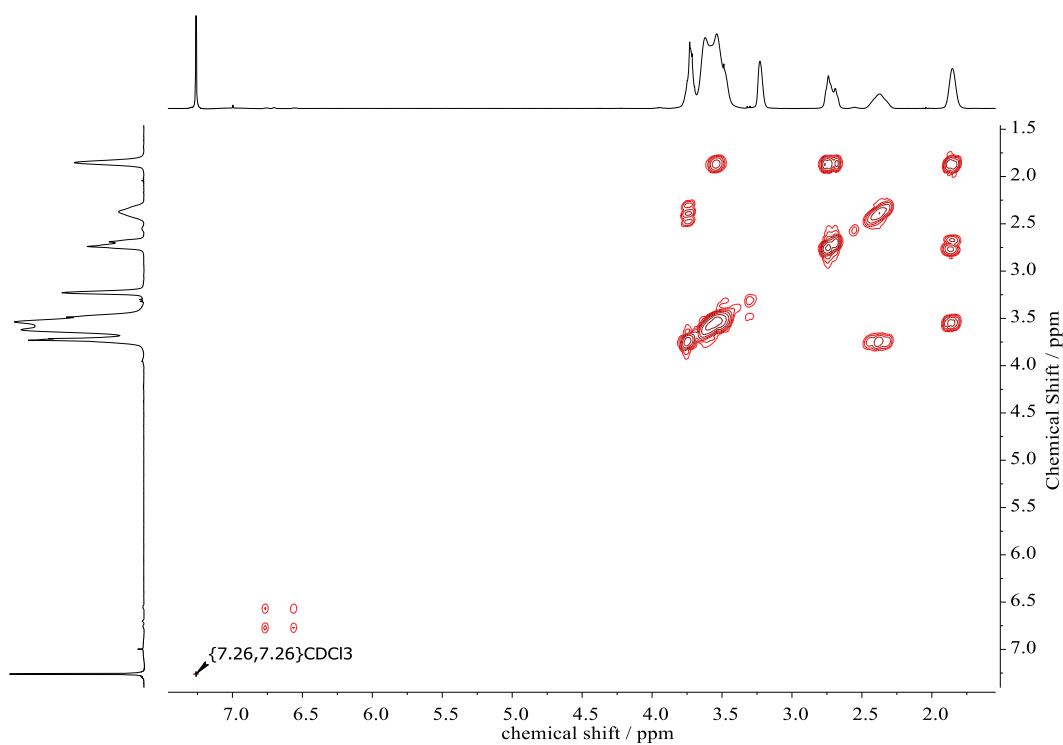
Figure S9. ^{1}H, ^{1}H COSY NMR spectrum (400 MHz, C*D*Cl$_3$) of thioglycolic acid-modified P(AGE$_{0.58}$-*co*-TDFOGE$_{0.40}$-*co*-CaGE$_{0.02}$) (entry B, **Table 2**).
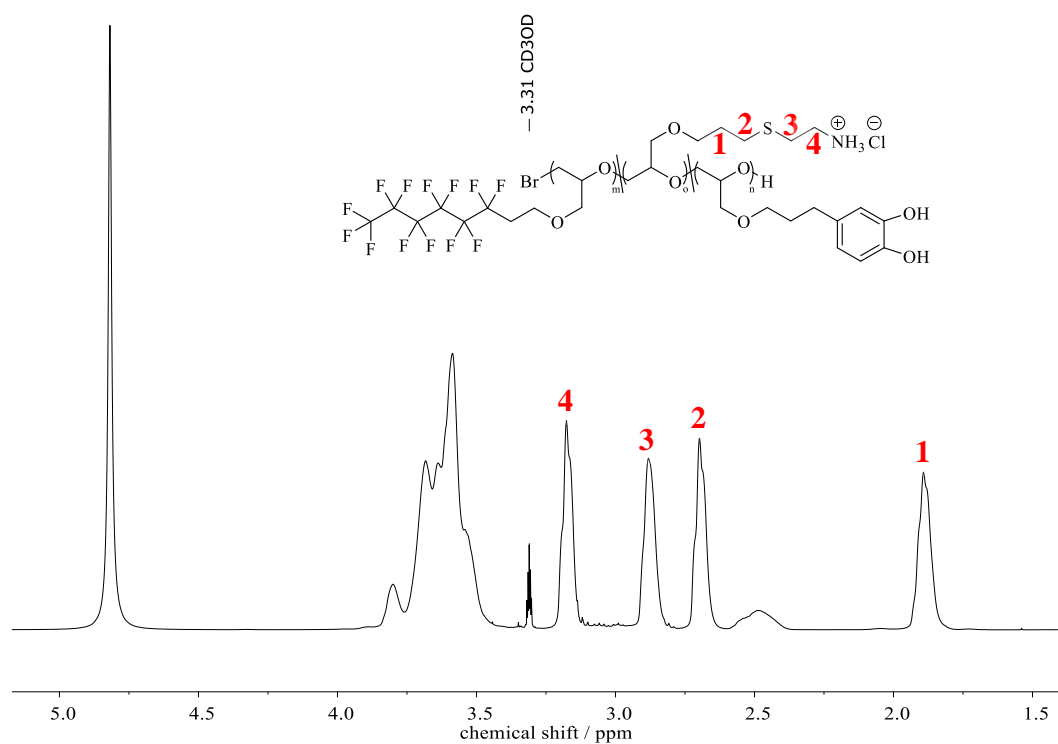
Figure S10. Relevant sections of ^{1}H NMR spectrum (400 MHz, CD_3OD) of cysteamine hydrochloride-modified P(AGE$_{0.79}$-*co*-TDFOGE$_{0.19}$-*co*-CaGE$_{0.02}$) (entry A, **Table 2**).
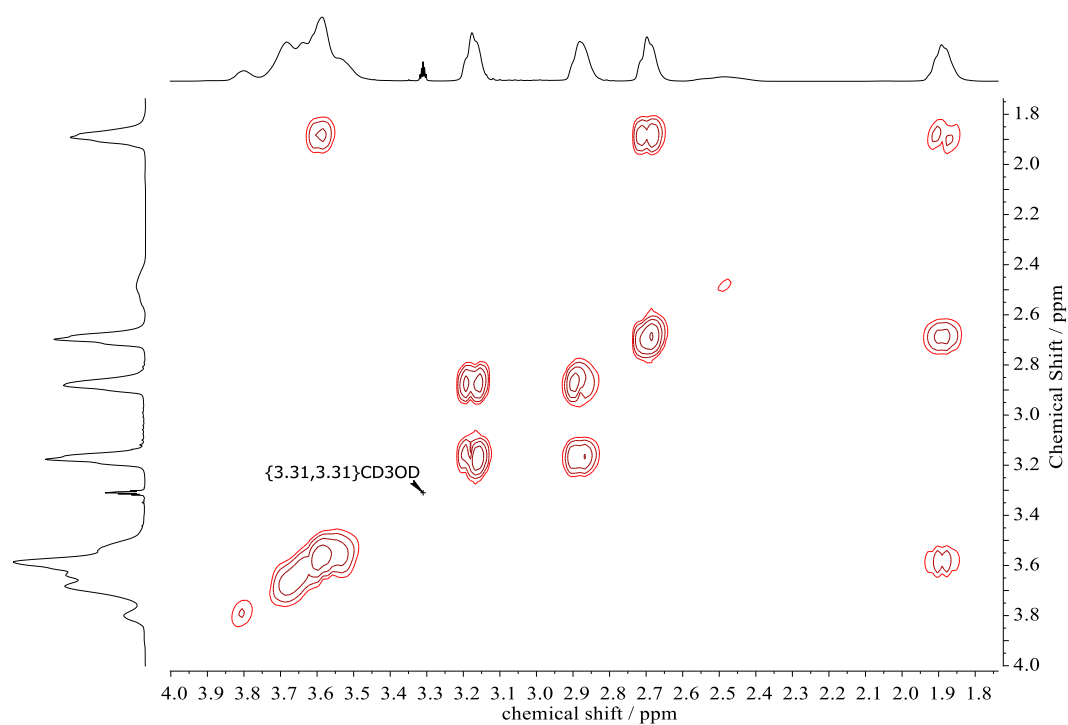
Figure S11. ^{1}H, ^{1}H COSY NMR spectrum (400 MHz, CD_3OD) of cysteamine hydrochloride-modified P(AGE$_{0.79}$-*co*-TDFOGE$_{0.19}$-*co*-CaGE$_{0.02}$) (entry A, **Table 2**).
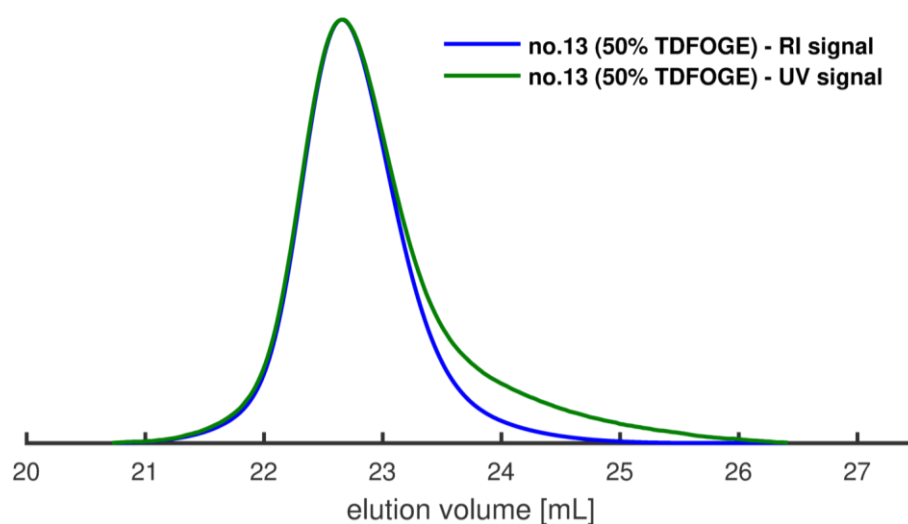
Figure S12. SEC traces (THF, PEG standards) of superimposed RI (blue) and UV (green) signals of of *lin*P(G$_{0.48}$-*co*-TDFOGE$_{0.50}$-*co*-CaGE$_{0.02}$) (entry 6, **Table 1**).
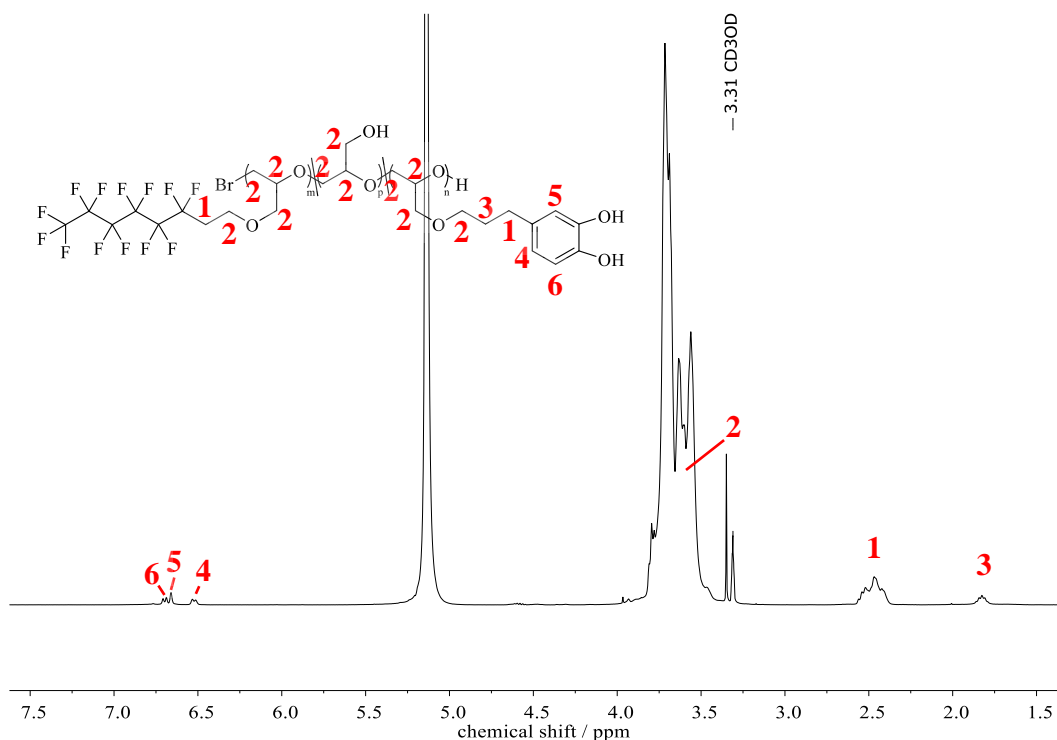
Figure S13. ^{1}H NMR spectrum (400 MHz, C*D*$_3$O*D*) of *lin*P(G$_{0.48}$-*co*-TDFOGE$_{0.50}$-*co*-CaGE$_{0.02}$) (entry 6, **Table 3**) after the removal of the protecting groups. TFA was added to the solution to suppress turbidity.
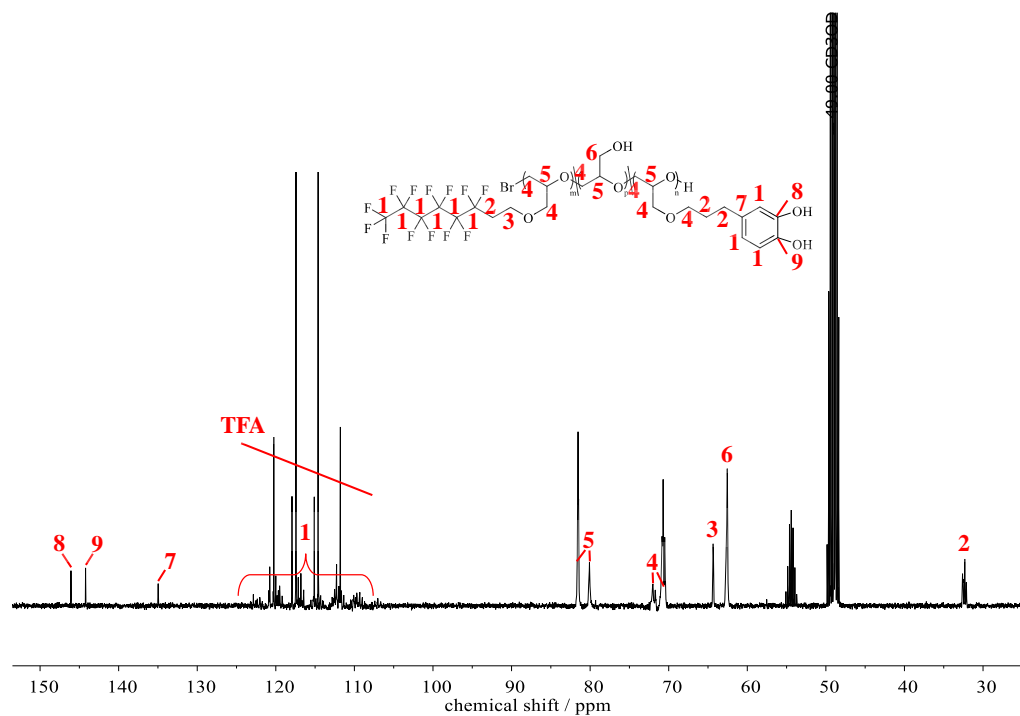
Figure S14. ^{13}C NMR spectrum (100 MHz, CD_3OD) of *lin*P(G$_{0.48}$-*co*-TDFOGE$_{0.50}$-*co*-CaGE$_{0.02}$) (entry 6, **Table 3**) after the removal of the protecting groups. TFA was added to the solution to suppress turbidity.
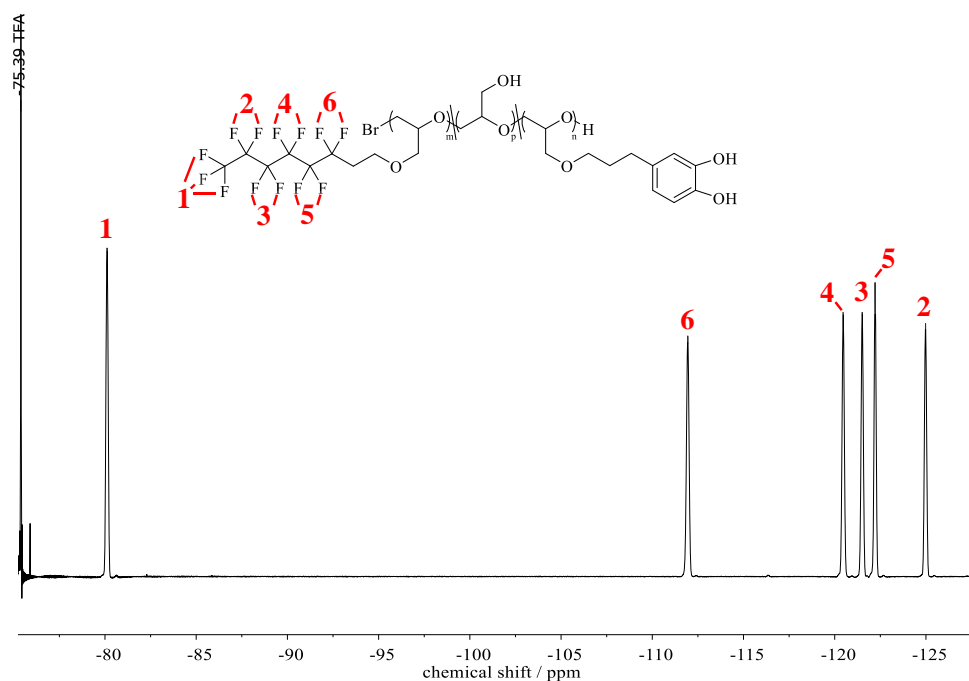
Figure S15. ^{19}F NMR spectrum (377 MHz, CD_3OD) of *lin*P(G$_{0.48}$-*co*-TDFOGE$_{0.50}$-*co*-CaGE$_{0.02}$) (entry 6, **Table 3**) after the removal of the protecting groups. TFA was added to the solution to suppress turbidity and as external reference and set to -75.39 ppm according to Tian and co-workers.[1] Assignment of signals based on literature.[2]
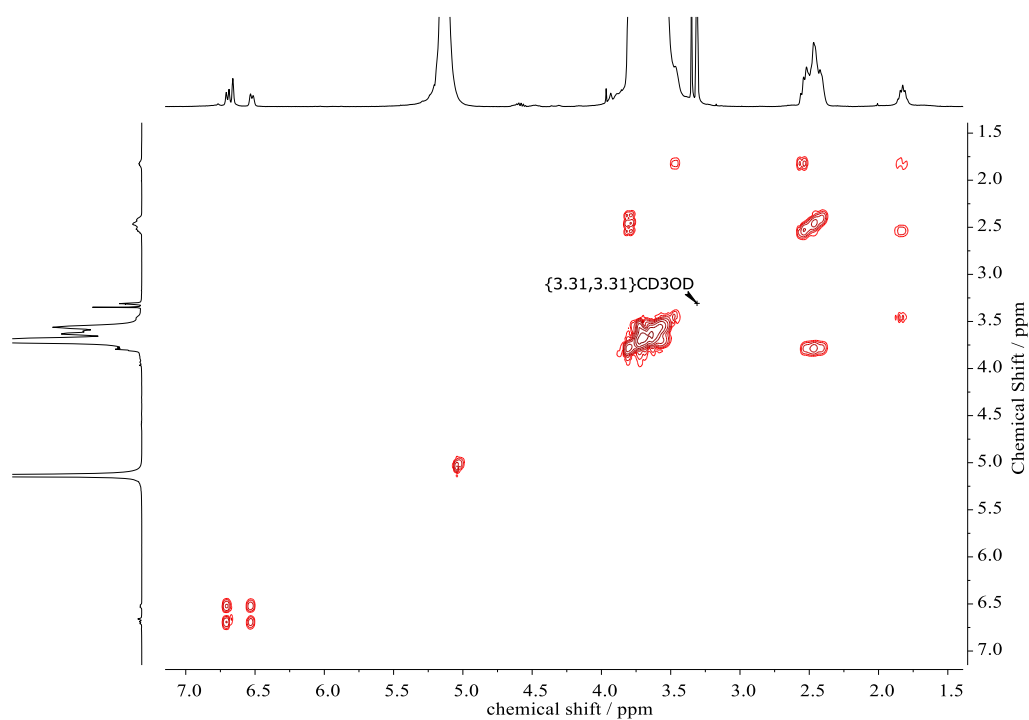
Figure S16. ^{1}H, ^{1}H COSY NMR spectrum (400 MHz, CD_3OD) of *lin*P(G$_{0.48}$-*co*-TDFOGE$_{0.50}$-*co*-CaGE$_{0.02}$) (entry 6, **Table 3**) after the removal of the protecting groups. TFA was added to the solution to suppress turbidity.
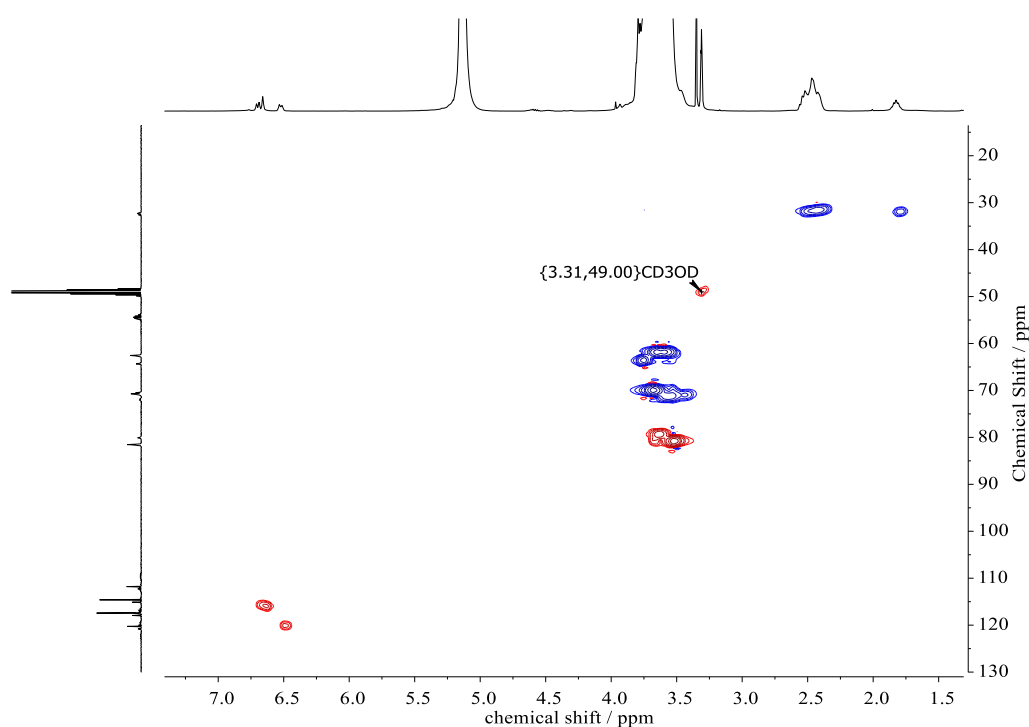
Figure S17. ^{1}H, ^{13}C HSQC NMR spectrum (400 MHz, CD_3OD) of *lin*P(G$_{0.48}$-*co*-TDFOGE$_{0.50}$-*co*-CaGE$_{0.02}$) (entry 6, **Table 3**) after the removal of the protecting groups. TFA was added to the solution to suppress turbidity. Color of the signals indicates the phase information (red: methine proton, blue: methylene protons).
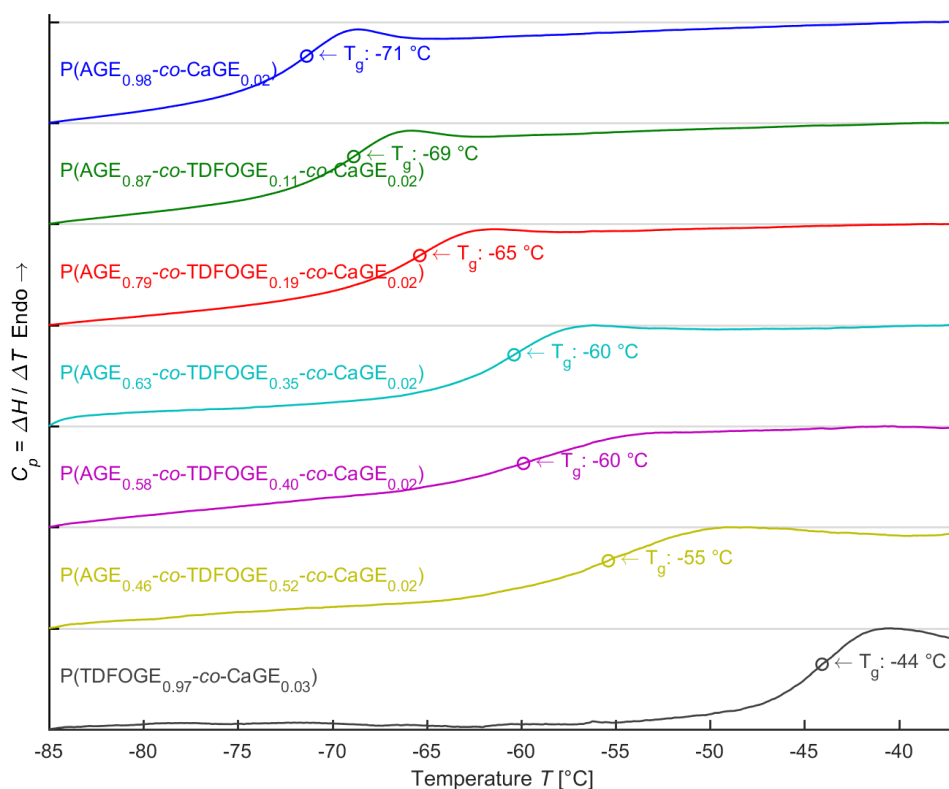
Figure S18. Flowcharts for P(AGE$_{0.98}$-*co*-CaGE$_{0.02}$) (entry 1, Table 1), P(TDFOGE$_{0.97}$-*co*-CaGE$_{0.03}$) (entry 7, **Table 1**) copolymers and P(AGE-*co*-TDFOGE-*co*-CaGE) (entries 2−6, **Table 1**) terpolymers.
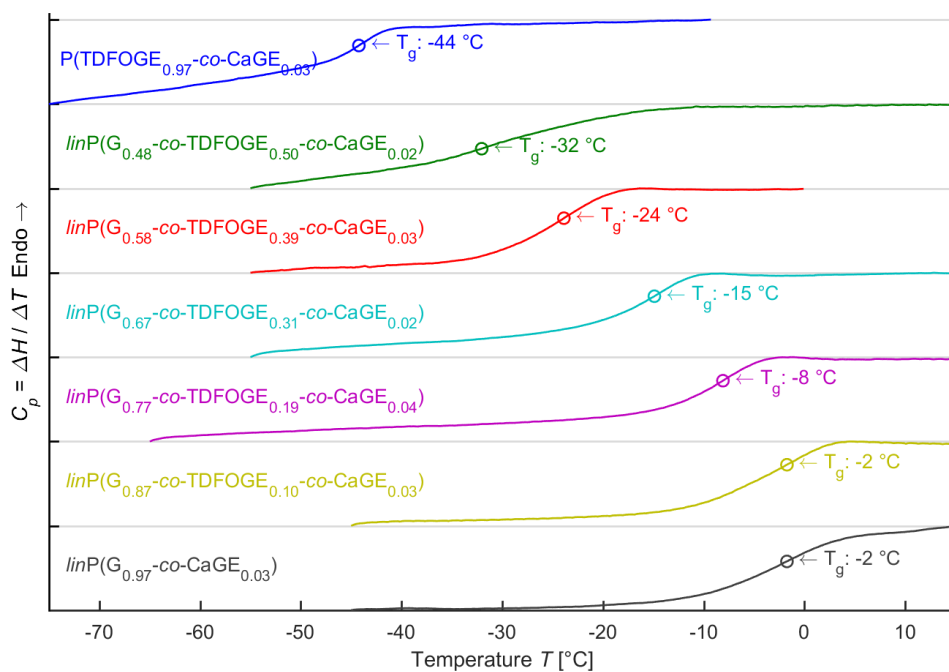
Figure S19. Flowcharts for P(TDFOGE$_{0.97}$-*co*-CaGE$_{0.03}$) (entry 7, **Table 1**), *lin*P(G$_{0.97}$-*co*-CaGE$_{0.03}$) (entry 1, **Table 3**) and *lin*P(G-*co*-TDFOGE-*co*-CaGE) (entries 2−6, **Table 3**) terpolymers.

SI-REFERENCES

(1) Shi, P.; Li, D.; Li, J.; Chen, H.; Wu, F.; Xiong, Y.; Tian, C. Application of Site-Specific 19 F Paramagnetic Relaxation Enhancement to Distinguish two Different Conformations of a Multidomain Protein. *J. Phys. Chem. Lett.* **2012**, *3*, 34–37, DOI: 10.1021/jz201480g.

(2) Zhang, H.; Pan, J.; Hogen-Esch, T. E. Synthesis and Characterization of One-Ended Perfluorocarbon-Functionalized Derivatives of Poly(ethylene glycol)s. *Macromolecules* **1998**, *31*, 2815–2821, DOI: 10.1021/ma9712256.

5. Appendix

A1.   Design of Multi-Aldehyde-Functional Poly(ethylene glycol) Establishes a Rich and Versatile Post-Polymerization Chemistry

Jan Blankenburg[‡§], Kamil Maciol[‡], Christoph Hahn[‡], Holger Frey[‡]*

‡ Institute of Organic Chemistry, Johannes Gutenberg University Mainz, Duesbergweg 10-14, 55128 Mainz, Germany

§ Graduate School Materials Science in Mainz, Staudinger Weg 9, 55128 Mainz, Germany

*(H.F.) E-Mail: hfrey@uni-mainz.de

Unpublished results.

The Supporting Information is given in the PhD thesis of Jan Blankenburg.

ABSTRACT

Two novel epoxide monomers 3,3-dimethoxy-propanyl glycidyl ether (DMPGE) and 3,3-dimethoxy-2,2-dimethylpropanyl glycidyl ether (DDPGE) for the introduction of multiple aldehyde functionalities into the poly(ethylene glycol) (PEG) backbone were developed. The acetal protecting group for the aldehyde-functionality is stable against the harsh, basic conditions present during the anionic ring-opening polymerization (AROP). Both monomers could be homopolymerized as well as copolymerized statistically with ethylene oxide (EO) in a controlled fashion. Polymers with molecular weights (M_n) in the range of 4,500 g/mol to 20,100 g/mol and low dispersities (M_w/M_n) between 1.06 and 1.14 have been synthesized. The polymers were characterized by SEC, ^{1}H NMR and regarding their thermal properties. Furthermore, the controlled character of the polymerization was verified by MALDI-TOF. To study the distribution of the acetal functionalities along the polyether chain, the copolymerization with ethylene oxide was monitored by real-time ^{1}H NMR kinetic experiments for both monomers. These measurements revealed almost random distribution of the comonomers with reactivity ratio pairs $r_{EO} = 0.96$, $r_{DMPGE} = 1.04$ and $r_{EO} = 1.20$, $r_{DDPGE} = 0.83$. The acetal functionalities of DMPGE-polymers could be successfully addressed by hydrazone-formation. DDPGE-copolymers could be successfully deprotected in acidic media and further transformations yielded aldehyde-, ester-, and nitrile-functionalized PEG while maintaining a dispersity below 1.1. Consequently, these monomers are a highly interesting building blocks for the synthesis of multi-functional PEG.

TABLE OF CONTENTS GRAPHICS
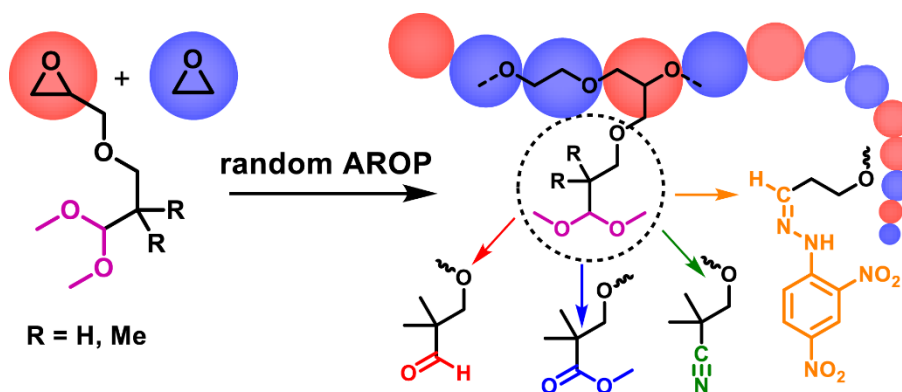
INTRODUCTION

The extraordinary properties of polyethylene glycol (PEG) such as high biocompatibility and water solubility render it an ideal candidate for biomedical applications.[1] Furthermore, the flexible polyether backbone and low glass transition fit the requirement for the soft segment component in polyurethane foams perfectly.[2] A drawback for bioconjugation or tailoring material properties is the chemically inert polyether backbone of PEG, which is resistant to post polymerization reactions. To overcome these limitations, only the terminal hydroxyl groups are available for modification reactions. In the past, this lack of functionality has been increased by copolymerizing ethylene oxide (EO) with functional epoxide monomers to create multi-functional PEGs.[3,4] In this manner, many functionalities could be introduced into the polyether backbone and the polymer properties thereby customized for the targeted application. However, challenging for this strategy are the harsh, basic conditions employed in the anionic ring-opening polymerization (AROP), which need to be tolerated by the functional group without side reactions. Only a few functionalities fulfill this requirement and therefore lead to well-defined polymers. Successfully established for the AROP are monomers containing vinyl and allyl ethers, tertiary amines, acetals and thioethers.[4–6] Acetals have been proven to be a good choice for masking hydroxyl groups during the polymerization. In this way monools[7], diols[8] and catechols[9] can be liberated in acidic conditions after the polymerization. A strategy to incorporate other functionalities, is the monomer-activated method carried out under milder conditions according to Carlotti and Deffieux.[10–12] This expands the scope of tolerated functionalities extensively. As reported by Herzberger *et al.* epicyanohydrin could be (co)polymerized and its nitrile functionalities transformed by post polymerization reactions into amides, amines and carboxylates.[13] Drawbacks of the monomer-activated method are the use of cytotoxic aluminum salts, a broadened distribution and non-uniform end groups. Therefore, block copolymers are usually not accessible. Furthermore, copolymerization of a glycidyl ether with EO leads to strong gradient in the case of the activated monomer mechanisms. In contrast, the same copolymerization via AROP yields a perfect random distribution of the functionalities.[14] For these reasons, the AROP of EO and other epoxide derivatives is still the best choice to get a well-defined polyether with defined architectures.[15,16] Motivated by this fact, this work aimed to expand the compatible functionalities for AROP.

Aldehyde functional polymers are interesting due to their high reactive aldehyde moiety e.g. for bioconjugation. Sokolovskaya *et al.* synthesized in a 4-step synthesis a protected aldehyde epoxide-monomer with a photolabile acetal group. However, the degree of polymerization was

limited and broad distributions were obtained otherwise.[17] PEG with aldehyde terminus has been used for the PEGylation of drugs via imine formation with the N-Terminus of proteins.[3,18] A direct employment of aldehydes in the AROP would lead to side reactions as aldol condensations or acetal formation and therefore undefined products. By using an acetal protected aldehyde as an initiator in AROP and subsequent deprotection a terminal aldehyde functionality could be introduced.[19] Multiple aldehyde functionalities in polymers are of interest as cross linkable hydrogels and for post-polymerization modification.[20–22]

In this work we present two novel monomers with acetal protected aldehydes which can be polymerized in a controlled manner in the conditions of the AROP. Statistical copolymers with EO and homopolymers were synthesized with narrow dispersities (M_w/M_n) in the range of 1.06 and 1.14 (Scheme 1). The acetal functionality of DMPGE polymers could be addressed via hydrazone formation. It could be shown that the deprotection of polymers of the DMPGE lead to undesirable side products, which was the motivation of a further improvement of the monomer and the development of the second monomer DDPGE. This improvement allowed the aldehydes to be liberated in acidic conditions from the acetal protecting groups and to be oxidized in acidic media to ester functionalities. The released aldehyde moieties could be successfully transformed into nitrile functionalities.
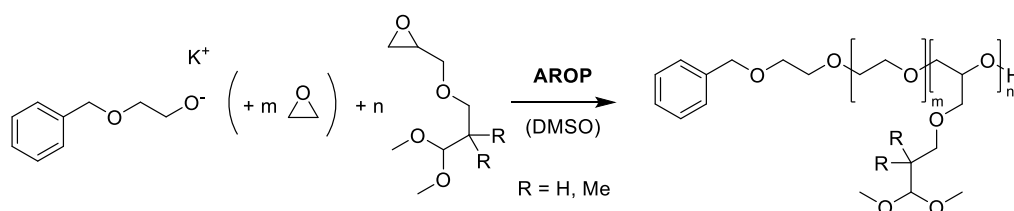
Scheme 1. Synthesis strategy of homopolymers and copolymer with EO of DMPGE and DDPGE.

EXPERIMENTAL SECTION

Reagents. Solvents and reagents were generally purchased from Acros Organics, TCI, Sigma-Aldrich, or Fluka and used as received, unless otherwise stated. Deuterated solvents were received from Deutero GmbH.

Instrumentation. ^{1}H NMR (400 MHz), ^{13}C NMR (100 MHz) were recorded on a Bruker Avance II 400 (400 MHz, 5 mm BBFO-SmartProbe with z-gradient and ATM, SampleXPress 60 sample changer) and referenced internally to the proton signal of the deuterated solvent. Solid K_2CO_3 was added to CDCl$_3$ when measuring acetal containing compounds to prevent hydrolysis of the protective groups by acid traces. For real-time ^{1}H NMR kinetic experiments an Avance III HD 400 from Bruker was used, which is equipped with a 5 mm BBFO-SmartProbe (Z-gradient probe), ATM and SampleXPress 60.

Size exclusion chromatography (SEC) was performed at 50 °C in dimethylformamide (DMF) with 1 g/L lithium bromide as an eluent on an Agilent 1100 Series equipped with Polymer Standards Service (PSS) HEMA columns with 300/100/40 Å porosity, using a RI detector. Molecular weights were determined by calibration with polyethylene glycol standards by PSS.

Differential scanning calorimetry (DSC) measurements were carried out under a nitrogen atmosphere using a PerkinElmer DSC 8500 in the temperature range of −95 °C to 95 °C, with heating rates of 20 °C/min for the first and 10 °C/min for the second heating run. The heat flow of the second heating cycle was used for the analysis.

MALDI-TOF Measurements were performed on a Shimadzu Axima CFR MALDI-TOF or a Bruker Rapiflex. Samples were prepared with alpha-cyano-4-hydroxycinnamic acid (CHCA) or trans-2-[3-(4-tert-Butylphenyl)-2-methyl-2-propenylidene]malononitrile (DCTB) as matrix and potassium trifluoroacetate as cationization agent.

3-3-Dimethoxy-propan-1-ol (I): 3-3-Dimethoxy-propan-1-ol was synthesized from 3-3-dimethoxy-propionic acid methyl ester in a slightly modified known procedure.[23] 9.22 g Lithium aluminum hydride (0.25 mol, 1.2 eq.) was suspended in 250 mL diethyl ethyl ether and stirred. The flask was cooled in an ice/water bath to 0 °C and a solution of 30 g 3-3-Dimethoxy-propionic acid methyl (0.2 mol, 1 eq) in 100 mL diethyl ether was added dropwise. After the complete addition, the mixture was stirred for an hour, allowing the mixture to reach room temperature. The reaction was then quenched by slow addition of 25 mL 1 M aqueous sodium hydroxide solution and stirred for 30 minutes. The white solid was removed by filtration and

washed several times with diethyl ether. The organic phase was dried with Na_2SO_4 and the solvent removed under reduced pressure, to give the product with sufficient purity in 95 % yield. ^{1}H NMR (400 MHz, $CDCl_3$): δ (ppm) 4.55 (t, J = 5.6 Hz, 1H, -CH(OMe)$_2$), 3.75 – 3.68 (m, 2H, -CH_2-OH), 3.36 (s, 6H, C(OCH_3)$_2$), 1.87 (q, J = 5.6 Hz, 2H, -CH$_2$-CH_2-CH(OMe)$_2$).

3-3-Dimethoxy-propanyl glycidyl ether (DMPGE): 10 g of 3-3-Dimethoxy-propan-1-ol (**I**) (83 mmol, 1 eq) and 13.1 mL epichlorohydrin (167 mmol, 2 eq) were added to 100 mL 50 wt% aqueous sodium hydroxide. The reaction mixture was heated to 40 °C and stirred vigorously for 24 h. The reaction mixture was extracted three times with 50 mL diethyl ether. The organic phase was washed with brine until the washings were neutral, dried with Na_2SO_4 and the solvent removed under reduced pressure. DMPGE was obtained in high purity by distillation in high vacuum in a yield of 56 % and stored over molecular sieves 4 Å. ^{1}H NMR (400 MHz, $CDCl_3$): δ (ppm) 4.53 (t, J = 5.8 Hz, 1H, -CH(OMe)$_2$), 3.71 (dd, J = 11.5, 3.0 Hz, 1H, ring–C$H_{2,a}$O-), 3.55 (qt, J = 9.4, 6.5 Hz, 2H, -OCH_2CH$_2$), 3.37 (dd, J = 11.6, 5.9 Hz, 1H, ring–C$H_{2,b}$O-), 3.33 (d, J = 0.6 Hz, 6H, C(OCH_3)$_2$), 3.14 (ddt, J = 5.8, 4.1, 2.8 Hz, 1H, CH_{ring}), 2.79 (dd, J = 5.0, 4.2 Hz, 1H, C$H_{2a,ring}$), 2.60 (dd, J = 5.1, 2.7 Hz, 1H, C$H_{2b,ring}$), 1.89 (td, J = 6.4, 5.8 Hz, 2H, -CH$_2$-CH_2-CH(OMe)$_2$).

3-Hydroxy-2,2-dimethylpropanal (A): 3-Hydroxy-2,2-dimethylpropanal was prepared in slightly modified procedure of Acerbis *et al.*.[24] 81,8 mL of a 37% aqueous formaldehyde solution (1.1 mol, 1.1 eq.) and 91.3 mL isobutyraldehyde (1 mol, 1 eq.) were mixed and cooled in ice water bath to 0 °C. 69.1 g K_2CO_3 (0.5 mol, 0.5 eq.)was carefully added to keep the temperature below 20 °C. The reaction was then stirred at room temperature for 2 hours. The solidified mixture was dissolved in chloroform and the organic layer washed with brine. The organic layer was dried with Na_2SO_4 and the solvent removed under reduces pressure. The product was obtained in 79% yield as a colorless liquid. Note, that solidification on standing is due to dimerization of the product by formation of the cyclic hemiacetal[25]. The reversible dimerization did not interfere with the following steps. ^{1}H NMR (400 MHz, $CDCl_3$): δ (ppm) 9.52 (s, 1H, CHO), 3.62 (s, 2H, -CH_2-), 1.10 (s, 6H, -CH_3)

3,3-Dimethoxy-2,2-Dimethylpropanol (B): 3,3-Dimethoxy-2,2-dimethylpropanol was prepared analogously to the procedure of Johnson *et al.*.[26] 50 g of 3-Hydroxy-2,2-dimethylpropanal (**A**) (0.49 mol, 1 eq), 107 mL of trimethyl orthoformate (0.98 mol, 2 eq.) and 4.22 g *p*-toluenesulfonic acid (24 mmol, 0.05 eq.) were dissolved in 350 mL Methanol and stirred for 24 hours. The mixture was brought to basic pH by addition of 20 mL concentrated aqueous K_2CO_3 solution and diluted with 80 mL brine. Methanol was removed in vacuo and the product

extracted with diethyl ether. The organic phase was washed with brine, dried with Na_2SO_4 and the solvent removed under reduced pressure. The crude liquid product was obtained in 66 % yield and could be used without further purification. ^{1}H NMR (400 MHz, CDCl$_3$): δ (ppm) 4.02 (s, 1H, -CH(OMe)$_2$), 3.53 (s, 6H, C(OCH_3)$_2$), 3.43 (s, 2H, -CH_2-), 0.92 (s, 6H, C(CH_3)$_2$).

3,3-Dimethoxy-2,2-propanyl glycidyl ether (DDPGE): 25 g 3,3-Dimethoxy-2,2-dimethylpropan-1-ol (**B**) (0.17 mol, 1 eq.) and 2.23 g 18-crown-6 (8 mmol, 0.05 eq) were dissolved in 50 mL Benzene. 50 mL of aqueous KOH solution (50 wt%) and 26.5 mL epichlorohydrin (0.34 mol, 2 eq.) were added. The mixture was then vigorously stirred for 4 h at room temperature. The product was extracted three times with 100 mL diethyl ether. The combined extracts were washed with brine until the washings were neutral. The organic layer was dried with Na_2SO_4 and the solvents removed under reduced pressure. The crude product was distilled in high vacuum to yield 53 % liquid DDPGE in high purity. The product was stored over molecular sieves 4 Å. ^{1}H NMR (400 MHz, CDCl$_3$): δ (ppm) 4.09 (s, 1H, -CH(OMe)$_2$), 3.67 (dd, J = 11.7, 2.9 Hz, 1H, ring–C$H_{2,a}$O-), 3.48 (d, J = 1.2 Hz, 6H, C(OCH_3)$_2$), 3.33 (dd, J = 11.7, 5.8 Hz, 1H, ring–C$H_{2,b}$O-), 3.24 (q, J = 8.7 Hz, 2H, -CH_2-), 3.11 (ddt, J = 5.7, 4.1, 2.8 Hz, 1H, CH_{ring}), 2.77 (dd, J = 5.1, 4.2 Hz, 1H, C$H_{2a,ring}$), 2.58 (dd, J = 5.1, 2.7 Hz, 1H, C$H_{2b,ring}$), 0.88 (s, 6H, C(CH_3)$_2$).

Preparation of the initiator solution: To reduce working steps one initiator solution for several copolymerization was prepared. First, 100 mg of 2-(Benzyloxy)ethanol (0.66 mmol, 1 eq.) was mixed with 6.4 mg of KO^{t}Bu (0.59 mmol, 0.9 eq.) and dissolved in a 6 mL benzene/methanol 5:1 mixture and dried overnight at room temperature under reduced pressure while stirring. The flask was then flushed with argon and dissolved in 30 mL dry dimethyl sulfoxide.

S*tatistical copolymerization for P(EO-co-DMPGE) and P(EO-co-DDPGE) copolymers:* In the following, an exemplary synthesis protocol for the P(EO$_{39}$-*co*-DDPGE$_{43}$) copolymers is described. 10 ml of the previously prepared initiator solution (corresponds to 33 mg 2-(Benzyloxy)ethanol (0.22mmol, 1 eq.) was added under argon flow in a dry Schlenk flask. Then, 1.8 g of DDPGE (8.7 mmol, 40 eq.) (or DMPGE respectively) were added via syringe, the solution immediately frozen in a cooling bath of liquid nitrogen and ethanol to -100 °C and then the flask was evacuated. 0.4 mL ethylene oxide (8.7 mmol, 40 eq.) was distilled under vacuum into a graduated ampule cooled to -100 °C and subsequently into the reaction flask. The valved flask was closed and heated to 40 °C. The copolymerization was carried out under stirring for 24 h at 40 °C to ensure complete conversion of the comonomers. Then 10 mL brine and 30 mL dichloromethane were added to the reaction mixture. The aqueous phase was

separated and washed four more times with brine. The organic phase was dried with K_2CO_3 and the solvent removed under reduces pressure. Last traces of DMSO were removed by stirring at 60 °C in high vacuum for 24 h. Typical yields of the liquid to solid products after isolation were >90%.

^{1}H NMR Kinetics: A solution of 30 mg partially deprotonated 2-(Benzyloxy)ethanol in 1 mL DMSO-d_6 was prepared following the protocol from above. 0.1 mL of this solution was transferred via syringe into a dried Norell S-500-VT-7 NMR tube (equipped with a Teflon stop-cock). The solution was frozen in liquid nitrogen and 0.5 mL DMSO-d_6 added. Then, 20 eq. of DMPGE (or DDPGE) were introduced to the NMR tube. The frozen NMR tube was evacuated and 40 eq. of EO were distilled in the cold. The NMR tube was sealed and allowed to reach room temperature. To homogenize the mixture, it was shaken vigorously before placement in the NMR spectrometer. Spectra were measured on a Bruker Avance III HD spectrometer equipped with a 5 mm BBFO SmartProbe and an ATM as well as a SampleXPress 60 auto sampler. The sample temperature was set to 40 °C and a spectrum recorded every 30 s with one scan until the complete disappearance of the epoxide signals.

Homopolymers PDMPGE and PDDPGE: 50 mg 2-(Benzyloxy)ethanol (0.33 mmol, 1 eq.) and 18.4 mg KO^{t}Bu (0.16 mmol, 0.5°eq) was dissolved in 6 mL of a benzene and methanol 5:1 mixture. While stirring at room temperature high vacuum was applied. After removal of the solvents, the mixture was stirred overnight in high vacuum at room temperature. 20 eq. of DMPGE or DDPGE were then added and the polymerization carried out at 60 °C for 24 h in bulk. The products were slightly yellow viscous oils in yields ≥95 %.

Acidic hydrolysis of acetal groups to aldehydes: A slightly modified procedure adopted from Danishefsky *et al.* was used to hydrolyze the acetal groups to aldehydes in the copolymers.[27] The procedure is shown here exemplary on the copolymer P(EO$_{160}$-*co*-DDPGE$_{17}$). 50 mg (1 eq.) copolymer ($M_{eq} = M_n / n$(DDPGE)) and 100 mg pyridinium *p*-toluenesulfonate (5 eq.) were dissolved in a mixture of 5 mL acetone and 0.5 mL water. The solution was stirred at 50 °C for 20 h. 5 mL concentrated NaHCO$_3$ was added and the solution concentrated with a nitrogen stream. The residue was extracted with 20 mL DCM. The organic phase was washed twice with 5 mL of brine, dried with Na$_2$SO$_4$ and the solvent removed under reduced pressure. The product was dried in high vacuum, yielding 70 % of the deprotected polymer. ^{1}H NMR confirmed the quantitative conversion of the acetal groups to aldehydes.

Oxidation of acetal groups to methyl ester groups: The general procedure for oxidation of aldehydes in acidic conditions was directly applied to the protected polymers.[28,29] The procedure is shown here exemplary on the copolymer P(EO$_{160}$-*co*-DDPGE$_{17}$). 100 mg (1 eq.) of the copolymer ($M_{eq} = M_n / n$(DDPGE)) and 276 mg Oxone (5 eq.) were dissolved in 4 mL methanol. The solution was stirred at 50 °C for 20 h. 5 mL concentrated NaHCO$_3$ was added. The residue was extracted with 40 mL dichloromethane. The organic phase was washed twice with 10 mL of Brine, dried with Na$_2$SO$_4$ and the solvent removed under reduced pressure. The product was dried in high vacuum. ^{1}H NMR-spectroscopy proofs the quantitative oxidation of the acetal group, the yield was ≥80 %.

Transformation of acetal groups into hydrazone functionalities: Brady's test[30] was directly performed with the acetal protected polymers.[31] 400 mg of 2,4-dinitrophenylhydrazine was dissolved in concentrated sulfuric acid. While stirring, 3 mL water was added slowly and the solution diluted with 10 mL absolute ethanol. 100 mg Polymer was dissolved in 1 mL absolute ethanol and added to the solution. The precipitated solid was separated by filtration and washed several times with cold absolute ethanol. After drying in vacuum, orange-red powder could be recovered in typically yields around 30 %.

Oxidation of aldehyde groups to nitrile groups: The direct transformation of aldehydes into nitriles was applied to aldehyde functionalized PEG which was yielded from the procedure above.[32] 20 mg of deprotected P(EO$_{160}$-*co*-DDPGE$_{17}$) was dissolved in a mixture of 0.4 mL ammonia solution (28 %) and 0.05 mL Tetrahydrofuran. 12 mg Iodine were added and the mixture stirred until the brownish color almost completely disappeared (1 hour). Then a solution of 10 mg Na$_2$S$_2$O$_3$ in 0.2 mL water was added and the mixture thoroughly mixed. 10 mL dichloromethane and 2 mL were added. The organic phase was separated, dried with Na$_2$SO$_4$ and the solvent removed to yield the nitrile product in quantitative yield.

Angeli-Rimini test for aldehydes[33]: 20 mg of deprotected P(EO$_{160}$-co-DDPGE$_{17}$) was dissolved in 1 mL methanol. 12 mg of benzenesulfohydroxamic acid and 0.07 mL 2 N sodium hydroxide solution were added while stirring. The solution was stirred for 15 minutes and then 0.1 mL 2 N hydrochloric acid were added. Addition of aqueous FeCl$_3$ solution produced a deeply red colored solution, which confirmed the conversion of the aldehyde functionalities into hydroxamic acid groups.

RESULTS AND DISCUSSION

A.　　Monomer synthesis

Acetal groups are well established for AROP of epoxides to protect hydroxyl groups during polymerization. Ethoxyethyl glycidyl ether (EEGE) and 1,2-isopropylidene glyceryl glycidyl ether (IGG) are monomers which can be polymerized a controlled way and release hydroxyl groups under acidic treatment.[7,8] Both monomers release a low molecular weight carbonyl compound as side product during acidic hydrolysis. The previous shown stability and easy cleavage inspired the development of an acetal containing epoxide which can liberate an aldehyde group which stays bound to polymer backbone. This concept has been already established for the initiation of the polymerization of EO with an acetal protected aldehyde alcohol.[19] In this work, DMPGE was the first design of an epoxy monomer with an acetal protected aldehyde group. The monomer was synthesized according to Scheme 2. In the first step the dimethoxy ester was reduced to the corresponding alcohol **I**. The alcohol was treated with Epichlorohydrin under basic conditions to yield the monomer DMPGE. The reaction with a phase transfer catalyst produced a side product due to an elimination reaction of epichlorohydrin, which showed to be problematic to separate due to similar boiling points of product and side product.[34] By refraining from using phase transfer catalyst no side product due to elimination reactions was formed. ^{1}H and ^{13}C NMR spectra of the purified monomer by distillation are shown Figure S1 and Figure S2.
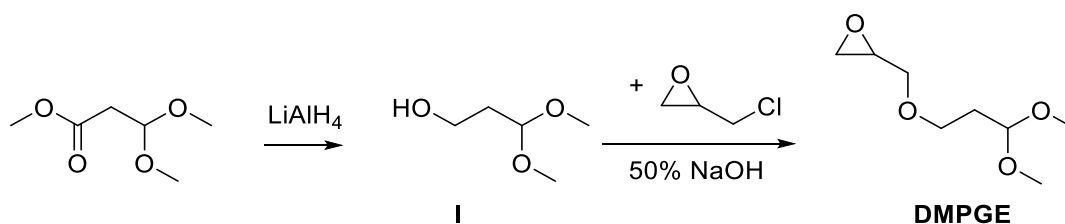
Scheme 2: Synthetic route for DMPGE.

DMPGE could be successfully employed in homo- and copolymerization with EO under conditions of AROP. However, attempts to hydrolyze the acetal group in the polymer directly led to side reactions as described in detail later. These side reactions are connected to the tendency of the deprotected aldehyde to tautomerize into the enol form and therefore can be successfully prevented for aldehydes without acidic alpha protons. This was the motivation for the development of DDPGE, which is a slightly modified version of the DMPGE, with two methyl groups instead of protons in alpha position to the aldehyde.
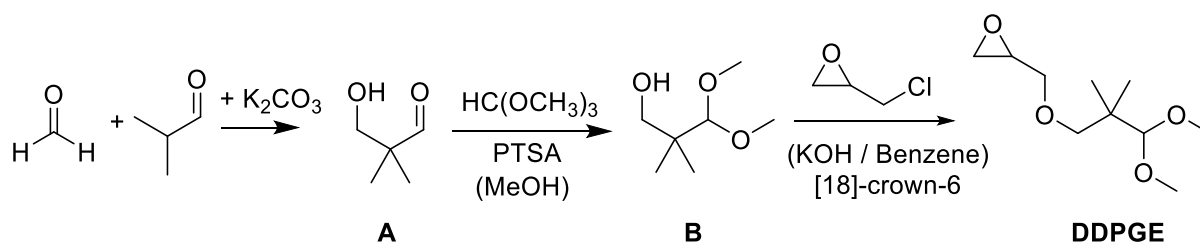
Scheme 3. Synthetic route of DDPGE.

As DDPGE does not possess acidic alpha protons, cross-linking via aldol condensation in its deprotected state is not possible. Furthermore, a reverse oxa-michael addition is also prevented.[35] The synthesis strategy is outlined in Scheme 3, starting from the aldol condensation of formaldehyde and isobutyraldehyde. The synthesized aldol adduct **A** is transformed into the dimethoxy acetal by trimethyl orthoformate. The dimethoxy alcohol **B** is then used to synthesize the corresponding glycidyl ether DDPGE under basic conditions with the phase transfer catalyst 18-crown-6. In contrast to the DMPGE glycidyl ether synthesis, phase transfer catalysis is required due to the nonpolar nature of the alcohol. As described above, phase transfer catalysis may lead to an elimination side reaction of epichlorohydrin. The side reaction could be repressed by using crown ether instead of tributyl ammonium bromide.[34] The product could be isolated in high purity by distillation, as confirmed by ^{1}H and ^{13}C NMR (Figure S3 and Figure S4). As predicted, the deprotection problems experienced in the case of DMPGE polymers could be successfully prevented with the development of DDPGE.

B.   Anionic ring opening (co)polymerization

To synthesize multifunctional PEGs with acetal functionalities statically distributed along the polyether chain, copolymerization with ethylene oxide (EO) were performed according to Scheme 1. Partly deprotonated 2-(benzyloxy)ethanol with potassium as counter ion was chosen to ensure molecular weight determination via end group analysis in ^{1}H NMR. DMSO was used as a solvent for the statistical copolymerization. The copolymerization was performed with both monomers in various ratios from 5−57 mol% and molecular weights between 9,800 and 20,100 g/mol with dispersities below 1.1. Additionally, both monomers could be homopolymerized without a solvent to yield polymers with molecular weights of 5700 and 4500 g/mol and dispersities below 1.2. These results strongly indicate that both monomers can be polymerized in a controlled fashion. The characterization data of these polymers is summarized in Table 1 and the corresponding SEC traces are shown in Figure 1. Exemplary ^{1}H NMR spectra

of the copolymers are shown in Figure S5 and Figure S6. The molecular weights determined by SEC are underestimated in comparison the molecular weights determined by end group analysis in ^{1}H NMR. This is due to the different elution behavior of the PEG standards and the copolymers. The thermal properties of the synthesized polymers were studied by DSC measurements. The determined glass transition temperatures T_g and melting points T_m of the polymers are summarized in Table 1. As apparent from the PDMPGE$_{17}$ homopolymer the glass transition temperature of the DMPGE units is very similar to these of PEG. Consequently, all glass transition temperatures of the DMPGE copolymers are in the narrow range between -62 °C and -64 °C. The additional methyl groups of DDPGE monomer increase the glass transition of the PDDPGE$_{21}$ homopolymer to -46 °C well above the T_g of PEG. This result in glass transition temperatures of the DDPGE copolymers in the range between -52 °C and -45 °C. Only the copolymers with a comonomer content below 10 % exhibit a melting point of the PEG domain. For higher comonomer ratios the PEG segments are too disturbed to pack into ordered crystalline domains.

Table 1. Characterization data of synthesized polymers.

polymer sample	ratio / mol%§	M_n / g mol^{-1} th	M_n /g mol^{-1} §	M_n /g mol^{-1} $^#$	M_w/ M_n $^#$	T_g / °C	T_m / °C
P(EO$_{173}$-co-DMPGE$_{11}$)	6	10300	9800	6400	1.06	-62	14
P(EO$_{179}$-co-DMPGE$_{20}$)	10	11600	11600	6100	1.06	-62	24
P(EO$_{214}$-co-DMPGE$_{60}$)	22	15600	20100	8500	1.09	-63	/
P(EO$_{42}$-co-DMPGE$_{56}$)	57	11600	11900	6900	1.10	-64	/
PDMPGE$_{17}$	100	3700	3200	1300	1.12	-68	/
P(EO$_{193}$-co-DDPGE$_{11}$)	5	10600	10900	4700	1.08	-52	36
P(EO$_{160}$-co-DDPGE$_{17}$)	10	9400	10700	4600	1.08	-54	20
P(EO$_{39}$-co-DDPGE$_{43}$)	52	10100	10600	3700	1.08	-45	/
PDDPGE$_{21}$	100	4300	4500	2200	1.13	-46	/

§Determined by ^{1}H NMR (400 MHz, CDCl$_3$ or DMSO-d$_6$); $^#$determined by SEC (eluent: DMF, calibration: PEG)
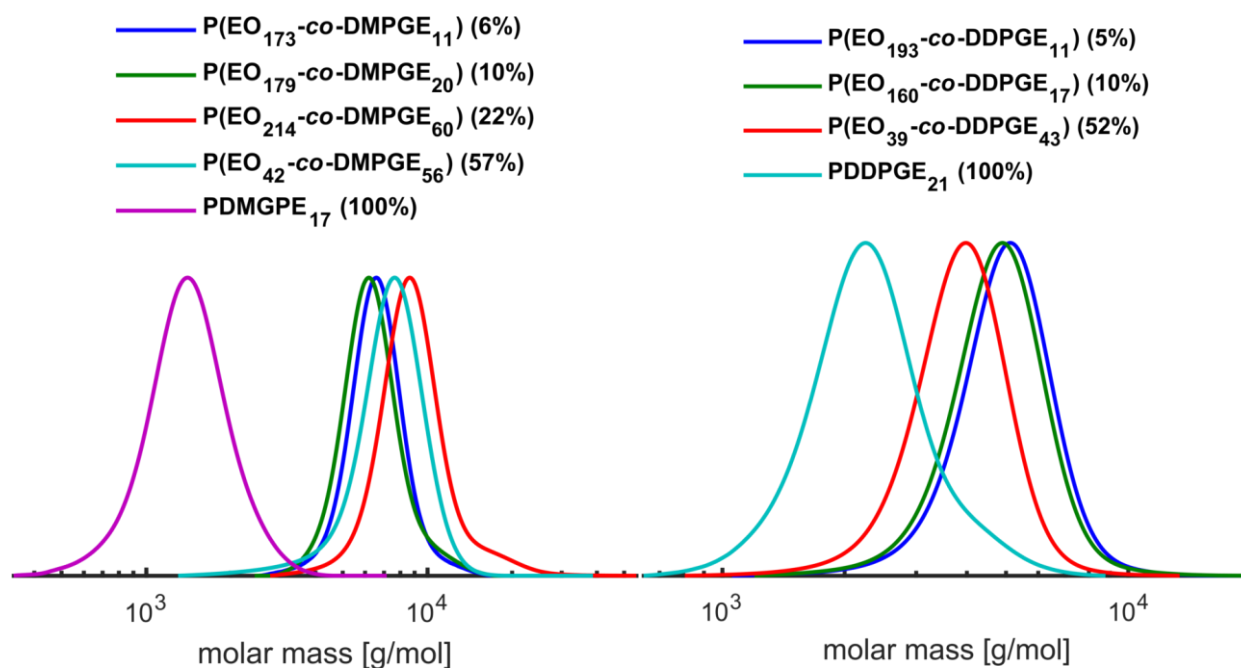
Figure 1. SEC traces (DMF, PEG-calibration) of synthesized (co)polymers of DMPGE (left) and DDPGE (right).

To further proof the controlled character of the polymerization of the two monomers mass spectrometry was used. MALDI-TOF of the homopolymers could be assigned to the expected peaks of the 2-(benzyloxy)ethanol-initiated chains as described in recent work (Figure 2).[36] The possible assignment of the signals confirms the controlled polymerization of both monomers with defined end groups takes place. The determined degree of polymerization by the assignment of the peaks is slightly smaller compared to the one determined by NMR due to mass discrimination effects. On the other hand, the determined weights are higher than the molecular weights determined by SEC with PEG-calibration. This also underlines the different elution behavior of these copolymers in comparison to PEG.
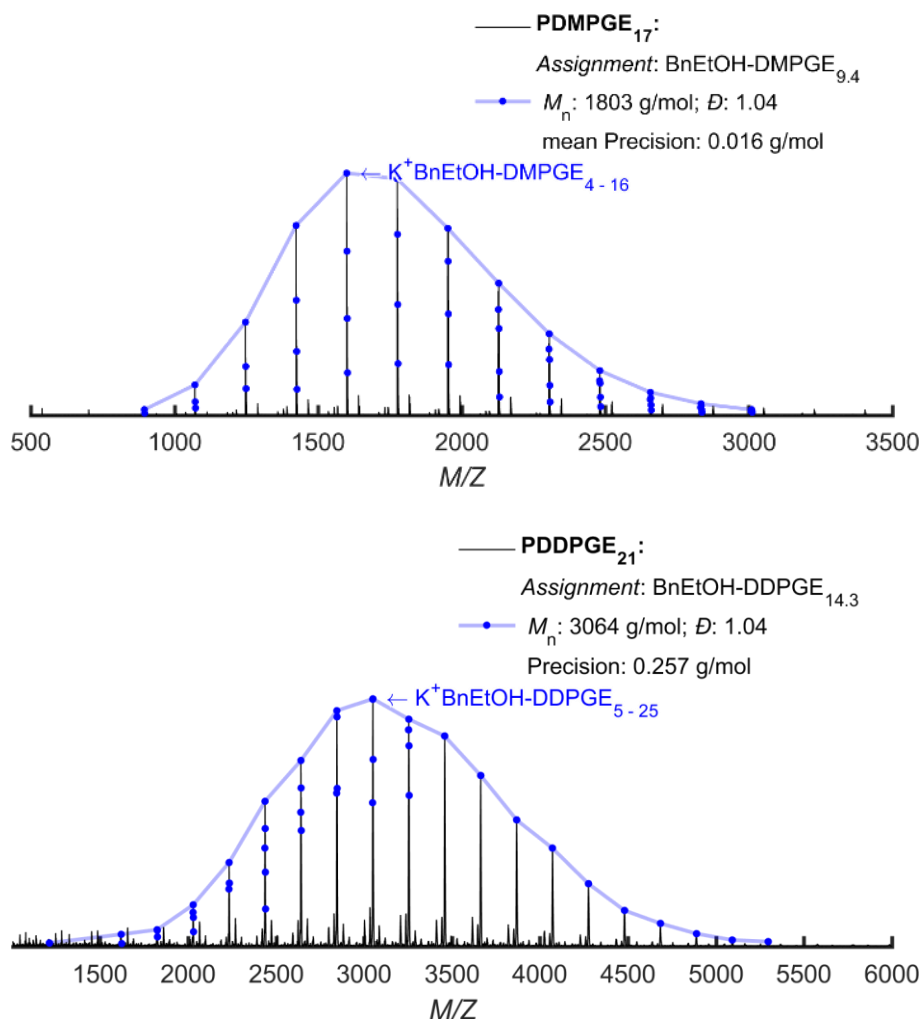
Figure 2: MALDI TOF spectra of PDMPGE$_{17}$ (top) and PDDPGE$_{21}$ (bottom) homopolymers with assignment of the peaks.

C. Kinetic investigation

The copolymerization of the two monomers with EO were investigated by *in-situ* ^{1}H NMR kinetic studies to gain a deeper understanding of the copolymer microstructure. The epoxide signals which are highlighted in Figure S7 and Figure S8 were monitored during the full conversion of the copolymerization. Reactivity ratios can be evaluated from this data as shown in previous works.[36,37] As the reactivity ratios are very close to one, the composition shift is minimal in the case of the copolymerization of EO and DMPGE. Therefore, only the non-terminal model could be applied.[38] The resulting reactivity ratios of the Jaacks fit are r_{EO}= 0.96 and r_{DMPGE} = 1.04 (Figure S9).[39] This implies a random incorporation of EO and DMPGE in the copolymerization. The bulkier DDPGE showed a little deviation from these results. The reactivity ratios determined by Jaacks-fit are r_{EO}= 1.20 and r_{DDPGE} = 0.83 (Figure S10).[39] In this

case a composition shift was observed and the terminal Meyer-Lowry model could be fitted to the conversion data. The determined reactivity ratios from the Meyer-Lowry fit are r_{EO}= 1.19 and r_{DDPGE} = 0.83 (Figure S11) are in very good agreement with the Jaacks-fit.[40] The slightly higher reactivity of DMPGE compared to the bulkier DDPGE probably due to sterically hinderance. Similar reactivity ratios were observed by Niederer *et al.* for the bulky Catechol Acetonide Glycidyl Ether (CAGE) in the copolymerization with EO.[9] However, both monomers are very close to an ideal random copolymerization as shown in the copolymerization diagrams (Figure 3). The simulated distribution of functionalities along the polymer chain shows an almost randomly distribution for both cases (Figure S12).
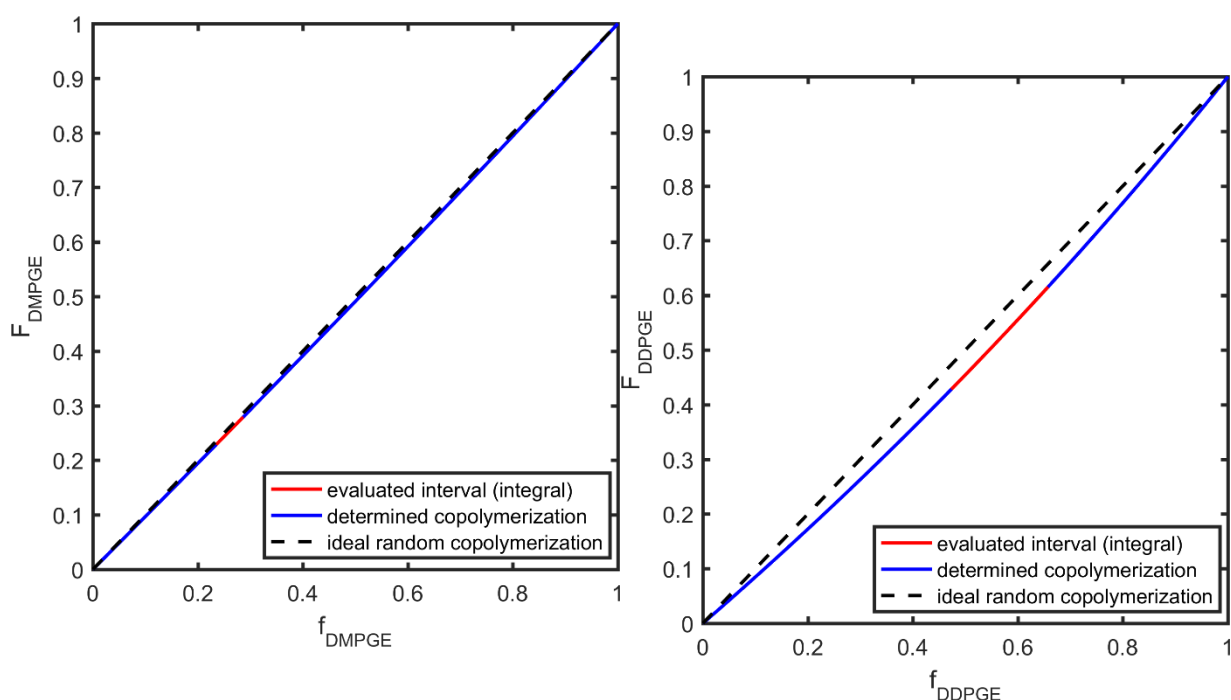
Figure 3. Copolymerization diagrams obtained by ^{1}H NMR kinetic experiments of EO and DMPGE (left) and EO and DDPGE (right).

D. Post polymerization modification reactions.
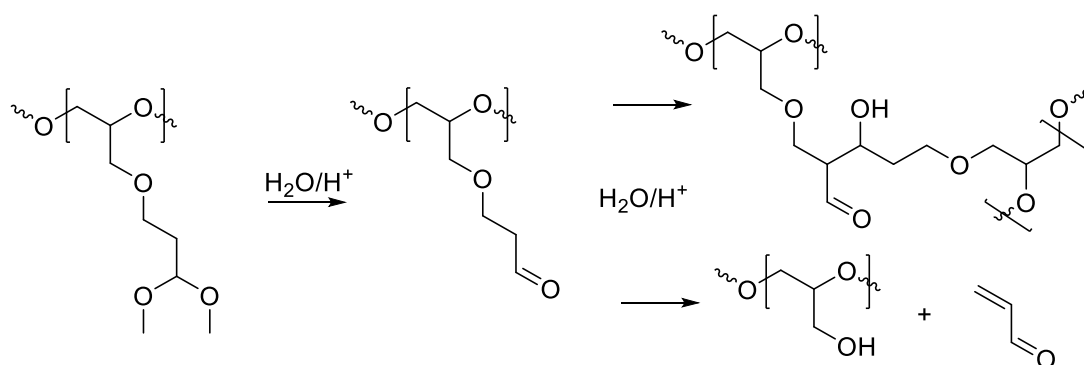
Scheme 4. Possible side reactions occurring during the acidic deprotecting of DMPGE-polymers.

As mentioned before the hydrolysis of the (co)polymers of DMPGE to yield defined multi aldehyde functional polyether was not successful. For this purpose, different deprotection methods were attempted. By using pyridinium *p*-toluene sulfonate[27] no soluble product could be recovered from the reaction mixture, due to crosslinking via aldol reactions catalyzed by the acidic conditions (Scheme 4). A high molecular weight distribution due to crosslinking could be observed in the deprotection attempt of a block copolymer (Figure S13). Similar observation of aldol reactions were made previously for multi aldehyde functional polyoxazolines by Taton and coworkers.[20] In a very mild deprotecting route with iodine in acetone,[41] the formation of acrolein could be observed in the ^{1}H NMR spectrum (Figure S14). This confirms the occurrence of a reverse oxa-Michael addition as shown in Scheme 4.[35,42] However, under acidic conditions which form the aldehyde *in-situ*, the acetals in the PDMPGE-homopolymers could be successfully transformed by the reaction with dinitro phenyl hydrazine. The formation of the polyhydrazone product causes a large shift in molecular weight distribution in SEC (Figure 4) and was confirmed further in the corresponding ^{1}H NMR spectrum (Figure S15).
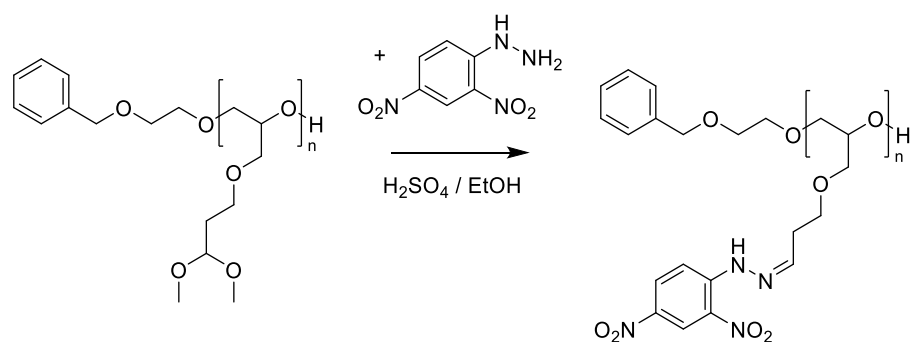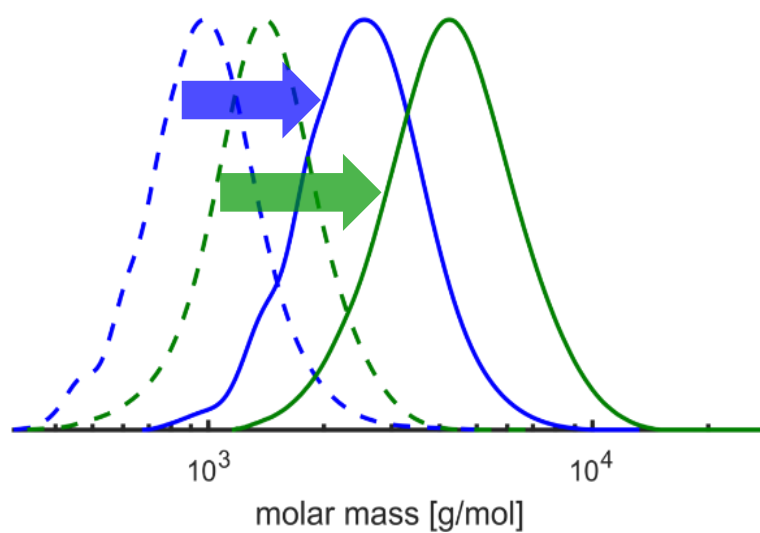
Figure 4: Top: Transformation of Acetal functionalities into hydrazone. Bottom: Shift in SEC traces of transformed PDMPGE homopolymers.
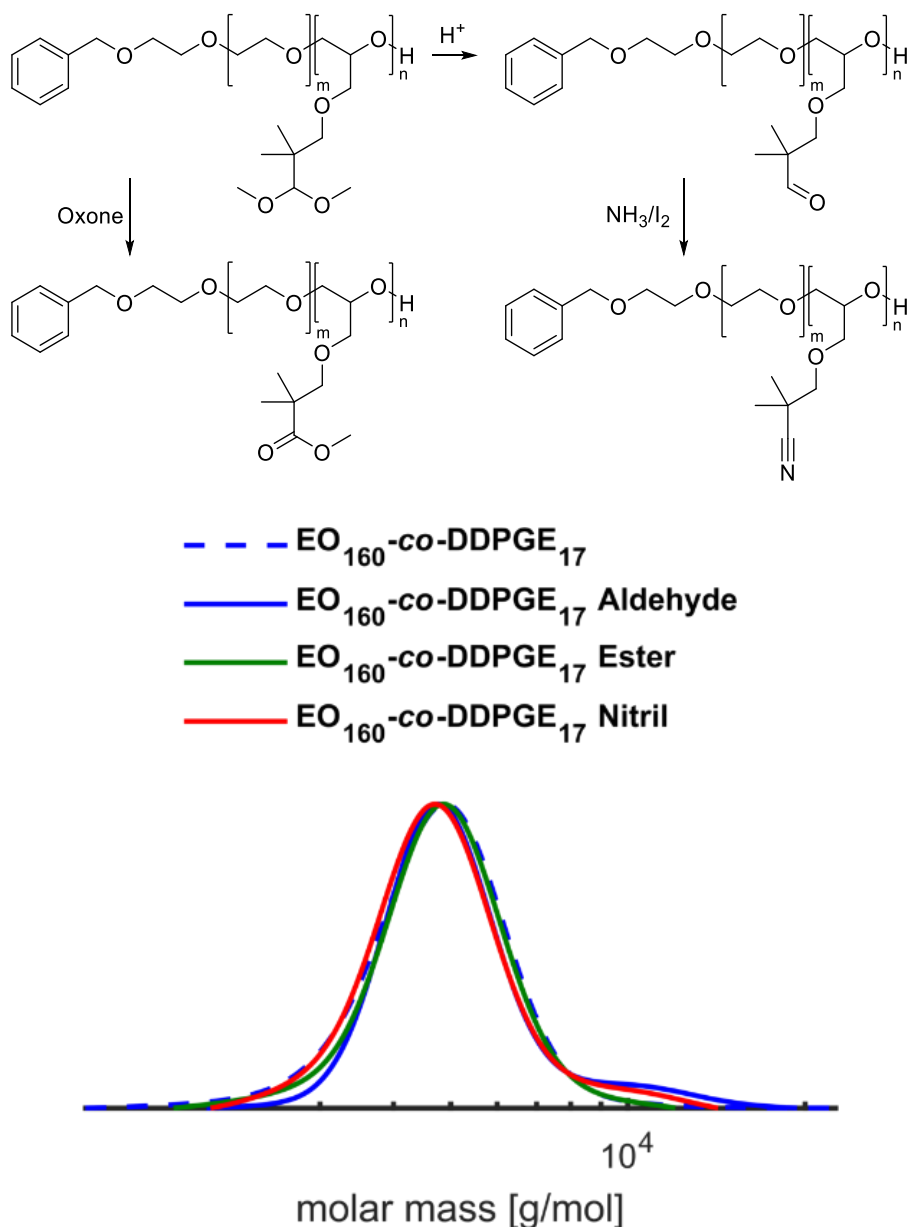
Figure 5. Left: Reaction scheme of post polymerization modification reactions. Right: SEC traces of corresponding polymers.

The mentioned side reactions motivated the shift of focus to polymers of the second developed monomer DDPGE, where no undesired side reactions were observed. The synthesized P(EO$_{160}$-co-DPPGE$_{17}$) was used to show possible post-polymerization reactions. These reactions were performed according to the Scheme in Figure 5. The ^{1}H NMR spectra which verify the modification are shown in Figure S16. The corresponding SEC traces are shown in Figure 5 and confirm that the monomodal distribution of the copolymers stays below a dispersity of 1.1 for all modifications. In contrast to the DMPGE polymers, the acetals of the P(EO-co-DDPGE) copolymers could be hydrolyzed by treatment with pyridinium p-toluene sulfonate to release the aldehyde functionalities.[27] The ^{1}H NMR spectrum in Figure S16 shows clearly the shift of

the single proton next to the acetal (labeled d) at 4.0 ppm to 9.5 of the corresponding aldehyde. The release of the aldehyde moieties shifts the protons at the two methyl groups in alpha position (labeled c) from 0.9 to 1.0 ppm. The IR spectrum shows the vibration of the carbonyl bond at 1728 cm^{-1} (Figure S17). Aldehydes are also known to be easily oxidized to the corresponding carboxylic acid.[28] Due to the acidic conditions of the Oxone oxidation, the acetal functionality can be directly transformed into the carboxylic acid methyl ester. This can be seen in the ^{1}H NMR spectra in Figure S16 by the disappearance of the single proton (labeled d) and the shift of methyl groups (labeled c) from 0.9 to 1.2 ppm. The IR spectrum proofs the presence of a carbonyl group with the vibration at 1731 cm^{-1} (Figure S17). The previously described aldehyde functional PEG could be oxidized in a second post-polymerization reaction to the nitrile in a mixture of ammonia and iodine.[32] In this case as for the ester the peak of the single proton d disappears and the methyl-groups (labeled c) shift from 1.0 to 1.3 ppm (Figure S16). The IR spectrum shows the nitrile group with the vibration at 2237 cm^{-1} (Figure S17). Herzberger *et al.* have shown that multi nitrile-functional could be synthesized by copolymerization of EO and epicyanohydrin via the activated monomer mechanism and could be transformed into amide and amine functional PEG.[13] These post-polymerization reactions could be also applied in the future to the nitrile functional PEG synthesized in this work, and so make these functionalities accessible via AROP. As aldehydes are highly reactive many more post polymerization reactions are possible. A chemical test for the presence of aldehydes is the Angeli-Rimini reaction, which oxidizes the aldehyde to the corresponding hydroxamic acid. The hydroxamic acid forms deep red colored complexes with Iron(III).[33] The positive test solution of the aldehyde functionalized PEG is shown in Figure S18, where some of the formed complexes of Iron and hydroxamic acid functionalized PEG could be transferred to the organic layer of dichloromethane.

CONCLUSION

In this work the two monomer DMPGE and DDPGE were developed with the aim to introduce multiple aldehyde functionalities into a PEG backbone. Both monomers are based on acetal protected aldehyde connected to an epoxide, which can be polymerized by AROP.

It could be shown that homo- and copolymerization of both monomers in various ratio with EO were successful and yielded well-defined polymers with low dispersity ($M_w/M_n < 1.2$). The microstructure of the copolymers was investigated by *real-time* ^{1}H NMR kinetics, revealing an almost random copolymerization in both cases. It became evident that the deprotection of DMPGE polymers was difficult due to side reactions, leading to cross-linking and degradation of the polymers. Nevertheless, DMPGE acetal functionalities could be successfully addressed by hydrazone formation. These results motivated further development of the monomer DDPGE which could repress the side reactions. The deprotected form does not possess acidic alpha-protons and thus preventing the side reactions. This enabled the quantitative deprotecting of DDPGE copolymers, while maintaining low dispersities ($M_w/M_n < 1.1$) and paved the way to various other post polymerization reactions. Besides the deprotection to the aldehyde, the acetal could be successfully oxidized to the methyl ester and the aldehyde-functionalities transformed into multi-nitrile functional PEG.

The insights in the structural features needed to incorporate multiple aldehyde functionalities into PEG will be also highly valuable for bioconjugation. The use of this system in biomedical application will be part of the future work. Furthermore, the new monomer DDPGE offers the possibility to introduce many functionalities into PEG which before were not easily accessible via AROP.

ACKNOWLEDGMENT

REFERENCES

(1) *Poly(Ethylene Glycol) Chemistry: Biotechnical and Biomedical Applications;* Harris, J. M., Ed.; Topics in Applied Chemistry; Springer US: Boston, MA, s.l., 1992.

(2) Engels, H.-W.; Pirkl, H.-G.; Albers, R.; Albach, R. W.; Krause, J.; Hoffmann, A.; Casselmann, H.; Dormish, J. Polyurethanes: Versatile materials and sustainable problem solvers for today's challenges. *Angew. Chem. Int. Ed. Engl.* **2013**, *52*, 9422–9441, DOI: 10.1002/anie.201302766.

(3) Herzberger, J.; Niederer, K.; Pohlit, H.; Seiwert, J.; Worm, M.; Wurm, F. R.; Frey, H. Polymerization of Ethylene Oxide, Propylene Oxide, and Other Alkylene Oxides: Synthesis, Novel Polymer Architectures, and Bioconjugation. *Chemical reviews* **2016**, *116*, 2170–2243, DOI: 10.1021/acs.chemrev.5b00441.

(4) Mangold, C.; Wurm, F.; Frey, H. Functional PEG-based polymers with reactive groups via anionic ROP of tailor-made epoxides. *Polym. Chem.* **2012**, *3*, 1714, DOI: 10.1039/c2py00489e.

(5) Wilms, V. S.; Frey, H. Aminofunctional polyethers: smart materials for applications in solution and on surfaces - Supporting Information. *Polym. Int.* **2013**, *62*, 849–859, DOI: 10.1002/pi.4496.

(6) Herzberger, J.; Fischer, K.; Leibig, D.; Bros, M.; Thiermann, R.; Frey, H. Oxidation-Responsive and "Clickable" Poly(ethylene glycol) via Copolymerization of 2-(Methylthio)ethyl Glycidyl Ether. *J. Am. Chem. Soc.* **2016**, *138*, 9212–9223, DOI: 10.1021/jacs.6b04548.

(7) Taton, D.; Le Borgne, A.; Sepulchre, M.; Spassky, N. Synthesis of chiral and racemic functional polymers from glycidol and thioglycidol. *Macromol. Chem. Phys.* **1994**, *195*, 139–148, DOI: 10.1002/macp.1994.021950111.

(8) Wurm, F.; Nieberle, J.; Frey, H. Synthesis and Characterization of Poly(glyceryl glycerol) Block Copolymers. *Macromolecules* **2008**, *41*, 1909–1911, DOI: 10.1021/ma702458g.

(9) Niederer, K.; Schüll, C.; Leibig, D.; Johann, T.; Frey, H. Catechol Acetonide Glycidyl Ether (CAGE): A Functional Epoxide Monomer for Linear and Hyperbranched Multi-Catechol Functional Polyether Architectures. *Macromolecules* **2016**, *49*, 1655–1665, DOI: 10.1021/acs.macromol.5b02441.

(10) Billouard, C.; Carlotti, S.; Desbois, P.; Deffieux, A. "Controlled" High-Speed Anionic Polymerization of Propylene Oxide Initiated by Alkali Metal Alkoxide/Trialkylaluminum Systems. *Macromolecules* **2004**, *37*, 4038–4043, DOI: 10.1021/ma035768t.

(11) Labbé, A.; Carlotti, S.; Billouard, C.; Desbois, P.; Deffieux, A. Controlled High-Speed Anionic Polymerization of Propylene Oxide Initiated by Onium Salts in the Presence of Triisobutylaluminum. *Macromolecules* **2007**, *40*, 7842–7847, DOI: 10.1021/ma070288d.

(12) Brocas, A.-L.; Mantzaridis, C.; Tunc, D.; Carlotti, S. Polyether synthesis: From activated or metal-free anionic ring-opening polymerization of epoxides to functionalization. *Prog. Polym. Sci.* **2013**, *38*, 845–873, DOI: 10.1016/j.progpolymsci.2012.09.007.

(13) Herzberger, J.; Frey, H. Epicyanohydrin: Polymerization by Monomer Activation Gives Access to Nitrile-, Amino-, and Carboxyl-Functional Poly(ethylene glycol). *Macromolecules* **2015**, *48*, 8144–8153, DOI: 10.1021/acs.macromol.5b02178.

(14) Herzberger, J.; Leibig, D.; Liermann, J. C.; Frey, H. Conventional Oxyanionic versus Monomer-Activated Anionic Copolymerization of Ethylene Oxide with Glycidyl Ethers: Striking Differences in Reactivity Ratios. *ACS Macro Lett.* **2016**, *5*, 1206–1211, DOI: 10.1021/acsmacrolett.6b00701.

(15) Staudinger, H.; Schweitzer, O. Über hochpolymere Verbindungen, 20. Mitteil.: Über die Poly-äthylenoxyde. *Ber. dtsch. Chem. Ges. A/B* **1929**, *62*, 2395–2405, DOI: 10.1002/cber.19290620879.

(16) Flory, P. J. Molecular Size Distribution in Ethylene Oxide Polymers. *J. Am. Chem. Soc.* **1940**, *62*, 1561–1565, DOI: 10.1021/ja01863a066.

(17) Sokolovskaya, E.; Barner, L.; Bräse, S.; Lahann, J. Synthesis and on-demand gelation of multifunctional poly(ethylene glycol)-based polymers. *Macromol. Rapid Commun.* **2014**, *35*, 780–786, DOI: 10.1002/marc.201300909.

(18) Pfister, D.; Morbidelli, M. Process for protein PEGylation. *J. Controlled Release* **2014**, *180*, 134–149, DOI: 10.1016/j.jconrel.2014.02.002.

(19) Nagasaki, Y.; Kutsuna, T.; Iijima, M.; Kato, M.; Kataoka, K.; Kitano, S.; Kadoma, Y. Formyl-Ended Heterobifunctional Poly(ethylene oxide): Synthesis of Poly(ethylene oxide) with a Formyl Group at One End and a Hydroxyl Group at the Other End. *Bioconjugate Chem.* **1995**, *6*, 231–233, DOI: 10.1021/bc00032a012.

(20) Legros, C.; Pauw-Gillet, M.-C. de; Tam, K. C.; Lecommandoux, S.; Taton, D. Aldehyde-functional copolymers based on poly(2-oxazoline) for post-polymerization modification. *Eur. Polym. J.* **2015**, *62*, 322–330, DOI: 10.1016/j.eurpolymj.2014.08.026.

(21) Patenaude, M.; Campbell, S.; Kinio, D.; Hoare, T. Tuning gelation time and morphology of injectable hydrogels using ketone-hydrazide cross-linking. *Biomacromolecules* **2014**, *15*, 781–790, DOI: 10.1021/bm401615d.

(22) Xu, Q.; A, S.; McMichael, P.; Creagh-Flynn, J.; Zhou, D.; Gao, Y.; Li, X.; Wang, X.; Wang, W. Double-Cross-Linked Hydrogel Strengthened by UV Irradiation from a Hyperbranched PEG-Based Trifunctional Polymer. *ACS Macro Lett.* **2018**, *7*, 509–513, DOI: 10.1021/acsmacrolett.8b00138.

(23) Chang Seok Lee; Tae Hee Lee; Sook Kyung Yoon; Jeung Soon Choi; Yong Jin Jang; Sung Wook Kim; Hye Kyung Chang; Mi Jeong Park; Tae Hun Kim; Young Ha Ahn *et al.* Fused heterocyclic compound WO2010027236A2, 2010.

(24) Acerbis, S.; Beaudoin, E.; Bertin, D.; Gigmes, D.; Marque, S.; Tordo, P. Leveled Steric Effect in Alkoxyamines of SG1-Type. *Macromol. Chem. Phys.* **2004**, *205*, 973–978, DOI: 10.1002/macp.200300240.

(25) Törmäkangas, O. P.; Koskinen, A. M.P. Monoalcoholates of 1,3-diols as effective catalysts in the Tishchenko esterification of 1,3-dioxan-4-ols. *Tetrahedron Lett.* **2001**, *42*, 2743–2746, DOI: 10.1016/S0040-4039(01)00277-5.

(26) Johnson, P. R.; White, J. D. Condensation of crotonic and tiglic acid dianions with aldehydes and ketones. *J. Org. Chem.* **1984**, *49*, 4424–4429, DOI: 10.1021/jo00197a019.

(27) Danishefsky, S. J.; Masters, J. J.; Young, W. B.; Link, J. T.; Snyder, L. B.; Magee, T. V.; Jung, D. K.; Isaacs, R. C. A.; Bornmann, W. G.; Alaimo, C. A. *et al.* Total Synthesis of Baccatin III and Taxol. *J. Am. Chem. Soc.* **1996**, *118*, 2843–2859, DOI: 10.1021/ja952692a.

(28) Travis, B. R.; Sivakumar, M.; Hollist, G. O.; Borhan, B. Facile oxidation of aldehydes to acids and esters with Oxone. *Organic letters* **2003**, *5*, 1031–1034, DOI: 10.1021/ol0340078.

(29) Curini, M.; Epifano, F.; Marcotullio, M. C.; Rosati, O. Oxone®: A Convenient Reagent for the Oxidation of Acetals. *Synlett* **1999**, *1999*, 777–779, DOI: 10.1055/s-1999-2703.

(30) Brady, O. L.; Elsmie, G. V. The use of 2:4-dinitrophenylhydrazine as a reagent for aldehydes and ketones. *Analyst* **1926**, *51*, 77, DOI: 10.1039/an9265100077.

(31) Becker, H. G. O; Beckert, R. *Organikum: Organisch-chemisches Grundpraktikum*, 23. Aufl.; Wiley-VCH: Weinheim, [Great Britain], 2009.

(32) Talukdar, S.; Hsu, J.-L.; Chou, T.-C.; Fang, J.-M. Direct transformation of aldehydes to nitriles using iodine in ammonia water. *Tetrahedron Lett.* **2001**, *42*, 1103–1105, DOI: 10.1016/S0040-4039(00)02195-X.

(33) Gattermann, L.; Wieland, H.; McCartney, W. *Laboratory methods of organic chemistry*; Macmillan, 1937.

(34) Gu, X.-P.; Ikeda, I.; Okahara, M. Stereoselective Formation of Allyl Ethers by Reaction of Epoxides with Organic Chlorides under Liquid-Solid Phase-Transfer Catalysis. *BCSJ* **1987**, *60*, 667–672, DOI: 10.1246/bcsj.60.667.

(35) Nising, C. F.; Bräse, S. The oxa-Michael reaction: from recent developments to applications in natural product synthesis. *Chem. Soc. Rev.* **2008**, *37*, 1218–1228, DOI: 10.1039/b718357g.

(36) Blankenburg, J.; Wagner, M.; Frey, H. Well-Defined Multi-Amino-Functional and Stimuli-Responsive Poly(propylene oxide) by Crown Ether Assisted Anionic Ring-Opening Polymerization. *Macromolecules* **2017**, *50*, 8885–8893, DOI: 10.1021/acs.macromol.7b01324.

(37) Rieger, E.; Blankenburg, J.; Grune, E.; Wagner, M.; Landfester, K.; Wurm, F. R. Controlling the Polymer Microstructure in Anionic Polymerization by Compartmentalization. *Angew. Chem. Int. Ed. Engl.* **2018**, *57*, 2483–2487, DOI: 10.1002/anie.201710417.

(38) Wall, F. T. The Structure of Vinyl Copolymers. *J. Am. Chem. Soc.* **1941**, *63*, 1862–1866, DOI: 10.1021/ja01852a016.

(39) Jaacks, V. A novel method of determination of reactivity ratios in binary and ternary copolymerizations. *Makromol. Chem.* **1972**, *161*, 161–172, DOI: 10.1002/macp.1972.021610110.

(40) Meyer, V. E.; Lowry, G. G. Integral and differential binary copolymerization equations. *J. Polym. Sci. A Gen. Pap.* **1965**, *3*, 2843–2851, DOI: 10.1002/pol.1965.100030811.

(41) Sun, J.; Dong, Y.; Cao, L.; Wang, X.; Wang, S.; Hu, Y. Highly efficient chemoselective deprotection of O,O-acetals and O,O-ketals catalyzed by molecular iodine in acetone. *J. Org. Chem.* **2004**, *69*, 8932–8934, DOI: 10.1021/jo0486239.

(42) Büttner, F. Über β-Methoxybutyraldehyd und α-Methylolcrotonaldehyd. II. Mitteilung über den Aufbau des Isoprenskeletts aus Crotonaldehyd und Formaldehyd. *Ann. Chem. Pharm.* **1953**, *583*, 184–190, DOI: 10.1002/jlac.19535830113.

A2. Ketone Functionalized Aliphatic Polycarbonates Based on Carbon Dioxide

Markus Scharfenberg[1]*, Kamil Maciol*[1]*, Holger Frey*[1,*]

[1] Institute of Organic Chemistry, Organic and Macromolecular Chemistry, Duesbergweg 10-14, Johannes Gutenberg University Mainz, 55128 Mainz, Germany

*E-Mail: hfrey@uni-mainz.de

Unpublished results.

The Supporting Information is given in the PhD thesis of Markus Scharfenberg.

ABSTRACT

Well-defined poly((ketone dioxolane glycidyl ether)-*co*-(propylene) carbonate) (P(KDGEC-*co*-PC) gradient terpolymers, with adjustable ketone dioxolane glycidyl ether (KDGE) content in the range of 2 – 100%, are prepared using (*R*,*R*)-(salcy)-Co(III)Cl as catalyst in a solvent-free synthesis, based directly on carbon dioxide and tailored epoxides. After cleavage of the acid-labile ketal protecting groups, a novel aliphatic polycarbonate is obtained (poly((ketone glycidyl ether)-*co*-(propylene) carbonate) (P(KGEC-*co*-PC)). The materials are comprehensively investigated by various NMR spectroscopy methods, SEC, DSC and TGA. The polycarbonates have molecular weights up to $14,200\ \text{g·mol}^{-1}$ with moderate size distributions of 1.11 – 1.55. Glass transition temperatures between 31 °C and –14 °C represents the high amorphous character. Thermal degradation studies reflect the huge stability effect of the glycidyl ethers. The free ketones were investigated with respect to their successful addressability with carboxylic acid hydrazides.

TABLE OF CONTENTS GRAPHICS
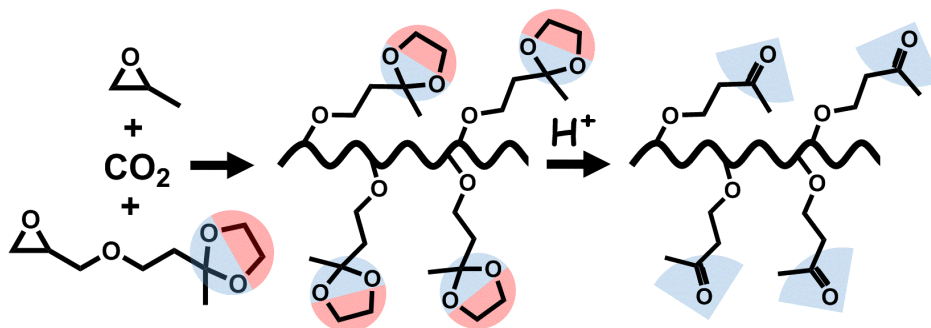
INTRODUCTION

Carbon dioxide is non-toxic, non-flammable, economical and easily acquirable in industrial scale in high purity. It can be used as C_1 feedstock in the organic chemistry. Due to its stability and low reactivity its usage is limited.[1,2] Since the discovery of the immortal CO_2/epoxide polymerization by Inoue *et al.* in 1969 aliphatic polycarbonates directly based on carbon dioxide and epoxides are producible.[3,4] Aliphatic polycarbonates are biocompatible and biodegradable. The most known polycarbonates made from CO_2 are poly(propylene oxide) (PO) and poly(cyclohexene oxide) (CHO). Important applications of aliphatic polycarbonates in general are ceramic binders, coatings, packing materials, adhesives and their use in the biomedical area, due to their biodegradability to non-toxic substances.[5,6] Therefore, aliphatic polycarbonates could be ideal systems for drug delivery applications.

However, their scope of application is limited, because of their low degree of functiona-lization.[7,8] This limitation can be solved by incorporation of functional groups via tailored epoxides.[9–13] Furthermore, the range of functional groups can be increased drastically by polymer analogous conversions, which is a powerful synthetic tool in the polymer chemistry.[14,15] Ketones and aldehydes are an important functional group for covalent attachment in a post polymerization reactions. Due to their high reactivity, many different successful modifications with molecules, e.g. drugs and others, are possible.[16–22] However, ketone or aldehyde functional aliphatic polycarbonates are rare in the literature. More precisely, only aldehydes are existing in the side chains using the polymerization of six membered cyclic carbonates.[21,22] Zelikin *et al.* developed a synthesis of aliphatic polycarbonates based on six membered cyclic carbonates with ketones in the backbone.[23] The ketone groups are protected by methyl ketals during the polymerization and are deprotected subsequently.[23–26] The addressing is also possible in the backbone.[23,27,28] To the best of our knowledge, aliphatic polycarbonates directly based on carbon dioxide and epoxides, functionalized with aldehydes or ketones, are unknown in literature so far.

Here we synthesized novel, aliphatic ketone functionalized polycarbonates in a solvent-free polymerization of carbon dioxide and KDGE (ketone dioxolane glycidyl ether) as a protected ketone-functional glycidyl ether (Figure 1). Furthermore, PO was used to tailor the thermal behavior, the thermal stability and the degree of functionalization. In addition to that, com-prehensive deprotection studies in acidic solution were done without any degradation of the acid-labile polycarbonate backbone. The free ketones groups were addressed with benzyl hydrazide in a proof of principle study.

Figure 1. Synthesis of P(KDGEC-*co*-PC) based on ketone dioxolane glycidyl ether, propylene oxide and carbon dioxide and concluding acid cleavage of the dioxolane protecting group to obtain P(KGEC-*co*-PC).

EXPERIMENTAL SECTION

Materials, instrumentation and further synthetic procedures are described in the Supporting Information.

Synthesis of P(KDGEC-*co*-PC). *General procedure:* KDGE and PO were distilled over CaH_2 under reduced pressure prior to use. A 100 mL Roth autoclave was dried under vacuum at 40 °C for 24 h. Propylene oxide (0.74 mL, 10.6 mmol), KDGE (0.4 mL, 2.3 mmol), (*R,R*)-(salcy)-Co(III)Cl (6.8 mg, 0.011 mmol) and [PPN]Cl (6.1 mg, 0.011 mmol) were mixed with a stir bar inside the autoclave under inert gas atmosphere. The mixture was stirred under CO_2 pressure of 50 bar at 30 °C for 23 h. The crude product was dissolved in 8 mL benzene and was washed with 2 mL aqueous 5% HCl solution. Before separation, 2 mL brine were added. The organic layer was separated and precipitated in cold methanol three times. The colorless product was collected by centrifugation and dried under reduced pressure; yield 78%. ^{1}H NMR (CDCl$_3$, 400 MHz): δ (ppm) = 4.99 – 4.84 (CH backbone), 4.23 – 3.97 (CH$_2$ backbone), 3.88 – 3.76 (OC*H*$_2$C*H*$_2$O), 3.57 – 3.41 (C*H*$_2$OC*H*$_2$), 1.88 – 1.80 (CH$_2$C*H*$_2$C), 1.30 – 1.14 (CH$_3$ PPC + PKDGEC), 1.14 – 1.08 (CH$_3$ PPC terminal unit). ^{13}C NMR (CDCl$_3$, 100 MHz): δ (ppm) = 154.43 – 154.12 (C=O), 108.85 (*C*CH$_3$), 74.39 (CH PKDGEC), 72.45 (CH PPC), 69.25 (CH$_2$ backbone PKDGEC), 69.06 (CH$_2$ backbone PPC), 68.54 (CH*C*H$_2$O), 67.67 (O*C*H$_2$CH$_2$), 64.60 (OCH$_2$*C*H$_2$O), 38.57 (OCH$_2$*C*H$_2$), 24.41 (*C*H$_3$C), 16.27 (*C*H$_3$CH).

Deprotection of P(KDGEC-*co*-PC). *General procedure:* For the Deprotection P(KDGEC-*co*-PC) (100 mg) was dissolved in 4 mL acetone and 2 mL 5% HCl/MeOH solution were added. The mixture was stirred for 15 min. The mixture was precipitated in cold methanol and the solid product was collected by centrifugation. The product P(KGEC-*co*-PC) was precipitated three times and dried under reduced pressure; the deprotection was nearly quantitative. ^{1}H NMR (CDCl$_3$, 400 MHz): δ (ppm) = 5.03 – 4.91 (CH backbone), 4.42 – 4.03 (CH$_2$ backbone), 3.72 – 3.65 (OC*H*$_2$CH$_2$), 3.63 – 3.56 (CHC*H*$_2$O), 2.67 – 2.60 (OCH$_2$C*H*$_2$), 2.13 (C*H*$_3$C=O), 1.32 – 1.26 (CH$_3$ PPC), 1.19 – 1.15 (CH$_3$ PPC terminal unit). ^{13}C NMR (CDCl$_3$, 100 MHz): δ (ppm) = 206.81 (CH$_3$*C*=O), 154.27 (O*C*=O), 74.24 (CH backbone PKGEC), 72.42 (CH backbone PPC), 69.05 (CH$_2$ backbone PPC), 68.77 (CH*C*H$_2$O), 66.55 (O*C*H$_2$CH$_2$), 65.91 (CH$_2$ backbone PKGEC), 43.46 (OCH$_2$*C*H$_2$), 30.53 (*C*H$_3$C), 16.24 (*C*H$_3$CH).

Functionalization with Benzyl hydrazide. The functionalization was done according to Yang *et al.*.[18] For the functionalization P(KGEC$_{15\%}$-*co*-PC$_{85\%}$) (100 mg) (Table 1, sample 4), benzyl hydrazide (37.8 mg) and DMF (2 mL) were mixed with a stir bar overnight. Then the mixture

was heated up to 60 °C for 1 h. The solution was precipitated two times in cold methanol, collected by centrifugation and dried under reduced pressure over night. ^{1}H NMR (CD$_2$Cl$_2$, 400 MHz): δ (ppm) = 7.86 – 7.74 (arom. *o*-H), 7.58 – 7.39 (arom. *m/p*-H), 5.09 – 4.87 (CH backbone), 4.44 – 3.97 (CH$_2$ backbone), 3.84 – 3.65 (OC*H$_2$*CH$_2$), 3.63 – 3.54 (CHC*H$_2$*O), 2.71 – 2.54 (OCH$_2$C*H$_2$*), 2.19 – 2.03 (C*H$_3$*C=N), 1.41 – 1.20 (CH$_3$ PPC), 1.19 – 1.10 (CH$_3$ PPC terminal unit).

RESULTS AND DISCUSSION

A. Synthesis and Characterization

In the current work, the one-pot synthesis of well-defined aliphatic polycarbonates is described. The incorporation of ketone groups in the side chains after deprotection is reported. To the best of our knowledge, this is the first time that ketones are incorporated in an aliphatic polycarbonate directly using carbon dioxide and epoxides via immortal CO_2/epoxide polymerization. The catalyst system (*R,R*)-(salcy)-Co(III)Cl and bis(triphenylphosphine)iminium chloride ([PPN]Cl) was chosen because of the alternating incorporation of CO_2 and epoxide, and very narrow size-distributions.[29] The protected ketone functional epoxide is ketone dioxolane glycidyl ether (KDGE) and was developed in our group.[16] Its characterization data are in the Supporting Information (Figure S2–3). Beside KDGE, PO was chosen, because of being a standard monomer for the polymerization with carbon dioxide and the described catalyst system, and its absence of functional groups.[2,29,30] Furthermore, the comonomer PO and its aliphatic polycarbonates are well known and well investigated.[31–33] By varying the ratio of KDGE and PO, the number of protected ketone groups was adjustable.
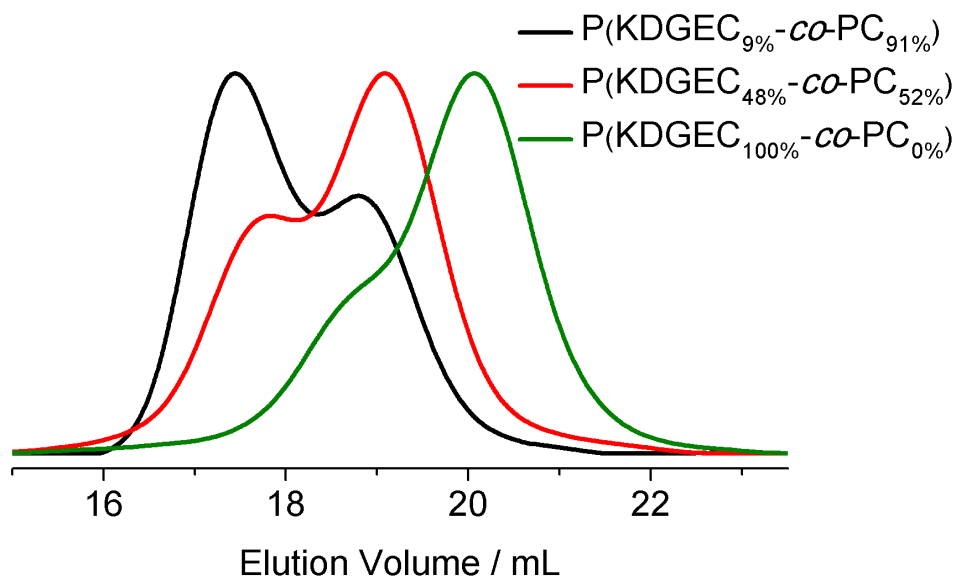
Figure 2. SEC results of representative P(KDGEC-*co*-PC) samples (Table 1, samples 3, 8 and 9) using DMF as eluent and PEG calibration.

All reactions were performed under 50 bar CO_2 pressure for 23 h at 30 °C in a solvent-free one-pot synthesis. Using FT-IR measurements the existence of aliphatic polycarbonates and the cyclic side product could be determined using the carbonyl stretch vibrations at 1798 cm^{-1} (cyclic carbonate) and 1747 cm^{-1} (linear carbonate) (Figure S4). The crude polymer could be

purificated by precipitation. A colorless product was received (Figure S5). These polymers are soluble in common organic solvents like acetone, acetonitrile, methylene chloride, chloroform, THF, DMSO, DMF or benzene. They are insoluble in polar solvents like water, methanol or ethanol and nonpolar solvents like diethyl ether or pentane. Molecular weights between 4,000 g·mol^{-1} and 14,200 g·mol^{-1} determined by SEC were obtained. The polymers have moderate size distributions of 1.22 – 1.47 and are bimodal (Figure 2 and Figure S6). A bimodal distribution is typical for this kind of polymerization and is already described by several groups.[29,34–37] The comparatively low molecular weights using 100% glycidyl ether as epoxide monomer are according to the literature.[9] Table 1 summarizes the SEC results and the composition of the prepared polycarbonates. The composition was calculated using ^{1}H NMR spectroscopy.

Table 1. Overview of all characterization data for all P(KDGEC-*co*-PPC) copolymers.

Sample	Composition [a]	M_n / g mol^{-1} [b]	Đ [b]
1	PPC	9,400	1.26
2	P(KDGEC$_{2\%}$-*co*-PC$_{98\%}$)	14,200	1.29
3	P(KDGEC$_{9\%}$-*co*-PC$_{91\%}$)	9,700	1.24
4	P(KDGEC$_{15\%}$-*co*-PC$_{85\%}$)	10,600	1.35
5	P(KDGEC$_{22\%}$-*co*-PC$_{78\%}$)	10,300	1.47
6	P(KDGEC$_{26\%}$-*co*-PC$_{74\%}$)	9,700	1.36
7	P(KDGEC$_{39\%}$-*co*-PC$_{61\%}$)	5,700	1.29
8	P(KDGEC$_{48\%}$-*co*-PC$_{52\%}$)	7,300	1.31
9	PKDGEC	4,500	1.22

[a] Terminology: Indices represent the percent of the respective repeating unit (rounded to integer), determined by ^{1}H NMR spectroscopy, [b] determined by SEC in DMF calibrated with a PEG standard.

The samples were comprehensively investigated with ^{1}H, ^{13}C and 2D NMR spectroscopy (Figure 3 and Figure S7–10). The incorporation of ether-defects can be excluded, because of the absence of further signals around 3.0 ppm in the ^{1}H NMR spectrum. Therefore, an alternating incorporation of epoxides and carbon dioxide can be proven by ^{1}H NMR. Besides the signals of the polycarbonate backbone at 4.99 – 4.84 ppm (methine group (i + j)) and

4.23 – 3.97 ppm (methylene group (g + h)) the signals of the KDGEC side chain are clearly visible. The signal of the protecting group appears at 3.88 – 3.76 ppm (f) and the signal of the methylene group at the ketal shifts to 1.88 – 1.80 ppm (c). The shifts of the methylene units at the ether group appear at 3.57 – 3.41 ppm (d + e). Both methyl groups have signals at 1.30 – 1.14 ppm (a + b). ^{13}C and 2D NMR spectroscopy also confirm the successful synthesis of P(KDGEC-*co*-PC) polymers. The carbonate signal at 154.43 – 154.12 ppm is clearly detectable. The distribution of KDGEC and PC units in the polycarbonates were also investigated using ^{1}H NMR spectroscopy. Several polymerizations were performed using the same reaction mixture (KDGE:PO, 1:9), but were stopped after different reaction times. In the first two hours, the incorporation of KDGE is much higher than expected (up to 42% instead of 10%) (Figure S11). However, after 23 h only 9% KDGEC was incorporated. The microstructure of the obtained aliphatic polycarbonates is a clear gradient with a perfect alternation of epoxide and carbon dioxide.
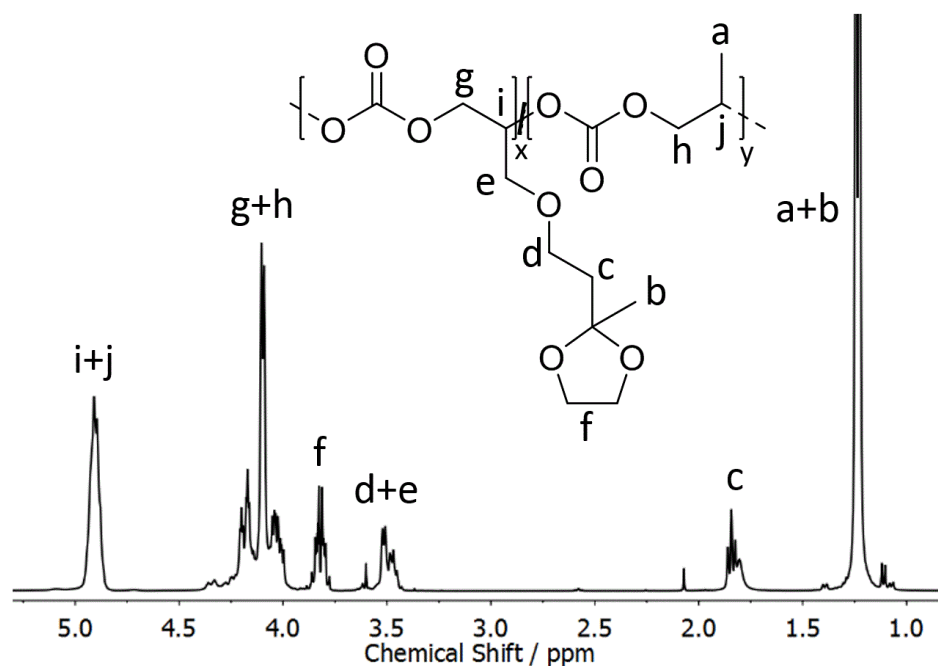
Figure 3. ^{1}H NMR spectrum of P(KDGEC$_{9\%}$-*co*-PC$_{91\%}$) (Table 1, sample 3) (400 MHz, CDCl$_3$).
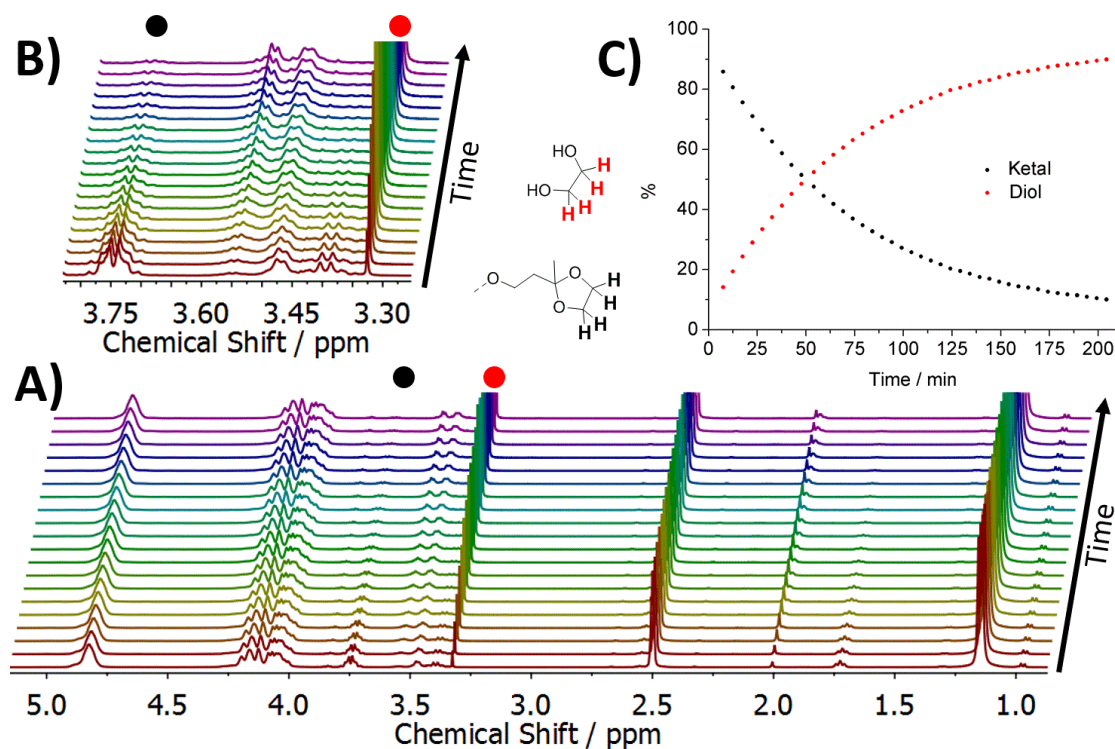
Figure 4. Online ^{1}H NMR deprotection study of P(KDGEC$_{9\%}$-*co*-PC$_{91\%}$) (Table 1, sample 3) with 2.3% DCl in DMSO-d$_6$ (400 MHz). A) Overlay of spectra of the ^{1}H NMR kinetic study. B) Zoom in, showing the decrease of the ketal signal (black dot) and the increase of the diol signal (red dot). C) Comparison of the protection group ketal (black) and the cleaved diol (red) depending on the reaction time.

For deprotection of the ketone group a work up under weak acidic conditions was performed. A detailed investigation of this step is important because of the acid-labile carbonate backbone structure. Figure 4A shows the online ^{1}H NMR spectroscopy study of the deprotection. The sample was measured each 5 min after a starting period of 7 min. A zoom in (B) shows the decreasing of the protecting group (black dot) and the increasing of the diol group (red dot) more detailed. A half-life period ($t_{1/2}$) of 50 min in DMSO-d$_6$ was calculated (Figure 4C). The reaction slows down with conversion. The intensity of both backbone signals do not change during the whole reaction period. Furthermore, no signals of cyclic carbonates appears during the reaction. This indicates that no depolymerization of the backbone occurs.
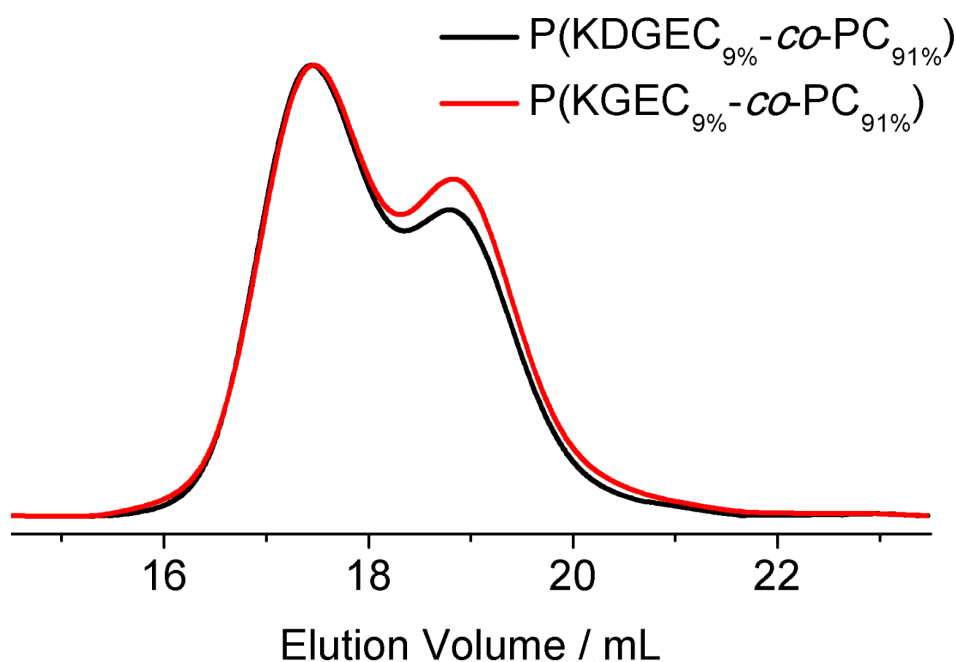
Figure 5. SEC traces of P(KDGEC$_{9\%}$-*co*-PC$_{91\%}$) (Table 1, sample 3) in comparison with P(KGEC$_{9\%}$-*co*-PC$_{91\%}$) (Table S1, sample 3) using DMF as eluent and PEG calibration.

A comprehensive investigation of the deprotected ketone functional polycarbonates (P(KGEC-*co*-PC)) was performed using NMR spectroscopy and is shown in the Supporting Information (Figure S12–16). Due to deprotection, a clear shift of the methyl group`s signal to 2.13 ppm is detectable. FT-IR measurements give a further hint for the successful deprotection by appearing of a new carbonyl signal (Figure S17). The SEC results of the deprotected polycarbonates are a further proof for a stable backbone (Figure S18). Hydrolysis of the carbonate groups is a second degradation possibility besides depolymerization. Hydrolysis increases the size distribution to higher elution volumes. Figure 5 illustrates the SEC traces of a protected and unprotected sample. Both have a similar distribution. The acidic conditions do not result neither in depolymerization nor in hydrolysis of the polycarbonate backbone.

All characterization data of all deprotected polycarbonates are summarized in Table S1. Polymers with molecular weights between 3,100 g·mol^{-1} and 14,000 g·mol^{-1} were prepared. Moderate narrow size distributions of 1.11 to 1.55 were obtained. After purification, the ketone functional polycarbonates are colorless and solid materials (Figure S5). The solubility in various solvents is comparable to the protected pendants.

B. Thermal Properties and Stability

The thermal behavior of the protected and deprotected ketone functional polycarbonates were studied using differential scanning calorimetry (DSC). The DSC results are summarized in Table 2 and the DSC curves are shown in the Supporting Information (Figure S19–20). As expected, no melting point was detectable. This aliphatic polycarbonates have a high amorphous character.

Table 2. Overview of the glass transition temperatures (left: protected; right: unprotected) and the thermal degradation temperatures (protected).

Sample	Composition [a]	T_g / °C [b]		T_d / °C [c]
1	PPC	31		225
2	P(KGEC$_{2\%}$-co-PC$_{98\%}$)	16	28	249
3	P(KGEC$_{9\%}$-co-PC$_{91\%}$)	14	26	268
4	P(KGEC$_{15\%}$-co-PC$_{85\%}$)	11	20	269
5	P(KGEC$_{22\%}$-co-PC$_{78\%}$)	14	19	270
6	P(KGEC$_{26\%}$-co-PC$_{74\%}$)	10	17	270
7	P(KGEC$_{39\%}$-co-PC$_{61\%}$)	2	1	266
8	P(KGEC$_{48\%}$-co-PC$_{52\%}$)	3	5	274
9	PKGEC	-2	-14	291

[a] Terminology: Indices represent the percent of the respective repeating unit (rounded to integer), determined by ^{1}H NMR spectroscopy, [b] determined by differential scanning calorimetry (DSC) with a heating rate of 10 K·min^{-1}; left: protected; right: unprotected, [c] determined by thermogravimetric analysis (TGA) with a heating rate of 10 K·min^{-1}.

In Figure 6 the glass transition temperatures of P(KDGEC-co-PC) (black) and P(KGEC-co-PC) (red) copolymers are plotted against the percent of KDGEC and KGEC units, respectively. The T_g values of the protected polymers decreases with increasing amount of KDGEC units from 31 °C (0% KDGEC) down to –2 °C (100% KDGEC). The gradient slows down up to 100% KDGEC. Also, the T_g of the deprotected polymers decreases with higher KGE content from 31 °C (0%) to –14 °C (100%). The gradient is steeper compared to the gradient of the protected counterparts, and regardless of the composition. The decreasing in both materials can be explained by the loss of dipole-dipole interactions of the polycarbonate backbones because of

bulky side chains. The higher glass transition temperatures of KGE containing polycarbonates compared to their protected counterparts up to 50% KGEC units illustrates the rise of dipole-dipole interactions of the ketone groups. Obviously, the effect of additional dipole-dipole interactions is less pronounced compared to the effect of bulky side chain group over 50% KGEC. Due to the bulky side chain group of the ketone is less bulky compared to the ketal, the T_g of PKDGEC homopolymer is higher than PKGEC homopolymer. Furthermore, it has to be mentioned that the T_gs are additionally influenced by the molecular weight.[38]
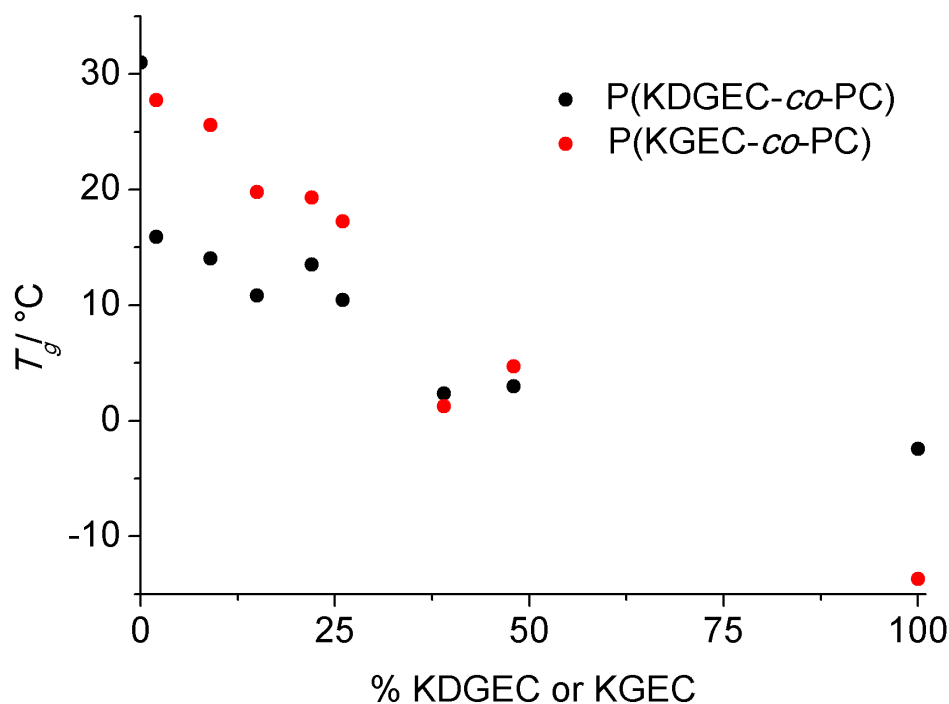
Figure 6. Glass transition temperatures (T_g) of all P(KDGEC-*co*-PC) (black) and P(KGEC-*co*-PC) (red) samples (Table 2, samples 1–9) depending on the amount of KDGEC or KGEC units.

Beside the thermal behavior also the thermal degradation was studied. Table 2 gives an overview of the degradation temperatures (T_d) of all KDGEC samples. The degradation temperature under nitrogen increases from 225 °C to 291 °C with increasing KDGE content. Representative TGA curves are shown in Figure S21 and the T_ds are plotted vs. percent of KDGEC units in Figure S22. The T_d has a steep rise with low amount of KDGE (225 °C for 0% until 268 °C for 9%), followed by a less steep increase until 291 °C for 100%. An increase was expected. It is already well known that the thermal degradation of aliphatic 1,2-polycarbonates is depending on the stiffness, the length and flexibility of the side chain, intermolecular dipole interactions, degree of alternation and the number of repeating units.[39,40] In the current work the length and flexibility of the side chains play the most important role. The thermal degradation of short polycarbonates (around 26,900 g·mol^{-1}) is dominated by deploymerization via backbiting of the OH-endgroup.[39] The formation of five membered rings on this

way is suppressed by bulky side chains like KDGEC units. Obviously, a small amount is already essential. Increasing thermal stability was also observed by Gu *et al.* for glycidyl ether containing aliphatic polycarbonates.[11]

C. Functionalization with Benzyl Hydrazide

Aliphatic polycarbonates based on carbon dioxide and tailored epoxides are an interesting research field for many applications, e.g. in surface coatings or biomedical purposes, because of their biocompatibility and biodegradability. However, established polycarbonates like poly(propylene carbonate) or poly(cyclohexane carbonate) are unfunctionalized and therefore limited in their use. Functional groups can be used as smart points of attack to change several properties of the polymer.[9,13–15,41,42] The addressability of ketone groups was confirmed by functionalization with benzyl hydrazide as a model compound. $P(KGEC_{15\%}$-*co*-$PC_{85\%})$ (Table S1, sample 4) was dissolved in DMF with benzyl hydrazide and stirred overnight at room temperature. Purification was done by precipitation in cold methanol after 1 h at 60 °C. The conversion was proved by ^{1}H NMR spectroscopy and SEC. Figure S23 shows the ^{1}H NMR spectrum of functionalized $P(KGEC_{15\%}$-*co*-$PC_{85\%})$ in methylene chloride. Additional signals of the aromatic group appears at 7.80 ppm and 7.49 ppm. Furthermore, a shift of the adjacent methyl group is visible (1.97 ppm). Figure S24 illustrates the SEC elugram of the same sample based on both RI and UV detector. Usually aliphatic polycarbonates are not UV active. However, due to the attached phenyl groups, the multifunctional polycarbonate generates an UV signal. It is obviously that every single polymer chain is addressed, due to the overlapping of the RI and the UV signals detected elugram. The ^{1}H NMR spectroscopy and the SEC measurement together verify addressing of the ketone groups in the side chains. Using this method many different systems, for instance dyes or drugs, could be linked to the polycarbonates in a smooth and gentle way.

CONCLUSION

Ketone functional aliphatic polycarbonates were synthesized via immortal CO_2/epoxide polymerization. To the best of our knowledge, this is the first time that ketone groups were incorporated in aliphatic polycarbonates formed directly from carbon dioxide and tailored epoxides. First, ketal functionalized polycarbonates were prepared using carbon dioxide, propylene oxide and ketone dioxolane glycidyl ether in a solvent-free one-pot procedure. The polymers had a perfectly alternating structure of epoxide and carbon dioxide, and a gradient regarding the used epoxides. The amount of ketal side chains was adjusted by varying the comonomer ratio of PO and KDGE. Polymers with molecular weights between 4,000 $g \cdot mol^{-1}$ and 14,200 $g \cdot mol^{-1}$ and moderate size distributions of 1.22 – 1.47 were obtained. The incorporation of glycidyl ethers increased the thermal stability significantly. In the second step, the ketal protecting group was removed using slightly acidic conditions to obtain the free ketone groups. Detailed deprotection kinetics proofs the successful conversion without degradation of the acid-labile backbone. The protected and unprotected polycarbonates were characterized comprehensively by ^1H, ^{13}C and various 2D NMR spectroscopy techniques, SEC and FT-IR measurements. Furthermore, their thermal behavior was studied regarding the comonomer amount and the functional group. The glass transition temperatures were adjusted between 31 °C and –14 °C. In a proof of principle study, the ketone groups were addressed successfully by benzyl hydrazide. This general method opens the pathway for attachment of many different dyes, drugs and other molecules to the biodegradable polycarbonates. The additional facile deprotection in smooth acidic solution expand the scope of application of aliphatic polycarbonates in the area of surface coatings, biomedicine purposes and drug delivery.

REFERENCES

(1) Herzberger, J.; Niederer, K.; Pohlit, H.; Seiwert, J.; Worm, M.; Wurm, F. R.; Frey, H. Polymerization of Ethylene Oxide, Propylene Oxide, and Other Alkylene Oxides: Synthesis, Novel Polymer Architectures, and Bioconjugation. *Chem. Rev.* **2016**, *116*, 2170–2243, DOI: 10.1021/acs.chemrev.5b00441.

(2) Hay, J.N.; Sabir, M.; Steven, R.L.T. Crystallization kinetics of high polymers. Polyethylene oxide—Part I. *Polymer* **1969**, *10*, 187–202, DOI: 10.1016/0032-3861(69)90030-5.

(3) Wetton, R. E.; Allen, G. The dynamic mechanical properties of some polyethers. *Polymer* **1966**, *7*, 331–365, DOI: 10.1016/0032-3861(66)90028-0.

(4) Bailey, F. E.; Koleske, J. V. *Poly(ethylene oxide)*; Academic Press: New York, 1976.

(5) Fruijtier-Pölloth, C. Safety assessment on polyethylene glycols (PEGs) and their derivatives as used in cosmetic products. *Toxicology* **2005**, *214*, 1–38, DOI: 10.1016/j.tox.2005.06.001.

(6) Dingels, C.; Schömer, M.; Frey, H. Die vielen Gesichter des Poly(ethylenglykol)s. *Chem. unserer Zeit* **2011**, *45*, 338–349, DOI: 10.1002/ciuz.201100551.

(7) Abuchowski, A.; van Es, T.; Palczuk, N. C.; Davis, F. F. Alteration of immunological properties of bovine serum albumin by covalent attachment of polyethylene glycol. *J. Biol. Chem.* **1977**, *252*, 3578–3581.

(8) Abuchowski, A.; McCoy, J. R.; Palczuk, N. C.; van Es, T.; Davis, F. F. Effect of covalent attachment of polyethylene glycol on immunogenicity and circulating life of bovine liver catalase. *J. Biol. Chem.* **1977**, *252*, 3582–3586.

(9) Pfister, D.; Morbidelli, M. Process for protein PEGylation. *J. Control. Release* **2014**, *180*, 134–149, DOI: 10.1016/j.jconrel.2014.02.002.

(10) *Die Pharmaindustrie: Einblick - Durchblick - Perspektiven;* Fischer, D.; Breitenbach, J., Eds., 4. Auflage; Springer Spektrum: Berlin, 2017.

(11) Almeida, M.; Magalhães, M.; Veiga, F.; Figueiras, A. Poloxamers, poloxamines and polymeric micelles: Definition, structure and therapeutic applications in cancer. *J. Polym. Res.* **2018**, *25*, 248, DOI: 10.1007/s10965-017-1426-x.

(12) Pitto-Barry, A.; Barry, N. P. E. Pluronic® block-copolymers in medicine: from chemical and biological versatility to rationalisation and clinical advances. *Polym. Chem.* **2014**, *5*, 3291–3297, DOI: 10.1039/C4PY00039K.

(13) Bodratti, A. M.; Alexandridis, P. Formulation of Poloxamers for Drug Delivery. *J. Funct. Biomater.* **2018**, *9,* DOI: 10.3390/jfb9010011.

(14) Dumortier, G.; Grossiord, J. L.; Agnely, F.; Chaumeil, J. C. A review of poloxamer 407 pharmaceutical and pharmacological characteristics. *Pharm. Res.* **2006**, *23*, 2709–2728, DOI: 10.1007/s11095-006-9104-4.

(15) Lee, S. M. *Dictionary of composite materials technology*; Technomic Publ: Lancaster, 1989.

(16) Thompson, M. S.; Vadala, T. P.; Vadala, M. L.; Lin, Y.; Riffle, J. S. Synthesis and applications of heterobifunctional poly(ethylene oxide) oligomers. *Polymer* **2008**, *49*, 345–373, DOI: 10.1016/j.polymer.2007.10.029.

(17) Louai, A.; Sarazin, D.; Pollet, G.; François, J.; Moreaux, F. Properties of ethylene oxide-propylene oxide statistical copolymers in aqueous solution. *Polymer* **1991**, *32*, 703–712, DOI: 10.1016/0032-3861(91)90484-Z.

(18) Müller, S. S.; Moers, C.; Frey, H. A Challenging Comonomer Pair: Copolymerization of Ethylene Oxide and Glycidyl Methyl Ether to Thermoresponsive Polyethers. *Macromolecules* **2014**, *47*, 5492–5500, DOI: 10.1021/ma501280k.

(19) Tonhauser, C.; Alkan, A.; Schömer, M.; Dingels, C.; Ritz, S.; Mailänder, V.; Frey, H.; Wurm, F. R. Ferrocenyl Glycidyl Ether: A Versatile Ferrocene Monomer for Copolymerization with Ethylene Oxide to Water-Soluble, Thermoresponsive Copolymers. *Macromolecules* **2013**, *46*, 647–655, DOI: 10.1021/ma302241w.

(20) Alkan, A.; Thomi, L.; Gleede, T.; Wurm, F. R. Vinyl ferrocenyl glycidyl ether: An unprotected orthogonal ferrocene monomer for anionic and radical polymerization. *Polym. Chem.* **2015**, *6*, 3617–3624, DOI: 10.1039/C5PY00404G.

(21) Song, J.; Palanikumar, L.; Choi, Y.; Kim, I.; Heo, T.-y.; Ahn, E.; Choi, S.-H.; Lee, E.; Shibasaki, Y.; Ryu, J.-H. *et al.* The power of the ring: a pH-responsive hydrophobic epoxide monomer for superior micelle stability. *Polym. Chem.* **2017**, *8*, 7119–7132, DOI: 10.1039/C7PY01613A.

(22) Herzberger, J.; Kurzbach, D.; Werre, M.; Fischer, K.; Hinderberger, D.; Frey, H. Stimuli-Responsive Tertiary Amine Functional PEGs Based on N,N -Dialkylglycidylamines. *Macromolecules* **2014**, *47*, 7679–7690, DOI: 10.1021/ma501367b.

(23) Aresta, M.; Dibenedetto, A. Utilisation of CO2 as a chemical feedstock: Opportunities and challenges. *Dalton Trans.* **2007**, *28*, 2975–2992, DOI: 10.1039/b700658f.

(24) Sakakura, T.; Choi, J.-C.; Yasuda, H. Transformation of carbon dioxide. *Chem. Rev.* **2007**, *107*, 2365–2387, DOI: 10.1021/cr068357u.

(25) Inoue, S.; Koinuma, H.; Tsuruta, T. Copolymerization of Carbon Dioxide and Epoxide with Organometallic Compounds. *Macromol. Chem. Phys.* **1969**, *130*, 210–220, DOI: 10.1002/macp.1969.021300112.

(26) Inoue, S. Copolymerization of Carbon Dioxide and Epoxide: Functionality of the Copolymer. *J. Macromol. Sci., Pure Appl. Chem.* **1979**, *13*, 651–664, DOI: 10.1080/00222337908056679.

(27) Zhu, K. J.; Hendren, R. W.; Jensen, K.; Pitt, C. G. Synthesis, Properties, and Biodegradation of Poly(1,3-trimethylene carbonate). *Macromolecules* **1991**, *24*, 1736–1740, DOI: 10.1021/ma00008a008.

(28) Yan, H.; Cannon, W.R.; Shanefield, D. J. Thermal decomposition behaviour of poly(propylene carbonate). *Ceram. Int.* **1998**, *24*, 433–439, DOI: 10.1016/S0272-8842(97)00032-1.

(29) Welle, A.; Kröger, M.; Döring, M.; Niederer, K.; Pindel, E.; Chronakis, I. S. Electrospun aliphatic polycarbonates as tailored tissue scaffold materials. *Biomaterials* **2007**, *28*, 2211–2219, DOI: 10.1016/j.biomaterials.2007.01.024.

(30) Rieger, B.; Amann, M. *Synthetic biodegradable polymers*; Advances in polymer science 245; Springer: Berlin, 2012.

(31) Hilf, J.; Scharfenberg, M.; Poon, J.; Moers, C.; Frey, H. Aliphatic Polycarbonates Based on Carbon Dioxide, Furfuryl Glycidyl Ether, and Glycidyl Methyl Ether: Reversible Functionalization and Cross-Linking. *Macromol. Rapid Commun.* **2014**, *36*, 174–179, DOI: 10.1002/marc.201400504.

(32) Geschwind, J.; Frey, H. Poly(1,2-glycerol carbonate): A Fundamental Polymer Structure Synthesized from CO2 and Glycidyl Ethers. *Macromolecules* **2013**, *46*, 3280–3287, DOI: 10.1021/ma400090m.

(33) Gu, L.; Qin, Y.; Gao, Y.; Wang, X.; Wang, F. Hydrophilic CO2 -based biodegradable polycarbonates: Synthesis and rapid thermo-responsive behavior. *J. Polym. Sci. Part A: Polym. Chem.* **2013**, *51*, 2834–2840, DOI: 10.1002/pola.26672.

(34) Wu, G.-P.; Xu, P.-X.; Lu, X.-B.; Zu, Y.-P.; Wei, S.-H.; Ren, W.-M.; Darensbourg, D. J. Crystalline CO2 Copolymer from Epichlorohydrin via Co(III)-Complex-Mediated Stereospecific Polymerization. *Macromolecules* **2013**, *46*, 2128–2133, DOI: 10.1021/ma400252h.

(35) Tsai, F.-T.; Wang, Y.; Darensbourg, D. J. Environmentally Benign CO2-Based Copolymers: Degradable Polycarbonates Derived from Dihydroxybutyric Acid and Their Platinum-Polymer Conjugates. *J. Am. Chem. Soc.* **2016**, *138*, 4626–4633, DOI: 10.1021/jacs.6b01327.

(36) Hauenstein, O.; Agarwal, S.; Greiner, A. Bio-based polycarbonate as synthetic toolbox. *Nat. Commun.* **2016**, *7*, 11862, DOI: 10.1038/ncomms11862.

(37) Deng, K.; Wang, S.; Ren, S.; Han, D.; Xiao, M.; Meng, Y. A Novel Single-Ion-Conducting Polymer Electrolyte Derived from CO2-Based Multifunctional Polycarbonate. *ACS Appl. Mater. Interfaces* **2016**, *8*, 33642–33648, DOI: 10.1021/acsami.6b11384.

(38) Maciol, K.; Blankenburg, J.; Frey, H. Ketone Dioxolane Glycidyl Ether (KDGE): Access to Well-Defined Ketone Functional Poly(ethylene glycol). *in preparation* **2017**.

(39) Blankenburg, J.; Maciol, K.; Hahn, C.; Frey, H. Multi Aldehyde Functional Poly(ethylene glycol) - A Versatile Platform for Post-Polymerization Modifications. *in preparation* **2017**.

(40) Yang, S. K.; Weck, M. Modular Covalent Multifunctionalization of Copolymers. *Macromolecules* **2008**, *41*, 346–351, DOI: 10.1021/ma702052k.

(41) Legros, C.; Pauw-Gillet, M.-C. de; Tam, K. C.; Lecommandoux, S.; Taton, D. Aldehyde-functional copolymers based on poly(2-oxazoline) for post-polymerization modification. *Eur. Polym. J.* **2015**, *62*, 322–330, DOI: 10.1016/j.eurpolymj.2014.08.026.

(42) Taubmann, C.; Luxenhofer, R.; Cesana, S.; Jordan, R. First aldehyde-functionalized poly(2-oxazoline)s for chemoselective ligation. *Macromol. Biosci.* **2005**, *5*, 603–612, DOI: 10.1002/mabi.200500059.

(43) Ke, X.; Coady, D. J.; Yang, C.; Engler, A. C.; Hedrick, J. L.; Yang, Y. Y. pH-sensitive polycarbonate micelles for enhanced intracellular release of anticancer drugs: A strategy to circumvent multidrug resistance. *Polym. Chem.* **2014**, *5*, 2621, DOI: 10.1039/c3py01784b.

(44) Heo, G. S.; Cho, S.; Wooley, K. L. Aldehyde-functional polycarbonates as reactive platforms. *Polym. Chem.* **2014**, *5*, 3555–3558, DOI: 10.1039/C4PY00456F.

(45) Zelikin, A. N.; Zawaneh, P. N.; Putnam, D. A functionalizable biomaterial based on dihydroxyacetone, an intermediate of glucose metabolism. *Biomacromolecules* **2006**, *7*, 3239–3244, DOI: 10.1021/bm060544e.

(46) Zawaneh, P. N.; Doody, A. M.; Zelikin, A. N.; Putnam, D. Diblock copolymers based on dihydroxyacetone and ethylene glycol: synthesis, characterization, and nanoparticle formulation. *Biomacromolecules* **2006**, *7*, 3245–3251, DOI: 10.1021/bm0605457.

(47) Weiser, J. R.; Zawaneh, P. N.; Putnam, D. Poly(carbonate-ester)s of dihydroxyacetone and lactic acid as potential biomaterials. *Biomacromolecules* **2011**, *12*, 977–986, DOI: 10.1021/bm101342p.

(48) Simon, J.; Olsson, J. V.; Kim, H.; Tenney, I. F.; Waymouth, R. M. Semicrystalline Dihydroxyacetone Copolymers Derived from Glycerol. *Macromolecules* **2012**, *45*, 9275–9281, DOI: 10.1021/ma302311h.

(49) Barrett, D. G.; Yousaf, M. N. Poly(triol α-ketoglutarate) as Biodegradable, Chemoselective, and Mechanically Tunable Elastomers. *Macromolecules* **2008**, *41*, 6347–6352, DOI: 10.1021/ma8009728.

(50) Iha, R. K.; van Horn, B. A.; Wooley, K. L. Complex, degradable polyester materials via ketoxime ether-based functionalization: Amphiphilic, multifunctional graft copolymers and their resulting solution-state aggregates. *J. Polym. Sci. Part A: Polym. Chem.* **2010**, *48*, 3553–3563, DOI: 10.1002/pola.24132.

(51) Cohen, C. T.; Chu, T.; Coates, G. W. Cobalt Catalysts for the Alternating Copolymerization of Propylene Oxide and Carbon Dioxide: Combining High Activity and Selectivity. *J. Am. Chem. Soc.* **2005**, *127*, 10869–10878, DOI: 10.1021/ja051744l.

(52) Kember, M. R.; Buchard, A.; Williams, C. K. Catalysts for CO2/epoxide copolymerisation. *Chem. Commun.* **2010**, *47*, 141–163, DOI: 10.1039/c0cc02207a.

(53) Darensbourg, D. J. Switchable catalytic processes involving the copolymerization of epoxides and carbon dioxide for the preparation of block polymers. *Inorg. Chem. Front.* **2017**, *4*, 412–419, DOI: 10.1039/C7QI00013H.

(54) Paul, S.; Zhu, Y.; Romain, C.; Brooks, R.; Saini, P. K.; Williams, C. K. Ring-opening copolymerization (ROCOP): synthesis and properties of polyesters and polycarbonates. *Chem. Commun.* **2015**, *51*, 6459–6479, DOI: 10.1039/c4cc10113h.

(55) Taherimehr, M.; Pescarmona, P. P. Green polycarbonates prepared by the copolymerization of CO2 with epoxides. *J. Appl. Polym. Sci.* **2014**, 41141(1)-41141(17), DOI: 10.1002/app.41141.

(56) Seong, J. E.; Na, S. J.; Cyriac, A.; Kim, B.-W.; Lee, B. Y. Terpolymerizations of CO2, Propylene Oxide, and Various Epoxides Using a Cobalt(III) Complex of Salen-Type Ligand Tethered by Four Quaternary Ammonium Salts. *Macromolecules* **2010**, *43*, 903–908, DOI: 10.1021/ma902162n.

(57) Anderson, C. E.; Vagin, S. I.; Xia, W.; Jin, H.; Rieger, B. Cobaltoporphyrin-Catalyzed CO2 /Epoxide Copolymerization: Selectivity Control by Molecular Design. *Macromolecules* **2012**, *45*, 6840–6849, DOI: 10.1021/ma301205g.

(58) Geschwind, J.; Frey, H. Stable, Hydroxyl Functional Polycarbonates With Glycerol Side Chains Synthesized From CO2 and Isopropylidene(glyceryl glycidyl ether). *Macromol. Rapid Commun.* **2013**, *34*, 150–155, DOI: 10.1002/marc.201200682.

(59) Darensbourg, D. J. Copolymerization of Epoxides and CO2: Polymer Chemistry for Incorporation in Undergraduate Inorganic Chemistry. *J. Chem. Educ.* **2016,** DOI: 10.1021/acs.jchemed.6b00505.

(60) Couchman, P. R. A theory of the molecular-mass dependence of glass transition temperatures for polydisperse homopolymers. *J Mater Sci* **1980**, *15*, 1680–1683, DOI: 10.1007/BF00550584.

(61) Li, X. H.; Meng, Y. Z.; Zhu, Q.; Tjong, S. C. Thermal decompostition characteristics of poly(propylene carbonate) using TG/IR and Py-GC/MS techniques. *Polym. Degrad. Stab.* **2003**, *81*, 157–165.

(62) Thorat, S. D.; Phillips, P. J.; Semenov, V.; Gakh, A. Physical properties of aliphatic polycarbonates made from CO2 and epoxides. *J. Appl. Polym. Sci.* **2003**, *89*, 1163–1176, DOI: 10.1002/app.12355.

(63) Martín, C.; Kleij, A. W. Terpolymers Derived from Limonene Oxide and Carbon Dioxide: Access to Cross-Linked Polycarbonates with Improved Thermal Properties. *Macromolecules* **2016**, *49*, 6285–6295, DOI: 10.1021/acs.macromol.6b01449.

(64) Subhani, M. A.; Köhler, B.; Gürtler, C.; Leitner, W.; Müller, T. E. Light-mediated curing of CO2-based unsaturated polyethercarbonates via thiol–ene click chemistry. *Polym. Chem.* **2016**, *7*, 4121–4126, DOI: 10.1039/C6PY00458J.

(65) Ren, J. M.; McKenzie, T. G.; Fu, Q.; Wong, E. H. H.; Xu, J.; An, Z.; Shanmugam, S.; Davis, T. P.; Boyer, C.; Qiao, G. G. Star Polymers. *Chem. Rev.* **2016**, *116*, 6743–6836, DOI: 10.1021/acs.chemrev.6b00008.

(66) Hadjichristidis, N.; Pitsikalis, M.; Iatrou, H.; Driva, P.; Sakellariou, G.; Chatzichristidi, M. Polymers with Star-Related Structures. *Polymer Science: A Comprehensive Reference*; Elsevier, 2012; pp 29–111.

(67) Knoll, K.; Nießner, N. Styrolux+ and styroflex+ - from transparent high impact polystyrene to new thermoplastic elastomers: Syntheses, applications and blends with other styrene based polymers. *Macromol. Symp.* **1998**, *132*, 231–243, DOI: 10.1002/masy.19981320122.

(68) Adhikari, R.; Michler, G. H.; Goerlitz, S.; Knoll, K. Morphology and micromechanical deformation behavior of styrene-butadiene block copolymers. III. Binary blends of asymmetric star block copolymer with general-purpose polystyrene. *J. Appl. Polym. Sci.* **2004**, *92*, 1208–1218, DOI: 10.1002/app.20119.

(69) Matmour, R.; Gnanou, Y. Synthesis of complex polymeric architectures using multilithiated carbanionic initiators—Comparison with other approaches. *Prog. Polym. Sci.* **2013**, *38*, 30–62, DOI: 10.1016/j.progpolymsci.2012.08.003.

(70) Hadjichristidis, N.; Pispas, S.; Iatrou, H.; Pitsikalis, M. Linking Chemistry and Anionic Polymerization. *COC* **2002**, *6*, 155–176, DOI: 10.2174/1385272023374463.

(71) Hadjichristidis, N.; Pitsikalis, M.; Pispas, S.; Iatrou, H. Polymers with complex architecture by living anionic polymerization. *Chem. Rev.* **2001**, *101*, 3747–3792.

(72) Hadjichristidis, N.; Iatrou, H.; Pitsikalis, M.; Mays, J. Macromolecular architectures by living and controlled/living polymerizations. *Prog. Polym. Sci.* **2006**, *31*, 1068–1132, DOI: 10.1016/j.progpolymsci.2006.07.002.

(73) Higashihara, T.; Hayashi, M.; Hirao, A. Synthesis of well-defined star-branched polymers by stepwise iterative methodology using living anionic polymerization. *Prog. Polym. Sci.* **2011**, *36*, 323–375, DOI: 10.1016/j.progpolymsci.2010.08.001.

(74) Booth, C. Polymer fractionation. A comparison of successive precipitation fractionation and precipitation chromatography. *J. Polym. Sci.* **1960**, *45*, 443–450, DOI: 10.1002/pol.1960.1204514613.

(75) Kohler, A.; Zilliox, J. G.; Rempp, P.; Polacek, J.; Koessler, I. Investigations on fractionation and polydispersity of anionically prepared star-shaped polystyrenes. *Eur. Polym. J.* **1972**, *8*, 627–639, DOI: 10.1016/0014-3057(72)90138-3.

(76) Hirao, A.; Goseki, R.; Ishizone, T. Advances in Living Anionic Polymerization: From Functional Monomers, Polymerization Systems, to Macromolecular Architectures. *Macromolecules* **2014**, *47*, 1883–1905, DOI: 10.1021/ma401175m.

(77) Hadjichristidis, N.; Guyot, A.; Fetters, L. J. Star-Branched Polymers. 1. The Synthesis of Star Polyisoprenes Using Octa- and Dodecachlorosilanes as Linking Agents. *Macromolecules* **1978**, *11*, 668–672, DOI: 10.1021/ma60064a010.

(78) Le Khac Bi; Fetters, L. J. Synthesis and properties of block copolymers. 3. Polystyrene-polydiene star block copolymers. *Macromolecules* **1976**, *9*, 732–742.

(79) Floudas, G.; Pispas, S.; Hadjichristidis, N.; Pakula, T.; Erukhimovich, I. Microphase Separation in Star Block Copolymers of Styrene and Isoprene. Theory, Experiment, and Simulation. *Macromolecules* **1996**, *29*, 4142–4154, DOI: 10.1021/ma951762v.

(80) Roovers, J.; Zhou, L. L.; Toporowski, P. M.; van der Zwan, M.; Iatrou, H.; Hadjichristidis, N. Regular star polymers with 64 and 128 arms. Models for polymeric micelles. *Macromolecules* **1993**, *26*, 4324–4331, DOI: 10.1021/ma00068a039.

(81) Pennisi, R. W.; Fetters, L. J. Preparation of asymmetric 3-arm polybutadiene and polystyrene stars. *Macromolecules* **1988**, *21*, 1094–1099, DOI: 10.1021/ma00182a041.

(82) Perny, S.; Allgaier, J.; Cho, D.; Lee, W.; Chang, T. Synthesis and Structural Analysis of an H-Shaped Polybutadiene. *Macromolecules* **2001**, *34*, 5408–5415, DOI: 10.1021/ma001608v.

(83) Frater, D. J.; Mays, J. W.; Jackson, C.; Sioula, S.; Efstradiadis, V.; Hadjichristidis, N. A kinetic study of the formation of polystyrene stars using 1,2-bis(trichlorosilyl)ethane. *J. Polym.*

Sci. B Polym. Phys. **1997**, *35*, 587–594, DOI: 10.1002/(SICI)1099-0488(199703)35:4<587:AID-POLB6>3.0.CO;2-N.

(84) Lee, H. C.; Lee, W.; Chang, T.; Yoon, J. S.; Frater, D. J.; Mays, J. W. Linking Reaction Kinetics of Star Shaped Polystyrene by Temperature Gradient Interaction Chromatography. *Macromolecules* **1998**, *31*, 4114–4119, DOI: 10.1021/ma971751x.

(85) Bi, L.-K.; Fetters, L. J. Synthesis and Properties of Block Copolymers. 3. Polystyrene-Polydiene Star Block Copolymers. *Macromolecules* **1976**, *9*, 732–742, DOI: 10.1021/ma60053a010.

(86) Fetters, L. J.; Kiss, A. D.; Pearson, D. S.; Quack, G. F.; Vitus, F. J. Rheological behavior of star-shaped polymers. *Macromolecules* **1993**, *26*, 647–654, DOI: 10.1021/ma00056a015.

(87) Burns, A. B.; Register, R. A. Strategies for the Synthesis of Well-Defined Star Polymers by Anionic Polymerization with Chlorosilane Coupling and Preservation of the Star Architecture during Catalytic Hydrogenation. *Macromolecules* **2016**, *49*, 2063–2070, DOI: 10.1021/acs.macromol.5b02764.

(88) Roovers, J.; Hadjichristidis, N.; Fetters, L. J. Analysis and dilute solution properties of 12- and 18-arm-star polystyrenes. *Macromolecules* **1983**, *16*, 214–220, DOI: 10.1021/ma00236a012.

(89) Roovers, J. E. L.; Bywater, S. Preparation and Characterization of Four-Branched Star Polystyrene. *Macromolecules* **1972**, *5*, 384–388, DOI: 10.1021/ma60028a010.

(90) Roovers, J. E. L.; Bywater, S. Preparation of Six-Branched Polystyrene. Thermodynamic and Hydrodynamic Porperties of Four- and Six-Branched Star Polystyrenes. *Macromolecules* **1974**, *7*, 443–449, DOI: 10.1021/ma60040a010.

(91) Morton, M.; Fetters, L. J.; Pett, R. A.; Meier, J. F. The Association Behavior of Polystyryllithium, Polyisoprenyllithium, and Polybutadienyllithium in Hydrocarbon Solvents. *Macromolecules* **1970**, *3*, 327–332, DOI: 10.1021/ma60015a011.

(92) Grune, E.; Johann, T.; Appold, M.; Wahlen, C.; Blankenburg, J.; Leibig, D.; Müller, A. H. E.; Gallei, M.; Frey, H. One-Step Block Copolymer Synthesis versus Sequential Monomer Addition: A Fundamental Study Reveals That One Methyl Group Makes a Difference. *Macromolecules* **2018**, *51*, 3527–3537, DOI: 10.1021/acs.macromol.8b00404.

(93) Greiner, A.; Wendorff, J. H. Electrospinning: a fascinating method for the preparation of ultrathin fibers. *Angew. Chem.* **2007**, *46*, 5670–5703, DOI: 10.1002/anie.200604646.

(94) Huang, Z.-M.; Zhang, Y.-Z.; Kotaki, M.; Ramakrishna, S. A review on polymer nanofibers by electrospinning and their applications in nanocomposites. *Composites Science and Technology* **2003**, *63*, 2223–2253, DOI: 10.1016/S0266-3538(03)00178-7.

(95) Li, D.; Xia, Y. Electrospinning of Nanofibers: Reinventing the Wheel? *Adv. Mater.* **2004**, *16*, 1151–1170, DOI: 10.1002/adma.200400719.

(96) Feng, S.-Q.; Shen, X.-Y.; Fu, Z.-Y.; Ji, Y.-L. Studies on the electrospun submicron fibers of SIS and its mechanical properties. *J. Appl. Polym. Sci.* **2009**, *114*, 1580–1586, DOI: 10.1002/app.30700.

(97) Grune, E.; Appold, M.; Müller, A. H. E.; Gallei, M.; Frey, H. Anionic Copolymerization Enables the Scalable Synthesis of Alternating (AB) n Multiblock Copolymers with High Molecular Weight in n /2 Steps. *ACS Macro Lett.* **2018**, *7*, 807–810, DOI: 10.1021/acsmacrolett.8b00390.

(98) Spencer, R. K. W.; Matsen, M. W. Domain Bridging in Thermoplastic Elastomers of Star Block Copolymer. *Macromolecules* **2017**, *50*, 1681–1687, DOI: 10.1021/acs.macromol.7b00078.

A3.   Synthesis of linear polyglycerols with tailored degree of methylation by copolymerization and the effect on thermorheological behavior

Christian Schubert [a,b], Philip Dreier [b], Thong Nguyen [a], Kamil Maciol [b], Jan Blankenburg [b,c], Christian Friedrich [a,*], Holger Frey [b,*]

[a] Freiburg Materials Research Center (FMF) and Institute of Macromolecular Chemistry, Albert Ludwig University of Freiburg, 79104 Freiburg, Germany

[b] Institute of Organic Chemistry, Johannes Gutenberg University Mainz, Duesbergweg 10-14, 55128 Mainz, Germany.

[c] Graduate School Material Science in Mainz, Staudinger Weg 9, 55128 Mainz, Germany.

*E-Mail: christian.friedrich@fmf.uni-freiburg.de, hfrey@uni-mainz.de

Available via the Polymer´s website:

https://www.sciencedirect.com/science/article/pii/S0032386117305050?via%3Dihub

Synthesis of linear polyglycerols with tailored degree of methylation by copolymerization and the effect on thermorheological behavior

CrossMark

Christian Schubert [a, b], Philip Dreier [b], Thong Nguyen [a], Kamil Maciol [b], Jan Blankenburg [b, c], Christian Friedrich [a, *], Holger Frey [b, **]

[a] Freiburg Materials Research Center (FMF), Institute of Macromolecular Chemistry, University of Freiburg, Freiburg, Germany
[b] Institute of Organic Chemistry, Organic and Macromolecular Chemistry, University of Mainz, Mainz, Germany
[c] Graduate School Material Science in Mainz, Staudinger Weg 9, 55128, Mainz, Germany

ABSTRACT

We introduce a two-step strategy for the synthesis of linear polyglycerols (linPG-OH$_x$/OMe$_y$) with an adjustable degree of methylation ($y = \frac{DM}{100}$). Ethoxy ethyl glycidyl ether (EEGE) and glycidyl methyl ether (GME) were copolymerized via the "activated monomer" polymerization technique, using tetraocty-lammonium bromide (NOct$_4$Br) as an initiator and triisobutylaluminum (i-Bu$_3$Al) as a catalyst under mild conditions. Subsequent acidic cleavage of the acetal protective groups generates linear polyglycerols with different degree of methylation (DM) by varying the GME comonomer content between 10 and 91%. Size exclusion chromatography (SEC) evidenced good control over molecular weight and narrow to moderate polydispersity (PDI = 1.2−1.8). ^{1}H NMR spectroscopy confirmed ideally random copolymerization of EEGE and GME (*in situ* ^{1}H-NMR kinetics) and provided perfect agreement of the comonomer content with the targeted values. Thermoresponsive behavior in solution and lowering of cloud points with increasing degree of methylation was observed. Furthermore, the differently methylated polyglycerols were investigated with respect to their rheological properties in the melt. Comparison with the fully hydroxylated and permethylated polyglycerol provides new insights into the dynamic behavior of functional polyethers. A tremendous influence of DM on zero-shear viscosity and differences of up to 5 decades were observable at the same reference temperature (273 K). The trend of glass transition temperature and zero-shear viscosity in dependency of degree of methylation was described by mixing rules. To understand the changes in zero-shear viscosity, the "sticky" Rouse model was applied and led to an estimated association lifetime of stickers, i.e. hydroxyl groups of $\tau_s = 4.9{\pm}1.8\ \mu s$.

© 2017 Elsevier Ltd. All rights reserved.

1. Introduction

In the past decade, linear polyglycerol (linPG-OH) has attracted interest in both academia and industry as a high potential biocompatible material [1]. The high number of functional groups combined with excellent aqueous solubility and biocompatibility renders linPG a good alternative to poly(ethylene glycol) (PEG), which is widely used in cosmetics, pharmaceutical and biomedical applications. Due to the more demanding synthesis of linPG that relies on protected glycidol derivatives, compared to its hyperbranched analogue, hbPG [2,3] linPG-OH will be mainly considered for specialty applications [1]. Taton et al. [4] reported the first synthesis of linPG with M$_n$ up to 30 kg/mol via anionic ring opening polymerization of ethoxyethyl glycidyl ether (EEGE), which is prepared by the addition of a vinyl ether to glycidol according to Fitton et al. [5] Acidic cleavage of the protective group subsequent to polymerization results in linear polyglycerol. Furthermore, protected glycidyl ethers, like *tert*-butyl glycidyl ether (*t*BGE), allyl glycidyl ether (AGE) and trimethylsilyl glycidyl ether (TMSGE) were polymerized to obtain linPG after deprotection [1]. EEGE is established as the most suitable monomer, since acidic cleavage of protective groups is easily achieved. Möller et al. [6] prepared copolymers with the different protected glycidyl ethers, which are selectively cleavable using different deprotection methods, respectively. Using two orthogonal protective groups,

---

they were able to control the number of hydroxyl groups and degree of functionalization in selective post polymerization reactions. In a further study the same group investigated the harsh reaction conditions of the alkali metal alkoxide initiated glycidyl ether polymerization. Side reactions as a consequence of the high basicity, leading to the formation of allyl alkoxides, limit molecular weights (P(EEGE) < 14 000 g/mol) [7]. A major advance for this polymerization was presented by Deffieux, Carlotti et al. [8] Their approach is based on a monomer activating catalyst, i.e. triisobutylaluminum (*i*-Bu₃Al), and an ammonium halide (e.g., NOct₄Br) as a weakly basic initiator. Due to the activation of the epoxide, bromide as a rather weak nucleophile is capable of initiating the polymerization under mild reaction conditions, i.e., at temperatures below 0 °C. Thus, side reactions are avoided and preparation of *lin*PG with molecular weights up to 85 kg/mol via polymerization of EEGE is possible [9]. A recent review article summarizes several applications of this polymerization technique, enabling polymerization of less reactive and sterically hindered epoxides [10].

Polymerization of methylated glycidol, glycidyl methyl ether (GME) by the activated monomer strategy provides the fully permethylated linear polyglycerol P(GME), whereas the anionic ring-opening polymerization of GME leads only to molecular weights up to 3000 g/mol [11,12]. Labbé et al. presented the first homo-polymerization affording high molecular weight (100 000 g/mol) P(GME) via the activated monomer polymerization and investigated its lower critical solubility temperature (LCST) behavior in water [13]. Beside some studies concerning the thermoresponsive behavior [12,14,15] and biocompatible surface coating properties [11,16,17], hardly any research concerning the GME homo- and copolymerization has been reported. Müller et al. [18] synthesized a series of thermoresponsive poly(glycidylmethyl ether-*co*-ethylene oxide) copolymers P(GME-co-EO) via the monomer activated strategy. Incorporating different GME comonomer contents, it was possible to tune the melting point and the degree of crystallization of PEG. Furthermore, the LCST of the different copolymers could be varied in the range of 55 °C–98 °C. In a recent publication, Heinen et al. found a random incorporation of the monomers for copolymers of (GME) and ethyl glycidyl ether (EGE) synthesized by the activated monomer polymerization and investigated the thermoresponsive properties [19].

The thermorheological properties of P(GME), i.e. methylated linear polyglycerol (*lin*PG-OMe), together with the linear polyglycerol (*lin*PG-OH) were investigated in a broad range of molecular weights in our recent publication [20]. In this study, permethylated *lin*PG-OMe was prepared in post polymerization reactions via methylation of *lin*PG-OH. However, partial methylation of linear polyglycerol employing the common methylation under phase transfer conditions is not possible [20–22].

Due to the amorphous structure and the low glass transition, the pair of *lin*PG-OH and its permethylated analogue offers an ideal model system to investigate the thermal behavior of hydrogen bonding polymers and their non-associating counterparts. The association interactions cause a delay in relaxation times, which can be described by the sticky Rouse or sticky reptation models [23–25]. In this model the lifetime and number of stickers affects the mobility of the chains and therefore determines the thermorheological properties. While most studies devoted to the sticky Rouse model were performed in solution [26–28], only little research has been performed in the melt state [29,30].

In this work we present a further development of our recent thermorheological study of linear polyglycerol [20] and its methylated counterpart by providing linear polyglycerols with adjustable degree of methylation (DM). For this purpose, we synthesized P(EEGE)-*co*-P(GME) with defined comonomer content and generated linear polyglycerol with varied DM after subsequent acidic
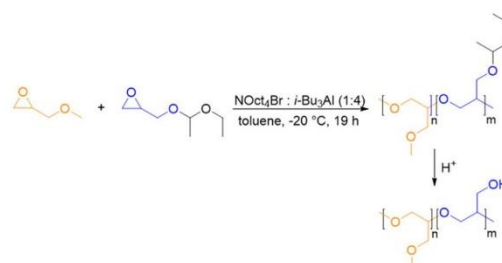
Scheme 1. Synthesis of P(EEGE-*co*-GME) via the activated monomer polymerization. Acidic cleavage of the protective groups results in linear polyglycerol copolymers with deliberately varied degree of methylation (DM).

cleavage, as illustrated in Scheme 1.

2. Experimental part

2.1. Instrumentation

¹H NMR spectra were recorded on a Bruker AC300 (at 300 MHz) or Bruker Avance-II 400 (400 MHz) and are referenced internally to residual proton signals of the deuterated DMSO-d_6 solvent. *In situ* copolymerization kinetics were measured on a Bruker Avance III HD 400 spectrometer equipped with a 5 mm BBFO SmartProbe (Z-gradient probe) and an ATM as well as a SampleXPress 60 auto sampler. For SEC measurements in DMF (containing 0.25 g L^{-1} of lithium bromide as an additive), an Agilent 1100 series was used as an integrated instrument including a PSS HEMA column ($10^6/10^4/10^2$ Å porosity) and an UV and RI detector. Calibration was achieved with polystyrene standards provided by Polymer Standards Service (PSS). DSC diagrams were recorded on a NETZSCH DSC 204 F1 in the range of –80 to 0 °C at a rate of 10 K min^{-1}. Cloud points were determined in deionized water at a concentration of 5 mg/mL and a heating rate of 1 K/min C using a Jasco V-630 photo spectrometer containing a Jasco ETC-717 Peltier element. The relative intensity of transmitted light ($\lambda = 500$ nm) was measured in dependence of temperature (1 point per 0.1 K). The cloud point was determined as the onset of transmission breakdown.

The glass transition temperature (T_g) was determined from the maximum of the first derivative of heat flow during the second heating process. Samples were dried for 48 h at 80 °C in vacuum before measurements. Rheological properties were measured on an Anton Paar Physica MCR-301 under nitrogen atmosphere with an 8 mm plate-plate geometry. Temperature-dependent oscillatory measurements were carried out in a frequency range between 0.1 and 100 rad/s with deformations of 10% for the highest temperatures down to 0.01% at temperatures close to T_g. The temperature range was individually chosen for every sample, starting at +25 °C down to temperatures close to the individual T_g of the samples. Temperature steps were 10 K at high temperatures, whereas steps of 2 K were chosen at temperatures close to T_g. Master-curves were constructed by shifting of isotherms relative to a reference temperature (here $T_g + 50$ K) using the commercially available IRIS Rheo-Hub 2008 software [31].

2.2. Materials

All reagents and solvents were purchased from Acros Organics, Sigma-Aldrich and TCI and used as received, unless otherwise mentioned. Ethoxy ethyl glycidyl ether (EEGE) was prepared as described by Fitton et al. [5] Toluene was dried over sodium and

was kept in a flask under vacuum until usage. Triisobutylaluminum (*i*-Bu$_3$Al, 1 M in toluene, Aldrich) was used without further purification. Tetraoctylammonium bromide (TOAB) (NOct$_4$Br, >99%, Aldrich) was used without further purification and dissolved in dry toluene (0.22 M). Glycidyl methyl ether (GME, >85%, TCI) was distilled twice over CaH$_2$ at reduced pressure using a Vigreux column and stored in a fridge. EEGE and GME were purified by cryotransfer over calcium hydride (CaH$_2$) directly prior to use. All polymerization reactions were performed under inert gas atmosphere.

2.3. Sample preparation for in situ ^{1}H NMR kinetic studies

50 mg tetraoctylammonium bromide (TOAB) was dissolved in 2 mL benzene in a dried 10 mL-Schlenk tube and stirred under vacuum for 30 min at 60 °C. The solvents were removed under high vacuum for 24 h. Then, 0.5 mL dry toluene-d_8 were added. 0.1 mL of the initiator solution (TOAB, 1 equiv.) was added under argon atmosphere in a dried Norell S-5-400-VT-7 NMR tube, followed by 0.9 mL toluene-d_8. Subsequently, 41 μL GME (25 equiv.) and 66 μL EEGE (25 equiv.) were then added, which were previously dried over CaH$_2$ and distilled. The mixture was cooled down with an acetone/dry ice bath for 15 min and 83 μL *i*-Bu$_3$Al solution (1.1 M in toluene, 5 equiv.) was injected via syringe. After sealing with a Teflon stop-cock, the cooled tube was repeatedly shaken vigorously to homogenize the solution before placing in the NMR spectrometer with the probe gas flow adjusted to −20 °C. After the temperature in the probe head was stable (~10 min, ΔT = 0.1 K), the first spectrum was recorded. Sample spinning was turned off. Spectra were recorded with 16 scans at 2 min-intervals. The measurement was stopped after full conversion (1.5 h). SEC data of the isolated copolymer are shown in SI-Fig. 4.

2.4. Synthesis of P(EEGE-co-GME) random copolymers

In a Schlenk flask equipped with a magnetic stirrer, the desired amount of EEGE and GME (16 vol %) was dissolved in dry toluene. The reaction mixture was cooled down to −20 °C and the initiator TOAB (1 mL, 0.22 M in dry toluene) was added. Under vigorous stirring the catalyst *i*-Bu$_3$Al (0.8 mL, 1 M in toluene) was slowly added via syringe. The mixture was allowed to warm up to room temperature. After 19 h the reaction was stopped by adding methanol (5 mL). The solvent was removed under reduced pressure and the polymers were obtained as colorless, highly viscous liquids.

2.5. Deprotection of P(EEGE-co-GME) random copolymers to obtain linPG-OH/OMe

A 20 wt.-% solution of the copolymer in methanol was stirred with the anionic exchange resin Dowex 50WX8 at room temperature for 5 d to cleave the acetal protective groups. After filtration and removal of the solvents, the polymer was dissolved in methanol and precipitated twice into diethyl ether.

3. Results and discussion

3.1. Synthesis and molecular characterization

In Scheme 1, the synthetic route employed for linear polyglycerol with different degrees of methylation is shown. The copolymerization of EEGE and GME with subsequent acidic cleavage of the acetal protective group leads to a linear polymer structure consisting exclusively of linear hydroxylated and methylated glycerol units. The degree of methylation depends on the incorporated amount of GME.

The polymerization was carried out according to the activated monomer polymerization strategy [9], which is illustrated in Scheme 2. The mixture of the monomers together with the initiator TOAB in dry toluene was cooled down to −20 °C and the catalyst *i*-Bu$_3$Al was added to start the reaction. In contrast to a literature procedure for P(EO-co-GME) copolymers [18], the ratio of catalyst (*i*-Bu$_3$Al):initiator(TOAB) 4:1 could be kept constant for all comonomer compositions providing very good reaction control. The reaction mixture was allowed to warm up to room temperature, and after 19 h the addition of methanol was used to terminate the polymerization. As described by Müller et al. [18], removal of the hydrolyzed initiator NOct$_4$OH subsequent to the polymerization represents a challenge. Since column chromatography or precipitation, as described in literature [18] was not suitable for the series of EEGE/GME copolymers, accurate dialysis against methanol led to the best results, i.e., no initiator salt was observable by ^{1}H NMR spectroscopy. Acidic removal of the acetal protective group provided *lin*PG-OH/OMe with different degrees of methylation in dependency of incorporated GME. The subscript numbers of the polymer description indicate the ratio of EEGE/GME and OH/OMe groups, respectively in mol %.

Table 1 lists all P(EEGE-co-GME) copolymers with their molecular weights and comonomer composition. The composition of the copolymers reflected the monomer fractions of the feed. Copolymers with monomodal molecular weight distribution and low polydispersity (1.2–1.4) were obtained and the monomer content of GME was continuously varied between 10% and 90%. The ratio of monomer to initiator (100:1) was kept constant for all copolymerizations. Since the EEGE monomer exhibits a higher molar mass than GME, the theoretical molecular weights of the copolymers decrease with increasing amount of GME incorporated. Molecular weights were determined by SEC (DMF, PS standards), and all SEC traces were monomodal, as shown in Fig. 1 (left). The molecular weights obtained are slightly higher than the calculated values. This is explained by the different hydrodynamic radius of the copolymers compared to the polystyrene standard. Moreover, after acidic cleavage of the protective groups, SEC measurements of samples containing different amounts of hydroxyl groups were only comparable to a very limited extent, no matter which standard was used. Polymer-solvent and polymer-polymer interactions are affected by hydrogen bonding, and hydroxyl groups influence the hydrodynamic radius and thereby the retention time in the column. Therefore, the molecular weights of the deprotected copolymer samples were calculated on the basis of the protected precursor materials by ^{1}H NMR spectroscopy. Molecular weights of the *lin*PG-OH/OMe samples are summarized in Table 2.

Determination of exact molecular weights by ^{1}H NMR spectroscopy is not possible, because in the activated monomer approach precise calculation of the chain length based on a functional initiator is not possible due to the lack of end group fidelity of the method. Nevertheless, ^{1}H NMR spectroscopy allows to follow the successful acidic cleavage of the protective groups. Fig. 1 (right, top) shows the spectra of a typical copolymer before and after the removal of the protective groups. The methyl groups a,b (1.25–1.00 ppm) and the acetal proton (4.65 ppm) disappear completely and no side products, i.e. ethanol or acetaldehyde, are observable. Furthermore, the amount of EEGE/GME and OH/OMe groups after acidic cleavage can be calculated using ^{1}H NMR spectroscopy by comparison of the signal of the methyl group with the acetal protons or the hydroxyl groups. The determined composition of the copolymers by ^{1}H NMR spectroscopy is in excellent agreement with the comonomer content in the monomer feed. The composition of all polymers is shown as subscript numbers in the sample names in Table 2. Fig. 1 (right, bottom) shows the ^{1}H NMR spectra of deprotected *lin*PG-OH/OMe with
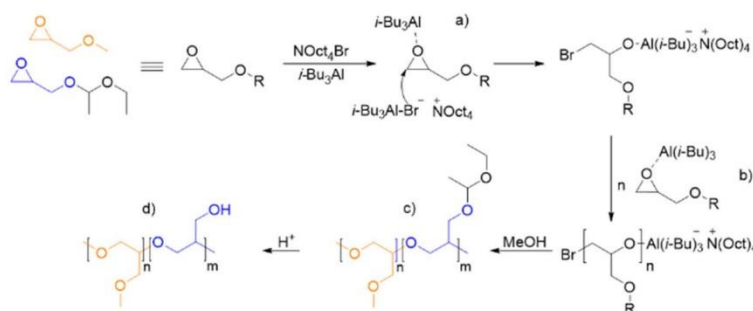
Scheme 2. Reaction mechanism of the activated monomer anionic polymerization [9]. a) Monomer activation, "ate" complex formation and nucleophilic attack of bromide. b) Monomer insertion steps c) The addition of methanol stops the reaction. d) Subsequent acidic cleavage provides *lin*PG-OH with different degrees of methylation that are determined by the amount of GME incorporated.

Table 1
P(EEGE-*co*-GME) copolymers with their composition, targeted values, molecular weight, and PDI.

no.	Composition[a]	EEGE(theo.)	GME(theo.)	$M_{n\,(theo.)}$ [g/mol]	M_n[b] [g/mol]	PDI[b]
1	P(EEGE$_{0.90}$-co-GME$_{0.10}$)	90	10	14 000	15 400	1.2
2	P(EEGE$_{0.80}$-co-GME$_{0.20}$)	80	20	13 500	13 300	1.3
3	P(EEGE$_{0.69}$-co-GME$_{0.31}$)	70	30	12 900	13 700	1.3
4	P(EEGE$_{0.64}$-co-GME$_{0.36}$)	60	40	12 300	14 200	1.2
5	P(EEGE$_{0.45}$-co-GME$_{0.55}$)	50	50	11 700	15 000	1.2
6	P(EEGE$_{0.40}$-co-GME$_{0.60}$)	40	60	11 100	12 500	1.3
7	P(EEGE$_{0.31}$-co-GME$_{0.69}$)	30	70	10 600	13 300	1.4
8	P(EEGE$_{0.09}$-co-GME$_{0.91}$)	10	90	9400	12 400	1.3

[a] Composition determined via ^{1}H NMR by integration of acetal group (c) compared to methyl group (d) of GME as shown in Fig. 1 (top,right).
[b] Molecular weight and molecular-weight distribution characterized by SEC (DMF, PS standards).

Table 2
*lin*PG-OH/OMe copolymers with molecular weight, degree of methylation (DM), PDI and glass transition temperature.

no.	Composition[a]	M_n[b] [g/mol]	$M_{n\,(theo.)}$[c] [g/mol]	PDI	DM [%]	T_g [K]
i	*lin*PG-OH$_{0.90}$/OMe$_{0.10}$	12 800	8300	1.2	10	253
ii	*lin*PG-OH$_{0.80}$/OMe$_{0.20}$	12 600	7600	1.3	20	253
iii	*lin*PG-OH$_{0.69}$/OMe$_{0.31}$	13 100	8300	1.3	31	246
iv	*lin*PG-OH$_{0.64}$/OMe$_{0.36}$	14 100	9200	1.4	36	244
v	*lin*PG-OH$_{0.45}$/OMe$_{0.55}$	12 100	10 400	1.3	55	234
vi	*lin*PG-OH$_{0.40}$/OMe$_{0.60}$	10 200	9300	1.4	60	234
vii	*lin*PG-OH$_{0.31}$/OMe$_{0.69}$	12 400	10 600	1.4	69	232
viii	*lin*PG-OH$_{0.09}$/OMe$_{0.91}$	8800	11 400	1.8	91	221

[a] Composition determined via ^{1}H NMR by integration of hydroxyl group (g) compared to methyl group (d) of GME as shown in Fig. 1 (top,right).
[b] Molecular weight and molecular-weight distribution characterized by SEC (DMF, PS standards).
[c] Theoretical molecular weight was calculated on the basis of the EEGE content determined by ^{1}H NMR and the molecular weight of the P(EEGE-*co*-GME).

varying amounts of GME. When increasing the incorporated amount of GME, the signal of the methyl group d (3.25 ppm) increases and the hydroxyl group g (4.50 ppm) disappears.

Good agreement between targeted and measured values was found, evidencing control over molecular weight and comonomer content. However, random comonomer incorporation is vital to provide comparable structures for the ensuing thermorheological investigations. In a recent work of Herzberger et al. [32] on the kinetics of the monomer-activated anionic ring opening

copolymerization by *in situ* ^{1}H NMR spectroscopy strongly tapered copolymer structures for EO and EEGE were observed. In the current work two similar glycidyl ethers, i.e. GME and EEGE were employed. Thus, the reactivities are most likely similar. Recent results of Heinen et al. [19] revealed a truly random copolymerization of GME and GEE (glycidyl ethyl ether) via the monomer-activated polymerization technique. To study the microstructure of P(EEGE-*co*-GME) copolymers, *in situ* ^{1}H NMR kinetics measurements were performed at −20 °C. For the evaluation, the integral ratios of the signals for the acetal group of EEGE (4.56 ppm) and the methoxy group of GME (3.09 ppm) were compared (for the exact calculation, see SI-Fig. 1). Fig. 2 shows the plotted monomer concentration against the monomer conversion, indicating nearly ideally random incorporation of both comonomers. It also shows that GME is incorporated slightly faster. From the data, the *r*-parameters (reactivity ratios) were determined according to Jaacks [33] ($r_{GME} = 1.11$, $r_{EEGE} = 0.90$) and Kelen-Tüdos [34] ($r_{GME} = 1.33$, $r_{EEGE} = 1.02$), which can be found in SI-Table 1 and SI-Figure 2 and 3. The results are consistent with the previous observation, and both methods show an almost ideal random incorporation of the comonomers. Oxophilicity and thus complexation of the *i*-Bu$_3$Al catalyst by EEGE can may be responsible for the slightly faster incorporation of GME [9,32].

These results are confirmed by the triad sequence analysis by ^{13}C NMR spectroscopy according to a literature procedure for P(EO-*co*-GME) [18]. Fig. 3 shows the ^{13}C NMR spectra of 3 differently methylated samples (10, 55, 91%). In contrast to P(EO-*co*-GME), the signals of all triads overlap due to the very similar backbone structure. Nevertheless, a signal assignment of the homo-triads can be achieved. M represents the signals of GME, while H is used as an abbreviation for the glycerol unit. Unfortunately, quantitative determination of signals intensities of the homo-triads is not possible due to the overlap with the hetero-triads. The probability of homo-triads like H-H$_b$-H decreases with increasing the GME content. The enlarged sections in Fig. 3 show that with increasing the GME content the intensity of triad H-H$_b$-H decreases, accompanied by a clear change of signal shape and a slight field shift, indicating clear disappearance of the homo-triad. Similar observations are made for the GME triads (M-M$_b$-M and M-M$_a$-M). Even the methylene signal apart from the backbone (H$_c$) and the methoxy group (M$_d$) show a slight high field shift.

3.2. Thermoresponsive properties in aqueous solution

In a recent publication Müller et al. [18] investigated the

332   C. Schubert et al. / Polymer 121 (2017) 328–339
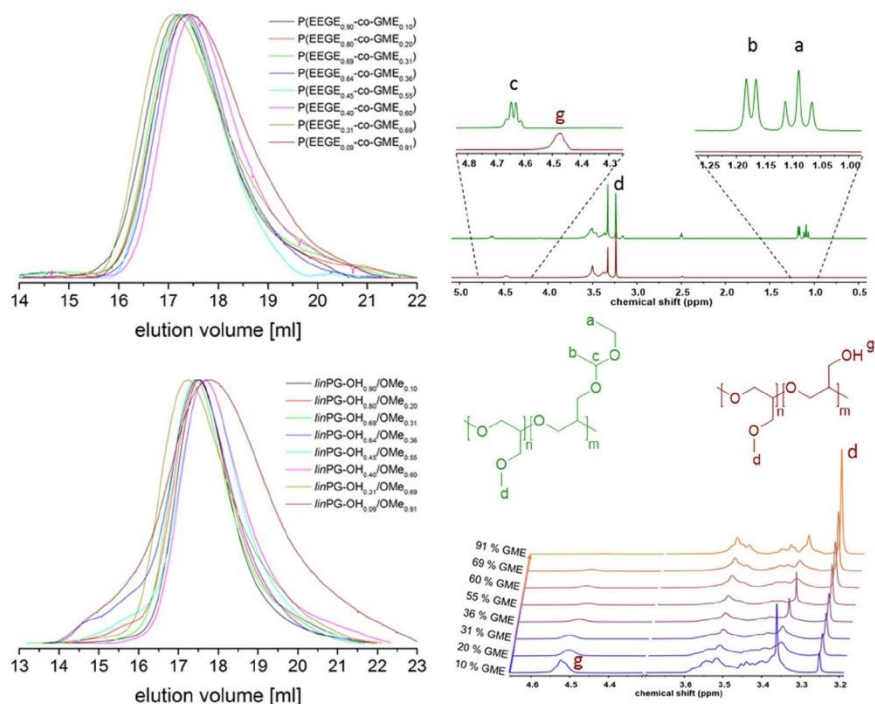
Fig. 1. SEC traces (DMF, PS standards) of all P(EEGE-*co*-GME) polymers (left, top) and of the corresponding linPG-OH/OMe polymers (left, bottom) after acidic cleavage. The subscript numbers represent the respective comonomer content in mol%. ^{1}H NMR spectra in DMSO-d_6 of P(EEGE$_{0.45}$-*co*-GME$_{0.55}$) (right, top) and the resulting *lin*PG-OH$_{0.45}$/OMe$_{0.55}$ co-polymers after acidic cleavage are shown as well. ^{1}H NMR spectra in DMSO-d_6 of all *lin*PG-OH/OMe with varying amounts of GME are also displayed (bottom, right).
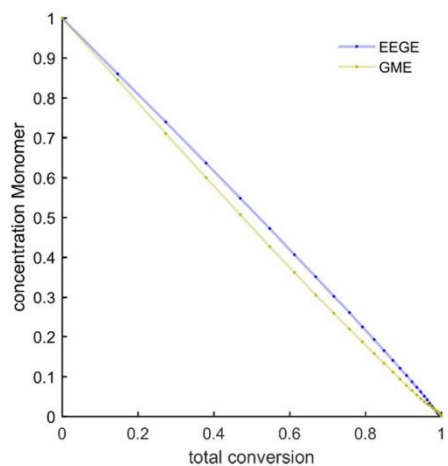
Fig. 2. Monomer concentrations in the copolymerization of GME and EEGE plotted against total monomer conversion determined by ^{1}H NMR in toluene-d_8 at −20 °C, applying the monomer-activated anionic ring-opening polymerization.

thermoresponsive behavior of P(GME-*co*-EO) copolymers in aqueous solution. Since linear glycerol moieties may be viewed as functional analogues of ethylene glycol units, the temperature dependent solubility of the series of *lin*PG-OH with different degree of methylation was intriguing. Fig. 4 (top) shows the temperature dependency of the intensity of transmitted laser light for the two highest methylated (90 and 69%) *lin*PG-OH samples, exhibiting cloud points of 61 and 91 °C, respectively. As expected, an increase of the degree of methylation leads to lowering of the cloud point. In contrast to P(GME-*co*-EO) copolymers, which still exhibit LCST behavior with GME contents as low as 42%, no cloud point below 100 °C was observable for our samples with degrees of methylation below 69%, due to the high aqueous solubility of the glycerol units.

Due to the high polarity and the H-bond formation of hydroxyl groups, all *lin*PG-OH samples are very well soluble in water, even with rather high degree of methylation. Fig. 4 (bottom) illustrates a comparison of our data with cloud points of P(GME-*co*-EO) found by Müller et al. [18] The 90% methylated polyglycerol fits well into the linear dependency of cloud points from P(GME-*co*-EO). Inter-estingly, the small amount of hydroxyl groups in this material does not show a significant effect on the cloud point compared to the P(GME-*co*-EO), whereas the 69% methylated *lin*PG-OH samples exhibits a significantly higher cloud point, indicating enhanced solubility of this polymer in water as a result of hydrogen bonds of the hydroxymethyl group.
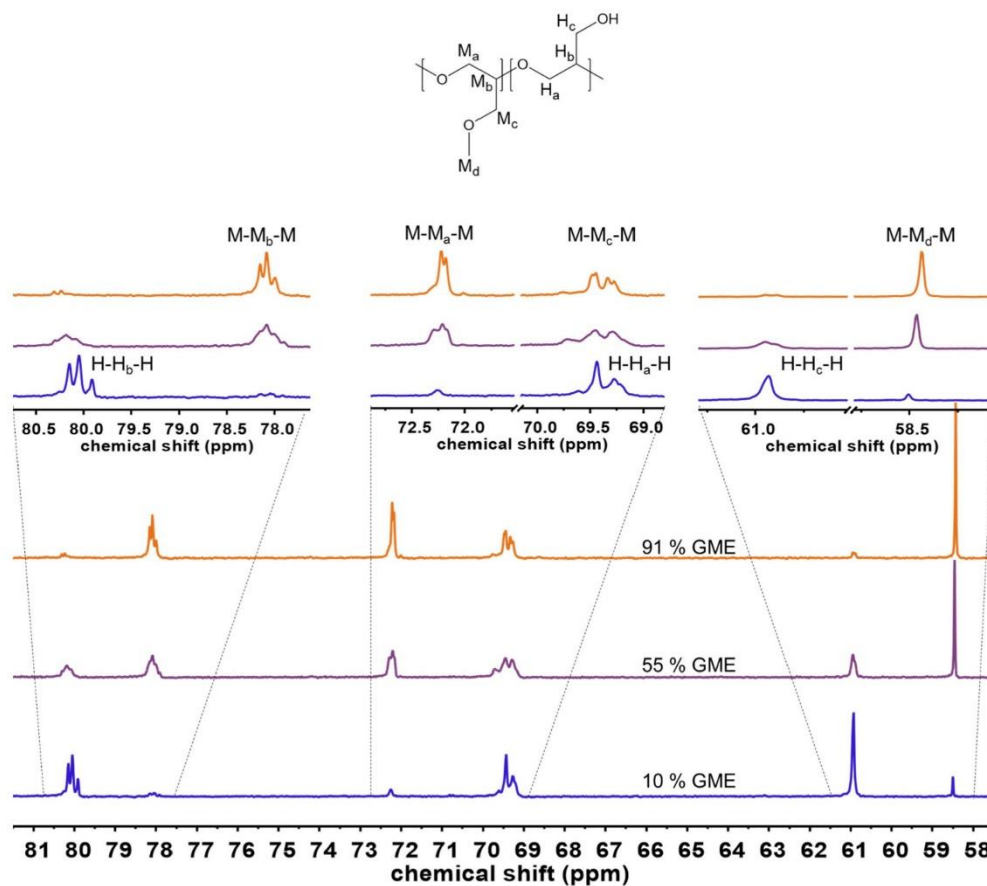
Fig. 3. ^{13}C NMR spectra of 3 samples of *lin*PG-OH/OMe in DMSO-d_6 with varying amounts of GME (91, 55, and 10%). Glycidol units are referred to as H$_{a/b/c}$ and GME units correspond to M$_{a/b/c}$.

3.3. Glass transitions

In Fig. 5 the glass transition temperature is shown in dependency of the degree of methylation. The data show monotonous, linear character. From our previous publications we provide the T_g–data for the full hydroxylated linear polyglycerols (blue data point) and its methylated counterpart (orange data point) [20]. The T_g decreases linearly upon increasing the degree of methylation and drops by 50 K overall, as observed for a similar pair of polymers, i.e. poly(vinyl alcohol) (PVA - T_g = 304 K [35]) and poly(vinyl methyl ether) (PVME - T_g = 240 K [36] to 250 K [37]).

A linear dependency of T_g on the amount of hydrogen bonding side groups was also described by Lewis et al. [38] who investigated several carboxylate functionalized poly(*n*-butyl acrylate) polymers. They correlated the steepness of the slope with the strength of hydrogen-bonding. As we found a significantly smaller slope, the strength of hydrogen-bonding arising from hydroxyl groups is clearly lower than the strength arising from carboxylate interactions. This fact is also supported by recent calculations of Miao et al. [39].

Usually the dependence of T_g on the composition of random copolymers is described by mixing rules such as the Gordon-Taylor or Fox equations [40,41]. These mixing rules correlate with the weight comonomer content and lead to a nonlinear relationship. In the present case the degree of methylation represents the molar fraction of GME. Although, the molar mass of repeating units of glycidol (74 g/mol) and GME (88 g/mol) is rather similar, the latter equations (Gordon-Taylor or Fox) do not describe the dependency well. In contrast, the Di Marzio-Gibbs equation [42] correlates the T_g with the molar fraction of flexible bonds in the comonomer backbone. Zhang et al. [43] used the DM equation (1) for the special case that both repeating units exhibit equal numbers of flexible bonds in both monomers, which results in the following linear mixing rule for T_g :

$$T_g = xT_{g_{OH}} + yT_{g_{OMe}} \tag{1}$$
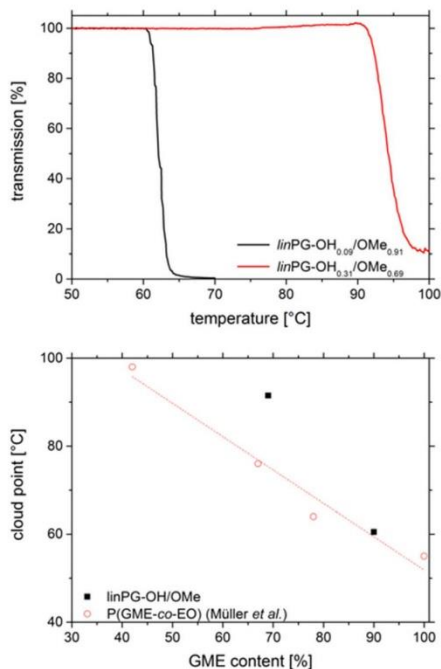
Fig. 4. Cloud point determination via turbidimetry for two *lin*PG-OH samples with different degree of methylation (top). Comparison of cloud points with data from literature for P(GME-*co*-EO) copolymers (bottom) [18].
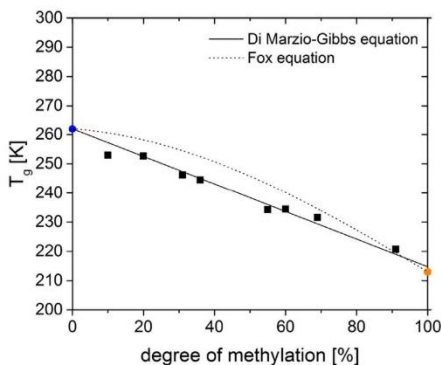
Fig. 5. Glass transition temperature T_g in dependence of degree of methylation. The data was fitted by Di Marzio-Gibbs equation (1), solid line. The dotted line represents the fit of the Fox equation.

In this equation, *x* and *y* represent the mole fraction of the co-monomers, and $T_{g_{OH}}$ and $T_{g_{OMe}}$ are the respective glass transitions of the homopolymers. Due to the similarity of both comonomers in our case having 3 flexible bonds, this equation can be applied to our data as well. The excellent agreement supports applicability of this mixing rule and is an indication of the good reaction control and

random incorporation of the comonomers, which is in agreement with the NMR results. For block structures one would expect two separate glass transition temperatures corresponding to the respective homopolymers [44].

3.4. Linear viscoelasticity

In the following, we investigate the impact of hydroxyl groups and the degree of methylation on the thermorheological properties of the partially methylated linear polyglycerol samples. For this purpose, rheological measurements were performed for all samples and Booij-Palmen-Plots (BPP) (top) and the resulting master curves (bottom) are shown in Fig. 6 for low degree of methylation (10%) and highly (69%) methylated linear polyglycerol. As reported in our previous publications [20,45], the isotherms overlap well in the terminal zone, allowing us to construct master curves. The choice of a reference temperature of 50 K above the glass transition temperature appears to be optimal for that purpose and enables to compensate for T_g effects in the analysis of material parameters.

A considerable violation of time—temperature superposition is observed in the transitional region, which corresponds to module values between 1 and 100 MPa. This failure is attributed to the temperature dependence of segmental relaxation, which is different from that of terminal relaxation [46,47] and is not related to the presence of hydroxyl groups, as already discussed for *lin* and *hb* polyglycerols [20,45]. All samples exhibit a distinct minimum of the $\delta(|G^*|)$ curves, which is in the range between the fully hydroxylated *lin*PG-OH and its permethylated counterpart.
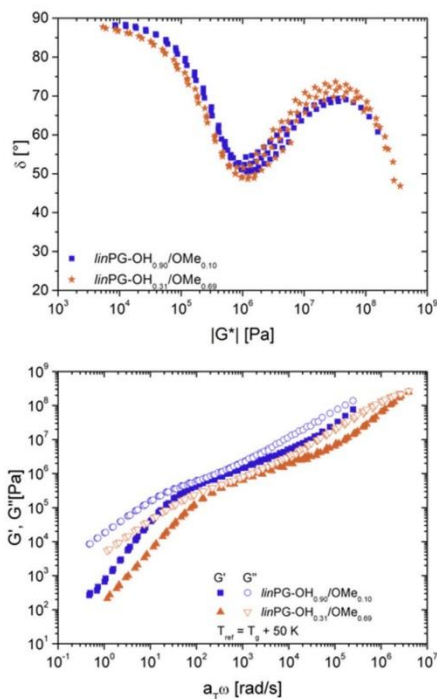
Fig. 6. Booij-Palmen-Plots of a 10% and 69% methylated copolymer sample (top) and master curves together at T_g +50 K (bottom, b_T = 1).

The scatter observed in Fig. 6 (top) has almost no impact on the presentation of data in the double logarithmic plot, for which reasonable master curves could be constructed. Fig. 6 (bottom) shows the result for the two samples. The terminal flow region $(G' \sim \omega^2, G'' \sim \omega^1)$ at low frequencies is followed by an intermediate region with slopes of G' and G'' in the range of 0.5, pointing to the presence of Rouse behavior. This fact is in accordance with the course of $tan(\delta)$ being always >1, indicating the absence of entanglements, which was expected based on the molecular weight regime studied.

3.5. Temperature dependence of dynamic response

According to the time temperature superposition principle, the isotherms measured by oscillatory rheometry were horizontally shifted to a master curve. The influence of vertical shifting is described in our recent publications [20,45] and is negligible compared to the results of horizontal shifting only. In Fig. 7 all WLF-parameters together with the data for the fully hydroxylated linear polyglycerol (blue data) and the methylated counterpart (orange data) is shown in dependence of the degree of methylation at a reference temperature of 50 K above the individual T_g of each polymer. A non-monotonous transition from neat linPG-OH to linPG-OMe is observed. For associating polymers, the viscosities

and relaxation times, and therefore shift factors and WLF-parameters do not only depend on free volume, i.e. packing effects, but also on associative interactions between the hydroxyl groups, i.e. energetic effects. By applying a modified WLF Equation (2) [45,48,49], we discuss modified WLF-parameters c_{1m}^0 and c_{2m}^0 at a reference temperature T_0.

$$\log a_T = -\frac{c_{1m}^0 (T - T_0)}{c_{2m}^0 + T - T_0} \tag{2}$$

$$c_{1m}^0 = c_{1f}^0 + c_{1E}^0 \text{ with } c_{1E}^0 = \frac{E_i}{2.3 R T_0} \cdot \frac{T_0 - T_V}{T_0} \text{ and } c_{2m}^0 = c_{2f}^0 = c_2^0 \tag{3}$$

The modified WLF-parameter c_{1m}^0 considers both the dependency of packing effects by free volume represented by c_{1f}^0 and an interaction energy expressed by c_{1E}^0 [45,48,49]. These factors are additive and can hardly be separated. Upon an increase of the degree of methylation, c_{1m}^0 becomes equal to c_{1f}^0, as the permethylated sample cannot interact via hydrogen bonds. The c_2^0 − parameter remains unchanged by this modification.

Fig. 7 (top) shows the c_{1m}^0 values in dependency of DM at $T_g + 50$ K. Surprisingly, c_{1m}^0 decreases strongly up to a DM of 40%, where a slight minimum is followed by a plateau region. If we assume that the free volume and packing frustration is not affected by increasing the DM, c_{1f}^0 in Equation (3) remains constant, i.e., the contribution of the interaction energy is of a non-linear character. For degrees of methylation from 40 to 90% we do not observe a significant change in interaction energy. On a molecular scale, this fact can be explained on basis of inter- and intramolecular interactions. We assume that for the DM exceeding 40% no intermolecular hydrogen bonds are formed, whereas for low DM < 40% the formation of intermolecular hydrogen bonds becomes possible. Therefore, the difference between the plateau and the value for the fully methylated sample can be understood as an interaction energy for the intramolecular hydrogen bonds. As mentioned before, the factors influencing c_{1m}^0 can hardly be separated, thus an estimation of E_i for intramolecular interactions is not possible in a general way. Based on the determination of activation energy, which will be described later, a rough estimation has been carried out.

A similar trend can be observed for the course of c_2^0, which is shown in Fig. 7 (bottom). Here again, a strong decrease in the c_2^0 value up to a DM of 40% is observable. The mentioned minimum is more pronounced in this case, but within the error of the data a plateau can be observed for c_2^0 as well. In a recent publication, Dudowicz et al. [50] demonstrated the universality of the WLF parameters. Applying their findings that the c_2^0 parameter correlates with cohesive molecular interactions and the degree of chain stiffness, expressed by the backbone bending energy, we can explain the course of c_2^0 in an analogous manner to c_{1m}^0. Obviously the effectivity of hydrogen bonding becomes significantly lower upon increasing the degree of methylation. This fact is already observable for a low degree of methylation. As mentioned before, the possibility to form intramolecular hydrogen bonds decreases, inducing higher flexibility of the chains.

3.6. Activation energy

A key parameter derived from the modified WLF model is the activation energy at infinite temperature $E_a^\infty = 2.303 \cdot R \cdot c_{1m}^0 c_2^0$. In Fig. 8 the activation energy is shown in dependency of the DM. As the c_{1m}^0 and c_2^0 values decrease by increasing the degree of
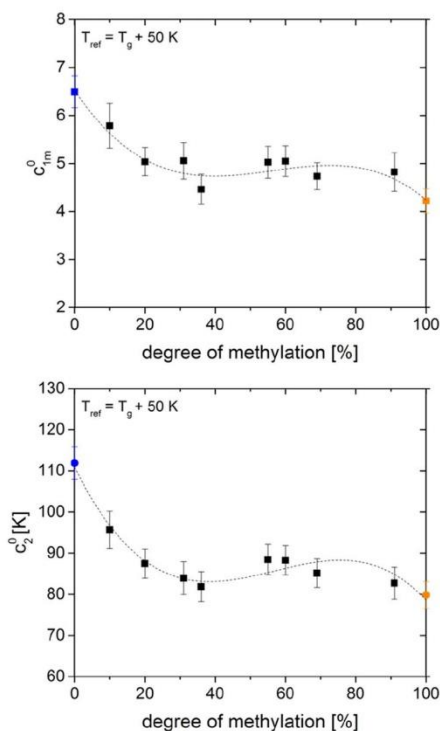
Fig. 7. Dependence of c_{1m}^0 (top) and c_2^0 (bottom) on the degree of methylation at $T_g + 50$ K. The dotted lines are plotted in order to guide the eye. The blue data point represents the value of linPG-OH, and the orange data point represents the data of linPG-OMe [20].
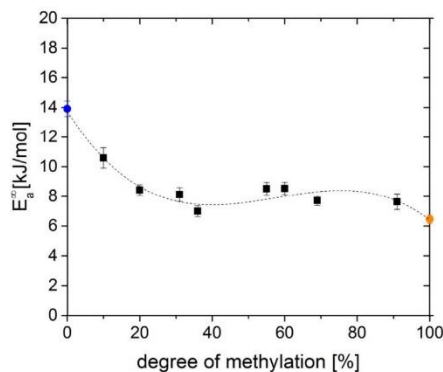
Fig. 8. Activation energy at infinite temperature in dependency of degree of methylation. The dotted lines are plotted in order to guide the eye.

Fig. 9. Zero-shear-viscosity at 273 K in dependency of the degree of methylation. The values were corrected according to equation (6) with M_{ref} = 10 000 g/mol.

methylation, the product of both multiplied with $2.303 \cdot R$ shows the same trend with a strong decrease up to a DM of 40% followed by a plateau region. In literature, Müller et al. [51] and McKee et al. [52] found also higher activation energies at infinite temperature of their associating polymers compared to their non-associating counterparts. Applying equation (3) for the description of c^0_{1m}, we can estimate an interaction energy E_i by calculating difference in activation energy of the fully hydroxylated and its permethylated analogue, which amounts to ≈ 8 kJ/mol. For strongly hydrogen bonding copolymers of n-butyl acrylate and a 2-ureido-4[1H]-pyrimidinone values up to 20 kJ/mol were found by Feldman et al. [29].

The differences in E_a^∞ of the "plateau"-value and the value for the permethylated PGME sample can be traced back to the interaction energy for intramolecular hydrogen bonds, as mentioned in the previous section. Therefore, we estimate the contribution of intramolecular hydrogen bonds to approximately 1.5 kJ/mol.

3.7. Characteristic material parameter: the zero shear viscosity η_0

The zero shear viscosity η_0 is the limiting value of $\eta'(\omega)$ at vanishing frequencies, as defined in equation (4). By fitting the data with the Carreau-Yasuda-equation (5) [53,54], the zero shear viscosity could be determined for all samples, even those, for which the plateau is not fully developed.

$$\eta_0(T) = \lim_{\omega \to 0} \eta'(\omega, T) = \lim_{\omega \to 0} \frac{G''(\omega, T)}{\omega} \qquad (4)$$

$$\eta' = \frac{\eta_0}{(1 + a\omega^\alpha)^\beta} \qquad (5)$$

a, α, β are the Carreau-Yasuda parameters. For a given reference temperature, the zero shear viscosity depends on molecular weight and the degree of methylation. To determine the functional dependence of the zero shear viscosity on the degree of methylation only, one has to fix the molar mass of all polymers at a certain reference value, M_{ref}. We choose $M_{ref} = 10 000$ g/mol, and according to $\eta_0 = K \cdot M_n^\alpha$ with $\alpha \approx 1$ for unentangled polymers we obtain a corrected viscosity value:

$$\eta_{0_{corr}} = \eta_0 \cdot \frac{M_{ref}}{M_n} \qquad (6)$$
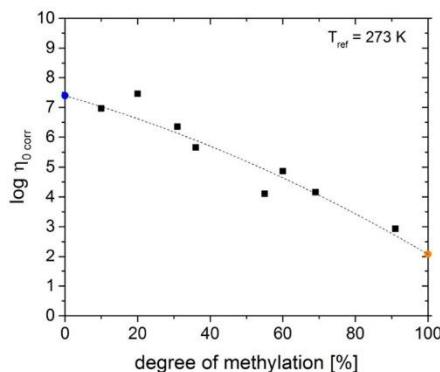
In Fig. 9, the corrected zero-shear-viscosities of all samples together with the data for the linear polyglycerol homopolymer (blue data) and the methylated counterpart are shown in dependence of the degree of methylation at a constant temperature of 273 K. For this comparison, we have chosen a reference temperature common to all samples (273 K) to illustrate the massive effect of hydrogen bonds on the samples viscosity. At this reference temperature η_0 drops by over 5 decades in a non-linear manner. The course of the zero-shear-viscosity with increasing degree of methylation is described quantitatively on the basis of a nonlinear quadratic mixing rule (equation (7)), which was recently applied by Zhang et al. [43].

$$\log(\eta_0) = x \, \log(\eta_{0_{OH}}) + y \, \log(\eta_{0_{OMe}}) + x \cdot y \, \log(\eta_{0_{mix}}) \qquad (7)$$

In this equation x and y are the mole fractions of the hydroxyl and methylated hydroxyl groups with their corresponding zero-shear-viscosities $\eta_{0_{OH}}$ and $\eta_{0_{OMe}}$. $\eta_{0_{mix}}$ represents a "mixing" term, which amounts to $\eta_{0_{mix}} = 1 \cdot 10^2 Pa \cdot s$.

For high degrees of methylation (60–100%) only the course of the zero-shear viscosity may be considered as linear. This observation is in accordance to other polymers containing different hydrogen-bonding moieties, i.e. carboxyl functionalized poly(n-butyl acrylate) polymers, for which the increase in viscosity was even more pronounced [38]. This can be attributed to the stronger interaction of the carboxyl groups in comparison to the hydroxyl groups. Moreover, these polymers were investigated with respect to the Cross relaxation time $\tau_a (= 2\pi \cdot a^{1/\alpha})$. For this purpose the authors fitted their complex viscosity η^* data by the empirical Cross model [55], equation (8), which is closely related to the Carreau-Yasuda-equation (5).

$$\eta^* = \frac{\eta_0}{1 + \left(\frac{\tau_a \cdot \omega}{2\pi}\right)^{1-n}} \qquad (8)$$

In Fig. 10, the dependency of the Cross relaxation time τ_a on the degree of methylation at 273 K is given. The linear trend observed is in good qualitative agreement with the literature results for carboxyl functionalized poly(n-butyl acrylate) polymers [38]. Again, the increase in this time with DM is much stronger for carboxylate functionalized polymers in comparison to the series of polyglycerols in question. Furthermore, we are able to show viscosities and times in a complete range of mole fractions, going from
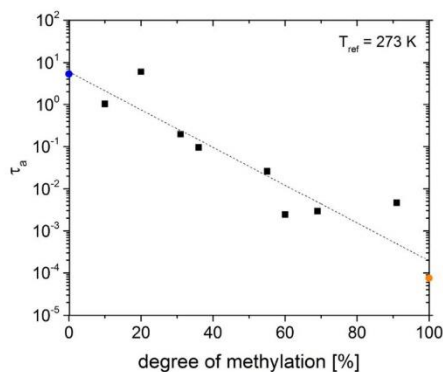
Fig. 10. Cross relaxation time τ_a in dependency of DM at 273 K. A dotted line is shown in order to guide the eye.

0 to 100 mol % of H-bonding monomers, confirming their trend for low degrees of methylation and for the fully hydroxylated homo-polymer sample as well.

In the following we examine the zero-shear viscosity at a reference temperature of 50 K above the glass transition to compensate for T_g effects in the analysis of material parameters. As can be seen from the comparison of results presented in Fig. 11, here as a relative viscosity, with those from Fig. 9, the T_g-effect is tremendous: In the first case the viscosity increases by more than 5 decades, while in the second case the increase is in the range of two decades only. Moreover, the comparison at equal distance to T_g breaks the monotonicity of the curve and leads to the appearance of a maximum at around DM = 20–30%. This maximum can be understood, if one uses an empirical nonlinear mixing rule for the relative viscosity:

$$\log\left(\frac{\eta_{0_{OH}}}{\eta_{0_{OMe}}}\right) = \left[a_0^\beta\cdot(1-y) + a_1^\beta\cdot y + a_2^\beta\cdot(1-y)\cdot y\right]^{\frac{1}{\beta}} \quad (9)$$

with $a_0 = \log(\eta_{rel,y=0})$, $a_1 = \log(\eta_{rel,y=1})$, $a_2 = \log(\eta_{rel\ mix})$, and $y = \frac{DM}{100}$. The corresponding fit curve is presented in Fig. 11 in purple with $a_0 = 1.37 \pm 0.26$, $a_1 = 0.0 \pm 0.24$, $a_2 = 5.0 \pm 2.3$ and
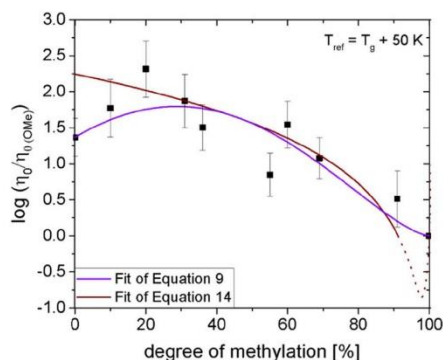
Fig. 11. Zero shear viscosity ($T_g + 50$ K) in dependency of the degree of methylation.

$\beta = 0.66 \pm 0.26$. Even though the fit is satisfactory in the whole composition range, this kind of description lacks a sound structural basis.

For associating polymer systems, the dependency of the zero-shear viscosity on the DM can be described with the sticky Rouse model, at least in a certain DM-range [28]. This model considers the dynamics of the formation and break of temporary network points induced by stickers, in our case OH-groups. Neglecting entanglement effects Chen et al.[56] derived an expression for the shear relaxation modulus G(t) of associating chains (Equation (10)), considering that stickers exhibit an association lifetime τ_s, which causes a delay in terminal relaxation time of the polymer compared to the non-modified polymer.

$$G_r^{ass}(t) = \int_0^\infty W(M)\cdot\frac{\rho RT}{M}\left\{\sum_{p=1}^{N_s} e^{-\frac{t}{\tau_s\left(\frac{M}{pM_s}\right)^2}}\right.$$
$$\left. + \sum_{N_s+1}^{N} e^{-\frac{t}{\tau_0\left(\frac{M}{pM_0}\right)^2}}\right\}dM \quad (10)$$

In this equation $N_s = \frac{M}{M_s}$ is the number of (Rouse-)strands between stickers, i.e., hydroxyl-groups of a chain having a molecular weight M. $M_s = \frac{M_n}{DP\left(1-\frac{DM}{100}\right)}$ is the average molecular weight of a strand between hydroxyl groups, and W(M) is molecular weight distribution. M_0 represents the molecular weight of the elementary Rouse segment, $N = \frac{M_n}{M_0}$, and τ_0 is the monomer relaxation time. According to equation (9) and simplifying the equation for monodisperse polymers $M = M_n$, the zero-shear viscosity can be written as:

$$\eta_0 = \int_0^\infty G_r^{ass}(t)dt = \frac{\rho RT}{M_n}\left\{\sum_{p=1}^{\frac{M_n}{M_s}}\tau_s\left(\frac{M_n}{pM_s}\right)^2 + \sum_{p=\frac{M}{M_s}+1}^{\frac{M_n}{M_0}}\tau_0\left(\frac{M_n}{pM_0}\right)^2\right\} \quad (11)$$

We consider only the leading terms to the sums to obtain the simplest expression for the zero-shear-viscosity

$$\eta_0 = \frac{\rho RT}{M_n}\left[\tau_s\left(\frac{M_n}{M_s}\right)^2 + \tau_0\left(\frac{M_n}{\left(\frac{M_n}{M_s}+1\right)M_0}\right)^2\right]. \quad (12)$$

For non-associating polymers ($\tau_s = 0$ and $M_s \to \infty$) the first term becomes zero and we obtain:

$$\eta_{0_{OMe}} = \frac{\rho RT}{M_n}\cdot\tau_0\left(\frac{M_n}{M_0}\right)^2$$

and for associating polymers

$$\eta_{0_{OH}} = \frac{\rho RT}{M_n}\cdot\left[\tau_s\left(\frac{M_n}{M_s}\right)^2 + \tau_0\left(\frac{M_n}{\left(\frac{M_n}{M_s}+1\right)\cdot M_0}\right)^2\right]. \quad (13)$$

Correlating both equation (13) by dividing $\eta_{0_{OH}}$ through $\eta_{0_{OMe}}$ and expressing M_s by the degree of methylation DM (mole fraction of methyl groups), we obtain:

Tetraalkylammonium salts/propylene oxide controlled anionic polymerization, Macromol. Symp. 226 (2005) 61—68, http://dx.doi.org/10.1002/masy.200550806.

[9] M. Gervais, A.-L. Brocas, G. Cendejas, A. Deffieux, S. Carlotti, Synthesis of linear high molar mass glycidol-based polymers by monomer-activated anionic polymerization, Macromolecules 43 (2010) 1778—1784, http://dx.doi.org/10.1021/ma902286a.

[10] J. Herzberger, K. Niederer, H. Pohlit, J. Seiwert, M. Worm, F.R. Wurm, H. Frey, Polymerization of ethylene oxide, propylene oxide, and other alkylene oxides: synthesis, novel polymer architectures, and bioconjugation, Chem. Rev. 116 (2016) 2170—2243, http://dx.doi.org/10.1021/acs.chemrev.5b00441.

[11] M. Weinhart, I. Grunwald, M. Wyszogrodzka, L. Gaetjen, A. Hartwig, R. Haag, Linear poly(methyl glycerol) and linear polyglycerol as potent protein and cell resistant alternatives to poly(ethylene glycol), Chem. Asian J. 5 (2010) 1992—2000, http://dx.doi.org/10.1002/asia.201000127.

[12] S. Aoki, A. Koide, S.-i. Imabayashi, M. Watanabe, Novel Thermosensitive polyethers prepared by anionic ring-opening polymerization of glycidyl ether derivatives, Chem. Lett. (2002) 1128—1129, http://dx.doi.org/10.1246/cl.2002.1128.

[13] A. Labbé, S. Carlotti, A. Deffieux, A. Hirao, Controlled polymerization of glycidyl methyl ether initiated by onium salt/triisobutylaluminum and investigation of the polymer LCST, Macromol. Symp. 249—250 (2007) 392—397, http://dx.doi.org/10.1002/masy.200750409.

[14] S. Reinicke, J. Schmelz, A. Lapp, M. Karg, T. Hellweg, H. Schmalz, Smart hydrogels based on double responsive triblock terpolymers, Soft Matter (2009), http://dx.doi.org/10.1039/b900539k.

[15] A. Labbé, A.-L. Brocas, E. Ibarboure, T. Ishizone, A. Hirao, A. Deffieux, S. Carlotti, Selective ring-opening polymerization of glycidyl methacrylate: toward the synthesis of cross-linked (Co)polyethers with thermoresponsive properties, Macromolecules 44 (2011) 6356—6364, http://dx.doi.org/10.1021/ma201075n.

[16] M. Weinhart, T. Becherer, N. Schnurbusch, K. Schwibbert, H.-J. Kunte, R. Haag, Linear and hyperbranched polyglycerol derivatives as excellent bioinert glass coating materials, Adv. Eng. Mat. 13 (2011) B501—B510, http://dx.doi.org/10.1002/adem.201180012.

[17] K. Hoger, T. Becherer, W. Qiang, R. Haag, W. Friess, S. Kuchler, Polyglycerol coatings of glass vials for protein resistance, Eur. J. Pharm. Biopharm. (2013) 756—764, http://dx.doi.org/10.1016/j.ejpb.2013.04.005.

[18] S.S. Müller, C. Moers, H. Frey, A challenging comonomer pair: copolymerization of ethylene oxide and glycidyl methyl ether to thermoresponsive polyethers, Macromolecules 47 (2014) 5492—5500, http://dx.doi.org/10.1021/ma501280k.

[19] S. Heinen, S. Rackow, A. Schäfer, M. Weinhart, A perfect match: fast and truly random copolymerization of glycidyl ether monomers to thermoresponsive copolymers, Macromolecules 50 (2017) 44—53, http://dx.doi.org/10.1021/acs.macromol.6b01904.

[20] C. Osterwinter, C. Schubert, C. Tonhauser, D. Wilms, H. Frey, C. Friedrich, Rheological consequences of hydrogen bonding: linear viscoelastic response of linear polyglycerol and its permethylated analogues as a general model for hydroxyl-functional polymers, Macromolecules 48 (2015) 119—130, http://dx.doi.org/10.1021/ma501674x.

[21] R. Haag, J.-F. Stumbé, A. Sunder, H. Frey, A. Hebel, An approach to Core—Shell-Type architectures in hyperbranched polyglycerols by selective chemical differentiation, Macromolecules 33 (2000) 8158—8166, http://dx.doi.org/10.1021/ma000831p.

[22] R.M. Nouguier, M. Mchich, Alkylation of pentaerythritol and trimethylolpropane, two very hydrophilic polyols, by phase-transfer catalysis, J. Org. Chem. 50 (1985) 3296—3298, http://dx.doi.org/10.1021/jo00218a010.

[23] L. Leibler, M. Rubinstein, R.H. Colby, Dynamics of reversible networks, Macromolecules 24 (1991) 4701—4707, http://dx.doi.org/10.1021/ma00016a034.

[24] F. Tanaka, S.F. Edwards, Viscoelastic properties of physically crosslinked networks. 1. Transient network theory, Macromolecules 25 (1992) 1516—1523, http://dx.doi.org/10.1021/ma00031a024.

[25] M. Rubinstein, A.N. Semenov, Dynamics of entangled solutions of associating polymers, Macromolecules 34 (2001) 1058—1068, http://dx.doi.org/10.1021/ma0013049.

[26] D. Xu, S.L. Craig, Scaling laws in supramolecular polymer networks, Macromolecules 44 (2011) 5465—5472.

[27] T. Annable, R. Buscall, R. Ettelaie, D. Whittlestone, The rheology of solutions of associating polymers: comparison of experimental behavior with transient network theory, J. Rheol. 37 (1993) 695—726, http://dx.doi.org/10.1122/1.550391.

[28] M. Rubinstein, A.N. Semenov, Thermoreversible gelation in solutions of associating polymers. 2. Linear dynamics, Macromolecules 31 (1998) 1386—1397, http://dx.doi.org/10.1021/ma970617+.

[29] K.E. Feldman, M.J. Kade, E.W. Meijer, C.J. Hawker, E.J. Kramer, Model transient networks from strongly hydrogen-bonded polymers, Macromolecules 42 (2009) 9072—9081, http://dx.doi.org/10.1021/ma901668w.

[30] R. Stadler, L. Lucca Freitas, Thermoplastic elastomers by hydrogen bonding 1. Rheological properties of modified polybutadiene, Colloid & Polym. Sci 264 (1986) 773—778, http://dx.doi.org/10.1007/BF01500752.

[31] H.H. Winter, M. Mours, The cyber infrastructure initiative for rheology, Rheol.

Acta 45 (2006) 331—338, http://dx.doi.org/10.1007/s00397-005-0041-7.

[32] J. Herzberger, D. Leibig, J.C. Liermann, H. Frey, Conventional oxyanionic versus monomer-activated anionic copolymerization of ethylene oxide with glycidyl ethers: striking differences in reactivity ratios, ACS Macro Lett. 5 (2016) 1206—1211, http://dx.doi.org/10.1021/acsmacrolett.6b00701.

[33] V.V. Jaacks, Eine neue Methode zur Bestimmung von Copolymerisationsparametern, Makromol. Chem. 105 (1967) 289—291, http://dx.doi.org/10.1002/macp.1967.021050129.

[34] T. Kelen, F. Tüdos, Analysis of the linear methods for determining copolymerization reactivity ratios. I. A new improved linear graphic method, J. Macromol. Sci. Part A - Chem. 9 (1975) 1—27, http://dx.doi.org/10.1080/00222337508068644.

[35] A.L. Agapov, Y.Y. Wang, K. Kunal, C.G. Roberston, A.P. Sokolov, Effect of polar interactions on polymer dynamics, Macromolecules 45 (2012) 8430—8437.

[36] J.E. Mark, Physical Properties of Polymers Handbook. Temperature Dependence of the Viscoelastic Response of Polymer Systems, second ed., Springer, New York, 2007.

[37] T.P. Lodge, Viscoelastic properties of highly entangled poly(vinyl methyl ether), Macromolecules 30 (1997) 3694—3695, http://dx.doi.org/10.1021/ma961019i.

[38] C.L. Lewis, K. Stewart, M. Anthamatten, The influence of hydrogen bonding side-groups on viscoelastic behavior of linear and network polymers, Macromolecules 47 (2014) 729—740, http://dx.doi.org/10.1021/ma402368s.

[39] K. Miao, Y. Hu, B. Zha, L. Xu, X. Miao, W. Deng, Hydroxyl versus carboxyl substituent: effects of competitive and cooperative multiple hydrogen bonds on concentration-controlled self-assembly, J. Phys. Chem. C 120 (2016) 14187—14197, http://dx.doi.org/10.1021/acs.jpcc.6b03920.

[40] M. Gordon, J.S. Taylor, Ideal copolymers and the second-order transitions of synthetic rubbers. i. non-crystalline copolymers, J. Appl. Chem. 2 (1952) 493—500, http://dx.doi.org/10.1002/jctb.5010020901.

[41] T.G. Fox, Influence of diluent and of copolymer composition on the glass temperature of a polymer system, Bull. Am. Phys. Soc. (1956) 123—125.

[42] E.A. Dimarzio, J.H. Gibbs, Glass temperature of copolymers, J. Polym. Sci. A Polym. Chem. 40 (1959) 121—131, http://dx.doi.org/10.1002/pol.1959.1204013609.

[43] Z. Zhang, H.R. Kricheldorf, C. Friedrich, Thermorheological and mechanical properties of copolymers of lactide, isosorbide, and different phthalic acids, Macromol. Rapid Commun. 36 (2015) 262—268, http://dx.doi.org/10.1002/marc.201400489.

[44] H. Daimon, H. Okitsu, J. Kumanotani, Glass transition behaviors of random and block copolymers and polymer blends of styrene and cyclododecyl acrylate. I. glass transition temperatures, Polym. J. Polym. J. 7 (1975) 460—466, http://dx.doi.org/10.1295/polymj.7.460.

[45] C. Schubert, C. Osterwinter, C. Tonhauser, M. Schömer, D. Wilms, H. Frey, C. Friedrich, Can hyperbranched polymers Entangle?: effect of hydrogen bonding on entanglement transition and thermorheological properties of hyperbranched polyglycerol melts, Macromolecules 49 (2016) 8722—8737, http://dx.doi.org/10.1021/acs.macromol.6b00674.

[46] J.R. Dorgan, D.M. Knauss, H.A. Al-Muallem, T. Huang, D. Vlassopoulos, Melt rheology of dendritically branched polystyrenes, Macromolecules 36 (2003) 380—388, http://dx.doi.org/10.1021/ma020612z.

[47] C. Tonhauser, D. Wilms, Y. Korth, H. Frey, C. Friedrich, Entanglement transition in hyperbranched polyether-polyols, Macromol. Rapid Commun. 31 (2010) 2127—2132, http://dx.doi.org/10.1002/marc.201000473.

[48] S. Kästner, Zur Frage der Abhängigkeit der Relaxationszeit des dielektrischen Verhaltens der Polymeren vom freien Volumen, J. Polym. Sci. C Polym. Symp. 16 (1967) 4121—4131, http://dx.doi.org/10.1002/polc.5070160752.

[49] L. De Lucca Freitas, R. Stadler, Thermoplastic elastomers by hydrogen bonding 4. Influence of hydrogen bonding on the temperature dependence of the viscoelastic properties, Colloid & Polym. Sci 266 (1988) 1095—1101, http://dx.doi.org/10.1007/BF01414399.

[50] J. Dudowicz, K.F. Douglas, K.F. Freed, The meaning of the "universal" WLF parameters of glass-forming polymer liquids, J. Chem. Phys. 142 (2015) 14905—14907, http://dx.doi.org/10.1063/1.4905216.

[51] M. Müller, U. Seidel, R. Stadler, Influence of hydrogen bonding on the viscoelastic properties of thermoreversible networks: analysis of the local complex dynamics, Polymer 36 (1995) 3143—3150, http://dx.doi.org/10.1016/0032-3861(95)97877-l.

[52] M.G. McKee, C.L. Elkins, T. Parl, T.E. Long, Influence of random branching on multiple H-bonding in Polyalkylmethacrylates, Macromolecules 38 (2005) 6015—6023.

[53] P.J. Carreau, Rheological equations from molecular network theories, Trans. Soc. Rheology (1957-1977) 16 (1972) 99—127, http://dx.doi.org/10.1122/1.549276.

[54] K. Yasuda, R.C. Armstrong, R.E. Cohen, Shear flow properties of concentrated solutions of linear and star branched polystyrenes, rheologica acta, Rheol. Acta 20 (1981) 163—178, http://dx.doi.org/10.1007/BF01513059.

[55] J.F. Vega, S. Rastogi, G.W.M. Peters, H.E.H. Meijer, Rheology and reptation of linear polymers. ultrahigh molecular weight chain dynamics in the melt, J. Rheol. 48 (2004) 663—678, http://dx.doi.org/10.1122/1.1718367.

[56] Q. Chen, G.J. Tudryn, R.H. Colby, Ionomer dynamics and the sticky Rouse model, J. Rheol. 57 (2013) 1441—1462, http://dx.doi.org/10.1122/1.4818868.

A4. Rapid One-Pot Synthesis of Tapered Star Copolymers via Ultra-Fast Coupling of Polystyryllithium Chain Ends

Philipp von Tiedemann,[a,b] *Kamil Maciol*,[a] *Jasmin Preis*,[c] *Paweł Sajkiewicz*,[d] *Holger Frey*[a,*]

[a] Institute of Organic Chemistry, Johannes Gutenberg University, Duesbergweg 10-14, 55128 Mainz (Germany)

[b] Graduate School Materials Science in Mainz, Staudinger Weg 9, 55128, Mainz (Germany)

[c] PSS Polymer Standards Service GmbH, In der Dallheimer Wiese 5, 55120 Mainz (Germany)

[d] Institute of Fundamental Technological Research, Polish Academy of Sciences, Adolfa Pawińskiego 5b, 02-106 Warsaw (Poland)

*E-Mail: hfrey@uni-mainz.de

To be submitted.

ABSTRACT

A highly efficient stoichiometric coupling of sterically hindered polystyryllithium (PS-Li) chain ends was achieved using tetra[3-(chloro-dimethylsilyl)propyl]silane (TCDMSPS) as the linking agent. Based on the disparate reactivities of isoprene (I, $r_I = 11.0$) and styrene (S, $r_S = 0.049$) in the anionic copolymerization in nonpolar media, poly(isoprene$_{0.5}$-$grad$-styrene$_{0.5}$) (P(I$_{0.5}$-$grad$-S$_{0.5}$)) tapered 4-arm star copolymers were synthesized in only two steps. The tapered 4-arm star copolymers ($M_w^{targeted} = 40$ to 160 kg mol^{-1}) were synthesized with high star functionalities f ($M_{w,star}/M_{w,arm} = 3.68 – 3.98$), low dispersities ($Đ = 1.08 – 1.15$) and minimal residual precursor content (2-8 wt%) without fractionation or other purification methods. Coupling kinetics measurements revealed that for the synthesis of poly(styrene) (PS) 4-arm stars (12 kg mol^{-1}) a coupling efficiency of 98% was already achieved within just 2 minutes. Nanofibers were processed via electrospinning. All star polymers were analyzed by size exclusion chromatography (SEC) viscometry with universal calibration (UC) as well as NMR spectroscopy.

TABLE OF CONTENTS GRAPHICS
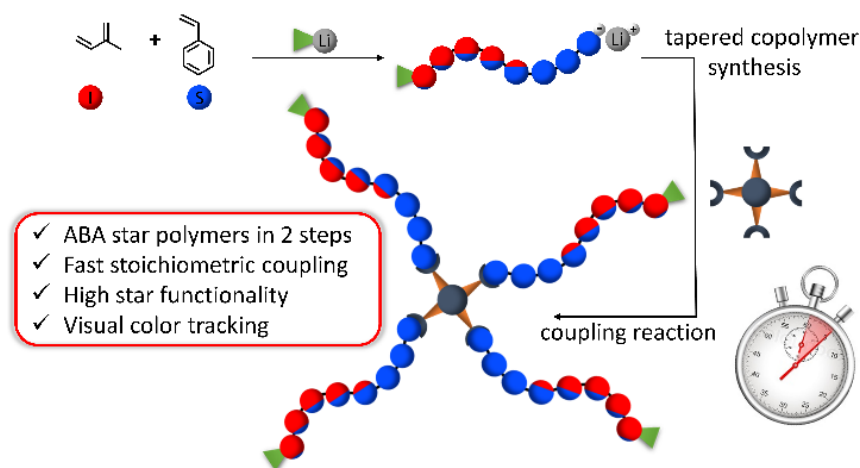
INTRODUCTION

Star-shaped polymers represent an outstanding class of materials as they intrinsically exhibit an extraordinary set of properties (e.g.: low viscosity in melt and solution, lower melting temperatures) compared to their linear analogs[1] rendering them suitable for many commercial applications. In the field of thermoplastic elastomers, star-shaped polymers are highly established for commercial products such as Solprene® (Phillips)[2] and Styrolux® (BASF).[3] Both materials are based on specially designed polymer architectures, combining properties like high stiffness, sufficient toughness and transparency.

Relying on anionic living polymerization, the so-called "arm-first" method is a versatile and well-established synthetic route towards complex star polymer architectures. The alternative "core-first" method requires multifunctional anionic initiators, which to date do not meet the strict requirements for the synthesis of well-defined star polymers.[4] Therefore, established procedures oftentimes rely on multifunctional di- or tri-chlorosilane moieties (with a number of x functional groups) as an electrophilic linking agent for the coupling reaction of living polymer chains.[5] In 1962 Morton and coworkers were the first to demonstrate the feasibility of this concept.[6] Whereas the coupling with chlorosilanes is known to proceed with almost no side reactions benzyl bromide or chloride linking agents suffer from problems like metal-halogen exchange, benzyl proton abstraction and single electron transfer reactions.[7] Anyhow the coupling step is generally very slow and prone to impurities.[5,8] In order to obtain star polymers with high functionality ($f \approx x$) usually a large excess (typically 100%) of the living polymer chains and a very low concentration of the coupling agent solution is needed. Due to these major drawbacks these coupling reactions always yield a mixture of products with different numbers of arms ($x > f > 1$). Consequently, the resulting star polymers have to be subjected to repeated fractionation in order to isolate the desired star-shaped polymer.[9] By means of this established procedure star polymers with a variety of different architectures have been synthesized.[10] For many star polymer syntheses, polyisoprenyllithium (PI-Li)[11] or polybutadienyllithium (PB-Li)[12,13] was utilized to increase the coupling efficiency based on the reduced steric hindrance of the polymer chain ends. Therefore, a typical synthesis strategy involves the end capping of the living polymer chains with a few units of butadiene[14] right before the coupling step in order to increase the coupling efficiency. Via this approach Fetters, Roovers, Hadjichristidis and others prepared star-branched polymers with arm numbers ranging from 4 to 128 via coupling with multifunctional chlorosilanes.[2,12,15] Anyhow, so far very long reaction times (up to 8 weeks)[12] were always necessary for a quantitative coupling in such complex syntheses. Register and

coworkers recently reported that the coupling of PI-Li with 2,2,4,4,6,6-hexachloro-2,4,6-trisilaheptane can be dramatically accelerated by the addition of small amounts of tetrahydrofuran (THF).[16]

In contrast, quantitative coupling of PS-Li[17,18] still presents a considerable challenge due to the steric demand and the more pronounced charge delocalization at the polymer chain end compared to PI-Li originating from the phenyl ring. Hence, long reaction times (more than 2 weeks) have been reported for the coupling of PS-Li with 1,2-bis(methyldichlorosilyl)ethane and higher reaction temperatures (48 °C) combined with demanding glass blowing techniques (break seal) were so far indispensable.[18] Therefore, a synthetic strategy for the rapid and direct coupling of PS-Li is very desirable as this would result in three major accomplishments: (i) avoiding an additional step of introducing butadiene prior to coupling, (ii) visual color tracking of the proceeding coupling reaction due to the orange colored PS-Li chain ends and (iii) the rapid synthesis of block like tapered star copolymers as a one-pot reaction in only two steps (initiation of the comonomer mixture and stoichiometric coupling).

As this approach allowed to circumvent exceedingly long coupling times high vacuum procedures, break seal and fragile glasbulb techniques would no longer be the only method to access complex model star polymers.

EXPERIMENTAL PART

Reagents

Chemicals and solvents were purchased from commercial suppliers (Acros, Sigma-Aldrich, Fisher Scientific, Alfa Aesar). Deuterated solvents were obtained from Deutero GmbH. Isopropyl alcohol and methanol were used as received without further purification.

Instrumentation

^{1}H NMR spectra (400 MHz) were recorded on a Bruker Avance II 400 spectrometer equipped with a 5 mm BBFO-SmartProbe with z gradient and ATM, as well as a SampleXPress 60 sample changer. All spectra are referenced internally to residual proton signals of the deuterated solvent. For *in situ* ^{1}H NMR kinetics measurements a Bruker Avance III HD 400 spectrometer equipped with a 5 mm BBFO SmartProbe (Z-gradient probe) and an ATM as well as a SampleXPress 60 auto sampler was used.

Size exclusion chromatography (SEC) measurements were performed using a SECurity 1260 Series, equipped with a SDV column set from PSS (PSS SDV 5μm ID 8.0 mm x 50 mm, PSS SDV 5μm (1 000Å, ID 8.0 mm x 300 mm), PSS SDV 5μm (100 000Å, ID 8.0 mm x 300 mm), PSS SDV 5μm (1 000 000Å, ID 8.0 mm x 300 mm). A SECurity 1260 isocratic pump and a SECurtiy GPC 1260 standard autosampler was used. Tetrahydrofuran (THF) was used as the mobile phase (flow rate: 1 mL min^{-1}) and as the solvent. The measurements were carried out at 23 °C with a SECurity GPC 1260 UV-VIS detector (275 nm) and a SECurity on-line viscometer DVD 1260 detector. Poly(styrene) standards PSS-psskitd-06) were provided by PSS for calibration. The reported molecular weights and molecular weight distributions were calculated by universal calibration (UC). All samples were allowed to dissolve for 8 hours at 23 °C prior to the injection of 100 μl. Every sample was injected thrice. The results were evaluated without any correction for instrumental spreading. The software PSS WinGPC UniChrom 8.3 was used for the data analysis.

For the sample preparation for scanning electron microscopy (SEM) analysis, a SEM specimen stub was covered with adhesive carbon tape (NEM Tape, Nisshin EM. Co. Ltd.). A small piece of the 4-arm star copolymer nonwovens were glued onto the tape and coated twice for 2 minutes each with a thin layer of gold using a sputter coater (DII-29030SCTR Smart Coater, JEOL). The microscopic examinations of the fiber morphologies were conducted on a JEOL JSM-

6010PLUS/LV scanning electron microscope with an acceleration voltage of 7 kV (secondary electron imaging mode, working distance: 10 mm, spot size: 50). To calculate the fiber diameter distribution, diameters of 100 fibers were determined using the software ImageJ and evaluated with OriginPro 9.0 (OriginLab Corporation).

Linking agent synthesis: Tetra[3-(chloro-dimethylsilyl)propyl]-silane

The linking agent tetra[3-(chloro-dimethylsilyl)propyl]silane (TCDMSPS) as synthesized according to a literature procedure from Muzafarov and coworkers.[19]

To the stirred solution of dimethylchlorosilane (41.10 g, 473 mmol) and 0.1 mL Karstedt's catalyst (2% in xylene) in anhydrous n-hexane (75 mL) was added dropwise a solution of tetraallyl silane (7.0 g, 36.4 mmol) in anhydrous n-hexane (15 mL). The conversion of the reaction was monitored by 1H NMR spectroscopy by the disappearance of the signals of the allyl protons (δ (ppm) = 4.841 (t, 2H) and 5.741 (m, 1H)). When the conversion reached 100% the reaction mixture was concentrated under reduced pressure and the residue was fractionated under vacuum to yield tetra[3-(dimethyl-chlorosilyl)propyl]silane as a colorless oil. Yield: 16.55 g, (80%).

^{1}H NMR (400 MHz, CDCl3) δ (ppm) = 1.54 – 1.38 (m, 8H, Hc), 0.92 (t, 8H, Hb), 0.69 – 0.59 (m, 8H, Hd), 0.43 (s, 24H, Ha). 13C NMR (100 MHz, CDCl3) δ (ppm) = 23.75 (Cb), 17.93 (Cc), 16.76 (Cd), 1.99 (Ca).

Synthesis of poly-(styrene) and poly(isoprene-grad-styrene) 4-arm star polymers

All polymerizations were carried out in 100 mL Schlenk flasks sealed with a teflon stopper in dry cyclohexane at room temperature in an argon-filled glovebox (MBraun UNILAB, <0.1 ppm of O_2 and <0.1 ppm of H_2O). Cyclohexane was purified by stirring over diphenylhexyllithium (adduct of *sec*-butyllithium and 1,1-diphenylethylene) and vacuum transferred into the polymerization reactor. Styrene (or styrene together with isoprene, 50:50 molar ratio) was dried by stirring over CaH_2 for 24 h followed by distillation into the polymerization flask. The flask was transferred into a glovebox and the monomer/solvent (20 wt%) mixture was initiated by *sec*-butyllithium (1.3 M in cyclohexane/hexane 92/8) via 1 mL syringe. The solution was stirred overnight to ensure full monomer conversion. The next day a small amount of the linear

polymer precursor was sampled out via glass pipette and terminated with methanol (degassed with argon for 1 h prior to use). According to the removed amount, the linking agent was weighted out carefully (0.25 eq. based on the amount of initiator used) and was added dropwise as a stock solution in THF (dried over sodium benzophenone ketyl and vacuum transferred) (100 eq. / eq. (Li)) to the living polymer. The coupling reaction was let run until decolorization occurred and then terminated by adding 1 mL of degassed methanol by a syringe. To precipitate the polymer the mixture was added dropwise into a 10-fold excess of isopropyl alcohol with a small amount of BHT for stabilization. The precipitate was separated by filtration and dried under reduced pressure.
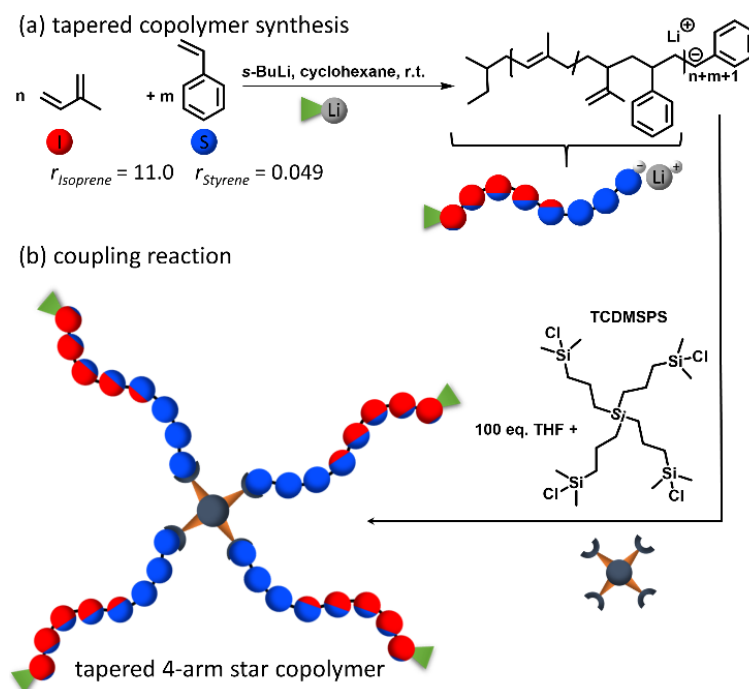
Scheme 1 (a) One-pot synthesis of tapered copolymers from isoprene/styrene and resulting microstructure; (b) coupling reaction with TCDMSPS towards tapered 4-arm star tapered copolymers.

Preparation of 4-arm star copolymer nanofibers

The $P(I_{0.5}\text{-}grad\text{-}S_{0.5})$ 4-arm star copolymer (118.8 ± 2.0 kg mol^{-1}) was dissolved in a mixture of THF and DMF (80:20, v/v) with a concentration of 30% w/w at room temperature. A rotating drum was used as collector (diameter: 2 cm, length: 13 cm), which was attached with an aluminium foil. The distance between needle tip (type 23G) and collector was 10 cm. Electrospinning was performed horizontally at a voltage of 17 kV, a flow rate of 1.75 mL h^{-1} and a collector rotation speed of 292 rpm. The low rotation speed did not result in alignment of the fibers. During the process the temperature was 22.9 °C and the humidity $36 \pm 5\%$.

RESULTS AND DISCUSSION

In this work we report the use of novel tetra-functional, mono-chlorosilyl-based coupling agents for the ultra-fast linking of living carbanionic polymer chains. To the best of our knowledge to date the use of multifunctional mono-chlorosilanes have not been reported for the synthesis of star-branched polymers (except carbosilane dendrimers[19]) via the "arm-first" approach although coupling of living polymer chains with many different multifunctional di- or tri-chlorosilanes has been exploited intensively over the past decades. We demonstrate the one-pot synthesis of PS and P($I_{0.5}$-*grad*-$S_{0.5}$) 4-arm star tapered copolymers (Scheme 1) based on near quantitative, stoichiometric coupling of living PS-Li chain ends with TCDMSPS as a linking agent. The extraordinary high coupling speed and efficiency is governed by three parameters: (i) the maximized reactivity of the chlorosilane compound by using mono-chloro-dimethyl functional groups, (ii) the separation of the reactive chlorosilyl moieties by alkyl spacers and (iii) addition of the linking agent as a stock solution in THF to facilitate the dissociation of the PS-Li dimer complexes formed in nonpolar media.[20] Capitalizing on these principles, defined star polymers with high functionality ($f = 3.68 \pm 0.1$ to 3.98 ± 0.1) were synthesized in high yields ($> 90\%$), avoiding demanding purification, with a low amount of residual precursor ($2-8$ wt%).

The statistical copolymerization and coupling reaction were carried out in all-glass reactors with teflon stopcocks at $23\,°C$ in cyclohexane in a glove box. To prepare PS 4-arm star polymers or P($I_{0.5}$-*grad*-$S_{0.5}$) 4-arm star tapered copolymers, styrene or a I/S mixture of the desired monomer ratio was initiated by *sec*-butyllithium. In case of the tapered copolymer synthesis, the characteristic color change of colorless PI-Li to the orange PS-Li marks the successful crossover from one living chain end to another. Once full monomer conversion was attained, the precursor was sampled out (see experimental part for details) and the successive coupling reaction was performed by adding TCDMSPS as the linking agent dropwise via syringe, dissolved in 100 eq. of THF (calculated with regard to the amount of used s-BuLi). It is important to note, that the dropwise addition yielded more defined star polymers than the simple batch addition. The titration method for polyisoprenyllithium introduced by Register and coworkers[16] was also examined for the coupling of polystyryllithium. In this case a lower coupling efficiency and star functionality was attained even when adding the coupling agent over a very long period (5 hours) via a syringe pump. When the orange color of the PS-Li chains had disappeared the reaction mixture was terminated with degassed methanol to ensure quenching of residual chlorosilane moieties. The addition of methanol is essential to react

potential leftover Si-Cl groups to Si-O-Me, to prevent coupling into Si-O-Si bonds after hydrolysis with H_2O to Si-OH in the precipitation step. After precipitation of the star polymer in isopropanol no further fractionation or purification was applied. All stars and linear polymers were characterized by SEC-viscometry with UC in THF with each sample being injected thrice and the obtained molecular weights (M_w) averaged. The results indicate that all star polymers within error range exhibit a high star functionality f immediately after the coupling reaction, which for many applications renders further purification redundant. For the PS linear precursor (Table 1, sample 1) and the PS 4-arm star (Table 1, sample 2) the measured molecular weights (M_w) were found to be close to those targeted. A star functionality of 3.98 ± 0.1 was achieved directly after the coupling reaction without further fractionation, subsequent to polymer precipitation.

Table 1 Synthesis results of PS linear and 4-arm star polymers coupled with TCDMSPS

Sample	$M_w^{targeted}$ / kg mol^{-1}	M_w^a / kg mol^{-1}	f^b	$Đ^c$
1	3	4.1 ± 0.1	-	1.03
2	12	16.3 ± 0.1	3.98 ± 0.1	1.08

[a] Determined by SEC (averaged triple inject) viscometry in THF (UV signal) and UC, [b] star functionality calculated by $f = M_{w,star} / M_{w,arm}$, [c] determined by SEC in THF (UV signal).

The SEC traces (Fig. 1) reveal that based on the very high coupling efficiency virtually no intermediate materal is formed. Low dispersities ($Đ = 1.03 – 1.08$) for the linear polymer precursor as well as for the resulting star polymer were obtained. Here, a small increase in dispersity can be observed, which is attributed to a low (< 2 wt% by numerical integration) amount of uncoupled linear precursor polymer.
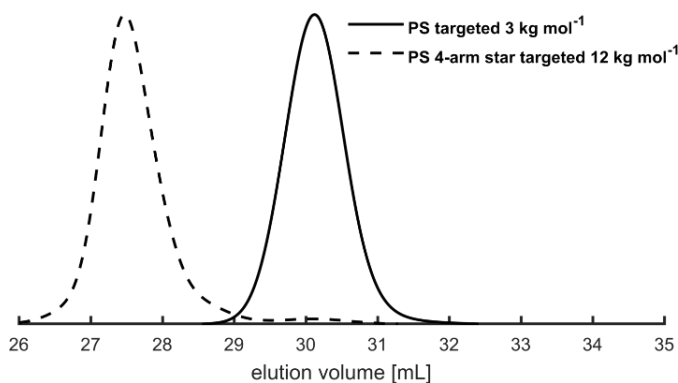

Fig. 1 SEC traces (THF, UV signal); dashed line PS 4-arm star targeted 12 kg mol^{-1}, solid line PS precursor, targeted 3 kg mol^{-1}.

According to the measured amount of residual precursor based on numerical integration by GPC, the ^{1}H NMR characterization (Figure S7) is in good agreement with the coupling efficiency. Based on the integral of the methyl protons (δ = - 0.14 to - 0.47 ppm) from TCDMSPS the efficiency was calculated to be 98% for the coupling reaction.

The coupling kinetics was investigated in a detailed manner by sampling out aliquots from the proceeding coupling reaction with glass pipettes and successive termination of the living polymers with degassed methanol in a glove-box. The samples were analyzed via SEC-viscometry and UC in THF and the star functionality ($f = M_{w,\text{star}}/M_{w,\text{arm}}$) was plotted as a function of coupling time (Fig. 2).
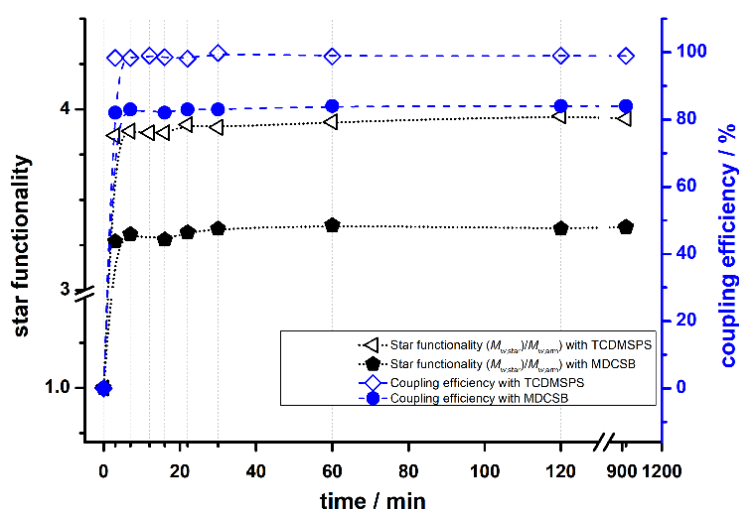
Fig. 2 Coupling kinetics for the synthesis of PS 4-arm star polymer (targeted 12 kg mol^{-1}) using TCDMSPS and MDCSB as the linking agent

To our surprise, this kinetics analysis revealed that already after 2 minutes a remarkably high coupling efficiency (98%) was reached and even after long reaction times (20 h) no further increase was observed. Small variations of the star functionality are attributed to the signal to noise ratio of the viscometer signal. It is interesting to note that after 2 minutes coupling time the solution remained slightly colored (light yellow), however strong turbidity from precipitated LiCl indicated the coupling reaction. The faint color vanished only after several days, indicating that the very few leftover living polymer chains were still active before being terminated. We propose that a very small amount of residual chlorosilyl moieties at the centre of the star polymers is highly sterically shielded after coupling of the living polymer chains to the core. In comparison, the coupling reaction of polystyryllithium (same molecular weight) with 1,4-Bis(methyldichlorosilyl)butane (MDCSB) as a commercially available di-chlorosilane linking agent resulted in a decrease in star functionality of 17% (Fig. 2) although all coupling conditions were kept the same as for the coupling with TCDMSPS. Although the coupling kinetics were

found to be equally fast to TCDMSPS the SEC analysis (Figure S9) revealed a significant low molecular weight shoulder doubtlessly resulting from star polymer side products with intermediate functionality $(4 > f > 1)$. The molecular weight dispersity of the resulting star polymer increased to 1.15 and an averaged star functionality of 3.30 ± 0.1 was only achieved.

From these results we conclude that TCDMSPS is a highly reactive linking agent, permitting ultra-fast coupling of sterically demanding, living PS-Li chain ends when added as a stock solution in THF. This fact can be explained by the high reactivity of the mono-chloro dimethyl silane groups that are separated from each other by alkyl spacers and thereby are more reactive for the subsequent linking of living carbanionic polymer chains. Based on these findings, $P(I_{0.5}$-$grad$-$S_{0.5})$ 4-arm star tapered copolymers with molecular weights ranging from 50.0 ± 1.1 to 118.8 ± 2.0 kg mol^{-1} and low dispersities $(Đ = 1.06 – 1.15)$ (Table 2, sample 1-6) were synthesized to confirm applicability of the concept for the synthesis of more complex polymer architectures with higher molecular weights. The linear gradient copolymer precursors were synthesized based on the disparate reactivity ratios of isoprene (I, $r_I = 11.0$) and styrene (S, $r_S = 0.049$) in apolar media, which we recently investigated in detail.[21] Similar to the synthesized PS 4-arm star, it was found that the measured molecular weights (M_w) were close to those targeted and high star functionalities ($f = 3.68 \pm 0.1$ to 3.98 ± 0.1, Table 2, samples 2, 4, 6) were rapidly achieved.

The SEC traces of the $P(I_{0.5}$-$grad$-$S_{0.5})$ 4-arm star tapered copolymers (Fig. 3) showed only a very low amount of residual precursor after the finished coupling reaction.
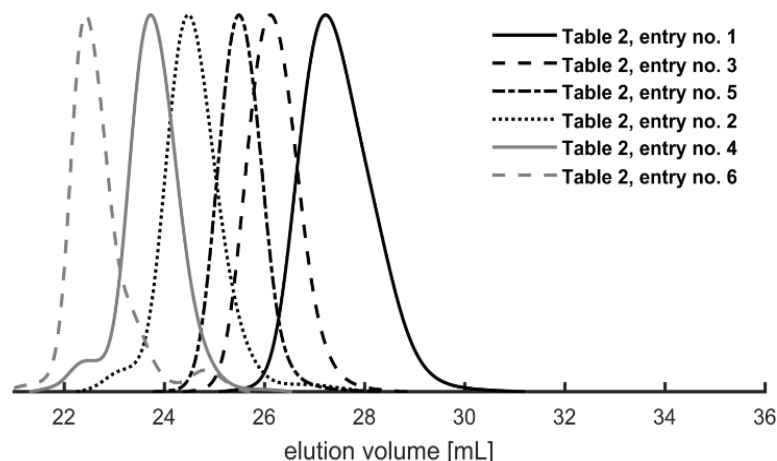

Fig. 3. Elution traces from SEC viscometry with universal calibration (UC) (THF, UV signal) of $P(I_{0.5}$-$grad$-$S_{0.5})$ 4 arm star tapered copolymers targeted 40 - 120 kg mol^{-1} (left) and $P(I_{0.5}$-$grad$-$S_{0.5})$ linear precursors targeted 10 - 30 kg mol^{-1} (right).

The star polymer with 118.8 ± 2.0 kg mol-1 (Table 2, sample 6) is the only sample for which a small low molecular weight shoulder was observed in the SEC trace (Fig. 3).

Table 2 Synthesis results of P(I$_{0.5}$-*grad*-S$_{0.5}$) 4-arm star tapered copolymers (50/50 molar ratio).

Sample	$M_w^{targeted}$ / kg mol^{-1}	M_w^a / kg mol^{-1}	f^b	$Đ^c$
1	10	12.2 ± 0.1	-	1.09
2	40	50.0 ± 1.1	3.98 ± 0.1	1.15
3	15	20.3 ± 0.1	-	1.08
4	60	74.7 ± 1.2	3.68 ± 0.1	1.06
5	30	31.6 ± 0.3	-	1.11
6	120	118.8 ± 2.0	3.92 ± 0.1	1.08

[a] Determined by SEC (averaged triple inject) viscometry in THF (UV signal) with UC, [b] star functionality calculated by $f = M_{w,star} / M_{w,arm}$, [c] determined by SEC in THF (UV signal).

Further, the star polymers (Table 2, sample 2, 4, 6) showed a small feature at low SEC elution time when the viscosity detector was utilized. This effect was neither observed for the tapered precursors (Table 2, sample 1, 3, 5), nor for pure PS or pure PI star polymers, thus hinting at a particular effect originating from the tapered copolymer microstructure. Furthermore, this effect was not present when only standard SEC detectors (UV, RI) were used (Figure S12).

Based on the introduced 4-arm star tapered copolymers many more complex macromolecular architectures are thinkable. Expanding this synthetic approach to thermoplastic elastomers (TPEs) in the end also requires an applicable processing method for this special type of polymers. Typical thermal processing procedures represent a convenient method once polydienes have been hydrogenated. Whereas the hydrogenation step is well established for many kinds of linear macromolecules it represents a considerable challenge for star polymers. Postpolymerization modification protocols such as catalytic hydrogenation are known to degrade the star architecture at the core (Si-C bond scission).[22] Thus, a processing procedure which excludes this additional and problematic step is very desirable. Therefore, the synthesized gradient star copolymers were subjected to electrospinning as an alternative processing method.[23] In contrast to thermal processing, electrospinning represents a gentle method for preventing thermo-oxidative degradation of polydienes as it can be operated at room temperature. Defined fibers with an averaged diameter of 0.99 µm were obtained from a

30 wt% THF/DMF (80:20, v/v)[24] solution (Fig. 4) when the P($I_{0.5}$-*grad*-$S_{0.5}$) 4 arm star tapered copolymer (Table 2, sample 6, $M_w = 118.8 \pm 2.0$ kg mol^{-1}) was used.
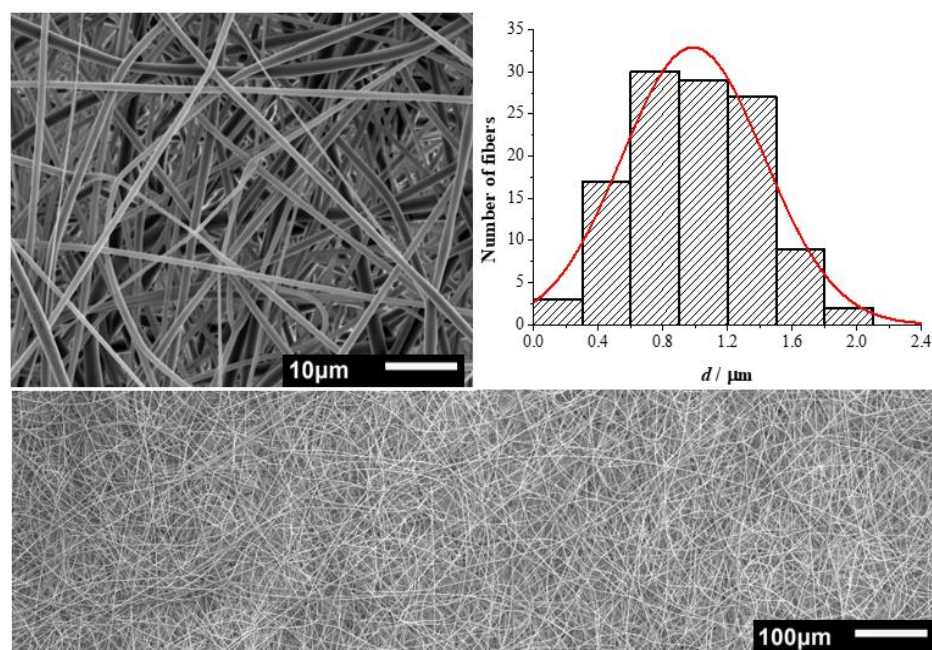

Fig. 4 SEM image of electrospun P($I_{0.5}$-*grad*-$S_{0.5}$) 4 arm star tapered copolymer nanofibers (Table 2, sample 6, $M_w = 118.8 \pm 2.0$ kg mol^{-1}), zoom (top left corner) and distribution of the fiber diameters ($d_{mean} = 0.99$ µm, $\sigma_{Std.Dev.} = 0.88$ µm) (top right corner).

CONCLUSIONS

In conclusion, we report a scalable one-pot synthesis of defined PS and P(I0.5-grad-S0.5) 4-arm star tapered copolymers without the need for glass blowing techniques (break seal) or demanding purification, relying on the ultra-fast coupling of PS-Li chain ends with the tetra-functional TCDMSPS as a highly reactive linking agent. In principle, only two reaction steps (initiation of the comonomer mixture and stoichiometric coupling) are required, rendering the established additional introduction of a few units of butadiene or isoprene redundant. Since the conversion of this coupling reaction can be visually tracked by the decrease of the orange color of the PS-Li chain ends, this synthetic approach holds great promise. Not only for the coupling of many other living polymers but also for a variety of industrial applications as the typically reported long reaction times for the coupling of PS-Li can be drastically reduced from weeks to minutes. Extending this general principle for the successful coupling of multiblock copolymers[25] to multiblock stars is a topic of ongoing research in our group. As these materials exhibit excellent material properties, originating from a high bridging fraction (v_b) of chains that link together the microdomains, they become suitable for many applications in the field of thermoplastic elastomers (TPEs).[26]

ACKNOWLEDGEMENTS

REFERENCES

1   J. M. Ren, T. G. McKenzie, Q. Fu, E. H. H. Wong, J. Xu, Z. An, S. Shanmugam, T. P. Davis, C. Boyer and G. G. Qiao, *Chem. Rev.*, 2016, **116**, 6743–6836.

2   N. Hadjichristidis, M. Pitsikalis, H. Iatrou, P. Driva, G. Sakellariou and M. Chatzichristidi, in *Polymer Science: A Comprehensive Reference*, Elsevier, 2012, pp. 29–111.

3   a) K. Knoll and N. Nießner, *Macromol. Symp.*, 1998, **132**, 231–243; b) R. Adhikari, G. H. Michler, S. Goerlitz and K. Knoll, *J. Appl. Polym. Sci.*, 2004, **92**, 1208–1218;

4   R. Matmour and Y. Gnanou, *Prog. Polym. Sci.*, 2013, **38**, 30–62.

5   N. Hadjichristidis, S. Pispas, H. Iatrou and M. Pitsikalis, *COC*, 2002, **6**, 155–176.

6   M. Morton, T. E. Helminiak, S. D. Gadkary and F. Bueche, *J. Polym. Sci.*, 1962, **57**, 471–482.

7   A. Hirao and N. Haraguchi, *Macromolecules*, 2002, **35**, 7224–7231.

8   a) N. Hadjichristidis, M. Pitsikalis, S. Pispas and H. Iatrou, *Chem. Rev.*, 2001, **101**, 3747–3792; b) N. Hadjichristidis, H. Iatrou, M. Pitsikalis and J. Mays, *Prog. Polym. Sci.*, 2006, **31**, 1068–1132; c) T. Higashihara, M. Hayashi and A. Hirao, *Prog. Polym. Sci.*, 2011, **36**, 323–375;

9   a) C. Booth, *J. Polym. Sci.*, 1960, **45**, 443–450; b) A. Kohler, J. G. Zilliox, P. Rempp, J. Polacek and I. Koessler, *Eur. Polym. J.*, 1972, **8**, 627–639;

10   A. Hirao, R. Goseki and T. Ishizone, *Macromolecules*, 2014, **47**, 1883–1905.

11   a) N. Hadjichristidis, A. Guyot and L. J. Fetters, *Macromolecules*, 1978, **11**, 668–672; b) L. K. Bi and L. J. Fetters, *Macromolecules*, 1976, **9**, 732–742; c) G. Floudas, S. Pispas, N. Hadjichristidis, T. Pakula and I. Erukhimovich, *Macromolecules*, 1996, **29**, 4142–4154;

12   J. Roovers, L. L. Zhou, P. M. Toporowski, M. van der Zwan, H. Iatrou and N. Hadjichristidis, *Macromolecules*, 1993, **26**, 4324–4331.

13   a) R. W. Pennisi and L. J. Fetters, *Macromolecules*, 1988, **21**, 1094–1099; b) S. Perny, J. Allgaier, D. Cho, W. Lee and T. Chang, *Macromolecules*, 2001, **34**, 5408–5415;

14   a) D. J. Frater, J. W. Mays, C. Jackson, S. Sioula, V. Efstradiadis and N. Hadjichristidis, *J. Polym. Sci. B Polym. Phys.*, 1997, **35**, 587–594; b) H. C. Lee, W. Lee, T. Chang, J. S. Yoon, D. J. Frater and J. W. Mays, *Macromolecules*, 1998, **31**, 4114–4119;

15   a) L.-K. Bi and L. J. Fetters, *Macromolecules*, 1976, **9**, 732–742; b) L. J. Fetters, A. D. Kiss, D. S. Pearson, G. F. Quack and F. J. Vitus, *Macromolecules*, 1993, **26**, 647–654;

16   A. B. Burns and R. A. Register, *Macromolecules*, 2016, **49**, 2063–2070.

17   a) J. Roovers, N. Hadjichristidis and L. J. Fetters, *Macromolecules*, 1983, **16**, 214–220; b) J. E. L. Roovers and S. Bywater, *Macromolecules*, 1974, **7**, 443–449;

18   J. E. L. Roovers and S. Bywater, *Macromolecules*, 1972, **5**, 384–388.

19   E. A. Rebrov, I. D. Leshchiner and A. M. Muzafarov, *Macromolecules*, 2012, **45**, 8796–8804.

20   M. Morton, L. J. Fetters, R. A. Pett and J. F. Meier, *Macromolecules*, 1970, **3**, 327–332.

21   E. Grune, T. Johann, M. Appold, C. Wahlen, J. Blankenburg, D. Leibig, A. H. E. Müller, M. Gallei and H. Frey, *Macromolecules*, 2018, **51**, 3527–3537.

22   J. M. Carella, J. T. Gotro and W. W. Graessley, *Macromolecules*, 1986, **19**, 659–667.

23   a) A. Greiner and J. H. Wendorff, *Angew. Chem.*, 2007, **46**, 5670–5703; b) Z.-M. Huang, Y.-Z. Zhang, M. Kotaki and S. Ramakrishna, *Composites Science and Technology*, 2003, **63**, 2223–2253; c) D. Li and Y. Xia, *Adv. Mater.*, 2004, **16**, 1151–1170;

24   S.-Q. Feng, X.-Y. Shen, Z.-Y. Fu and Y.-L. Ji, *J. Appl. Polym. Sci.*, 2009, **114**, 1580–1586.

25   E. Grune, M. Appold, A. H. E. Müller, M. Gallei and H. Frey, *ACS Macro Lett.*, 2018, **7**, 807–810.

26   R. K. W. Spencer and M. W. Matsen, *Macromolecules*, 2017, **50**, 1681–1687.

Curriculum Vitae

███████████████

████████████████████████████████ ████████████
████████████████████████

████████████████████████████████ ████████████
███████████████████████████████

████████████████████████████████ ████████████
██████████████████████████████████████

████████████████████

████████████████████████████████ █████████████
███████████████████████████████
██████████████████████████████

████████████████████████████████ ████████████
████████████████
███

███████████████████████████████ █████
██████████████████████████████████████

███████████████████

████████████████████████████████ ██████████████
██████████████████████████████████████ ██████████
██████████████████████████████████████ █████
  ████████████████
  ████████████████
  ██████████████████████

███████████

███
██   █████

████████████████████████████████████

██████████████   ██
██████████████   ███
                      ███████████████████████████████████████
██████████████   ██
                      ████████████████████████████████████
██████████████   ████████████████████████████████████

███████████████████████████

██
██
███████████████████████████

██████   ███████   ████   ██████████   ██   █████████████   ██████
██

██
██
████████████████████████████████████

Publications

Maciol, K.; Linden, G.; Blankenburg, J.; Schmolke, W.; Seiffert, S.; Frey, H. "Design of a Novel Epoxide Monomer for pH-Sensitive Poly(ethylene glycol) Hydrogels via Acid-Labile and Crosslinkable Allyl Side Groups" *to be submitted*

Maciol, K.; Blankenburg, J.; Urschbach, M.; Leibig, D.; Frey, H. "Ketone Dioxolane Glycidyl Ether: Synthesis of Multi-Ketone-Functional Poly(ethylene glycol) as a Promising Candidate for Bioconjugation and Reversible Hydrogels" *to be submitted*

Maciol, K.; Schüttner, S.; Blankenburg, J.; Johann, T.; Frey, H. "Glycidyl Cinnamate: Copolymerization with Glycidyl Ethers, *in-situ* NMR Kinetics and Photocrosslinking" *Submitted to Macromolecules.*

Maciol, K.; Blankenburg, J.; Fischer, K.; Bros, M.; Gleede, T.; Wurm, F. R.; Frey, H. "Ethoxy Butoxy Vinyl Glycidyl Ether: Reactive and Cleavable Multi-Vinyl Ether-Functional Poly(ethylene glycol)s for Drug Delivery Applications" *Submitted to Biomacromolecules.*

Maciol, K.; Dänzer, T.; Keth, J.; Blankenburg, J.; Frey, H. "Epoxy Undecane Methacrylate: A Symbiosis of Methacrylates and Poly(ethylene glycol)" *to be submitted.*

Maciol, K.; Frey, H. "Synthesis of Perfluoroalkyl-Bearing Polyether, Their Characterization and Application as Coating for Glass Slides" *to be submitted.*

Blankenburg, J.; **Maciol, K.**; Hahn, C.; Frey, H. "Design of Multi-Aldehyde-Functional Poly(ethylene glycol) Establishes a Rich and Versatile Post-Polymerization Chemistry" *to be submitted.*

Scharfenberg, M.; **Maciol, K.**; Frey, H. "Ketone Functionalized Aliphatic Polycarbonates Based on Carbon Dioxide" *to be submitted.*

Schubert, C.; Dreier, P.; Nguyen, T.; **Maciol, K.**; Blankenburg, J.; Friedrich, C.; Frey, H. "Synthesis of linear polyglycerols with tailored degree of methylation by copolymerization and the effect on thermorheological behavior." *Polymer* **2017**, *121*, 328–339.

Von Tiedemann, P.; **Maciol, K.**; Preis, J.; Sajkiewicz, P.; Frey, H. "Rapid One-Pot Synthesis of Tapered Star Copolymers via Ultra-Fast Coupling of Polystyryllithium Chain Ends" *to be submitted.*

Von Tiedemann, P.; Blankenburg, J.; **Maciol, K.**; Johann, T.; Müller, A. H. E.; Frey, H. "Copolymerization of Isoprene with para-Alkylstyrene Monomers: Disparate Reactivity Ratios and the Shape of the Gradient" *Submitted to Macromolecules.*

Blankenburg, J.; Kersten, E.; **Maciol, K.**; Kaiser, T.; Wagner, M.; Zarbakhsh, S.; Frey, H. "No Legroom for Comonomers in the Double Metal Cyanide (DMC) Catalysis: Extensive in situ NMR Kinetic Studies on the Copolymerization of Propylene Oxide" *unpublished results.*

Blankenburg, J.; Kersten, E.; **Maciol, K.**; Wagner, M.; Zarbakhsh, S.; Frey, H. "Highly Relevant Polyether Copolymers: The Microstructure of Poly(propylene oxide-*co*-ethylene oxide) Copolymers is Controlled by the Polymerization Method" *unpublished results*.